USDA
United States Department of Agriculture

Proceedings

22nd International Nondestructive Testing and Evaluation of Wood Symposium

Quebec City, Canada
2022


Photo by Gadiel Lazcano on Unsplash


Photo by Julie Boulanger on Unsplash


Photo by Gadiel Lazcano on Unsplash

Forest Service, Forest Products Laboratory
Université Laval
Forest Products Society
International Union of Forest Research Organizations

General Technical Report
FPL–GTR–290

May
2022

Abstract

The 22nd International Nondestructive Testing and Evaluation of Wood Symposium was hosted by the Université Laval in Quebec City, Canada, May 24–27, 2022. This symposium was a forum for those involved in nondestructive testing and evaluation (NDT/NDE) of wood and brought together many international researchers, NDT/NDE users, suppliers, representatives from various government agencies, and other groups to share research results, products, and technology for evaluating a wide range of wood products, including standing trees, logs, structural lumber, engineered wood products, and wood structures. Networking among participants encouraged international collaborative efforts and fostered the implementation of NDT/NDE technologies around the world. A special on-line session was conducted to accommodate individuals who could not attend in-person due to the ongoing COVID-19 pandemic. The technical content of the 22nd symposium is captured in these proceedings. Full-length, in-depth technical papers for most of the oral presentations, along with abstracts for all the oral and poster presentations, are published herein. The papers were not peer reviewed and are reproduced here as they were submitted by the authors.

Keywords: Nondestructive evaluation, nondestructive testing, wood properties, wood products, logs, trees, wood structures

May 2022

Wang, Xiping; Ross, Robert J., eds. 2022. Proceedings: 22nd International Nondestructive Testing and Evaluation of Wood Symposium. General Technical Report FPL-GTR-290. Madison, WI: U.S. Department of Agriculture, Forest Service, Forest Products Laboratory. 324 p.

A limited number of free copies of this publication are available to the public from the Forest Products Laboratory, One Gifford Pinchot Drive, Madison, WI 53726-2398. This publication is also available online at www.fpl.fs.fed.us. Laboratory publications are sent to hundreds of libraries in the United States and elsewhere.

The Forest Products Laboratory is maintained in cooperation with the University of Wisconsin.

Contents

Proceedings

22nd International Nondestructive Testing and Evaluation of Wood Symposium

Quebec City, Canada
May 24–27, 2022

Edited by

Xiping Wang, Research Forest Products Technologist
Robert J. Ross, Supervisory Research General Engineer
USDA Forest Service, Forest Products Laboratory, Madison, Wisconsin, USA

Preface

The International Nondestructive Testing and Evaluation of Wood Symposium Series started in Madison, Wisconsin, USA, in 1963. Since its inception, 21 symposia have been held in various countries around the world, including Brazil, China, Germany, Hungary, Switzerland, and the United States.

The 22nd International Nondestructive Testing and Evaluation of Wood Symposium was hosted by the Université Laval. It was held in Quebec City, Canada, May 24–27, 2022. This symposium was a forum for those involved in nondestructive testing and evaluation (NDT/NDE) of wood and brought together many international researchers, NDT/NDE users, suppliers, representatives from various government agencies, and other groups to share research results, products, and technology for evaluating a wide range of wood products, including standing trees, logs, structural lumber, engineered wood products, and wood structures. Networking among participants encouraged international collaborative efforts and fostered the implementation of NDT/NDE technologies around the world.

After opening comments from the International Nondestructive Testing and Evaluation of Wood Symposium Organizing Committee, participants were welcomed by the Executive Vice-Rector and Vice-Rector of Academic and Student Affairs at Université Laval, Dr. Robert Beauregard.

During the symposium's banquet, special recognition awards were presented to Dr. Alexis Achim, Professor at Université Laval and Director of the Renewable Materials Research Centre in Canada, for his leadership as a co-chair in organizing the event, and to Ms. Claude Durocher and Dr. Rosilei Garcia, Research Associates at Université Laval, for their supporting efforts. Special recognition awards were also presented to Dr. R. Bruce Allison for his distinguished service in the symposium series and efforts to extend the field of nondestructive evaluation to practicing arborists and to Mr. Frank Rinn for his outstanding technology transfer efforts in the field of nondestructive evaluation of wood.

Prior to the Symposium, a technical workshop, "Nondestructive Testing and Evaluation of Wood for Cultural Uses," was conducted on May 24, 2022, and followed by a visit to the Gene-H.-Kruger Building and the Université Laval's TELUS Stadium. The Gene-H.-Kruger building is the hub of teaching, innovation, and development of wood sciences at Université Laval. It provides a showcase for the use of engineered wood products in construction, elements of which are featured in the labs, classrooms, meeting venues, and administrative buildings that are part of this 8,000 m^2 complex. The TELUS stadium is part of a large-scale project, the regional expansion project of the PEPS sports building at Université Laval. The stadium has a magnificent main frame constructed of glued-laminated timber and is an example of sustainable construction. This structural choice avoided the emission of around 1,500 tonnes of CO_2.

An excellent post-symposium Old Quebec Cultural Heritage tour was held on May 28, 2022. This tour of Old Quebec, guided by historian David Mendel and architect Émile Gilbert, provided a perspective of the wooden heritage of Quebec City and included visits to the Dufferin Terrace, Ursuline Chapel, Holy Trinity Anglican Cathedral, interior courtyard of the *Petit Séminaire de Québec,* Université Laval School of Architecture, Augustine's Monastery, and General Hospital.

The technical content of the 22nd symposium is captured in the following proceedings. Full-length, in-depth technical papers for the oral presentations and several of the oral and poster presentations are published herein. The papers were not peer reviewed and are reproduced here as they were submitted by the authors.

The organization of the proceedings follows that of the sessions at the 22nd symposium. Technical sessions covered the following topics:

1. Nondestructive Characterization of Wood and Wood-Based Materials
2. In-Forest Wood Quality Assessments
3. NDE for Urban Trees
4. NDE of Sawn Logs for Optimal Utilization
5. Advanced Grading Technologies for Solid Wood and Engineered Wood Products
6. Condition Assessment of Historic Wood Artifacts and Structures
7. Mixed Session (Online)
8. Poster Session

Note that a special online session was conducted to accommodate individuals who could not attend in-person due to the ongoing COVID-19 pandemic.

We express our sincere appreciation and gratitude to members of the Organizing Committee, International Nondestructive Testing and Evaluation of Wood Symposium Series, for their efforts in making this symposium a success:

Dr. Laszlo Bejo, University of West Hungary, Hungary
Dr. Raquel Gonçalves, University of Campinas, Brazil
Dr. Francisco Arriaga Martitegui, Universidad Politécnica de Madrid, Spain
Dr. Robert J. Ross, FPL and Michigan Technological University, USA
Dr. Udo H. Sauter, Forest Research Institute Baden-Württemberg, Germany
Dr. C. Adam Senalik, FPL, USA
Dr. Xiping Wang, FPL, USA
Dr. Houjiang Zhang, Beijing Forestry University, China

We thank the International Union of Forest Research Organizations (IUFRO), Forest Products Society, USDA Forest Products Laboratory, and Université Laval for their support. Thanks also go to the following organizations for providing financial support in the form of sponsorships:

Mississippi State University
FPInnovations

A very special thank you to Claude Durocher and Rosilei Aparecida Garcia for their outstanding efforts—without their efforts, this meeting would not have been possible. Thanks for being wonderfully gracious hosts!

We thank the following staff at FPL for their outstanding efforts in preparing these proceedings: Jim Anderson and Barb Hogan.

A note of thanks to the many individuals who prepared papers for inclusion in the symposium. Your dedication and efforts make this symposium series a success!

We hope that these proceedings provide inspiration to those who read its papers. And welcome to new participants in the global wood NDT/NDE family!

Dr. Robert J. Ross and Dr. Alexis Achim
Symposium Co-Chairs

General Session

In-Forest Wood Quality Assessments—Where Are We with NDT Technologies?

Xiping Wang *
USDA Forest Service Forest Products Laboratory, Madison, Wisconsin, USA, xiping.wang@usda.gov

Robert J Ross
USDA Forest Service Forest Products Laboratory, Madison, Wisconsin, USA, robert.j.ross.@usda.gov

* Corresponding author

Abstract

Recent research and development on nondestructive testing technologies has brought the in-forest assessments of wood and fiber properties of standing trees into forest management, resource evaluation, harvesting operation, and efficient wood utilization. Significant values are associated with the wood and fiber quality of our forests for the production of structural lumber, engineered wood products (such as glulam, LVL, and CLT), and pulping and paper. Rapid and nondestructive measurements on trees allow this value to be realized through better silvicultural practices, as well as the allocation of resources to highest value users and application of best processing methods. This paper provides an overview of recent research and development on in-forest wood quality assessments using emerging precision-based nondestructive technologies with a focus on forest resource evaluation and wood utilization. These include, but are not limited to, SilviScan™, near infrared, DiscBot, acoustic waves, and resistance drilling. A brief discussion is followed on how these technologies and the knowledge obtained from them can support the development of the next generation of forests, e.g. through tree breeding and silviculture.

Keywords: wood and fiber properties, wood quality, standing trees, forest resources, silviculture, genetic improvement

Introduction

Efficient wood production and utilization requires knowing the wood quality attributes of forest resources relevant to various end uses, prescribing appropriate silvicultural treatments that positively influence wood quality, and then, at the time of harvesting, sorting and allocating standing timbers to the most appropriate markets (Wang et al. 2007a; Amishev and Murphy 2018; Briggs et al. 2008). The field of forestry has many widely accepted field tools, sampling procedures, and models for gathering and summarizing data and making projections of growth, yield, and tree size; however, counterparts for wood quality assessment have lagged behind (Briggs et al. 2008). One of the reasons for this lag has been a lack of simple field tools permitting rapid collection of wood quality data from trees in a stand or sample plot.

The traditional method for evaluating wood quality in standing trees is to extract core samples from living trees using an increment borer, analyzing growth trends based on inspection of the ring patterns, and measuring basic wood properties (density and stiffness) in a laboratory (Cown 2006; Wiemann and Williamson 2013; Gao et al. 2017). This procedure has been used by foresters around the world for many years for defining wood quality of forest resources. The main disadvantages of this method are as follows: first, it is time consuming and labor intensive, which often prevents its use because of the high cost

involved; and second, the tree is wounded in the coring process even though it has been practiced as a ″nondestructive″ sampling procedure. To achieve rapid, reliable, and economical wood quality assessment in trees, forest managers and landowners are interested in implementing more robust nondestructive testing technologies in field operations. Nondestructive is a relative term, because damage is done whenever the protective covering of bark is compromised; the term is used in comparison with sampling methods that require the felling of trees.

In this paper, we provide a brief overview of the research and development of nondestructive evaluation technologies for assessing wood quality of standing trees, highlighting several emerging precision-based nondestructive technologies (SilviScan™, near infrared, DiscBot, acoustic waves, and resistance drilling) and their applications in resource evaluation, harvesting operation, forest management, and tree genetic improvement.

Emerging nondestructive technologies

SilviScan™ system

Since the 1990s, there has been a steady increase in the development of tools for nondestructive assessment of wood quality in trees prior to harvesting. One significant development has been the SilviScan™ system specifically designed for characterizing many wood and fiber properties by taking core samples from trees and then conducting scanning and post analysis in the laboratory (Evans and Ilic 2001; Evans and Kibblewhite 2002). This instrument, as shown in Figure 1, was developed by Dr. Robert Evans and his team in CSIRO, Australia to meet the requirements of plantation assessment and breeding programs. It involves several measurement principles, including microscopic image analysis (tracheid and fiber diameters, vessel size and position, ring boundary position, ring orientation), x-ray densitometry (density profile, fiber tilt, ring boundary position), and x-ray diffractometry (microfibril angle (MFA), tracheid and fiber 3D orientation, cellulose crystallite width) (Figure 2). This laboratory instrument system can generate a series of high-resolution wood property data from the same wood sample, including wood density, stiffness, microfibril angle, and tracheid properties such as tracheid diameter, coarseness, and cell wall thickness. All SilviScan™ data can be related to individual annual rings so that detailed ″tree property maps″ can be developed, allowing quantification of the effects of site, silvicultural treatment, or genotype.

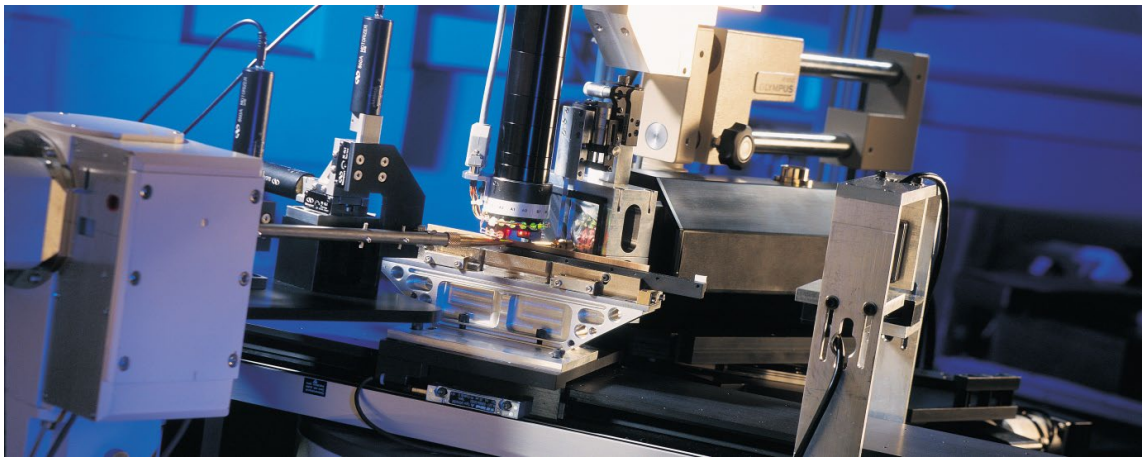

Figure 1. SilviScan system developed by Dr. Robert Evans and his team in CSIRO, Australia (Schimleck et al. 2019. Photo credit: Robert Evans)

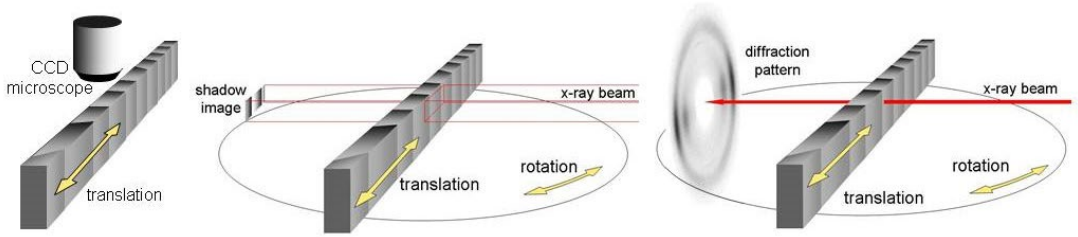

Figure 2. The three analysis components of SilviScan (Cell Scanner, Densitometer, Diffractometer) (Schimleck et al. 2019).

Currently there are three SilviScan™ systems in operation, one in the University of Melbourne, Australia; one in Innventia, Stockholm, Sweden; and one in FP Innovations, Vancouver, Canada. These three systems are now being used for a range of basic and applied research and commercial programs, providing test data to researchers around the world. These three systems together are capable of measuring 10,000 samples per year. The main advantage of SilviScan™ is that it can nondestructively assess a large number of trees and produce high resolution wood property profiles from pith to bark and along the tree height. Drawbacks are that it is a laboratory instrument with a relatively high cost requiring the user to have specialized knowledge and expertise to run the scanning process and interpret the results.

Near infrared (NIR) spectroscopy

Near infrared (NIR) spectroscopy is another laboratory technique that can be used to assess the wood quality of standing trees. Similar to SilviScan™, it requires taking core samples or wood chips from trees and then conducting scanning in the laboratory. Near-infrared is the region of the electromagnetic spectrum immediately after the visible region with the wavelength range of 780–2500 nm. NIR spectroscopy can measure the chemical composition of a material very rapidly, with minimum sample preparation. The technique was originally developed for use in biomedical applications. It has also been thoroughly investigated for use in the forest products industry, and it is particularly well-suited to quality control and process monitoring in pulp production (So et al. 2004). Many studies have been performed to explore the potential of using NIR spectroscopy to characterize wood and fiber properties, specifically linking the wood chemistry to a range of properties, such as tracheid length, density, microfibril angle, and physical and mechanical properties (So et al. 2004; Schimleck et al. 2019).

One of the most successful applications of NIR spectroscopy is in the estimation of genetic parameters, particularly those related to pulp production (Schimleck et al. 2019). In-forest wood quality assessment can potentially be achieved using spectra collected on standing trees (Figure 3) or in the lab based on spectra collected from a milled increment core. Utilizing milled increment cores to estimate whole-tree properties has been the most common approach and it has been demonstrated that spectra from milled breast height cores can provide good calibrations for estimating whole-tree properties (Schimleck et al. 2005, 2006). This approach has been adopted by several forest industry companies to assess progeny in their breeding programs (Meder et al. 2010).

However, there are some challenges in implementation of NIR spectroscopy. For example, data interpretation and post-processing can be complicated and require expertise; calibration must be maintained and updated. There are also issues related to calibration accuracy and applicability in harsh environmental conditions outside of the laboratory. Sandak et al. (2016) provide many practical recommendations for the successful application of this technique.

Figure 3. NIR acquisition on standing trees using a handheld device (Meder et al. 2010. Photo credit: Roger Meder).

DiscBot system

Although taking pith-to-bark core samples enables the radial patterns of wood property variation to be understood, such an approach does not capture the circumferential variation that exists in internal wood properties. In addition, the sample collection and preparation costs may also make it impractical to take core samples from multiple heights up the stem of a tree, thus making it difficult to capture the longitudinal variation. To address some of these challenges, Scion—the New Zealand Forest Research Institute Limited, has developed a new semi-automated platform, the DiscBot (Figure 4), for the rapid and cost-effective assessment of wood properties on cross-sectional discs (Schmleck et al. 2019; Moore 2018). With the DiscBot, a disc is systematically moved under each of five measurement stations to collect data on disc size and shape, spiral grain angle, density, wood chemistry and microfibril angle. Data are collected at high resolution to give two-dimensional wood property maps for the sample. By scanning multiple discs within a single stem, the DiscBot can produce intra-stem wood property maps that provide a more complete picture of the full extent of variation that exists (Figure 5). These data and subsequent simulations provide greater insights into the full impacts of silvicultural practices, environment, and genetics on wood quality of the forest resources.

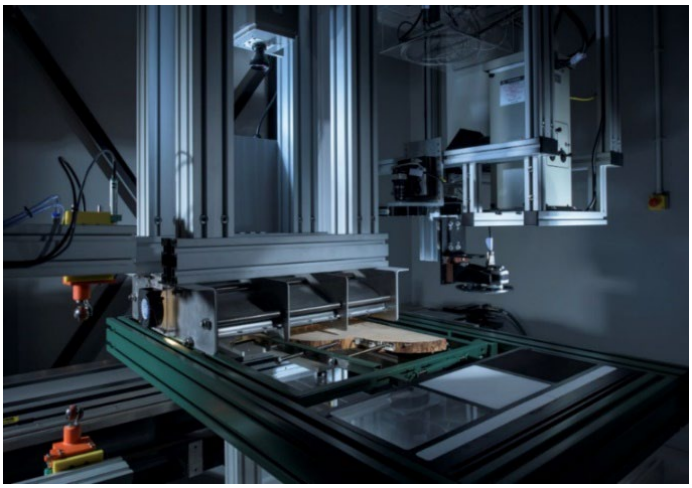

Figure 4. Scion's (New Zealand Forest Research Institute Limited) DiscBot (Moore 2018; Schimleck et al. 2019. Photo credit: John Moore).

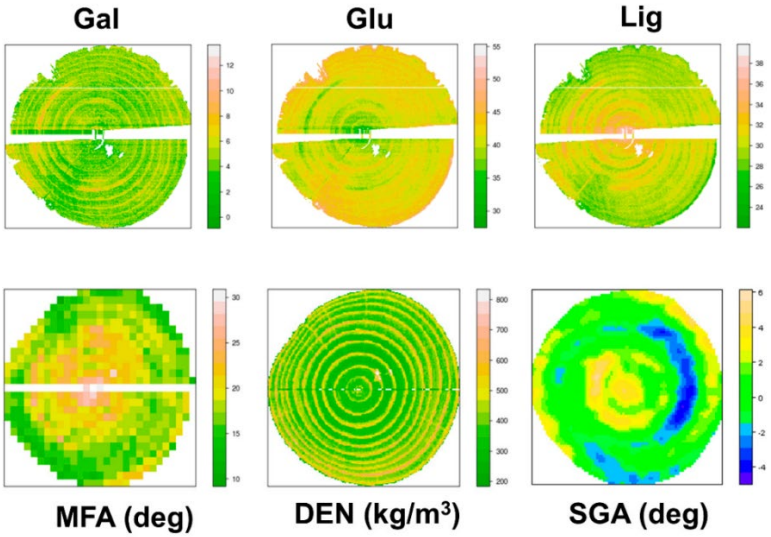

Figure 5. Examples of wood property maps produced by the DiscBot for galactan content (Gal), glucose content (Glu), lignin content (Lig), microfibril angle (MFA), density (DEN), and grain angle (SGA) (Schimleck et al. 2019).

Time-of-flight (TOF) acoustic technique

Another example is the development and commercialization of standing tree acoustic tools for assessing wood stiffness in trees (Wang et al. 2001, 2007a; Carter et al. 2005, 2013). The concept of using acoustic wave velocity as an effective measure of wood quality has been widely recognized in the forest products industry (Wang et al. 2007a, 2017b; Carter et al. 2005; Carter 2011; Harris and Andrews 1999). A resonance-based acoustic method, with a single sensor gauged with the material end, has been successfully used to grade structural timber, logs, poles, and wood-based composite materials (such as laminated veneer lumber and glued laminated timber) (Harris et al. 2002; Wang et al. 2006; Achim et al. 2011). However, the resonance-based acoustic tool cannot be used on standing trees because it requires two end-cut surfaces for compressional waves to reverberate between. To measure acoustic velocity on standing trees, a time-of-flight (TOF) acoustic wave technique was developed to gauge two sensor probes with a tree trunk by inserting the probes into the sapwood (Wang 1999; Huang 2005; Wang et al. 2008; Divos 2010; Huang 2000). In tree acoustic measurement, an impact impulse is introduced by a hammer impact on the start probe and TOF readings can be obtained by analyzing the receiving signals of the start and stop sensor probes (Wang 1999; Wang et al. 2008; Huang 2000; Addis et al. 2000).

The TOF acoustic method has been validated through various field and laboratory experiments. Hand-held standing tree acoustic tools have been commercialized (Figure 6) and are currently used by many research organizations and forest companies around the world, providing a means for silviculturists, forest managers, and planners to predict the stiffness potential of trees and stands prior to harvest, which enables management, planning, harvesting, and wood processing to be carried out in a way that maximizes extracted value from forests. The latest development on acoustic wave technology is the automated acoustic optimization system integrated into the processor head of a harvesting machine (Figure 7), allowing the processor head to acoustically test a stem and obtain its stiffness prior to making a log length cutting decision (Carter et al. 2013). The system allows wood producers to cut logs according to the measured stiffness, match logs to their requirements, and therefore extract more value from the trees. This automated acoustic optimization system has gone through experimental trials in UK, Australia, New Zealand, and the U.S. and it has shown improved precision over the head-held tool—ST300. While ready for operational application, the system still needs the harvest head manufacturers to adopt the technology and fully integrate it into their harvest head design.

(a) (b) (c)

Figure 6. Measuring acoustic velocity in standing trees. a) Prototype of TOF measurement system; b) Hitman ST300 (fibre-gen, Ltd.); c) Fakopp TreeSonic (Fakopp Enterprise Bt.).

(a) (b)

Figure 7. Harvesting machine with an automated acoustic optimization system. a) Harvesting operation; b) Hitman PH330 processor head (Photo credit: Peter Carter).

Resistance drilling

Resistance drilling is another method that has been extensively studied for its use in assessing wood quality of standing trees. The resistance drilling tool is an electronic micro-drill system that measures the relative resistance profile as a thin drill bit is driven into wood (Figure 8). The technique operates on the principle that drilling resistance is directly related to the density of the material being tested (Rinn et al. 1996). A resistance drilling tool consists of a power drill unit, a thin spade-type drill bit, and an electronic device that can be connected to a computer or a portable printer. As the needle drill bit cuts into the wood in a linear path, the drilling resistance is measured by recording the power consumption. The trace of change in drilling resistance is recorded as a digital representation display. This method was originally designed to characterize the radial density variation within a tree. However, resistance drilling tools have mostly been used for urban tree decay detection and wood structure inspection (Wang and Allison 2008; Allison and Wang 2015; Rinn 2012; Ceraldi et al. 2001; Ross et al. 2004).

Figure 8. Electronically regulated resistance drilling in a standing tree using a Resistograph® tool (Photo credit: Frank Rinn).

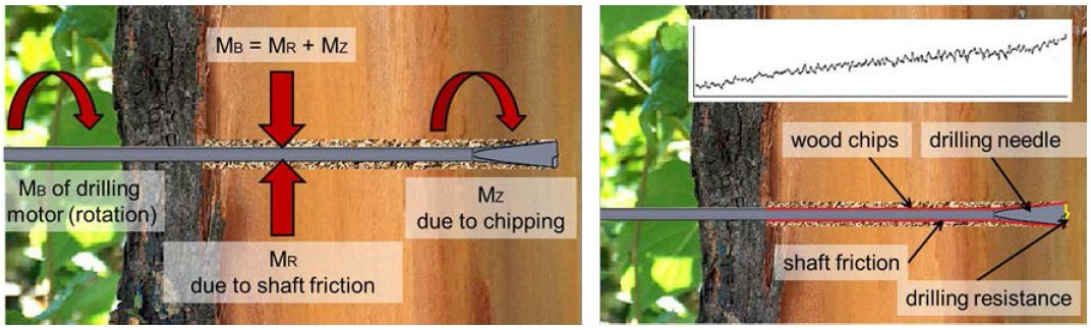

Figure 9. Illustration of resistance drilling process in a standing tree. The wood chips accumulate inside the cutting channel and cause friction on the needle shaft, leading to an increase in drilling resistance (Nutto and Biechele 2015).

Recent improvements in resistance drilling instruments have prompted research efforts to evaluate the potential of using resistance drilling to estimate the wood density of standing trees, particularly in tree genetic improvement programs. One of the challenges in assessing wood density of trees using a resistance drilling tool is the effect of friction. As illustrated in Figure 9, during the resistance drilling process, the wood chips can build up inside the cutting channel and cause friction on the needle shaft, which leads to an increase in drilling resistance (Nutto and Biechele 2015; Sharapov et al. 2017). New research has offered potential solutions to improve the accuracy of resistance measurement by developing friction models and using the models to remove the shaft friction from the original resistance profiles (Wang 2017; Downes et al. 2018). More research is needed to characterize the friction levels for different tree species.

NDT technologies for tree decay detection

Tree decay, or tree rot, is common to many tree species in forests. Internal tree decay, if goes undetected, can destroy lignin and cellulose in a tree trunk rapidly and cause significant loss to forest owners and timber buyers. It is estimated that for all the timber harvested annually in the United States, heartwood decay fungi destroy about 30% of the timber volume (Tainter and Baker 1996). The economic loss caused by heartwood decay is most significant for the hardwood trees that are used to produce appearance-grade

veneer products. Early detection of internal decay in hardwoods could provide a significant benefit to the industry in terms of making accurate quality assessments and volume estimates and use of the resource. It can also help foresters in prescribing silvicultural treatments for improved management decision-making and thus help maintain a healthy forest. Researchers have developed various methods and tools for nondestructively testing trees for internal decay. These methods include simple visual inspection, single path stress wave timer, multi-sensor acoustic tomography, microdrills, ground penetrating radar, and x-ray scanning etc. A general review of these technologies can be found in Allison and Wang 2015 and Allison et al. 2020.

Conclusions

The research and development of nondestructive evaluation technologies for assessing wood quality of standing trees is still ongoing. Recent technology advances have brought the operational assessment of wood and fiber properties of standing trees into resource evaluation, harvesting operation, forest management, and tree genetic improvement. Significant values are associated with wood and fiber quality in wood supply chain for production of structural lumber, engineered wood products (such as glulam, LVL and CLT), and pulping and paper. Rapid and nondestructive measurements on trees allow this value to be captured through better decision-making, allocation of resources to highest value users, and application of best processing methods.

References

Achim, A.; Paradis, N.; Carter, P.; Hernandez, R.E. 2011. Using acoustic sensors to improve the efficiency of the forest value chain in Canada: A case study with laminated veneer lumber. Sensors 11: 5716–5728.

Addis, T.; Buchanan, A.H.; Walker, J.C.F. 2000. Selecting trees for structural timber. Holz Roh-Werkst 58: 162–167.

Allison, R.B.; Wang, X. 2015. Nondestructive testing in the urban forest. In: Ross, R.J., Ed. Nondestructive Evaluation of Wood, 2nd ed.; General Technical Report FPL-GTR-238; Department of Agriculture, Forest Service, Forest Products Laboratory: Madison, WI, USA, pp. 77–86.

Allison, R.B.; Wang, X.; Senalik, C.A. 2020. Methods for nondestructive testing of urban trees. Forests 11, 1342; doi:10.3390/f11121341.

Amishev, D.; Murphy, G.E. 2018. In-forest Assessment of veneer grade Douglas-fir logs based on acoustic measurement of wood stiffness. For. Prod. J. *58*:42–47.

Briggs, D.G.; Thienel, G.; Turnblom, E.C.; Lowell, E.; Dykstra, D.; Ross, R.J.; Wang, X.; Carter, P. 2008. Influence of thinning on acoustic velocity of Douglas-fir trees in western Washington and western Oregon. In: Proceedings of the 15th International Symposium on Nondestructive Testing of Wood, Duluth, MN, USA, 10–12 September 2007; Forest Products Society: Madison, WI, USA; pp. 113–123.

Carter, P. 2011. Real-time measures of wood quality—Transition from research to application. In: Proceedings of the 17th International Nondestructive Testing and Evaluation of Wood Symposium, Sopron, Hungary, September 14–16, 2011; pp. 34–39.

Carter, P.; Briggs, D.; Ross, R.J.; Wang, X. 2005. Acoustic testing to enhance western forest values and meet customer wood quality needs. In: Harrington, C.A., Schoenholtz, S.H., Eds. Productivity of Western

Forests: A Forest Products Focus; PNW-GTR-642; USDA Forest Service, Pacific Northwest Research Station: Portland, OR, USA, 2005; pp. 121–129.

Carter, P.; Wang, X.; Ross, R.J. 2013. Field application of processor head acoustic technology in forest harvest operations. In: Proceedings of the 18th International Nondestructive Testing and Evaluation of Wood Symposium, Madison, WI, USA, September 24–27, 2013; pp. 7–14.

Ceraldi, C.; Mormone, V.; Ermolli, E.R. 2001. Resistographic inspection of ancient timber structures for the evaluation of mechanical characteristics. Mater. Struct. 34: 59–64.

Cown, D.J. 2006. Wood quality in standing timber—Evolution of assessment methods in plantations. In: Kurjatko, S., Kudela, J., Lagana, R., Eds. Proceedings of the 5th IFRUO Symposium "Wood Structure and Properties 06", Sliac-Sielnica, Slovakia, 3–6 September 2006; pp. 11–17.

Divos, F. 2010. Acoustic tools for seedling, tree and log selection. In: Proceedings of the Future and Quality Control for Wood & Wood Products, Edinburgh, UK, May 4–7, 2010; p. 5.

Downes, G.M.; Lausberg, M.; Potts, B.M.; Pilbeam, D.L.; Bird, M.; Bradshaw, B. 2018. Application of the IML Resistograph to the infield assessment of basic density in plantation Eucalypts. Aust. For. 81: 177–185, doi:10.1080/00049158.2018.1500676.

Evans, R.; Ilic, J. 2001. Rapid prediction of wood stiffness from microfibril angle and density. For. Prod J. *51*:53–57.

Evans, R.; Kibblewhite, R.P. 2002. Controlling wood stiffness in plantation softwoods. In: Beal, F.C., Ed. Proceedings of the 13th International Symposium on Nondestructive Testing of Wood, University of California, Berkeley Campus, California, USA, August 19-21, 2002; Forest Products Society: Madison, WI, USA, 2002; pp. 67–74.

Gao, S.; Wang, X.; Wiemann, M.C.; Brashaw, B.K.; Ross, R.J.; Wang, L. 2017. A critical analysis of methods for rapid and nondestructive determination of wood density in standing trees. Ann. For. Sci. *74*, 27, doi:10.1007/s13595-017-0623-4.

Harris, P.D.; Andrews, M.K. 1999. Tools and acoustic techniques for measuring wood stiffness. In: Proceedings of the 3rd Wood Quality Symposium: Emerging Technologies for Evaluating Wood Quality for Processing, Forest Industry Engineering Association: Rotorua, New Zealand, 1999.

Harris, P.; Petherick, R.; Andrews, M. Acoustic Resonance Tools. 2002. In: Proceedings of the 13th International Symposium on Nondestructive Testing of Wood, Berkeley, CA, USA, August 19–21, 2002; pp. 195–201.

Huang, C.L. 2000. Predicting lumber stiffness of standing trees. In: Proceedings of the 12th International Symposium on Nondestructive Testing of Wood, University of Western Hungary, Sopron, Hungary, September 13–15, pp. 173–179.

Huang, C.L. 2005. System and method for measuring stiffness in standing trees. U.S. Patent No. 6,871545, March 29, 2005.

Meder, R.; Trung, T.; Schimleck, L.; Schimleck, L. 2010. Seeing the wood in the trees: Unleashing the secrets of wood via near infrared spectroscopy. J. Near Infrared Spectrosc. 18, 3.

Moore, J. 2018. DiscBot—A new automated system for measuring wood properties on discs. In: Proceedings of the IUFRO Technical Workshop "New Advances in Nondestructive Evaluation of Wood", Beijing, China, 7–9 May 2018.

Nutto, L.; Biechele, T. 2015. Drilling resistance measurement and the effect of shaft friction—Using feed force information for improving decay identification on hard tropical wood. In: Ross, R.J., Gonçalves, R., Wang, X., Eds. Proceedings of the 19th International Nondestructive Testing and Evaluation of Wood Symposium; General Technical Report FPL-GTR-239; Department of Agriculture, Forest Service, Forest Products Laboratory: Madison, WI, USA, pp. 154–161.

Rinn, F. 2012. Basics of micro-resistance drilling for timber inspection. Holztechnologie 53: 24–29.

Rinn, F.; Schweingruber, F.H.; Schar, E. 1996. Resistograph and x-ray density charts of wood comparative evaluation of drill resistance profiles and x-ray density charts of different wood species. Holzforschung 50: 303–311.

Ross, R.J.; Brashaw, B.K.; Wang, X.; Pellerin, R.F. 2004. Wood and timber condition assessment manual; Forest Products Society: Madison, WI, USA.

Sandak, J.; Sandak, A.; Meder, R. 2016. Assessing trees, wood and derived products with near infrared spectroscopy: hints and tips. J. Near Infrared Spectrosc. 24, 485–505.

Sharapov, E.; Wang, X.; Smirnova, E. 2017. Drill bit friction and its effect on resistance drilling measurements in logs. In: Proceedings of the 20th International Nondestructive Testing and Evaluation of Wood Symposium, Madison, WI, USA, September 12–15, 2017; Gen. Tech. Rep. FPL-GTR-249. Department of Agriculture, Forest Service, Forest Products Laboratory: Madison, WI, USA; pp. 413–423.

Schimleck, L.R.; Kube, P.D.; A Raymond, C.; Michell, A.J.; French, J. 2005. Estimation of whole-tree kraft pulp yield of Eucalyptus nitens using near-infrared spectra collected from increment cores. Can. J. For. Res. 35, 2797–2805.

Schimleck, L.R.; Rezende, G.D.S.P.; Demuner, B.J.; Downes, G.M. 2006. Estimation of whole-tree wood quality traits using near infrared spectra from increment cores. Appita J. 59, 231.

Schimleck, L.; Dahlen, J.; Apiolaza, L.A.; Downes, G.; Emms, G.; Evans, R.; Moore, J.; Pâques, L.; Van den Bulcke, J.; Wang, X. 2019. Non-destructive evaluation techniques and what they tell us about wood property variation. Forests *10*, 50.

So, C.; Via, B.K.; Groom, L.H.; Schimleck, L.R.; Shupe, T.F.; Kelley, S.S.; Rials, T.G. 2004. Near infrared spectroscopy in the Forest Products Industry. For. Prod. J. 54: 6–16.

Tainter FH, Baker FA. 1996. Principles of forest pathology. John Wiley & Sons, New York, NY. 803 pp

Wang, X. 1999. Stress wave-based non-destructive evaluation (nde) methods for wood quality of standing trees. Ph.D. Dissertation, Michigan Technological University, Houghton, MI, USA, 1999; p. 187.

Wang, X. 2017. Partial resistance drilling to assess wood density in trees. In: Proceedings of the 20th International Nondestructive Testing and Evaluation of Wood Symposium, Madison, WI, September 12–15, 2017; Gen. Tech. Rep. FPL-GTR-249; U.S. Department of Agriculture, Forest Service, Forest Products Laboratory: Madison, WI, USA; pp. 22–35.

Wang, X.; Allison, R.B. 2008. Decay detection in red oak trees using a combination of visual inspection, acoustic testing, and resistance microdrilling. Arboric. Urban For. 34: 1–4.

Wang, X.; Carter, P.; Ross, R.J.; Brashaw, B.K. 2007a. Acoustic assessment of wood quality of raw forest materials—a path to increased profitability. For. Prod. J. *57*:6–14.

Wang, X.; Ross, R.J.; Carter, P. 2007b. Acoustic evaluation of wood quality in standing trees: Part 1. Acoustic wave behavior in standing trees. Wood Fiber Sci. 39: 28–38.

Wang, X.; Ross, R.J.; Mattson, J.A.; Erickson, J.; Forsman, J.W.; Geske, E.A.; Wehr, M.A. 2006. System for and method of performing evaluation techniques on a log or round timber. U.S. Patent No. 7,043,990, May 16, 2006.

Wang, X.; Ross, R.J.; McClellan, M.; Barbour, R.J.; Erickson, J.R.; Forsman, J.W.; McGinnis, G.D. 2001. Nondestructive evaluation of standing trees with a stress wave method. Wood Fiber Sci. 33: 522–533.

Wang, X.; Sharplin, N.; Carter, P.; Ross, R.J. 2008. Method and apparatus for evaluation of standing timber. U.S. Patent No. 7,418,866 B2, September 2, 2008.

Wiemann, M.C.; Williamson, G.B. 2013. Biomass determination using wood specific gravity from increment cores. General Technical Report FPL-GTR-225; Department of Agriculture, Forest Service, Forest Products Laboratory: Madison, WI, USA, p. 7.

Industrial CT Scanning in Wood Research

José Couceiro *
Luleå University of Technology, Wood Science and Engineering, Forskargatan 1, 931 87 Skellefteå, Sweden, jose.couceiro@ltu.se

Lars Hansson
Department of Ocean Operations and Civil Engineering, Faculty of Engineering, Norwegian University of Science and Technology, 6025 Ålesund, Norway, lars.hansson@ltu.se

Dick Sandberg
Luleå University of Technology, Wood Science and Engineering, Forskargatan 1, 931 87 Skellefteå, Sweden, dick.sandberg@ltu.se

Enrico Ursella
Microtec GmbH, Venice, Italy, enrico.ursella@microtec.eu

* Corresponding author

Abstract

The X-ray computed tomography (CT) lab at Wood Science and Engineering (WSE) has been a cutting-edge facility in wood research: drying, thermal modification, sorting, and machining. Since the mid-1990s, the research at Luleå University of Technology has produced more than 50 doctorate theses and hundreds of projects have supported the improvement of processes in the wood-industry sector. Nowadays, industrial CT scanners and other X-ray technologies are installed in sawmills around the globe. Nevertheless, there has always been a mismatch between the technologies used in industrial environments and in research. In research, CT technology has mostly been based on medical equipment, which comes with quite hindering limitations caused by the low doses of radiation required and by certain characteristics in the visualisation of tissues. For wood research, the objective has to be versatility and freedom. An industrial prototype of a CT scanner developed by Microtec (Bressanone/Brixen, Italy) has been installed in the laboratories of WSE in Skellefteå. The advantages of this equipment are the wider range of acceleration voltages, the unlimited scanning time, and the possibility to obtain raw data instead of non-disclosed ready-processed images, as is the case with medical technology. The new Microtec Mito scanner has shown great capabilities, with voxel volume of 0.3x0.3x0.3 mm^3 and the possibility to scan large specimens, such as entire logs, with great accuracy. The laboratory is currently being developed so that wood drying processes and thermal modification can be performed and scanned. The goal is to develop further the cutting-edge research that WSE has been performing during the last 30 years, with more accurate results and great opportunities that this new technology provides in the form of more access to the image generation process. This presentation gives insight into the first year of tests of this equipment, its capabilities, and future projects.

Keywords: X-ray CT, computed tomography, industrial CT, wood drying, thermal modification

Session 1

Nondestructive Characterization of Wood and Wood-Based Materials

Effects of Microwave Radar Sensor Distance and Material Thickness on Density and Moisture Content Determination

Laszlo Bejo *
Institute of Wood Engineering, University of Sopron, Sopron, Hungary, bejo.laszlo@uni-sopron.hu

Mihaly Jakocs
University of Sopron, Sopron, Hungary, alceyaon@gmail.com

Ahmed Altaher Omer
Institute of Wood Engineering, University of Sopron, Sopron, Hungary,
Altaher.Omer.Ahmed.Ahmed@phd.uni-sopron.hu

* Corresponding author

Abstract

According to our earlier research, measuring the microwave attenuation and propagation time across the thickness of wood allows the simultaneous determination of wood moisture content and density, using one relatively simple and quick measurement. Results seem to be independent of wood species. On the road to developing a practical measurement system, the next step is to assess various other influencing factors that need to be considered when calibrating the instrument. Small clear specimens of eight different species and different thicknesses ranging from 5 to 50 mm were conditioned to different moisture content levels below the fiber saturation point (FSP) and were measured with a microwave radar. The distance of the sensors, as well as the position of the specimens were varied to assess the sensitivity of the method to these factors.

Keywords: moisture content, density, microwave radar, propagation time, signal attenuation

Comparison between Static Modulus of Elasticity and Nondestructive Testing Moduli of Elasticity in White Spruce and Lodgepole Pine Wood

Cyriac S. Mvolo*
Canadian Wood Fibre Centre, Canadian Forest Service, Natural Resources Canada, Edmonton, Alberta, Canada, cyriac.mvolo@nrcan-rncan.gc.ca

James D. Stewart
Canadian Wood Fibre Centre, Canadian Forest Service, Natural Resources Canada, Edmonton, Alberta, Canada, jim.stewart@nrcan-rncan.gc.ca

Ahmed Koubaa
Institut de recherche sur les forêts, Université du Québec en Abitibi-Témiscamingue, Rouyn-Noranda, Quebec, Canada, ahmed.koubaa@uqat.ca

* Corresponding author

Abstract

Static bending tests to measure modulus of elasticity (MOE_{ST}) provide an indicator of the structural performance of a finished product; however, these tests are slow and expensive. Tests to measure MOE using non-destructive testing [MOE_{NDT}] provide alternatives to MOE_{ST} tests. MOE_{NDT} measured by two methods (SilviScan [MOE_{SS}] and time of flight [MOE_{TOF}]) have been compared with MOE_{ST}. Stress wave speed (SWS) relationships with MOE_{ST} have also been evaluated. Simple linear regression of MOE_{SS}, MOE_{TOF}, and SWS produced coefficients of determination (R^2) with greater explanatory power than did multiple linear regressions including growth rate or other wood fibre attributes. Simple linear regression from MOE_{TOF} and MOE_{SS} on MOE_{ST} had lower R^2 for lodgepole pine than for white spruce; however, the converse was true for SWS. SWS had the highest R^2 (89%) and MOE_{SS} the lowest R^2 (47%) with MOE_{ST} in lodgepole pine. The results were tool and species specific.

Keywords: Modulus of elasticity, stress wave speed, juvenile wood, mature wood

1 Introduction

It has become essential to have up-to-date information on the variation of wood products mechanical properties in general, and their stiffness or modulus of elasticity (MOE) in particular. This information should take into account the differences between juvenile wood (JW) and mature wood (MW). The 3-point static bending test is the traditional means for measuring static modulus of elasticity (MOE_{ST}) in woody material, as described in (1) (Brancheriau et al. 2002). Measuring MOE_{ST} is an expensive, time-consuming, and destructive process. Therefore, many studies have focussed on developing tools and techniques for rapid, non-destructive, and cost-effective measurement of mechanical properties that could be used as substitutes for static bending tests; the speed of sound transmission and attenuation (Wang et al. 2004) and the SilviScan technology (Evans 1999) are among the most promising.

$$MOE_{ST} = \left(\frac{L^3}{4eh^3}\right) \times k \quad (1)$$

Where L is sample length (span), e is sample width, h is sample height, $k = \frac{|\Delta P|}{|\Delta f|}$ is indentation coefficient, P is applied load and f is deflection at midspan.

Acoustic time of flight (TOF) is a method used to measure acoustic velocity (Schimleck et al. 2019). The stress wave is induced by a transmitting probe, travels through the wood, and is detected by a receiving probe located at a known distance (d) from the transmitter. The time taken by the stress wave to first reach the receiving probe, known as TOF (Mora et al. 2009), is then used to compute the stress wave speed (SWS), as described in (2). SWS is used in the one-dimensional wave equation (3), which establishes the relationships among TOF modulus of elasticity (MOE_{TOF}), SWS, and gravimetric wood density (WD) (Wang et al. 2004). SilviScan is a tool composed of several proven technologies, which allows assessment of a range of wood and fibre attributes (WFA) in an automated, rapid, cost-effective, and non-destructive way (Evans 1999). SilviScan MOE (MOE_{SS}) is obtained through a combination of X-ray densitometry, X-ray diffraction and image analysis, as described in (4) (Evans 1999).

$$SWS = \frac{\mathrm{d}}{\mathrm{TOF}} \quad (2)$$

$$\mathrm{MOE_{TOF}} = \mathrm{SWS}^2 \times WD \quad (3)$$

Where d is sample length (distance), TOF is time of flight, and WD id wood density.

$$\mathrm{MOE_{SS}} = A \times (I_{CV} \times \rho)^{B} \quad (4)$$

Where I_{cv} is the coefficient of variation of the intensity of the X-ray diffraction profile, ρ is the wood density obtained from X-ray densitometry, A is a scaling factor and B is an exponent to allow for curvature.

There is a good correlation between MOE_{TOF} and MOE_{ST}. MOE_{TOF} generally exceeds MOE_{ST} by 8% to 15% in many species (Wang et al. 2004). However, it is not uncommon for the measurement of MOE using non-destructive testing [MOE_{NDT}] to be lower than the measurement of MOE_{ST}. Due to the anisotropic nature of wood, MOE_{TOF} is highest in the longitudinal direction, followed by the radial radiation and lowest in the tangential direction (Schimleck et al. 2019). The longitudinal MOE_{TOF} is negatively influence by knots, moisture content (MC), tree height, branches and bark. There is a good correlation between MOE_{SS} and MOE_{ST} (Defo et al. 2010). Defo et al. (2010) found high correlations for both small clear battens (r = 0.80 to 0.82) and lumber (r = 0.79) of balsam fir and black spruce. However, the results were species specific, indicating the need to validate the suitability of SilviScan for use in each species of interest.

Although a close relationship exists between MOE_{NDT} values computed using different technologies, MOE_{NDT} values do vary according to the technology used (Liang and Fu 2007). White spruce (*Picea Glauca* (Moench) Voss) and lodgepole pine (*Pinus contorta* Dougl. ex. Loud.) are prominent components of the commercial forest land base in western Canada; they are principally used for lumber production and are of vital economic importance to the Canadian forestry industry (Nienstaedt and Zasada 1990). Cost-effective and validated tools for measuring the mechanical properties of wood are essential for optimizing the use of this important resource. The objective of this study was to compare MOE_{SS} and MOE_{TOF} to MOE_{ST} for both lodgepole pine and white spruce, and to compare SWS to MOE_{ST}.

2 Material and methods

2.1 Material

Ten lodgepole pine trees and 10 white spruce trees were used in this study (Table 1). The lodgepole pine trees were harvested from the MacKay thinning trial, Alberta, in 2016. These trees were part of a fire-origin stand. White spruce trees were harvested from several long-term monitoring plots in natural untreated forest stands near Calling Lake, Alberta, in 2016. All trees were of the codominant social class.

Table 1 Tree-level average values of modulus of elasticity (MOE) obtained from SilviScan, time of flight (TOF), and static bending tests for lodgepole pine and white spruce, presented in decreasing order using SilviScan MOE values.

TreeID	Tree age (years)	Transition age (years)	JWP (%)	DBH (cm)	Tree height (m)	MOE_{SS} (GPa)	MOE_{ST} (GPa)	MOE_{TOF} (GPa)	MFA (°)	RD (kg/m^3)	WD (kg/m^3)	RW (mm)	SWS (m/s)
Lodgepole pine													
Pl 1	70	21	10.8	15.7	18.5	18.38	13.84	9.52	10.3	519.9	628.8	1.1	3892
Pl 2	71	13	11.6	15.3	19.5	17.79	12.04	7.04	7.5	461.7	521.9	0.9	3671
Pl 3	72	20	17.1	16.7	20.6	17.62	12.39	7.58	7.3	467.9	547.3	0.9	3721
Pl 4	72	44	54.2	18	20.8	17.39	14.38	8.47	6.4	426.6	543.4	0.9	3948
Pl 5	74	34	38.8	17	21.9	16.57	12.74	7.87	10.1	470.8	542.8	1.1	3807
Pl 6	70	12	14.8	13.2	16.2	16.44	10.70	7.11	9.0	451.6	572.5	0.8	3525
Pl 7	73	29	36.1	17.8	21	16.30	10.60	6.68	8.2	424.2	514.1	0.9	3606
Pl 8	70	29	31.7	14.2	17	15.86	13.42	8.1	8.0	436.5	575.5	0.8	3766
Pl 9	71	38	50.1	15.3	17	14.45	9.21	5.63	9.1	402.4	453.2	0.8	3524
Pl 10	69	13	10.4	14.5	19.7	13.26	10.56	7.11	12.8	430.0	543.3	0.9	3619
Average	71.2	25.4	27.6	15.8	19.2	16.40	12.04	7.51	8.9	449.2	543.8	0.9	3706
White spruce													
Sw 1	107	36	23.2	34.9	29	15.23	9.89	6.71	9.0	390.0	430.2	1.4	3948
Sw 2	153	18	2.0	41.8	28.7	14.02	9.84	6.48	8.4	368.5	427.5	1.1	3890
Sw 3	107	23	6.5	34.8	24.7	13.90	9.18	6.01	10.7	382.8	492.7	1.4	3498
Sw 4	107	15	5.1	35.5	25.6	13.81	8.69	5.86	8.7	351.6	411.3	1.4	3773
Sw 5	78	18	6.8	24.3	27.6	13.19	9.74	6.56	10.4	362.6	434.1	1.6	3884
Sw 6	55	13	3.0	30.5	24.9	12.67	9.39	5.99	11.9	368.9	407.2	2.4	3835
Sw 7	148	28	15.0	32	26.8	12.39	10.15	7.64	19.4	452.6	508.3	1.0	3869
Sw 8	75	40	33.7	26.9	24.1	12.15	7.36	5.06	12.5	362.0	413.6	1.5	3496
Sw 9	55	15	6.8	32.7	21.9	8.93	7.61	4.61	15.2	301.5	352.2	2.6	3619
Sw 10	51	8	0.7	39.5	24.5	8.92	5.97	4.26	14.6	297.7	341.6	3.3	3535
Average	93.6	21	10.3	33.3	25.8	12.52	8.78	5.92	12.1	363.8	421.9	1.8	3735

Note: Pl, lodgepole pine; Sw, white spruce; JWP, juvenile wood proportion computed from SilviScan ring width at breast height, assuming a circular shape for all trees; DBH, diameter at breast height; MOE_{SS}, SilviScan modulus of elasticity; MOE_{ST}, static modulus of elasticity; MOE_{TOF}, TOF modulus of elasticity; MFA, microfibrils angle; RD, wood density measured with X-ray densitometry using SilviScan3; WD, wood density measured gravimetrically from battens; RW, ring width measured with X-ray densitometry using SilviScan3; SWS, stress wave speed measured with the Picus instrument.

2.2 Testing methods

A 5-cm-thick disk was collected at breast height from every felled tree, air dried in the laboratory at the Northern Forestry Centre, Edmonton, Alberta, and sent to the EvaluTree laboratory of FPInnovations, Vancouver, British Columbia, for Silviscan analysis. A 12 by 12 mm radial block was taken from pith to bark of each disk, extracted with acetone to remove resins and then conditioned to 8% equilibrium moisture content. A 2 by 7 mm strip was sawn from each block and used to measure WFA with SilviScan. MOE_{SS} was calculated from wood density and X-ray diffraction metrics as described in (4).

A 60-cm bolt was cut just above the disk and used to prepare small clear battens for static bending measurement according to the guidance for secondary method specimens (25 by 25 by 410 mm) in ASTM-D-143. One to 6 pith-free battens per bolt were collected, depending on the tree's diameter and defects. These were shipped to the Université du Québec en Abitibi-Témiscamingue (UQAT) for further processing. Acoustic velocity was measured on the battens with a through transmission test method using the point-to-point measurement mode on a Picus 3 TOF Acoustic Tomograph developed by Argus

Electronic Gmbh, and mainly used to detect decay and cavities in standing trees non-invasively. The tapping pin of an electronic radio hammer was bound to one nail, and the wave was induced by gently hitting the tapping pin with the electronic hammer. One receiving magnetic sensor was bound to the other nail. To avoid reproducibility and accuracy issues, the Picus TOF instrument was operated within a few days by a single user, who inserted all probes parallel to the small clear batten edges and tried to keep the same impact angle and impact strength of the hammer. The longitudinal SWS was computed automatically by the Picus and the average of 5 hits was recorded as the SWS for the batten in question.

After the SWS measurement, a universal testing machine (Zwick/Roell, model Z020) with 20 kN capacity and equipped with an extensometer was used for the 3-point bending test according to the guidance for secondary method specimens in ASTM-D-143. After testing, a 25-mm cube was taken at 1 cm from the batten edge and weighed to 0.001 g precision with a Mettler Toledo scale (model XS204). These cubes were then oven dried at 103°C in a Quincy Lab drying oven (model 40 GC) to determine the batten's MC. Another small sample was cut from the batten and sanded. After sanding, these samples were conditioned in the Labocon at the same condition as the battens, weighed with an Ohaus Precision scale to 0.01 g precision and measured with an electronic caliper to 0.01 mm precision for WD determination. MOE_{ST} was computed with the Zwick using (1), and MOE_{TOF} was calculated from SWS and WD as described in (3).

2.3 Statistical analyses

The lodgepole pine and the white spruce datasets were partitioned into JW and MW based on the MOE transition age calculated using a linear-linear segmented model (Wang and Stewart 2013). Linear regressions proved efficiency in converting MOE measurements from a testing method to another, and were used to compare MOE_{TOF}, MOE_{SS}, and SWS to MOE_{ST}. Analyses were performed separately for the JW and the MW zones, and by combining these two subsamples. Additionally, a database that included those tree rings that had MOE values obtained with all three technologies was created.

3 Results and discussion

3.1 Tree characteristics, radial pattern and average values

The TA and JWP variation within species and between species in this study (Table 1) were consistent with earlier studies (Wang and Stewart 2013). MOE_{SS} increased to about 75 and 45 growth rings from the pith for white spruce and lodgepole pine, respectively, where it started decreasing with age. These MOE_{SS} radial patterns were consistent with previously described patterns in spruce (Alteyrac et al. 2006) and pine (Wang and Stewart 2013). The MOE_{SS} values were similar to those previously reported for lodgepole pine (Wang and Stewart 2013 [5–19 GPa]) and white spruce (Sattler and Stewart 2016 [4–18 GPa]). The MOE_{TOF} was lower than the previously reported value for lodgepole pine lumber (Liang and Fu 2007 [15 GPa]). The MOE_{ST} values were comparable to those previously reported for lodgepole pine (Jessome 2000 [11 GPa]; Liang and Fu 2007 [11.7 GPa]) and white spruce (Jessome 2000 [9.93 GPa]; Sattler et al. 2014 [4–14 GPa]).

As expected, wood density (RD) determined by SilviScan using X-ray densitometry were different from wood density (WD) determined gravimetrically (Table 1). However, these values are not strictly comparable, because SilviScan samples were extracted radial strips, while unextracted longitudinal battens were used to determine WD. The RD values that we observed in this study were similar to those previously reported for lodgepole pine (Mansfield et al. 2009 [275–575 kg/m^3]) and white spruce (Middleton et al. 2000 [275–413 kg/m^3]). The WD values were higher than those previously reported for lodgepole pine (412 kg/m^3) and white spruce (372 kg/m^3) by Jessome (2000). This difference may be explained by sampling, as we used small samples collected avoiding defects and branch traces. Most of

these samples were closer to the pith than to the bark. The radial pattern of pines and spruces wood density belongs to the type II as described by Panshin and de Zeuuw (1980), in which the closer to the pith, the higher the wood density. The average SWS values found in this study for lodgepole pine and white spruce, respectively (Table 1), were comparable to the 3292 m/s and 3486 m/s values reported by Wang et al. (2004) for western hemlock and Sitka spruce, respectively. The faster stress wave transmission in spruce compared to pine, and the associated lower MOE_{TOF} agreed with values reviewed by Ross and Pellerin (2015).

3.2 Comparisons of MOE measurement methods

The largest variability found with MOE_{SS} may be explained by the fact that the SilviScan measurement was done at a finer scale, allowing a better capture of MOE variation. The lowest variation found with the acoustic TOF equipment may have been because the longitudinal wave in our samples travels preferentially through the earlywood, where both wood density and stiffness are lower, and SWS passes with lower velocity (Haines et al. 1996).

This higher MOE_{SS} value compared to MOE_{ST} value is consistent with findings from previous studies on black spruce and balsam fir (Defo et al. 2010). The lowest MOE_{TOF} may have been because our samples were too short for the equipment used. The longitudinal acoustic velocity was found to diminish below a length/width ratio of 20 (Bucur 2006). The length/width ratio for secondary method specimens in ASTM-D-143 used in this study is 16.4. Acoustic TOF are usually designed for probes being inserted at about a meter of distance one from the other in field environment (Schimleck et al. 2019). Our probes were inserted at about 0.4 m one from the other. Even for samples having the same length/width ratio, the longitudinal acoustic velocity diminishes with shorter samples. This was explained by mode conversion phenomena in infinite solid vs. rod (Bucur 2006). Following this reasoning, despite the care taken in selecting our samples, one can expect branch traces and small knots to significantly reduce MOE_{TOF} (Bucur 2006) in these short battens than it would do in longer samples. A more appropriate setup for stress wave measurements using secondary method specimens designed for ASTM-D-143 may be using a digital oscilloscope.

Our finding that values were higher for MOE_{ST} than for MOE_{TOF} for both species is consistent with findings from a previous study comparing MOE_{TOF} and axial compression MOE on 3-year-old radiata pine clones (Lindström et al. 2004). Despite the common observation that MOE_{NDT} exceeds MOE_{ST}, some studies have found a higher MOE_{ST} than MOE_{NDT}. Despite the discrepancies among MOE values, the results obtained with all three technologies followed the expected pattern produced with MOE_{SS}. Also, when one looks at our trees ranked according to their MOE_{SS} values (Table 1), all 3 technologies followed the same overall decreasing trend, in accordance with a previous report (Lindström et al. 2004). Finally, all 3 technologies produced the expected overall increasing relationships with wood density and SWS (Haines et al. 1996) and the expected overall decreasing relationship with MFA (Lindström et al. 2004).

MOE values were higher in lodgepole pine than in white spruce, independent of the measurement technique and wood zone considered. These differences in MOE between species, and with all 3 technologies, are consistent with previous reports (Wang et al. 2004). It confirms that any comparison between MOE values must take the tree species and the measurement technologies and operating conditions into account. The similarity between matched-rings and mean-disc MOE values while using SilviScan suggests that one could sample only a few selected rings from pith to bark and have a representative value of mean pith-to-bark MOE. As expected, MOE_{SS} values were higher and less variable in MW than in JW.

3.3 Comparison between MOE values

Despite the differences in measurement modality and scale noted above, the estimations of static MOE from either of the NDT methods were linear and gave significant and useful predictions (Table 2, Figure 1). The R^2 values between the TOF and static methods presented in Table 2 were in the same range as correlations previously reported in other coniferous species (Lindström et al. 2004; Liang and Fu 2007). However, these values were slightly lower than the 0.98 found by Bell et al. (1954) and the 0.91 found by Wang et al. (2004) using a laboratory setup with an oscilloscope. This advocate for using purposely designed experimental technique for measuring MOE_{TOF} in laboratory environment.

Table 2 Parameters and statistics from regression models estimating static modulus of elasticity from time of flight modulus of elasticity (MOE_{TOF}), SilviScan modulus of elasticity (MOE_{SS}) and stress wave speed (SWS).

Species/modality	Mean disc			Matched-rings		
	Intercept	Slope	R^2 %	Intercept	Slope	R^2 %
Lodgepole pine						
SWS	-26.80	0.010	89	-27.57	0.011	72
MOE_{TOF}	1.81	1.363	81	0.97	1.482	71
MOEss	0.31	0.715	47	4.75	0.459	67
White spruce						
SWS	-13.61	0.006	61	-15.58	0.006	55
MOE_{TOF}	1.37	1.253	88	0.04	1.478	82
MOEss	2.34	0.515	62	0.89	0.604	75

Note: All parameter estimates were significant at $p \leq 0.01$. SWS, stress wave speed; MOE_{TOF}, time of flight modulus of elasticity; MOEss, SilviScan modulus of elasticity.

The lower R^2 values between the SilviScan and static methods than those between the TOF and static technologies (Table 2) was expected, because the static and TOF technologies used the same longitudinal battens, while SilviScan samples were radial strips. Lodgepole pine JW MOE measured with the SilviScan equipment explained 57 % (p value: 0.01) of mean tree MOE measured with the static equipment. White spruce SilviScan JW MOE failed to explain mean tree static MOE variation (R^2: 29 % and p value: 0.11).

The R^2 values between SWS and MOE_{ST} were higher than both the R^2 between MOE_{TOF} and MOE_{ST} and the R^2 between MOE_{SS} and MOE_{ST}. SWS has been presented as a valuable and flexible way to estimate MOE non-destructively, both in standing trees and in lumber (Liang and Fu 2007). It is particularly appealing because it allows users to estimate the mechanical properties of wood more quickly and cheaply than by also measuring wood density. However, one may conclude that the higher performance of SWS is species specific, because it was not found with white spruce.

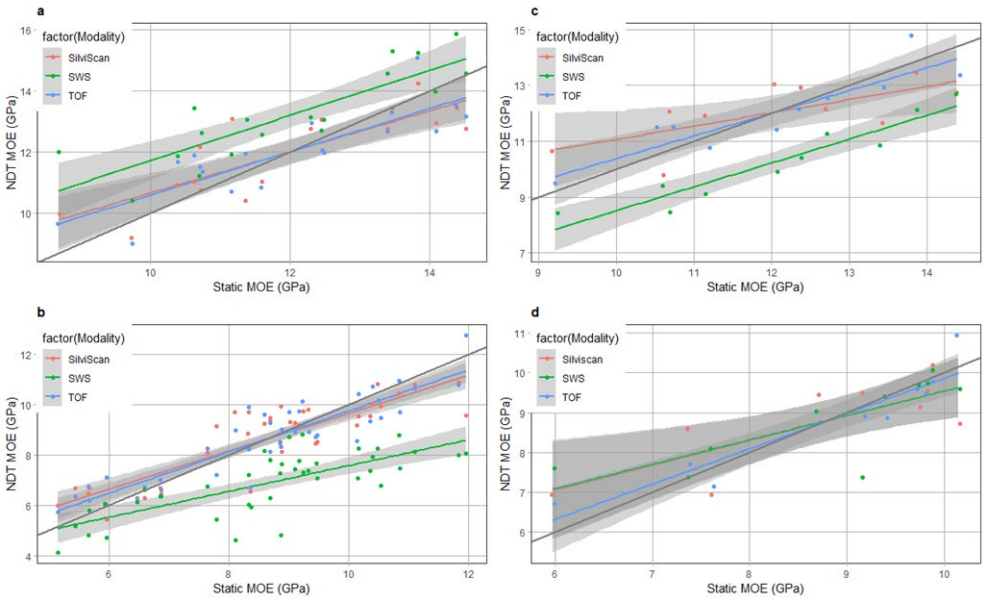

Figure 1 Predicted modulus of elasticity (MOE) from non-destructive testing (NDT) techniques, SilviScan, time of flight (TOF), and stress wave speed (SWS) versus observed static MOE for matched-rings of lodgepole pine (a), matched-rings of white spruce (b), disc mean of lodgepole pine (c), and disc mean of white spruce (d); the grey line is the 1:1 regression line and standard errors are represented by the grey zones

MOE values predicted from SilviScan and TOF equipment had a consistent pattern, and their confidence intervals largely overlapped across all databases (Figure 1), supporting the use of these technologies to estimate MOE_{ST} from MOE_{NDT}. Both MOE_{SS} and MOE_{TOF} overestimated MOE_{ST} for lower MOE value and underestimated MOE_{ST} for higher MOE values, in agreement with previous findings (Mora et al. 2009). MOE predicted from SWS did not show a consistent pattern across databases. It overestimated (Figure 1a), underestimated (Figures 1b and 1c), and both overestimated MOE_{ST} for lower MOE values and underestimated MOE_{ST} for higher MOE values (Figure 1d). The lack of consistency among MOE values predicted from SWS across sampling strategies, together with the species-specific performance discussed earlier and its distinct confidence intervals, suggests that more testing is still required with SWS, using a laboratory designed setup, before sound conclusions can be drawn.

3 Conclusion

The objective of this study was to compare measurements of the modulus of elasticity (MOE) determined with SilviScan (MOE_{SS}) and acoustic time of flight (MOE_{TOF}) equipment with measurements of standard static MOE (MOE_{ST}) for lodgepole pine and white spruce. MOE_{SS} values were highest, followed by MOE_{ST}, and MOE_{TOF} was the lowest MOE values. The high explanatory power of the regression models relating MOE_{ST} and both MOE_{TOF} and MOE_{SS} are evidence that both non-destructive testing (NDT) tools can be confidently used as alternatives to standard static bending testing. Contrary to lodgepole pine, SWS relationship with MOE_{ST} was not strong in white spruce, suggesting that more testing is required with this technology before sound conclusions can be drawn. Overall, this study confirmed that coefficients of determination between static and NDT MOE are species and tool specific.

Acknowledgements

The authors thank the Canadian Wood Fibre Centre (CWFC) for funding. They also acknowledge the work of Jared Salvail (CWFC) in carrying out the field work and that of William Belhadef (Université du Québec en Abitibi-Témiscamingue) in the static and TOF measurement of modulus of elasticity. The

support of Sharon Meredith (Foothills Growth and Yield Association) was instrumental in carrying out this research.

References

Alteyrac, J.; Cloutier, A.; Ung, C. [and others]. 2006. Mechanical properties in relation to selected wood characteristics of black spruce. Wood Fiber Scien 38:229-237

Bell, E.R.; Peck, E.C.; Krueger, N.T. 1954. Modulus of elasticity of wood determined by dynamic methods. Report n° 1977. USDA, Forest Service, Forest Products Laboratory, Madison, Wisconsin, U.S.

Brancheriau, L.; Bailleres, H.; Guitard, D. 2002. Comparison between modulus of elasticity values calculated using 3 and 4 point bending tests on wooden samples. Wood Sci Technol 36:367-383.

Bucur, V. Acoustics of Wood, 2nd ed.; Springer Series in Wood Science, Springer-Verlag Berlin Heidelberg, 2006; p. XVIII, 394

Defo, M.; Duchesne, I.; English, B. 2010. Element 5: Sensing Attributes for Value Chain Optimization – Validation of Silviscan modulus of elasticity. Report, FPInnovations, Vancouver, BC, Canada.

Evans, R. 1999. A variance approach to the x-ray diffractometric estimation of microfibril angle in wood. APPITA J 52:283-294

Haines, D.W.; Leban, J.M.; Herbé, C. 1996. Determination of Young's modulus for spruce, fir and isotropic materials by the resonance flexure method with comparisons to static flexure and other dynamic methods. Wood Sci Technol 30:253-263. doi:10.1007/BF00229348

Jessome, A.P. 2000. Résistance et propriétés connexes des bois indigènes au Canada. SP 514-F, Forintek Canada Corp., Sainte-Foy, QC, Canada

Liang, S.Q.; Fu, F. 2007. Comparative study on three dynamic modulus of elasticity and static modulus of elasticity for Lodgepole pine lumber. J Forestry Res 18:309-312 doi:10.1007/s11676-007-0062-4

Lindström, H.; Harris, P. Sorensson, C.T. [and others]. 2004. Stiffness and wood variation of 3-year old Pinus radiata clones. Wood Sci Technol 38:579-597

Mansfield, S.D.; Parish, R.; Di Lucca, C.M. [and others]. 2009. Revisiting the transition between juvenile and mature wood: a comparison of fibre length, microfibril angle and relative wood density in lodgepole pine. Holzforschung 63:449-456. doi:10.1515/hf.2009.069

Middleton, G.R.; Munro, B.D.; Sadlish, J. 2000. Influence of Growth Rate on Strength and Related Wood Properties of Boreal White Spruce. Forintek Canada Corp., Vancouver, B.C.

Mora, C.R.; Schimleck, L.R.; Mahon, J.M. [and others]. 2009. Relationships between acoustic variables and different measures of stiffness in standing *Pinus taeda* trees. Can J Forest Res 39:1421-1429

Nienstaedt, H.; Zasada, J.C. 1990. *Picea glauca* (Moench) Voss White Spruce. In: Burns, R.M.; Honkala, B.H. (eds) Silvics of North America. Vol. 1. Conifers, USDA, Forest Service, Agriculture Handbook 654, pp 204-226, Washington, DC, USA

Panshin, A.J.; de Zeuuw, C. 1980. Textbook of Wood Technology: Structure, Identification, Properties, and Uses of the Commercial Woods of the United States and Canada, 4th ed.; McGraw-Hill Book. p. 722.

Ross, R.J.; Pellerin, R.F. 2015. Inspection of Timber Structures Using Stress Wave Timing Nondestructive Evaluation Tools. In: Ross, R. J. (Ed.). Nondestructive evaluation of wood: 2nd edition. General Technical Report FPL-GTR-238. Madison, WI: USDA, Forest Service, Forest Products Laboratory, pp 5-19.

Sattler, D.F.; Comeau, P.G.; Achim, A. 2014. Within-tree patterns of wood stiffness for white spruce (*Picea glauca* (Moench) Voss) and trembling aspen (*Populus tremuloides* Michx.). Can J Forest Res 44:162-171.

Sattler, D.F.; Stewart, J.D. 2016. Climate, location, and growth relationships with wood stiffness at the site, tree, and ring levels in white spruce in the Boreal Plains ecozone. Can J Forest Res 46:1235-1245.

Schimleck L et al. (2019) Non-destructive evaluation techniques and what they tell us about wood property variation. *Forests* 2019, 10(9), 728; https://doi.org/10.3390/f10090728

Wang, M.; Stewart, J.D. 2013. Modeling the transition from juvenile to mature wood using modulus of elasticity in lodgepole pine. West J Appl For 28:135-142. doi:10.5849/wjaf.12-026

Wang, X.; Ross, R.J.; McClellan, M. [and others]. 2004. Strength and stiffness assessment of standing trees using a nondestructive stress wave technique. USDA, Forest Products Laboratory, research paper FPL−RP−585 Madison, WI.

Evaluation of Elastic Constants of Oil Palm Wood using Ultrasonic Measurement

Katja Fruehwald-Koenig
Department for Production Engineering and Wood Technology, OWL University of Applied Sciences and Arts, Lemgo, Germany, katja.fruehwald@th-owl.de

Benedikt Faust
Department for Production Engineering and Wood Technology, OWL University of Applied Sciences and Arts, Lemgo, Germany, benedikt.faust@th-owl.de

Abstract

200 million m³ oil palm trunks per year are still a "waste by-product". For generating added-value, material modelling and product optimization and therefore knowledge of the elastic properties are required. Apart from Young´s modulus parallel to the vascular bundles, the elastic properties of oil palm wood are not known. The applicability of ultrasonic testing (time of flight of three longitudinal, six shear and three quasi-shear wave measurements) for the characterization of all 12 elastic constants of oil palm wood having various densities was investigated under the assumption of an orthotropic material behavior. For the evaluation, the simplified uncorrected and the full stiffness inversion method were used. The lack of correlation between the density and the ultrasonic velocity when using flat transducers questions the applicability of this method for oil palm wood.

Keywords: oil palm wood, elastic constants, ultrasonic measurement, time of flight

Introduction

Background

The application of simulations using analytical and numerical methods is increasing in R&D and the wood processing industry, especially concerning the optimized composition of engineered wood products based on solid wood lamellas or veneers (e.g. GLT, CLT), as well as combinations of wood with other materials. Fruehwald-Koenig and Heister (2022) give an overview of the availability of oil palm wood, it´s micro-structure and macro-mechanical properties determined by mechanical testing in regard to tension ($f_{t,0}$, $E_{t,0}$, $f_{t,90}$), compression ($f_{c,0}$, $f_{c,90}$) and bending (f_m, E_m). They show that oil palm wood is inhomogeneous, the elastomechanical properties depend amongst others on the density, the position within the trunk and probably on the moisture content (the latter was not examined). Oil palm wood exhibits anisotropic material behavior. Killmann and Lim (1985) assumed, that the characteristic values in radial and tangential direction are equal because of the anatomic structure. The proof for a transversely isotropic material model has not been provided yet for oil palm wood. Therefore, small size, defect free test specimen are considered idealized as an orthotropic material using a right-angled coordinate system with clearly different properties along the three main axes longitudinal, radial and tangential and three planes of symmetry formed by the axes. For elastic numerical modelling, twelve elastic constants (3 E, 3 G and 6 ν) must be known. Young´s modulus of oil palm wood parallel to the vascular bundles (E_L) was determined by Fathi (2014), Fruehwald-Koenig (2019), Fruehwald-Koenig and Heister (2022). Karlinasari et al.

(2019), Srivaro et al. (2018) and Srivaro et al. (2019). All other eleven elastic constants are not determined for oil palm wood till now. Najmie et al. (2011) determined the ultrasonic velocity in longitudinal, radial and tangential direction without calculating the Young´s moduli.

Determination of Elastic Constants

No special test methods and standards are currently available for the determination of the elastic constants on oil palm wood; therefore, the methods for common wood species (mechanical testing, vibration test, ultrasonic testing) are considered. The determination of the elastic constants of orthotropic materials by **mechanical testing** is widespread and characterized by many variants. According to various standards, Young´s modulus of wood is determined using compression and tensile tests. On oil palm wood, Young's modulus in compression parallel to the vascular bundles ($E_{c,0}$) was determined by Fathi (2014), Srivaro et al. (2018) and Srivaro et al. (2019); Fruehwald-Koenig and Heister (2022) determined the Young's modulus in tension parallel to the vascular bundles ($E_{t,0}$) according to DIN 52188 (1979). The determination of the Poisson´s ratios is often made in the course of tensile and compression tests. Several test methods for the mechanical determination of the shear modulus of solid wood and wood based panels have been investigated: the measurement on shear cubes, the picture frame method. on (notched) shear blocks with single or double shear section, with two-plate compression shear tests, with a fixture consisting of the tested specimen glued between two steel or plywood plates, with Iosipescu test respectively with Arcan test, with compression, torsion or bending test. Determining the shear properties using mechanical testing has challenges, is complicated and imprecise, because it is difficult to generate a pure shear stress and to measure the corresponding strains (Keunecke et al. 2007; Kollmann 1951; Petermann 1941).

The three E and three G moduli of solid wood can be determined **with longitudinal, flexural and torsional vibration and modal analysis**. Fruehwald-Koenig (2019) shows the applicability of longitudinal and flexural vibration for the determination of E_L on oil palm wood. The determination of all elastic constants of an orthotropic material by mechanical or vibration test is only possible with considerable effort using several test methods and using a wide variety of specimen geometries. According to Keunecke et al. (2007), the particular advantage of the **ultrasonic time-of-flight method** is that all 9 or 12 elastic constants can be determined with one method and on just a few test specimens. Using small specimen geometries (when using high frequencies) also enables a better approximation to the assumed orthotropic material model (Bachtiar et al. 2017; Bucur and Archer 1984; Crespo et al. 2017; Gonçalves et al. 2011a; Hering et al. 2012; Jiang et al. 2018; Keunecke et al 2007; Ozyhar et al 2013; Sinclair and Farshad 1987). Furthermore, small specimen are also an advantage because of the large density gradient of oil palm wood within the cross section (Koelli 2016). When using the “full stiffness inversion” (FSI) method, Poisson's constants are also calculated by determining the transit times at different angles between the symmetry axes, but the validity of the results of these calculations is doubted in the literature (Bachtiar et al. 2017; Bucur and Archer 1984; Gonçalves et al. 2011a; Gonçalves et al. 2011b; Ozyhar et al. 2013). So far, only Fruehwald-Koenig (2019) and Karlinasari et al. (2019) determined E_L of oil palm wood on rod-shaped specimens using low-frequency longitudinal waves parallel to the vascular bundles and only using the simplified uncorrected (SU) method.

Research Question and Assumptions

The following considerations are based on the hypothesis that oil palm wood is an unidirectional long-fiber-reinforced composite and is orthotropic (details on the validation of the composite material model for oil palm wood cf. Fruehwald-Koenig and Heister (2022)). Therefore, aim of this study is to investigate the applicability of ultrasonic testing (time of flight of three longitudinal, six shear and three quasi-shear wave measurements) to determine the elastic constants of oil palm wood (3 E, 3 G and 6 ν) depending on the location within the trunk and the density. In analyzing the ultrasound data, the elastic moduli can only

be accurately estimated from stiffness data if the Poisson's ratios are available (Ozyhar et al. 2013). Because no Poisson´s ratios are available for oil palm wood so far, two data evaluation techniques, which differ in the way to incorporate the Poisson's ratios, are used according to Bachtiar et al. (2015) (full-stiffness-inversion, FSI, and simplified uncorrected, SU).

Material

Oil palms of the subspecies tenera (*Elaeis guineensis* JACQ. var. tenera) were felled at an average age of 33 years and a trunk height of approx. 12 m on a plantation near Labis in the state of Johor, Malaysia. The root collar was removed at a height of 0.7 m above ground. The trunks were exported in frozen state to Germany and cut into four sections (further processed into boards) and approx. 100 mm thick disks at various heights. The disks used for this investigation were dried for several weeks at 40…60°C and then stored in standard climate at 20 °C, 65% rel. humidity (DIN 50014-20/65-1 according to DIN 50014 (2018)). In order to avoid an influence of different densities and therefore different elastomechanical properties within a test specimen, small test specimen dimensions were chosen. The ultrasonic measurements were carried out on four different type of cuboid specimens, corresponding to specific material planes (figure 2 in Bachtiar et al. (2015)). Each specimen type was manufactured with an edge length of 15 mm. Table 1 gives an overview of the specimens. Two series of specimens were produced from two trunks. In series A, specimen types I to IV were produced; numerous specimens were destroyed during manufacture by tearing out the vascular bundles from the parenchyma tissue (most of which were specimen type II, III and IV). When evaluating the TOF for series A it turned out, that for densities below 200 kg/m³ the evaluation showed significant uncertainties or was even impossible due to the high damping and scattering effect. Therefore, all test specimens of series A below a density of 200 kg/m³ were excluded (and not shown in table 1). In series B, only type I specimens were produced. The determined density of all 187 test specimens available for the investigation was 208…462 kg/m³ for series A and 123…318 kg/m³ for series B. While the lower limit agrees well with the density of the oil palm wood published in the literature, e. g. Koelli (2016), the maximum values are lower due to the manufacturing process of the test specimens. Before testing, all specimens were stored to constant weight in standard climate 20°C, 65 % relative humidity (DIN 50014-20/65-1 according to DIN 50014 (2018)).

Table 1—Overview on test specimens

series	specimen type acc. to Bachtiar et al. (2015)	height within the trunk from the bottom	# of specimen					Σ
			distance to the cortex [mm]					
A			**22.5**	**67.5**	**112.5**			
	I	0.7 m	4	4	4			12
		2.9 m	3	4	0			7
		5.3 m	0	2	0			2
	II	0.7 m	4	4	4			12
	III	0.7 m	4	4	4			12
	IV	0.7 m	4	4	4			12
			distance to the cortex [mm]					
B			**18.5**	**48.5**	**78.5**	**108.5**	**138.5**	
	I	0.5 m	13	13	12	12	11	61
		2.9 m	5	4	9	10	0	28
		5.5 m	7	11	11	12	0	41

Methods

For each test specimen, the density was determined according to DIN 52182 (1976). The TOF measurements were carried out using the Epoch 650 flaw detector with a through-transmission technique

and Olympus C103 transducer with a diameter of 13 mm and a frequency of 1 MHz for longitudinal waves and Olympus V153 transducer with a diameter of 13 mm and a frequency of 1 MHz for transverse waves. For series A, the transducers were pressed manually onto the specimen with a contact pressure of around 30 N without coupling agent. Due to sometimes considerable difficulties in the evaluation of transverse wave measurements on test specimens with a very low density and/or poor surface quality, only for these test specimens small amounts of honey were used as a couplant agent. For series B, a constant contact pressure of the transducers was ensured by using a holding device. The time of flight of three longitudinal and six shear waves was measured along the principal axes resp. planes (on specimen type I according to figure 2 in Bachtiar et al. (2015)) and three quasi-shear waves measured at a 45° angle to the principal axes (on cube specimen type II to IV according to figure 2 in Bachtiar et al. (2015)). The (from transmission length divided by TOF) calculated velocities were used to calculate the elastic constants by full stiffness inversion (FSI) and simplified, uncorrected (SU) data evaluation technique as described in Bachtiar et al. (2015) and Bachtiar et al. (2017). For the FSI evaluation, only the complete sets of test specimens (for which specimens I to IV were available) were used, whereas for the SU evaluation all available test specimens of type I were used.

Results and Discussion

Young´s Moduli

The plots of the Young´s moduli related to density are shown in figure 1. Young´s moduli determined by FSI are lower than that determined by SU (on average E_L -17 %, E_R -51 %, E_T -53 %), which is in accordance with e. g. Bachtiar et al. (2017) and Bucur (2006). For E_L both values (FSI and SU) are much higher than the results determined by compression test from Fathi (2014), by compression and beding test by Srivaro et al. (2018) and Srivaro et al. (2019), by tension test from Fruehwald-Koenig and Heister (2022), by ultrasonic testing (SU) and bending test on bar shaped specimen from Karlinasari et al. (2019), by ultrasonic testing (SU), longitudinal and flexural vibration and bending test on bar shaped specimen from Fruehwald-Koenig (2019). Young´s modulus parallel to the vascular bundles (E_L) depends strongly on the density (figure 1 a). Young´s modulus in tangential direction (E_T) shows a moderate dependance on the density and Young´s modulus in radial direction (E_T) seems to be independent from the density (figure 1 b). The partly strong dependency of the Young´s moduli determined using SU can be explained by the calculation $E = \rho \cdot c^2$. The ultrasonic speed (c) hardly shows any dependence on the density (table 2) and thus represents a constant (therefore, the SU-determined Young´s modulus is linear proportional to the density). The relationship between E_L resp. E_T and the density is lower for FSI than for SU (figure 1 a and b). This can be explained according to Bachtiar et al. (2017) with the matrix inversion and the very different influence on the Young´s modulus by the respective off-diagonal parameters, which – as shown by Bucur and Archer (1984) – lead to high measurement uncertainties during the evaluation. In addition in figure 1, the Young´s moduli determined by FSI are shown over the mean density of the test specimen set. E_L and E_T incease with increasing density by linear regression, which is in contrast to the power law equation for E_L from tension test shown Fruehwald-Koenig and Heister (2022).

In contrast to the results in this investigation, the ultrasonic time-of-flight measurements **parallel to the vascular bundles (E_L)** with conical transducers on rod-shaped specimens with longitudinal waves by Fruehwald-Koenig (2019) for oil palm wood and by Wolters et al. (2015) for coconut palm wood lead to medium to good correlations between the density and ultrasonic velocity. When coupling with conical or point contact transducers, the ultrasonic velocity depends on the properties of the material to which it is coupled. Therefore, the variance between several measurements on the same palm wood specimen is higher than with flat transducers (which record the fastest part of the sound wave over the transducer diameter), depending on whether the coupling is made to a vascular bundle (with high density) or parenchyma (with low density). This higher variance is confirmed by a measurement system analysis (MSA) from Fruehwald-Koenig (2019). Therefore, the correlation between density and ultrasonic velocity in

Fruehwald-Koenig (2019) and Wolters et al. (2015) could have arisen from the fact, that with increasing density (which in case of oil palm wood correlates with an increased proportion of vascular bundles) the probability is increased to couple to a vascular bundle and thereby determine a higher ultrasonic velocity. When using flat transducers (which couple both – vascular bundles and parenchyma), the “fastest” signal (from the vascular bundles, which physically represent a continuous waveguide) is recorded. Therefore, the TOF determined with flat transducers would not correlate to the specimen density but only to the vascular bundles properties. Small variations in the values can be explained by the different secondary wall thicknesses and the associated density of the vascular bundles over the cross-section and the height of the trunk (Fathi 2014). This is in accordance with Burmester (1965), who stated that the ultrasonic velocity corresponds to the "zone most permeable to sound" (in case of his investigation the latewood proportion). This research hypothesis also explains the higher Young´s modulus and ultrasonic speed determined in this investigation compared to the values from the literature (see above).

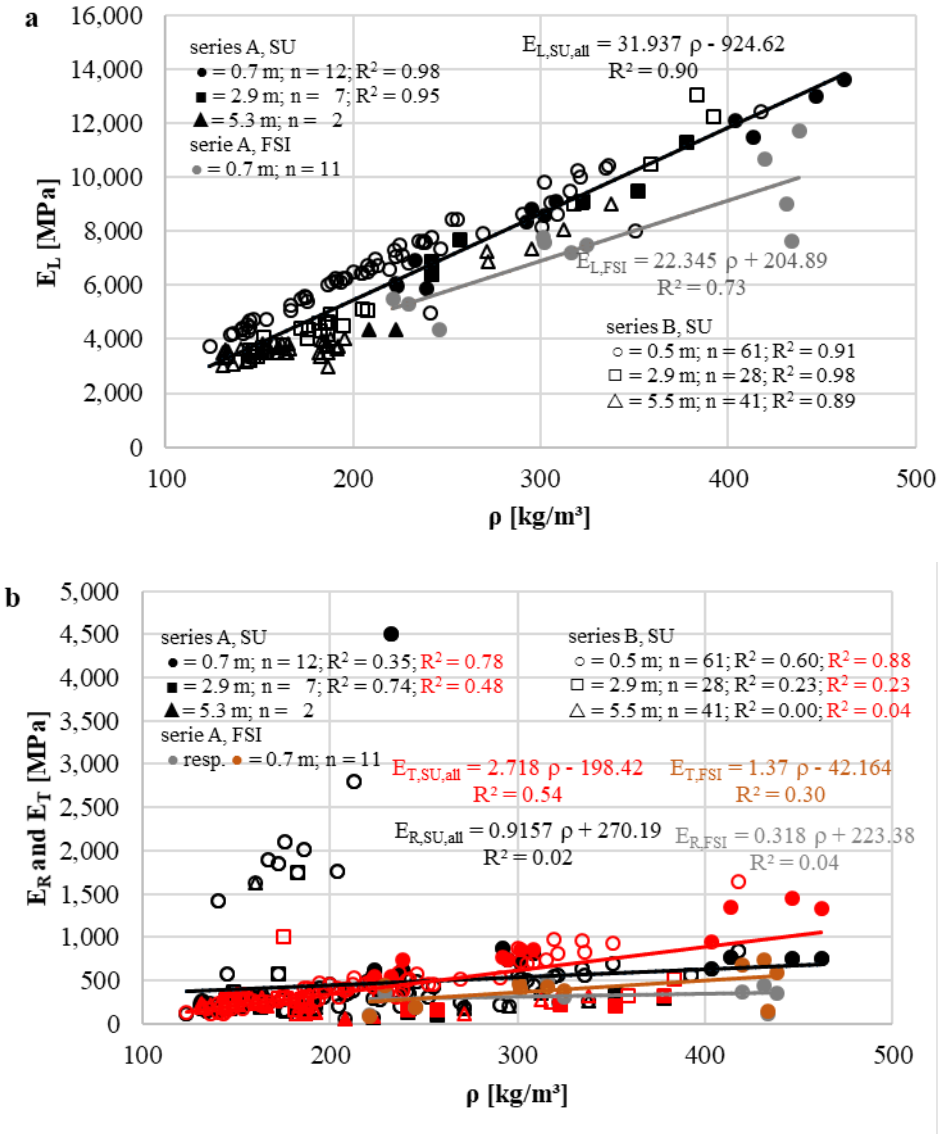

Figure 1— Young´s moduli (E) calculated by SU and FSI data evaluation technique against the density (ρ);
a Young´s moduli longitudinal to the vascular bundles (E_L),
b Young´s moduli perpendicular to the vascular bundles (E_R and E_T)

Table 2—Coefficient of determination (R^2) between ultrasonic velocity (c) and density (ρ)

series	height [m]	# specimen	coefficient of determination (R^2)								
			c_{LL}	c_{RR}	c_{TT}	c_{LR}	c_{RL}	c_{LT}	c_{TL}	c_{RT}	c_{TR}
A	0.7	12	0.22	0.22	0.28	0.01	0.03	0.10	0.07	0.27	0.35
	2.9	7	0.02	0.28	0.05	0.30	0.35	0.08	0.51	0.16	0.22
	5.3	2									
B	0.5	61	0.09	0.04	**0.64**	0.02	0.11	0.04	0.42	0.16	0.08
	2.9	28	**0.77**	0.00	0.19	0.04	0.04	0.16	0.37	0.20	0.17
	5.5	41	0.03	0.19	0.34	0.26	0.01	0.17	0.14	0.45	0.24

Young´s moduli in **tangential (E_T) and radial (E_R) direction** are of the same order of magnitude (figure 1b), because the ultrasonic velocity depends on the most direct path through the low-density parenchyma, in which as few vascular bundles as possible block the way of the wave. Due to the foam-like parenchyma cells (Gibson 2012) and the resulting almost non-directional structure of the parenchyma tissue, the ultrasonic velocity (table 3) and therefore the Young´s moduli within the RT plane are very similar.

Table 3—Mean ultrasonic ultrasonic velocity in dependence of the trunk height

series	height [m]	mean ultrasonic speed [m/s]								
		c_{LL}	c_{RR}	c_{TT}	c_{LR}	c_{RL}	c_{LT}	c_{TL}	c_{RT}	c_{TR}
A	0.7 m	5,326	1,746	1,649	1,153	844	1,191	896	905	925
	2.9 m	5,318	841	859	1,333	559	1,286	583	560	583
	5.3 m	4,490	565	581	1,004	481	1,177	516	486	472
B	0.5 m	5,565	1,498	1,356	1,113	723	1,180	742	792	787
	2.9 m	4,981	1,350	1,313	1,179	644	1,146	662	790	793
	5.5 m	4,787	1,221	1,119	1,082	644	1,075	643	672	659

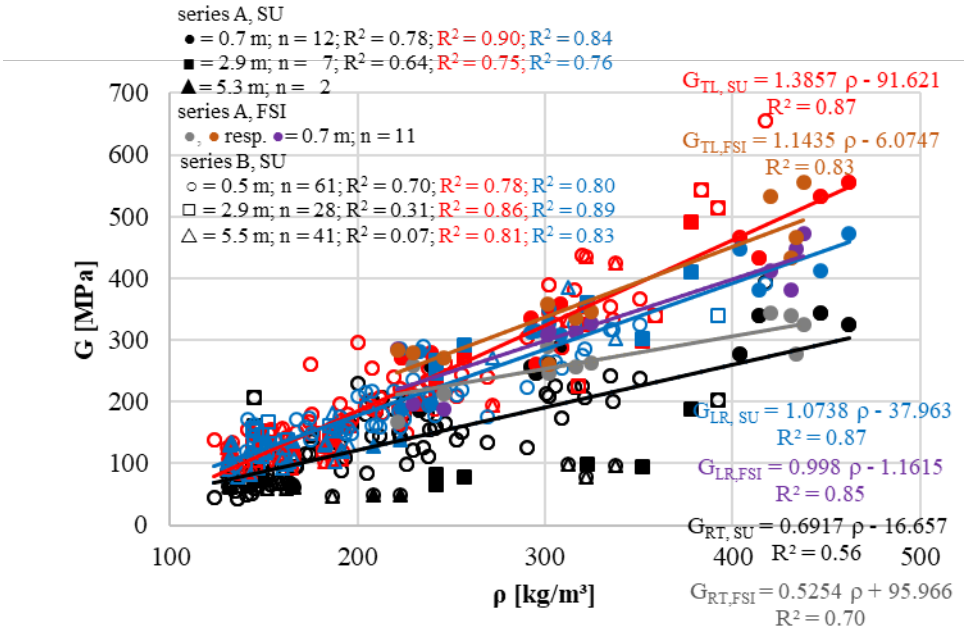

Figure 2— Shear moduli (G) calculated by SU and FSI data evaluation technique against the density (ρ)

Shear Moduli

The plots of the shear moduli related to density are shown in figure 2, the shear moduli are dominated by the parenchyma. The transverse wave velocities are significantly lower than the longitudinal waves in the same direction of propagation (table 3). The velocities depend mainly on the direction of propagation (longitudinal > radial = tangential) and are independent from the direction of polarisation. The very similar ultrasonic velocities within the RT/TR plane allow the assumption that oil palm wood is transversely isotropic (similar to an unidirectional fiber composite material).

Poisson´s ratios

The plot of the Poisson´s ratios related to density is shown in figure 3. The Poisson's ratios are independent from the density, because strains are density-dependent via the Young´s modulus. With a uniform, density-dependent, linear change in the Young´s modulus in the longitudinal and radial/ tangential direction, the ratio of these remains constant. The consequence is, that the ratio of active and passive expansion must also remain constant with changing densities.

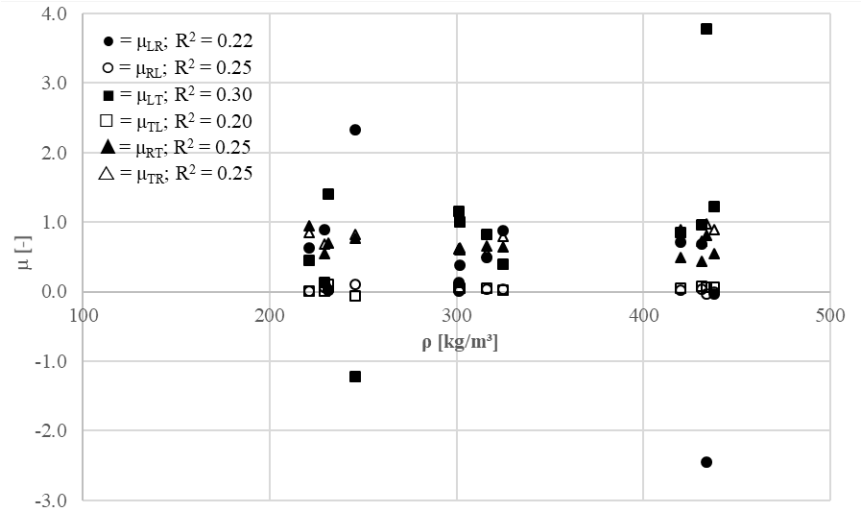

Figure 3— Poisson´s ratios (μ) calculated by FSI data evaluation technique against the density (ρ)

Table 4 shows the mean values for Poisson's ratios and their comparison with dynamically and mechanically determined values from the literature, the Poisson's ratios for dicotylendons are confirmed. But – as described in the literature for Poisson´s ratios determined by UT-FSI – only individual values show a tendency to match, not all six Poisson´s ratios agree with each other. This inequality is much less pronounced in the literature for mechanical test results. The high variation coefficients of up to 279 %, partially negative values and values whose absolute value is > 1 (in the case of μ_{LT} even > 3), figure 3, are confirmed by the literature (e. g. Kohlhauser and Hellmich (2012)). The high uncertainties in the determination can be explained with the high measurement uncertainties in directions outside the symmetry axes (Bucur and Archer 1984). For oil palm wood, these measurement uncertainties appear to occur in particular in measurement planes that include the longitudinal axis. The CV of the two measurements in the RT-plane are still high at 22 % and 34 %, but far lower than the other four values (CV = 97…279 %). Values > 3 cannot be found in the studied literature. However, in experiments with unidirectional fiber composites, Wooh and Daniel (1991) found that with a few degrees of deviation between the symmetry axes, the Poisson´s ratios can exceed the correct value by a factor of up to 10. Furthermore, Bachtiar et al. (2017) explain the high uncertainties with the numerical method of matrix inversion. They show that by changing

the ultrasonic velocity used to calculate the stiffness coefficients by just 0.5…2 %, the calculated Poisson's ratios vary up to 30 %.

Table 4—Poisson´s ratios from FSI from series A and their comparison with dynamically and mechanically determined values from the literature

	μ_{LR}	μ_{RL}	μ_{LT}	μ_{TL}	μ_{RT}	μ_{TR}	**wood specie**
mean value	0.389	0.026	0.911	0.044	0.647	0.707	oil palm
standard deviation	1.085	0.033	1.140	0.042	0.142	0.239	
CV	279 %	128 %	125 %	97 %	22 %	34 %	
literature (dynamically)							
Crespo et al. (2017)	0.390	0.048	0.460	0.033	0.670	0.380	eucalyptus
Goncalves (2011a)	1.231	0.344	0.271	0.024	0.459	0.222	eucalyptus
Bucur and Archer (1984)	0.255	0.022	2.350	0.043	1.700	0.377	spruce
Ozyhar et al. (2013)	0.04	0.08	0.11	2.26	0.23	1.02	birch
literature (mechanically)							
Bodig und Jayne (1982)	0.37	0.04	0.5	0.027	0.67	0.33	hardwood
Goncalves et al. (2011a)	0.333	0.038	0.780	0.060	0.420	0.300	eucalyptus
Bachtiar et al. (2017)	0.257	0.055	0.242	0.042	0.734	0.321	cherry

Conclusions

Since there is no linear relationship between the density and the ultrasonic velocity (and the ultrasonic velocity seems to be more or less a constant), the applicability of the ultrasonic transit time measurements with high frequency flat transducers for determination of the elastic constants must be questioned. Further investigation on the influence of the cell wall properties (thickness and density) of the vascular bundles and parenchyma cells and the influence of the position within the trunk (cross section and height) on the ultrasonic velocity is necessary. If an influence of the cell wall properties or the position within the trunk exists, this method could be suitable to determine Young´s moduli and shear moduli (with optimization in regard to the evaluation criteria, improvements in the coupling quality and better measurement resolution). The influence of (high) measurement uncertainties when determining the off-diagonal stiffness values by ultrasonic testing on the determination of Young´s moduli by FSI should be examined (in particular whether this leads to a non-linear error of the calculated Young´s moduli compared to those calculated according to SU). For reliable Poisson´s ratios of oil palm wood, a comprehensive determination using static testing seems to be necessary.

Author Contributions

B.Sc. Benedikt Faust did the UT-measurements in the laboratory and the FSI-calculations. Prof. Katja Fruehwald-Koenig had the idea, worked on the theoretical background, supervised the laboratory work, made the analyses and wrote the paper.

Acknowledgments

The project was funded by the German Federal Ministry of Education and Research through the “Bioökonomie International 2017” project “Oilpalmsugar (031B0767A)”. The procurement of the oil palm material was supported by the Malaysian Timber Industry Board (MTIB) and the Fibre and Biocomposite Development Centre (FIDEC) represented by Dr. Loh Yueh Feng as well as Profina Plywood Sdn Bhd.

References

Bachtiar, E.V.; Sanabria, S.J.; Niemz, P. 2015. Elastic characteristics of wood by means of ultrasonic waves and mechanical test. Wood Science-Annual Meeting: 12-19.

Bachtiar, E.V.; Sanabria, S.J.; Mittig, J,P,; Niemz, P. 2017. Moisture-dependent elastic characteristics of walnut and cherry wood by means of mechanical and ultrasonic test incorporating three different ultrasound data evaluation techniques. Wood Science and Technology, 51:47-67.

Bodig, J.; Jayne, B.A. 1982. Mechanics of wood and wood composites. Van Nostrand Reinhold Company, New York, 712 p.

Bucur, V. 2006. Acoustics of Wood. Springer, 393 p.

Bucur, V.; Archer, R. 1984. Elastic constants for wood by an ultrasonic method. Wood Science and Technology, 18:255-265.

Burmester, A. 1965. Zusammenhang zwischen Schallgeschwindigkeit und morphologischen, physikalischen und mechanischen Eigenschaften von Holz. Holz als Roh- und Werkstoff, 23(6): 227-236.

Crespo, J.; Aira, J.R,; Vázquez, C.; Guaita, M. 2017. Comparative Analysis of the Elastic Constants Measured via Conventional, Ultrasound, and 3-D Digital Image Correlation Methods in Eucalyptus globulus Labill. BioResources, 12:3728-3743.

DIN 50014:2018. Normalklimate für Vorbehandlung und/oder Prüfung – Festlegungen. Beuth Verlag, Berlin, 7 p.

DIN 52182:1976. Prüfung von Holz – Bestimmung der Rohdichte. Beuth Verlag, Berlin, 3 p.

DIN 52188:1979. Prüfung von Holz – Bestimmung der Zugfestigkeit parallel zur Faser. Beuth Verlag, Berlin, 3 p.

Fathi, L. 2014. Structural and Mechanical Properties of the Wood from Coconut Palms, Oil Palms and Date Palms. Dissertation, University of Hamburg, 181 p.

Fruehwald-Koenig, K. 2019. Properties and Grading of Oil Palm Lumber. In: Wang, N.; Sauter, U.; Ross, R.J. (Ed.) Proceedings 21th International Nondestructive Testing and Evaluation of Wood Symposium, Freiburg, Germany, 24.-27.09.2019, U.S. Department of Agriculture, Forest Service, Forest Products Laboratory, Madison, WI, General Technical Report FPL–GTR–272: 204-212.

Fruehwald-Koenig, K.; Heister, L. 2022. Macromechanical and Micromechanical Behavior of Oil Palm Wood (Elaeis guineensis JACQ.) - Part 1: Tensile, Compression and Bending Properties. Publication in preparation.

Gibson, L.J. 2012. The hierarchical structure and mechanics of plant materials. J. R. Soc. Interface 9(76): 2749-2766.

Gonçalves, R.; Trinca, A.J.; Cerri, D.G.P. 2011a. Comparison of elastic constants of wood determined by ultrasonic wave propagation and static compression testing. Wood and Fiber Science, 43:64-75.

Gonçalves, R.; Trinca, A.J.; Cerri, D.G.P.; Pellis, B.P. 2011b. Elastic constants of wood determined by ultrasound wave propagation. Proceedings of 17th Symposium Nondestructive Testing of Wood, 14.-16.09.2011, Sopron, Hungary:435-441.

Hering, S.; Keunecke, D.; Niemz, P. 2012. Moisture-dependent orthotropic elasticity of beech wood. Wood Science and Technology, 46:927-938.

Jiang, J.; Bachtiar, E.V.; Lu, J.; Niemz, P. 2018. Comparison of moisture-dependent orthotropic Young's moduli of Chinese fir wood determined by ultrasonic wave method and static compression or tension tests. European Journal of Wood and Wood Products, 76:953-964.

Karlinasari, L., Ritonga, R.P.; Maddu, A. 2019. Prediction of Bending and Hardness Strength Properties of Oil Palm (Elaeis guineensis Jacq.) Trunk using Nondestructive Evaluation of Ultrasonic Testing Method. In: Wang, N.; Sauter, U.; Ross, R.J. (Ed.) Proceedings 21th International Nondestructive Testing and Evaluation of Wood Symposium, Freiburg, Germany, 24.-27.09.2019, U.S. Department of Agriculture, Forest Service, Forest Products Laboratory, Madison, WI, General Technical Report FPL–GTR–272:277-282

Keunecke, D.; Sonderegger, W.; Pereteanu, K.; Lüthi, T.; Niemz, P. 2007. Determination of Young's and shear moduli of common yew and Norway spruce by means of ultrasonic waves. Wood Science and Technology, 41:309-327

Killmann, W.; Lim, S.C. 1985. Anatomy and Properties of Oil Palm Stem. Proceedings NATIONAL SYMPOSIUM OF OIL PALM BY-PRODUCTS, Kuala Lumpur, Malaysia, Report No. 87

Kohlhauser, C.; Hellmich, C. 2012. Determination of Poisson's ratios in isotropic, transversely isotropic, and orthotropic materials by means of combined ultrasonic-mechanical testing of normal stiffnesses: Application to metals and wood. European Journal of Mechanics-A/Solids, 33:82-98

Koelli, N. 2016. Density and Moisture Distribution in Oil Palm Trunks from Peninsular Malaysia. BSc-Thesis, University of Hamburg, 52 p.

Kollmann, F. 1951. Technologie des Holzes und der Holzwerkstoffe 1. Band. 2. Auflage, Springer Verlag, Berlin, Göttingen, Heidelberg, 1050 p.

Najmie, M.; Khalid, K.; Sidek, A.; Jusoh, M. 2011. Density and ultrasonic characterization of oil palm trunk infected by Ganoderma boninense disease. Measurement Science Review 11(5): 160-164.

Ozyhar, T.; Hering, S.; Sanabria, S.J.; Niemz, P. 2013. Determining moisture-dependent elastic characteristics of beech wood by means of ultrasonic waves. Wood Science and Technology, 47:329-341.

Petermann, H. 1941. Schubversuche mit Kiefernholz. Holz als Roh-und Werkstoff, 4:141-150

Sinclair, A.; Farshad, M. 1987. A comparison of three methods for determining elastic constants of wood. Journal of Testing and Evaluation, JTEVA, 15(2):77-86.

Srivaro, S.; Matan, N.; Lam, F. 2018. Property gradients in oil palm trunk (Elaeis guineensis). Journal of Wood Science, 64:709-719.

Srivaro, S.; Cherdchim, B.; Pasztory, Z. 2019. Bending and Compressive Properties of Finger-jointed Oil Palm Wood Products. BioResources, 14:6341-6352.

Wooh, S.C.; Daniel, I.M. 1991. Mechanical characterization of a unidirectional composite by ultrasonic methods. The Journal of the Acoustical Society of America, 90:3248-3253.

Wolters, M.; Huels, T.; Solbrig, K.; Fruehwald-Koenig, K. 2015. Nondestructive evaluation of coconut palm wood by means of ultrasonic and natural frequency methods. In: Ross, R. J.; Gonçalves, R.; Wang, X. (Ed). 19th International Nondestructive Testing and Evaluation of Wood Symposium. Rio de Janairo, U.S. Department of Agriculture, Forest Service, Forest Products Laboratory, Madison, WI. General Technical Report FPL–GTR–239: 618-625.

Estimation of the Moisture Content in Wood by Combination of Neutron and X-Ray Imaging

José Couceiro
Luleå University of Technology, Wood Science and Engineering, Forskargatan 1, 931 87 Skellefteå, Sweden, jose.couceiro@ltu.se

Lars Hansson
Department of Ocean Operations and Civil Engineering, Faculty of Engineering, Norwegian University of Science and Technology, 6025 Ålesund, Norway, laha@ntnu.no

David Mannes
Paul Scherrer Insitute (PSI), Villigen, Switzerland, david.mannes@psi.ch

Peter Niemz
ETH Zürich, Institute for Building Materials, Stefano-Franscini Platz 3, 8093 Zürich, Switzerland; Luleå University of Technology, Wood Science and Engineering, Forskargatan 1, 931 87 Skellefteå, Sweden, niemzp@retired.ethz.ch

Dick Sandberg
Luleå University of Technology, Wood Science and Engineering, Forskargatan 1, 931 87 Skellefteå, Sweden, dick.sandberg@ltu.se

Abstract

Recent advances in image processing and X-ray computed tomography (CT) led to substantial development in the non-destructive estimation of the moisture content (MC) in wood, but a real-time technique is not yet available. The use of dual-energy CT has been proposed, but not yet proven due to the similarities of X-ray attenuation in wood and water. Neutron imaging (NI) provides an opportunity due to the large difference in the interactions of neutrons with hydrogen and carbon. The equipment available at the Paul Scherrer Institute (Switzerland) makes it possible to scan wood simultaneously with both neutron and X-rays in a climate chamber, so that changes in the moisture distribution with time can be studied through both methods. The aim of these studies was to increase basic knowledge of how the use of neutrons and X-rays in combination can be applied to study wood-moisture interactions and moisture flow in wood and wood-based products. Wood specimens conditioned to different MCs have been exposed to varying climate conditions and scanned with both techniques in the three main anatomical directions. The results have been processed by an advanced image-processing algorithm for MC calculation from both NI and X-ray imaging data. A preliminary analysis of the results suggests that the NI technique may be used to estimate MC with an accuracy equivalent to that of CT-based techniques, but further analyses and statistical studies are needed.

Keywords: neutrons, industrial X-ray computed tomography, dual energy, timber drying

Introduction

Recent advances in image processing in combination with discrete or computed tomography (CT) X-ray techniques have led to a substantial development of non-destructive detection of internal features of logs and sawn timber in industrial applications. The accuracy of X-ray measurements needs, however, to be

improved to be able to take full advantage of these techniques to give, for example, the accurate detection of properties and structures in the wood material as a basis for the further optimisation of sawing, drying, product sorting and grading, etc. It is a great challenge in image processing to assess the water present in green wood since water and wood have very similar X-ray attenuation coefficients (Couceiro et al. 2019), making it difficult to distinguish wood features when liquid water is present. From basic studies of moisture behaviour in wood in different climate environments using a combination of neutron and X-ray sources, we believe that the industrial X-ray detection in wood applications can be improved.

Due to the high hydrogen content of water, neutrons are more suitable for detecting water in, for example, wood, but neutrons and neutron sources are, at least for the foreseeable future, not suitable for industrial use for health and safety reasons. The investment and operating costs of the neutron facilities are also very high and the number of facilities in the world is limited. One such facility is available at the Paul Scherrer Institute (PSI) in Villigen, Switzerland. The equipment available at the Laboratory for Neutron Scattering and Imaging at PSI makes it possible to scan wood simultaneously with both neutron and X-rays in a climate chamber and to study the evolution of moisture distribution over time with both sources.

The overall purpose of this project is threefold: (1) to compare the information obtained from X-ray and neutron imaging, and to studying how this information can be combined and used to improve the X-ray CT-scanner detection at the CT WOOD laboratory at Wood Science and Engineering, Luleå University of Technology in Skellefteå, Sweden, (2) to study surface phenomena when drying with the help of neutron radiation, since technologies based solely on X-ray cannot properly represent the surface due to the so-called Gibbs phenomenon, and (3) to study moisture transport through adhesive bond-lines and wood-welding joints under varying humidity and temperature conditions above and below 0°C.

This paper focuses on the central question that must be solved before more detailed studies are carried out on wood: whether the moisture level of the wood can be continuously determined in the experiments described here, when it is expressed as the dry weight moisture content (MC) according to:

$$\omega = \frac{m_\omega - m_0}{m_0} \tag{1}$$

where ω is the MC, m_ω is the mass of the wood at the MC ω, and m_0 is the dry mass of wood.

Theory

The attenuation of a neutron or X-ray beam is dependent on the properties of the material through which the beam is travelling, as described by the Beer-Lambert law:

$$T = \frac{I}{I_0} = e^{-\int_0^l \Sigma(z)dz} \tag{2}$$

where T is the extent to which the material transmits the beam, I is the intensity of the attenuated beam, I_0 is the initial intensity of the beam, $\Sigma(z)$ is the linear attenuation coefficient and l is the is the path length of the beam through the material. According to Jackson and Hawkes (1981), the attenuation coefficient of a material can be expressed as the sum of the gravimetric proportions of the attenuation of each of its components, so that the attenuation coefficient for wood can be expressed as:

$$\sum_{i=1}^{n} \Sigma_i z_i = \Sigma_w z_w + \Sigma_h z_h + \Sigma_{v.s} z_{v.s} \tag{3}$$

where Σ_w is the linear attenuation coefficient of wood (w), Σ_h is the linear attenuation coefficient of water (h), $\Sigma_{v.s}$ is the linear attenuation coefficient of the void space ($v.s$), z_w is the thickness of the discrete layer

of dry wood, z_h is the thickness of the discrete layer of water and $z_{v.s}$ is the thickness o the discrete layer of the void space. Neglecting the transmission of the void space and rewriting Eq. 2, the transmission over a certain time (i) can be described by:

$$T_i = e^{-(\Sigma_w z_w + \Sigma_h (z_h)_i)} \tag{4}$$

Considering the definitions of density for dry wood, compact wood and water, Eq 1 can be expressed as a function of time (i):

$$\omega = \frac{\rho_h (z_h)_i}{\rho_{c.w} z_w} \tag{5}$$

where ρ_h is the density of water, z_h is the thickness of the discrete layer of water present in the specimen, $\rho_{c.w}$ is the density of compact wood, and z_w is the thickness of the discrete layer of wood. If the MC is known on two occasions:

$$\omega_i = \frac{\rho_h (z_h)_i}{\rho_{c.w} z_w} \tag{6}$$

$$\omega_{n+1} = \frac{\rho_h (z_h)_{n+1}}{\rho_{c.w} z_w} \tag{7}$$

where n is the number of measurements, the thickness of the discrete layer of wood z_w can be expressed as:

$$z_w = \frac{\rho_h ((z_h)_{n+1} - (z_h)_i)}{\rho_{c.w} (\omega_{n+1} - \omega_i)} \tag{8}$$

By using the Hounsfield scale, the density of wood can be calculated from the X-ray data as:

$$\rho \approx 1000 \frac{\mu - \mu_h}{\mu_h - \mu_{v.s}} + 1000 \tag{9}$$

where μ is total linear attenuation coefficient, $\mu_{v.s}$ is the linear attenuation coefficient of air, and μ_h is the linear attenuation coefficient of water. Since the attenuation coefficient of a material can be expressed as the sum of the gravimetric proportions of each of its components, the density can be expressed by:

$$\rho \approx 1000 \frac{\left(\frac{\mu_w z_w + \mu_h z_h + \mu_{v.s} z_{v.s}}{z}\right) - \mu_h}{\mu_h - \mu_{v.s}} + 1000 \tag{10}$$

where the μ_w is the linear attenuation coefficient of wood. When a given wood specimen undergoes a change in moisture, approximately only the change in the spatial distribution of water z_h takes place. Thus, the neutron transmission of a reference piece of wood can be expressed as:

$$T_i = e^{-(\Sigma_w z_w + \Sigma_h (z_h)_i)} \tag{11}$$

Dividing the transmission at a certain point in time (T_{n+1}) by the transmission for the reference piece of wood (T_i), the change in the spatial distribution of water can be expressed as:

$$((z)_{n+1} - (z)_i) = -\frac{ln\left(\frac{T_{n+1}}{T_i}\right)}{\Sigma_h} \quad (12)$$

The thickness of the discrete layer of wood z_w can thus be estimated if neutron scanning has been carried out on two occasions, where the test piece has undergone a moisture change. If the MC is known on these two occasions, the MC can be calculated at all times where a neutron image is determined. Rearranging Eq. 8 and combining it with Eq. 12, the MC variation over time can be estimated as:

$$\omega_{i+1} - \omega_i = \frac{\rho_h}{\rho_{c.w} z_w \Sigma_h}((z_h)_{i+1} - (z_h)_i) \quad (13)$$

If the initial value of the MC is uncertain, it is possible to estimate this uncertainty if the dry density of the wood, the MC at the end of the experiment, the thickness of the test piece in the neutron beam direction and the thickness of the discrete layer of water at the beginning and at the end are known. By rearranging equation (13) and using the definitions for the compact density of wood and the density of dry wood, the MC at the start of the experiment can be estimated as:

$$\omega_1 = \omega_{n+1} - \frac{\rho_h}{\rho_{d.w} z \Sigma_h}((z_h)_{n+1} - (z_h)_1) \quad (14)$$

Materials and methods

Specimens of green Scots pine (*Pinus sylvestris* L.) sapwood with dimensions of 10 x 10 x 50 mm were used. The specimens were cut with specific orientations in relation to the three main anatomical directions of wood – longitudinal (L), radial (R) and tangential (T) –, so that four types of specimens were prepared, giving different possible relations between growth-ring orientation and the neutron and X-ray beam directions, as shown in Figure 1. All the specimens were taken from the same region in one tree and cut in a way so that they matched each other as well as possible with respect to the orientation of the growth rings. The specimens were sealed using aluminium tape along four of their sides so that the moisture uptake and drying could take place only in one direction, perpendicular to the beam (Figure 1). The specimens were conditioned to different MCs or kept in the green condition and sealed in plastic film to avoid uncontrolled MC changes prior to the experiments.

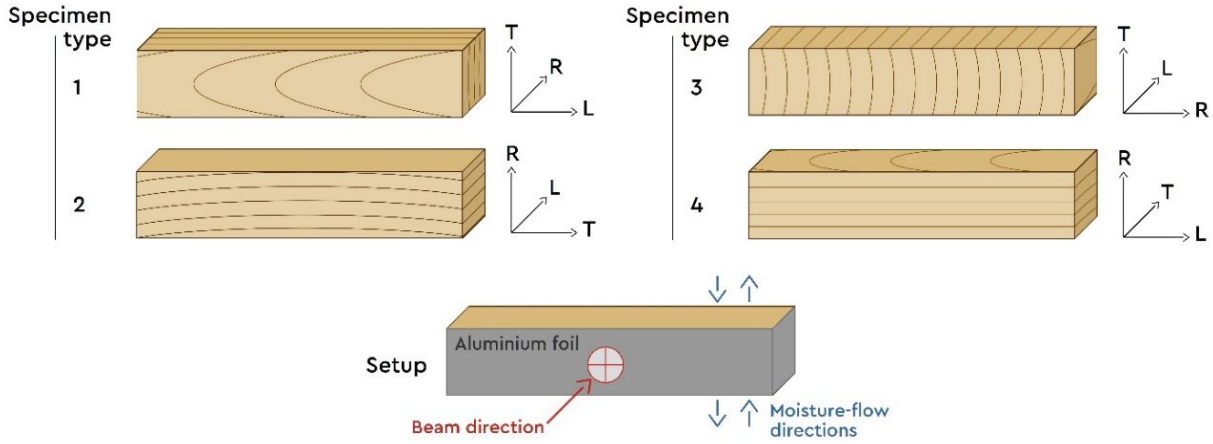

Figure 1—The configurations of specimens (types 1 to 4) used in the experiments, and their positions relative to the beam direction and the moisture flow, due to the restriction of moisture movement with aluminium foil sealing.

The experiments were performed at the NEUTRA beamline at Paul Scherrer Institute, Villigen, Switzerland. The experimental setup consisted of a specially designed climate chamber (Mannes et al. 2017), which was mounted in the Neutron/X-ray beamline, followed by a scintillator-camera based detector (cf. Lämmlein et al 2019). The specimens were placed in an aluminium rack which holds up to eight specimens and were placed inside the climate chamber (Figure 2).

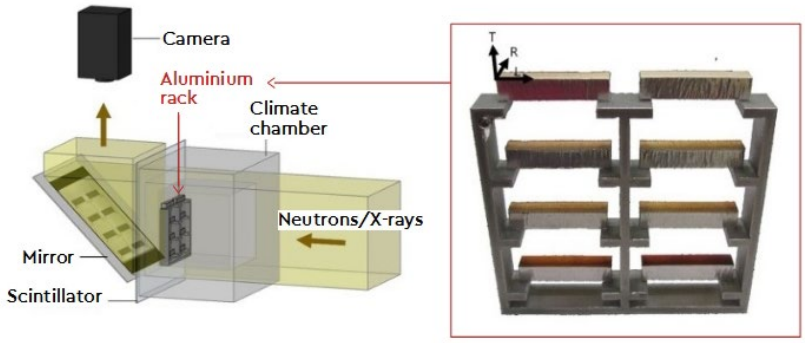

Figure 2—Experimental setup (cf. Lämmlein et al. 2019).

The specimens were weighed in order to calculate gravimetrically their initial average MC and then placed on the aluminium rack inside the climate chamber. They were then scanned under an 18-hour cycle with varying relative humidity (RH) at a constant temperature of 60°C. The initial RH in the chamber was, after a 30 min stabilisation regime at 76% RH, 90% (5.5 h), and it was then lowered stepwise (2x4 h) to a final 30% (4 h).

Since images obtained contain anomalies, they had to be processed before using them for the calculations. This processing entails open beam correction to decrease the noise and black body correction (Boillat et al. 2018; Carminati et al. 2019a) to reduce the scattering effects. These image processing steps are implemented in the software Kiptool (Carminati et al. 2019b).

Results and discussion

The results of the MC calculations showed considerable discrepancies compared to what was expected based on the equilibrium MC (EMC) of the climate over time (Figure 3). The results for only 2 of the 8 specimens were chosen for an in-depth analysis, both corresponding to specimen type 2, designated as specimen A and B. These are pointed out in Figure 3 and shown in Figure 4 as neutron images. Specimen A had an initial MC slightly over 0%, whereas specimen B had an initial MC of almost 120% (green state).

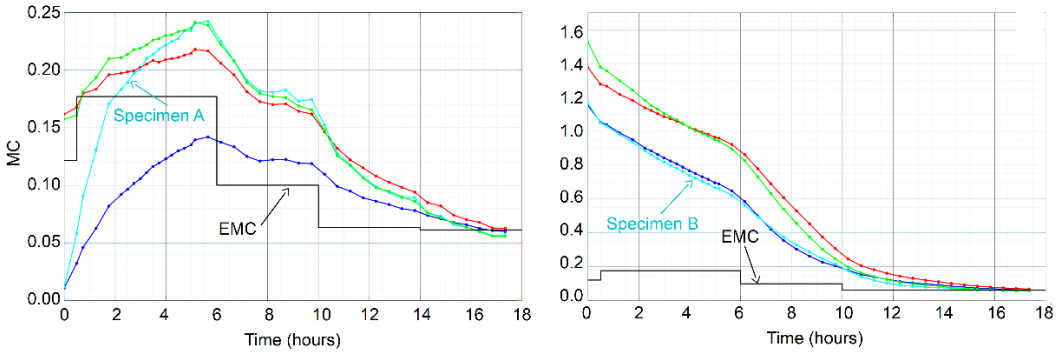

Figure 3—Evolution of the MC of the 8 specimens (left: low initial MC, type 1-4 and, right: initial green MC, type 1-4) during the experiment, and the equilibrium EMC corresponding to the climate in the chamber over time. Specimens A and B are indicated.

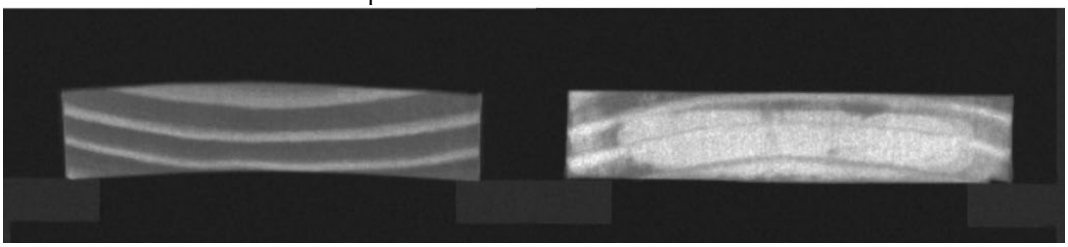

Figure 4—Neutron imaging of specimens A (left) and B (right) at Time = 0 h, with water movement taking place in the radial direction. High brightness in the images indicates large attenuation of the beam interacting with the specimen, thus high MC. In specimen B it can clearly be seen that the surface region of the specimens has dried before the start of the neutron scanning.

The unexpected errors in the MC calculation mentioned in the theory section may be due to small MC differences within the specimen at the start of the experiment. These differences appear to play a much greater role than expected in the accuracy of the calculations. Even when the specimens were conditioned, handling them before the experiment seems to have caused a water uptake or drying sufficiently high for the surfaces to show a higher/lower MC than the core of the specimens. To correctly estimate the initial MC at the pixel level, these moisture differences must be taken into consideration. These moisture differences can be estimated by dividing the specimen into regions, in this case three layers, and calculating the MC and density independently for each of them with help of X-rays, and then using Eq. 14 to estimate the initial MC of each layer. This method was applied for specimens A and B, and the results show that the layer-wise MC estimation, as shown in Figure 5, leads to a more accurate result in relation to the EMC at a given time.

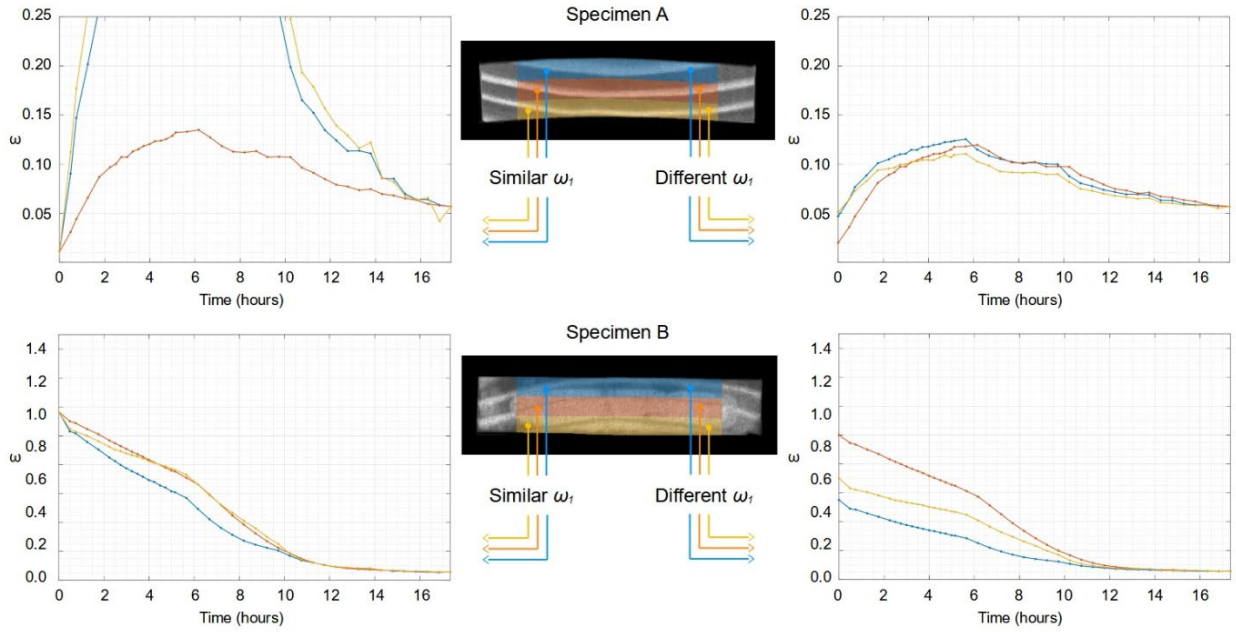

Figure 5—Difference in the prediction of MC over time between a similar initial MC (ω_1) (left) and an initial MC estimated separately for three different regions (right), for specimen A (top) and specimen B (bottom).

Specimen A was oven-dried, so its initial MC should be quite similar, but due to possible differences between the surface and core regions, the MC estimation based on different initial MCs seems more plausible during the entire climate cycle. In the case of specimen B, even if the bottom left-hand graph in Figure 5 seems to be more plausible than the bottom right-hand graph due to the apparently more similar MCs in the three different regions, that is not the case. The initial MC that was originally estimated as a single value for the entire piece is clearly shown in Figure 4 not to be a correct assumption (note the brighter colour in the centre of the specimen and the darker colour closer to the edges). When the initial MC was estimated separately for the three regions shown in Figure 5, the initial MC of specimen B seemed to match the image in Figure 4 more accurately, as does the evolution of the MC towards a more homogeneous MC as the climate change proceeds.

Conclusions

The combination of neutron and X-ray imaging is a powerful tool for estimating the MC in wood at a very detailed level. MC calculations were found to have considerable discrepancies compared to what was expected based on the EMC of the climate over time, and the known initial conditions of the wood specimens. This has been shown to be because the initial MC was not correctly estimated. By dividing the wood into three different regions during the image analysis, the initial MC could be estimated separately for each region and the MC could be estimated a more accurately. The method and technique shown in this study will be used for a complete statistical analysis of the data collected in this project, and the method will be developed as a tool for future projects in the field of wood and water interactions.

Acknowledgments

The authors gratefully acknowledge the considerable support of CT WOOD, a research program at Luleå University of Technology in Skellefteå for the development of X-ray computed tomography applications for use in the forest products industry.

References

Boillat, P., Carminati, C., Schmid, F. [and others]. 2018. Chasing quantitative biases in neutron imaging with scintillator-camera detectors: A practical method with black body grids. Optics Express. 26(12): 15769-15784.

Carminati, C., Boillat, P., Schmid, F. [and others]. 2019a. Implementation and assessment of the black body bias correction in quantitative neutron imaging. PLoS One. 14(1): e0210300.

Carminati, C., Strobl, M., Kaestner, A. 2019b. KipTool, a general purpose processing tool for neutron imaging data. SoftwareX, 10, 100279.

Couceiro, J., Lindgren, O., Hansson, L. [and others]. 2019. Real-time wood moisture-content determination using dual-energy X-ray computed tomography scanning. Wood Material Science & Engineering. 14(6): 437-444.

Jackson, D. F., Hawkes, D. J. 1981. X-ray attenuation coefficients of elements and mixtures. Physics Reports. 70(3): 169-233.

Lämmlein, S. L., Mannes, D., Van Damme, B. [and others]. 2019. The influence of multi-layered varnishes on moisture protection and vibrational properties of violin wood. Scientific Reports. 9(1): 1-9.

Mannes, D., Schmid, F., Wehmann, T., & Lehmann, E. 2017. Design and applications of a climatic chamber for in-situ neutron imaging experiments. Physics Procedia. 88: 200-207.

Nondestructive Model for Predicting the Mechanical Properties of Wood in South West, Nigeria

Lawrence Aguda*
Forest Products Development and Utilization Department, Forestry Research Institute of Nigeria, Jericho, Ibadan, Oyo State, Nigeria. aguda.lo@frin.gov.ng

Misirat Bakare
Forest Products Development and Utilization Department, Forestry Research Institute of Nigeria, Jericho, Ibadan, Oyo State, Nigeria. bakare.mb@frin.ng

Ige Oluwagbemiga
Social and Environmental Forestry Department, University of Ibadan, Ibadan, Oyo State, Nigeria. igeup@yahoo.com

Abstract

Destructive method of testing has been a popular method for determining the mechanical properties of wood in most part of West Africa as a result of non-availability of equipment for Non Destructive Test (NDT). Data for the study were collected from four age series of *Tectona grandis* plantation: 10, 15, 20 and 25 years old using the destructive testing method. Samples were collected from *Tectona grandis* plantation at Onigambari forest reserve, Ibadan, Oyo State, Nigeria. A stand was harvested from each age series and samples were taken at the base, middle and top and further partitioned into inner wood, centre wood and outer wood. Investigation was carried out to determine the strength properties using a computer control electronic universal testing machine. Data collected were subjected to regression analysis at $\alpha_{0.05}$ to predict the mechanical properties for the age series 30, 35, 40 and 45 years old. The result revealed that non-linear regression model (Power) was adjudged the best for the prediction following least root mean square error and highest Adjusted coefficient of determination. This implied that NDT-Power model can be used to determine mechanical properties of Teak in southwest Nigeria.

Keywords: Non-destructive, destructive, mechanical properties, *Tectona grandis*, prediction, model.

Introduction

Wood is one of the oldest, most versatile, and most lightweight renewable resources that has been accepted and conditioned for structural and construction applications on its stiffness properties (Green 2001, Smith and Snow 2008, Ramage et al. 2017). The strength properties of wood considered for construction purposes may be generally assessed through visual grading; however, it is scientifically determined through assessing the mechanical properties. Mechanical properties are characterized by the response of a material to externally applied forces (Murugan 2020). Furthermore, it was highlighted that static modulus of elasticity (sMOE), bending strength, and parallel compression strength are the most sought-after mechanical properties for assessing the strength of wood. (Vernay 2000, Messaoudene *et al*. 2008). Mechanical methods such as resistance drilling, screw withdrawal, hardness test (Nowak et al. 2021), and the use of a Universal Testing Machine (UTM) have been adopted for measuring the strength properties of wood. Notwithstanding, the common method of determining the mechanical properties of wood is through the use of the UTM. This method is considered expensive, demanding high maintenance cost; it is time consuming

about 10 minutes per sample and also damages the wood samples, thus rendering an undesirable effect. In contrast, nondestructive testing technology aims to have no effect on the appearance, internal structure, or usability of ancient wooden components; thus, it represents a significant improvement from conventional timber and wooden material testing methods.

Nondestructive testing (NDT) and nondestructive evaluation (NDE) of materials is constantly evolving. This is especially true in the area of wood and fiberbased materials. For example, early research on NDT/NDE technologies for wood products focused on methods for assessing the performance characteristics of structural lumber in North America. The NDT techniques, equipment, and evaluation procedures that resulted from those efforts are now in widespread use. Currently, world wide research and development efforts are underway to examine the potential use of a wide range of NDT technologies for evaluating wood and wood based materials from the assessment of standing trees to in-place structures. In recent years, methods such as X-ray scanning, Pilodyn , vibration methods, stress waves, drilling resistance, and ultrasonic waves for the nondestructive testing of internal defects, researchers have determined that stress wave and impedance meter testing methods are the most suitable for defect detection because of their convenience, security, and effective visualization of results. The international forest products research communi ty is responding to these driving forces by conducting NDT/NDE research to provide the technologies needed to address these challenges. This article presents a sample of the ongoing NDT/NDE research efforts being conducted in several areas of the world.

Materials and methods

The study area

This study was carried out on *Tectona grandis* plantation in Onigambari Forest Reserve (Fig.1). It is located on latitude 7^0 25' and 7^0 55'N and longitude 3^0 53' and 3^0 9'E within the low land semi-deciduous forest belt of Nigeria and covers a total land area of 17,984ha. The reserve is divided into two: natural and plantation forests. The natural forest is made up of indigenous species such as *Terminalia spp*, *Triplochiton scleroxylon*, *Irvingia garbonensis, Treculia africana,* among others while the plantation forest is made up of mainly exotic species such as G*melina arborea* and *Tectona grandis*. The topography of the study area is generally undulating, lying at altitude between 90m and 140m above sea level. The annual rainfall ranges between 1200mm to 1300mm spreading over March to November. The dry season is severe and the relative humidity is low and average annual temperature is about 26.4^0C**.**

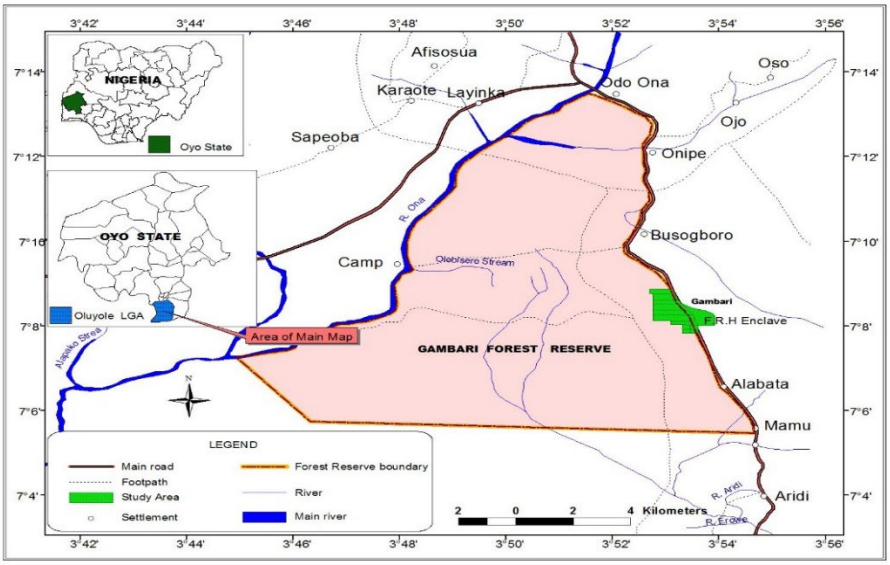

Fig 1: Map of Gambari forest reserve

Sampling selection and preparation for the destructive test

One standing tree were felled from each age series (10, 15, 20 and 25) and their merchantable heights were measured. Bolts (70cm long) were cut from each tree at the base (10%), middle (50%), and top (90%) of the merchantable length as shown in fig 2. Twelve bolts were then taken to the sawmilling section of the Department of Forest Products Development and Utilization (FPD&U), Forestry Research Institute of Nigeria (FRIN), Ibadan, for conversion. Planks were obtained from all the bolts, and they were taken to the Wood Workshop Section for further conversion to test samples. Samples for impact bending, compression strength, shear strength, modulus of elasticity and modulus of rupture were taken.

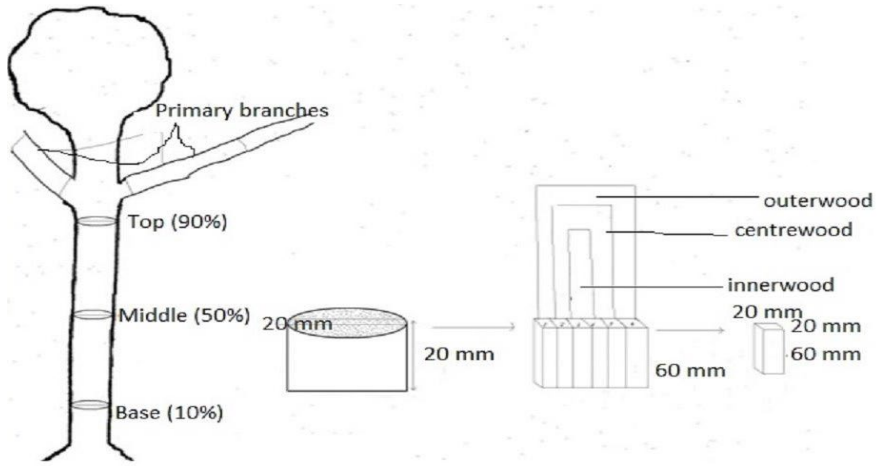

Fig. 2. The selected parts of samples

Equipment Used for destructive evaluation

A computer control electronic universal testing machine manufactured by Jinan Hensgrand Instrument Co., Ltd. in Jinan, China with model number WDW-50 was used for the mechanical properties determination.

The non-destructive model

Five models were selected as candidate models (Table 1) for this study to predict the wood mechanical properties. The data were divided into two sets, 70% of the data set (calibrating set) were used to fit the non-destructive models, while the remaining 30% was used for model validation as described by Akindele, (1990) and Ige, *et al*., (2019). Linear and Non-linear regression models were used in fitting the models.

Table 1: Evaluated models

Model No	Model Name	Function
1	Simple Linear	$MP = a + Age$
2	Power	$MP = aAge^{b}$
3	Saturation	$MP = aAge/(b + Age)$
4	Growth Rate	$MP = aAge/(b + Age)$
5	Exponential	$MP = ae^{bAge}$

MP = Mechanical Properties (Impact bending, Modulus of Rupture, etc), a and b = regression constants and e = exponential

Model Evaluation and Comparison

Model evaluation and comparison are important aspects of model development. It is imperative that some examination of a model be made at all stages of model design, fitting and implementation. Therefore, a thorough evaluation of model involves several steps, which include two major ones often called verification and validation. In tree growth modeling, the two steps usually denote qualitative and quantitative tests of model respectively.

Model Verification

Model verification involves examination of the structure and properties of a model. As a matter of fact, model verification implicitly means comparing and evaluating candidate models. Model evaluation should be convincing enough to boost user's confidence.
According to Ige (2017) and Soares *et al* (1994), a thorough evaluation should include the following aspects:

- Examine the model and its components for logical consistency and biological realism (Oderwald and Hans, 1993)
- Ascertain the statistical properties of the model in relation to data
- Characterize errors in terms of magnitude (i.e confidence intervals), residuals and contributions by each model component to total error
- Test, using statistical approaches for bias and precision of the model, goodness-of-fit and patterns in, and distribution of residuals (Mayer and Butler, 1993)
- Identify model components with the greatest influence on predictions.

These analyses need not be sequential. All relevant aspects should, however, be examined in each model component and in the assembled model. The models that will be developed in this study will be evaluated using the following statistical tests:

a. The Mean Square Error (MSE). This is a measure of the spread of the data and therefore an indication of the precision of the predicted response. The suited and best model must have least MSE value. This is expressed as:

b.

$$MSE = \frac{RSS}{n - p} \quad \ldots\ldots\ldots\ldots\ldots\ldots\ldots\ldots\ldots\ldots\ldots\ldots 1$$

c. The Adjusted Square Multiple Correlation Coefficients (R_a^2). The model with highest value is adjudged the best. This is given as:

$$R_a^2 = 1 - \text{MSE}\left[\frac{n - 1}{n - p}\right]$$

$$R_a^2 = 1 - \text{MSE}\left[\frac{n - 1}{TSS}\right] \quad \ldots\ldots\ldots\ldots\ldots\ldots\ldots\ldots\ldots\ldots 2$$

Where:
p = number of parameters in the model
n = number of observations
RSS = Residual sum of square

TSS = Correlated total sum of squares

d. Akaike information criterion (AIC). Model with least AIC is always selected as the best. The AIC is of the form:

$$AIC = 2k - 2*\ln(L) \quad \ldots\ldots\ldots\ldots\ldots\ldots\ldots\ldots\ldots\ldots\ldots\ldots 3$$

Where:
K = number of estimated parameters in the model
ln = Natural logarithm
L = the maximized value of the likelihood function for the model

e. Paired sample Student T-test

$$t = \frac{\bar{X}_1 - \bar{X}_2}{S_{X_1X_2} \cdot \sqrt{\frac{2}{n}}} \quad \ldots\ldots\ldots\ldots\ldots\ldots\ldots\ldots\ldots\ldots\ldots\ldots 4$$

$$S_{X_1X_2} = \sqrt{\frac{1}{2}(S_{X_1}^2 + S_{X_2}^2)} \quad \ldots\ldots\ldots\ldots\ldots\ldots\ldots\ldots\ldots\ldots 5$$

where
$\overline{X}$ = Means for prediction model and real data respectively
$S_{X1\&X2}$ = Pooled standard deviation
The significance of each regression coefficient in the models was tested using the Student t-test (eq 4). The t-values will be compared with the critical value of t at $\alpha = 0.05$ level. Where t-calculated for the regression coefficient exceeded the critical value of t, the independent variable will be considered significant and vice-versa. Thus, it was possible to drop out any of the insignificant independent variables from the models and carry out further regressions based on only significant independent variables.

Model Validation

It is important to subject the models formulated to a process of validation before inferences about the real world obtained from them can be used with confidence. Validation involves the testing and comparing of the model output with what is observed in the real world (Reynolds *et al* 1981). This requires that the prediction model be compared with the real-world data that are independent of the real data used in the construction of the models. In cases where the collection of new data is to be avoided, an alternative procedure is to split the original data into two sets; the first being called the calibrating set and the second the validation set. The calibrating set is used to construct the models while the validation set is used to test them (Maltamo and Kangas, 2008).
In forest growth models, fewer data are often used for validation (e.g. West (1981) reserved a quarter of their data while Akindele (1990) and Akinnagbe (2001)) reserved one third of their data). The validation data set should contain sufficient replications to enable the natural variability to be expressed. Hence, in this study, one third of the data set from each age series will be set aside as the validation set while the rest of the data will be use in calibrating the models.

The selected equations were used to predict values for the test plantations. The values were compared with the observed values (i.e values from the validation set) and the differences were expressed as model bias. The t-test procedure was used to compare the predicted values with the observed values from the validation data as done by Goulding (1979), Adesoye (2002) and Ige (2017). For a valid model, the comparison should indicate that the observed and the predicted are not significantly different at 5% probability level

Results and discussions

Table 2: Summary of mean values of destructive method

Property	Age series			
		Base (10%)	**Middle (50%)**	**Top (90%)**
Impact Bending (N/mm^2)	**10**	40.12	39.88	38.28
	15	43.65	42.61	42.61
	20	45.76	44.29	44.22
	25	46.98	46.98	46.95
Modulus of Elasticity (N/mm^2)	**10**	7600	7600	7562
	15	8119	8111	7820
	20	8405	8367	8230
	25	8555	8429	8421
Modulus of Rupture (N/mm^2)	**10**	60.32	58.23	58.02
	15	66.78	66.38	64.23
	20	61.02	61.02	58.91
	25	74.09	72.77	72.41
Max Shear Strength (N/mm^2)	**10**	10.43	10.22	10.06
	15	11.21	11.19	11.19
	20	13.22	13.33	13.18
	25	14.98	14.34	14.31
Max Compression Strength Parallel-to-grain (N/mm^2)	**10**	38.87	38.48	38.39
	15	39.43	39.21	39.03
	20	42.67	42.61	42.61
	25	45.66	45.35	45.31

Table 3: Models parameters and fit Indices for Impact Bending

Model No	Model Name	a	b	RSME	AIC	R^2adj	Rank	Validation t-Test
			Base					
1	Simple Linear	0.0009120	1.8397808	0.06302	-2199.619	0.7049	6	
2	Power ($IB = 0.001Age^{0.0005}$)	0.001130	0.0005256	0.0109	-2855.692	0.9487	1	0.0214^{ns}
3	Saturation	-0.09721	0.01035	0.0595	-2293.47	0.7372	4	
4	Growth Rate	-0.2447	0.0059	0.0480	-2642.177	0.8285	2	
5	Exponential	-0.3468	0.0181	0.0516	-2526.98	0.8024	3	
			Middle					
1	Simple Linear	-0.2190	0.02679	0.0601	-2277.216	0.7319	4	
2	Power ($IB = -7.887Age^{2.210}$)	-7.8868	2.2096	0.0016	-3164.567	0.87564	1	0.0199^{ns}
3	Saturation	-0.2190	-6.164e^{-05}	0.0601	-2277.216	0.7319	4	
4	Growth Rate	0.01673	3.857e^{-05}	0.0479	-2649.053	0.8295	3	
5	Exponential	4.760e^{-05}	1.666	0.0466	-2693.595	0.8388	2	
			Top					
1	Simple Linear	-0.0896	0.0121	0.0447	-596.0443	0.7441	5	
2	Power ($IB = -6.931Age^{1.863}$)	-6.93120	1.8632	0.0246	-710.3751	0.8723	1	0.0122^{ns}
3	Saturation	-0.1178	0.0001	0.04843	-567.7031	0.7443	4	
4	Growth Rate	2.204e^{-02}	3.510e^{-05}	0.0347	-687.3545	0.8384	3	
5	Exponential	8.188e^{-05}	1.756	0.0345	-688.8525	0.8446	2	

ns = not significant at 5% probability level

Table 4: Models parameters and fit Indices for Modulus of Elasticity

Model No	MODEL NAME	a	b	RSME	AIC	R^2adj	Rank	Validation t-Test
			Base					
1	Simple Linear	0.00048	2.0040	0.0418	-620.5406	0.7861	5	
2	Power ($MOE = -0.002Age^{0.001}$)	-0.00248	0.0005	0.0218	-820.6407	0.9182	1	0.0918^{ns}
3	Saturation	-0.0598	0.0057	0.0419	-619.6953	0.7933	4	
4	Growth Rate	-0.0970	-0.0079	0.0316	-717.9074	0.8912	2	
5	Exponential	-0.3428	0.0195	0.0349	-684.0188	0.8861	3	
			Middle					
1	Simple Linear	0.0011	1.8103	0.0763	-483.335	0.7327	3	
2	Power ($MOE = -0.014Age^{0.0006}$)	$1.365e^{-02}$	$5.513e^{-04}$	0.0566	-489.0783	0.8102	1	0.0632^{ns}
3	Saturation	-0.2543	0.02780	0.0751	-488.5178	0.7511	2	
4	Growth Rate	-0.24752	0.0017	0.0618	-569.557	0.5527	5	
5	Exponential	-0.407095	0.0195	0.06248	-566.3715	0.5529	4	
			Top					
1	Simple Linear	-0.0463	0.0024	0.07004	-518.1987	0.3913	5	
2	Power ($MOE = -7.816Age^{2.205}$)	-7.8159	2.2053	0.2984	92.39956	0.8551	1	0.0710^{ns}
3	Saturation	-0.0492	0.0007	0.0660	-543.5202	0.5128	3	
4	Growth Rate	$8.397e^{-03}$	$4.238e^{-05}$	0.05035	-658.5046	0.7495	2	
5	Exponential	$3.363e^{-05}$	1.7420	0.04878	-670.8719	0.4644	4	

ns = not significant at 5% probability level

Table 5: Models parameters and fit Indices for Modulus of Rupture

Model No	MODEL NAME	a	b	RSME	AIC	R^2adj	Rank	Validation t-Test
			Base					
1	Simple Linear	2.725e-04	2.222	0.04351	-792.181	0.4808	4	
2	Power ($MOR = -0.026Age^{0.0006}$)	-2.586e^{-02}	5.994e^{-04}	0.01308	-996.8074	0.6724	1	0.0337^{ns}
3	Saturation	-0.1475	0.0134	0.0428	-799.0405	0.4536	5	
4	Growth Rate	-0.1215	-0.0033	0.0334	-913.3599	0.6063	2	
5	Exponential	-0.3148	0.0191	0.0346	-897.2451	0.5181	3	
			Middle					
1	Simple Linear	-2.107e-01	2.421e^{-02}	0.04677	-757.593	0.5061	5	
2	Power ($MOR = -8.531Age^{2.436}$)	-8.53089	2.4362	0.0276	-965.83311	0.7332	1	0.0813^{ns}
3	Saturation	-2.107e^{-01}	4.317e^{-05}	0.04677	-757.593	0.6061	4	
4	Growth Rate	8.843e^{-03}	3.855e^{-05}	0.03506	-892.2844	0.6442	3	
5	Exponential	4.869e^{-05}	1.765	0.03428	-901.8554	0.7068	2	
			Top					
1	Simple Linear	0.0004091	2.0755677	0.06615	-506.9894	0.7860	5	
2	Power ($MOR = -0.016Age^{0.0006}$)	-1.623e^{-02}	5.512e-04	0.03582	-708.9438	0.9897	1	0.0102^{ns}
3	Saturation	-0.1842712	0.0170375	0.06499	-512.962	0.7941	4	
4	Growth Rate	-0.2163	-0.0015	0.04606	-647.6201	0.9062	2	
5	Exponential	-0.3999	0.0186	0.0478	-633.9994	0.8961	3	

ns = not significant at 5% probability level

Table 6: Models parameters and fit Indices for Max Shear strength

Model No	MODEL NAME	a	b	RSME	AIC	R^2adj	Rank	Validation t-Test
			Base					
1	Simple Linear	-2.287e-01	2.774e-02	0.07147	-475.5342	0.7462	4	
2	Power ($MSS = -8.129Age^{2.292}$)	-8.12942	2.29165	0.0365	-666.3395	0.9159	1	0.0821^{ns}
3	Saturation	-2.287e-01	-5.856e-05	0.07147	-475.534	0.7461	5	
4	Growth Rate	1.781e-02	$3.865e^{-05}$	0.05306	-593.9003	0.8635	3	
5	Exponential	4.552e-05	1.561	0.04795	-632.8062	0.8941	2	
			Middle					
1	Simple Linear	0.879356	0.18362	4.5420	936.4631	0.3587	5	
2	Power ($MSS = 3.366Age^{-8.408}$)	3.36554	-8.40790	4.0529	910.1653	0.6364	1	0.0992^{ns}
3	Saturation	28.6925	7.9806	4.3883	926.4997	0.4052	2	
4	Growth Rate	25.7600	0.0699	4.4678	931.2228	0.3795	3	
5	Exponential	29.05019	1.47728	4.4753	931.7580	0.3774	4	
			Top					
1	Simple Linear	0.023	0.072	0.072	-703.245	0.6874	5	
2	Power ($MSS = 0.021Age^{14.75}$)	0.0212	14.75	0.019	-794.873	0.8953	1	0.0331^{ns}
3	Saturation	0.055	-0.120	0.021	-7837.97	0.7991	2	
4	Growth Rate	0.024	6.738	0.063	-780.688	0.7914	3	
5	Exponential	0.025	2.314	0.066	-751.016	0.6904	4	

ns = not significant at 5% probability level

Table 7: Models parameters and fit Indices for Max Compression Strength Parallel-to-grain (N/mm^2)

Model No	Model Name	a	b	RSME	AIC	R^2adj	Rank	Validation t-Test
			Base					
1	Simple Linear	0.026	0.012	0.064	-774.031	0.8912	2	
2	Power ($MCSP = 0.024Age^{1.063}$)	0.024	1.063	0.031	-785.026	0.8993	1	0.0211^{ns}
3	Saturation	0.024	0.172	0.069	-731.929	0.8901	3	
4	Growth Rate	0.0455	0.032	0.401	302.536	0.8684	4	
5	Exponential	0.055	0.031	0.403	303.149	0.8591	5	
			Middle					
1	Simple Linear	0.094	0.004	0.128	-29.005	0.9631	2	
2	Power ($MCSP = 0.043Age^{0.035}$)	0.043	0.035	0.024	-333.043	0.9872	1	0.0618^{ns}
3	Saturation	0.044	0.030	0.415	320.839	0.8771	3	
4	Growth Rate	0.044	0.031	0.426	336.639	0.8704	4	
5	Exponential	0.045	0.032	0.430	342.025	0.8683	5	
			Top					
1	Simple Linear	0.044	0.032	0.0429	-841.285	0.8628	2	
2	Power ($MCSP = 0.045Age^{0.032}$)	0.045	0.032	0.0367	-844.539	0.8698	1	0.0912^{ns}
3	Saturation	0.024	6.738	0.0632	-780.688	0.8144	3	
4	Growth Rate	0.025	2.314	0.0661	-751.016	0.7904	4	
5	Exponential	0.026	0.012	0.0682	-714.031	0.7712	5	

ns = not significant at 5% probability level

Conclusions

The results in Table 3 – 7 revealed the models statistics summary observed in the study. It was deduced that Power model performed the best for all the mechanical properties assessed at different tree height position. The model verification test further confirmed the selected models as good and reliable candidate and recommended for further use. Model is now a daily routine used in forestry for predicting growth and yield, modeling diameter distributions, basal area model and tree crown model and many more (Ogana *et al*., 2015). Models are simply used for prediction and projection. Several studies had opined that decision of the management of the forest are often predetermined on information about current and future resources condition (Ige, 2017). As such, this study has directed effort in obtaining prediction models for Non-destructive method in determining different mechanical properties of Gmelina wood at different tree height position. Studied have shown that adding of age to tree growth functions improves the predictability of the model (Maleki *et al.,* 2015 and Ige, 2017). For the study area it was observed that power gave better estimation of wood mechanical properties and its effect on the growth of such trees. Values gotten for the root mean square error of all the models are very small and high values was gotten for the adjusted coefficients of determination shows that the model form is well adapted and biological realistic which also agrees with what was reported by Ige and Adesoye (2017).

References

Adesoye, P.O (2002). Integrated system of forest stand models for *Nauclea diderrichii* in Omo forest reserve, Nigeria. Ph.D thesis, Department of Forest Resources Management, University of Ibadan, Nigeria. 174p.

Akindele, S. O. (1990). Site quality assessment and yield equation for Teak plantation in the dry forest zone of Nigeria. Ph.D Thesis, Department of Forest Resources Management, University of Ibadan, Nigeria. 180p

Akinnagbe, A. (2001). Stem diameter distribution model in Akure forest reserve, Nigeria. M.Tech Thesis submitted to the Department of Forestry and Wood Technology, Federal University of Technology, Akure pp 14 - 56

Goulding, C.J. (1979). Validation of growth models used in forest management *N.Z.J* 24:108-124Pp.

Ige P. O. (2017): Development of Models For Assessing the Slenderness of *Triplochiton Scleroxylon* K. Schum Stands in Oniganbari Forest Reserve, Nigeria.. *Nigerian Journal of Forestry,47 (2)44 - 50*

Ige, P.O. and Adesoye, P.O., (2017). Assessment of Non-Spatially explicit competition indices effects on Diameter Growth of Gmelina arborea Roxb. Stands in Omo Forest Reserve, Nigeria. *Journal of Forests and Forest Products*, 10, pp.106-118.

Maleki, K., Kiviste, A., and Korjus, H. (2015). Analysis of individual tree competition on diameter growth of silver birch in Estonia. *Forest Systems*, *24*(2), 8.

Maltamo, M. and A. Kangas. (2008). Methods based on k-nearest neighbor regression in estimation of basal area diameter distribution. *Can. J. For. Res*. 28:1107-1115

Mayer, D.G and D.G Butler (1993). Statistical Validation. *Ecological Modelling* 68: 21-32

Oderwald, R.G and R.P. Hans (1993). Corroborating models with model properties. *Forest Ecology and Management* 62: 271-283

Ogana, F.N., Osho, J.S.A. and Gorgoso-Varela, J.J., (2015). Comparison of Beta, Gamma Weibull distributions for characterising tree diameter in Oluwa Forest Reserve, Ondo state, Nigeria. *Journal of Natural Sciences Research*, *5*(4), pp.28-36.

Reynolds, M. R., Burkhart, H. E. and Daniels, R. F. (1981). Procedures for Statistical Validation of Stochastic Simulation Models. *Forest Science* Vol. 27 No. 2. 349-364

Soares, P; M. Tome; J.P, Skovsgaard and J.K. Vanclay (1994). Evaluating a growth model for forest management using continuous forest inventory data. *Forest Ecology and Management* 71(3)

West, P.W. (1981). Estimation of height, bark thickness and plot volume in re-growth eucalyptus forest. *Aust For Res* 9:295–308.

Comparative Estimation of Acoustic Velocity and Strength Properties of Down Pine Trees Using Near Infrared Spectroscopy

Munkaila Musah*
Forest Products Development Center, Auburn University, Auburn, AL, USA, mzm0263@auburn.edu

Javier Hernandez Diaz
Forest Products Development Center, Auburn University, Auburn, AL, USA, jah0189@auburn.edu

Dana Mitchell
USDA Forest Service, Southern Research Station, Auburn, AL, USA, dana.mitchell@usda.gov

Mathew Smidt
USDA Forest Service, Southern Research Station, Auburn, AL, USA, mathew.smidt@usda.gov

Yucheng Peng
Forest Products Development Center, Auburn University, Auburn, AL, USA, yzp0027@auburn.edu

Tom Gallagher
School of Forestry and Wildlife Sciences, Auburn University, Auburn, AL, USA

Maria S. Peresin
Forest Products Development Center, Auburn University, Auburn, AL, USA, soledad.peresin@auburn.edu

Brian Via
Forest Products Development Center, Auburn University, Auburn, AL, USA, brianvia@auburn.edu

* Corresponding author

Abstract

Near infrared reflectance (NIR) spectroscopy was used to determine the acoustic velocity and strength properties of down pine trees in the southern coastal plains of the United States. Three different acoustic measurements (longitudinal, transverse, and offset or opposite-face method) from the acoustics velocity determined by Time-of-Flight (TOF) measurement and the increment core samples obtained from the thirty down loblolly pine trees were used in the study. NIR spectra were obtained using a fiber probe on the radial surface of each core to rapidly predict the speed of sound and strength properties of the down trees from the Time-of-Flight acoustic estimations. The NIR prediction was moderately good for the transverse and offset methods. The predictability was 0.67 for offset measurement and 0.65 for transverse. The longitudinal measurement recorded the least prediction ($R^2 = 0.42$) with the standard error of prediction (SEP) of 0.305 degrees and mean property value of 3.498. The dry density from the increment cores had a moderate variance percentage (60%), whiles the green density recorded a low variance percentage (42%) from the multiple linear regression (MLR) of the reduced model of the density properties. The results of the acoustic model indicated that NIR spectroscopy has a potentially useful role in the measurement of the acoustic velocity and strength properties of down trees; however, further development of the method is still necessary to reach acceptable accuracy.

Key words: Near infrared spectroscopy, Down trees, Acoustic velocity, Strength properties

Nondestructive Determination of the Within-Ring Wood Dynamic Modulus of Elasticity for Black Spruce and Jack Pine‡

Wassim Kharrat
Centre de Recherche sur les Matériaux Renouvelables, Université Laval, Ville de Québec, QC G1V 0A6, Canada, wassim.kharrat.1@ulaval.ca

Ahmed Koubaa
Institut de Recherche sur les Forêts, Université du Québec en Abitibi-Témiscamingue, Rouyn-Noranda, QC J9X 5E4, Canada, ahmed.koubaa@uqat.ca

Mohamed Khlif
École Nationale d'Ingénieurs de Sfax, Université de Sfax, Sfax, Tunisia, khlifmohamed@yahoo.fr

Chedly Bradai
École Nationale d'Ingénieurs de Sfax, Université de Sfax, Sfax, Tunisia, chedly.bradai.enis@gmail.com

‡ *This manuscript is a short version of a published manuscript in Forests: https://doi.org/10.3390/f10070569*

Abstract

Ultrasonic measurement is a widely used approach for the nondestructive determination of wood elastic properties, including the dynamic modulus of elasticity (DMOE). The latter is calculated from wood density and ultrasonic wave propagation velocity. Using the average wood density to estimate the DMOE introduces significant imprecision considering the important variation of this property. For accurate DMOE evaluation, we developed a device to measure the ultrasonic wave velocity in wood with the same resolution as the X-ray densitometer for density measurement. Data from the X-ray densitometry and the ultrasonic device determined the radial and the within-ring wood density and DMOE variations. High-order polynomials modeled the within-ring wood density and DMOE variations for black spruce and jack pine. Predicted and measured wood density and DMOE data were highly correlated. The earlywood (EW) to latewood (LW) transition, defined as the inflection point, was determined to compute EW and LW width, density, and DMOE data. High correlations between ring, EW, and LW densities and DMOE are found. The practical implications of the results are discussed, namely the ease of determination of the EW and LW elastic properties, the evaluation of the impact of several forest management practices on the wood mechanical properties, and a better understanding of their variations.

Keywords: ultrasonic wave velocity; nondestructive assessment; wood density; dynamic modulus of elasticity; within-ring variation.

Introduction

Wood quality is the result of physical and chemical characteristics a tree possesses that enable it to meet the property requirements for different end products" (Mitchell 1961). Wood density is considered to be the most important wood quality attribute. It is one of the most widely used parameters to predict the wood's mechanical and physical properties (Koubaa et al. 2002). However, wood quality attributes are

highly variable due to within tree, tree-to-tree, site variations, and genetic, environmental, and physiological factors (Panshin and de Zeeuw 1980). In the same species, variations in wood density also result from variations in anatomical characteristics such as earlywood and latewood width. Wood density, defined as the ratio of the wood mass to volume, is expressed in kilograms per cubic meter (kg/m3). This definition does not consider variations due to biological processes such as earlywood and latewood formation, juvenile wood formation, or environmental conditions. Modern nondestructive measurement methods such as X-ray densitometry are widely used to assess the effect of this variation on wood density and growth.

Within ring wood density profiles, obtained with X-ray densitometry, generally provide ring density (RD), earlywood density (EWD), latewood density (LWD), ring width (RW), and earlywood width (EWW), and latewood width (LWW). These parameters have been determined for many wood species, such as European oak (Zhang et al. 1994), black spruce (Koubaa et al. 2002), and Thuja occidentalis (Bouslimi et al. 2014). Within wood, density profiles are used to determine the use-specific suitability of wood, especially for high value-added applications (Zhang et al. 1994, Zobel and Van Buijtenen 1989). Intra-ring wood density variation can also indicate wood uniformity and provide information about the wood growth process and the wood fiber yield (Zobel and Van Buijtenen 1989, Pernestal et al.1995).

Earlywood and latewood properties depend on the earlywood–latewood transition point (E/L). Several methods have been reported in the literature to determine the E/L, notably Mork's index (Mork 1928). Pernestål et al. (1995) and Ivkovic and Rosenberg (2004) used modified spline functions to model within ring wood density profiles. The E/L transition was defined using a numerical derivative method. Koubaa et al. (2002) demonstrated that high-order polynomial functions consider both profiles and within ring density variation for E/L estimation. These functions gave consistent estimates of the E/L transition point, with correlation coefficients between measured and predicted density well above 0.90 for the 6th order polynomial. These results are significant because modeled within ring wood density profiles can simplify the modeling of final wood product properties (Ivkovic and Rosenberg 2004). Although wood density is considered the most important wood quality attribute, elastic properties are important, especially for engineering design (Bucur and Archer 1984). The wood DMOE, an elastic constant describing wood mechanical behavior, is computed from the wood density and the ultrasonic wave velocity (Hassan et al., 2013). Ultrasonic wave velocity measurement is one of the most widely used nondestructive methods to assess the strength properties of living trees, logs, sawn timbers, and wood-based materials due to its rapidity, flexibility, portability, cost-effectiveness, and ease of use (Najafi et al. 2005, Brashaw et al. 2009, Chiu et al. 2013, Proto et al. 2017). Wood DMOE has been determined using ultrasonic wave velocity parallel to the grain direction and wood density based on the mass-to-volume ratio of specimens (Hassan et al., 2013, Chiu et al., 2013, Proto et al., 2017, Horáček and Tippner, 2012). However, no study has investigated ring wood DMOE profiles to determine variations between earlywood and latewood DMOE. A nondestructive method based on X-ray densitometry and ultrasonic wave velocity measurements was proposed to determine within ring wood DMOE profiles.

This study aims to develop a nondestructive method to determine within ring wood DMOE profiles; model within ring wood density and DMOE profiles in black spruce and jack pine wood using high-order polynomial functions (Koubaa et al. 2002), and analyze correlations between wood density, and DMOE.

Materials and Methods

Materials

The experimental material used in this study consisted of subsamples from previous studies on the wood quality of jack pine (Park et al. 2009) and black spruce (Ourais 2012) sampled from even-aged stands in

the Abitibi region, Québec, Canada. Discs were sampled from eight black spruce and eight jack pine trees at breast height. Bark-to-bark samples passing through the pith were extracted from each disc from were sawn to extract thin strips (15 to 20 mm wide and 1.57 to 1.9 mm thick). The strips were extracted with cyclohexane/ethanol (2:1) solution for 24 hours and then with distilled water for another 24 hours to remove extractives (Grabner et al. 2005). Then, the strips were air-dried under pressure to prevent warping. Samples were then conditioned to 8% equilibrium moisture content before wood density and ultrasonic wave propagation time measurements.

Wood Ring Density and Width Measurements

A QTRS-01X Tree-Ring Scanner (Quintek Measurement Systems, Knoxville, TN, USA) measured the density (RD) and width (RW) for each ring using from pith to bark. The QTRS passes thin strips from increment cores through an accurately collimated soft X-ray beam using a precisely controlled stepping system and linear bearing carriage at a 40 μm resolution. Rings from pith to bark were scanned in air-dry conditions.

Wood Ultrasonic Wave Velocity Measurement

An in-house device measured the ultrasonic wave propagation time with a resolution of 40 μm, the same as that used in X-ray densitometry experiments. The device consists of a motorized linear translation stage that holds the sample and is controlled by a microcontroller. The wood sample's ultrasonic wave propagation time is measured between a parallel ultrasonic transmitter (Spot Weld Transducer) and a receiver transducer (Fingertip Contact Transducer CF).

The ultrasonic wave propagation time was measured on samples using a Masterscan 380 (Sonatest Inc., Texas) equipped with 10 MHz frequency transducers. Ultrasonic waves were applied to the samples through two transducers (transmitting and receiving). A coupling agent, petroleum jelly, served to aid the transmission of the transducer pulses into the test samples.

A correction factor (C_f; s) was applied to calculate the ultrasonic wave velocity in the wood samples to consider the transport time of the electric waves within the measuring circuit. A Plexiglas sample having the same thickness as the wood samples (2 mm) was used as a reference to determine the correction factor (Hernández et al. 1998). The DMOE (in MPa) was determined according to equation 1

$$\mathrm{DMOE} = \rho \times V^2 \times 10^{-6} \quad (1)$$

where ρ is the wood density measured by X-ray densitometry [kg/m^3], and V is the ultrasonic wave velocity.

Modeling Within ring Wood and DMOE Profiles and Statistical Analysis

Matlab software (R2016a, The MathWorks, Inc.) determined the within-ring wood density and DMOE profiles at 40 μm resolution. Sixth order polynomial functions modeled the within ring wood density and DMOE profiles for black spruce and jack pine. The E/L transition, defined as the inflection point obtained from the within-ring density and DMOE profiles, is obtained by equalling the second derivative of the polynomial function to zero according to the method described by Koubaa et al. (2002).

Correlation analysis between measured traits was conducted using R software (Version 2.15.0 R, R Development Core Team, 2012) for black spruce and jack pine.

Results and Discussion

Radial and within ring Profiles of Wood Density and Dynamic Modulus of Elasticity

Figure 1 shows the typical radial and within ring density and DMOE profiles for jack pine. Figure 2 shows the similar patterns of within-ring density and DMOE variations for black spruce and jack pine. Wood density and DMOE increase slowly in earlywood to reach a maximum in latewood. Both properties decrease at about mid-latewood width to reach a minimum at the boundary between two growth rings. Even at the ring level, the similarity between within-ring density and DMOE profiles confirms the close relationship between wood density and stiffness.

(**a**)

(**b**)

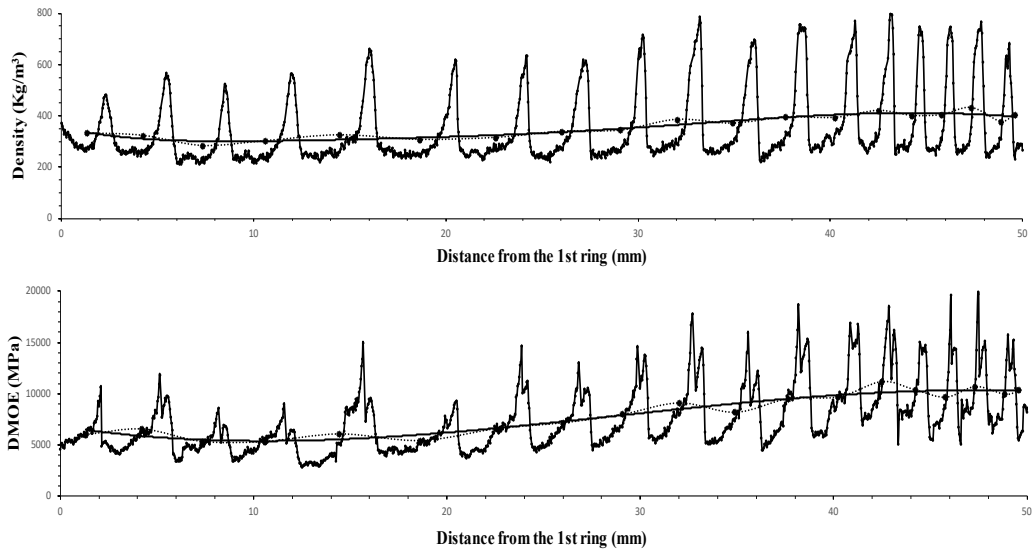

Figure 1. Examples of jack pine profiles showing radial variation in (a) wood density and (b) DMOE in (from ring 2 to 19).

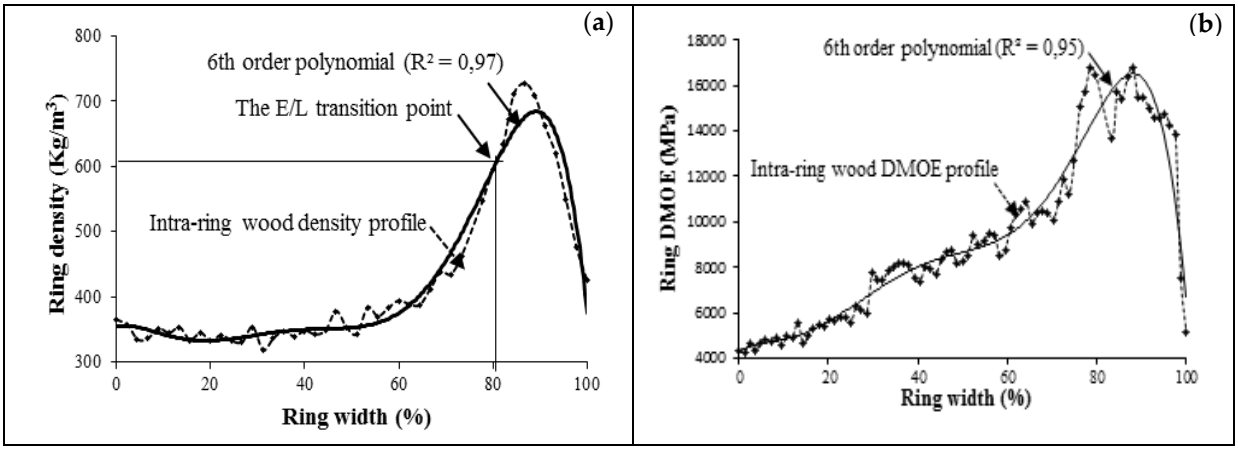

Figure 2. Examples of within-ring profiles and the fits obtained with the 6th order polynomials for (a) ring density in jack pine and (b) DMOE in Jack pine.

The modeling approach suggested by Koubaa et al. (2002) modeled the DMOE profiles of the black spruce and jack pine samples (Figure 2). The correlation coefficients obtained between the measured and predicted ring density data range from 0.88 to 1.00 (Table 1). In agreement with previous findings (Koubaa et al. 2002), these results indicate that the 6th order polynomial models can well describe the within ring density variation for black spruce and jack pine. Table 1 also indicates that high-order polynomials fit the within ring DMOE profiles for black spruce and jack pine well. The correlation coefficients between measured and predicted DMOE data ranged from 0.80 to 0.99 (Table 1). These results indicate that high-order polynomials can describe DMOE profiles for the 2 species well.

The Earlywood–Latewood Transition

Table 2 shows that E/L transition density is highly variable, as indicated by the large standard errors (Table 2). The E/L transition density of the 10th annual ring from the pith varied from 541 to 655 kg/m^3 and from 548 to 672 kg/m^3 in black spruce and jack pine, respectively (Table 2). These results agree with previous findings for black spruce (Koubaa et al. 2005) and jack pine (Park et al. 2009).

The E/L transition density defined by the inflexion point method is variable and higher than the threshold density for jack pine. Thus, the earlywood and latewood width and density defined by the inflexion point method will differ from those defined by the threshold method. Earlywood width, defined by the inflexion point method, will be greater, whereas latewood width will be smaller. Consequently, the latewood proportion defined by the inflexion point method will be lower. These results are in good agreement with Koubaa et al. (2002). The same method determined the DMOE of the ring, earlywood, latewood, and E/L transition. The E/L transition DMOE was highly variable. For example, at the 10th annual ring, the DMOE ranged from 9261 to 15798 MPa for black spruce and 11162 to 15950 MPa for jack pine (Table 2).

Table 1. Average, standard variation (between parenthesis) and range of Pearson's coefficient of determination between measured and predicted within-ring density and dynamic modulus of elasticity values from the 6th order polynomial models for different rings for black spruce and jack pine

	Ring from pith			
	5	10	15	20
	Wood density profiles			
	Black spruce			
Average profiles	0.96 (0.02)	0.97 (0.02)	0.96 (0.02)	0.97(0.02)
Range	0.88-0.99	0.91-0.99	0.91-0.99	0.92-1.00
	Jack pine			
Average profiles	0.96 (0.02)	0.95 (0.02)	0.97 (0.02)	0.98 (0.01)
Range	0.92-0.98	0.90-1.00	0.89-0.99	0.96-0.99
	Dynamic modulus of elasticity profiles			
	Black spruce			
Average profiles	0.92 (0.03)	0.94 (0.04)	0.95 (0.03)	0.95 (0.02)
Range	0.82-0.99	0.88-0.99	0.86-0.99	0.91-0.99
	Jack pine			
Average profiles	0.89 (0.04)	0.93 (0.02)	0.93 (0.03)	0.94 (0.02)
Range	0.80-0.97	0.88-0.98	0.82-0.99	0.91-0.99

Table 2. Average (Av), range (Ra), and standard variation for wood density, and wood DMOE at the earlywood–latewood transition as defined by the inflexion method for different rings.

	Black Spruce			Jack pine		
	Ring number from the pith					
	5	10	20	5	10	20
	Density at the earlywood latewood transition					
Av (kg/m^3)	580 (33)	596 (20)	600 (29)	520 (49)	612 (49)	614 (48)
Ra (kg/m^3)	536-653	541-655	547-649	433-623	548-672	482-674
	Dynamic modulus of elasticity at the earlywood latewood transition					
Av (MPa)	13404 (2111)	13623 (1945)	15388 (1862)	9752 (1413)	12883 (1174)	14950 (1858)
Ra (MPa)	10437-17650	9261-15798	13075-18448	6431-12193	11162-15950	11238-17061

Relationships between Density and DMOE

RD is positively correlated to earlywood (EWD) and latewood density (LWD) (Table 3). For both species, the correlation coefficients between RD and EWD are higher than between RD and LWD. These results agree with previous findings for black spruce (Koubaa et al., 2000). Similarly, the correlations between ring DMOE and earlywood DMOE are higher than those between ring DMOE and latewood DMOE in both species. High positive relationships were found between ring DMOE and earlywood and latewood DMOE for both species (Table 3).

Table 3. Pearson's coefficient of correlations (r) between the different traits for black spruce (upper row) and jack pine (lower row).

	RD	EWD	LWD	RDMOE	EWDMOE	LWDMOE
RD		0.91***	0.37*	0.45**	0.44**	0.33*
EWD	0.85***		0.11 ns	0.4**	0.46**	0.18 ns
LWD	0.75***	0.48**		0.18 ns	0.09 ns	0.49**
RDMOE	0.79***	0.65**	0.66***		0.98***	0.85***
EWDMOE	0.73***	0.65**	0.57**	0.98***		0.75***
LWDMOE	0.74**	0.54**	0.80***	0.89***	0.78***	

* Significant at $\alpha = 0.05$; ** Significant at $\alpha = 0.01$; *** Significant at $\alpha = 0.001$; ns not significant. RD: ring density, EWD: earlywood density,. LWD: latewood density, RDMOE: ring dynamic modulus of elasticity, EWDMOE: earlywood dynamic modulus of elasticity, LWDMOE: latewood dynamic modulus of elasticity.

Practical implications

A rapid, nondestructive method determined the density of wood and DMOE based on X-ray densitometry and ultrasonic wave velocity measurements. This method enabled the experimental determination of earlywood and latewood elastic behavior. The available studies on the earlywood and latewood elastic properties used fastidious experimental procedures (Jeong et al. 2009, Roszyk et al. 2016, Cramer et al. 2005, Moliński et al. 2014, Mott et al. 2002, Vehniäinen 2008, Jeong and Hindman 2010). This method offers the possibility of rapid investigation of the multiscale variation of the wood elastic properties from the ring to the stand. It will be highly useful in studying the impact of intensive forest management practices on the wood's mechanical properties.

The impact of intensive forest management on wood mechanical properties has received little attention due to sample size constraints, the destructive nature of assessment methods, and the lack of effective tools for rapid, nondestructive characterization of these properties at the ring level. Nondestructive

assessment is essential for understanding the impact of intensive forest management practices on wood mechanical properties and the physiological and biological processes involved in wood strength development (Russo et al., 2019). Enhanced growth through intensive forest management can significantly diminish the wood's mechanical properties due to several biological factors, including increased earlywood proportion and the production of larger cells with thinner walls. Several anatomical and physical characterization studies have demonstrated the impact of intensive forest management strategies on earlywood, latewood, and overall wood properties (Jeong and Hindman 2010). The developed method allows nondestructive measurement of within ring wood DMOE and provides deeper insights into wood strength development and its relationship to wood density. This relationship is critical for effective forest management strategies (Proto et al., 2017, Russo et al., 2019).

The developed method will be very helpful in understanding the rupture mechanism in wood. Understanding mechanical properties variations at the earlywood-latewood scale will eventually allow a better knowledge of wood's areas of weakness to optimize the in-service performance of wood products and the mechanical wood processing such as pulping and oriented strand board (OSB) manufacturing.

Conclusions

A nondestructive method based on X-ray densitometry and ultrasonic wave velocity measurement provided radial and within ring profiles of wood density and dynamic modulus of elasticity jack pine and black spruce. Sixth order polynomials models described the within ring profiles and served to define the earlywood–latewood transition density and DMOE in both species. This study examined the correlation coefficients between the ring, EW, LW density, and wood DMOE. Positive correlations are found between wood density and DMOE at the ring, earlywood, and latewood.

Acknowledgments

The authors thank the Canada Research Chair Program, the NSERC-UQAT-UQAM Industrial Chair in Sustainable Forest Management, the MITACS Scholarship Program, and the Canadian Wood Fiber Center for funding. We are also grateful to Gilles Villeneuve and Williams Belhadef for their invaluable technical assistance. The authors also thank Besma Bouslimi and Zahia Ait-Si-Said for assistance with X-ray density measurements.

References

Bouslimi, B.; Koubaa, A.; Bergeron, Y. 2014. Anatomical properties in Thuja occidentalis: Variation and relationship to biological processes. International Association of Wood Anatomists Journal. 35(4), 363-384.

Brashaw, B.K.; Bucur, V.; Divos, F.; Gonçalves, R.; Lu, J.; Meder, R.; Pellerin, R.F.; Potter, S.; Ross, R.J.; Wang, X.; Yin,Y. 2009. Nondestructive testing and evaluation of wood: A Worldwide Research Update. Forest products journal. 59(3), 7-14.

Bucur, V.; Archer, R.R. 1984. Elastic constants for wood by an ultrasonic method. Wood Science and Technology. 18, 255–265.

Chiu, C.M.; Lin, C.H.; Yang, T.H. 2013. Application of nondestructive methods to evaluate mechanical properties of 32-Year Old Taiwan Incense Cedar (Calocedrus formosana) wood. BioResources. 8(1), 688-700.

Cramer, S.; Kretschmann, D.; Lakes, R.; Schmidt, T. 2005. Earlywood and latewood elastic properties in loblolly pine. Holzforschung. 59(5), 531–538.

Grabner, M.;Wimmer, R.; Gierlinger, N.; Evans, R.; Downes, G. 2005. Heartwood extractives in larch and effects on X-ray densitometry. Canadian Journal of Forest Research. 35(12), 2781-2786.

Hassan, K.T.; Horacek, P.; Tippner, J. 2013. Evaluation of stiffness and strength of Scots Pine wood using resonance frequency and ultrasonic techniques. BioResources. 8(2), 1634-1645.

Hernández, R.; Koubaa, A.; Beaudoin, M.; Fortin, Y. 1998. Selected mechanical properties of fast-growing poplar hybrid clones. Wood and Fiber Science. 30(2), 138-147.

Horáček, P.; Tippner, J. 2012, Nondestructive evaluation of static bending properties of Scots Pine wood using stress wave technique. Wood Research. 57(3), 359-366.

Ivkovic, M.; Rosenberg, P. 2004. A method for describing and modeling of within-ring wood density distribution in clones of three coniferous species. Annals of forest science. 61(8), 759-769.

Jeong, G.Y.; Hindman, D.P. 2010. Modeling differently oriented loblly pine strands incorporating variating intraring properties using a stochastic finite element method. Wood and Fiber Science. 42(1), 51-61.

Jeong, G.Y.; Zink-Sharp, A.; Hindman, D.P. 2009. Tensile properties of earlywood and latewood from loblolly pine (Pinus taeda) using digital image correlation. Wood and Fiber Science. 41(1), 51–63.

Koubaa, A.; Isabel, N.; Zhang, S.Y.; Beaulieu, J.; Bousquet, J. 2005. Transition from juvenile to mature wood in black spruce (Picea Mariana (Mill.) B.S.P.). Wood and Fiber Science. 37(3), 445-455.

Koubaa, A.; Tony Zhang, S.Y.; Makni, S. 2002. Defining the transition from earlywood to latewood in black spruce based on intra-ring wood density profiles from X-ray densitometry. Annals of forest science. 59(5-6): 511-518.

Koubaa, A.; Zhang, S.Y.; Isabel, N.; Beaulieu, J.; Bousquet, J. 2000. Phenotypic correlations between juvenile mature wood density and growth in black spruce. Wood and Fiber Science. 32(1), 61-71.

Mitchell, H. A.1961. Concept of Intrinsic Wood Quality and Nondestructive Methods for Determining Quality in Standing Timber, Forest Service, U.S. Report No 2233, Forest Products Laboratory: Madison, WI, USA.

Moliński, W.; Roszyk, E.; Puszyński, J. 2014. Variation in mechanical properties within individual annual ring of the resonance spruce wood [Picea abies (L.) Karst]. Drvna Industrija. 65(3), 215–223.

Mork, E. 1928. Die qualität des fichtenholzes unterbesonderer rücksichtnahme auf schleif-und papierholz. Papier-Fabrikant, 26, 741-747.

Mott, L.; Groom, L.; Shaler, S. 2002. Mechanical properties of individual southern pine fibers. Part II. Comparison of earlywood and latewood fibers with respect to tree height and juvenility. Wood and Fiber Science. 34(2), 221–237.

Najafi, S.K.; Bucur, V.; Ebrahimi, G. 2005. Elastic constants of particleboard with ultrasonic technique. Materials Letters. 59(16), 2039-2042.

Ourais, M. 2012. Variations intra-arbres de la largeur du cerne, de la masse volumique du bois et des propriétés morphologiques des trachéides de l'épinette noire (Picea Mariana (MILL.) B.S.P) avant et après traitements sylvicoles. Rouyn-Noranda, QC, Université du Québec en Abitibi-Témiscamingue. 85 p. M.S. thesis.

Panshin, A.J.; De Zeeuw, C. 1980. Textbook of Wood Technology. McGraw-Hill Book Co. New York, NY. p. 772.

Park, Y.I.D.; Koubaa, A.; Brais, S.; Mazerolle, M.J. 2009. Effects of cambial age and stem height on wood density and growth of jack pine grown in boreal stands. Wood and Fiber Science. 41(4), 346-358.

Pernestal, K.; Jonsson, B.; Larsson, B. 1995. A simple model for density of annual rings. Wood Science and Technology. 29, 441-449.

Proto, A.R.; Macri, G.; Bernardini, V.; Russo, D.; Zimbalatti, G. 2017. Acoustic evaluation of wood quality with a non destructive method in standing trees: A first survey in Italy. Forests, 10, 700-706.

Roszyk, E.; Molinski, W.; Kaminski, M. 2016. Tensile properties along the grains of earlywood and latewood of Scots pine (Pinus Sylvestris L.) in dry and wet state. BioResources. 11(2), 3027–3037.

Russo, D.; Marziliano, P.A.; Macri, G.; Proto, A.R.; Zimbalatti, G.; Lambardi, F. 2019. Does Thinning Intensity Affect Wood Quality? An Analysis of Calabrian Pine in Southern Italy Using a Nondestructive Acoustic Method. Forests.10(4), 303: 1-16.

Vehniäinen, A. 2008. Single Fiber Properties: A Key to the Characteristic Defibration Patterns from wood to Paper Fibers. Helsinki, Finland: Helsinki University of Technology. Ph.D. Thesis.

Zhang, S.Y.; Nepveu, G.; Owoundi, R.E. 1994. Intratree and intertree variation in selected wood quality

Zobel, B.J.; Van Buijtenen, J.P. 1989. Wood Variation: Its Causes and Control. Berlin, Germany: Springer: p. 363.

Session 2

In-Forest Wood Quality Assessments

Using Time-of-Flight Acoustic Velocity to Assess the Modulus of Elasticity and Bending Strength Properties of White Spruce from Tree Improvement Experiments

Iman Rashidi-Jouybari
Département des sciences du bois et de la forêt, Centre de recherche sur les matériaux renouvelables, Université Laval, Québec, QC, G1V 0A6, Canada, Iman.rashidijouybari.1@ulaval.ca

Alexis Achim
Département des sciences du bois et de la forêt, Centre de recherche sur les matériaux renouvelables, Université Laval, Québec, QC, G1V 0A6, Canada, alexis.achim@sbf.ulaval.ca

Patrick Lenz
Canada Research Chair in Forest Genomics, Forest Research Centre, Qc, Quebec, Canada, patrick.lenz@nrcan-rncan.gc.ca

Jean Beaulieu
Département des sciences du bois et de la forêt, Centre de recherche sur les matériaux renouvelables, Université Laval, Québec, QC, G1V 0A6, Canada, jean.beaulieu@sbf.ulaval.ca

Jean Bousquet
Département des sciences du bois et de la forêt, Centre de recherche sur les matériaux renouvelables, Université Laval, Québec, QC, G1V 0A6, Canada, Jean.Bousquet@sbf.ulaval.ca

Abstract

Although acoustic tools are commonly used to estimate wood stiffness (MOE) in standing trees, the derived relationships vary in accuracy. In this study, we aimed to investigate the efficiency of acoustic velocity to predict the mean individual and family-level values of MOE in white spruce (*Picea glauca* [Moench] Voss) from a 21-year-old tree improvement trial consisting of two sites. A total of 190 white spruce trees were targeted from two different genetic improvement plantations established in Quebec, Canada. Standing tree acoustic velocity was assessed using the ST300 tool, which measures the time-of-flight of a longitudinal stress wave between two probes inserted in the tree stem. Dynamic stiffness (MOE_d) was calculated using two different estimates of density (i.e., a constant for green wood density (MOE_{dGD}) and a measure density at 8% relative humidity (MOE_{dRH}). From each tree, two samples of 2.5*2.5*40.60 cm were collected at breast height (1.3 m) to measure static bending stiffness (MOE_s). In the Normandin site, compared to the site Valcartier, Moderate levels of correlation (R^2 = 0.34 to 0.42) between MOE_{dGD}, MOE_{dRH} and MOE_s were obtained at the individual tree level plantation, while stronger levels of correlation (R^2 = 0.57 to 0.60) were obtained at the family level. Results showed that MOE_d calculated based on density at 8% relative humidity (RH) allowed a better prediction of stiffness at both sites. Further, the Pearson correlation matrix also revealed strong correlations between MOE_s and MOE_{dRH} of r= 0.65 and r=0.77 at the individual tree and family levels, respectively. Values of MOE_d estimated at 8% RH were in good agreement with static MOE values measured on solid wood samples, and had lower bias compared with MOE_d estimates based on a constant green wood density. Results also show that predicting bending strength properties at the family level is more accurate that making

predictions at the individual level. This method confirms that MOE_{dRH} corresponds 57-60% to the static MOE, while it is easily obtainable at very low cost can potentially be used to in tree improvement programs in which MOE is a trait of interest.

Keywords: Modulus of elasticity (MOE), Non-destructive (NDE), Prediction, Standing tree measurement, green wood density.

Introduction

White spruce (Picea glauca [Moench] Voss) is a prominent component of boreal conifer forests in North America. It has a large natural range spreading from Newfoundland to Alaska. It can be described as a boreal and sub-boreal species with a high life expectancy, low mortality and relatively high shade tolerance, with an ability to disperse huge crops of seed on a periodic basis (Gärtner et al. 2011). In addition to its ecological importance, white spruce is one of the species that feeds commercial wood production from Canada's boreal forest, as well as a value chain dedicated to products such as pulp and paper and dimension lumber (Zhang and Koubaa 2008, Lenz et al. 2013, Mvolo et al. 2019). White spruce plantation has been a key part of Canadian forest management efforts since the 1950s (Stiell 1976), and to date, significant resources have been devoted to improving tree plantation initiatives in order to increase seedling stock (Pelletier and Pitt 2008). However, the wood quality of the planted trees at harvest remains uncertain (Krajnc et al. 2019). To promote suitable wood properties for specific applications such as structural construction materials, knowledge of wood physical and mechanical qualities must be acquired and implemented into tree breeding programmes. Destructive, semi-destructive, and nondestructive measuring techniques can be used for this purpose (Ettelaei et al. 2019).

The modulus of elasticity (MOE), which is a component of the stiffness of the material within the elastic deformation range, or the modulus of rupture (MOR), a component of strength of the material based on maximum force loaded, are the key mechanical properties used by engineers and architects to determine end-use applications (Green et al. 1999). Modulus of elasticity (MOE), which is a component of the stiffness of the material within the elastic deformation range, or modulus of rupture (MOR), a component of strength of the material based on maximum force loaded, are the key mechanical properties used by engineers and architects to determine end-use applications (Green et al. 1999). Both MOE and MOR values are driven by the intrinsic characteristics of wood such as microfibril angle (MFA), spiral grain, cell wall thickness, fiber length, latewood proportion, ring width, and density (Cave and Walker 1994, Alteyrac et al. 2006), all of which vary systematically among species and within tree stems both radially and longitudinally (Lachenbruch et al. 2011, Zobel and Van Buijtenen 2012). Wood density is often considered as a key indicator of timber performance for structural end-uses (Panshin and De Zeeuw 1964) due to its linear relationship with MOE (Bowyer et al. 2007). More recent assessments have highlighted the important contribution of MFA as this variable explained more than 70% of the variation in MOE in black spruce (*Picea mariana* (Mill.) B.S.P.) (Alteyrac et al. 2006). As a general trend in conifers, MOE increases from pith to bark (Xu and Walker 2004, Auty et al. 2016), and also tends to increase with height in tree for a given ring number from the pith (Xu and Walker 2004). Predious studies have reported that tree-scale characteristics can be used to predict tree-level MOE such as morphological properties (Lei et al. 2005, Lenz et al. 2013), or crown ratios (Kuprevicius et al. 2013) or growth rate (Psaltis et al. 2021). While merchantable logs are harvested from a variety of stand types, including natural forests, conventional plantations, and intensively managed plantations, with varying rotation ages, growth rates, and wood quality traits, there is a need to segregate trees and logs according to lumber quality for improved decision-making in the forest value chain.

Destructive testing methods are the commonly used to measure wood MOE and MOR, typically on single pieces of lumber. In addition to altering the properties of the specimen, such procedures can be costly and

time consuming (Tanasoiu et al. 2002). Nondestructive assessment techniques (NDT) can be used to determine the material's physical and mechanical qualities on standing trees and logs without causing any structural damage (Agrawal and Choudhari 2010). NDT has been extensively used in lumber grading in North America and around the world since the 1960s (Murphy and Cown 2015, Ross 2015). Many indirect and non-destructive methods have been developed to facilitate the evaluation of wood quality traits on standing and/or felled trees (Wessels et al. 2011, Wang et al. 2013, Vössing and Niederleithinger 2018). For instance, near infrared spectroscopic analyses for the prediction of wood chemical composition (Acquah et al. 2015) or the assessment of mechanical wood traits (Fundova et al. 2019, Fathi et al. 2020). Density estimations can also be obtained through Pilodyn pin penetration or drill resistance (Fundova et al. 2018, Vlad et al. 2018). Several studies have also reported reliable predictions of MOE using different NDT techniques (Galligan and McDonald 2000, Lenz et al. 2013). Notably, measures of the transit time of flight of sound waves between two piezoelectric sensors penetrating approximately one centimeter into standing trees, also known as Acoustic velocity (AV), provide dynamic estimates of the modulus of elasticity (MOE_d). This method is both rapid and easy to implement compared to traditional destructive mechanical testing methods but results are generally limited to the localized nature of stress-wave propagation (Fischer et al. 2015, Bucur 2017). Also, despite the fact that mechanical properties (i.e., static stiffness and strenght) of lumber pieces may be affected by the occurrence of knots, depending on their size and location (Panshin and De Zeeuw 1964, Bowyer et al. 2007), Chauhan and Walker (2006) reported that they have very little impact on dynamic stiffness obtained by acoustic velocity since the wave tends to take the fastest route around local defects (Chauhan and Walker 2006). Therefore, acoustic velocity measurement gives a mean estimate of MOE over the testing area in which the probes were used (Chauhan and Walker 2006).

Several studies have confirmed the positive relationship between acoustic measurements and wood stiffness on standing trees. For instance, moderate to strong relationships were reported in white spruce (62%) (Lenz et al. 2013), Norway spruce (Picea abies) (58-60%) (Chen et al. 2015), Douglas-fir (Pseudotsuga menziesii (Mirb.) Franco) (0.53) (Lachenbruch et al. 2010), loblolly pine (Pinus tuedu) (0.49) (Butler et al. 2017). In another study, Fathi et al. (2020) showed that wave velocity was highly sensitive to the moisture content and density of wood. Based on results obtained for different wood species, the application of acoustic velocity for the evaluation of mechanical wood properties opens opportunities to improve the efficiency of tree and log sorting for the production of valuable high stiffness structural lumber and veneer. (Ivković et al. 2009, Eckard et al. 2010, Wang et al. 2013).

Acoustic wave tools are being implemented operationally in various tree improvement programs, especially for fast growing coniferous species (Apiolaza 2009). However, due to the visco-elastic behavior and attenuation of wood, the correlation between dynamic MOE and static MOE are not yet fully understood (Beall 2002, Chauhan and Sethy 2016). Previous studies have also shown that some physical and mechanical properties of wood such as stiffness and density are strongly dependent on moisture content (MC) (Rohanová et al. 2010, Senalik et al. 2014, Montero et al. 2015). Yet, the effect of MC on acoustic velocity remain unclear (Sanabria et al. 2011), despite the fact that its influence has clearly been demonstrated.

With a view to facilitate the operational implementation of AV testing in genetic improvement programs, the current study was designed to address some of the knowledge gaps associated with to the effects of MC and wood density variation on field-based estimations of dynamic MOE. Standing tree acoustic velocity tools were used to evaluate the accuracy of dynamic MOE predictions in two 20-year-old white spruce genetic trials with contrasting stand densities. The specific objectives of the study were to: (i) understand the effect of density estimates obtained from green wood density or at 8% MC on the accuracy of static MOE predictions, (ii) evaluate the effect of plantation density on prediction accuracy.

Materials and methods

Experimental sites

The study site consisted of two polycross progeny trials of white spruce located in two different regions of Quebec, Canada. At the time of sampling, the mean stand age was 20 years old. The first site is located in Valcartier (site VaL, Lat. 46o 58′ N, Long. 71o 28′ W, Elev. 212 m, planted in 1996) in the sugar maple bass wood bioclimatic domain in the eastern part of Quebec and the second site is in Normandin (site NOR, Lat. 48o 50′ N, Long. 72o 31′ W, Elev. 122 m, planted in 1997) located in the balsam fir-yellow birch bioclimatic domain further to the North. The experiments were both laid out into a randomised complete block design with four blocks per site. Four single-tree plots per family were established as subblocks in an interlocking structure in each block to allow for systematic thinning (Libby and Cockerham, 1980). The distances between the planted seedlings were 1.5 m × 1.8 m and 2 m × 2 m at Valcartier and Normandin, respectively.

Sample preparation and testing

Sampling material

Thirty-eight polycross families were sampled for a total of 189 trees that were felled during a systematic thinning of the genetic trials. Mortality led to a slight variation in the number of trees per family and site that were available for the experiment. At both sites, diameter at breast height (DBH, measured 1.3 m from ground level), tree height and acoustic velocity (AV, assessed between 30 cm and 1.3 m from the ground) were measured at age 19, (i.e., measured in 2015 at Valcartier and in 2016 at Normandin). Increment cores were collected from the south facing side of trees at breast height for wood density and ring width (RW) measurements. For the destructive assessment of wood flexural properties, trees were felled, and two standardised samples were sawn from each tree in a stem section located just above breast height (Figure 1). A short log was collected above breast height (1.3 m), transported, and stored at Laval University's Renewable Materials Research Centre.

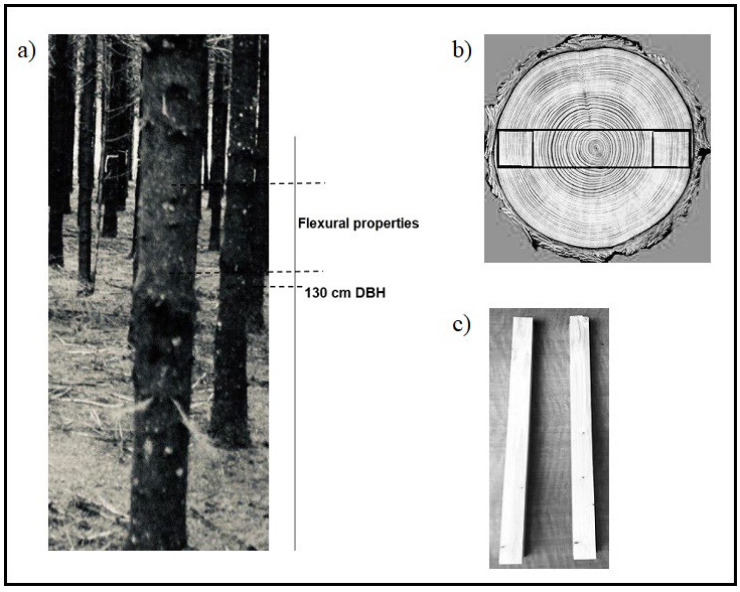

Figure 1—Sample preparation for wood flexural properties, including: where the samples were taken from tree stem (a), where the samples were taken radially (b), final samples (c)

Flexural properties

Specimens were prepared from both sides of a radial slab sawn in the north to south direction on the standing tree. On both sides, specimens were extracted as close to the bark as possible (Figure 1) and were prepared with final dimensions of 2.54 cm × 2.54 cm × 40.64 cm. They were then stored for two months in a conditioning chamber (60 percent relative humidity at 20 °C) until the moisture content stabilised.

Three-point loading was used to perform static bending tests in accordance with ASTM standard (ASTM 1997). Specimen supports were positioned 38.1 cm apart for a 15:1 span to depth ratio. The load was applied to the tangential–longitudinal face nearest to the pith at a speed of 2.5 mm/min. Static bending tests were performed on the specimens using an Instron universal testing machine with a 50 kN load cell. MOE values were calculated using equation 1:

$$MOE = \frac{l^3(F_{40\%} - F_{10\%})}{4bh^3(u_{40\%} - u_{10\%})} \quad (1)$$

where l is the span of supports, $F_{40\%}$ and $F_{10\%}$ are forces at the 40% and 10% level of the maximum force F_{max}, b is the width of the cross-section of sample and h is height of the sample, $u_{40\%}$ and $u_{10\%}$ are deflections at forces $F_{40\%}$ and $F_{10\%}$.

Wood density

A twin-blade pneumatic saw was used to cut the increment cores to a thickness of 1.68 mm. They were also Soxhlet extracted overnight with acetone and conditioned to an estimated moisture content of 8% before being analysed (Ukrainetz et al. 2008). Wood density profiles were determined by x-ray densitometry at a resolution of 25 μm with a QTRS-01X Tree Ring Analyzer (Quintek Measurement Systems Inc., Knoxvile, TN, USA). Tree ring boundaries were determined with the internal algorithm of the Quintek software. In the current study, area-weighted means of wood density and ring width were computed for each increment core.

Acoustic Velocity

Acoustic velocity (AV) was measured on standing trees at age 19 using the Hitman ST300 device (Fibregen, Christchurch, New Zealand) (Huang 2005). A hammer impact was used to create a mechanical stress wave in the lower probe inserted in the standing tree, which was then detected with a receiver in the top probe (Paradis et al. 2013). In the analysis, we used an average of 24 observations from each tree. The measurements were collected at each research site during a two-week period in June/July 2012 to minimise temperature and moisture content changes that could have altered the speed of sound waves passing through stems (Gao et al. 2013). The acoustic velocity recorded by the device was used to calculate the MOE_{dGD} and MOE_{dRH} according to equations 2 and 3:

$$MOE_{dGD} = \rho_{GD} V^2 \quad (2)$$

$$MOE_{dRH} = \rho_{RH} V^2 \quad (3)$$

where MOE_d is dynamic modulus of elasticity, ρ_{GD} is the estimated density of green wood (ρ_{GD} was considered to be constant at 1000 kg/m^3), ρ_{RH} is the density at 8% relative humidity obtained by Silviscan, and V is the acoustic velocity.

Statistical analyses and model development

All statical of analysis were conducted using the nlme library (Pinheiro et al. 2015) of the R statistical programming environment (Team 2013).

Results and discussion

From a total of 189 trees representing 38 polycross families tested on two experimental sites, two wood flexural measurements were obtained and an average per tree was used for further analyses. The final model-fitting datasets consisted of 265 samples from 143 trees at Valcartier and 81 samples from 46 trees at Normandin. Mean stand, and specimen characteristics as well as the mean distribution based on cambial age of static wood stiffness for both sites are summarised in Table 1 and Figure 2.

The mean values of dynamic stiffness for MOE_{dGD} and MOE_{dRH} varied from 9317 to 13678 MPa and from 3554 to 5312 MPa, respectively (Table 1). MOE_{dGD} were higher than those of MOE_s, while the opposite was true for MOE_{dRH} and MOE_s. This is attributable mainly to the density estimates that were used in equations 2 and 3. In reality, fresh-cut wood density should be used to estimate dynamic MOE. MOE_{dGD} and MOE_{dRH} should therefore be interpreted as indices of MOE_d rather than direct measurements. Overestimations of dynamic MOE calculated based on green wood density has also been reported in previous studies (Rohanová et al. 2010, Güntekin and Aydin 2016, Ettelaei et al. 2019). Authors attributed the overestimation of MOE based on green wood density to the fact that above the fiber saturation point (FSP), the additional free water in the cell lumen, cavities and porosity increases the weight of the material with little or no alteration to the the wood structure (Essien et al. 2018, Korkmaz and Büyüksarı 2019), while it affects sound propagation. According to Sandoz (1993), the MC influence is 8 times stronger below the FSP. Above the fibre saturation point, velocity reduces by less than 2% per unit increase in moisture content, whereas density grows exponentially per unit increase in moisture content (Essien et al. 2018). In another study by Chauhan and Sethy (2016), dynamic stiffness was 125% greater that MOE_s. Due to such overestimation, acoustic velocity methods have been recommended for pre-harvesting or screening of trees rather than attempting to obtain accurate estimates of MOE (Raymond et al. 2008). This recommendation is in line with the idea the MOE_d values reported in this study should be considered as indices of MOE.

Both MOE_d estimates, density, AV and tree height had higher values in Valcartier, while static wood stiffness and DBH were higher at Normandin. On average, MOEs was 6.13% higher at Normandin than Valcartier. The opposite trend was observed for height growth and wood density with values being 13.65% and 1.57% higher, respectively at Valcartier than Normandin. Trees in the Valcartier site were planted at a narrower spacing, resulting in higher height and density due to lower juvenile wood content (Alteyrac et al. 2006).

Table 1—Trait means and variation among 189 trees tested on two sites. Measured traits are whole tree dynamic MOE based on green wood density and density at 8%RH (MOE_{dGD} and MOE_{dRH}), static MOE (MOE_s), average wood density (Density), diameter at breast height (DBH), tree height (Height), acoustic velocity (AV), and average ring width (RW).

Trait	Units	Valcartier *(n= 143 trees)*			Normandin *(n= 46 trees)*		
		Age	Mean	SD	Age	Mean	SD
MOE_s	MPa	20	8492	1719.84	20	9013	1644.98
MOE_{dGD}	MPa	20	13678	2396.13	20	9317	2014.38
MOE_{dRH}	MPa	20	5312	1049.54	20	3554	800.05
Density	Kg/m^3	20	387.4	25.40	20	381.5	27.25
DBH	mm	19	113.5	20.4	19	135.9	27.2
Height	cm	19	957.2	136.7	19	842.4	175.2
AV	km/s	19	368.4	32.8	19	303.3	34.96

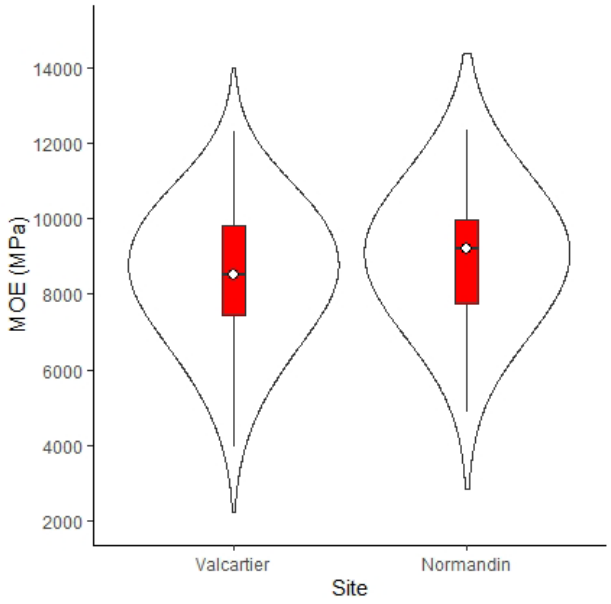

Figure 2 —Solid wood sample characteristics, mean distribution of MOE for both sites.

Relationships between static and dynamic MOE at the individual tree level

Single-variable linear regression models were built to correlate the static bending MOE values and NDT outputs MOE_{dGD} and MOE_{dRH} values for both sites. The regression parameters and relationship for each parameter are presented in Table 2 and Figure 3. The coefficients of determination (R^2) ranged from 0.14-0.42. The results are lower than those obtained in previous studies as Lenz et al. (2013) reported R^2 values of 24 and 53% for 15- and 32-year-old white spruce trees, respectively. Higher values were also reported in Norway spruce (58-60%) (Chen et al. 2015), Douglas fir (0.53) (Lachenbruch et al. 2010) and loblolly pine (0.49) (Butler et al. 2017). MOE_{dRH} gave better predictions of MOE_s at both sites. For both dynamic MOE estimates, R^2 values were higher at Normandin compared to Valcartier.

Table 2— Regression model outputs for predictions of static MOE at the family level using two dynamic MOEs

	Site	Intercept	Slope	R^2	p-value
MOE_{dGD}	Valcartier	4843^{***}	0.26^{***}	0.14	4×10^{-6}
MOE_{dRH}	Valcartier	5234.84^{***}	0.61^{***}	0.14	4×10^{-6}
MOE_{dGD}	Normandin	4578.94^{***}	0.48^{***}	0.34	2×10^{-5}
MOE_{dRH}	Normandin	4275.33^{***}	1.33^{***}	0.42	10^{-6}

Signifiant codes: '***', 0.001 '**', 0.01 '*', 0.05 '.', 0.1 ' ' 1.

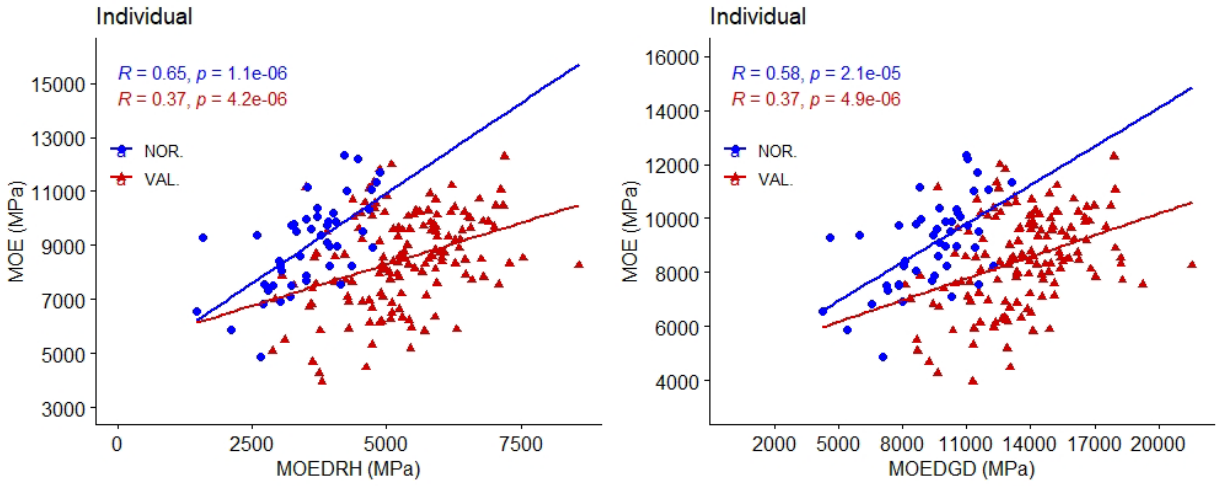

Figure 3 —Linear regression and relationship between MOE_s and both MOE_{dRH} and MOE_{dGD} at the level of individual trees

Relationship between static and dynamic MOE at the family level

Single-variable linear regression analyses for static bending MOE and dynamic MOE estimates at the family level are presented in Table 3 and Figure 4. Values of R^2 were in the range of 0.31-0.60, which are consistent with previous studies (Lachenbruch et al. 2010, Lenz et al. 2013, Chen et al. 2015, Butler et al. 2017). Lenz et al. (2011) reported that the variations explained by the fixed effects of similar models at the family level were between 27.6 and 29.3% and 64.7 and 66.0%, for 15- and 32-year-old white spruce, respectively. Similarly, to regressions at the individual tree level, MOE_{dRH} had the highest fit with static MOE values. This is in consistent with other studies, which reported that acoustic wave velocity had a lower correlation with MC above the fiber saturation point (MC > 30%), resulting in a gradual reduction in velocity beyond the FSP (Yang et al. 2015, Stewart et al. 2021). Again, better predictions of static MOE were obtained at Normandin than Valcartier. This indicates that the dynamic MOE estimation method employed in this work gave reasonably precise and dependable predictions of static MOE at the family level. It could therefore be used as a tool for selection in genetic improvement programs.

Table 3— Regression model outputs for predictions of static MOE at the tree level using two dynamic MOEs

	Site	Intercept	Slope	R^2	p-value
MOE_{dGD}	Valcartier	2062.48	0.46^{***}	0.31	3×10^{-4}
MOE_{dRH}	Valcartier	2137.35	1.19^{***}	0.36	7×10^{-5}
MOE_{dGD}	Normandin	2971.17^{*}	0.64^{***}	0.57	10^{-5}
MOE_{dRH}	Normandin	2855.40^{*}	1.71^{***}	0.60	5×10^{-6}

Signifiant codes: '***', 0.001 '**', 0.01 '*', 0.05 '.', 0.1 ' ' 1.

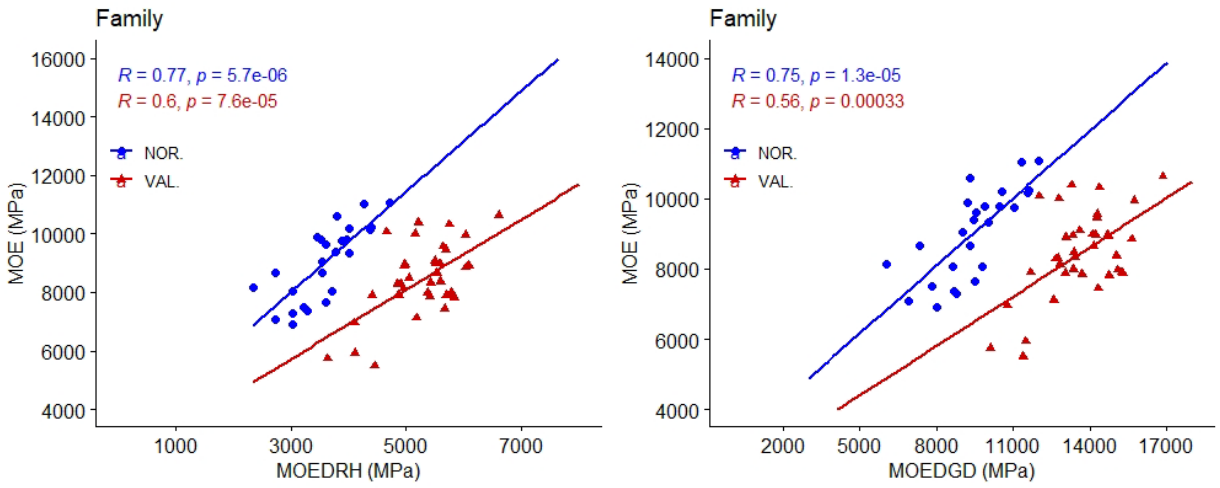

Figure 4—Linear regression and relationship of MOE_s to MOE_{dRH} and MOD_{dGD} at the family level

Conclusion

This study investigated the reliability of dynamic MOE estimated by commercial NDT techniques in predicting the static bending MOE value white spruce stands. Based on the results, we conclude that dynamic MOE obtained by acoustic tools can be used to predict static MOE. The highest coefficient of determination (R^2) was 60%. Furthermore, the dynamic MOE calculated based on density obtained at 8% RH, compared to the green wood density, can better predict the static MOE. We also found that stand density can negatively influence the output of acoustic velocity, as a result the dynamic MOE. In our case, site Normandin with lower stand density provided better prediction ability on static bending. Finally, our results suggest that predicting static MOE value with the given outputs, NDT tools have great potential to be implemented as an in-field quality control as well as for early selection purposes.

Acknowledgments

We thank Gaëtan Daoust, René Paquet, Daniel Plourde, the late Serge Légaré (Natural Resources Canada) and all staff of the Ministère des Forêts, de la Faune et des Parcs du Québec who participated in trial establishment and data collections over the years, in particular Martin Perron, André Rainville and Guildo Gagnon, as well as many collaborators and students. Thanks to Éric Dussault, Philippe Labrie, Marie Deslauriers, Esther Pouliot, Jean-François Légaré (Natural Resources Canada) and François Beaulieu (Canada Research Chair in Forest Genomics, Univ. Laval) for help with wood sampling and phenotypic assessments of test trees. We are grateful to staff at Laval University, including Benoît St-Pierre, Daniel Bourgault, Luc Germain for wood sample preparation according to the testing standards as well as Normand Paradis for their crucial help with the analyses of wood flexural properties. Our thanks to Sébastien Clément and Jason Miccocci (Natural Resources Canada) for help with databasing and statistical analyses of quantitative trait data.

Reference

Acquah, G. E., B. K. Via, O. O. Fasina and L. G. Eckhardt (2015). "Non-destructive prediction of the properties of forest biomass for chemical and bioenergy applications using near infrared spectroscopy." Journal of Near Infrared Spectroscopy **23**(2): 93-102.

Agrawal, G. and N. Choudhari (2010). "Non-destructive testing of wood using ultrasonic Technique." International Journal of Signal and Imaging Systems Engineering **3**(3): 195-207.

Alteyrac, J., A. Cloutier, C.-H. Ung and S. Zhang (2006). "Mechanical properties in relation to selected wood characteristics of black spruce." Wood and Fiber Science **38**(2): 229-237.

Alteyrac, J., A. Cloutier and S. Zhang (2006). "Characterization of juvenile wood to mature wood transition age in black spruce (Picea mariana (Mill.) BSP) at different stand densities and sampling heights." Wood Science and Technology **40**(2): 124-138.

Apiolaza, L. A. (2009). "Very early selection for solid wood quality: screening for early winners." Annals of Forest Science **66**(6): 1-10.

ASTM (1997). " American Society For Testing and Materials–ASTM. Annual book of ASTM standards." Denver's, (D143-94-Standard methods of testing small, clear specimens of timber). Philadelphia: ASTM: 23–53.

Auty, D., A. Achim, E. Macdonald, A. D. Cameron and B. A. Gardiner (2016). "Models for predicting clearwood mechanical properties of Scots pine." Forest Science **62**(4): 403-413.

Beall, F. (2002). "Overview of the use of ultrasonic technologies in research on wood properties." Wood science and Technology **36**(3): 197-212.

Bowyer, J., R. Shmulsky and J. Haygreen (2007). Forest products and wood science–an introduction. 131-134, Blackwell Publishing, Ames, Iowa, USA.

Bucur, V. (2017). Acoustics of wood, CRC press.

Butler, M. A., J. Dahlen, T. L. Eberhardt, C. Montes, F. Antony and R. F. Daniels (2017). "Acoustic evaluation of loblolly pine tree-and lumber-length logs allows for segregation of lumber modulus of elasticity, not for modulus of rupture." Annals of forest science **74**(1): 1-15.

Cave, I. and J. Walker (1994). "Stiffness of wood in fast-grown plantation softwoods: the influence of microfibril angle." Forest products journal **44**(5): 43.

Chauhan, S. and A. Sethy (2016). "Differences in dynamic modulus of elasticity determined by three vibration methods and their relationship with static modulus of elasticity." Maderas. Ciencia y tecnología **18**(2): 373-382.

Chauhan, S. and J. Walker (2006). "Variations in acoustic velocity and density with age, and their interrelationships in radiata pine." Forest Ecology and Management **229**(1-3): 388-394.

Chen, Z.-Q., B. Karlsson, S.-O. Lundqvist, M. R. García Gil, L. Olsson and H. X. Wu (2015). "Estimating solid wood properties using Pilodyn and acoustic velocity on standing trees of Norway spruce." Annals of Forest Science **72**(4): 499-508.

Eckard, J. T., F. Isik, B. Bullock, B. Li and M. Gumpertz (2010). "Selection efficiency for solid wood traits in Pinus taeda using time-of-flight acoustic and micro-drill resistance methods." Forest Science **56**(3): 233-241.

Essien, C., B. K. Via, Q. Cheng, T. Gallagher, T. McDonald and L. Eckhardt (2018). "Determining the predictive accuracy of whole tree modulus of elasticity (MOE) of 14-year-old loblolly pine using density and dynamic MOEs estimated by three different acoustic tools." European Journal of Wood and Wood Products **76**(5): 1535-1546.

Essien, C., B. K. Via, T. Gallagher, T. McDonald and L. Eckhardt (2018). "Distance error for determining the acoustic velocity of standing tree using tree morphological, physical and anatomical properties." Journal of the Indian Academy of Wood Science **15**(1): 52-60.

Ettelaei, A., M. Layeghi, H. Z. Hosseinabadi and G. Ebrahimi (2019). "Prediction of modulus of elasticity of poplar wood using ultrasonic technique by applying empirical correction factors." Measurement **135**: 392-399.

Fathi, H., V. Nasir and S. Kazemirad (2020). "Prediction of the mechanical properties of wood using guided wave propagation and machine learning." Construction and Building Materials **262**: 120848.

Fischer, C., G. I. Vestøl, A. Øvrum and O. A. Høibø (2015). "Pre-sorting of Norway spruce structural timber using acoustic measurements combined with site-, tree-and log characteristics." European Journal of Wood and Wood Products **73**(6): 819-828.

Fundova, I., T. Funda and H. X. Wu (2018). "Non-destructive wood density assessment of Scots pine (Pinus sylvestris L.) using Resistograph and Pilodyn." PloS one **13**(9): e0204518.

Fundova, I., T. Funda and H. X. Wu (2019). "Non-destructive assessment of wood stiffness in Scots pine (Pinus sylvestris L.) and its use in forest tree improvement." Forests **10**(6): 491.

Galligan, W. L. and K. A. McDonald (2000). "Machine grading of lumber: practical concerns for lumber producers." Gen. Tech. Rep. FPL–GTR–7 (Revised). Madison, WI: US Department of Agriculture, Forest Service, Forest Products Laboratory. 39 p.: ill.; 28 cm. **7**.

Gao, S., X. Wang, L. Wang and R. B. Allison (2013). "Effect of temperature on acoustic evaluation of standing trees and logs: Part 2: Field investigation." Wood and Fiber Science **45**(1): 15-25.

Gärtner, S. M., V. J. Lieffers and S. E. Macdonald (2011). "Ecology and management of natural regeneration of white spruce in the boreal forest." Environmental Reviews **19**(NA): 461-478.

Green, D. W., J. E. Winandy and D. E. Kretschmann (1999). "Mechanical properties of wood. Wood handbook: wood as an engineering material." Forest Products Laboratory.

Güntekin, E. and T. Y. Aydin (2016). "Prediction of bending properties for some softwood species grown in Turkey using ultrasound." Wood Research **61**(6): 993-1002.

Huang, C.-L. (2005). System and method for measuring stiffness in standing trees, Google Patents.

Ivković, M., W. J. Gapare, A. Abarquez, J. Ilic, M. B. Powell and H. X. Wu (2009). "Prediction of wood stiffness, strength, and shrinkage in juvenile wood of radiata pine." Wood Science and Technology **43**(3): 237-257.

Korkmaz, O. and Ü. Büyüksarı (2019). "Effects of moisture content on mechanical properties of micro-size oak wood." BioResources **14**(4): 7655-7663.

Krajnc, L., N. Farrelly and A. M. Harte (2019). "The effect of thinning on mechanical properties of Douglas fir, Norway spruce, and Sitka spruce." Annals of Forest Science **76**(1): 1-12.

Kuprevicius, A., D. Auty, A. Achim and J. P. Caspersen (2013). "Quantifying the influence of live crown ratio on the mechanical properties of clear wood." Forestry **86**(3): 361-369.

Lachenbruch, B., G. Johnson, G. Downes and R. Evans (2010). "Relationships of density, microfibril angle, and sound velocity with stiffness and strength in mature wood of Douglas-fir." Canadian Journal of Forest Research **40**(1): 55-64.

Lachenbruch, B., J. R. Moore and R. Evans (2011). Radial variation in wood structure and function in woody plants, and hypotheses for its occurrence. Size-and age-related changes in tree structure and function, Springer**:** 121-164.

Lei, Y., S. Zhang and Z. Jiang (2005). "Models for predicting lumber bending MOR and MOE based on tree and stand characteristics in black spruce." Wood Science and Technology **39**(1): 37-47.

Lenz, P., D. Auty, A. Achim, J. Beaulieu and J. Mackay (2013). "Genetic improvement of white spruce mechanical wood traits—early screening by means of acoustic velocity." Forests **4**(3): 575-594.

Lenz, P., J. MacKay, A. Rainville, A. Cloutier and J. Beaulieu (2011). The influence of cambial age on breeding for wood properties in Picea glauca. Tree Genet Genomes 7: 641–653.

Montero, M., J. De la Mata, M. Esteban and E. Hermoso (2015). "Influence of moisture content on the wave velocity to estimate the mechanical properties of large cross-section pieces for structural use of Scots pine from Spain." Maderas. Ciencia y tecnología **17**(2): 407-420.

Moreno Chan, J., J. C. Walker and C. A. Raymond (2011). "Effects of moisture content and temperature on acoustic velocity and dynamic MOE of radiata pine sapwood boards." Wood Science and Technology **45**(4): 609-626.

Murphy, G. and D. Cown (2015). "Stand, stem and log segregation based on wood properties: a review." Scandinavian Journal of Forest Research **30**(8): 757-770.

Mvolo, C. S., A. Koubaa, J. Beaulieu, A. Cloutier, M. Defo and M.-C. Yemele (2019). "Phenotypic correlations among growth and selected wood properties in white spruce (Picea glauca (Moench) Voss)." Forests **10**(7): 589.

Panshin, A. J. and C. De Zeeuw (1964). "Textbook of wood technology."

Paradis, N., D. Auty, P. Carter and A. Achim (2013). "Using a standing-tree acoustic tool to identify forest stands for the production of mechanically-graded lumber." Sensors **13**(3): 3394-3408.

Pelletier, G. and D. G. Pitt (2008). "Silvicultural responses of two spruce plantations to midrotation commercial thinning in New Brunswick." Canadian Journal of Forest Research **38**(4): 851-867.

Pinheiro, J., D. Bates, S. DebRoy and D. Sarkar (2015). "R Core Team. 2015. nlme: linear and nonlinear mixed effects models. R package version 3.1-120." R package version: 3.1-120.

Psaltis, S., C. Kumar, I. Turner, E. J. Carr, T. Farrell, L. Brancheriau, H. Bailléres and D. J. Lee (2021). "A new approach for predicting board MOE from increment cores." Annals of Forest Science **78**(3): 1-16.

Raymond, C. A., B. Joe, D. W. Anderson and D. J. Watt (2008). "Effect of thinning on relationships between three measures of wood stiffness in Pinus radiata: standing trees vs. logs vs. short clear specimens." Canadian Journal of Forest Research **38**(11): 2870-2879.

Rohanová, A., R. Lagaňa and V. Vacek (2010). "Static and dynamic modulus of spruce structural timber." Annals of Warsaw University of Life Sciences-SGGW, Forestry and Wood Technology(72): 229-232.

Ross, R. J. (2015). Nondestructive evaluation of wood, Government Printing Office.

Sanabria, S. J., R. Furrer, J. Neuenschwander, P. Niemz and U. Sennhauser (2011). "Air-coupled ultrasound inspection of glued laminated timber."

Sandoz, J. (1993). "Moisture content and temperature effect on ultrasound timber grading." Wood Science and Technology **27**(5): 373-380.

Senalik, A. C., G. Schueneman and R. J. Ross (2014). "Ultrasonic-based nondestructive evaluation methods for wood: a primer and historical review." USDA Forest Service, Forest Products Laboratory, General Technical Report, FPL-GTR-235, 2014; 36 p. **235**: 1-36.

Stewart, J. D., R. Koppenaal, A. Lalumière and R. J. Whitehead (2021). "Predicting wood stiffness of lodgepole pine trees using acoustic tools and green density." The Forestry Chronicle **97**(1): 52-64.

Stiell, W. (1976). "White Spruce: artificial regeneration in Canada." White Spruce: artificial regeneration in Canada.(FMR-X-85).

Tanasoiu, V., C. Miclea and C. Tanasoiu (2002). "Nondestructive testing techniques and piezoelectric ultrasonics transducers for wood and built in wooden structures." Journal of Optoelectronics and Advanced Materials **4**(4): 949-957.

Team, R. C. (2013). "R: A language and environment for statistical computing."

Ukrainetz, N. K., K. Ritland and S. D. Mansfield (2008). "Identification of quantitative trait loci for wood quality and growth across eight full-sib coastal Douglas-fir families." Tree Genetics & Genomes **4**(2): 159-170.

Vlad, R., M. Zhiyanski, L. Dincă, C. G. Sidor, C. Constandache, G. Pei, A. Ispravnic and T. Blaga (2018). "Assessment of the density of wood with stem decay of Norway spruce trees using drill resistance." Comptes rendus de l'Academie Bulgare des Sciences **71**(11).

Vössing, K. J. and E. Niederleithinger (2018). "Nondestructive assessment and imaging methods for internal inspection of timber. A review." Holzforschung **72**(6): 467-476.

Wang, X., S. Verrill, E. Lowell, R. J. Ross and V. L. Herian (2013). "Acoustic sorting models for improved log segregation." Wood and Fiber Science **45**(4): 343-352.

Wessels, C., F. Malan and T. Rypstra (2011). "A review of measurement methods used on standing trees for the prediction of some mechanical properties of timber." European Journal of Forest Research **130**(6): 881-893.

Xu, P. and J. Walker (2004). "Stiffness gradients in radiata pine trees." Wood Science and Technology **38**(1): 1-9.

Yang, H., L. Yu and L. Wang (2015). "Effect of moisture content on the ultrasonic acoustic properties of wood." Journal of forestry research **26**(3): 753-757.

Zhang, S. and A. Koubaa (2008). Softwoods of eastern Canada: Their silvics, characteristics, manufacturing and end-uses, FPInnovations.

Zobel, B. J. and J. P. Van Buijtenen (2012). Wood variation: its causes and control, Springer Science & Business Media.

Nondestructive Characterization of Sugar Maple Wood Decay and Dynamic Modulus of Elasticity by Acoustic Tomography

Achraf Ammar*
Institut de recherche sur les forêts, Université du Québec en Abitibi-Témiscamingue, Rouyn-Noranda, QC, Canada, achraf.ammar@uqat.ca

Ahmed Koubaa*
Institut de recherche sur les forêts, Université du Québec en Abitibi-Témiscamingue, Rouyn-Noranda, QC, Canada, ahmed.koubaa@uqat.ca

Dorra Gassara
École Nationale d'Ingénieurs de Sfax, Université de Sfax, Sfax, Tunisia, dorra.gassara@gmail.com

Yves Bergeron
Institut de recherche sur les forêts, Université du Québec en Abitibi-Témiscamingue, Rouyn-Noranda, QC, Canada, yves.bergeron@uqat.ca

Pierre Grondin
Ministère des Forêts, de la Faune et des Parcs, Québec, QC, Canada, Pierre.Grondin@mffp.gouv.qc.ca

David Voyer
Ministère des Forêts, de la Faune et des Parcs, Québec, QC, Canada, David.voyer@mffp.gouv.qc.ca

* Corresponding author

Abstract

Sugar maple wood is highly prized for appearance and structural applications. However, the presence of decay in maple causes considerable decreases in its stem value and wood properties. Thus, the general objective was to evaluate the potential of acoustic tomography to detect decay in sugar maple trees and evaluate its impact on wood mechanical properties. Specific objectives were: 1) to characterize the proportion of decay by acoustic tomography; 2) to evaluate the impact of decay on the static and dynamic (DMOE) modulus of elasticity; 3) to evaluate the potential of acoustic tomography to predict the impact of decay on the mechanical properties of sugar maple wood. Fifty-three trees were sampled from two sites in La Tuque (Quebec). The sound propagation speed in wood and its density determined the DMOE. Eighteen sugar maple trees were sampled and felled from two sites in Abitibi-Témiscamingue (Quebec). Their parallel compression and flexural properties were measured on clear wood samples (ASTM D143). The trees' DMOE was also measured by acoustic tomography and ultrasound methods to investigate the relationship between the wood moduli of elasticity measured by destructive and nondestructive methods. Acoustic tomography accurately predicted the proportion of decay in sugar maple trees. The DMOE measured on standing trees correlates well to the static and DMOE measured on destructive samples. Decay has a significant negative impact on the mechanical properties of sugar maple wood that can reach up to 60% reduction depending on the decay stage. Practical implications include the effectiveness of acoustic tomography in predicting the wood quality and economic value of sugar maple stands.

Keywords: sugar maple, wood decay, nondestructive characterization, acoustic tomography, dynamic modulus of elasticity

Introduction

Sugar maple is a specific hardwood species of the forests of northeastern North America (Baral, 2016) and specifically in Canada (Natural Resources Canada, 2020). This species has an important economic weight appreciated for its syrup and good quality wood. Sugar maple wood is sought after mainly because of its hardness, fiber density, and light color (MFFP 2020).

In general, due to its mechanical and physical properties, wood is among the most exploited materials in the world. The quality of the attributes of this material is directly related to the final application. Indeed, for foresters, the wood quality depends on the shape and size of the trees. At the same time, for the lumber industries, it is defined according to the quality of the logs, i.e., diameter, taper, presence of knots, etc. (Zhang, 2003). For the construction industry, the quality of wood depends mainly on its stiffness (Wang et al., 2017).

Nevertheless, its biological character weakens its potential for wood users. Indeed, wood is a biobased material subject to degradation due to exposure to pathogens (fungi, bacteria, insects) or environmental conditions (light, heat, humidity, etc.). Specifically, sugar maples are exposed to various pathogens, causing less than 40% losses, mainly white-rot fungi (Basham and Morawski, 1964).

In this context, the presence of decay in maples causes a considerable decrease in stem quality and degradation of the mechanical and physical properties of the wood (Bouslimi, 2014).

To avoid the misuse of wood and ensure the wood's safety standards, the forest industry aims to find effective and fast solutions to inspect the wood before felling, during processing, and in-service (Zhang, 2003). Hence the interest of researchers and industrialists in developing reliable and accurate methods of wood quality assessment before the felling stage, which will allow a better evaluation of wood properties, especially its mechanical properties. This evaluation will lead to more efficient use of the available wood according to its characteristics and fields of application. This type of evaluation can indeed be done using destructive tools, but it isn't easy, limiting the scope of its application. In addition, the preparation of the samples and the measurement of the wood properties of these tools are very time-consuming. In some applications, it is important to regularly inspect the current condition of the wood without affecting its functional characteristics (Nowak et al., 2015; Wang et al., 2017). In addition, the use of nondestructive tools to assess the mechanical properties of wood has many advantages, including mobility, speed, application in various atmospheric and field conditions, and cost savings when compared to traditional destructive tools (De Oliveira et al., 2005; Wang et al., 2017).

The objective of this study was to evaluate the potential of acoustic tomography for nondestructive characterization of the effect of wood stain and decay on wood mechanical properties. In particular, this project aims to determine the variation of the modulus of elasticity with the wood's state (stained or sound). These moduli are evaluated by nondestructive methods, namely the ultrasonic method and the acoustic tomography, and the destructive methods, such as the parallel static compression test and the three-point bending test. On the one hand, these evaluations make it possible to establish relationships between static and dynamic moduli of elasticity. On the other hand, they make it possible to develop models for predicting static moduli. However, acoustic tomography is generally used to predict the proportion and location of decay in standing trees. Few studies have examined the potential of this technique to predict mechanical properties. Therefore, this project will examine the reliability of this technique for predicting the static behavior of wood.

Materials and methods

Materials

Sugar maple trees were randomly selected from four sites in La Tuque and Abitibi-Témiscamnigue regions, Québec. Two types of sampling were conducted: 1) Nondestructive sampling, where 53 standing

trees were sampled from the La Tuque sites during summer 2019. These trees are analyzed by acoustic tomography. From each tree, a six-millimeter bark-to-pith) increment core was sampled at 1.3 m height for X-Ray densitometry measurements; 2) Destructive sampling, where 18 trees were harvested from two sites in the Abitibi-Témiscamingue region, Québec (9 trees per site), for destructive characterization results. From each tree, 18 logs of 70 cm in length were collected between 1.3 m and 2m. They were used first for acoustic tomography and then to prepare the test samples for parallel compression and three-point bending. The dimensions of the test samples were according to the ASTM D143 standard. The samples were air-dried to an equilibrium moisture content of 8%.

The proportion of decay in trees measurement

The present study measured decay proportion by acoustic tomography and visual inspection for 18 cross-sections of sugar maple trees taken at diameter at breast height (DBH). Acoustic tomography detects cavities and decay within trees by measuring sound wave propagation velocities in the wood (Göcke, 2017; Son et al., 2021). This technique involves mounting several sensors (depending on tree diameter) around the perimeter of a cross-section of the tree trunk. Each sensor is connected to a nail driven lightly into the bark. Each time, one of the sensors is removed by tapping on its nail by the tomograph hammer (transmitter of the wave), and the other sensors act as receivers of the sound wave. Thus, the sensors recorded the propagation times of the waves induced by the small blows of the hammer. The relative velocities of the sound are thus calculated with these data. Consequently, a dense network of velocities is obtained over the entire cross-section and represented on a tomogram. The latter provides a mesh of different colors indicating the presence or absence of cavities or decay foci inside the tree and the percentage of rotten or hollow wood (Göcke, 2017). As for the visual method, decay proportions are calculated using Image J software that allows manual selection of decayed areas and subsequently allows measurement of their surfaces.

X-Ray density measurement

Density was measured at the ring scale (core) for the first sampling using the X-ray densitometer and at the test specimen scale for the second sampling by measuring each compression test specimen. In addition, for both scales, moving from pith to bark, decayed, discolored, and sound portions of the wood were properly identified for each tree to measure the average density of each portion.

The assessment of ring density is performed using X-ray densitometry (Quintek Measurements System (QMS)). This instrument is equipped with a video camera that scans the rings of samples from pith to bark based on X-ray attenuation with a linear resolution of 0.01 mm. The Tree Ring Analyser software generates a density profile for each sample, which provides the radial or annual variations of the density. This profile makes it possible to determine the density of the initial and final wood rings and the cambial age of the trees. Matlab software modeled the intra-ring wood density profiles.

Static moduli of elasticity measurements

The static moduli of elasticity in bending ($SMOE_F$) and parallel compression ($SMOE_C$) were measured according to the ASTMD143 standard. The modulus of elasticity in three-point bending ($SMOE_F$) and parallel compression ($SMOE_C$) were measured using a universal testing machine with a capacity of 20 kN (ZWICK Roell, Germany). The dimensions of the test specimen were measured to the nearest 0.01 mm and weighed to the nearest 0.01g for bulk density determination. The averages of all mechanical properties were determined for each decay class (C1: discolored; C2: decayed; C3: advanced decay). The relative ratio of mechanical property loss was calculated.

Ultrasonic measurements

The ultrasonic measurements were conducted on parallel compression test samples using the Sonatest Mastercam 380 ultrasound generator (Sonatest Inc., Texas, USA). Ultrasonic waves were applied to the samples through two 10 MHz transducers attached to both ends of the test specimen, one of which is a transmitter and the other a receiver. The device measures the wave propagation time. The ultrasonic $DMOE_U$ depends on two parameters, the specimen's bulk density (ρ_a) and the wave propagation velocity (V_b) ($DMOE_U=\rho_a V_b^2$).

Acoustic tomography

The acoustic tomography was used to detect and assess the proportion of decay zones and measure the $DMOE_T$ in standing trees. The device gives sound propagation speed at different wood zones (V_b). X-Ray density gives the variation of the trees' radial wood density (ρ). X-ray and acoustic tomography data give the $DMOE_T$ ($DMOE_U=\rho V_b^2$) for the different wood zones (sound, discolored and decayed) according to Equation 1.

Results and discussion

The proportion of decay in trees

The tomograph did not detect any decay in 11 trees among the 18 sampled ones. In the remaining 7 trees, there was a good agreement between the percentage of decay measured visually and by the acoustic tomography (Figure 1) ($r = 0.87$ /R^2=0.76). These results agree with previous findings for white oak and hickory (Gilbert and Smiley 2004) that reported a correlation coefficient of 0.90 between visual and acoustic tomography decay proportions. Thus, the acoustic tomography can detect the decay location and proportion in agreement with previous reports (Gilbert and Smiley, 2004; Dudkiewicz and Durlak, 2021; Martiansyah et al., 2022).

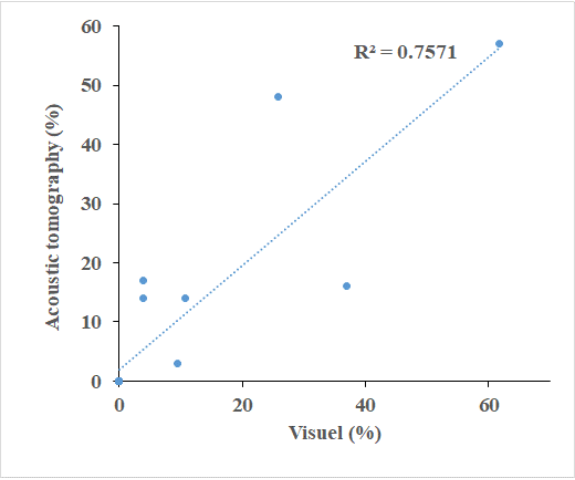

Figure 1: Relationship between the proportion of decay measured visually and by acoustic tomography

Intra-tree variation of density and dynamic modulus of elasticity

An overview of the intra-tree variation of the DMOE and the density is presented in Figure 2. The abscissa axis is taken randomly, and its values are not representative. We notice a periodic repetition of a peak throughout the sample for both quantities. Each peak represents one of the characteristics of the

growth ring apart from its composition of initial wood and final wood. Moreover, for each growth ring, both quantities increase progressively at the level of the initial wood, reaching their maximum at about half of the final wood. Afterward, these two properties start to decrease progressively until reaching minimum values at the border between two consecutive annual rings.

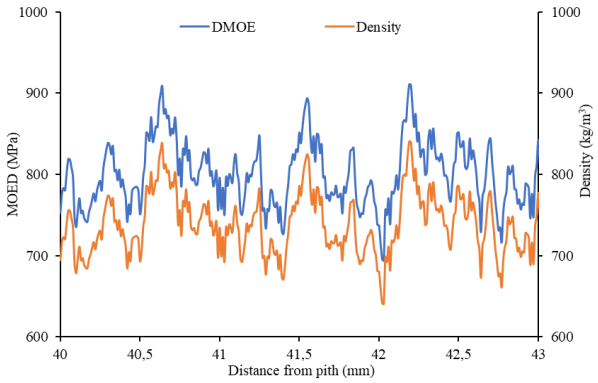

Figure 2: Example of DMOE and density variation along with the increment core

Effect of discoloration/caries on the studied properties

Figure 3 shows the impact of discoloration/decay on wood density (Figure 3 a), the static moduli of elasticity in bending (Fig. 3b) and in parallel compression (Fig. 3c) and ultrasonic ($DMOE_U$, Fig. 3d) and acoustic tomography ($DMOE_T$, Fig. 3e) dynamic moduli of elasticity of sugar maple.

The density shows a relatively small variation for the three decay classes as it decreases by 4% for C1, 3% for C2, and C3. The $SMOE_F$ presents a loss of 20% for the very decayed class, 23% for the decayed class, and 11% for the colored class. Regarding the $MOES_C$, it presents a drop of 27% for C1, 31% for C2, and 23% for C3. The $MOED_U$ shows a decrease of 14% for the very decayed and decayed classes and a 1% decrease for the colored class. The $DMOE_T$ shows a loss of 60%, 38%, and 12%, respectively, for the three classes. Since DMOE depends on the speed of sound propagation (Equation 1), the decrease in these two moduli is due to the slow sound wave propagation speed in the discolored or decayed area. Indeed, the decay or defect in the wood causes a deviation of the sound signal, which explains the increase in propagation time and, consequently, the decrease in the propagation speed of the wave and DMOE (Feio, 2005).

Relationships between static and dynamic MOEs

Figure 4 shows the relationships between the static and the dynamic moduli of elasticity measured by ultrasonic and acoustic tomography methods. The relationships' coefficients of determination between the $DMOE_T$ determined by acoustic tomography and the static MOEs in flexion (Fig. 4a, R^2=0.60), parallel compression (Fig. 4b, R^2=0.51), and $DMOE_U$ determined by ultrasound $DMOE_U$ (Fig. 4c, R^2=0.61.). It is worthy that only a few investigations examined the potential of acoustic tomography to determine elastic wood properties.

The $DMOE_T$ values measured by the tomograph are low compared to the dynamic modulus ($MOED_U$) and the static moduli in flexion (MOESF) and parallel compression ($MOES_C$). The higher frequencies of the ultrasound method than that of the acoustic tomography is a plausible explanation. Given that the propagation velocity of the sound wave is directly proportional to the frequency, the modulus of elasticity, which is proportional to the square of the velocity, decreases as the frequency decreases (Sales et al., 2011). The velocities measured by acoustic tomography ranged from 494 m/s to 1245 m/s. These values are comparable to the velocities measured on beech, ranging from 460 m/s to 2350 m/s (Martinis et al., 2004).

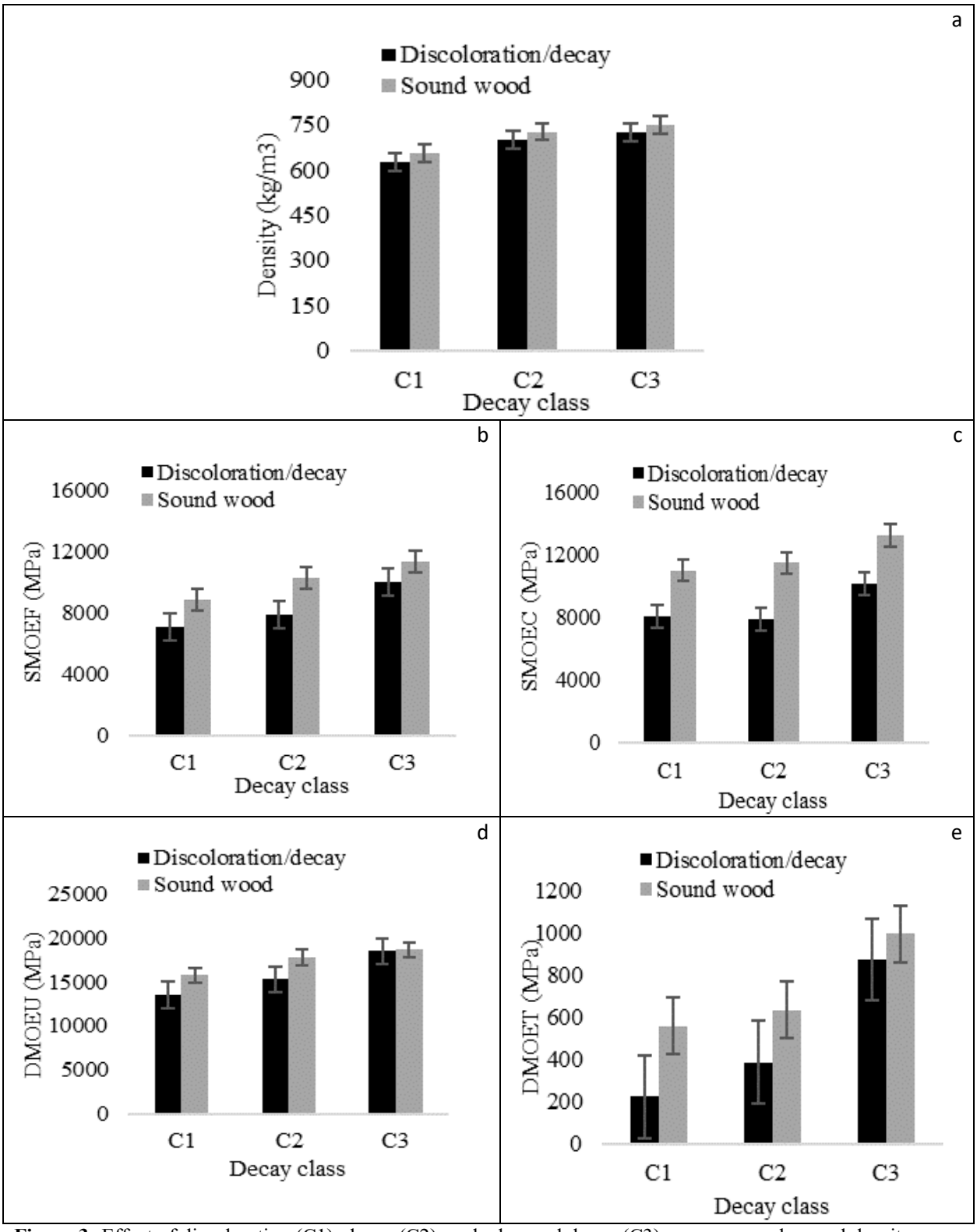

Figure 3: Effect of discoloration (C1), decay (C2), and advanced decay (C3) on sugar maple wood density (a); static moduli of elasticity in flexion, $SMOE_F$ (b), in parallel compression $SMOE_C$ (c), and dynamic moduli of elasticity determined by ultrasonic wave propagation, $DMOE_U$ (d) and acoustic tomography $DMOE_T$ (e)

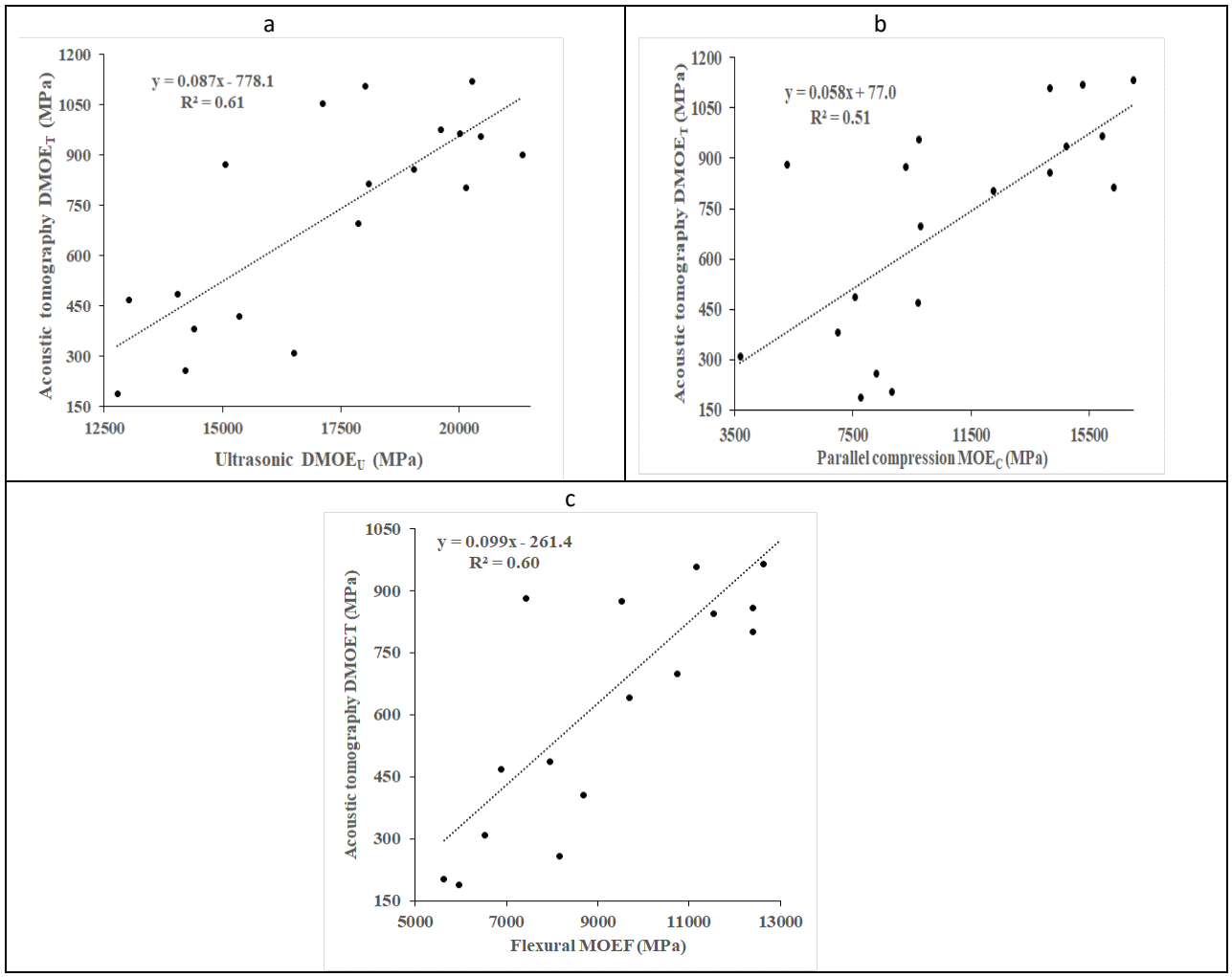

Figure 4: Relationships between the static and dynamic moduli of elasticity a) Flexural DMOE$_F$ vs. Acoustic tomography DMOE$_T$ b) Parallel compression MOE$_C$ vs. DMOE$_T$, c) Ultrasonic DMOE$_U$ vs. and DMOE$_T$.

Conclusions

Acoustic tomography accurately predicted the proportion of decay and the dynamic modulus of elasticity in sugar maple trees. The incidence of decay had a much more important impact on the static and dynamic moduli of elasticity than wood density. Close relationships are found between static and dynamic moduli of elasticity.

Acknowledgments

The authors acknowledge the financial contribution of the *Ministère des forêts, de la Faune et des parcs du Québec* (MFPP), the Natural Science and Engineering Research Council of Canada (NSERC), and the Canada Research Chair Program.

References

Basham, J., et Morawski, Z. 1964. Cull studies. The defects and associated basidiomycete fungi in the heartwood of living trees in the forests of Ontario. Publication, Département foresterie, Canada, No 1072, 67p.

Bouslimi, B. 2014. Variation intra-arbre, intrasites et intrasites des attributs de la qualité du bois Thuya occidental (Thuja occidentalis). Thèse de doctorat, Université Abitibi-Témiscamingue, Rouyn-Noranda, 395p.

De Oliveira Feio, A. J. 2005. Inspection and Diagnosis of Historical Timber Structures: NDT Correlations and Structural Behaviour. Universidade do Minho Escola de Engenharia.

Gocke, L. (2017). Picus Sonic Tomograph: Software Manual Q74. Argus Electronic GmbH, Rostock, Germany, 91p.

Dudkiewicz, M., et Durlak, W. 2021. Sustainable Management of Very Large Trees with the Use of Acoustic Tomography. Sustainability, 13(21), 12315.

Feio, A. J. d. O. (2005). "Inspection and diagnosis of historical timber structures : NDT correlations and structural behaviour. " Thése de doctorat, University of Minho. 208p.

Gilbert, E. A., et Smiley, E. T. 2004. Picus Sonic tomography for the quantification of decay in white oak (*Quercus alba*) and hickory (*Carya* spp.). Journal of arboriculture, 30(5), 277-281.

Martiansyah, I., Zulkarnaen, R. N., Hariri, M. R., Hutabarat, P. W. K., et Wardani, F. F. 2022. Tree Health Monitoring of Risky Trees in the Hotel Open Space: A Case Study in Rancamaya, Bogor. Jurnal Sylva Lestari, 10(2), 180-201.

Martinis, R., Socco, L., Sambuelli, L., Nicolotti, G., Schmitt, O., et Bucur, V. 2004. Tomographie ultrasonore pour les arbres sur pied. Annals of forest science, 61(2), 157-162.

Nowak, T., Hamrol-Bielecka, K., et Jasienko, J. 2015. Nondestructive testing of wood-correlation of ultrasonic and stress wave test results in glued laminated timber members. Annals of Warsaw University of Life Sciences-SGGW. Forestry and Wood Technology, 92.

Sales, A., Candian, M., et de Salles Cardin, V. 2011. Evaluation of the mechanical properties of Brazilian lumber (Goupia glabra) by nondestructive techniques. Construction and Building Materials, 25(3), 1450-1454.

Son, J., Kim, S., Shin, J., Lee, G., et Kim, H. 2021. Reliability of nondestructive sonic tomography for detection of defects in old Zelkova serrata (Thunb.) Makino trees. Forest Science and Technology, 17(3), 110-118.

Wang, X., Senalik, C. A., et Ross, R. J. 2017. Proceedings: 20th International Nondestructive Testing and Evaluation of Wood Symposium. General Technical Report FPL-GTR-246. Madison, WI: U.S. Department of Agriculture, Forest Service, Forest Products Laboratory. 539 p.

Zhang, S. 2003. Wood quality attributes and their impacts on wood utilization, In Proceedings of XII World Forestry Congress, Quebec City, Canada, https://www.fao.org/3/xii/0674-b1.htm

Effect of Partial Harvesting on Growth, Density, and Dynamic Modulus of Elasticity of White Spruce in a Mixed Boreal Forest

Md Nazrul Islam
Forestry and Wood Technology Discipline, Khulna University, Khulna, Bangladesh, MD. NAZRUL
nazrul17@yahoo.com

Ahmed Koubaa*
Institut de recherche sur les forêts, Université du Québec en Abitibi-Témiscamingue, Rouyn-Noranda, QC, Canada, ahmed.koubaa@uqat.ca

Brian Harvey
Institut de recherche sur les forêts, Université du Québec en Abitibi-Témiscamingue, Rouyn-Noranda, QC, Canada, brian.harvey@uqat.ca

Suzanne Brais
Institut de recherche sur les forêts, Université du Québec en Abitibi-Témiscamingue, Rouyn-Noranda, QC, Canada, suzanne.brais@uqat.ca

* Corresponding author

Abstract

Several alternative practices to clear-cut harvesting treatments are being tested for their ability to accelerate stem growth in boreal and temperate forests. Partial harvesting removes the oldest and largest shade-intolerant broadleaf trees, which improves the ecological perspective of the forest by enhancing the ability of survival and proper growth of shade-tolerant conifers while gaining the economic value of the operation. This study aimed to determine the effect of partial harvesting intensity in mixed forests on the radial growth, density, and dynamic modulus of elasticity (DMOE) of white spruce (*Picea glauca* (Moench) Voss) wood of different social classes, i.e., suppressed, co-dominant, and dominant. X-ray densitometry served to measure ring (RW), earlywood (EWW), and latewood (LWW) widths, latewood percentage (LWP), and ring (RD), earlywood (EWD), and latewood (LWD) densities on radial increment cores. An ultrasonic wave propagation method assessed the DMOE. RW, EWW, LWW, and LWP increased, while RD decreased significantly with partial harvesting intensity. However, the effects were less prominent on LWD and EWD. The impact of harvesting intensity on RD was higher in co-dominant trees than in other social classes. Moreover, RD varied significantly without affecting the DMOE. The results suggest that partial harvesting increased the radial growth of remaining stems and reduced the wood density without negative effects on the DMOE.

Keywords: white spruce, partial harvesting, Ring density, wood density, dynamic modulus of elasticity, ultrasonic wave propagation, X-ray densitometry

Introduction

Many alternatives to clear-cutting are being tested in the boreal forest, ranging from dispersed retention to selective harvesting. The pattern and intensity of stem removal tend to depend on a proposition or specific silvicultural or conservation objectives. In boreal mixedwood stands, partial harvesting can remove shade-intolerant broadleaf trees while allowing survival and proper growth of shade-tolerant conifers (Comeau et al. 2005) and has been extensively tested across boreal forests (Gradowski et al. 2010).

While partial harvesting has been demonstrated to accelerate stem growth, it can negatively affect residual stems' wood quality and properties (Gendreau-Berthiaume et al., 2012). Stem growth response to harvesting intensity depends on several factors, including species traits, social status, harvesting intensity, and the composition of silvicultural treatment. Partial harvesting in Eastern Canada improved stem growth for several species (Gendreau-Berthiaume et al., 2012, Gagné et al., 2012; Goudiaby et al., 2012).

Wood density is an important indicator of mechanical properties (Panshin and de Zeeuw 1970), which are the most important wood attributes (WFA) for many end products (Mvolo et al. 2021). Elastic properties are also important besides wood density, especially for engineering design (Bucur 2006). Static and dynamic test methods can determine this stiffness or modulus of elasticity (MOE) (Divós and Tanaka 2005, Bucur 2006). The dynamic modulus of elasticity (DMOE) is increasingly used to assess wood quality for its rapidity and convenience (Kharrat et al., 2019, Mvolo et al., 2021). It is determined using ultrasonic wave velocity and density of the wood. Ultrasonic wave velocity measurement is widely used as a non-destructive method for assessing the strength properties of living trees, logs, sawn timbers, and wood-based materials because of its rapidity, flexibility, portability, cost-effectiveness, and ease of use (Proto et al. 2017). However, wood density varies within and between trees, sites, and genetic sources originating from genetic, environmental, and physiological factors (Panshin and De Zeeuw 1980). Several researchers (Divós and Tanaka 2005, Mvolo et al. 2021) established relationships between the static and dynamic MOE, and good correlations (R^2: 0.90–0.96) between the two MOE values have been determined.

The dynamic MOE is about 10% higher than the static MOE (Divós and Tanaka 2005), depending on the methods used. Mvolo et al. (2021) compared the MOE in static bending to the dynamic MOE measured by two non-destructive methods: the SilviScan and the ultrasonic time-of-flight methods for white spruce and lodgepole pine. This study indicated that the time-of-flight method had a higher correlation coefficient between the static and the dynamic MOEs. In addition, these coefficients of correlation varied between the two species. They concluded that the results of the wood non-destructive testing must be validated separately for each commercial tree species and each measurement method.

White spruce (*Picea glauca* (Moench) Voss), a relatively shade-tolerant (intermediately) conifer, is widely distributed in the boreal forests of North America. It is one of Canada's widest-ranging and most commercially important tree species and an important source of pulpwood and construction-grade lumber (Zhang and Koubaa 2008). Gagné et al. (2012) found that thinning had a significant positive effect on dominant and co-dominant 32-year-old white spruce stem volume, with no negative effects on wood density, MOE, or modulus of rupture for all commercial thinning intensities and social classes. Thinning increased the MOE by 50 % for dominant and 70 % for co-dominant white spruce when the thinning intensity was 35 % of the basal area.

This study aimed to determine the effects of partial harvesting on the wood quality of the residual stems in northwestern Quebec. The main objective was to assess the effects of varying intensities of partial harvesting of mixed wood stands and social status on the radial growth, wood density, and dynamic MOE of residual white spruce stems.

Materials and Methods

The study was carried out in Beauchatel Township (48°13′–48° 15′ N, 79° 16′–79° 19′ W.), 35 km west of Rouyn-Noranda, Quebec, Canada. The region is located in the Abitibi Lowlands Ecoregion of the western balsam fir-white birch bioclimatic subdomain (Saucier et al. 1998). The climate is continental, with an annual average temperature of 1.7°C and yearly precipitation of 883 mm, of which 625 mm of rain falls from April to November (Government of Canada, 2016). The forest is considered part of the boreal mixedwood. It contains intermediate to shade-tolerant boreal conifers, which often grow with shade-intolerant hardwoods such as aspen (*Populus tremuloides*) and white birch (*Betula papyrifera*).

The experiment was conducted in ≃70-year-old trembling aspen-dominated stands of fire origin with an average basal area (BA) of 43.5 m^2 ha^{-1} having the maximum DBH and height of trees were 30 cm and 25 m, respectively. Aspen accounted for 79 % of stand BA with a density of 662 stem ha-1 (≥3 cm diameter at breast height), and white spruce occupied 18 % of stand BA with a density of 734 stem ha^{-1}. In 2001–2002, four levels of partial harvesting, including one no-harvest treatment (control, C), were applied according to a completely randomized experimental design in 39 ha of forest. The three partial cut treatments were designed to remove respectively 60, 75, and 100 % of aspen BA and are respectively referred to as light (L), moderate (M), and total harvest (T). Forty 400-m^2 permanent circular sampling plots were distributed within the experimental area following different harvesting intensities.

Four plots were selected randomly from each treatment for 16 plots to determine tree response to partial harvesting. White spruce stems were classified into three social classes: dominant (D), co-dominant (CO), and suppressed (S) in each sampling plot, depending on the crown position in the canopy layer. Five stems (diameter ≥10 cm) were selected randomly from each social class, and 240 stems were selected for coring. Cores were collected.

Two 6-mm increment cores were taken at breast height from each selected tree for analysis and data collection. Cores were air-dried at room temperature and sawn to 1.57–1.9 mm thickness. Samples were extracted in cyclohexane/ethanol solution at a ratio of 2:1 (v/v) for 24 hours, followed by distilled water for another 24 hours. The extracted samples were air-dried and sanded with increasingly fine grades of sandpaper. Rings were scanned from bark to pith with a QTRS-01X Tree Ring Scanner (QMS, Knoxville, Tennessee). Incomplete or false rings and rings with compression wood or branch tracers were eliminated from the analysis. Rings were eliminated by analyzing computer-generated images and visual examination with a microscope after scanning. Scans were performed at 0.04 mm resolution.

The X-ray density analysis samples served for measuring the ultrasonic wave velocity using a Masterscan 380 (Sonatest Inc., Texas, USA). Measurements were made at a 10 MHz frequency on every 1.5 mm starting from the bark, according to the procedure reported by Kharrat et al. (2019). Plexiglas was used as reference material. The velocity is measured along the fibers' longitudinal direction. The X-Ray density data and the ultrasonic wave velocity data collected on the same sample and at the same sampling points were processed with Matlab software to calculate the dynamic modulus of elasticity (DMOE) using the following equation:

$$DMOE = \rho v^2 \qquad (1)$$

where ρ is the wood density and v is the ultrasonic wave velocity.
Average ring (RW), earlywood (EWW) and latewood (LWW) widths, latewood percentage (LWP), ring (RD), earlywood (EWD), and latewood (LWD) densities, and DMOE following different harvesting intensities were determined. Analyses of variance (ANOVA) were performed with linear models in a completely randomized to investigate the impact of harvesting intensity and social class on the growth and

wood quality attributes. All statistical tests were performed using SAS (version 9.2) at a 95 % confidence level.

Results

Harvesting intensity significantly affected RW, EWW, and LWW (Table 1). RW increased significantly with harvesting intensities, showing an average increase of 80.4 % 10 years after harvesting. RW did not change in the first year after harvesting but increased after that for all plots (Fig. 1A). However, harvested plots showed higher RW increment than control plots, with the highest increase for lightly harvested plots, followed by totally and moderately harvested plots. EWW also increased with harvesting intensities, with a similar trend to that for RW (Fig. 1B). LWW increased significantly after harvesting but at a slower rate than earlywood width (Fig. 1C). However, despite the slight decreasing tendency, harvesting intensity did not affect LWP (Fig. 1D). The slower increase rate of LWW compared to EWW explains this decreasing tendency.

Table 1. Analysis of Variance (F values) on the effects of harvesting intensity and social class on growth and wood quality attributes of white spruce in a mixed boreal forest in Quebec

	Growth attributes				**Wood quality attributes**			
	RW	EWW	LWW	LWP	RD	EWD	LWD	DMOE
Harvesting (H)	10.96**	8.74**	8.87**	1.86ns	3.89**	2.28ns	1.18ns	0.65ns
Social class (C)	2.49ns	4.93**	0.74ns	5.45**	1.44ns	0.20ns	4.41*	0.10ns
HxC	11.20**	1.03ns	1.26ns	0.70ns	2.15*	1.94ns	4.76**	0.16ns
HxCxYear	2.85**	5.42**	1.43ns	3.5**	9.03**	4.41**	17.62**	5.2**

* significant at α=0.05; ** Significant at α=0.01; ns : non significant at α=0.05

Each partial harvesting intensity showed a similar effect pattern for radial growth considering the social class. However, the results were very revealing when comparing social classes harvesting intensities. RW, RW, EWW, and LWW increased, but LWP decreased after harvesting for all social classes. The highest RW (Fig. 2A), EWW (Fig. 2B), and LWW (Fig. 2C) were found for dominant trees, followed by co-dominant and suppressed trees, before and after harvesting. However, once harvesting intensity was introduced as a factor for social status, lightly harvested plots showed greater responses than other harvesting intensities for all social classes.

Mean RD decreased from 511 kg/m^3 to 428 kg/m^3 after harvesting (Fig. 3a). RD for control plots remained approximately constant until 2007 and decreased after that. However, RD for partially harvested plots remained analogous until the second year of partial harvesting and then decreased rapidly thereafter. RD varied significantly with harvesting intensity. RD decrease was more evident in the harvested plots for 100 % hardwood removal than in lightly and moderately harvested plots.

Average EWD also decreased after harvesting intensities but at a slower rate than average RD for all treatments. EWD also varied significantly with harvesting intensity (Table 1). In contrast, LWD increased until six years after harvesting and decreased after that. EWD and LWD increased with increasing treatment intensity. However, the differences among intensities were not significant.

Density also varied with social status. Significant variation in RD with harvesting intensity was observed for three social classes. The LSD test (not shown) did not show any significant difference between suppressed and co-dominant or suppressed and dominant classes. Still, it showed differences between co-dominant and dominant social classes. EWD and LWD varied significantly with harvesting intensity for three social classes (Fig. 3b), with consistently higher LWD for the dominant class.

The DMOE increased for all plots after harvesting (Fig. 3c) but did not vary due to harvesting over time. An increasing tendency was found for DMOE for all plots before harvesting, which continued even after harvesting. The highest DMOE was found for control plots, followed by lightly, moderately, and totally harvested plots.

Harvesting intensity did not significantly affect the DMOE across social classes ($p = 0.1135$). The highest mean DMOE was found in suppressed trees in totally harvested plots (Fig. 3d). However, co-dominant trees showed the highest DMOE for all other plots.

The DMOE increased for all plots after harvesting (Fig. 3c) but did not vary due to harvesting over time. An increasing tendency was found for DMOE for all plots before harvesting, which continued even after harvesting. The highest DMOE was found for control plots, followed by lightly, moderately, and totally harvested plots. Harvesting intensity did not significantly affect the DMOE across social classes (Table 1). The highest mean DMOE was found in suppressed trees in totally harvested plots (Fig. 3d). However, co-dominant trees showed the highest DMOE for all other plots.

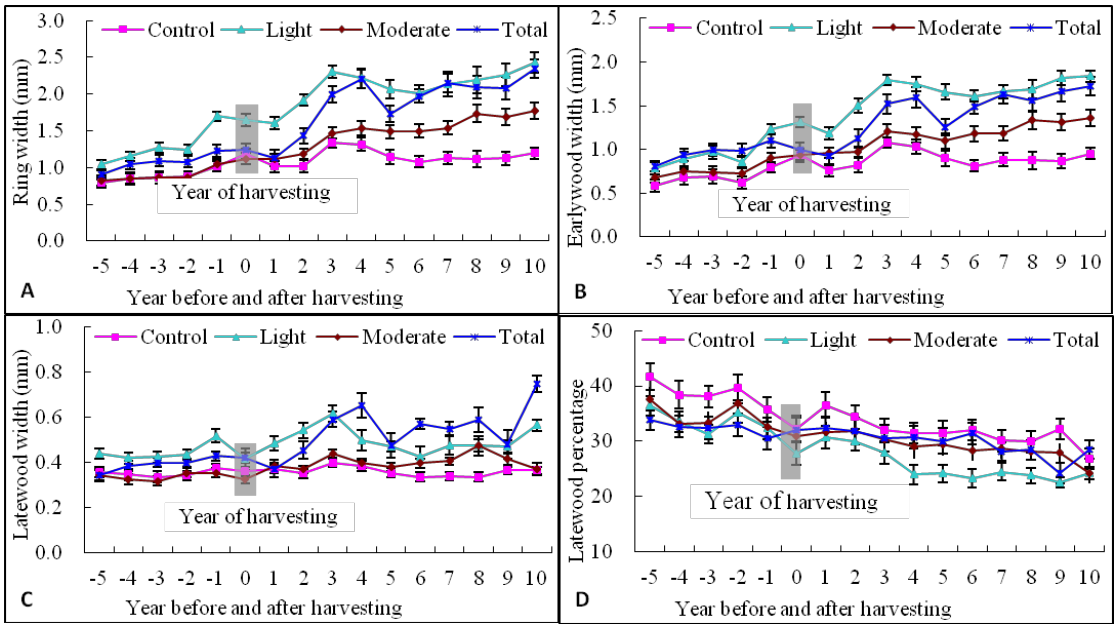

Figure 1. (A) Ring (RW), (B) Earlywood (EWW), (C) Latewood (LWW) widths, and (D) Latewood percentage (LWP) of white spruce with harvesting intensity before and after harvesting.

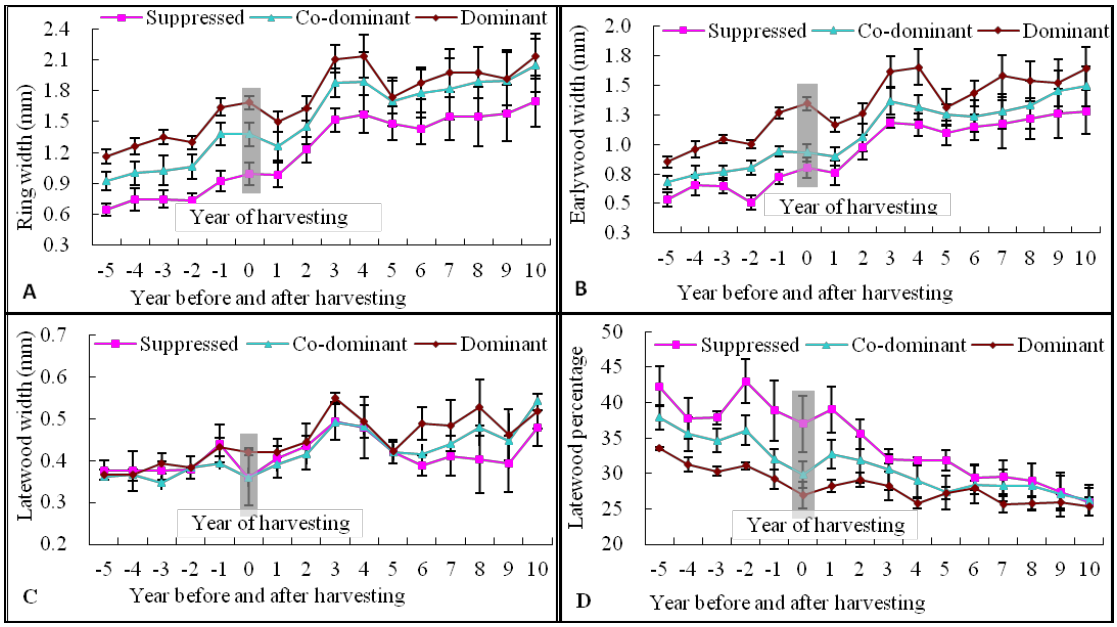

Figure 2. (A) Ring (RW), (B) Earlywood (EWW), (C) Latewood (LWW) widths, and (D) Latewood percentage (LWP) of white spruce for different social classes before and after harvesting.

Discussion

The growth of a tree and its wood properties, especially the mechanical properties, are critical for efficient forest management plans (Proto et al., 2017, Russo et al., 2019). Thus, determining the DMOE of living trees to predict the mechanical properties is important for identifying silvicultural practices' effects on wood quality. In the study, the residual trees showed increased radial growth following harvesting, characterized by a 1-year lag of no response, which agreed with the previous reports (Gagné et al., 2012, Gendreau-Berthiaume et al., 2012). However, there was a steep increase in radial growth after the lag period, as Thorpe and Thomas (2007) reported. The growth rate again decreased as the neighborhood competition increased. Vincent et al. (2009, 2011) reported that commercial thinning (CT) significantly increased the RW of black spruce. In Scots pine, CT increased RW by 40 % (Mörling 2002). In contrast, Gagné et al. (2012) reported that partial harvesting significantly affected the residual stem volume increment for dominant and co-dominant white spruce. In a given stand, dominant and co-dominant trees usually have a higher radial growth rate than suppressed trees, irrespective of stand density and site fertility (Tasissa and Burkhart 1997). Similarly, these dominant and co-dominant trees also show higher absolute thinning responses after moderate or heavy thinning than suppressed trees due to improved growing conditions (Peltola et al., 2007).

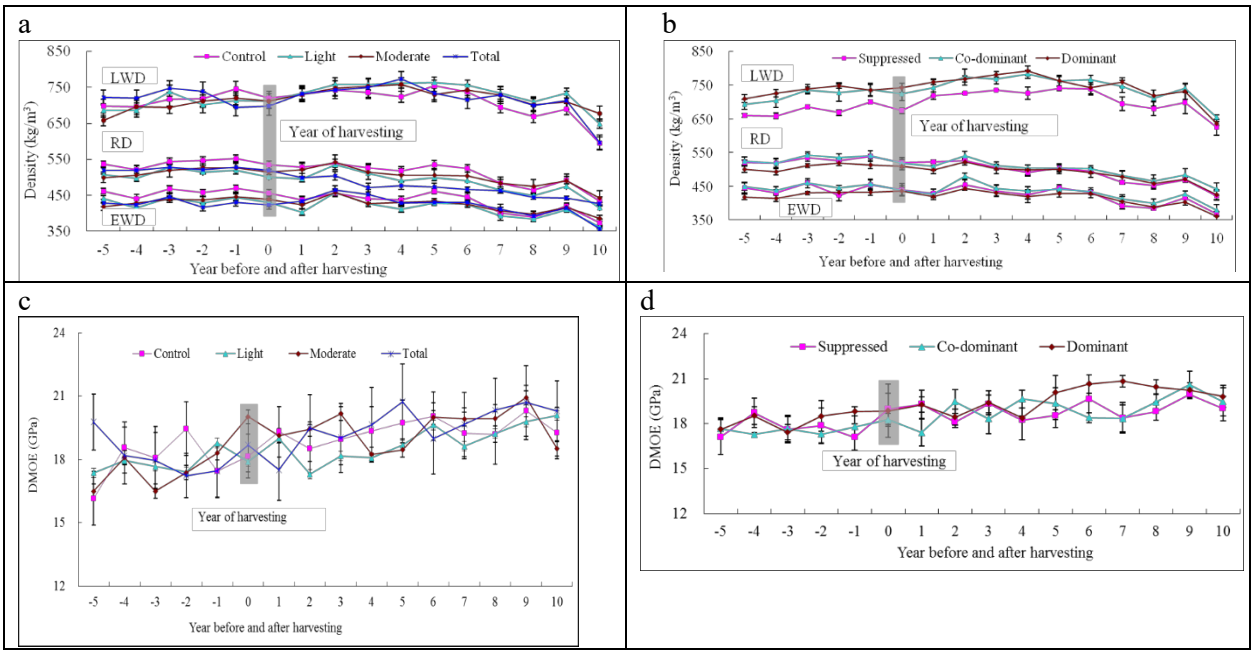

Figure 3. Effect of harvesting intensity and social class on density (RD, EWD, LWD) (a-b); and DMOE (c-d);

RD decreased after harvesting, and this variation was statistically significant for white spruce. Corriveau et al. (1987) also reported that the growth rate was negatively correlated with relative density in white spruce. Several authors have found reduced wood density after thinning and with increasing initial spacing in black spruce (Vincent et al. 2011) and Norway spruce (*Picea abies* (L.) H.Karst.) (Jaakkola et al. 2005). However, partial harvesting did not affect the density of different social classes of young white spruce stands (Gagné et al., 2012).

The average RD decreased significantly after harvesting. However, DMOE increased slightly but continuously after harvesting. Vincent et al. (2011) reported similar results for black spruce where MOE increased, but the variation was not significant due to partial cutting or thinning, although RD increased significantly. The velocity of the ultrasonic wave increased after harvesting, which was the reason for this negative relationship between RD and DMOE. The tracheid length and microfibril angle might vary after harvesting, which might cause this velocity variation of the ultrasonic wave (Hasegawa et al., 2011).

The dynamic MOE reported in the present study was higher than the general static MOE of white spruce, which is related to the testing method. Shan-qing and Feng (2007) studied static and dynamic MOE using three different methods (ultrasonic wave, stress wave, and longitudinal wave propagation) in lodgepole pine (*Pinus contorta* Douglas). They found the highest dynamic MOE using ultrasonic wave propagation.

Conclusion

White spruce showed a significant response to partial harvesting intensities. The response also differed significantly across social classes of stems. The results indicated that RD changed significantly after harvesting without concerning the harvesting intensity of white spruce. Although EWD and LWD varied across partial harvesting treatments, these differences were insignificant. Compared to unharvested controls, radial growth response was greatest in co-dominant stems, and RD varied significantly for this tree class. On the other hand, the change in DMOE was generally gradual and slow, with no significant increase due to partial harvesting. The significant decrease in density indicated that harvesting elicited a

substantial radial growth response on white spruce stems without affecting wood strength. Due to the high variability of biological resources, the impact of harvesting on radial growth, density, and dynamic modulus of elasticity (DMOE) needs to be investigated further to enhance our understanding of the effects of silvicultural treatments on these critical properties of wood quality.

References

Bucur V (2006) Acoustics of wood, 2nd ed. Springer, 2006.

Chave J, Coomes D, Jansen S, Lewis SL, Swenson NG, Zanne AE (2009) Towards a worldwide wood economics spectrum. Ecology Letters 12:351–366.

Comeau PG, Kabzems R, McClarnon J, Heineman JL (2005) Implications of selected approaches for regenerating and managing western boreal mixedwoods. Forestry Chronicle 81(4):559-574.

Corriveau A, Beaulieu J, Mothe F (1987) Wood density of natural white spruce populations in Quebec. Can J For Res 17:675-682.

Divós F, Tanaka T (2005) Relation between static and dynamic modulus of elasticity of wood. Acta Silv. Lign. Hung 1:105-110.

Gagné L, Lavoie L, Binot JM (2012) Croissance et proprietes mecaniques du bois apres eclaircie commerciale dans une plantation d'epinette blanche (*Picea glauca*) agee de 32 ans (in French). Can J For Res 42:291-302.

Gendreau-Berthiaume B, Kneeshaw DD, Harvey BD (2012) Effects of partial cutting and partial disturbance by wind and insects on stand composition, structure, and growth in boreal mixedwoods. Forestry 85(4):551-565.

Goudiaby V, Brais S, Berninger F, Schneider R (2012) Vertical patterns in specific volume increment along stems of dominant jack pine (*Pinus banksiana*) and black spruce (*Picea mariana*) after thinning. Can J For Res 42, 733-748.

Government of Canada. 2016. Canadian climate normals 1981–2010. Government of Canada, Ottawa, Ont.

Gradowski T, Lieffers VJ, Landhäusser SM, Sidders D, Volney J, Spence JR (2010) Regeneration of Populus nine years after variable retention harvest in boreal mixedwood forests. Forest Ecol Mgt 259:383–389.

Hasegawa M, Takata M, Matsumura J, Oda K (2011) Effect of wood properties on within-tree variation in ultrasonic wave velocity in softwood. Ultrasonics 51(3):296-302.

Jaakkola T, Mäkinen H, Saranpää P (2005) Wood density in Norway spruce. changes with thinning intensity and tree age. Can J For Res 35:1767–1778

Jozsa LA, Middleton GR (1994) A discussion of wood quality attributes and their practical implications. Special Publication No. SP-34, Forintek Canada Corp., Western Laboratory, Vancouver, B.C.

Kharrat W, Koubaa A, Khlif M, Bradai C (2019) Intra-Ring Wood Density and Dynamic Modulus of Elasticity Profiles for Black Spruce and Jack Pine from X-Ray Densitometry and Ultrasonic Wave Velocity Measurement. Forests 10(7):569.

Mörling T (2002) Evaluation of annual ring width and ring density development following fertilisation and thinning of Scots pine. Ann For Sci 59:29–40

Mvolo CS, Stewart JD, Koubaa, A (2021) Comparison between static modulus of elasticity, non-destructive testing moduli of elasticity and stress-wave speed in white spruce and lodgepole pine wood. Wood Material Sci & Engineering DOI: 10.1080/17480272.2021.1871949

Nicholas NS, Gregoire TG, Zedaker SM (1991) The reliability of tree crown position classification. Can J For Res 21:698-701.

Panshin AJ, de Zeeuw C (1970) Textbook of wood technology: structure, identification, properties, and uses of the commercial woods of the United States and Canada, McGraw-Hill series in forest resources. Mcgraw-Hill College, USA.

Panshin AJ, De Zeeuw C (1980) Textbook of Wood Technology; McGraw-Hill Book Co: New York, NY, USA, p. 772.

Peltola H, Kilpeläinen A, Sauvala K, Räisänen T, Ikonen VP (2007) Effects of early thinning regime and tree status on the radial growth and wood density of Scots pine. Silva Fennica 41(3):489–505.

Proto AR, Macri G, Bernardini V, Russo D, Zimbalatti G (2017) Acoustic evaluation of wood quality with a non-destructive method in standing trees: A first survey in Italy. IForest 10, 700–706.

Russo D, Marziliano PA, Macri G, Proto AR, Zimbalatti G, Lambardi F (2019) Does Thinning Intensity Affect Wood Quality? An Analysis of Calabrian Pine in Southern Italy Using a Non-Destructive Acoustic Method. Forests 10: 303.

Saucier JP, Bergeron JF, Grondin P, Robitaille A (1998) Les regions écologiques du uébec méridional. Third version. L'Aubelle 124:S1–S12.

Shan-qing L, Feng FU (2007) Comparative study on three dynamic modulus of elasticity and static modulus of elasticity for Lodgepole pine lumber. J For Res 18(4):309–312.

Tasissa G, Burkhart HE (1997) Modelling thinning effects on ring width distribution in loblolly pine (*Pinus taeda*). Can J For Res 27:1291–1301.

Thorpe HC, Thomas SC (2007) Partial harvesting in the Canadian boreal: success will depend on stand dynamic responses. Forestry Chronicle 83:319-325.

Vincent M, Krause C, Koubaa A (2011) Variation in black spruce (*Picea mariana* (Mill) BSP) wood quality after thinning. Annals For Sci 68:1115-1125.

Vincent M, Krause C, Zhang S (2009) Radial growth response of black spruce roots and stems to commercial thinning in boreal forest. Forestry 82:557-571.

Zhang, SY, Koubaa, A (2008). Softwoods of Eastern Canada: Their silvics characteristics, manufacturing, and end-uses. Special Publication SP-526E, FPInnovations, Forintek.

Effect of Silvicultural Practices on Basic Wood Density of Sugar Maple in Lake States Region

Chinmoyee Das
College of Forest Resources and Environmental Science, Michigan Technological University, Houghton, Michigan, USA, cdas2@mtu.edu

Peng Quan
College of Forest Resources and Environmental Science, Michigan Technological University, Houghton, Michigan, USA, pengq@mtu.edu

Xinfeng Xie *
College of Forest Resources and Environmental Science, Michigan Technological University, Houghton, Michigan, USA, xinfengx@mtu.edu

Yvette Dickinson
Scion (New Zealand Forest Research Institute), Rotorua, New Zealand, yvette.dickinson@scionresearch.com

Xiping Wang
Forest Products Laboratory, USDA Forest Service, Madison, Wisconsin, USA, xiping.wang@usda.gov

Robert J. Ross
Forest Products Laboratory, USDA Forest Service, Madison, Wisconsin, USA, robert.j.ross@usda.gov

Christel C. Kern
Northern Research Station, USDA Forest Service, Rhinelander, Wisconsin, USA, christel.c.kern@usda.gov

* Corresponding author

Abstract

The quality of wood in a tree is a critical factor in determining its engineering applications. Silvicultural practices and growing environment are known important factors influcencing wood quality. While much research has been done on softwood species on that regard, there is a knowledge gap for hardwoods between silvicultural practices and wood properties. The goal of this study was to elucidate the effects of silvicultural treatments on the basic density of hardwoods grown in Lake States region. We investigated the basic wood density of sugar maple in an existing long-term silvicultural trial at the Dukes Experimental Forest in northern Michigan, USA. The silvicultural treatments included clear-cut, 30cm diameter limit cut, 55cm diameter limit cut, group selection, 70% stocking cut with 17cm diameter limit, single tree selection cut, and an old-growth as the control. A total of 105 increment cores were extracted from the sampled trees and studied using SilviScan. The data of each growth ring were averaged for each core sample based on the ring area (ring area weighted average). The results showed that the clear cut (CC) and diameter limit 12 inch treatment could be relatively effective approaches to affecting the basic density of annual rings in sugar maple wood.

Keywords: increment cores, northern hardwood, nondestructive testing, silvicultural treatment, SilviScan, specific gravity.

Introduction

Wood quality is an important factor that determines the end use and value of wood products.[1] Thus, researchers have been seeking for effective ways to improve the wood quality. Silvicultural practices, such as regeneration methods and density management, are one type of the approaches to regulate wood quality.[2,3] Regeneration methods are long-term, stand-scale forest management plans to create a new group of trees in the stand. The regeneration methods can be classified into three categories based on the distribution of age classes present in a forest stand over the long-term, including even-aged (e.g., clearcut, shelterwood and seedtree system), multi-aged and uneven-aged (e.g., single tree and group selection) regeneration methods.[2] The effects of regeneration methods on tree form and wood grades have been studied previously. For example, the impacts of partial cutting techniques on the quality of sugar maple and yellow birch were investigated, and it was concluded that removing more trees during harvests could enable the residual trees to grow more epicormic branches.[4]

In addition to the regeneration methods, the effects of tree density management, usually involving planting spacing and thinning, on the tree form and wood properties were studied as well. Previous investigations found that decreasing tree density by thinning likely would increase the crown depth, size and density of knots, and proportion of tension wood.[3] As a result, the engineering properties of wood could be negtively impacted by the tree density management. It was also found that the type and severity of thinning may influence the log quality after partial cutting.[5] However, less attention was paid to the direct effects of silvicultural practice on the physical and mechanical perties of wood that is crucial for processing and utilization of the mateiral. Moreover, it should be noted that the regulation level of different silvicultural practices on the wood quality may be variable within wood species and among locations.[2]

The hardwoods growing in the North American Great Lakes Region have received less attention in terms of the effect of silvicultural treatments on their basic density.[5] The goal of this study was to elucidate the effects of silvicultural treatments on the basic density of hardwoods grown in Lake States region.

Experiments

Data collection

The sugar maple trees in an existing long-term silvicultural trial at the Dukes Experimental Forest in northern Michigan, USA were sampled for this study. The silvicultural treatments included clear-cut and thinning, 30cm diameter limit cut (DL12), 55cm diameter limit cut (DL22), group selection, 70% stocking cut with 17cm diameter limit, single tree selection cut, and an old-growth as the control. A total of 15 trees were selected from each treatment and the control stand and one increment core was taken from each tree. A total of 105 increment cores were collected and prepared for data collection using SilviScan, where the wood density of each growth ring were measured. The harvest times of each treatment were found in previous publications and records.[4,6,7,8]

Statistical analysis

The samples dating from 1927 to 2018 were divided into 5-year groups. Treatments include clear cut and thinning, DL22, Single tree selection, Group selection and 70% selection had wood harvesting done in certain years, these years were taken as reference points and statistical analysis was done for a set of 20 years including the reference/year of harvest, 10 years preceding and 10 years succeeding the year of harvest. While grouping the data the year of harvest was selected as the end of growing season. In order to maintain this throughout the study, in some cases the grouping of data is done with 4 or 6 years instead of 5. Similar approach was taken to analyze the data for the control samples as well. There are two parts in the statistical analysis: (1) the weighted mean of those data based on the annual ring area of the samples in each year; (2) analysis of variance ($\alpha = 0.05$) for the different treated sample groups using SPSS software. The

objective of the first part is to disclose the variation of the basic density of wood treated by different silvicultural strategies within the investigated years. The second part is aimed at demonstrating the significance of different silvicultural methods on the variation of the basic density compared to the control samples.

Results and Discussion

1. Clear cut (CC)

The basic wood densities of the annual rings of sugar maple for clear-cut (CC) treatment and control are shown in Figure 1. The basic densities of annual rings in maple wood were determined after the implemetation of CC treatment. After the CC treatment, the samples were then subjected to thinning in 2008 that was taken as the reference year here, and the effect of thinning treatment on wood density was investigated in 5 years within two groups before and after the reference year. More specifically, the basic wood densities of annual rings in CC treated maple appeared to be higher than that those in the control wood, indicating that CC treatment could increase the wood density of the annual rings in sugar maple. Among the CC treated maple wood, the average basic wood density value gradually decreased from 786.15 kg/m^3 of 1999-2003 group to 753.65 kg/m^3 of 2014-2018 group, and such variance was statistical significant (p value < 0.05). This reuslt suggests that the thinning treatement might not change the decreasing trend of basic wood density with increasing growth season in last 20 years.

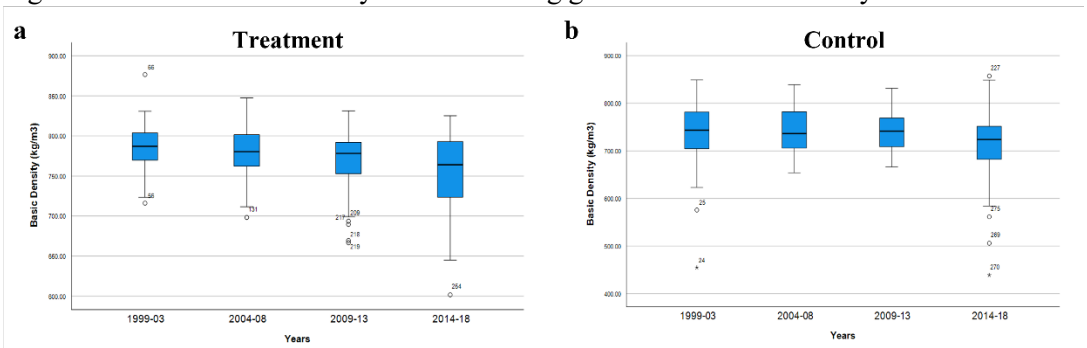

Figure 1. Basic wood density of sugar maple for last 20 years 1999-2018 with reference year 2008.

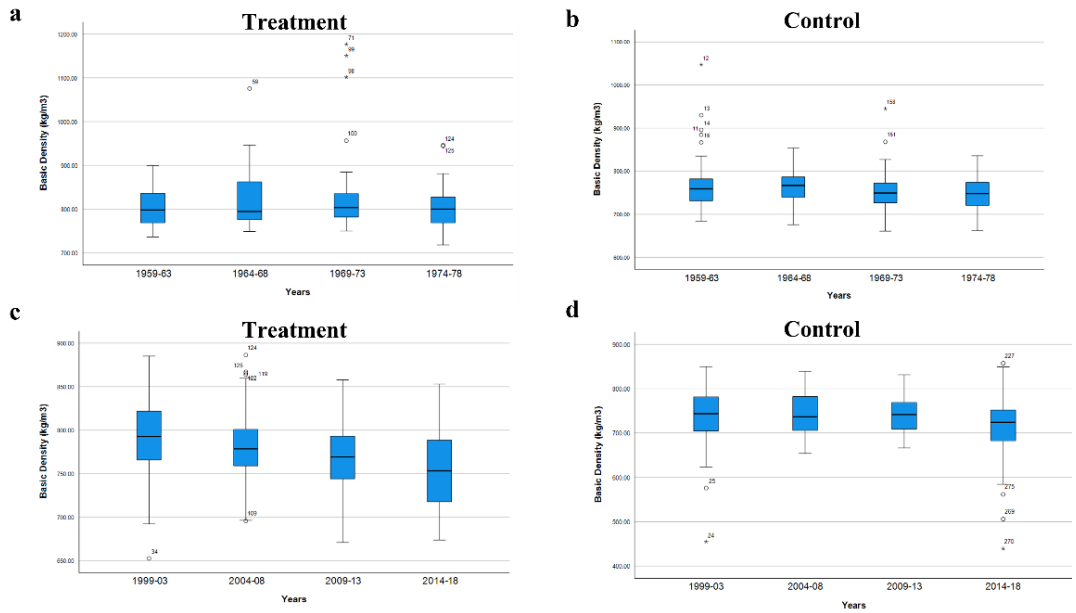

Figure 2. Basic wood density of sugar maple subject to treatment DL12.

2. 30cm diameter limit cut (DL12)

The basic wood densities of the annual rings of dugar maple for DL12 treatment and control are shown in Figure 2. In DL12 treatment, the wood were harvested in 1927, but most of the wood were younger than in 1950s. Hence, the analysis was done starting year 1959. The analysis was done for the first 20 years and the last 20 years as no other harvesting was done during the treatment period. In the first set of 20 years, the basic densities of the annual rings in maple wood after DL 12 treatment seems to be similar to that in control wood (Figure 2a and b). Moreover, the p value > 0.05 was obtained in terms of the basic density of DL 12 treated wood, suggesting that the variance among each 5-year group of treated maple wood was insignificant. In the last 20 years, the basic densities of annual rings in the DL 12 treated maple wood showed a decreasing trend (Figure 2c), and a significant difference (P value < 0.05) was observed btween 1999-03, 2014-2018, 2004-08, and 2014-18 annual rings. However, the basic densities of annual rings in control wood fluctuated with the increasing growth season in the last 20 years (Figure 2d). These results implied that the DL 12 treatment had negative impact on the basic density of maple wood in last 20 years but not affact them in the first 20 years.

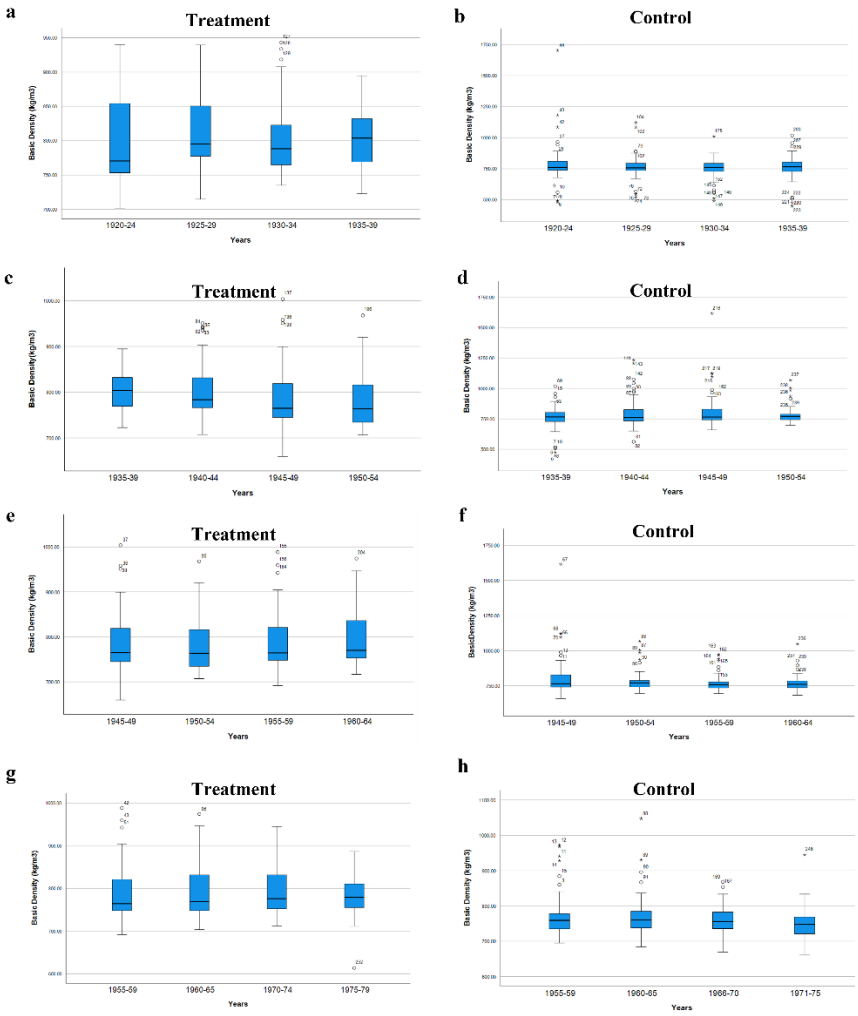

Figure 3. Basic density of maple wood samples subjected to treatment group selection.

3. Group Selection

The group selection treatment was implemented on sugar maple trees and the trees were harvested in the years 1929, 1944, 1954, and 1965, respectively. Figure 3 shows the basic density of annual rings in group selection treatment and control sugar maple wood. As shown in Figure 3b, d, f, and h, the basic densities

of annual rings in the control maple wood fluctuated with the increasing growth season regardless of growth periods. As for the group selection treated wood harvested in 1929 (Figure 3a), the basic densities of annual rings increased before the harvesting time. After the harvesting, the basic densities decreased in the first 5-years annual rings and then increased in the second 5-years annual rings. However, such variances were statistically insignificant as p value was greater than 0.05. Moreover, a reduction trend of basic density of annual rings was found with the progressing growth season of the sugar maple wood treated by the group selection in 1944 (Figure 3c), while the change in this case was not statistically significant as well (p value > 0.05). In contrast, the wood treated in 1954 tended to present a increase in the basic density of annual rings with the increasing growth season (Figure 3e). There was no significant effect of treatment on these samples as well (p value > 0.05). For the wood treated in 1965 (Figure 3g), the basic densities of annual rings appeared to increase in the investigated growth period. No significant effect of treatment was seen as indicated by p value greater than 0.05. These results demonstrated that the effect of group selection treatment on the basic density of annual rings in sugar maple wood was insignificant.

4. Single Tree Selection

The single tree selection (STS) treatment was implemented on the experimental plot in the years of 1927, 1953, and 1962, respectively. As shown in Figure 4b, d, and f, the maximum, median, and minimum basic densities of the annual rings in control maple wood slightly fluctuated within different investigated growth periods. In contrast, STS treated maple wood showed either a increase, decrease or fluctuation in basic densities of annual rings within the investigated growth periods (Figure 4a, c, and e). No significant treatment effect (p value > 0.05) was observed on the basic density of the 4 annual ring groups in 1918-1937 and 1954-1972, respectively, but a significant treatment effect (p value < 0.05) was observed on the basic density of 4 annual ring groups in 1945-1962. Overall, these results indicated that the effect of single tree selection treatment on the basic density of maple wood was insignificant.

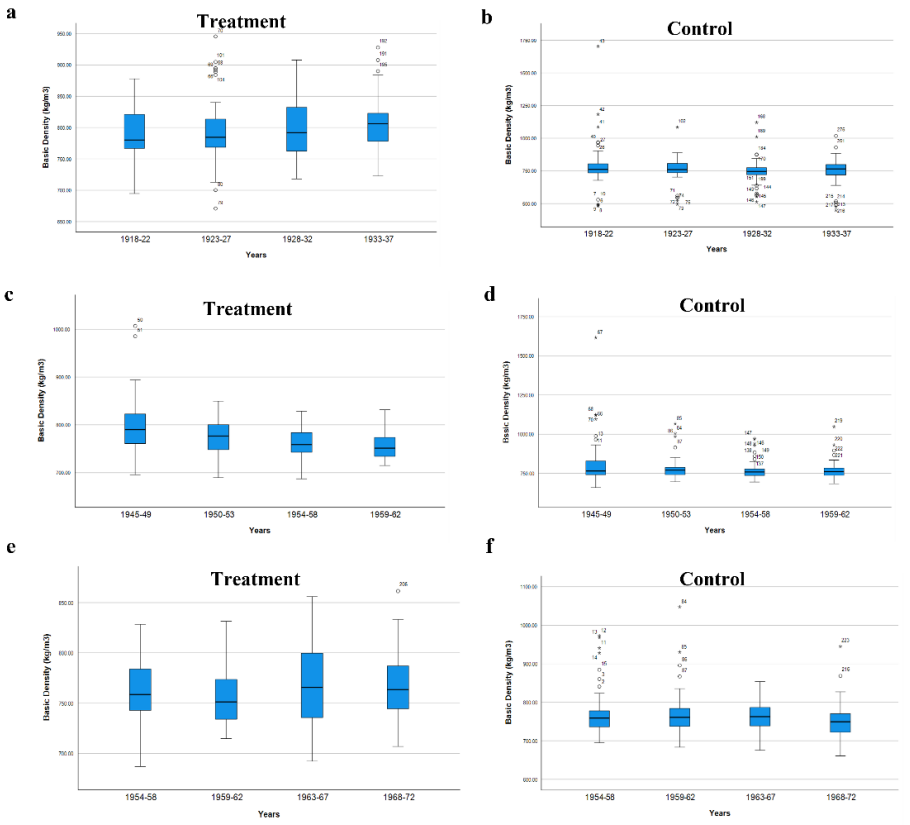

Figure 4. Basic density of maple wood samples subjected to treatment single tree selection.

5. 70% Selection

Figure 5 shows the basic density of annual rings of control and 70%-selection treated sugar maple wood. For the treated samples, 70% selection was conducted on sugar maple trees in the years of 1952 and 1962, respectively. As shown in Figure 5a, increases in the basic densities were observed in the 1953-58 annual rings after the treatment was implemented. However, such variances in the basic densities of sugar maple wood were statistically insignificant ($P > 0.05$). Moreover, the basic densities in 1963-67 and 1968-72 annual rings appeared to decline after the 70% selection treatment in 1962 (Figure 5c), but these reductions were statistically insignificant as well ($P > 0.05$). In contrary to the treated wood samples, the control samples showed slight fluctuations in the basic densities of annual rings within the investigated growth periods. These results suggest that 70%-selection treatment had an insignificant effect on the basic densities of sugar maple wood.

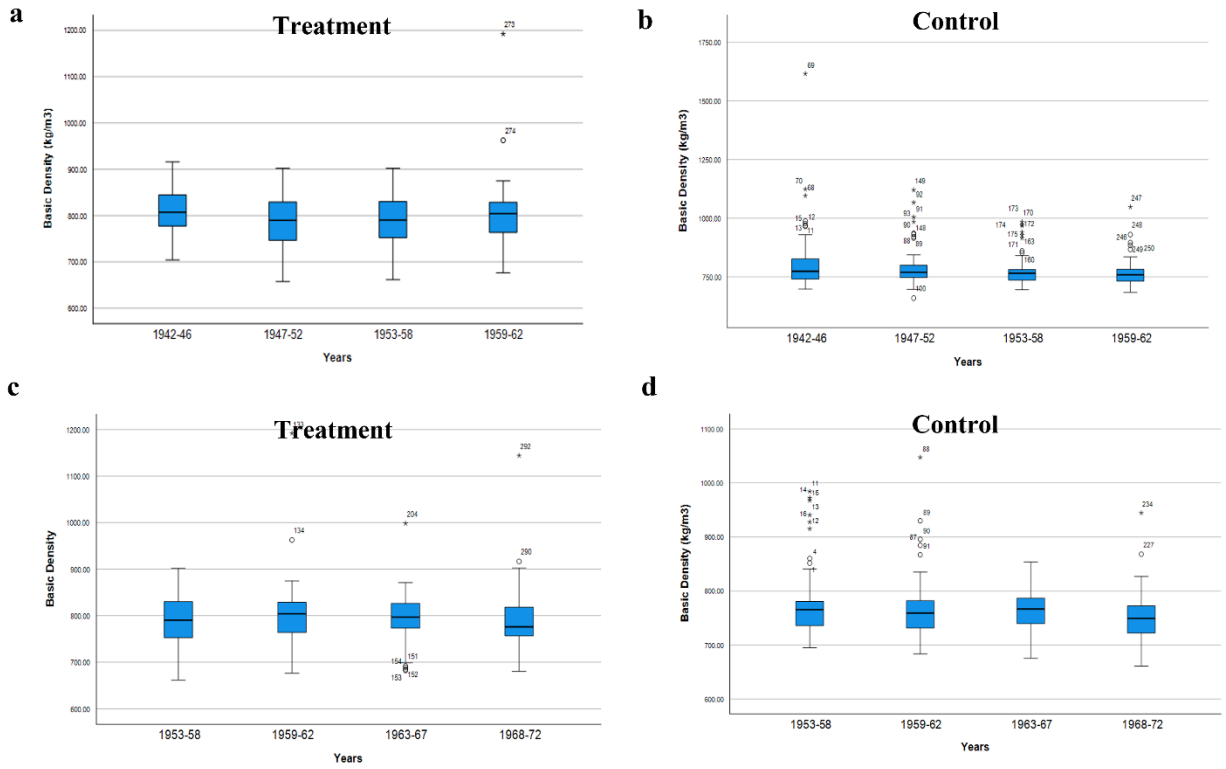

Figure 5. Basic density of maple wood samples subjected to treatment 70% selection.

6. 55cm diameter limit cut (DL22)

Figure 6 shows the basic density of annual rings in control and DL 22 treated sugar maple wood. The DL22 treatment was carried out on sugar maple trees in 1942, 1953, and 1962 years, respectively. As shown in Figure 6a, the basic densities of the 1944-48 annual rings seems to be higher than that 1939-43 annual rings. The treatment effect was seen to be significant as p value was determined to be lower than 0.05. Moreover, there was increase in the basic densities of the 1954-58 annual rings compared with that of 1949-53 annual rings (Figure 6c), while a slight reduction was found in the basic densities of the 1963-67 annual rings in comparison to that of 1959-62 annual rings (Figure 6e). However, these variations were statistically insignificant as their P values were higher than 0.05. It should be noted that overall the basic densities of annual rings in treated wood showed fluctuating trends which were also observed in that in control wood (Figure 6b, d, and f), further indicating that the variances of basic densities may not be caused by the DL 22 treatment.

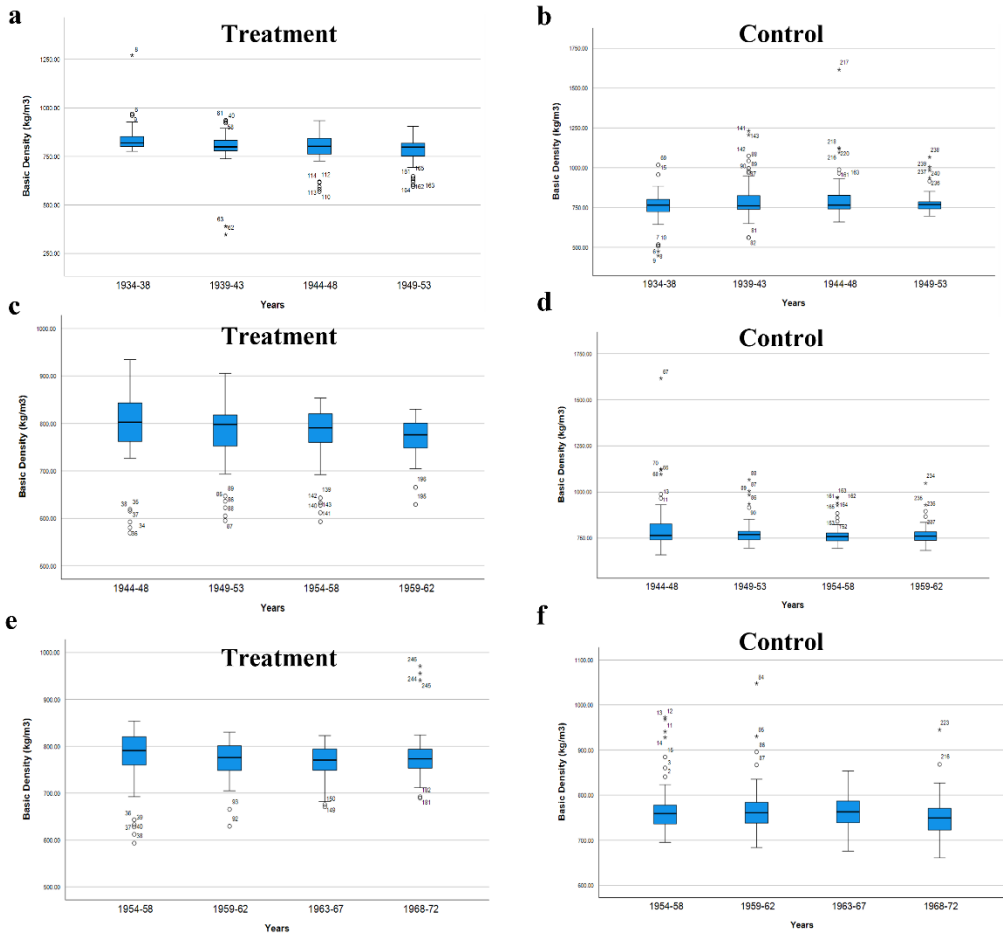

Figure 6. Basic density of maple wood samples subjected to treatment DL22.

Conclusion

The effects of six silvicultural treatments namely clear cut, group selection, 30cm diameter limit cut, 50cm diameter limit cut, group selection, and 70% selection were studied on the basic density of annual rings in sugar maple wood in Lake States Region. Among all the treatments, the clear cut (CC) and 30cm diameter limit cut treatment could be relatively effective approaches to affect the basic density of annual rings in sugar maple. More specifically, the CC treatment could improve the basic density of sugar maple, and the DL 12 treatment had negative impact on the basic density of sugar maple in last 20 years but did not affact them in the first 20 years.

Acknowledgements

This study was conducted through a cooperative research agreement (17-JV-11111133-018) between Michigan Technological University and USDA Forest Service and was partially funded by USDA Forest Service, Forest Products Laboratory and Northern Research Station.

References

[1] Ross, Robert J., and John R. Erickson. *Undervalued hardwoods for engineered materials and components*. Forest Products Society, 2005.

[2] Dickinson, Yvette, Xiping Wang, Jan Wiedenbeck, and Robert J. Ross. "Effects of Silvicultural Practices on Engineering Properties of Northern Hardwood Species of the Great Lakes Region." (2019).

[3] Zobel, Bruce J., and Johannes P. Van Buijtenen. *Wood variation: its causes and control*. Springer Science & Business Media, 2012.

[4] Eyre, Francis Howlett, and Walter Morrison Zillgitt. *Partial cuttings in northern hardwoods of the Lake States: Twenty-year experimental results*. No. 1076. The Department, 1953.

[5] Tubbs, C.H. 1977. Manager's handbook for northern hardwoods in the north-central states. Gen. Tech. Rep. NC-39. St. Paul, MN: U.S. Department of Agriculture, Forest Service, North Central Forest Experiment Station.

[6] Woods, Kerry and Christel C. Kern. Intermediate distrubances drive long-term fluctuation in old-growth forest biomass: na 840yr temperate forest record. Ecosphere, 2022 13(1)

[7] Kenefic, Laura S. and Christel C. Kern. The Remarkable Story of the Partial Cutting Study at the Dukes Experimental Forest. In Long-Term Silvicultural & Ecological Studies. Results for Science and Management: Volume 2. Ed. Ann E. Camp, Lloyd C. Irland, Charles J.W. Carroll. Yale University, 2013.

[8] Kenefic, Laura S. and Christel C. Kern. Early Northern Hardwood Silvicultural Research at the Duke Experimental Forest, Michigan. J. For. 2015 1113(2):258-261.

Differentiation of Eucalyptus Clone Seedlings by Nondestructive Tests and Machine Learning Methods

Rafael Gustavo Mansini Lorensani*
Valora Madeira Ltda – Campinas, São Paulo, Brazil, rafael@valoramadeira.com

Cinthya Bertoldo Pedroso
Laboratory of Nondestructive Testing – LabEND, College of Agricultural Engineering – FEAGRI – UNICAMP, Campinas, São Paulo, Brazil, cinthyab@unicamp.br

Raquel Gonçalves
Laboratory of Nondestructive Testing – LabEND, College of Agricultural Engineering – FEAGRI – UNICAMP, Campinas, São Paulo, Brazil, raquelg@unicamp.br

Isabela Constantino de Toledo
Laboratory of Nondestructive Testing – LabEND, College of Agricultural Engineering – FEAGRI – UNICAMP, Campinas, São Paulo, Brazil, i218077@dac.unicamp.br

Abstract

The correct management of raw materials in the pulp and paper industry impacts the resources to be used at each stage of the production chain, since edaphoclimatic factors and the inherent characteristics of each clone interfere in the final quality of the wood produced. Genetic tests to identify clones in cases of accidental mixing of clonal batches has been shown to be time-consuming, laborious and costly, but they are the means most used by wood modification companies today. Therefore, this research seeks to use results obtained from non-destructive tests applied to eucalyptus clone seedlings in the evaluation of several machine learning algorithms in order to act in the classification of eucalyptus clones. For this research, 28 eucalyptus clones, from a pulp and paper company, were evaluated according to their total height, base diameter, age and ultrasonic pulse propagation velocity using 7 machine learning algorithms (K-Nearest Neighbor, Decision Tree, Random Forest, Gradient Boosting, Xtreme Gradient Boosting, Superior Vector Machine and Neural Networks). All classification algorithms went through the hyperparameter optimization process and the classification resulting from each one of them was evaluated using the accuracy, precision, sensitivity and f1-score metrics. The Decision Tree algorithm was the one that presented all metrics above 79%, demonstrating the potential of using machine learning algorithms together with non-destructive tests in the classification of eucalyptus clones still in the seedling stage.

Keywords: machine learning, seedling, ultrasound.

Introduction

The prediction of properties of interest of the raw material used by the wood processing industries is shown to be an important management tool, as it impacts within the production cycle, the resources used as a whole, from the inputs used in nurseries and gardens, to the used in wood processing methods.

Previous results from the Research Group on Non-Destructive Testing of the Faculty of Agricultural Engineering (FEAGRI) evaluated the separation of clones by stiffness (Gonçalves et al. 2013) using ultrasound tests on trees, and the inference of wood properties from tests in seedlings (Gonçalves et al. 2018, Gonçalves et al. 2019). The results of the research developed by these authors, as well as most research on this subject, are evaluated only based on classical statistics.

Classical statistics, like any other analytical method, has advantages and limitations in understanding how the parameters analyzed evolve, as well as how they relate to each other.

Data mining techniques also have advantages and disadvantages, however, as they have in their libraries, tools capable of generating analyzes different from those generated by classical statistics, they allow the evaluation of parameters from new perspectives (Plas, 2016 and Guido et al. 2016).

Data Mining Methods

Basically, data mining methods are divided into two types: regression and classification methods. In regression models, we fit curves and/or surfaces to our data in order to obtain mathematical models that reproduce and represent the behavior of the data. In the classification models, we evaluate the variables in order to classify them into pre-established classes, according to known parameters.

Whether a regression model or a classification model, they all have a feature in common, which are the hyperparameters, which are nothing more than configurations, intrinsic to the models, that allow us to change the behavior, and consequently, the response time and its results. These hyperparameters can be the number of neighbors analyzed around each data, the number of decision trees calculated, the number of neurons in a network, the depth of a decision tree, among others.

Next, we describe the algorithms used in this research.

K-Nearest Neighbor (KNN)

The objective of this model is to classify the evaluated variables based on the class of their nearest neighbor. Most of the time it is more useful to take into account multiple neighbors, hence the name K-Nearest. Unlike some models, KNN does not present itself as a black box, being easy to interpret and configure, since it depends on few hyperparameters. (Cunningham and Delany, 2021; Zhang, 2016).

Decision Tree

A decision tree classifies the data of a set through a series of questions about the attributes contained in the database. Each question is contained in a “node” and is derived from “child nodes” for each possible answer to the question. The questions then form a hierarchy, encoded as an inverted tree. An item is classified according to a class following the path from the top node, the root, to a childless node, a leaf, according to the answers that apply to the data under consideration. A datum is assigned to the class that was associated with the leaf it hits (Kingsford and Salzberg, 2008; Ali et al, 2012).

Random Forest, Gradient Boosting, Xtreme Gradient Boosting

Often, when talking about data modeling, one thinks of building just a single strong predictive model. However, you can build a set of models for a specific learning task, using simpler models that do not use all the data in the set or that are generated sequentially, learning from the predecessor's mistakes.

In the case of Random Forest, numerous decision trees are generated, each using different variables, and for the final prediction, all results are evaluated and compiled into a global result. (Ali et al, 2012).

The Gradient Boosting technique is based on shallow decision trees with few nodes, which are generated not in parallel like Random Forest, but sequentially, also using a modified version of the original dataset. (Natekin and Knoll, 2013).

Xtreme Gradient Boosting is an improved version of Gradien Boosting, since for each generated model an error value associated with that model is computed. This technique aims to minimize this error without increasing bias, which would lead to overfitting, a model that performs very well with training data, but when confronted with new data does not present a satisfactory behavior (Chen and Guestrin, 2016).

Support Vector Machine

The Support Vector Machine technique works at the limits of data sets, at the interface between groups of data that are different from each other, in order to maximize the margin of separation of the different classes of data. For that, the model is able to make changes to the data, even changing the Cartesian planes that contain them, in order to find lines and/or surfaces that can separate the different classes of the database (Lorena and De Carvalho, 2007).

Redes Neurais

Neural networks are adaptive artificial systems, inspired by the processes that rule the functioning of the human brain. The elements that make up a neural network are nodes and connections. Each node has its own input, from which it receives communications from other nodes or data input; and its own output, which communicates with other nodes or with the final response. Each node has an activation function and each connection receives different weights. They generally have robustness in terms of data noise and a high capacity for generalization, but their training tends to be time consuming and synaptic weights do not accept interpretation (Grossi and Buscema, 2007).

Therefore, this research seeks to use results obtained from non-destructive tests applied to eucalyptus clone seedlings in the evaluation of several machine learning algorithms in order to act in the classification of eucalyptus clones.

Materials and Methods

During the research, results obtained from 28 clones, with different ages and planted in different locations in the state of São Paulo, were evaluated.

The clones were tested with ultrasound equipment (USlab, Agricef, Brazil - Figure 1a) and exponential transducers, whose tips were adapted during a doctoral research carried out by the research group. The adaptation was made to allow testing on the reduced size seedlings (Figure 1b). By means of the ultrasound test on seedlings of eucalyptus clones, it was possible to obtain the wave propagation time in each specimen (Figure 2a).

The height to the first bifurcation (h1), the total height (ht) and the diameters at the base (ground support - d1), at the central point of the stem (d2) and at the first fork (d2) were also measured in the trees. d3) (Figure 2b).

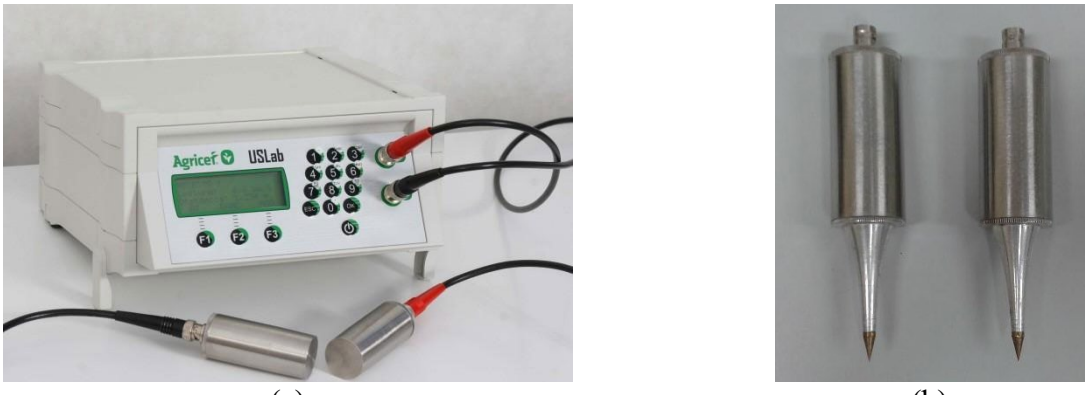

(a) (b)

Figure 1. Ultrasound equipment (a) and exponential transducers with modified tip to adapt to tests on small seedlings (b)

Figure 2. Dimensions obtained from the plant (a) and scheme of the ultrasound test performed on the clones (b)

All data were evaluated using data mining techniques, using the following algorithms: K-Nearest Neighbor (KNN), Decision Tree, Random Forest, Gradient Boosting, Xtreme Gradient Boosting, Superior Vector Machine and Neural Networks. Since this is an ongoing research, with data from a company, the code cannot be disclosed.

All data mining methods were set up according to Plas (2016) and Wes (2017) regarding the configuration of hyperparameters. Individual adjustments were made, model by model, to avoid overfitting or overfitting. Overfitting occurs when a model fits the training data very well, but is unable to predict new data. Underfitting occurs when the model cannot find relationships between the variables available in the training set and therefore the process is interrupted, even before confronting the test set.

To evaluate the data mining methods we used the confusion matrix (Table 1) and the concepts of accuracy, precision, sensitivity and F1-score.

Table 1. Example of a confusion matrix.

		PREDICTED	
		YES	**NO**
REAL	**YES**	True Positive (TP)	False Negative (FN)
	NO	False Positive (FP)	True Negative (TN)

The errors that we can have in models, as well as the successes are characterized as:

True Positives: correct classification of the Positive class;

False Negatives (Type II Error): error in which the model predicted the Negative class when the real value was Positive class;

False Positives (Type I Error): error in which the model predicted the Positive class when the real value was Negative class;

True Negatives: Correct classification of the Negative class.
After the model finishes classifying all inputs, the errors are counted and then it is possible to calculate metrics to evaluate it.

Accuracy (1): It represents the general performance of the model, showing among all the evaluations, which the model was right.

$$AC = \frac{TP + TN}{TP + TN + FP + FN} \quad (1)$$

Precision (2): Evaluating all positive ratings, how many are positive.

$$PR = \frac{TP}{TP + FP} \quad (2)$$

Recall (3): Among all the evaluations taken in the predicted values for the positive ratings, how many are correct.

$$RE = \frac{TP}{TP + FN} \quad (3)$$

F1-Score (4): Harmonic average between Precision and Sensitivity.

$$\mathrm{F1} = \frac{2 * \mathrm{PR} * \mathrm{RE}}{\mathrm{PR} + \mathrm{RE}} \quad (4)$$

Results

Since not all clones had the same structural configuration, some variables present gaps, as the age variation caused the lack of a more defined crown, therefore, the analyzed variables were: ultrasonic pulse propagation speed (v), diameter of ground fixing (db), total height (ht) and age (Table 2).

Table 2. Name (Clone), amount, mean ultrasonic pulse velocity (VM), mean base diameter (dbM) and mean total height (htM), with respective coefficients of variation (CV), and clone ages.

Clone	Amount	VM [m.s-1]	CV [%]	dbM [mm]	CV [%]	htM [cm]	CV [%]	Age [months]
AEC144	60	1721,1	2,30%	5,8	3,83%	22,9	2,53%	8/10/11
ARA6084	60	1168,0	3,39%	7,8	2,85%	24,5	2,37%	11/49
BA7346	90	1448,0	2,23%	6,8	2,64%	22,7	2,08%	13/14/15/16/17
CC05JAC	30	1397,5	4,00%	7,5	4,19%	20,0	4,09%	25
CC05JAC - 6825	90	1323,6	2,44%	7,0	2,58%	21,5	2,19%	15/67
CCJ05JAC	60	1295,8	3,05%	5,4	4,07%	18,5	3,12%	7/10
CCJ05JAC - MJ	30	1257,4	4,45%	8,9	3,51%	28,3	2,89%	67
FJ367	90	1169,8	2,76%	5,3	3,40%	20,3	2,32%	5/7/9/10/12/15
FJ460	180	1334,9	1,71%	5,8	2,21%	18,0	1,86%	1/2/3/5/6/9/10/12/15
FJ570	120	1231,4	2,27%	5,9	2,64%	19,2	2,13%	2/4/7/9/15
IPB013	90	1405,1	2,30%	4,0	4,51%	19,1	2,47%	1/2
IPB02	30	1395,7	4,01%	9,6	3,25%	22,2	3,69%	55/56
IPB29	30	1536,4	3,64%	6,1	5,16%	21,1	3,88%	14
IPB34	30	1535,3	3,64%	5,8	5,42%	23,3	3,52%	14
IPB58	150	1476,2	1,69%	6,0	2,32%	24,5	1,49%	3/4/5/6/8/11/14
SP1048	150	1409,2	1,78%	11,3	1,23%	32,1	1,14%	23/39/72/98/118
SP1049	210	1355,1	1,56%	12,2	0,97%	33,3	0,93%	28/41/77/81/97/114/
SP1318	30	2082,2	2,69%	13,1	2,39%	41,9	1,95%	61
SP1944	60	1566,2	2,53%	5,0	4,44%	26,8	2,16%	1/10
SP5173	120	1430,9	1,95%	5,2	3,02%	21,6	1,89%	4/5/7/10
SP5174	60	1483,0	2,67%	6,2	3,56%	20,8	2,78%	8/10/11
SP6079	60	1563,7	2,53%	7,4	3,00%	23,8	2,43%	15/18/27
SP6247	60	1203,2	3,29%	8,5	2,60%	24,4	2,37%	13/15/18/40
VCC975	32	1502,9	3,60%	4,3	6,97%	20,2	3,92%	1
VT05	90	1185,6	2,72%	7,3	2,47%	20,1	2,35%	4/37
VT06	60	1524,7	2,59%	6,8	3,25%	21,6	2,68%	3/74
VT07	90	1273,5	2,54%	8,4	2,15%	22,5	2,10%	11/49/98
VT07 - MJ	30	1045,4	5,35%	6,3	4,97%	17,2	4,76%	15

Some of the models did not perform very well, presenting low accuracies, as in the case of K-Nearest Neighbor and Superior Vector Machine (Table 3) and this may have occurred due to inherent limitations of the model or misconfigured hyperparameters. However, the other models presented all metrics above 73% (Table 3).

The model with the best performance was the Decision Tree, with metrics above 79% (Table 3), indicating a high success rate in the classification of clones. We can also mention that, as the model recall is high, we will not incur Type I (False Positive) errors. In this case, the Type I error is more harmful, from a financial and logistical point of view, because if we mistakenly classify a clone as belonging to a class other than its own, we can encourage its cultivation in better areas, expecting better results, occupying gardens and consuming resources with a genetic material that will not present the best results.

Table 3. Evaluation metrics obtained for each model considering data mining techniques

Modelo	**Acurácia**	**Precisão**	**Recall**	**F1-Score**
K-Nearest Neighbor	0,5623	0,5763	0,4997	0,5062
Decision Tree	0,8283	0,8166	0,8017	0,7979
Random Forest	0,7872	0,7833	0,7687	0,7642
Gradient Boosting	0,8176	0,8002	0,7910	0,7896
Xtreme Gradient Boosting	0,8119	0,7908	0,7919	0,7837
Superior Vector Machine	0,3526	0,5678	0,2738	0,3161
Redes Neurais	0,7356	0,7522	0,7357	0,7302

Conclusion

The Decision Tree model presented the best classification metrics when compared to the other tested algorithms.

Mathematical models that are based on data mining and machine learning concepts are not widely used in the field of inspection and classification of forest products and this research showed the opportunity that this line of work can represent for wood processing industries.

Acknowledgments

We thank the pulp and paper company Suzano for the logistical support and supply of eucalyptus clones for this research.

References

Gonçalves, R.; Lorensani, rR G. M.; Ruy, M.; Veiga, N. S.; Müller, G.; Alves, C. S.; and Martins, G. A. M. Evolution of Acoustical, Geometrical, Physical, and Mechanical Parameters from Seedling to Cutting Age in *Eucalyptus* Clones Used in the Pulp and Paper Industries in Brazil**. Forest Products Journal**: 2019, Vol. 69, No. 1, pp. 5-16. DOI: 10.13073/FPJ-D-17-00013.

Gonçalves, R.; Lorensani, R. G. M.; Merlo, E.; Santaclara, O.; Touza, M.; Guaita, M.; Lario, F. Modeling of wood properties from parameters obtained in nursery seedlings. **Canadian Journal of Forest Research.** 2018. DOI: 10.1139/cjfr-2017-0393

Gonçalves, R.; Batista, F. A. F.; Lorensani, R. G. M. Selecting eucalyptus clones using ultrasound test on standing trees. **Forest Prodcuts Journal.** 2013. 63(3/4): 112-118. DOI: 10.13073/FPJ-D-12-00114.

Guido, S. & Müller, A. Introduction to Machine Learning with Python. 2016. Disponível em <https://learning.oreilly.com/library/view/introduction-to-machine/9781449369880/ >.

Plas, J. V. Python Data Science Handbook. 2016. Disponível em: < https://jakevdp.github.io/PythonDataScienceHandbook/>.

Zhang, Z. Introduction to machine learning: K-nearest neighbors. **Annals of Translational Medicine.** 2016, Vol. *4*, No. 11. https://doi.org/10.21037/atm.2016.03.37

Cunningham, P., & Delany, S. J. K-Nearest Neighbour Classifiers-A Tutorial. In **ACM Computing Surveys.** 2021. Vol. 54, No. 6). Association for Computing Machinery. https://doi.org/10.1145/3459665

Kingsford, C., & Salzberg, S. L. What are decision trees? **In Nature Biotechnology.** 2008. Vol. 26, No. 9, pp. 1011–1012. https://doi.org/10.1038/nbt0908-1011

Ali, Jehad & Khan, Rehanullah & Ahmad, Nasir & Maqsood, Imran. Random Forests and Decision Trees. **International Journal of Computer Science Issues.** 2012. (IJCSI). 9.

Natekin, A., & Knoll, A. Gradient boosting machines, a tutorial. **Frontiers in Neurorobotics.** 2013. Vol. 7*,* No. Dec. https://doi.org/10.3389/fnbot.2013.00021

Chen, T., & Guestrin, C. XGBoost: A scalable tree boosting system. **Proceedings of the ACM SIGKDD International Conference on Knowledge Discovery and Data Mining**. 2016. 13-17-August-2016, 785–794. https://doi.org/10.1145/2939672.2939785

Lorena, Ana Carolina; DE CARVALHO, André C. P. L. F.. Uma Introdução às Support Vector Machines**. Revista de Informática Teórica e Aplicada**. 2007. Porto Alegre, RS, v. 14, n. 2, p. 43-67, dec. ISSN 21752745. https://doi.org/10.22456/2175-2745.5690.

Grossi, E., & Buscema, M. Introduction to artificial neural networks. **In European Journal of Gastroenterology and Hepatology.** 2007. Vol. 19, No. 12, pp. 1046–1054. https://doi.org/10.1097/MEG.0b013e3282f198a0

Distinction of Eucalyptus Planting Areas through Data Mining

Carolina Kravetz *
Laboratory of Nondestructive Testing – LabEND, College of Agricultural Engineering – FEAGRI – UNICAMP, Campinas, São Paulo, Brazil, carolinakra.12@gmail.com

Cinthya Bertoldo
Laboratory of Nondestructive Testing – LabEND, College of Agricultural Engineering – FEAGRI – UNICAMP, Campinas, São Paulo, Brazil, cinthyab@unicamp.br

Rafael Mansini Lorensani
Laboratory of Nondestructive Testing – LabEND, College of Agricultural Engineering – FEAGRI – UNICAMP, Campinas, São Paulo, Brazil, rafaelmansini@hotmail.com

Fernanda Trisltz Perassolo Guedes
Sylvamo do Brasil, Mogi Guaçu, São Paulo, Brazil, fernanda.guedes@sylvamo.com

* Corresponding author

Abstract

Wood, the main raw material for industries in the forestry sector, is influenced by the edaphoclimatic characteristics of plantation sites. This interference can cause changes in physical, chemical, mechanical and anatomic characteristics, influencing the final product quality. To anticipate knowledge about the quality of wood, nondestructive tests have been applied to freshly felled logs and even standing trees. One way to evaluate the results of these tests is through data mining, which has different algorithms that elaborate prediction models or data groupings. Thus, the objective of this work was, from nondestructive tests in three different clones of the genus Eucalyptus, to identify which variable has the highest degree of importance for the prediction model to differentiate two edaphoclimatic conditions of planting. Among the available algorithms, random forest was used for the elaboration of class prediction models, which provides a rank of the attributes that had the greatest importance in the obtained model. As a result of this work, analyzing the individuals with 1 year, in Clone A, the radial propagation velocity was the attribute that obtained the highest degree of importance in the prediction model, in Clones B was the perforation resistance and C the highlighted attribute was the longitudinal propagation velocity. A descriptive statistical analysis collaborated with the knowledge of the data distribution in the two regions, and in this work, it was possible to notice the interference of edaphoclimatic characteristics in the performed tests. Therefore, new field tests and laboratory tests will be carried out to understand the dynamics of the relationship between wood characteristics, nondestructive tests and edaphoclimatic characteristics.

Keywords: nondestructive tests, bagging, random forest

Introduction

The forest sector has wood as its main raw material, which is influenced by several factors throughout its growth. These interferences in its characteristics mainly affect the quality of the wood produced. In this way, monitoring the development of plantations is essential for the industry to obtain satisfactory results from its final products.

The quality of wood can be influenced according to the place of planting, due to the combination and interaction of several factors that change its physical, chemical and mechanical characteristics, and these changes directly interfere in industrial processes. Differences between locations are almost entirely due to interactions between environmental characteristics and these are not adequately measured to predict the type of wood that will be produced (ZOBEL & BUIJTENEN, 2012).

Faced with the need to monitor and anticipate knowledge of the quality of planting efficiently, the forestry sector needs more agile methods that allow decision-making and necessary actions to maintain the expected development. This would only be possible with the use of nondestructive methods, which have already been used by several authors to predict wood quality.

Lima et al (2006) and Gouvêa et al. (2011) performed nondestructive analyzes using equipment such as the penetrograph and the pilodyn, focused mainly on predicting the basic density of wood from different species and clones of the Eucalyptus genus, having obtained satisfactory results. Another promising test is the propagation of ultrasound waves, which can be used to anticipate knowledge of wood properties. This has emerged as an alternative to optimize costs for companies, as discussed by Lorensani (2017) and Bertoldo (2014).

In order to analyze the data resulting from the tests, in the forestry sector it is possible to find studies that used different data mining techniques. For example, in estimating the productivity of eucalyptus areas (BATISTA, 2020; ARAGÃO et al., 2018), in evaluating images of forest areas (NONATO & ABREU, 2020; ARAUJO & TORRESAN, 2013) and evaluating the quality of lumber through images (RODER et al., 2015).

Data mining consists of a collaborative process between man and machine, using a set of techniques aimed at exploring large databases. This is considered an exploratory activity, with which, from the search for patterns, it is possible to obtain predictive models or perform data grouping (CORTES et al., 2002). To make this analysis, different algorithms are used, which from the mathematical language, describe the actions that must be performed to solve a problem.

In this work, data mining techniques were applied in databases obtained through field tests carried out in trees belonging to a company in the pulp and paper area. This study is part of a project that has a partnership between this company and the Laboratory of Nondestructive Testing (LabEND) of the Faculty of Agricultural Engineering in the State University of Campinas (FEAGRI – UNICAMP).

The studies show that it is possible to correlate the results of the nondestructive tests with the characteristics of the wood. However, considering that the wood is influenced by the characteristics of the planting site, it is necessary to verify if these tests are sensitive to edaphoclimatic variations. Therefore, the objective of this work is to identify, among the results of the nondestructive tests carried out in the trees, which variable stands out to differentiate two distinct regions of Eucalyptus clone plantations, through the application of data mining techniques.

Methodology

For the work, three clones of *Eucalyptus* sp (A, B and C) cultivated in two regions (R1 and R2) with different soil and climate conditions were used. Region 1 has as main characteristics: the presence of latosols, which are considered more fertile, and greater precipitation. While Region 2 has sandy soils, which are considered less fertile and are areas with less precipitation. For each of the clones with different ages (1, 3 and 4 years) 30 individuals were selected, whose development was monitored during two periods: May and August/2021.

The monitoring of the development of trees in the field occurred through nondestructive tests such as: velocity of ultrasound waves and resistance to perforation, both performed at the breast height (about 1,30 meters from the soil).

To obtain the velocity of ultrasound waves in the trees, a test was carried out with ultrasound equipment (USLab, Agricef, Brazil) and exponential face transducers of 45 kHz frequency. The ultrasound tests on the trees were performed indirectly (longitudinal propagation velocity) and directly (radial propagation velocity).

To obtain the perforation resistance in the trees, a penetrograph (IML Resi PD Series 500) was used, with diametrical measurements in perpendicular positions, using the methodology described by Isik & Li (2003).

These results were organized into 9 sets of data, where each one belongs to a Eucalyptus clone in a different age. Each set has 60 instances. Table 1 describes the variables present in all data sets, where the Region attribute is considered the response variable.

Table 1 – Description of the variables used

Attributes/Variables	Unit	Type
Longitudinal propagation velocity	$m.s^{-1}$	numeric
Radial propagation velocity	$m.s^{-1}$	numeric
Perforation resistance	%	numeric
Region	R1/R2	nominal

The analyzes were performed using Weka software (Waikato Environment for Knowledge Analysis), developed by the University of Waikato in New Zealand. The databases were analyzed separately, but all went through the same processing steps. Initially the data were normalized at the pre-processing step, since each numerical attribute has a different amplitude, and for the analysis it is desirable that all variables have the same weight for the model. For this, the Z-score normalization was used, which assigns a mean equal to zero and a variance equal to one for all attributes, through the application of the following equation (1) (HAN et al., 2012):

$$Z = \frac{x_{i-}\bar{x}}{\sigma} \quad (1)$$

where Z is the instance normalized value, x_i is the instance initial value, $\bar{x}$ is the attribute mean value, and σ is the attribute standard deviation.

After this pre-processing step, the data were analyzed using the Random Forest (RF) algorithm, with the default parameters. This algorithm is considered a particular case of the technique called Bagging, which combines the results of models from several algorithms and aims to obtain a single prediction model where each classifier uses a random set of data (bootstrap). This technique allows for an increase in precision, as the combination of classifiers reduces the variance of each individual classifier. RF uses a set of decision trees, and considers fewer attributes for each division, so they are efficient in large databases (HAN et al., 2012; WITTEN et al., 2011).

Another advantage of this algorithm is the calculation of the importance of attributes in relation to the predicted model. Each decision tree chooses an initial variable that will separate the data into two regions, this chosen variable is the one that provides the highest estimate of improvement over the model, according to the squared error risk value. As the RF is formed by a set of trees, the measure of importance will be the average of these improvement values (HASTIE et al., 2008).

The nine databases, with the same composition of attributes, were analyzed separately through Random Forest to obtain a prediction model that identified the attribute that provides more information for classifying individuals between the R1 or R2 regions. The resulting models were analyzed according to accuracy, which gives us the model's global hit rate; with the kappa, which represents the agreement index, obtained from a relationship between the values that were predicted and those observed; and precision, which is calculated specifically for each class of response, providing the list of true positives across all results reported as positive, whether false or true. Therefore, the higher the numerical value of all these parameters, the better the evaluated model can be considered. About kappa, Landis and Koch (1977) suggest that above 0.61 the model has greater predictive power, thus this was the value used to evaluate the models.

Results and discussion

In the dataset of clone A – 1 year, the model had high value parameters (accuracy – 90.8%; kappa 0.81; Precision – 0.90 and 0.91), in clone A – 3 years and 4 years, was obtained a low values parameter, especially the kappa (accuracy – 76.6%; kappa 0.53; Precision – 0.78 and 0.75 and accuracy – 67.5%; kappa 0.35; Precision – 0.68 and 0.66, respectively). Therefore, was analyzed the sequence of attributes from the degree of importance just in relation to the prediction model of clone A - 1 year (Table 3).

Table 3 – Degree of importance of the attributes of the clone A – 1 year dataset.

Degree of importance	Attributes
0.54	Radial velocity (V_R)
0.42	Longitudinal velocity (V_L)
0.39	Perforation resistance (R_P)

Analyzing Table 3, it is possible to identify that the attribute that obtained the highest degree of importance in the model was the radial propagation velocity (V_R). As this variable is the one that has the greatest contribution to the classification of individuals, descriptive statistics (Table 4) were performed to understand their behavior in the two regions.

Table 4 – Descriptive statistics – Radial velocity (Clone A – 1 year)

	Radial Velocity ($m.s^{-1}$)						
Regions	Average	Stand. deviation	Minimum	Q1	Median	Q3	Maximum
R1	3006	532.8	2142	2690	2949	3179	4652
R2	2229	233.7	1683	2091	2195	2387	2744

In the dataset of clone B occurred the same as in clone A, where the model in 1 year had high value parameters (accuracy – 98.3%; kappa 0.96; Precision – 0.98 and 0.98), but in clone B – 3 years and 4 years, the parameters, especially kappa, had low values (accuracy – 75%; kappa 0.5; Precision – 0.74 and 0.75 and accuracy – 70%; kappa 0.4; Precision – 0.69 and 0.7, respectively). Thus, was analyzed the sequence of attributes from the degree of importance just for clone B-1 year (Table 5).

Table 5 – Degree of importance of the attributes of the clone B – 1 year dataset.

Degree of importance	Attributes
0.7	Perforation resistance (R_P)
0.47	Longitudinal velocity (V_L)
0.38	Radial velocity (V_R)

The attribute that obtained the highest degree of importance in the model for clone B – 1 year was the perforation resistance. To understand the behavior of this attribute in the two regions, was performed the descriptive statistics of it (Table 6).

Table 6 – Descriptive statistics – Perforation resistance (Clone B – 1 year)

	Perforation resistance (%)						
Regions	Average	Stand. deviation	Minimum	Q1	Median	Q3	Maximum
R1	6.4	0.8	5.1	5.9	6.4	6.8	10.9
R2	16.2	3.4	6.4	14.0	16.3	18.7	23.8

In the dataset of clone C the same pattern was presented, the model in 1 year had high value parameters (accuracy – 93.3%; kappa 0.86; Precision – 0.94 and 0.91), but in clone C – 3 years and 4 years, the kappa, again, had low values (accuracy – 76,6%; kappa 0.53; Precision – 0.76 and 0.76 and accuracy – 75%; kappa 0.5; Precision – 0.75 and 0.75, respectively). So, Table 7 presents the sequence of attributes from the degree of importance just for clone C-1 year.

Table 7 – Degree of importance of the attributes of the clone C – 1 year dataset.

Degree of importance	Attributes
0.47	Longitudinal velocity (V_L)
0.44	Radial velocity (V_R)
0.38	Perforation resistance (R_P)

In this case, the longitudinal propagation velocity was the attribute that obtained the highest degree of importance in the model. In Table 8 is presented the descriptive statistics of this variable to understand its behavior in the two regions.

Table 8 – Descriptive statistics – Longitudinal velocity (Clone C – 1 year)

	Longitudinal Velocity ($m.s^{-1}$)						
Regions	Average	Stand. deviation	Minimum	Q1	Median	Q3	Maximum
R1	3714	252.1	2809	3544	3736	3889	4249
R2	4023	469.0	1032	3866	4082	4286	4573

In general, the most important attribute for the clone A model was the radial velocity, for the clone B the perforation resistance and for the clone C the longitudinal velocity. To understand how these parameters behave, it is first necessary to remember that wood is a complex material, especially trees classified as hardwoods, such as Eucalyptus, due to the variety of anatomical elements that constitute it.

The propagation of ultrasound waves, as well as the perforation resistance, are influenced by the structure of the wood, with the anatomical elements of the trees being variable according to genetic material, silvicultural treatments and also due to the edaphoclimatic characteristics of the planting site. In this study it can be observed that during the analyzed period, region 1 had an accumulated precipitation of 187 mm, while in region 2 the accumulated precipitation was 19 mm. In the case of this research, the edaphoclimatic variations of the two study regions influenced the growth of plantations, as can be seen in the growth rate data, presented in Table 9.

Table 9 – Average growth rate of individuals

	Growth rate (%)	
Clones	Region 1	Região 2
A	11.06	2.36
B	8.79	3.37
C	13.68	7.12

Analyzing the growth rates, it is possible to observe that they were higher in region 1 for all clones. In situations of water restriction, as occurred in region 2, there is less growth and, consequently, there is a tendency of thickness cell walls. Câmara et al (2020) observed that the hydraulic architecture of some

Eucalyptus clones suffered variation, especially due to the reduction of precipitation, thus, changes were detected in the xylem anatomy, such as vessel wall thickness, adjacent double walls and implosion resistance of the vessels.

According to Wang et al. (2007) the properties and microstructure of the wood fiber interfere in the propagation of waves, which makes the process dynamic and complex. Bucur (1988) explains that the ultrasonic velocities can be influenced by the annual ring structure, because of the difference in the thickness of the wall-cells. In this way, the differences in the values of radial and longitudinal velocity, in clones A and C, may have happened due to the different edaphoclimatic conditions to which of these regions are submitted. It is worth noting that both clones presented higher ultrasound velocity values for the species, but Bertoldo (2011) and Lorensani (2011) found this same situation due to the predominance of juvenile wood.

Discussing about the penetrograph, its value is related to the penetration depth of the needle in the tree, therefore, when the material presents greater resistance to the needle entry, the higher the resulting value will be. This kind of result is commonly correlated with the material's basic density. Ribeiro (2018) confirmed the change in the basic density of Eucalyptus clones due to different edaphoclimatic conditions in the regions studied. And these changes are commonly caused by variations in wood anatomy such as cell wall thickness, proportion of fibers and vessels, etc. (Vidaurre et al, 2020). As presented the conditions of the regions studied in this work, the difference in perforation resistance found in clone B must have happened to the different edaphoclimatic conditions.

Conclusion

In this work, nondestructive tests were carried out on three clones of the genus Eucalyptus, with the aim of monitoring the development of trees located in two regions with distinct soil and climate characteristics. Using data mining techniques, the objective was to identify which variable stands out according to its degree of importance for the prediction model, in order to differentiate the two planting regions. Evaluating each data set separately, the Random Forest algorithm was used and the resulting models were evaluated according to the parameters: accuracy, kappa and precision. As a result, analyzing the individuals with 1 year, in Clone A, the radial propagation velocity was the attribute that obtained the highest degree of importance in the prediction model, in Clones B was the perforation resistance and C the highlighted attribute was the longitudinal propagation velocity. With the performance of a descriptive statistical analysis, the variables were evaluated individually and it was possible to verify the difference in the distribution of data that occurs in each region, affirming the choice made by the algorithm. As already discussed in other works, the soil and climate conditions interfere in the characteristics of the wood and in this work it was possible to evidence the interference of these conditions in the tests carried out. Therefore, new studies will be carried out to understand the dynamics of the relationship between wood characteristics, nondestructive tests and soil and climate characteristics.

Acknowledgments

We are grateful to the support of the Laboratory of Nondestructive Testing (LabEND), the employees of forest research from Sylvamo do Brasil and to the financial support from the National Council for Scientific and Technological Development (CNPQ).

References

Aragão, M. de A.; Santos, J. S.; Silva, M. L. M. da. 2018. Técnica de mineração de dados aplicada a estimação de volume de árvores de *Eucalyptus*. V Semana de Engenharia Flo restal da Bahia.

Araujo, L. S. & Torresan, F. E. 2013. Classificação de florestas plantadas e nativas a partir da análise orientada a objeto e técnica de mineração de dados em imagem geoeye. XI Congresso de Ecologia do Brasil. Porto Seguro, BA.

Batista, T. S. 2020. Redes neurais artificiais para quantificar o volume de madeira em espécies de eucalipto, com ampliação teórica da base de dados. Dissertação: Mestrado em Agronomia – Universidade Federal de Mato Grosso do Sul.

Bertoldo, C. Estimativa de propriedades de rigidez da madeira a partir de avaliação acústica na árvore e em toras recém abatidas. 2011. Dissertação: Mestrado em Engenharia Agrícola - Universidade Estadual de Campinas.

Bertoldo, C. 2014. Propriedades de Resistência e de Rigidez da madeira obtidas a partir da avaliação acústica na árvore. Tese: Doutorado em Engenharia Agrícola - Universidade Estadual de Campinas, Fundação de Amparo à Pesquisa do Estado de São Paulo.

Bucur, V. 1988. Wood structural anisotropy estimated by acoustic invariants. IAWA Bulletin, v. 9 (1), p. 67-74.

Câmara, A. P.; Vidaurre, G.B.; Oliveira, J.C.L.; Picoli, E.A.de T.; Almeida, M.N.F; Roque, R.M.; Tomazello Filho, M.; Souza, H.J.P.; Oliveira, T.R.; Campoe, O.C. 2020. Changes in hydraulic architecture across a water availability gradient for two contrasting commercial Eucalyptus clones. Forest Ecology and Management, 474.

Cortes, S. Da C; Porcaro, R. M.; Lifschitz, S. 2002. Mineração de Dados – Funcionalidades, Técnicas e Abordagens. PUC-RioInf.MCC10/02, Maio.

Gouvêa, A. de G.; Trugilho, P.F.; Gomide, J.L.; Silva, J. R. M.da.; Andrade, C.R.; Alves, I.C.N. 2011. Determinação da densidade básica da madeiras de eucalyptus por diferentes métodos não destrutivos. Revista Árvore, v. 35, n. 2, p. 349-358.

Han, J.; Kamber, M.; Pei, J. 2012. Data Mining – Concepts and Techniques. Elsevier. 3rd edition.

Hastie, T; Tibshirani, R.; Friedman, J. 2008. The elements of statistical learning – Data mining, Inference, and Prediction. Springer Series in Statistics. 2nd Edition.

Isik, F. and Li, B. L. 2003. Rapid assessment of wood density of live trees using the Resistograph for selection in tree improvement programs. Canadian Journal of Forest Research, 33(12), 2426-2435.

Landis, J. R. and Koch, G. G. 1977. The measurement of observer agreement for categorical data. Biometrics, 33(1), 159-174.

Lima, J. T; Hein, P. R. G.; Trugilho, P. F.; Silva, J. R. M. da. 2006. Adequação do resistograph para a estimativa da densidade básica da madeira de Eucalyptus. Madeira: Arquitetura e Engenharia, v. 7, n. 18.

Lorensani, R. G. M. 2011. Classificação de peças estruturais de eucalipto utilizando ultrassom. Dissertação: Mestrado em Engenharia Agrícola - Universidade Estadual de Campinas.

Lorensani, R. G. M. 2017. Antecipação do conhecimento de propriedades da madeira utilizando ensaios em mudas. Tese: Doutorado em Engenharia Agrícola - Universidade Estadual de Campinas.

Nonato, C. T. & Abreu, Y. V. de. 2020. Desenvolvimento de modelos de classificação de florestas plantadas para planejamento e tomada de decisão: Mineração de dados e Imagens de satélite. Life Editora. Campo Grande, MS. 124 p.

Ribeiro, M. D. dos S. B. 2018. Densidade básica da madeira de plantios florestais de Eucalyptus spp: Associações com variáveis do sítio e do plantio e estimativas com redes neurais artificiais. Tese: Doutorado em Agronomia – Universidade Estadual Paulista "Júlio de Mesquita Filho".

Roder, M.; Rossi, A. L. D.; Affonso, C. de O. 2015. Comparação de técnincas de aprendizado de máquina para a classificação da qualidade da madeira. 8º Congresso de extensão universitária da UNESP.

Vidaurre, G. B.; Silva, J. G. M. da; Moulin, J. C.; Carneiro, A. de C. O. 2020. Qualidade da madeira de eucalipto proveniente de plantações no Brasil. Edufes. 221 p.

Wang, X.; Ross, R. J.; Carter, P. 2007. Acoustic Evaluation of Wood Quality in Standing Trees. Part 1. Acoustic Wave Behavior. Wood Science and Technology, p. 28-38.

Witten, I. H.; Frank, E.; Hall, M. A. 2011. Data Mining – Practical Machine Learning Tools and Techniques. Elsevier. 3rd edition.

Zobel, B. J.; Buijtenen, J. P. 2012. Wood Variations: Its Causes and Control. Spring Science & Business Media. 363p.

Dynamic Modulus of Elasticity in *Calophyllum brasiliense* Cambess Trees from Bajo Calima - Colombia

Julio Bermúdez Escovar
Department of Wood and Forest Sciences, Laval University, Quebec, QC, Canada, julio.bermudez-escovar.1@ulaval.ca
Engineering department, University of Tolima, Ibagué, Tolima, Colombia, jcbermudez@ut.edu.co

Roger Hernández
Department of Wood and Forest Sciences, Laval University, Québec, QC, Canada, roger.hernandez@sbf.ulaval.ca

Alexis Achim
Department of Wood and Forest Sciences, Laval University, Québec, QC, Canada, alexis.achim@sbf.ulaval.ca

Claudia Cáceres
Department of Wood and Forest Sciences, Laval University, Québec, QC, Canada, alexis.achim@sbf.ulaval.ca

Abstract

The aceite maría tree (*Calophyllum brasiliense* Cambess) is a versatile species whose wood has good physical and mechanical properties, which places it in a privileged place for marketing in Colombia. This paper compares the dynamic modulus of elasticity (MOE) between trees grown in natural environments and in plantation forests. A total of 90 trees, 30 trees from natural forest (estimated age 26 years), and 60 trees from planted forests 34 years ago (with a spacing of 4x4 m and 5x5 m) were sampled. The results showed that there were no differences in MOE according to the cardinal orientation on the measured trees. The diameter at breast height (DBH) had a negative influence on the MOE in the longitudinal direction of the fiber, showing highly significant differences between the natural and planted forest. Between the forests planted at 4x4 m and 5x5 m, the significant differences were moderate. It's possible to predict MOE from DHB in the three types of forest. The stress wave speed (SWS) technique in standing trees can be successfully used for the non-destructive evaluation (NDE). These results allow the promotion of aceite marÍa plantations to market high-value products contributing to the sustainable management of Colombian tropical forests.

Keywords: *Calophyllum brasiliense*, natural and planted forests, MOE, DHB, SWS, NDE

Introduction

The aceite maría tree (*Calophyllum brasiliense* Cambess) is a versatile species whose wood has good physical and mechanical properties. For this reason, the aceite maría wood is currently replacing other high-priced woods in the Colombian market. The wood of this species exhibits visible growth rings, distinguished by having terminal parenchyma with denser areas of darker color. This is a diffuse-porous wood, vascular lines in the tangential longitudinal section (T), visible to the naked eye, with reddish color and tyloses are often present (Arévalo and Londoño 2005, Vásquez and Ramírez 2011). Regarding its

physical properties, aceite maría shows, great dimensional stability, presenting low levels of distortions or warping during drying according to the studies of (Bastidas *et al*. 1975) and (JUNAC 1981).
The Colombian wood industry, after a shortage of mahogany and Spanish cedar woods, has taken advantage of aceite maría wood because of its good mechanical properties to manufacture several structures for interior, furniture in general, canoes, parquet floors, bridges, truck bodies, tool handles, stair treads, poles and railway sleepers (mining), turned items, handrails, toys, handicraft, and veneer. Its use in the manufacture of musical string instruments stands out (Bárcenas 1995; Rojas 2008). The Bajo Calima is one of the regions in Colombia where the aceite maría species is marketed. This zone is characterized by high biodiversity and a high degree endemic (Martinez 2006). It is necessary to evaluate of wood properties of various species in the Bajo Calima region, including those of *C. brasiliense*, is required given that only two studies on this wood have been reported.

The evaluation of the mechanical properties of wood by non-destructive methods is mainly characterized by its speed and low cost and by not affecting the physical structure of the material under study. Among these methods, the stress waves have demonstrated the ability to determine dynamic modulus of wood (Kawamoto and Williams 2002; Pellerin and Ross 2002).

The objective of this study was to evaluate the dynamic modulus of elasticity (MOE) using non-destructive methods (SWS) of standing trees of *C. brasiliense* coming from natural forests and plantation forests. The moisture content and wood density of the trees were also calculated from increment cores. The results obtained will be used to increase the commercialization of high-value products. This will improve the rational use of aceite maría wood and help to prevent the depletion of tropical forests in Colombia.

Materials and methods

Study region

Bajo Calima is geographically located at 3°59 '57.20' north latitude and 76°58'28.29" west longitude, 27 km from the urban area of Buenaventura, Valle del Cauca province, between the Pacific Ocean and the Colombian Andes (Figure 1). Bajo Calima region has a rainfall of 7500 mm $year^{-1}$ without dry periods, an average annual temperature of 26 °C, relative humidity of 88%, and low sunlight for 712 hours $year^{-1}$. Secondary forests were created through exploitation according to the total clear-cutting method of primary forests from 1959 to 1993. The region is located in an equatorial bio-climatic zone between 40 and 70 meters above sea level. According to the climatic classification proposed by Koeppen, this corresponds to «humid tropical forest climate» or “humid climate” (Martínez 2006). The soils of the Bajo Calima region are of the Typic Dystrudepts type. These soils are deep, fine, and medium textured, well-drained, very acidic, with high aluminum saturation and very low fertility. (Forero 2014).

Sampling areas

The trees from natural forest were sampled from two zones (a and b) of secondary forests (Figure 1). Two zones were required in order to obtain 30 trees with a diameter at breast height (DBH) greater than 20 cm.

The plantation trees were sampled from an experimental plot with an area of 0.29 ha, located in the lower part of Calima river watershed, as shown in Fig. 1 (zone c). Trees were planted at two different distances (4x4 m and 5x5 m) as part of an agroforestry experiment for research purposes. The plantation was established in 1985 by students of the Forest Engineering Faculty of the University of Tolima at the Tropical Forest Center of Bajo Calima. A total of 60 trees were sampled, 30 with 4x4 m spacing and 30 with 5x5 m spacing.

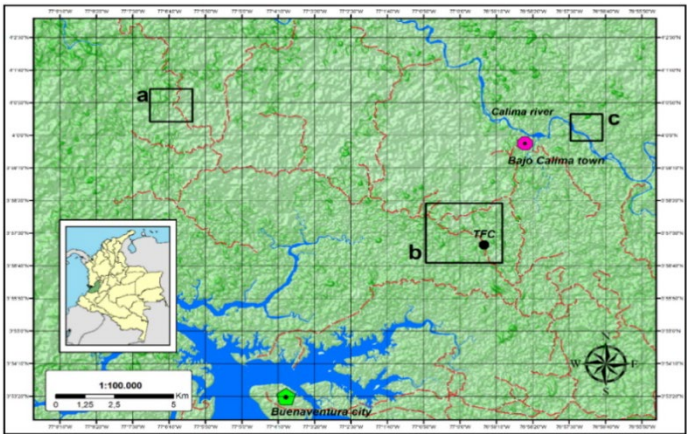

Figure 1— Study region and sampling areas in Bajo Calima - Colombia: zone **a** (natural environments trees); zone **b** (natural environments trees), zone **c** (planted trees), and Tropical Forest Center (***TFC***).

The selected trees for the measurement of stress wave velocity (SWS) are located in areas of low hills, on land belonging to the Community Council of Bajo Calima. The general information of the sites selected for this study is presented in Table 1.

Moisture content and density

The moisture content (MC) and density at the green state of the cores (ρ) were obtained on the same day that they were extracted. For this, the mass was taken using a precision balance of 0.001 g. The volume was measured by immersion in water with an accuracy of 0.01 g according to ASTM D2395 (2017).

Dynamic modulus of elasticity (MOE)

The MOE was evaluated using the SWS technology with the TreeSonic device (FAKOPP ™) that measured the stress wave time (SWT). Two transducers (transmitter and receiver) were inserted at an angle of about 45 degrees of the stem axis and at a 30 mm depth. The transducers were vertically aligned 1000 mm apart to introduce acoustic energy signals to the axis through a hammer having a mass of 200 g. The TreeSonic device was calibrated for each tree by selecting a random point in the stem in which eight readings of SWT were taken every 1000, 800, 600, 400, and 200 mm of distance. With this data, a simple linear regression between SWT (Y) and distance (x) was established according to the Equation 1 (Fakopp 2008).

$$Y = Ax \pm B \tag{1}$$

where B is the time correction factor that was used to find the SWS for each tree.

Two measurements were made per tree North or South (N/S) and East or West (E/W) depending on the land slope. Each measurement was taken between 1.3 m and 2.3 m in height. Eight SWT readings were made at each position and averaged. The standard deviation of the eight readings made should be less than ± 1.5 µs (Fakopp 2008). The value considered in the analysis was the average between the measurements obtained per tree. With the correction factor obtained and the average of TreeSonic measurements in each tree, the speed calculation was performed as follows (Equation 2) (Fakopp 2008):

$$v = \frac{1000 * d}{t \pm B} \tag{2}$$

where υ is wave speed (m s^{-1}), d is the distance between the two transducers (mm), t is SWT (µs), and $\pm B$ is the time correction factor (µs).

The MOE of each tree was calculated using Equation 3.

$$MOE = \rho * \upsilon^2 \quad (3)$$

where MOE is the dynamic modulus of elasticity at the green state (MPa), ρ is the green density (kg m^{-3}) and υ is stress wave speed (m s^{-1}).

Table 1 General information of the sites selected for sampling and recording of the data collected: NF: Natural Forest, PF: Plantation Forests, NA: Not Applicable, DHB: Diameter at breast height, TH: Tree Height, 1: Average, 2: Natural Forest come from the secondary forests and their age is estimated at 26 years, from 1993 (when logging was completed by Smurfit Kappa Cartón de Colombia in the Bajo Calima region) to 2019 (the year the trees were measured), 3: Forero (2014), TD: Typic Dystrudepts

Forest type	Tree spacing (m)	Sampling area	No. of trees	DHB[1] (cm)	TH[1] (m)	North latitude	West longitude	Elevation[1] (m)	Age[2] (years)	Soil type[3]
NF	NA	a	23	24	14	4°0'43"	77°6'38"	78	26	TD
		b	7	26	14	3°57'13"	76°59'27"	59	26	TD
PF	4x4	c	30	30	17	4°0'14"	76°57'15"	41	34	TD
	5x5	c	30	31	17			44		

Statistical analysis

Descriptive statistics for each forest type were calculated. First, an Analysis of Variance (ANOVA) was performed of the dynamic modulus of elasticity (MOE) was performed considering as sources of variation the cardinal orientation of the sides measured in each tree (N/S and E/W) and the forest types [NF and PF (4x4 m and 5x5 m)]. Subsequently, with the average of the measurements taken on each side of the trees (N/S and E/W), an analysis of covariance (ANCOVA) was applied, taking as co-variables the Diameter at Breast Height (DBH), Height of the Trees (HT), and the Density at green (ρ). A correlation analysis was performed on the average MOE of cardinal orientation with respect to DHB, TH, and (ρ) of *C. brasiliense* trees. A linear regression was applied between MOE and DBH for each forest type. Tests for significant differences between means were applied at a 95% confidence level when required. Data were analyzed with the Statistical Analysis System SAS® OnDemand for Academics (2021).

Results and discussion

The MOE of the trees from the plantation forest showed an average value of 15122 MPa (4x4 m) and 15341 MPa (5x5 m), higher than that of the natural forest trees (13564 MPa) (Table 2). The variation of MOE is 1286 MPa, 1107 MPa, and 1043 MPa in natural forest trees for the first value, plantation (4x4 m) in the second, and (5x5 m) in the third. The MOE shows a very low variability in the analyzed forests based on the coefficients of variation. Being the lowest the PF (5x5) with 6.8%, followed by PF (4x4) with 7.3%, and the highest variation is presented in the NF (9.5%) (Table 2).

The results presented are the average obtained between the MOE N/S and E/W of each tree, since there were no statistical differences between the MOE measurements depending on the position of the sides measured in each tree. This result is in agreement with the studies of (Madhoushi and Daneshvar 2016) for *Populus deltoides* trees. They found that cardinal position did not significantly affect the velocity of

stress waves in the trees and thus their dynamic MOE. These results confirm the use of the mean of the results obtained from the two positions used for this study.

The dynamic MOE in the NF (13564 MPa) is higher than the static MOE of *C. brasiliense* from the Bajo Calima region reported by (Bastidas *et al*. 1975) which was 9642 MPa (12% CH) and (JUNAC 1981) which was 11180 MPa in the green state (for samples from another region in Colombia). This behavior was also presented in the studies conducted by: (Mendoza 2017) who found a dynamic MOE of 19504 MPa in standing trees and a static MOE of 11112 MPa (12% CH) in the wood of *Tachigali colombiana* Dwyer species from Bajo Calima. (Yin *et al*. 2010) show that the MOE obtained by static bending was approximately 15.4% lower than the dynamic MOE in plantation trees of *Cunninghamia lanceolata*.

Table 2 Descriptive statistics of the data collected in the two forest types in 2019 of standing trees of *Calophyllum brasiliense* in Colombia: NF: Natural Forest, PF: Plantation Forest, MC: Moisture Content SD: Standard Deviation, SE: Standard Error, CV: Coefficient of Variation in %, DBH: Diameter at Breast Height, TH: Tree Height, ρ: Density in green state, MOE: Modulus of Dynamic Elasticity

Type of forest	No. of trees	Variable	Mean	SD	SE	CV
NF	30 (MC 81%)	DBH (cm)	24.5	3.2	0.6	13.1
		TH (m)	14.3	3.7	0.7	25.9
		ρ (kg m^{-3})	926	46	8	5,0
		MOE (MPa)	13564	1286	235	9.5
PF (4x4 m)	30 (MC 78%)	DBH (cm)	29.9	3.3	0.6	11.0
		TH (m)	17.4	2.4	0.4	13.8
		ρ (kg m^{-3})	1044	24	4	2.3
		MOE (MPa)	15122	1107	202	7.3
PF (5x5 m)	30 (MC 77%)	DBH (cm)	30.8	3.9	0.7	12.7
		TH (m)	17.9	2.1	0.4	11.7
		ρ (kg m^{-3})	1062	35	6	3.3
		MOE (MPa)	15341	1043	190	6.8

Other authors report that SWS techniques, generate stiffness measurements that are overestimated compared to those obtained in bending techniques, but that this should not be a limitation for their use (Chiu *et al*. 2012; Legg and Bradley 2016). Also, (Bertoldo 2011) for the *Pinus elliottii* species determined a MOE_d of 1787 MPa and a MOE_s of 5753 MPa.

The DBH, TH, and ρ variables have the same behavior as the MOE means in the different forests. The DBH showed greater variation in the PF (5x5 m) followed by PF (4x4 m) and NF. Tree Height (TH) and green density (ρ) showed higher variability in NF in relation to PF (5x5 m) and PF (4x4 m). According to the CV of DBH and ρ, the homogeneity of the data is higher in the PF (4x4 m) and lower in the NF. Regarding the TH the values are more homogeneous in the PF (5x5 m) with respect to the PF (4x4 m) and the NF (Table 2).

The Analysis of Variance (ANOVA) applied to the dynamic MOE considered as sources of variation the position of the sides measured on each tree (N/S and E/W) and the forest types [NF and PF (4x4 and 5x5 m)]. The results showed that there are no significant differences between the results obtained in the N/S location with respect to the E/W. Significant differences were also found between forest types. There are

significant differences between NF and PT (4x4 m and 5x5 m). The 1% difference in the dynamic modulus of elasticity between the two planting densities (4x4 m and 5x5 m) was not significant.

The stiffness of trees in natural environments was lower than that of planted trees, with significant differences. This may be due to several reasons:

- The age difference between trees in natural environments (26 years) and planted trees (34 years). Studies by (Auty and Achim 2008) for *Pinus sylvestris* and Wang (2013), have suggested that the effect of tree age on MOE should be taken into account. As trees age, their outer wood becomes stiffer. The angle of microfibrils decreases and the proportion of mature wood increases in the cross-section of a tree.
- A possible formation of reaction wood in trees from natural environments, as they were located on steeper slopes than planted trees. According to (Legg and Bradley 2016) in their review on measuring the stiffness of standing trees and (INIA 2018) in plantation trees of *Calycophyllum spruceanum*, found reaction wood. This decreases dynamic MOE, probably due to a high microfibril angle and lower strength.
- The effect of density on the MOE of trees in natural and planted environments. (Hernandez and Restrepo 1995) on *Alnus acuminata*; and (INIA 2018) on plantation trees of *Calycophyllum spriceanum*, found that in general terms, longitudinal stiffness, and therefore longitudinal velocity, increases with higher density. However, other authors such as (Bertoldo 2011) for *Pinus elliotti*, *Eucalyptus grandis*, and *Toona ciliata*; and (Reyes 2019) on *Anacardium excelsum*, report that density does not always have such a direct relationship with wood stiffness and strength.

Given the effects on wood stiffness of the characteristics discussed above, we can confirm that it is possible that planted aceite maría trees have higher stiffness than trees in natural environments.

With the average of the measurements taken on each side of the trees (N/S and E/W), an analysis of covariance (ANCOVA) was applied, taking as co-variables the Diameter at Breast Height (DBH), Height of the Trees (HT), and the Density in green (ρ). Table 3 shows a significant effect of DBH on forest types, presenting significant differences between them. The ANCOVA shows high significant differences between the BN and the BP (4x4 m and 5x5 m). There was a moderate significant difference in MOE between the two plantations (4x4 m and 5x5 m).

Table 3. ANCOVA for the dynamic MOE of standing *Calophyllum brasiliense* trees in Colombia, considering DBH, HT and ρ as co-variables in the different forest types: DF: Degrees of Freedom, P > F: Significance of the F ratio, *: Significance level $\alpha = 5\%$, n.s.: not significant

Source of variation	DF	F-value	P > F
DHB	1	184.86	<.0001*
HT	1	3.13	0.0825 n.s.
P	1	1.81	0.1843 n.s.
Forest Type	2	34.76	<.0001*

The effect of DBH on the MOE of natural forest trees compared to plantation trees coincides with that reported by: (Wang *et al*. 2007), (Proto *et al*. 2017) on *Pinus nigra*, (Madhoushi and Boskabadi 2019) on *Paulownia fortune*, they indicate that the diameter of the tree has a significant effect on the acoustic wave measurements and, therefore, with the dynamic MOE. Although for (Liu *et al* 2021) in the simulation of *Larix principis-rupprechtii* Mayr trees, the propagation of acoustic waves depends on both tree diameter and propagation distance. They found that in the range between 10 and 40 cm in diameter (transition phase) the acoustic velocity of the tree increases with increasing diameter. This is contrary to the results obtained in this study, which showed that as the diameter increases, the acoustic velocity and MOE decrease.

The correlation analysis on the average MOE of the cardinal orientation with respect to diameter at breast height (DBH) and dynamic MOE showed a negative correlation, with a strong magnitude and a highly significant effect on the forest types evaluated as shown in Table 4.

Table 4 shows a correlation between MOE and total height of plantation trees (4x4 and 5x5 m) negative, with a significant effect and a moderate magnitude for PF (5x5 m). Trees at 4x4 m have no significant effect and their magnitude is weak. The correlation in the NF was positive, weak, and with no significant effect. The density in the saturated state (ρ) and the MOE of the NP show a positive, weak correlation with no significant effect. In the plantation such correlation was positive, but for trees at 4x4 m spacing it was not significant with a moderate magnitude and in trees at 5x5 m spacing it was significant and with a strong magnitude as shown in Table 4.

Table 4 Pearson correlations of dynamic MOE of different forests with DBH, TA, and ρ of standing trees of *Calophyllum brasiliense* in Colombia: MOE: Dynamic Modulus of Elasticity, NF: Natural Forest, PF: Plantation Forest, DBH: Diameter at Breast Height, TH: Tree Height, ρ: Density in saturated state, *: Significance level α = 5%, n.s.: not significant

Source of variation	DAP	TH	ρ
MOE_{NF}	-0.75032	0.19273	0.10736
	<.0001*	0.3076 n.s.	0.5723 n.s.
$MOE_{PF\ (4x4\ m)}$	-0.86079	-0.16817	0.31136
	<.0001*	0.3744 n.s.	0.0940 n.s.
$MOE_{PF\ (5x5\ m)}$	-0.89654	-0.38950	0.67503
	<.0001*	0.0334*	<.0001*

The linear regressions obtained between MOE and DBH (a variable that presented a significant effect on ANCOVA and a better performance in the correlation analysis), show that it is possible to predict MOE from DBH in the types of forest evaluated. Figure 2 shows the linear regressions obtained for NF, PF (4x4 m) and PF (5x5 m). In the NF the coefficient of determination (R^2) obtained a value of 0.68 explaining the variation of the MOE in 68% from the DBH with a CV = 5.4%. The PF (4x4 m) has an R^2 = 0.78, therefore the DBH explains 78% of the variability of the MOE with a CV value of 3.2% and PF (5x5 m) shows an R^2 = 0.80, explaining the variation of the MOE by 80% from the DBH.

The models resulting from the linear regression analysis using DBH as the best predictor of MOE for each forest were as follows: MOE_{BN} = -319,94DAP + 21368, $MOE_{BP(4x4\ m)}$ = -270,41DAP + 23254, and $MOE_{BP(5x5\ m)}$ = -239,85DAP + 22717 (Figure 2). Taking the trees at 4x4 m and 5x5 m distance as a single plantation forest, the applied linear regression analysis showed an R2 value of 0.78, explaining the variability of the MOE by 78% with a CV = 3.1%. The resulting model was -246.54 DBH + 22774.

The correlation and regression results presented between dynamic MOE and diameter at breast height in both forest types (natural and plantation) are consistent with that reported by (Wang *et al*. 2007b), (Legga and Bradley 2016), (Reyes 2019) for *Anacardium excelsum*. They found a negative relationship between DHB and modulus of elasticity. Larger diameter trees have less stiffness than smaller diameter trees. Therefore, it is possible and interesting to predict MOE from DHB.

Conclusions

The stiffness of *Calophyllum brasiliense* tree stems was higher in plantation trees than in trees growing in natural environments. It is possible to predict MOE from DHB with an inverse relationship. Larger diameter trees had less stiffness than smaller diameter trees.

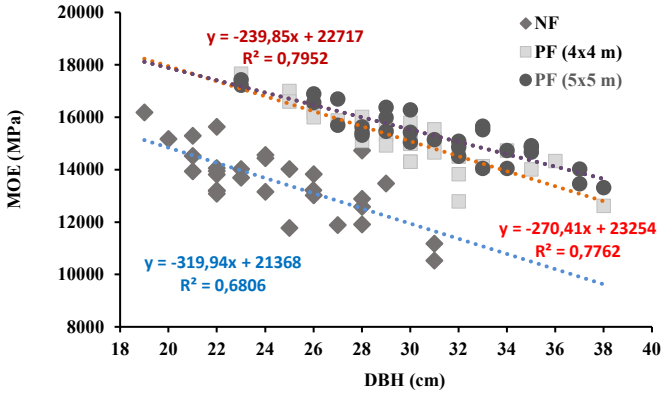

Figure 2 — Linear models to predict MOE from DBH in NF, PF (4x4 m) y PF (5x5 m).

The cardinal position where MOE was measured on the tree did not show any impact on its assessment. The effect of DBH on MOE showed high significant differences between the NF and the two plantation forests (4x4 m and 5x5 m). When comparing PF (4x4 m) with PF (5x5 m) the significant difference was moderate. Total height had no effect on the MOE of the different forest types.

The stress wave speed (SWS) technique in standing trees can be successfully used for the nondestructive assessment of wood stiffness among different forest types.

These results are of great practical interest, as they will allow the promotion of aceite maria plantations to market high-value products and contribute to the sustainable management of Colombian tropical forests.

Acknowledgments

The authors thank the Forest Engineer Willy Reyes, the students and officials of the Forest Engineering program at the Tropical Forest Center of the University of Tolima for their support in the field. The authors also thank Luc Germain and Paul Desaulniers for their technical assistance in the CRMR laboratories at Université de Laval.

References

Arévalo R, Londoño A (2005) Manual para maderas comerciales del Tolima. Universidad del Tolima. Ibagué (Colombia): 161 p.

ASTM D2395 – 17 (2017) Standard Test Methods for Density and Specific Gravity (Relative Density) of Wood and Wood-Based Materials. Copyright © ASTM International, United States: 13 p.

Auty D, Achim A (2008) The relationship between standing tree acoustic assessment and timber quality in Scots pine and the practical implications for assessing timber quality from naturally regenerated stands. Forestry: An International Journal of Forest Research, Vol. 81, No. 4. 475 – 487.

Bastidas A, Gómez F, Salcedo P, Chaparro R (1975) Propiedades físicas y mecánicas de doce especies del bosque muy húmedo tropical. Facultad de Ingeniería Forestal. Universidad del Tolima: 121.

Bertoldo C (2011) Estimativa de propriedades de rigidez da madeira a partir de avaliação acústica na árvore e em toras recém abatidas. Ph.D. thesis, Faculdade de Engenharia Agrícola. Universidade Estadual de Campinas. 85 p.

Chiu C, Lin C, and Yang T (2012) Application of nondestructive methods to evaluate mechanical properties of 32-year-old Taiwan incense cedar (Calocedrus formosana) wood. BioResources 8(1), 688–700.

Fakopp Enterprise Bt (2008) Treesonic microsecond timer User's guide. Hungary: 1 – 8.

Forero L (2014) Dinámica del bosque húmedo tropical en un periodo de 30 años de intervenciones y sus efectos en algunas variables edafológicas. Bajo Calima, Buenaventura, Colombia. Ph.D. thesis, Universidad Nacional de Colombia. Facultad de Ciencias Agropecuarias. Sede Palmira, Colombia: 110 p.

Hernández R, Restrepo G (1995) Natural variation in wood properties of Alnus acuminata H.B.K. grown in Colombia. Wood and Fiber Science by the Society of Wood Science and Technology, 27(1): pp. 41 – 48.

INIA (2018) Comportamiento del módulo de elasticidad de Capirona *Calycophyllum spriceanum* determinado con métodos no destructivos en plantaciones de 19 años. Subdirección de investigación y estudios especiales. Ministerio de agricultura y riego. Informe técnico N° 3. 22 p.

JUNAC (1981) Tablas de propiedades físicas y mecánicas de 24 especies de Colombia. Junta del Acuerdo de Cartagena (JUNAC PAD-REFORT)). Lima Perú: 120 p.

Legg M, Bradley S (2016) Measurement of stiffness of standing trees and felled logs using acoustics: A review. Journal Acoustical Society of America (JASA). 588 – 604.

Liu F, Zhang H, Wang X, Jiang F, Yu W, Ross R (2021) Acoustic wave propagation in standing tres - Part II. Effects of tree diameter and juvenile wood. Wood and Fiber Science, 53(2), pp. 95-108.

Madhoushi M, Boskabadi Z (2019) Relationship between the dynamic and static modulus of elasticity in standing trees and saw lumbers of Paulownia fortune planted in Iran. Universidad del BIO-Bio. Maderas Ciencia y tecnología, vol. 21, no 1. 35-44.

Madhoushi M, Daneshvar S (2016) Predicting the static modulus of elasticity in eastern cottonwood (Populus deltoides) using stress wave non-destructive testing in standing trees. European Journal of Wood and Wood Products volumen 74, 885 - 892

Martínez H (2006) Análisis ecológico silvicultura, con fines de manejo, del bosque secundario de la vereda las brisas, Buenaventura, Valle del Cauca. Ph.D. tesis, Facultad de Ciencias, Universidad del Valle: 199 p.

Mendoza V (2017) Pruebas no destructivas y destructivas de la madera de la especie *Tachigali colombiana* Dwyer (guamo querré) procedente del Bajo Calima municipio de Buenaventura, Colombia. Undergraduate thesis, Facultad de Ingeniería Forestal. Universidad del Tolima. Colombia. 85 p.

Proto A, Macrì G, Bernardini V, Russo D, Zimbalatti G (2017) Acoustic evaluation of wood quality with a non-destructive method. Forest Biogeosciences and Forestry, Vol. 10: pp. 700 – 706.

Reyes W (2019) Evaluación de los árboles de las especies Anacardium excelsum (caracolí) y Guarea guidonia (bilibil) mediante métodos no destructivos en un conjunto residencial de la ciudad de Ibagué-Tolima. Undergraduate thesis, Facultad de Ingeniería Forestal. Universidad del Tolima. 85 p.

Vásquez Á, Ramírez A (2011) Anatomía e identificación de maderas. Facultad de Ciencias Agropecuarias, Departamento de Ciencias Forestales, Laboratorio de Productos Forestales "Héctor Anaya López" Universidad Nacional de Colombia Sede Medellín: 70 p.

Wang X (2013) Acoustic measurements on trees and logs: a review. USDA Forest Products Laboratory. Wood Sci Technol. @Springer-Verlag (outside the USA). Madison, WI, USA, 47:965–975.

Wang X, Ross R. J, Carter P (2007) Acoustic evaluation of wood quality in standing trees. Part I. Acoustic wave behavior.Acoustic wave behaviour. Wood Fiber Sci. 39: 28-38.

Yin Y, Nagao H,·Liu X, Nakai T (2010) Mechanical properties assessment of Cunninghamia lanceolata plantation wood with three acoustic-based nondestructive methods. United States, Department of Agriculture, FOREST SERVICE, Forest Products Laboratory, General Technical FPL 25. 1979: 33 – 40.

Field Assessment of Downed Timber Strength Deterioration Rate and Wood Quality Using Acoustic Technologies

Munkaila Musah*
Forest Products Development Center, Auburn University, Auburn, AL, USA, mzm0263@auburn.edu

Javier Hernandez Diaz
Forest Products Development Center, Auburn University, Auburn, AL, USA, jah0189@auburn.edu

Dana Mitchell
USDA Forest Service, Southern Research Station, Auburn, AL, USA, dana.mitchell@usda.gov

Mathew Smidt
USDA Forest Service, Southern Research Station, Auburn, AL, USA, mathew.smidt@usda.gov

Tom Gallagher
School of Forestry and Wildlife Sciences, Auburn University, Auburn, AL, USA

Maria S. Peresin
Forest Products Development Center, Auburn University, Auburn, AL, USA, soledad.peresin@auburn.edu

Brian Via
Forest Products Development Center, Auburn University, Auburn, AL, USA, brianvia@auburn.edu

* Corresponding author

Abstract

Hurricane and tornado events cause significant damage to high-value timber in the United States each year. Forest managers and landowners are keenly interested in finding solutions to salvage and repurpose these downed timbers before they cause pest infestations and fire outbreaks, losing their value completely or increasing processing costs. To better understand the wood quality of downed timber, we used acoustic wave techniques as a nondestructive testing approach to assess the wood degradation rate of downed trees and determine the extent of fracture and voids in the damage regions. We monitored the acoustic velocity of the downed trees periodically for 12 consecutive months using a time-of-flight (TOF) acoustic method. Acoustic measurements were conducted in three different approaches, longitudinal, transverse, and off-set method. Wood density, age and the diameter at breast height (dbh) class measurement for the South (Chip-n-saw for dbh 8–11 in. and Sawtimber with dbh 12 in. and up) were used as predictive parameters of the downed trees.The results indicated positive relationships between tree dbh class, stand age, and all acoustic velocity measurement ($R^2 > 65\%$), except the longitudinal measuring technique ($R^2 = 45\%$). The regression coefficient from the repeated measures indicated that both age and diameter class have strong impact on the acoustic properties of the downed trees (P-value < 0.000). The Sawtimber dbh class recorded higher acoustic velocity compared to the chip-n-saw class. Generally, the acoustic measurements were able to detect fracture, voids, and massive decay in downed trees beyond the visible inspection; however, they showed a weak response in picking up subtle incremental deterioration as changes in certain environmental factors (rain, humidity, moisture) affect acoustic readings. The results of this study showed that acoustic wave methods have potential for use as a field evaluation tool for assesing the quality of downed trees.

Keywords: Acoustic velocity, Dbh class, Down timber, Non-destructive evaluation, Wood properties

Models for Predicting the Within-Tree Variation of Ultrasonic Velocity and Dynamic Modulus of Elasticity for Plantation Loblolly Pine

David Auty *
School of Forestry, Northern Arizona University, Flagstaff, Arizona, USA, David.auty@nau.edu

Joseph Dahlen
Warnell School of Forestry and Natural Resources, University of Georgia, Athens, Georgia, USA, jdahlen@uga.edu

Thomas L. Eberhardt
USDA Forest Service, Forest Products Laboratory, Madison, Wisconsin, USA, thomas.l.eberhardt@usda.gov

Laurence Schimleck
Wood Science and Engineering, Oregon State University, Corvallis, Oregon, USA, laurence.schimleck@oregonstate.edu

Nawa Pokhrel
Warnell School of Forestry and Natural Resources, University of Georgia, Athens, Georgia, USA, nawaraj.pokhrel@uga.edu

* Corresponding author

Abstract

Approximately 90 percent of conifer wood is comprised of longitudinal tracheids, which are responsible for water transportation and mechanical support of the standing tree. The anatomical and mechanical properties of tracheids vary within the tree, which ultimately impacts the utilization of the wood. Young trees contain a high proportion of low-stiffness corewood that can be attributed to high microfibril angle values in tracheid cell walls. As an alternative to expensive microfibril angle measurements using X-ray diffraction techniques, related properties such as dynamic modulus of elasticity (MOE_{dyn}) can be determined using a combination of wood specific gravity (SG) and ultrasonic velocity (USV), the latter measured at frequencies greater than 20 kHz. The objective of this study was to examine the within-tree variation in wood stiffness for loblolly pine grown in southeastern Georgia through assessment of SG, USV, and MOE_{dyn}. In total, 419 pith-to-bark radial strips collected from multiple height levels in 92 trees were processed to obtain matching SG (2-mm tall) and USV (8.2-mm tall) samples. Ring-by-ring SG was measured using X-ray densitometry and time-of-flight USV was measured at a 10-mm radial resolution from pith to bark. A subset of samples was sent to SilviScan to determine microfibril angle using X-ray diffraction. The relationship between microfibril angle and USV was strong ($R^2 = 0.91$, RMSE = 2.6°). Nonlinear mixed-effects models were developed to predict radial variation in SG, USV, and MOE_{dyn}. Fixed effects for the models, which included cambial age and height of disk within tree, had R^2 (pseudo) of 0.67 for SG (RMSE = 0.051), R^2 of 0.71 for USV (316 m/s), and R^2 of 0.69 for MOE_{dyn} (1.9 GPa). When combined with SG measurements from X-ray densitometry, acoustic velocity measurements from pith to bark are a powerful tool for assessing variability in wood stiffness.

Keywords: acoustic velocity, nondestructive testing, *Pinus taeda*, SilviScan, southern pine, wood and fiber quality, wood stiffness

Electric Resistance Tomograph: A Nondestructive Testing Approach to Valuation of High-Value Trees of India

B.N. Divakara*
Department of Silviculture Forest Management, Institute of Wood Science and Technology, Bangalore, Karnataka, India, bndsira@gmail.com

S. Chaithra
Department of Silviculture Forest Management, Institute of Wood Science and Technology, Bangalore, Karnataka, India, greenivyscarlet14@gmail.com

C. Balaji
Department of Silviculture Forest Management, Institute of Wood Science and Technology, Bangalore, Karnataka, India, balajich95216@gmail.com

*Corresponding author

Abstract

Electric resistance tomograph (ERT) is a promising nondestructive technique to noninvasively study the stems of standing trees. It allows insights into xylem properties based on the cross-sectional distribution of electrical resistivity that is governed by the wood's electrical conductance. ERT as a nondestructive tool can capture the complete assembly of the internal structure of the standing tree without harming the perpetual health of the tree. This multisensor channel system passes the required current to the tree based on its wood moisture and electrolyte content to sense the status of wood internally. By generating an electrical field to conduct the tests at different tree heights starting from ground level to clear bole height, a three-dimensional structure of any tree can be obtained and thereby the valuation of that tree can be analyzed with subsequent measurement of the electrical conductivity. The value of a tree, with certain years of a fixed financial rotation period especially for highly valued trees such as *Santalum album* and *Pterocarpus santalinus* within a tropical community, provides significant ecological, economic, and social benefits. Economic value may be defined as the monetary worth of a tree at a given time with the expectation of benefit, and the valuation of the tree can be estimated using ERT three-dimensional technology by deciphering the internal formation of the wood and its health. Therefore, ERT can be a nondestructive approach to estimating the value of highly valued trees in India.

Keywords: electric resistance tomograph, nondestructive testing, *Santalum album*, *Pterocarpus santalinus*

Session 3

NDE for Urban Trees

Tree Risk Assessment: A Systemic Approach Involving Nondestructive Techniques and Tree Biomechanics

Raquel Gonçalves *
Nondestructive Testing Laboratory (LabEnd), School of Agricultural Engineering (FEAGRI), University of Campinas (UNICAMP), Campinas, São Paulo, Brazil, raquelg@unicamp.br. * Corresponding author

Gustavo Garcia
LabEND, FEAGRI, Unicamp, gustavohlgarcia@gmail.com

Karen Freitas
LabEND, FEAGRI, Unicamp, karen.chris@gmail.com

Mariana Reis
LabEND, FEAGRI, Unicamp, ma.nagle.reis@gmail.com

Stella Palma
LabEND, FEAGRI, Unicamp, ssapalma@gmail.com

Camila Linhares
SERQ – Innovation and Competence Forest Centre, Sertã, Portugal, clinhares@serq.pt

Monica Ruy
Structural Wood Engineering Platform, University of Santiago of Compostela, Lugo, Lugo – Spain, m.ruy@usc.es

Abstract

The analysis of the risk of falling trees is complex, involving many different knowledge, such as the physical and mechanical properties of the different parts of the tree (root, trunk and branches), both in clean and deteriorated conditions; the forces acting on the standing tree, which trigger different types of efforts on roots, trunks and branches; the influence of aspects related to the surroundings and planting conditions; and the expected behavior of this tree subjected to such efforts. This complexity made the research group on nondestructive testing at the School of Agricultural Engineering of the University of Campinas, Brazil work, for years, on research at different levels (scientific initiation, master's, doctoral and postdoctoral) with a common focus. This work aims to briefly address the main results of this group involving the nondestructive characterization of wood from different parts of the tree and in different health conditions; the association of physical and mechanical parameters with those inferred using nondestructive field inspection techniques; the development of methodologies for the inference of wind loads on trees, involving the simplified calculation of the drag coefficient, the wind speed trunk profile and the crown geometry and area; and the development of a methodology for analyzing aspects of the surroundings that impact the stability of the tree and, finally, incorporating all these aspects into a proposal for a simplified simulation of the tree's behavior, using numerical methods, with a focus on the analysis of the risk assessment. It is expected, with this systemic approach, to introduce a methodological proposal that allows us to obtain results closer to the specific condition of trees and, thus, treatments or interventions that are also more specific, reducing, as far as possible, given the inherent complexities of this approach, accidents, or unnecessary tree suppression.

Keywords: tree inspection, ultrasound tomography, wood from root, branch, and stem characterization

Introduction

The urban system is composed of gray infrastructure (buildings, roads, pipes, etc.) and green infrastructure, basically composed of urban forest (Tomao et al. 2015). The urban forest brings countless benefits to cities, but they are often seen as risks because trees are living beings that age, get sick and die and, when they fall without warning, they cause accidents. Thus, for this system to be adequate, it is necessary to manage the old trees as well as the young ones that succeed them (Corona et al. 2011). In this context, the risk of falling has been the focus of many studies (Smiley et al. 2012, Tomao et al. 2015, Coelho-Duarte 2021), involving great complexity. Coelho-Duarte (2021) mentions that the first studies associated with the risk of trees began in the 1960s/1970s and that since the 1990s, different methods have been proposed. Visual methods were pioneers, and many manuals were published that allow risk recognition based on the defects and symptoms that can be identified (Pokorny 2003). Tomao et al. (2015) developed a tree risk index involving three dimensions: the hazard representing the probability of failure, the target value, and the potential for injury. Coelho-Duarte (2021) compared six methods of visual analysis in classifying the risk of falling, concluding that the inspector's experience, the location of trees and the characteristics of the species influence the efficiency of the analysis.

Our group began research in ultrasound in 1997, focusing on the classification of sawn wood, having been the first doctoral thesis defended in this area in 2001. In 2008, we began research in ultrasound applied to the forestry sector, with a focus on the classification of wood from the tree. In 2009, research began focusing on tree inspection.

The first focus of research on trees, aimed at inspection, arose from the need for a Brazilian company (Cikel), which carries out forestry exploration in the Amazon through certified management (Forest Stewardship Council - FSC). This company was interested in getting to know the trees with cavities before proceeding with selective cutting (management). In parallel, we know the company Tora Brasil, which operates in the luxury furniture market produced with tunks from forest management in the Amazon, also certified by the FSC. The furniture produced by this company considers the organic shape and imperfections, including cavities, existing in the trunks. In view of these characteristics (Figure 1), both companies needed to know the existence and positioning of cavities inside the standing trees and, later, the trunks.

Trunks in Cikel Company

Roche Farma, São Paulo, Brazil

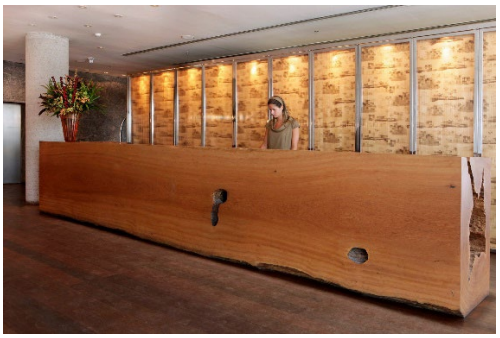

Hotel Fasano, Rio de Janeiro, Brazil

Figure 1— Cut trees with large internal hollows (Company Cikel) and furniture produced by Company Tora Brasil taking advantage of the organic shape and defects of the logs.

Thus, we started our research using ultrasound equipment (developed in our research group in partnership with the AGRICEF Company) and a pair of transducers. The equipment (Figure 2) was developed with high power (700 watts) with the possibility of operating at different frequencies (from 20 to 1000 kHz).

Figure 2— Ultrasound equipment and transducers adopted in our research

After the first publicity of our work with forest trees, opportunities to work with urban trees began to appear. Aware that, to know the phytosanitary state of a tree, it is necessary to associate knowledge and techniques, it was also necessary to address the association of techniques and equipment, which in the case of our group were visual analysis, drilling resistance and ultrasonic tomography. Additionally, no matter how good the results of an inspection, knowing the risk of a tree falling involves many other parameters, including the local surroundings and planting conditions, the performance of the wind, the properties of each part that composes it (roots, stem, and branches) and safety factors. To associate these parameters and thus respond more adequately about the risk of a tree, it was first necessary to invest in the knowledge of each parameter in isolation.

The objective of this work is to present a sequential overview used by our research group to systematize the progress in this tangle of knowledge and complexities, that is, the biomechanics of trees.

Systemic approach to the problem and main results

Regarding tomography, our approach has always been to evaluate the feasibility of using a more accessible technology for our country, and as we had already developed ultrasound equipment (Figure 1) based on the needs of wood (high power), we started the hypothesis that it would be possible to use this same equipment for tree inspections, making the technology cheaper when compared to the use of commercial tomographs already available in the international market.

For the tests on trees and logs, we studied different types of meshes (reticulate and diffraction) and different frequencies of transducers, and to obtain the images, we initially used an image software developed for remote sensing - ArcGis. This software allowed working with two types of interpolators – the inverse square of distance (ISD) and kriging (2009 to 2011). With the evolution of research (2015 to 2017), we developed specific software (ImageWood) for the application we wanted, studying two types of interpolators, the ISD and the ellipse method with and without compensation proposed by Du et al. (2015).

To adjust the fieldwork, we studied the minimum number of measurement points in the mesh, capable of maintaining the image quality without increasing the fieldwork too much. We also evaluated the feasibility of reducing the number of measurement repetitions on the same route (in two directions) from 2017 to 2022.

To advance our knowledge, we separately studied (2011 to 2014) the behavior of wave propagation in the presence of knots, pith, cavities caused by termites and biodeteriorations caused by fungi. This knowledge began to allow us to study a pattern of velocity variation (2015 to 2017) that effectively represented, through the association with colors, different conditions of the wood. Further advances, using quantitative analysis (confusion matrix) of the results, were made to obtain cutting velocities that represent variations in the properties of clean and deteriorated wood, associating macro and microscopic analyses and determinations of stiffness and density in different positions inside the trunk (2017 to 2022). For the microscopic analysis, we count on the collaboration of the Institute of Technological Research of the State of São Paulo (IPT), which has the experts and the appropriate equipment for microscopic analysis, mainly of deteriorated wood. Still focusing on improving image quality, using simplified methods and open technology, we studied the application of filters in the images.

The product of this step was the images produced with good definition and accuracy (Figure 2) using the manual measurement process with our ultrasound equipment and a pair of 45 kHz frequency transducers; diffraction mesh proposed by Divos and Divos (2005) with a number of points equal to 5 times the perimeter of the trunk; ellipse algorithm with velocity compensation proposed by Du et al. 2015; and median filter with 30 pixels for 6-point mesh, 25 pixels for 8-point mesh, and 20 pixels for meshes with more than 10 measurement points. We also concluded that measurements can be performed on each theoretical route in only one direction, with repetition in the opposite direction being performed only when signal problems are observed. The velocity ranges are always constructed as a function of the reference velocity, which, in our methodology, is the maximum (V_{max}) obtained in the section under inspection.

Considering that our tomography did not use an industrial tomograph with more complex embedded technology, it was necessary to act in several peripheral aspects to guarantee the effective quality of the image produced (2011 to 2022). Thus, we studied the issue of how to obtain the contour coordinates of irregular trunks necessary for insertion in the imaging software (2011 to 2016). The results allowed obtaining from more complex tools to be applied in more irregular trunks (with indentations) to macros

that allow simplifications (2017 to 2022) for the case of less irregular trunks, without significant losses in the quality of the images produced - Figure 3.

Seeking additional answers that could help researchers and users of acoustic tomography, we also compared the results of images produced through inspections of standing trees and disks in the laboratory, concluding that, using the adopted reference velocity methodology (V_{max}), the results of tomography obtained in the laboratory are equivalent to those obtained in the field. However, we found that there may be an influence of climatic parameters on tomographic images (2017 to 2022), caused by variations in sap flow flux and as a function of acoustoelastic parameters. If this influence is confirmed, studies will be needed to propose a velocity correction factor associated with the times of the day or year in which the measurements are performed.

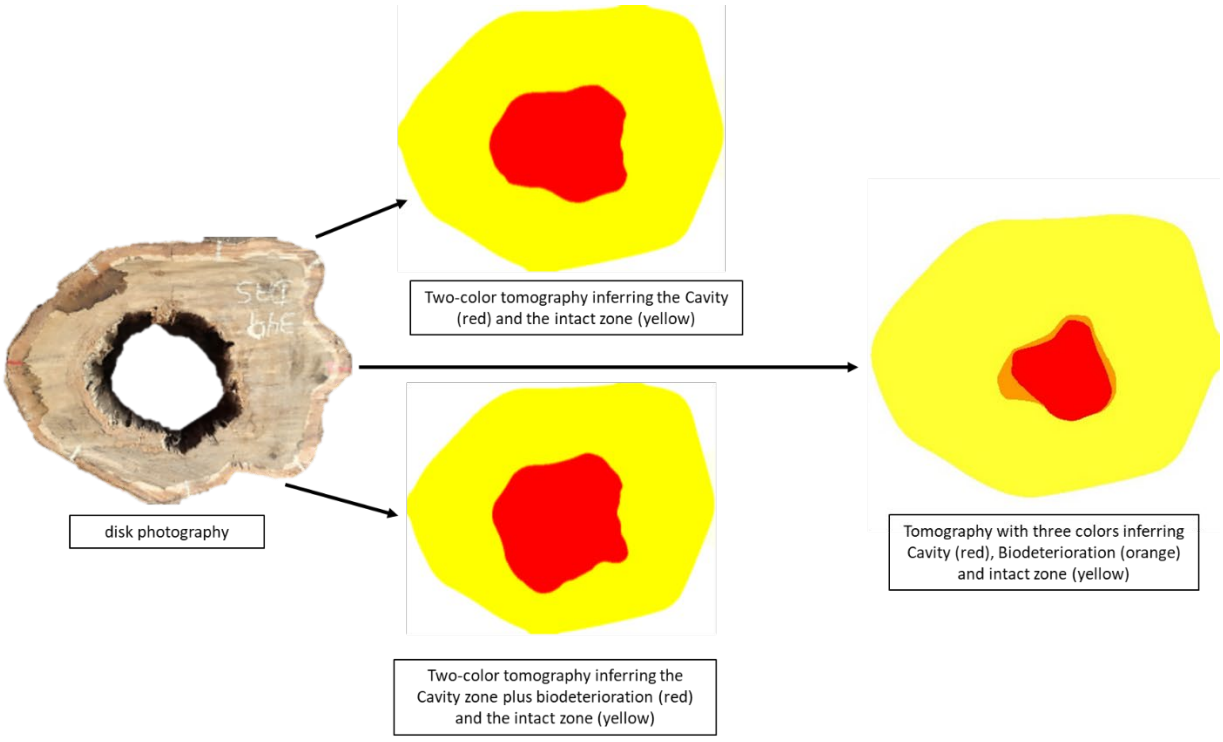

Figure 2— Results of images produced by ultrasonic tomography to infer cavity, biodeterioration and both zones

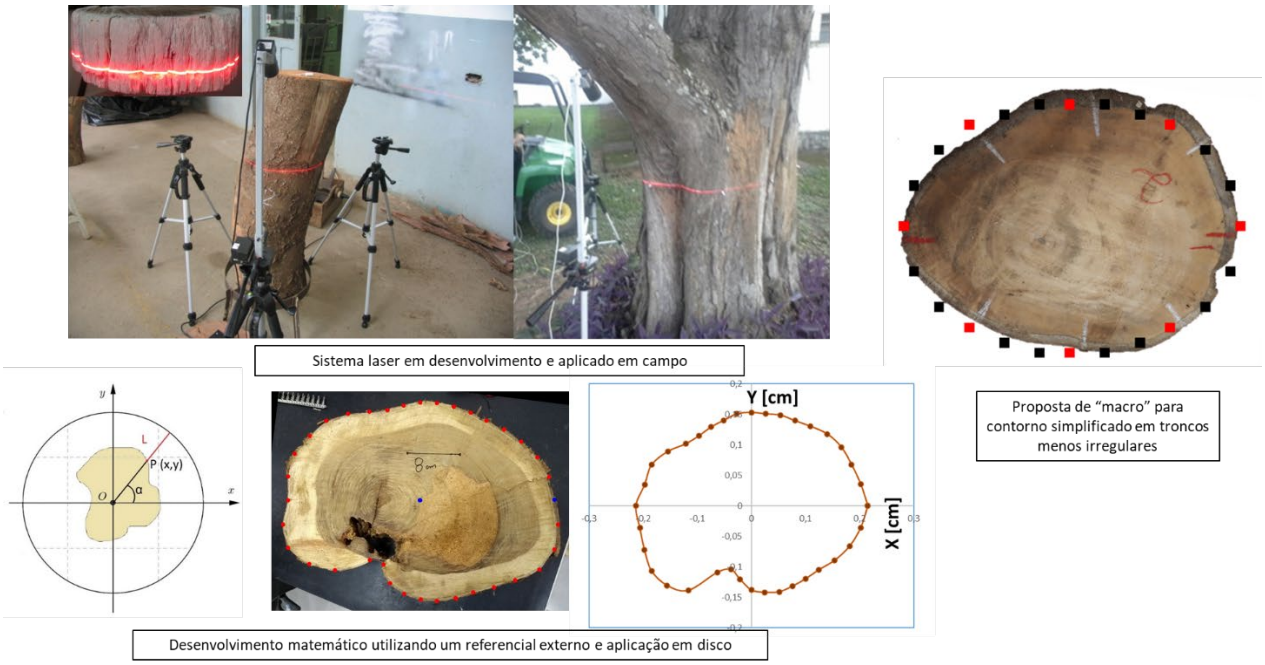

Figure 3— Development of techniques for obtaining, in the field, the contour coordinates of trunks

Aware that the risk of a tree falling involves many other parameters in addition to the condition of its trunk, we started to plan the use of computer simulation using the finite element method (FEM) to enable the composition of the parameters necessary for this complex analysis. In view of the complexity of an analysis that would consider the actual behavior of the tree and the actions that act on it, we are aware that our approximations are very simplified, which does not make it any less useful. The tree model must be simplified, but we can keep the wood properties closer to the real properties. Thus, we invested in proposing the characterization, by ultrasound, of the wood of the roots, branches and trunk (2016 to 2018), with determination of the complete stiffness matrix (3 longitudinal elasticity modules, 3 shear modules and 6 Poisson's coefficients) to feed the model made in the MEF.

It was also necessary to check how to consider the conditions of the roots of the tree. For this, we once again teamed up with the IPT, and in a joint project, we evaluated the soil of the bed (compaction) and the feasibility of obtaining the characteristics of the distribution of the roots around the tree (2018 to 2020). The study involved visual analysis, ultrasound, and stress waves to assess rooting distribution and a soil penetrometer.

For the construction of a tree model to be used in numerical simulation, in addition to the approximate knowledge of the distribution of roots and the properties of the soil containing the clod, it is necessary to consider the canopy architecture (2016 to 2018) and the adaptive characteristics of trees (tigmomorphogenesis) from 2018 to 2019.

For the numerical simulation, in addition to the tree model and its soil anchoring conditions, it is necessary to insert parameters related to the main loads to which it is subjected. As in our country we do not have snow loads, we invested in the analysis of gravitational and wind loads. For gravitational loads, dendrometric data easily measurable in the field and our previous findings (canopy architecture and thigmomorphogenesis) were sufficient, but it was necessary to work on the issue of wind action. For this, we started the work of gathering data from the literature that were sparse and carried out a study to

propose a simplified way of calculating the drag coefficient (2017 to 2019), once again in partnership with the IPT. The complexity of wind action on trees led us to deepen our knowledge by studying the drag force and the velocity distribution profile in the crown and stem considering different crown architectures (2018 to 2022).

With all these factors in hand, it was possible to propose models to be used in numerical simulation to infer the behavior of trees against the action of gravitational loads and wind (2017 to 2020). All of them are still mere simplifications in the face of the enormous complexity of the trees, but we have already considered important advances for our focus, which is the assessment of the risk of falling. These models grew in complexity in terms of tree representation (from the simplest to the most detailed), application of wind load, representation of the zone surrounding the roots and behavior of its different parts (root, stem and branches). To better assess the risk caused by a given action, it is important to know the safety factor, which is a complexity apart from trees and whose study we are currently involved in (2020 to 2024).

Thus, in the last 13 years, our group has been systematically developing research focusing on the biomechanics of trees to contribute to improving the scope of the inference of the risk of falling trees (Figure 4). The simulation models allow us to insert two types of tree architecture (monopodial and sympodial), to consider the differentiation and orthotropy of the wood of roots, branches, and trunk, to consider the properties of the soil and the dimensionality of the clod and, also, to insert into the stem defects inferred by tomography. As a result, displacements and normal and shear stresses are obtained along the trunk and, in possession of adequate safety factors for the trees, infer the risk of rupture.

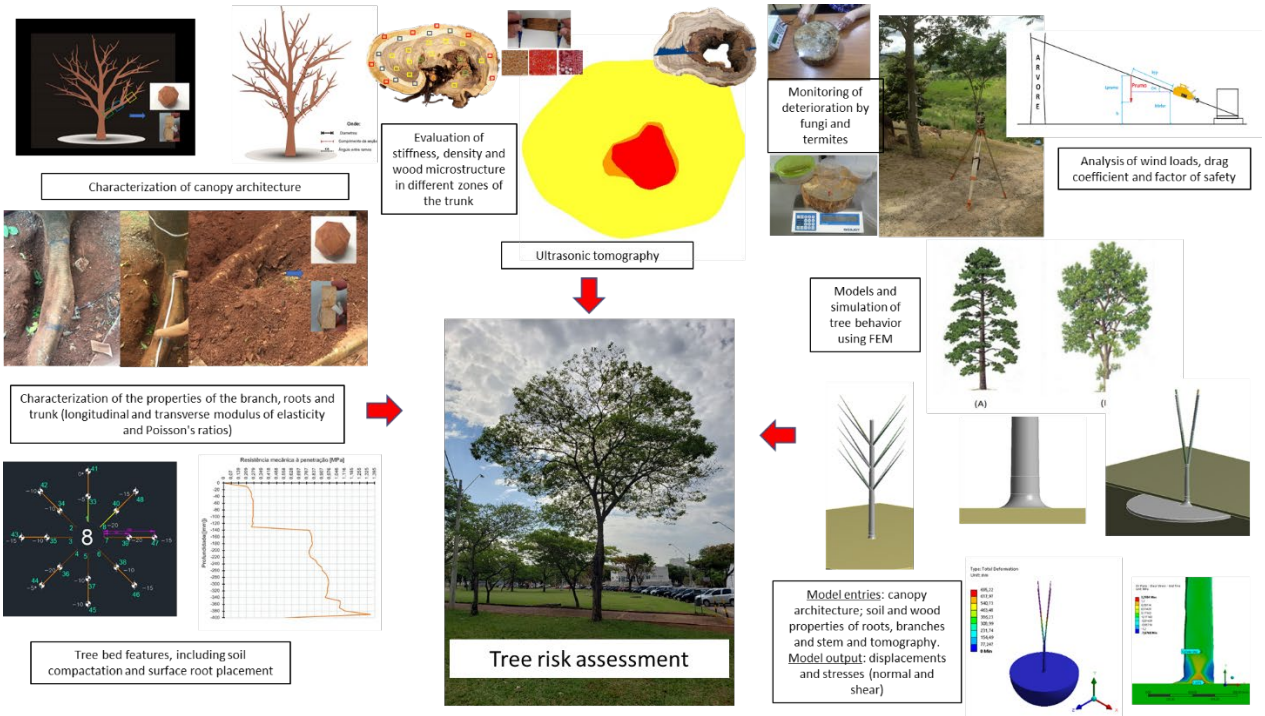

Figure 4— Systemic process of research related to tree biomechanics focusing on tree fall risk analysis

Conclusion

The research, systematically organized around a greater common objective, made it possible to advance and answer questions on different fronts and, thus, contribute to proposing a set of actions that, together, allow a more assertive assessment of the risk of falling.

Acknowledgments

In view of the years of research involved, we thank FAPESP (2008/00622-3, 2009/10319-9, 2011/08286-5, 2012/22599-9, 2015/05692-3, 2018/14386-1) and CNPq (305316/2008-7, 552681/2009-1, 426130/2018-9) for funding individual projects as well as scholarships and CAPES for scholarships and support for the Graduate Program (Código 001).

References

Coelho-Duarte, A.P.; Daniluk-Mosquera, G.; Gravina, V.; Vallejos-Barra, Ó.; Ponce-Donoso, M. 2021. Urban Forestry & Urban Greening. 59: 127005.

Corona, P., Chirici, G., McRoberts, R.E., Winter, S., Barbati, A. 2011. Contribution of large-scale forest inventories to biodiversity assessment and monitoring. Forest Ecol. Manage. 262, 2061–2069.

Divos, F.; Divos, P. 2005. Resolution of stress wave based acoustic tomography. In: 14th international symposium on nondestructive testing of wood Proceedings, Germany 309–314.

Pokorny, J.D., 2003. Urban Tree Risk Management: A Community Guide to Program Design and Implementation. Retrieved March 30th, 2020 from. USDA Forest Service.

Smiley, T.E., Matheny, N., Lilly, S., 2012. Qualitative Tree Risk Assessment. Arborist News 20 (6), 12–17.

Tomao, A.; Secondi, L.; Corona, P.; Giuliarelli, D.; Quatrini, V.; Agrimi, M. 2015. Can composite índices explain multidimensionality of tree risk assessment? A case study in an historical monumental complex. Urban Forestry & Urban Greening. 14: 456-465.

Use of Tomographic Images to Support the Inference of Strength Loss in Trunks Using Equations from Literature

Mariana Nagle dos Reis *
School of Agricultural Engineering – University of Campinas, São Paulo, Brazil,
ma.nagle.reis@gmail.com

Raquel Gonçalves
School of Agricultural Engineering – University of Campinas, São Paulo, Brazil,
raquel@feagri.unicamp.br

Camila Stephanie Fernandes Linhares
Coimbra University, Coimbra, State, Country, email@email.com

Abstract

Trees in urban environment are subject to failures that can cause human and material losses but knowledge of the phytosanitary status of trees helps to prevent accidents and is particularly important in urban context. Some equations are proposed in the literature to infer the strength loss. These equations are based on cavity and trunk diameter relation, or based on the remaining stem wall dimension. However, these equations have limitations, such as assuming only cavities, always centered, and not including the wood decay or eccentricities. It is expected that tomographic images represent, with relative accuracy, the dimension, and the position of biodeterioration inside the trunk. Therefore, the objective of this study was to quantitatively evaluate whether the use of ultrasonic tomography allow to improve the accuracy of the equations used to infer the strength loss of tree trunks with the presence of cavities and biodeteriorations. The results showed that ultrasonic tomography images allowed the equations to be closer to real conditions of the tree trunk, such as the inclusion of wood strength reduction from decay and the displacement of internal cavities in calculating the reduction of the moment of inertia.

Keywords: biodeterioration, mechanical stress, tree hazard, tree risk assessment

Introduction

The provision of urban green spaces and their associated benefits are important for sustainable urban development as far as ecological, economic, and social aspects are concerned (Jansson 2014). Urban forests provide benefits that may strengthen community resilience to climate change. Forested urban areas promote social interaction, and contribute to a sense of place and family for residents, resulting in more stable communities.

However, trees are subject to failure that may lead to their fall. In this context, knowledge of the phytosanitary status of trees helps to prevent accidents and is particularly important in urban environment due to possible human and material losses. Therefore, the inference of the likelihood of tree failure is very significant for the management of urban forests to define the best corrective treatment or suppression.

Studies have found that the extent of urban forest benefits and ecosystem services depends on several factors including: tree structure, health condition and physiology. It is strongly related to the presence of inner decays, which can lead to wood strength loss and, consequently, its decline. Hence, test methodologies are important to provide knowledge about the health, safety and structural conditions of trees and improve the measurement accuracy (Alani et al 2019, Vidal et al 2019, Li et al 2021, Salsabila et al 2021).

Some methods are consolidated in the detection of the external and internal conditions of trees, such as visual analysis (Giacomazzi et al 2020; Duarte et al 2021), the use of tomography (Brazee et al 2011; Rust 2022), and drilling resistance (Vlad et al 2018; Reis et al 2019). Tree trunks are subject to efforts directly from their weight and the weight of their branches and leaves (canopy). However, the most important and significant load comes from the wind, which have been considered frequent causes of mechanical failure in trees (Gonçalves et al 2020). The response of the tree to this load is dynamic in nature (Chan et al 2020; Jackson et al 2021). However, the complexity of this dynamic consideration makes many authors propose replacing the wind action by a horizontal load applied at the center of gravity of the canopy as a simplification (Gonçalves et al 2020).

Among the methods used to infer the falling tree risk, some equations have been proposed to quantify the strength loss using formulas (Wagener 1963; Coder 1989; Smiley and Fraedrich 1992; Mattheck and Kubler 1995). The main limitations of these equations to estimate the reduced load-bearing capacity are assumed that the cross-section's neutral axis corresponds to the centroid axis and only accounts for cavities and not decayed areas (Ciftci et al 2014; Reis et al. 2022). In this sense, Burcham et al (2019) and Reis et al. (2022) present interesting proposals for using ultrasonic tomography to increase the accuracy for predict the internal condition of trees.

Although all equations to infer the strength loss have been developed considering important simplifications of the geometry of the trunk and cavities, Equation 1 proposed by Coder (1989) is the most conservative for the inference of the strength loss (SL). This equation assumes concentric decayed and solid areas sharing the same centroid (Figure 1a) using the relation of the second moment of area of a cylinder of homogeneous and isotropic material and a hollow cylinder, both with a circular cross-section.

$$SL = \frac{d^4}{D^4} \tag{1}$$

d = internal cavity diameter; D = trunk diameter

Equation 2, proposed by Wagener (1963), is also based on reducing the second moment of area, but the author changed the exponent (four to three). The exponent change and the choice of this specific number (3) is unclear Burcham (2019).

$$SL = \frac{d^3}{D^3} \tag{2}$$

d = internal cavity diameter; D = trunk diameter

Equation 3, proposed by Smiley and Fraedrich (1992) and adapted from equation 3 (Wagener 1963), includes the consideration of open cavities (Figure 1b). According to Kane et al (2001), this is very important, as these cavities remove the outer rings, which are fundamental to trunk strength.

$$SL = \frac{d^3 + R \times (D^3 + d^3)}{D^3} \tag{3}$$

d = internal cavity diameter; D = trunk diameter; R = ratio between the length of the cavity opening (Cc) and the trunk circumference (C)

Mattheck and Kubler (1995) did not follow the same logic of using the reduction of the second moment of area in the inference of strength loss on the tree trunk. They used the concept of the relation between the residual wall thickness and the trunk radius (Equation 4), also considering the trunk as a cylinder.

$$SL = \frac{t}{Rs} \quad (4)$$

t = residual wall thickness; Rs = trunk radius

Thus, it is verified that all equations consider only the cavities, which effectively cause a reduction at the second moment of area. However, trees may have deteriorated regions associated or not associated with internal cavities which would affect its residual resistance. The use of tomographic images is one of the ways to evaluate both cavities and deteriorated areas inside the trunk. This methodology has proven to be efficient in detecting deteriorated areas (Reis 2017; Palma 2017).

It should also be noted that all Equations that use reductions at the second moment of area (Equations 1,2 and 3) consider that the cavity is centered. However, much higher inertia reductions occur when the cavity is eccentric, affecting the inference of the strength loss proposed by the equations.

Thus, the objective of this research was to evaluate whether the use of ultrasonic tomographic images improves the reach of the equations proposed in the literature for inferring the strength loss of trees due to the presence of cavities and decay. More details about this research can be seen at Reis et al. (2022).

Methodology

The samples used in this experiment consisted on 12 cross-sections of approximately 300 mm high from *Cenostigma pluviosum* (Sibipiruna) trees taken from the campus of the State University of Campinas – Unicamp in the city of Campinas, São Paulo, Brazil. These cross-sections had different types and stages of decay. Summary of the methodology used can be seen in the flowchart (Figure 1).

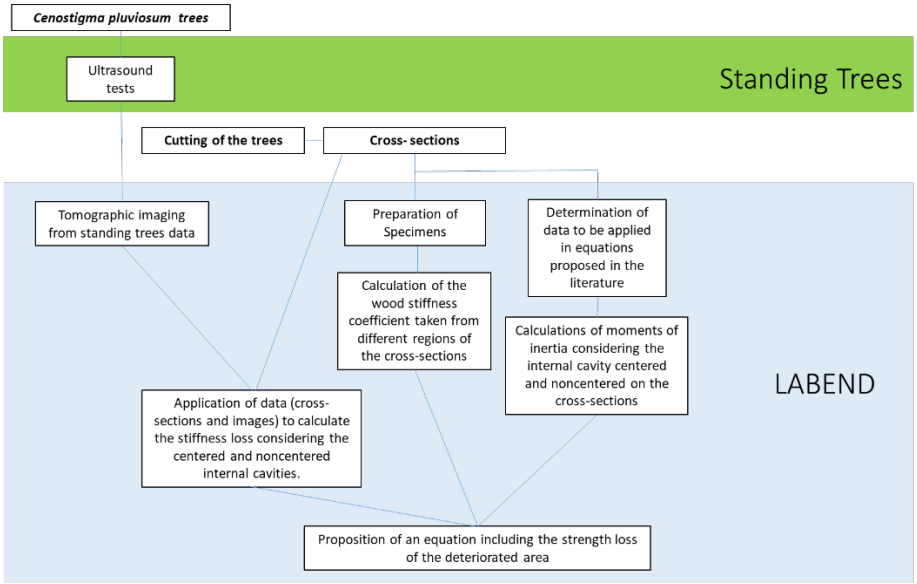

Figure 1 - flowchart of the methodology

The ultrasound tests were performed at breast height (1.3 m from the ground) in the standing trees using ultrasound equipment (USLab, Agricef, Brazil) and 45 kHz exponential face transducers applied using eight measuring-point diffraction mesh and radial wave propagation.

The tomographic imaging from standing tree data was processed using ImageWood 3.0, software developed by the LabEnd* research group (ImageWood 3.0). We adopted the interpolation system proposed by Du et al (2015), with velocity compensation, which has already been used in other studies, providing good results (Reis 2017; Palma 2017). To generate the tomographic image, velocity bands are associated with color bands. The maximum velocity (V_{max}) obtained in the analyzed cross-section was chosen as a reference. Based on this velocity, the ranges according to velocity variations (losses) were defined, assigning colors to elaborate the tomographic image. For the choice of velocity ranges, previous results from the literature were used (USDA 2014, Reis 2017; Palma 2017), which was distributed into four representative velocity loss ranges as can be seen in Figure 2.

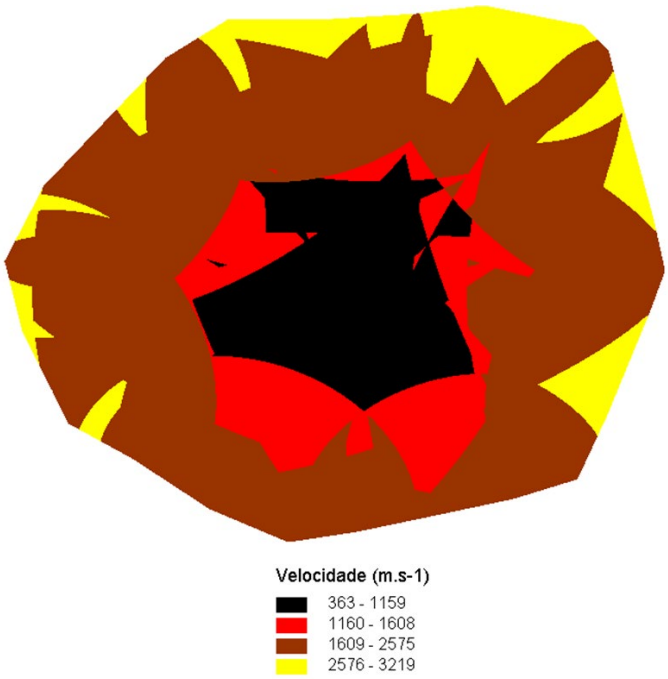

Figure 2 - Example of tomographic image.
Legend: 0 to 36% of V_{max} to represent zones with cavities (black); 36% to 50% of V_{max} to represent areas with deteriorated wood (red); 50 to 80% of V_{max} to represent healthy areas of heartwood (brown); and 80 to 100% of V_{max} to represent healthy areas of sapwood (yellow).

To prepare the specimens, approximately 300 mm high cross-sections extracted from the trees in the same position as the ultrasound measurements (Figure 3) were taken to the laboratory, where they were polished with sandpapers of different weights to highlight the areas with de-cays (D), healthy wood (HW) and cavities (Ca). The polished cross-sections were placed on a neutral surface to be photographed. After identifying each region, the specimens were properly removed from the cross-sections (D, HW).

The specimens in the saturated condition had their volume and weight measured to calculate the apparent density in the saturated condition ($\sigma_{sat}= m_{sat}/V_{sat}$). After the ultra-sound tests, the specimens were kiln dried until reaching the anhydrous condition, and as soon as they did, they were weighed once again to obtain the dry mass (md) with which the basic density was determined ($\sigma_{bas}= m_d/V_{sat}$).

The mechanical characterization of stiffness tests was carried out on specimens in the saturated condition removed from each of the regions under study. The ultrasound test, which allows the stiffness coefficient calculation, has been proposed for wood characterization since it directly correlates with the modulus of elasticity and allows testing in different dimensions of the specimen. The test was performed using ultrasound equipment (EP1000, Olympus, Japan) due to the transducer frequency function used in the tests, which, in turn, was a function of the size of the prismatic specimen. Thus, the transducer frequency (1 MHz) was adopted to ensure that the minimum ratio between wavelength and path length was greater than three, minimizing the interferences when the wave propagation does not occur in in-finite media (Bucur 2006). In addition, it was ensured that the transducer diameter (13 mm) was always limited to the cross-section of the specimen, minimizing the wall effect (Bucur 2006).

From the ultrasound test on the specimens, the propagation time of the waves (t) was obtained, and with the path length (dimension of the specimen in the direction of the wave propagation), the propagation velocity (V) was determined. To determine the stiff-ness coefficient in the longitudinal direction (C_{LL} – Equation 5), the basic density (ρ_{bas}) obtained in the specimen was used. In wood applications, the stiffness coefficient is generally calculated in the equilibrium humidity, and therefore, the apparent density in the same humidity condition is used. As the objective is the calculation of the CLL in a saturated condition, the use of the apparent density could falsely indicate high stiffness due to the water weight and not to the effective stiffness of the material. Resulting in a contrary response to what is expected for wood (Bucur 2006), to which stiffness decreases as moisture in-creases (Haygreen and Bowyer 1995).

$$C_{LL} = \rho_{BAS} \times V^2 \quad (5)$$

To calculate the equations proposed in the literature (Equations 1 to 4), the necessary parameters are the deteriorated zone average diameter (d); the bark-less trunk average diameter (D); the relation between the open cavity circumference and the trunk circumference (R); the thickness of the smallest wall remaining to the trunk (t); and the trunk radius (Rf) – Figure 1. Thus, to obtain these parameters, the photographs of the polished cross-sections and the tomographic images were used in ImageJ software, which enabled us to measure the areas with decays and cavities and those with a smaller remaining wall thickness of the trunk when there were cross-sections with cavities.

In general, tree trunks are not regular, but as shown above, the equations proposed in the literature simplify the calculation considering a cylindrical trunk with diameter D. To consider the irregularity, the value adopted for D was the average between the largest and smallest diameters of the trunk.

For cavities, the equations also adopt a hollow cylinder. However, these cavities can be even more irregular than the trunk under real conditions, making the adoption of a cylindrical geometry imply gross errors. Thus, we sought a calculation to obtain an equivalent circular cross-section that would allow us to use the equations while minimizing errors. For this, the dimensions of decays and cavities were measured in ImageJ using the tool “Measure”, which measures the selected region using a predetermined scale, which, in the case of this research, was the dimension of the largest diameter in the real cross-section. As they are neither cylinders nor homogeneous shapes, the measurements were selected in four positions, and the average was used as an equivalent circular cross-section (Figure 5).

Two situations were considered for the calculation using Equations 1 to 4: the first using the internal cavity diameter (d) and the second using the internal cavities plus the decayed areas that surrounded the cavities ($d_{cav+det}$). As a simplification for the strength loss calculation, the equations proposed (1 to 3) consider the trunk as a uniform cylinder with a central axis. When there is a cavity, they consider a hollow cylinder with a central axis.

To take into account that the cavity and the cavity plus decay may not be centered, calculations were made considering the eccentricity of these regions. To simplify the calculations, the eccentricity was

considered in only one of the axes (X or Y), adopting the axis with higher eccentricity. The eccentricity was calculated based on the thickness of the smallest wall remaining in the trunk. Having the eccentric position of the cavity or cavity plus the surrounding deteriorated area, we calculated the second moment of area (I) using the parallel axis theorem ($I = I_c + A\ d^2$), which considers the second moment of area of that element about its own centroid (Ic), the area of the element (A) and the distance (d) from the neutral plane (x-x or y-y) to the centroid of that element.

For each cross-section, the data of the average diameter (D), the internal cavity (d) and the internal cavity plus the surrounding decayed ($d_{cav}+d_{ec}$) were used to calculate the loss of the second moment of area considering the cavity centered or noncentered. This allows us to verify how much the consideration of the eccentricity influenced the strength loss obtained by the equations.

The Equation 3 can be rewritten as:

$$\frac{(d^3 + RD^3 - Rd^3)}{D^3} = \frac{d^3}{D^3} + R - \frac{Rd^3}{D^3} = (Equation2) + R - R(Equation2)$$

The proposed Equation 6 considers Equation 3 rewritten but, instead of the loss of the second moment of area proposed in Equation 2 (d^3/D^3), using concentric cavity, it proposes the calculation of the loss of the second moment area considering the eccentricity of the cavity (if there is).

$$SL = I_{exc} + R - RI_{exc} \quad (6)$$

The new equation proposed in this study, Equation 7, consisted in consider, in addition to the cavity with eccentricity (Equation 6), the loss of strength of the deteriorated zone (DL)

$$SL = (I_{exc} + R - RI_{exc}) + DL \quad (7)$$

As the specimens were tested by ultrasound and the results are related to stiffness (Equation 5), the relationship between strength (MOR) and stiffness was adapted from the equation proposed by Hassan (2013) to infer strength in clean and decayed wood.

Results and Discussion

From the ultrasonic tests, the average wood stiffness (C_{LL}) for specimens taken from clear wood was 92% superior than specimens taken from decayed wood and for bending strength (MOR) obtained using Hassan (2013) equation, the average loss of strength (SLD) was 34%.

Table 1 present the strength losses calculated using Equation 7 proposed in this research, considering the actual position of the cavity for the calculus of the second moment of area and not only cavities, but also biodeteriorations zones.

According to Kane et al 2001, strength losses inferred by Equation (1) (Coder 1989) from 20% to 45% indicate trees that need care, and above this value, they mean hazard trees. Strength loss pre-dictions above 33% by Equation 2 (Wagener 1969) indicate hazardous trees (Kane et al 2001). For strength losses predicted by Equation (3) (Smiley and Fraedrich 1992), from 20% to 33% indicate a risk when the tree presents, in addition to cavities, signs of decay (cracks, trunk thickening, etc.) and above 33% if they indicate only cavities (Kane et al 2001). For the inference proposed by (Mattheck and Kubler 1995), Equation (4), the tree is at risk when the calculated ratio is less than 0.3 (Kane et al 2001). Considering these limits, none of the cross-sections analyzed in this research would be considered at risk by Equations 1, 2 and 3. For Equation 4, as we always consider the smallest remaining wall thickness (t), the ratio value will already be zero whenever there is an open cavity, since t = zero. In this case, except for cross-section 7, using the tomographic data, the trees considered at risk coincided with the cross-sections (actual condition), a 92% hit. For cross-section 7, tomography centered the cavity, causing the thickness of the remaining wall to be greater than it is. This increased the ratio value.

Table 1— Strength loss percentage values using Equation 9 with data from cross-sections and tomographic images

Cross-sections	Data obtained from Cross-sections photography	Data obtained from Cross-sections tomography
1	0	8
2	13	17
3	0	0
4	0	0
5	36	48
6	14	17
7	19	10
8	8	8
9	18	21
10	39	43
11	3	4
12	39	40

As expected, the loss of the second moment of area considering the centered cavity results in values equal to those obtained using Equation 1, since this equation is based only on the second moment of area variation concept. On the other hand, the loss of the second moment of area calculated with the cavity in the actual eccentric position (if this is the case of the cavity) results in higher values than those obtained with the cavity centered or with Equation 1. For Equation 3, which considers the open cavity, the inferred strength losses are greater in cross-sections with these cavities.

By replacing the portion referring to Equation 2 with the stiffness losses considering the eccentricity of the internal cavity (Equation 6), we found that the percentage of strength loss increases. Using the same criteria for risk consideration as in Equation 2, with a limit of 20% for trees presenting decayed areas and cavities and 33% for trees with decay, we verified that the inference of risk was coincident for the data from the tomography or actual cross-section.

Equation 7 (Table 1) shows that considering the criteria mentioned above, cross-section 9 would not be at risk (strength loss was less than 20%), according to the actual cross-section data, but would be regarding the tomographic image data. Cross-sections 5, 10 and 12 would be at risk considering data from actual cross-sections or tomography (Table 1). Cross-sections 6 and 7 would only be considered at risk using Equation 4. Similar to Burcham et al (2019), with tomography being an assistant, our results also indicate that taking into account not only cavities but also the eccentricity of the damaged part, the results of strength loss are closer to the actual condition of the trunk.

Conclusions

The ultrasonic tomography images of the cross-sections allow us to propose a new equation to infer the loss of resistance of the trees, adding biodeterioration zones and also eccentricities, giving more realistic results.

Acknowledgments

The authors thank CAPES (Proc. 001) for the scholarship and CNPq (Proc. 426130/2018-9) for funding the research. We also thank scholarship holder Carlos Eduardo Bento for all the support in the laboratory tests.

References

Alani AM, Lantini L. 2019. Recent advances in tree root mapping and assessment using nondestructive testing methods: a focus on ground penetrating radar. Surveys in Geo-physics, 1-42. http://10.1007/s10712-019-09548-6

Brazee N; Marra RE; Goecke L; Wassenaer PV. 2011. Nondestructive assessment of internal decay in three hardwood species of northeastern North America using sonic and electrical impedance tomography. Forestry. 84(1): 33-39. http://dx.doi.org/10.1093/forestry/cpq040

Bucur V. 2006. Acoustics of wood. 2nd ed. Springer Verlag, New York.

Burcham DC; Brazee NJ; Marra RE; Kane B. 2019. Can Sonic Tomography Predict Loss in Load-Bearing Capacity for Trees with Internal Defects? A Comparison of Sonic Tomograms with Destructive Measurements. Trees. 33: 681–695.

Chan WC; Cui Y; Jadhav SJ; Khoo BC; Lee HP; Lim CWC; Gobeawan L; Wise DJ; Ge Z; Poh HJ; Raghavan V; Lin ES; Burcham DC. 2020. Experimental study of wind load on tree using scaled fractal tree model. Int J Mod Phys B. 34 (14n12): 2040087. https://doi.org/10.1142/S0217979220400871

Ciftci C; Kane B; Brena SF; Arwane SR. 2014. Loss in moment capacity of tree stems induced by decay. Trees. 28: 517–529. http://doi.org/10.1007/s00468-013-0968-8

Coder KD. 1989. Should you or shouldn't you fill tree hollows? Grounds Maintenance. 24(9): 68–70, 98–100.

Duarte APC; Daniluk-Mosquera G; Gravina V; Vallejos-Barra O; Ponce-Donoso M. 2021. Tree Risk Assessment: Com-ponent analysis of six visual methods applied in an urban park, Montevideo, Uruguay. Urban Fo Urban Green. 59: 127005. https://doi.org/10.1016/j.ufug.2021.127005

Du X; Li S; LiG; Feng H; Chen S. 2015. Stress Wave Tomography of Wood Internal Defects using Ellipse-Based Spatial In-terpolation and Velocity Compensation. BioResources. 10(3):3948-3962

Giacomazzi M; Silva EFLP; Hardt E. 2020. Diagnosis of urban trees on neighborhoods in the municipality of Tietê. Re-vista Ra'e Ga. 47(1): 35-48. http://doi.org/10.5380/raega

Gonçalves R; Linhares CSF; Yojo T. 2020. Drag Coefficient in Urban Trees. Trees. 35: 01951. http://doi.org/10.1007/s00468-019-01951-1

Haygreen JG; Bowyer JL. 1995. Forest Products and wood science. An introduction. 2nd ed. Iowa State University: Ames.

Hassan KTS; Horacek P; Tippner J. 2013. Evaluation of Stiffness and Strength of Scots Pine Wood Using Resonance Fre-quency and Ultrasonic Techniques. BioResources. 8(2): 1634-1645.

Jackson et al. 2014. The motion of trees in the wind: a data synthesis. Biogeosciences.18: 4059–4072. https://doi.org/10.5194/bg-18-4059-2021

Jansson M. 2014. Green space in compact cities: the benefits and values of urban ecosys tem services in planning. The Nordic Journal of Architectural Research 26(2):139-160.

Kane B; Ryan D; Bloniarz DV. 2001. Comparing Formulas that assess strength loss due to decay in trees. J. Arboric. 27(2): 78-86

Klein RW; Koeser AK; Hauer RJ; Hansen G; Escobedo FJ. 2019. Risk Assessment and Risk Perception of Trees: A Re-view of Literature Relating to Arboriculture and Urban Forestry. Arboric Urban For. 45(1): 23–33. http://doi.org/10.48044/jauf.2019.003

Li FX, Li M, Feng XG. 2021. High-Precision Method for Estimating the Three-Dimensional Green Quantity of an Urban Forest. Journal of the Indian Society of Remote Sensing, 1-11. http://10.1007/s12524-021-01316-7.

Mattheck C; Kubler H. 1995. Wood: The internal optimization of trees. Springer Verlag, Berlin.

Palma SSA. 2017.Pattern recognition in ultrasound generated images. Dissertation. University of Campinas – UNICAMP.

Reis MN. 2017. Association of nondestructive methods for tree inspection. Dissertation. University of Campinas – UNI-CAMP.

Reis M.; Gonçalves R; Garcia GHL; Manes L. 2019. Profiles of a Non-Calibrated Resistance Drill Compared with Dete-riorated Stem Cross Sections. Arbor Urban For. 45(1): 1–9. http://doi.org/10.48044/jauf.2019.001

Reis MN; Gonçalves R, Brazolin, S.; de Assis Palma, S.S. 2022. Strength Loss Inference Due to Decay or Cavities in Tree Trunks Using Tomographic Imaging Data Applied to Equations Proposed in the Literature. Forests 2022, 13, 596. https://doi.org/10.3390/f13040596

Rust S. 2022. Reproducibility of Stress Wave and Electrical Resistivity Tomography for Tree Assessment. Forests. 13: 295. https://doi.org/10.3390/f13020295

Salsabila R, Hariyadi H, Santoso N. 2021. Tree Health Management Strategy in Cianjur Urban Forest. Jurnal Sylva Lestari, 9(1), 86-103. http://10.23960/jsl1986-103

Smiley ET; Fraedrich BR. 1992. Determining strength loss from decay. Arboric J. 18 (4): 201-204.

United States Department of Agriculture (USDA) Wood and Timber Assessment Manual. 2ed. Madison. 2014.

Vidal D, Pitarma R. 2019. "Infrared thermography applied to tree health assessment: A review." Agriculture 9.7: 156. http://10.3390/agriculture9070156

Vlad R; Zhiyanski M; Dinc L; Sidor CG; Constandache C; Pei G; Ispravnic A; Blaga T. 2018. Assessment of the density of wood with stem decay of Norway spruce trees using drill resistance. Comptes rendus de l'Académie bulgare des sciences: sciences mathématiques et naturelles. 71(11): 1502-1510. http://doi.org/10.7546/CRABS.2018.11.09

Wagener WW. 1963. Judging Hazard from Native Trees in California Recreational Areas: A Guide for Professional Forest-ers. Berkeley, CA, USA, Pacific Southwest Forest and Range Experiment Station, Forest Service, US Department of Ag-riculture, PSW-P1, pp 1-29

Influence of the Manner of Obtaining Outline Coordinates of Irregular Discs in Tomographic Images

Stella Stopa Assis Palma
School of Agricultural Engineering – University of Campinas, Campinas, São Paulo, Brazil, ssapalma@gmail.com

Mariana Nagle dos Reis
School of Agricultural Engineering – University of Campinas, Campinas, São Paulo, Brazil, ma.nagle.reis@gmail.com

Raquel Gonçalves
School of Agricultural Engineering – University of Campinas, Campinas, São Paulo, Brazil, raquelg@g.unicamp.br

Abstract

Ultrasonic tomography has been widely used in tree inspections because it allows to obtain internal images of the stem relatively easily and without causing damage to the inspected material. For the application of the technique using measuring mesh, it is necessary to obtain coordinates of the outline of the stem. However, the morphology of the stem of many species, especially tropical leafy ones, can make it difficult to obtain outline coordinates, generating the need for the application of more complex technology. An alternative to overcome this difficulty is the use of approximate techniques, such as those that simplify the outline of the trunk, making approximations to fewer complex shapes and with better known geometric relationships. However, when promoting such approximations, there are changes in the wave propagation routes that, even if small, could cause interferences in the resulting image, since the calculation of velocities depends on the path lengths and wave propagation times, measured in microseconds. Thus, this research aimed to quantify, through the metrics of the confusion matrix, the interference of the method that approximates the irregular outline of the stem to an ellipse, in the image produced by the tomography. For this, tomographic images obtained from 12 disks with irregular shape, of *Cenostigma pluviosum DC. Gagnon & G.P.Lewis*, produced with the real and the approximate outline. The difference between the metrics obtained in the images using the two outlines indicated small differences, allowing us to conclude that the ease in applying the simplified method is rewarding.

Keywords: outline of trees, ultrasonic tomographic, urban trees.

Introduction

Acoustic tomography has been widely used as an important tool to support tree management decisions targeting the falling tree risk (Linhares et al. 2021; Gilbert et al. 2016), mainly due to its good results. Constant studies of data acquisition techniques and interpolation methods have been increasingly improving the images obtainance (Du et al. 2018). However, the cost is always associated with these improvements that end up delivering more sophisticated and high priced equipments, making its acess difficult to the communities with fewer resources.

The focus of the larger research from which this one is part, presents as one of the main objectives the elaboration of a simplified methodology both in terms of cost and operation, to obtain high quality

tomographic images, obtained with the use of a benchtop ultrasound equipment and post-processed images (Reis, 2022; Palma et al. 2018; Secco et al. 2012).

The methodology developed by the group consists of using the diffraction mesh proposed by Divos and Szalai (2002) on the chosen section of the trunk. However, for the wave propagation data to be converted into velocity, it is necessary to know the distance, or size of each theoretical route formed between the emitter and receiver transducer (Secco et al. 2012). Thus, it is necessary to know the outline coordinates of the studied section.

The coordinates could be easily obtained if the trees outline had regular shapes, however this is not what happens with most urban trees in Brazil (the research development site). However, these trees have in common geometries that approach an ellipse (Figure 1), which greatly facilitates the methodology, since the optainance of an elliptical shape computationally it is only necessary to measure the largest diameter, and the perpendicular diameter situated at the midpoint of the greater diameter.

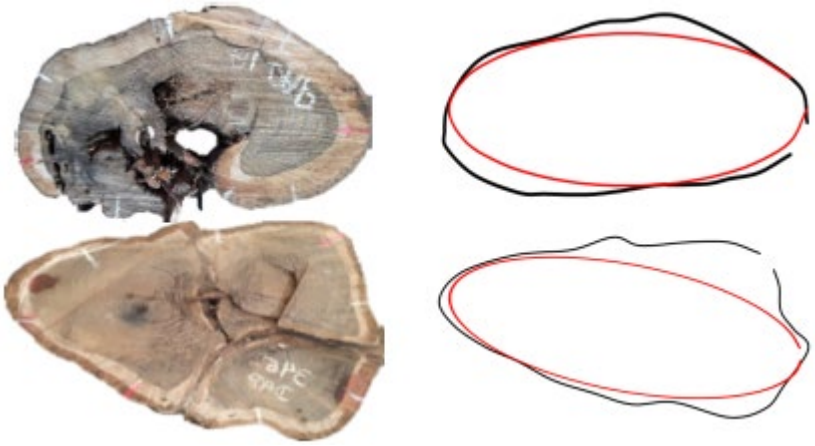

Figure 1- Example of irregular trunk outline in tree species used in urban areas (on the left) and representation of the real outline (in black) and generated from an elliptical outline generator (red) on the right.

However, the geometry simplification can result in differences in the routes lengths, so it is important to know how much this error can interfere the tomographic image generated to verify the possibility of using the simplified methodology. Therefore, this research aims to verify and evaluate, through the accuracy of the images, if there are significant interferences that prevent the adoption of the simplified outline methodology in relation to the results obtained with the use of the real outline of the trunk.

Materials and methods

Materials

For this study, five trees of the species *Cenostigma pluviosum DC Gagnon & G.P. Lewis* (Sibipiruna) were used. These trees were located on the Campus of the State University of Campinas, in the city of Campinas, State of São Paulo, Brazil ((22°49'03"S 47°04'11"W), and had a cutting authorization issued by the Environmental Department of the Campus as they presented a great falling risk. Thus, after carrying out the tests, the trees were removed and discs of approximately 300 mm high were extracted from the trunks on the tested sections.

For the wave propagation test, a benchtop ultrasound equipment USLab (Agricef ® - Brazil) was used, with 45 kHz dry-end transducers and a dendrometric caliper to measure the trunk diameters.

Methods

Inspections in the standing trees

The inspections were carried out in 12 sections from 5 different trees. The sections were taken 0.30 m from the ground (DAS), at breast height (1.30 m from the ground) and the height of the first bifurcation (H) when this bifurcation exceeded the breast height. In these sections, the perimeters (P) were measured to decide the number of points to be used in the mesh according to the methodology proposed by Palma (2022) (Table 1). The referred methodology indicates that the number of points (n) to be used in the diffraction mesh must be equal to five times the obtained perimeter (n = 5P).

Table 1— Perimeter of the tested sections and number of points in the configuration mesh

Tree	Section	P	n
1	1	2.52	14
	2	1.20	6
2	1	1.44	8
	2	1.48	8
3	1	1.10	6
	2	1.02	6
4	1	1.60	8
	2	1.47	8
	3	1.47	8
5	1	1.44	8
	2	1.48	8
	3	1.52	8

According to the perimeter measurements acquired (Table 1), different indications of the number of points to be used in the diffraction mesh were obtained. To keep the variables fixed, an average of n = 8 was adopted. With the number of points in the mesh defined, the demarcation of these points around the section was started.

The largest diameter of the tree is measured with the caliper and **point 1** is defined at its right jaw, according to the adopted mesh of 8 points, **point 5** will be at the other jaw. Then, the diameter perpendicular to the first is measured, in which we will have **point 3** at one end and **point 7** at the other, considering the increasing order of the points in the clockwise direction. The other points were marked equidistantly between the points already identified, totaling 8 points in their surroundings. And at these points, holes of 5 mm in diameter were made with the necessary depth to cross the bark, coupling the tip of the transducer to the wood.

The measurements were performed according to the methodology already used by the group, in which the emitter transducer is coupled to point 1, and the receiver transducer to point 2, and the reading is taken on the theoretical route (1-2).

Then the receiving transducer is coupled at point 3, and the procedure is repeated until point 8, then the emitter transducer is coupled at point 2 and the receiver at the other points for the other readings. The process is repeated until readings are taken on all routes and in both directions (eg 1-2 and 2-1).

Data processing for the image generation

For the generation of images, two spreadsheets are needed, one referring to the outline of the evaluated section and another referring to the wave propagation times of each of the theoretical routes of the diffraction mesh. In this research the outline acquisition was done with two different methods. The first one uses the image of the disk surface after cutting, which we call real outline, and the second is done by approximating the outline to an ellipse, a process called approximate outline.

The real outline was obtained using the ImageJ software, in which the photo of the disk surface is opened, and its scale is transformed from pixel to centimeters, based on the real measurements obtained in the field (routes 1-5 and 3- 7). Then, with the multipoint tool, the outline points are demarcated following the exact outline of the disk (Figure 2), and saved in a text file as x and y coordinates. This file obtained is the outline worksheet.

Figura 1- Plotting of the outline points on a photograph of the surface of the wooden disk to obtain the real outline coordinates.

The approximate outline was obtained with the use of a plugin for ImagJ, developed by a student of the group in its Scientific Initiation Program at the University. This plugin uses an algorithm that plots an ellipse from the dimensions of two axes, one being the largest diameter and the other perpendicular to it obtained in the field. This plugin also allows choosing the number of points to be used, so the adopted points and two more intermediate points are plotted to better adjust the outline (Figure 3). As a result, we get the plot of the points and the outline sheet in a text file just like the one obtained for the real image.

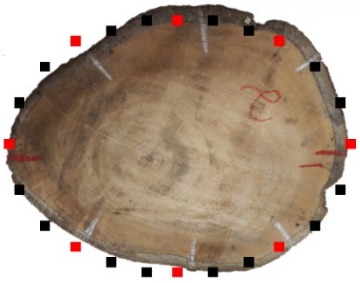

Figure 2 – Obtaining of the outline points by approaching an ellipse

From the outline sheets, both the actual and approximate outlines, the time sheets are created. They are obtained from the association of the outline coordinates forming the theoretical routes of wave propagation, where for each one is assigned its respective time obtained during the field tests.

Images generation

The images were generated by the ImageWood software. This software presents two interpolation algorithms, the inverse square distance method and the ellipse method with and without velocity compensation proposed by Du et al. (2015). The images of this research were generated by the ellipse method with velocity compensation. Previous studies (Palma, 2022) evaluated that the images generated by this interpolation method had best accuracy.

In the same study (Palma 2022), it was found that the velocity band for image generation associated with the use of a 25-pixel median filter, allowed inferring cavities (up to 40% of V_{max}) and cavity + biodeterioration (up to 45% of V_{max}). The maximum velocity referenced here corresponds to the maximum velocity obtained in each of the sections studied and by each of the outline methods. Thus, considering the two outline methods and the two speed ranges, 48 images were generated and subsequently filtered.

Confusion matrix

The generated images were compared with the real images of the disk surface quantitatively using the confusion matrix. This method was performed using a Python script proposed by Strobel et al. (2018), from which we used the accuracy method, which, as already evaluated in previous works (Palma 2022), is more suited to the evaluation proposed in this research.

The method is performed based on the comparison of two images (model and ROI) in an image that delimits the comparison field (internal points). All must have the same resolution, and be binary, where black is positive and white is negative. Thus, the ROI or region of interest is obtained from the binarization of the image generated by ImageWood and filtered (Figure 4). The image of internal-points is obtained from the same image used for the ROI, but showing the outline (Figure 4). The model that is the reference for the evaluation is obtained from the real image through color segmentation tools (Figure 4).

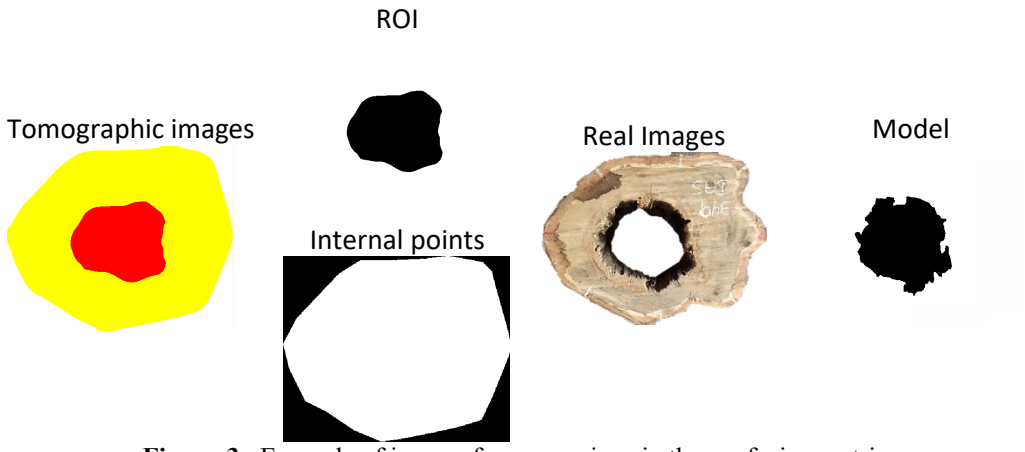

Figura 3 –Example of images for comparison in the confusion matrix

The Python script makes the comparison considering the four conditions proposed by Fawcett (2006), as shown in table 2 accompanied by the accuracy equation.

Table 2. Comparisons between Model and ROI pixels in the confusion matrix considering the delimitation given by the image of the internal points

	Pixels within the zone of interest in the real image	Pixels outside the zone of interest in the real image
Pixels within the zone of interest in the tomographic image	True Positive (VP)	False Positive (FP)
Pixels outside the zone of interest in the tomographic image	False Negative (FN)	True Negative (TN)

$$Acuracy = \frac{TP + VN}{TP + TN + FP + FN} \quad (1)$$

Velocity evaluation

The differences in velocities obtained with the use of the real and statistically approximated outlines were evaluated. The 336 velocity pairs obtained in the theoretical routes were considered. The statistical comparison was made using the confidence interval of the average of the differences between the velocities obtained with the two types of outline and also with the "t" test for comparing the means. In the case of the confidence interval, the velocities are considered statistically equivalent when zero belongs to the interval constructed with a 95% safety level. For the t test, the data are considered equal, with a security level of 95%, when the P-value of the test is greater than 0.05.

Results

Velocities

The average velocity obtained in the 336 pairs of theoretical routes was 1765 $m.s^{-1}$ for the exact outline and 1758 $m.s^{-1}$ for the approximate outline, and the statistical comparison showed a confidence interval of -110.4 $m.s^{-1}$; +125.0 $m.s^{-1}$ and the P-value of 0.90. Thus, the statistical analysis of the velocities obtained in the measurement routes using the exact or approximate outline of the trunk were statistically equivalent, with a 95% confidence level, which demonstrates that in general, with the adoption of an approximate outline, there were no significant changes in the speed behavior.

However, it is important to verify if these numerical differences will reflect in the generated image to the point of generating an interpretation error during the evaluation of a tree. Even with the use of commercial tomographs with a high degree of sophistication, it is necessary to use specific methodologies for species with highly irregular outlines in order not to incur tomography with serious errors (Gilbert et al., 2016).

Images

A total of 48 images were generated and filtered, 24 with the real outline, and 24 with the approximate outline and for each of the outline types 12 images for cavity inference and 12 for cavity inference associated with biodeterioration. These images were treated and quantitatively compared using the confusion matrix (Figure 5).

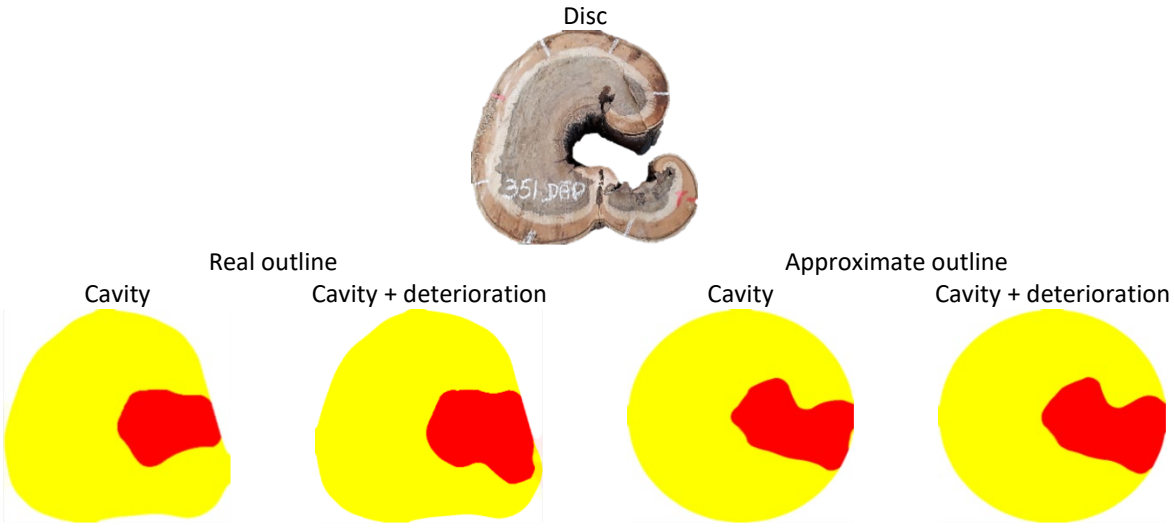

Figure 4 - Example of a generated image to a disk**.**

Most of the evaluated discs had cavities, and some were accompanied by deterioration. Thus, it was expected that the generated images presented areas in red representing these areas with cavities and/or deteriorated (Figure 5).

Despite showing the areas in red, it is necessary to assess whether they adequately represent the real image. The accuracy evaluations performed by the confusion matrix showed that for the images generated for inference of cavity zones with the real outline, the average was 88.8%, while for the images generated with the approximate outline the average was 87, 3%, the statistical comparison showed a confidence interval of -4.46; +7.7 and the P-value of 0.60. For the inference of the cavity + biodeterioration, despite having lower average accuracies, the values remained above 80%, which indicates good results, being 85.7% for the real outline and 83.8% for the approximate outline, in the comparison analysis the confidence interval was -6.9; +10.8 with a P-value of 0.66.

Conclusions

From a statistical point of view, the velocities obtained in the theoretical wave propagation routes were not affected by the use of simplified outline and the accuracy of the images generated with the exact outline of the disks presented values about 1% higher than those obtained with the images generated with the simplified outline. From a statistical point of view, there was no difference between the accuracies of the images.

Acknowledgments

The authors thank CNPq for the scholarship (Proc. 141067-2018-7) and for the research funding (Proc. 426130/2018-9). To the Higher Education Personnel Improvement Coordination – CAPES, for the scholarship for the internship in Spain (Process- 88887.467257/2019-00). The Research Support Foundation of the State of São Paulo - FAPESP, for funding LabEND research with which it was possible to purchase all the equipment used in the development of the research. To the student José Victor Gonçalves Cardoso, grantee of the PIBIC/SAE Program at the State University of Campinas, for his support in the essays.

References

Divos, F.; Szalai, L. 2002. Tree evaluation by acoustic tomography. *In: Proceedings of the 13th International symposium on nondestructive testing of wood,* WI: *Forest Products Society*, August 19– 21; Berkeley, CA, p. 251–256.

Du, Xiaochen et al. 2018. Image reconstruction of internal defects in wood based on segmented propagation rays of stress waves. Applied Sciences, v. 8, n. 10, p. 1778.

Du, X., Li, S., Li, G., Feng, H., Chen, S. 2015. Stress wave tomography of wood internal defects using ellipse-based spatial interpolation and velocity compensation. BioResources, 10(3), 3948-3962.

Gilbert, G. S., J. O. Ballesteros, C. A. Barrios-Rodriguez, E. F. Bonadies, M. L. Cedeño-Sánchez, N. J. Fossatti-Caballero, M. M. Trejos-Rodríguez, et al. 2016. Use of sonic tomography to detect and quantify wood decay in living trees. *Applications in Plant Sciences* 4(12): 1600060.

Linhares, Camila SF et al. 2021. Structural Stability of Urban Trees Using Visual and Instrumental Techniques: A Review. Forests, v. 12, n. 12, p. 1752, 2021.

Palma S.A.P. 2022. Interference of factors related to inspections of standing trees and data processing on the quality of images generated by ultrasonic tomography. University of Campinas – UNICAMP. Thesis.

Palma, S. S. A., Gonçalves, R., Trinca, A. J., Costa, C. P., dos Reis, M. N., Martins, G. A. 2018. Interference from knots, wave propagation direction, and effect of juvenile and reaction wood on velocities in ultrasound tomography. BioResources, 13(2), 2834

Reis M N. 2022. Quantitative analysis of the scope and contribution of field inspections in trees in the inference of wood biodeterioration. University of Campinas – UNICAMP.
Thesis. 95p.

Secco, C. B.; Gonçalves, R.; Cerri, D. G. P.; Vasques, E. C.; Batista, F. A. F. Behavior of ultrasonic waves in wood with presence of voids. *Cerne*, n. 18, v. 3, p.1-8, 2012.

Strobel, J. R. A.; de Carvalho, M. A. G.; Gonçalves, R.; Pedroso, C. B.; dos Reis, M. N.; Martins, P. S. Quantitative image analysis of acoustic tomography in woods. *European Journal of Wood and Wood Products*, 1-11, 2018.

Adjustment of Ultrasonic Tomography Velocity Ranges to Represent Variations within Tree Trunks Using Confusion Matrix Metrics

Stella Stopa Assis Palma *
School of Agricultural Engineering – University of Campinas, Campinas, São Paulo, Brazil, ssapalma@gmail.com

Mariana Nagle dos Reis
School of Agricultural Engineering – University of Campinas, Campinas, São Paulo, Brazil, ma.nagle.reis@gmail.com

Raquel Gonçalves
School of Agricultural Engineering – University of Campinas, Campinas, São Paulo, Brazil, raquelg@g.unicamp.br

Abstract

There are numerous of benefits related to the presence of urban forestry. However, attacks by biotic agents, such as xylophagous insects and fungi that can modify wood´s properties. To guarantee preservation and risk reduction to population, one must invest in research that evaluate the accuracy of the technological tools used in tree inspection. The objective of this research was to define a methodology to adjust velocity range to best represent the different regions (deterioration and cavities) inside the trunk generated by ultrasonic tomography images using metrics of the confusion matrix. Discs of *Cenostigma pluviosum DC. Gagnon & G.P.Lewis* with different types of biodeterioration were analyzed so that it was possible to create representative masks of these different regions so they could be compared to the tomographic images. The tomographic images were created using different ranges and median filter setting to narrow the best velocity range for each of the different regions using the confusion matrix methods. The results showed that the best velocity ranges to infer the position and size of the cavities were from 0% to 40% of the maximum velocity and from 40% to 45% of the maximum velocity for detect deteriorated zones. We conclude that the methodology using metrics from confusion matrix is very reliable to propose fine adjustments in parameter associations to be inferred through tomographic images.

Keywords: ultrasonic tomographic, urban trees, filters

Introduction

The urban landscape is composed of several elements, especially trees that bring numerous benefits such as thermal, acoustic, and scenic comfort, in addition to contributing to the local fauna (Locke and Baine 2015). At the same time that it brings benefits, it can bring risks due to its phytosanitary conditions, which makes it necessary to associate biological knowledge with the use of technical tools in the evaluation of trees (Arciniegas et al. 2014), ensuring the well-being of the population in its surroundings.

Several non-invasive techniques have been studied for the evaluation of urban trees (Wu et al. 2018). Among these techniques, there are those that work with imaging through wave propagation, such as ultrasonic tomography, which has shown good results, including the use of simplified technology and

methodology (Reis 2019, Palma et al. 2018, Strobel et al., 2018, Seco et al. 2010). The simplification of technology brings the benefit of cost reduction, however, it is necessary to guarantee the quality of results.

In the simplified methodology, we performed an ultrasound test with conventional equipment (not tomograph), applying the measurements manually in a diffraction mesh (Divos 2005) to obtain the wave propagation velocity in the evaluated section. Subsequently, the images are generated with a spatial interpolation method, which use velocity ranges represented by colors to generate a representative image of the wood conditions (Reis 2019, Palma et al. 2018, Seco et al. 2010).

Spatial interpolation allows us to obtain velocity values for all pixels of the evaluated section, based on neighboring velocities (Du et al. 2018) obtained from the mesh measurement routes. One of the ways to obtain greater precision is to increase the number of points in the diffraction mesh, making the mesh finer. However, this greatly increases the work in the field without increasing the image quality to the point of being compensating (Palma 2022). Another way to improve the quality of images is through the use of filters. The filter can be applied directly to the generated image to smooth the edges and reduce interference caused by the interpolation system (Palma 2022).

Image quality assessment can be done quantitatively using the confusion matrix (Strobel et al. 2018). This tool allows us, through metrics, to evaluate accuracy, precision, sensitivity, among others, by comparing pixels classified as positive and negative, resulting in four classes as proposed by (Fawcett 2006) (Table 1).

Table 1. Comparisons between Model and ROI pixels in the confusion matrix considering the delimitation given by the image of the internal points

	Pixels within the zone of interest in the real image	Pixels outside the zone of interest in the real image
Pixels within the zone of interest in the tomographic image	True Positive (VP)	False Positive (FP)
Pixels outside the zone of interest in the tomographic image	False Negative (FN)	True Negative (TN)

$$Acuracy = \frac{TP + VN}{TP + TN + FP + FN} \quad (1)$$

This research presents a methodological proposal applied to the species *Cenostigma pluviosum* (Sibipiruna) as a case study, for the definition of parameters related to the images produced by this technique.

Materials and methods

Materials

In this study, we used five trees of the species *Cenostigma pluviosum DC. Gagnon & G.P. Lewis* (Sibipiruna). These trees were located on the State University of Campinas Campus, in the city of Campinas, State of São Paulo, Brazil ((22°49'03"S 47°04'11"W), and were provided for study by the Environmental Department of the same University. For the wave propagation test, a benchtop ultrasound equipment USLab (Agricef ® - Brazil) was used, with 45 kHz dry tip transducers and a dendrometric caliper to measure the diameters.

Methods

Inspections in the standing tree

The inspections were carried out in 12 sections from 5 different trees. The sections were taken 0.30 m from the ground (DAS), at breast height (1.30 m from the ground) and the height of the first bifurcation (H) when this bifurcation exceeded the breast height. In these sections, the perimeters (P) were measured to decide the number of points to be used in the mesh according to the methodology proposed by Palma (2022) (Table 1). The referred methodology indicates that the number of points (n) to be used in the diffraction mesh must be equal to five times the obtained perimeter (n = 5P).

Once the number of points has been defined, the largest diameter of the tree is first measured with the caliper and point 1 is defined at one of the two jaws. Then, the other points were marked equidistantly (P/8) around the perimeter P. Holes of 5 mm in diameter were drilled with the necessary depth to go through the shell, allowing the transducer tip to be coupled to the wood.

The measurements were performed according to the methodology already used by the group, in which the emitter transducer is coupled to point 1, and the receiver transducer to point 2, and the reading is taken on the theoretical route (1-2). Then the receiving transducer is coupled at point 3, and the procedure is repeated until point 8, then the emitter transducer is coupled at point 2 and the receiver at the other points for the other readings. The process is repeated until readings are taken on all routes and in both directions (eg 1-2 and 2-1).

Data processing to the image generation

For the generation of images, two spreadsheets are needed, one referring to the outline of the evaluated section and another referring to the propagation times of the wave in each of the theoretical routes of the diffraction mesh. To generate the contour worksheet, we use the image of the disk surface after cutting. So, we open this image in ImageJ, change its pixel scale to centimeters, based on measurements obtained in the field. Then, with the multipoint tool, the contour points are demarcated following the exact contour of the disk (Figure 1), and saved in a text file with x and y coordinates, which corresponds to the contour worksheet.

Figure 1 - Example of an image with the points already demarcated to obtain the outline.

From the outline sheets, the time sheets are created. They are obtained by associating the wave propagation time, obtained in the field measurements, to the outline coordinates corresponding to the initial and final measurement points, forming the theoretical wave propagation routes.

Geration of images

The images were generated by the ImageWood software. This software features two interpolation algorithms, the Inverse Square Distance (IQD) method and the ellipse method with (MEC) and without velocity compensation (ME) proposed by Du et al. (2015). In this research, the images were generated by the two interpolation methods and for the ellipse method, in both conditions, with and without velocity compensation.

All images were generated using only two colors, as the analysis is performed using a binary confusion matrix. Therefore, we chose red to represent the region of interest and yellow for the rest of the cross section. Another condition to be adopted for image generation is the variation of the velocity range in relation to the maximum velocity obtained in the evaluated section. As one of the objectives of this research was to propose a methodology that would indicate the most suitable velocity range for cavity and/or cavity inference along with biodeterioration, the images were constructed considering increasing percentages (0% to 100% every 5%) of the maximum velocity (V_{max}).

The generated images present interferences due to the interpolation method. To reduce these interferences, we use the median filter, whose function is to soften impulsive noises without affecting the outline, by replacing the intensity of each pixel by the median of the neighboring intensities. To use this filter, the number of neighbors (25 pixels) proposed by Palma (2022) was used.

Confusion matrix

The generated images were compared quantitatively with the real images of the disc surface using the confusion matrix. This method was performed using a Python script proposed by Strobel et al. (2018). This method is performed based on the comparison of two images (model and ROI) in an image that delimits the comparison field (internal points).
The Python script makes the comparison considering the four conditions proposed by Fawcett (2006), as shown in table 1.

Evaluation of the Results

The analysis focused on the confusion matrix metrics. Thus, we analyzed the confusion matrix metrics in order to obtain the most adequate $\%V_{max}$ to infer zones of interest (Ca and Ca+Bio), seeking the maximum values. The comparison of images was also used to evaluate the different interpolators and the use or not of the filter.

Results and discussion

756 images were generated and filtered (Figure 3) totaling 1512 images evaluated by the confusion matrix.

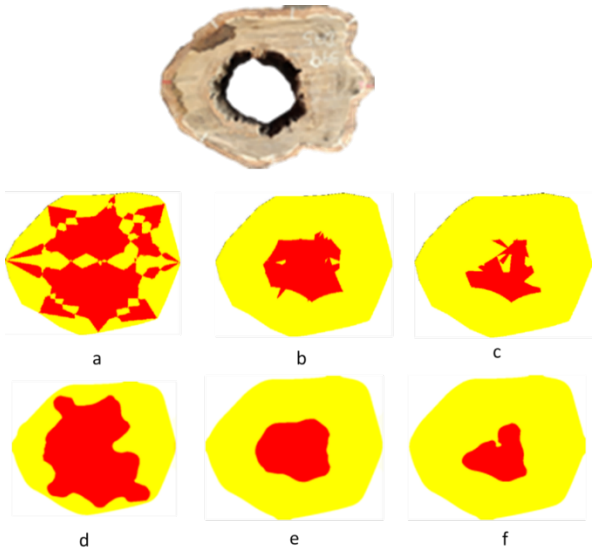

Figura 2- Example of disk photography and tomographic images obtained without applying a filter with IQD algorithms (a), Ellipse with compensation (b) and Ellipse without compensation (c) and with application of a filter with IQD algorithms (d), Ellipses with offset (e) and Ellipses without offset (f).

The graphs in Figures 3, 4, 5 and 6 show the behavior of each of the metrics for the images generated with the different interpolators and the variation of the velocity range as proposed in the methodology. The graphs obtained by the filtered images are also shown in comparison.

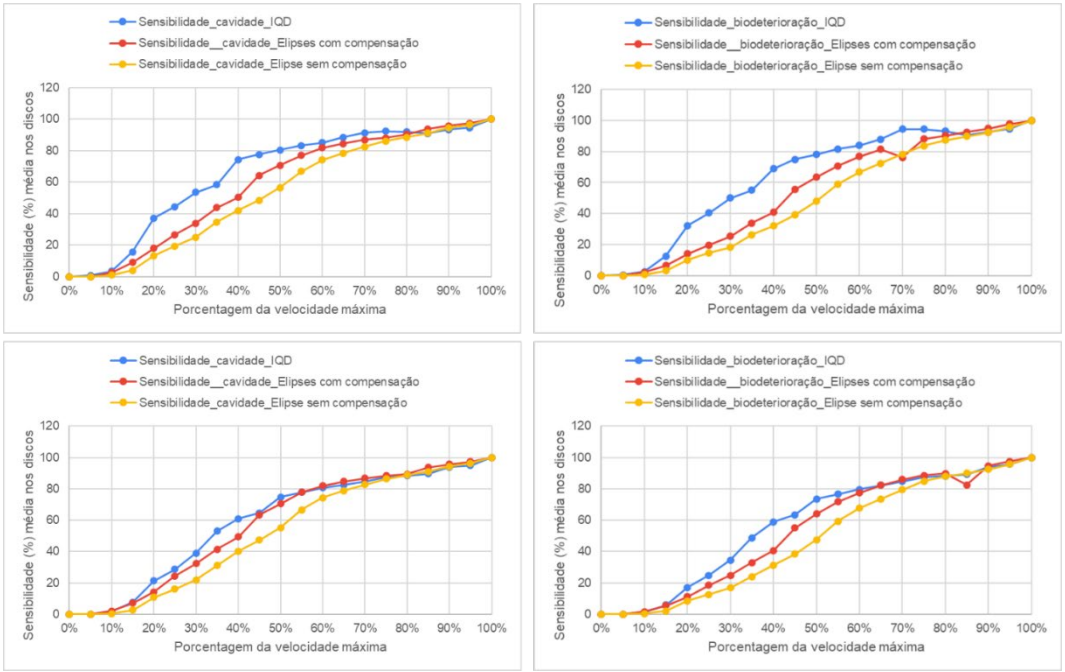

Figura 3- Example of disk photography and tomographic images obtained without applying a filter with IQD algorithms (a), Ellipse with compensation (b) and Ellipse without compensation (c) and with application of a filter with IQD algorithms (d), Ellipses with offset (e) and Ellipses without offset (f).

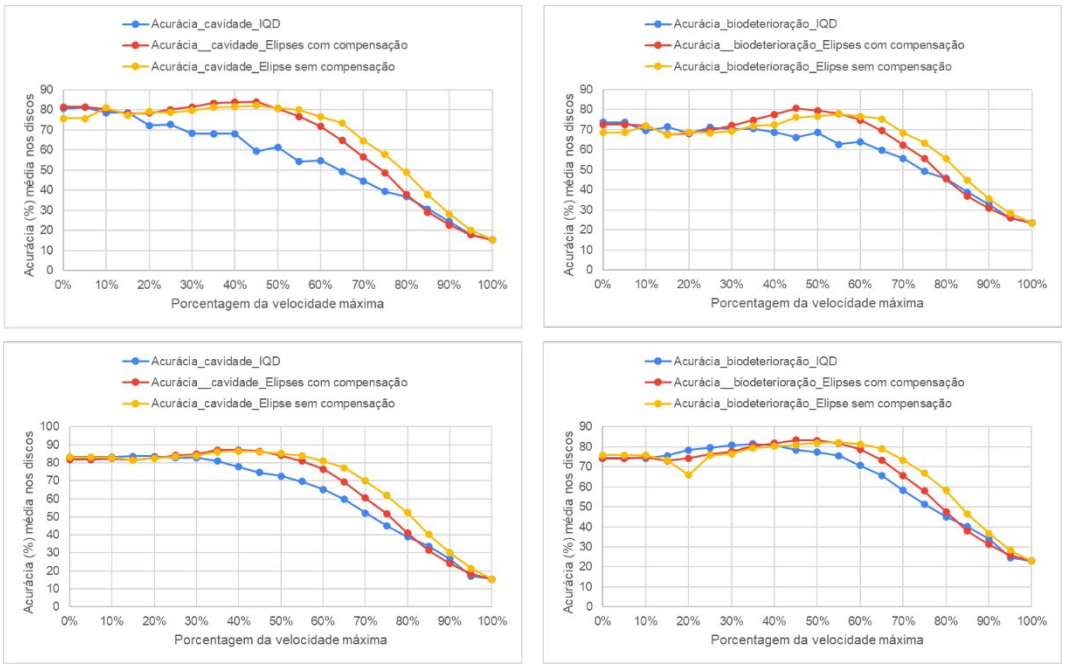

Figure 4 - Behavior of the Accuracy metric, obtained with the application of the confusion matrix for the cavity and the cavity plus biodeterioration as areas of interest, without the application of filters (upper graphics) and with the application of filters (lower graphics)

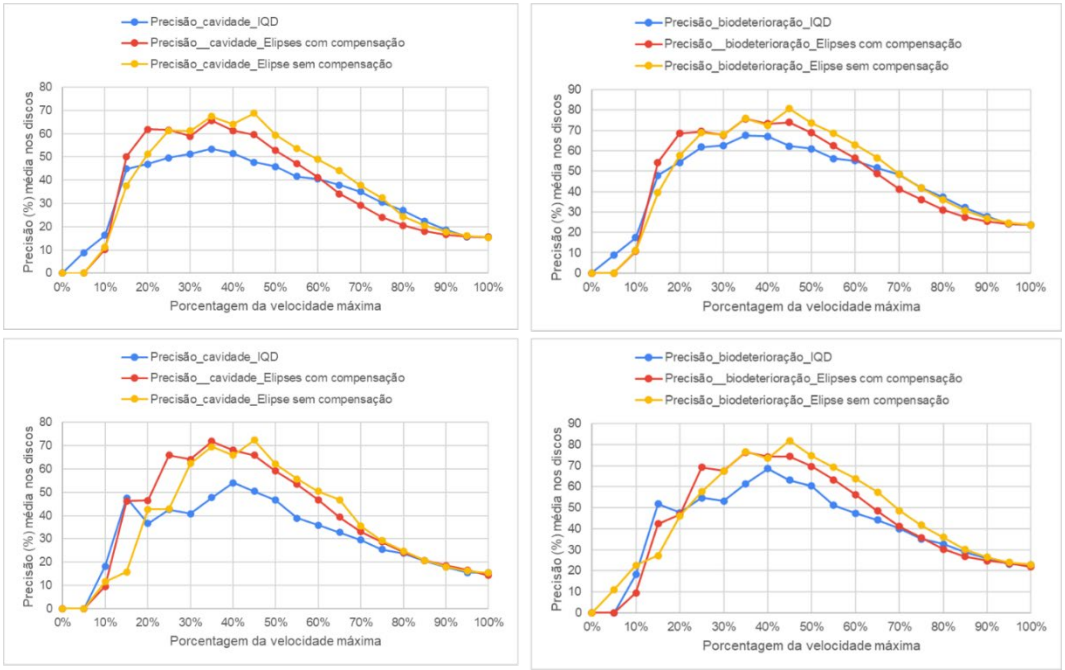

Figure 5 - Behavior of the metric Precision, obtained with the application of the confusion matrix for the cavity and the cavity plus biodeterioration as areas of interest, without the application of filters (upper graphics) and with the application of filters (lower graphics)

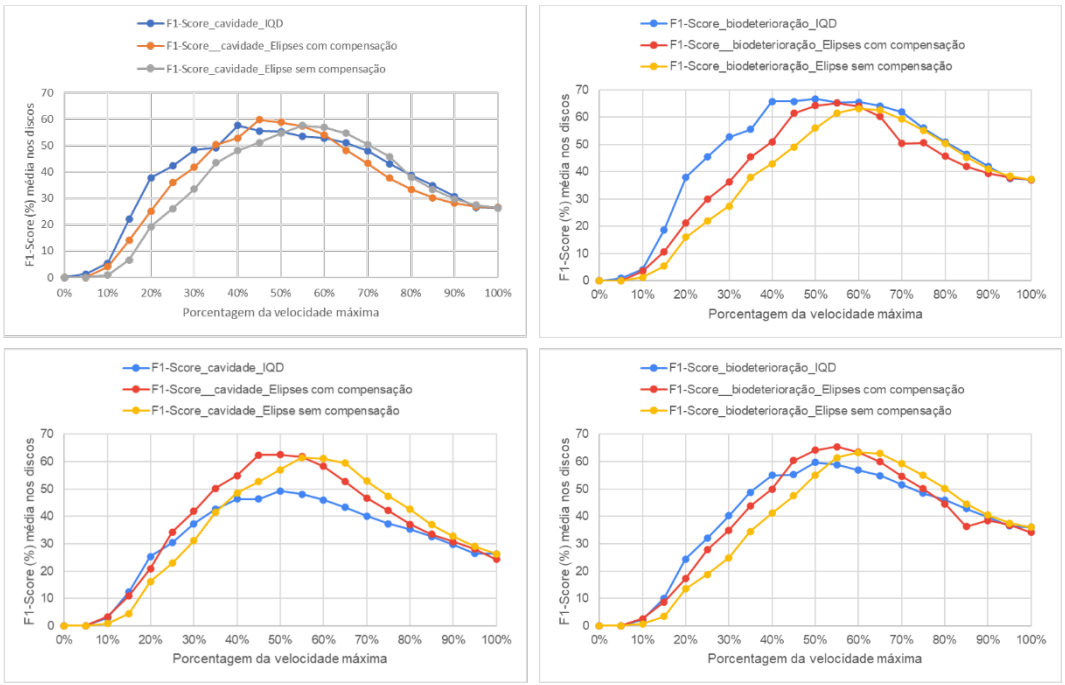

Figure 6 - Behavior of the F1-Score metric, obtained with the application of the confusion matrix for the cavity and cavity plus biodeterioration as areas of interest, without the application of filters (upper graphics) and with the application of filters (lower graphics)

Analyzing the results, we verified that the Accuracy was the metric that differentiated the region of interest and presented the best results considering all the interpolation algorithms.
Among the algorithms, the one that stood out with the best results was the ellipse method with velocity compensation, indicating that the best range of $\%V_{max}$ for the inference of cavities in ultrasonic tomography is from 0 to 40% and for the inference of cavities plus biodeterioration up to 45% (Figure 7). The application of the filter also increased the quality (Figure 7).

Figura 7 - Example of an image generated with 3 colors considering the cut velocitys for inference of Ca (up to 40%) and Ca+Bio (up to 45%) and filtered

Conclusions

The proposed methodology in this case study allowed us to conclude that the most suitable velocity range for the Cavity inference was up to 40% V_{max} and for Cavity associated with biodeterioration up to 45% V_{max}, and the interpolator with better results was the Ellipses Method with compensation. The use of filters improved image quality, and the most appropriate metric for evaluation was accuracy.

Acknowledgments

The authors thank CNPq for the scholarship (Proc. 141067-2018-7) and for the research funding (Proc. 426130/2018-9). To the Higher Education Personnel Improvement Coordination – CAPES, for the scholarship for the internship in Spain (Process- 88887.467257/2019-00). The Research Support Foundation of the State of São Paulo - FAPESP, for funding LabEND research with which it was possible to purchase all the equipment used in the development of the research.

References

Divos F, Divos P. 2005. Resolution of stress wave based acoustic tomography. 14th international symposium on non-destructive testing of wood, Germany 309–314

Du, Xiaochen et al. 2018. Image reconstruction of internal defects in wood based on segmented propagation rays of stress waves. Applied Sciences, v. 8, n. 10, p. 1778.

Du, X., Li, S., Li, G., Feng, H., Chen, S. 2015. Stress wave tomography of wood internal defects using ellipse-based spatial interpolation and velocity compensation. BioResources, 10(3), 3948-3962.

Fawcett T. 2006. An introduction to ROC analysis. Pattern Recogn Lett 27(8):861–874. https ://doi.org/10.1016/j.patre c.2005.10.010

Locke, D. H., & Baine, G. 2015. The good, the bad, and the interested: how historical demographics explain present-day tree canopy, vacant lot and tree request spatial variability in New Haven, CT. *Urban Ecosystems*, *18*(2), 391-409.

Palma S.A.P. 2022. Interference of factors related to inspections of standing trees and data processing on the quality of images generated by ultrasonic tomography. University of Campinas – UNICAMP. Thesis.

Palma, S. S. A., Gonçalves, R., Trinca, A. J., Costa, C. P., dos Reis, M. N., Martins, G. A. 2018. Interference from knots, wave propagation direction, and effect of juvenile and reaction wood on velocities in ultrasound tomography. BioResources, 13(2), 2834

Reis M N. 2022. Quantitative analysis of the scope and contribution of field inspections in trees in the inference of wood biodeterioration. University of Campinas – UNICAMP. Thesis. 95p.

Secco, C. B.; Gonçalves, R.; Cerri, D. G. P.; Batista, F. A. B. 2010. Evaluation of determined types in the detection of the internal condition of the wood by ultrasound. *Madeira: Arquitetura e Engenharia*, v.11(27), p.1-5.

Strobel, J. R. A.; de Carvalho, M. A. G.; Gonçalves, R.; Pedroso, C. B.; dos Reis, M. N.; Martins, P. S. Quantitative image analysis of acoustic tomography in woods. *European Journal of Wood and Wood Products*, 1-11, 2018.

Wu X, Li G, Jiao Z, Wang X (2018) Reliability of acoustic tomography and ground-penetrating radar for tree decay detection. Applications in Plant Science 6 (10): e1187. Doi:10.1002/aps3.1187

Visual Tree Assessment and Static Integrated Assessment Do Not Allow Breaking Safety Evaluation of Defective Stems of Mature Urban Trees

Frank Rinn*
Court Registered Expert for Tree and Timber Inspection, Heidelberg, Germany

* Corresponding author

Abstract

The well-known visual tree assessment (VTA) method promotes two criteria for evaluating the safety of trees: the ratio of the thickness (t) of the intact outer shell-wall divided by the local radius (R) should be higher than 1/3 for guaranteeing sufficient breaking safety ($t/R > 1/3$!) of decayed trunks. For intact trees, the ratio of total height (H) divided by the stem diameter at breast height (D) should be below 50 ($H/D < 50$!). A biomechanical analysis shows that these two criteria are not relevant and that the t/R rule is not applicable to defective mature urban trees, which are typically evaluated in terms of safety considering the following factors: (1) the cross-sectional shape is usually not circular; (2) the defects are usually not located in the center; and (3) the "allometric age effect". The widely used static integrated assessment (SIA) concept is not an alternative because it uses formulas that are valid only for thick-walled metal tubes with homogeneous material properties. Biomechanical science shows that SIA calculations deliver results that are inaccurate by factors of 10 or even more. Because of the highly anisotopic material properties of wood, a fundamentally different math has to be used to determine and evaluate the real load carrying capacity of decayed wooden trunks under bending loads. In addition, the SIA windload prediction contains huge estimation errors. In consequence, both methods are fundamentally wrong and/or inappropriate and thus should not be used to evaluate the safety of defective trunks of mature urban trees and should not be recommended by standards.

Keywords: VTA, SIA, shell-wall, tree-safety

Biomechanical and Mathematical Basics of "Allometric Self-Referencing" for Evaluating Breaking Safety of Defective Stems of Mature Urban Trees

Frank Rinn*
Court Registered Expert for Tree and Timber Inspection, Heidelberg, Germany

* Corresponding author

Abstract

Tree safety experts evaluate if a damaged mature urban tree has a significantly increased probability of breakage compared with the "normal condition" (intact tree). Only then, a risk reduction is required, by, for example, pruning. Thus, there is no need to determine absolute values of load carrying capacity and wind loads but only to compare the current tree with the same tree in an intact state. For mature urban trees, the total tree height H determines the wind load ($\sim H^3$) just as the trunk diameter D determines its load carrying capacity ($\sim D^3$). Thus, in first order, D^3/H^3 characterizes trunk breaking safety in changes with time. That's why most trees keep H/D approximately constant in the "exploration phase" (after juvenile growth and until maximum tree height is reached). Then, the trunk diameter continues to grow as long as the tree is alive, increasing the "basic safety" each year incrementally (allometric safety effect). Reductions in tree height caused by age and/or previous pruning increase the safety because of lower wind loads. The loss in mechanical load carrying capacity of a trunk cross section caused by defects is determined by wood-specific, anisotropic, and tomographic area integrals (compared with the intact state). Combining all these aspects allows the evaluation of a relative level of breakage safety of a defective trunk compared with the intact state, without the need of measuring or estimating any material properties or wind loads. This enables arborists to keep more mature trees longer with the same budget.

Keywords: allometry, self-referencing, tree safety

Dynamic Tree Stability: Improved Testing Methodology and Indications of Reliability

Laszlo Bejo *
Faculty of Forest Products Engineering and Creative Industries, University of Sopron, Sopron, Hungary
bejo.laszlo@uni-sopron.hu

Imre Sumegi
Fakivagas company, Balatonfüred, Hungary, sumegi.imre72@gmail.com

Ferenc Divos
Fakopp Enterprise Bt., Sopron, Hungary, divos@fakopp.com

* Corresponding author

Abstract

Dynamic tree stability assessment is a relatively new technique that has good potential to replace the more cumbersome and less productive static pulling test as the primary method of tree stability evaluation. The reliability of the new technique was greatly improved in recent years through introducing new statistical tools and approaches in the evaluation of the measurement results. This includes, a baseline correction using a median filter to eliminate the slow drift of the inclination sensors. The evaluation algorithm was also simplified by using the first member of the Taylor series for the tangential pressure-inclination function, reducing it to a simple linear approximation. This paper provides a detailed explanation concerning these changes.

The reliability of dynamic tree stability testing is inherently more difficult to evaluate than that of the static pulling test, where the ultimate load can be verified by pulling the tree over. However, in recent years, a significant body of experience was accumulated, which provides good indication concerning the consistency and accuracy of the dynamic method. Experimental evidence include the comparison of the dynamically measured parameters to static ultimate load testing results, the demonstration of the effect of foliage change through dynamic testing results, tracking the effect of root cutting through measuring dynamic safety, and results of high-wind measurements that allows the comparison of dynamic safety prediction to actual ultimate load indications found under dynamic conditions. Based on these case studies – described in detail in the paper – dynamic tree stability testing is an accurate and reliable tool for tree stability assessment, albeit the interpretation of the results requires in-depth expertise in the dynamic behavior of trees.

Keywords: Tree stability, Tree safety, Dynamic stability, Safety Factor, Uprooting

Introduction

Trees add much value to urban life: they offer stress relaxation, provide habitat for birds and insect, shade that reduces temperature in the summer, and capture carbon dioxide and dust particles. On the other hand, urban trees often grow in adverse conditions; hard pavement inhibits rainwater absorption into the soil, traffic around the trees leads to soil compaction, and air pollution impacts growth conditions adversely

(Shigo 1986). As trees go older, worsening condition and a possible loss of stability poses dangerous risk to both property, and human safety and health.
It is important to balance the important benefits of trees against the possible risk arising from tree breakage or uprooting of aging or diseased trees. Tree inspectors regularly assess the condition and stability of urban trees to assess these risks, and their recommendations often include specialized, instrumented tree inspection to assess the tree's safety against breakage and/or uprooting.

There are several methods available for assessing tree safety, including single-pass sound velocity measurement, acoustic and impedance tomography, and resistance drilling. Fewer methods are available for uprooting safety assessment. Some researchers proposed techniques for root mapping based on acoustic signal conduction through the roots, but this only works for large and shallow roots, as deeper accessing deeper roots is not possible from the surface (Buza and Divos 2016). The standard method for uprooting safety determination is the pulling test. This approach is based on simulating horizontal loads through a concentrated load introduced through a cable, and increased gradually, while measuring tree collar inclination, which allows the determination of the ultimate uprooting torque (Wessoly and Orb, 1998).

More recently, researchers examined the possibility of measuring trees under actual wind load conditions (Kent et al. 2016, Moore and Maguire 2008, etc). While the relationship between wind intensity and tree inclination is not as straightforward, as is the case of static pulling load, a statistical approach allows the evaluation of trees in a similar manner as the one used in the case of the pulling test. Earlier studies based on this approach demonstrated the principles and introduced some results and comparisons with static testing (Bejo et al. 2017, Fathi et al. 2019, 2020). Recent years has also brought several innovations that makes the evaluation of the dynamic test results more simple, and the accuracy and reliability of the evaluation also improved.

One drawback of dynamic testing is that its reliability is inherently difficult to evaluate. Low dynamic safety points to the risk of the tree falling over in high wind, but the proving the prediction requires an adverse weather event, with the right wind direction, within a relatively short time frame. In the meantime, static pulling test predictions are easily verified by pulling the tree over. However, in recent years, a significant body of experience was accumulated, which provides good indication concerning the consistency and accuracy of the dynamic method.

The purpose of this paper is twofold: 1) the paper will introduce recent advances in the evaluation of dynamic test results that make the evaluation of the results simpler, and the predictions more reliable than before, and 2) the results of some recent case studies provide further indications as to the reliability and accuracy of dynamic tree stability evaluation.

Dynamic tree evaluation – principle and recent improvements

The dynamic tree testing principle

The basic idea behind the dynamic tree evaluation technique has been described in detail in (Bejo et al., 2017). The technique was developed based on the uprooting safety determination method used with the static pulling test, whereby a safety factor value is determined, which compares the torque arising from the horizontal wind loads to the torque required to uproot the tree:

$$SF = \frac{M_{crit}}{M_{wind}}, \quad (1)$$

M_{crit} is the torque required for uprooting the tree, and it is determined from the load-inclination curve. The value is calculated by fitting a special second order tangential function that describes the relationship

between load and inclination while uprooting the tree to the relatively low values generated during the measurement. M_{wind} is calculated from the geometric parameters, the characteristic aerodynamic drag factor of the given species and expected high wind velocity value in the given geographic area. Since M_{wind} is always calculated relative to an expected high wind condition, *SF* is also valid for that wind velocity. Dynamic tree stability testing is based on collecting several wind intensity and inclination measurements over a period of several minutes, and calculating a statistical parameter (e.g. the average) of the collected values. The process is then repeated for several more periods, and the mean value pairs are used to create pressure-inclination curves, rather than the momentary pressure and inclination. The pressure-inclination curve created this way follows the same tangential relationship as the load-inclination curve obtained through the static pulling test. The analysis of the curve yields a critical pressure value, which is analogous to the critical torque, and can be compared directly to the maximum wind pressure that the tree will experience in high wind conditions. This reduces equation (1) to the ratio of the critical to maximum wind pressure. This eliminates the need for geometric parameters and aerodynamic drag factor. A more detailed explanation of the static and dynamic measurements is available in Bejo et al. 2017.

Dynamic tree stability measurement does not require cumbersome and heavy equipment, several trees can be measured simultaneously (as the anemometer used for testing may be some distance away from the trees), and the lack of geometric parameters and drag factor eliminates much of the uncertainty in the measurement. Most importantly: trees are examined in actual dynamic wind conditions, which promises a better approximation of the potentially dangerous high winds.

Dynamic tree testing was applied successfully in recent years in various scenarios. The accumulated practical experience pointed to possible ways to improve the outcome of the assessment, mainly through more efficient and more accurate evaluation of the collected data. These improvements are introduced for the first time in this paper.

Improving the accuracy and efficiency of the evaluation

Using various statistical parameters

Common sense dictates that using the average in each batch provides the best results when evaluating the batches of collected wind velocity and inclination values. However, in reality, other statistical parameters are more conducive to good correlation. Maximum load and inclination, in particular, proved to be much better than average values, and drastically improved the correlation coefficient. The FAKOPP DynaTree system has been using maximum, rather than average values since early in its development.

Applying baseline correction

When using the equipment over longer periods (measurement periods may take anywhere from 3 to 18 hours or more), some researchers reported an interdependence between the statistical window width and the resulting Safety Factor value. Since the safety of the tree does not depend on the size of the batches used to generate average (or maximum) values, this points to some unintended measurement inaccuracy. The explanation is the slight temperature-sensitivity of the inclinometers used in the measurement. This may introduce some bias when inclinometers are taken outside from a warm indoor environment, or due to daily temperature fluctuations.

A computational solution to this problem is applying a baseline correction when evaluating the data, using a one dimensional median filter to eliminate the slow drift on the inclination sensors. This removes any measurement bias, and effectively eliminates the dependence of the Safety Factor on the statistical time window. This new feature that was introduced in the latest versions of the Dynatree software (FAKOPP

2021) does not only eliminate this problem in future measurements, but may be applied retroactively to past datasets.

Simplified curve fitting procedure

In reality, the relationship between the maximum wind pressure and inclination values obtained from analyzing the data batches follows a special tangential formula, as follows:

$$\varphi = \frac{1}{3}\tan\left(\frac{100}{73.85}\frac{p}{p_{max}}\right) + \frac{1}{3}\left(\frac{p}{p_{max}}\right)^2 - \frac{1}{10}\left(\frac{p}{p_{max}}\right), \quad (2)$$

where φ and p are the maximum inclination and wind pressure within the batch, and p_{max} is the wind pressure required for uprooting the tree. We can use the measured pairs of φ and p values to fit the above curve, and then extrapolate to obtain p_{max}, which we then use to calculate the Safety Factor.

Unfortunately, fitting a relatively complex relationship like this requires much computation, and increases the evalution time. In most cases when taking dynamic mmeasurements, we obtain relatively low pressure and inclination values. In this region, a linear relationship provides good approximation (see **Fig. 1**). For this reason, we can apply a simplification of using the first member of the Taylor series for the tangent function, i.e. fitting a linear function. The slope of the line can be used to obtain the critical wind pressure based on equation (2).

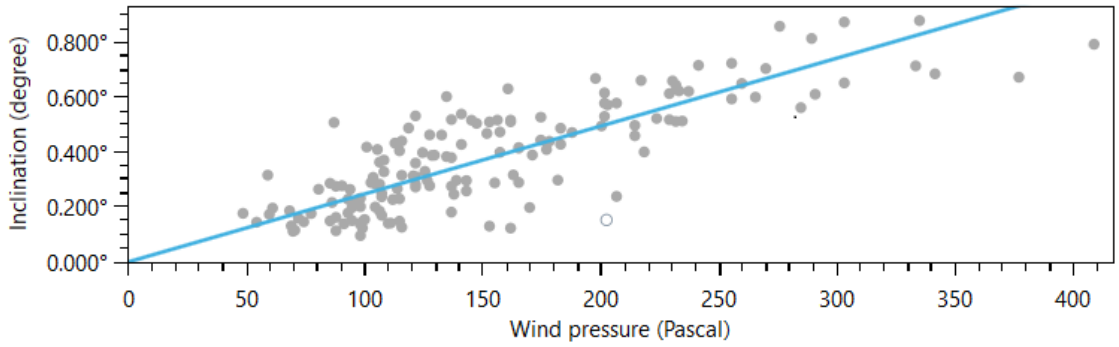

Figure 1—Maximum inclination and wind pressure values obtained through dynamic testing. As long as the inclination remains relatively low, a linear approximation can be used.

Practical examples for the reliability of dynamic tree stability testing

This chapter includes several case studies that underline the practical utility of dynamic tree stability testing. While it is extremely difficult to obtain direct evidence for the reliability of dynamic testing, due to the nature of the test, the results presented in this chapter are also indicative of the accuracy and reliability of the method.

Materials and methods

This chapter introduces a number of different experiments, carried out over a span of several years. The experimental setup was similar in all cases, with slight variations, as detailed below:

- Inclinometers: bubble type biaxial inclinometers, with sampling frequencies of 10 Hz and a resolution of 0.001 degree. The inclinometer is equipped with a data logger and GPS timer for precise synchronization of wind pressure and inclination data. Precise time data is stored together with measured data. A mounting plate with three pins and a ball head were used to attach the inclinometer at the bottom of the tree trunk. The inclinometer's operating range is ± 2 degrees.

After finishing data collection, we removed the screw. Data collection periods varied between 1 hour and 2 days.

- Anemometers: either cup type anemometers or ultrasonic anemometers were used for wind velocity measurements, with 1 Hz sampling rates. The anemometers were always positioned several meters above the tops of trees or nearby buildings, where their interference was negligible. Both instruments worked equally well for dynamic root evaluation. The anemometers were equipped with a data logger and a precise GPS-based clock. The distance between the anemometers and the measured trees varied, but was below 1000 m in all cases.
- Result evaluation was carried out using the DynaTree software of the FAKOPP Company (FAKOPP, 2021). The statistical window size was 5 minutes in each case. Each batch included 300 velocity data points and 3000 inclination data points, of which maximum values were used for the analysis. Older measurements were re-evaluated using the newest version of the software, to apply the median filter.

The number and species in each case study, as well as the wind direction, wind intensity and other circumstances varied between the various measurements, and will be given in each case study. However, wind intensity was always above 25 km/h, as required for the dynamic test.

Case study nr. 1 – Comparing static and dynamic stability test results

In the first case study, ten diseased ash trees were examined in 2018, in Donaudorf, Austria. The stability of the trees was measured in the same day using the DynaRoot system. After the dynamic measurement, all ten trees were measured by the pulling test as well. Pulling test was not stopped at 0.2 degrees of inclination as is customary; instead, trees were tested to failure by uprooting. This allowed the comparison of the critical loads estimated from the static and dynamic test results with the actual critical load obtain by uprooting. See (Fathi, 2019) for further details.

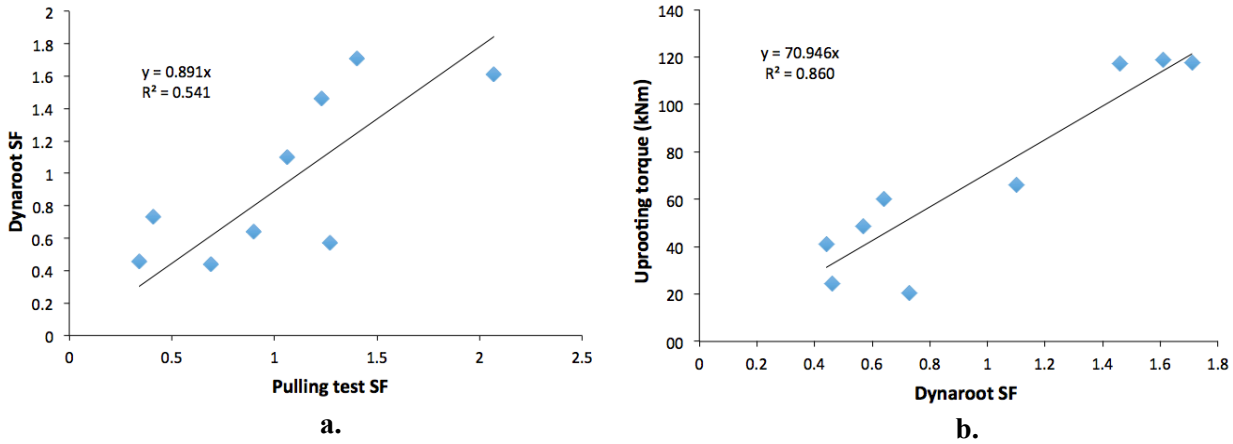

Figure 2—The relationship between the static and dynamic SF values (a) and between the dynamic SF and the measured ultimate torque values of 10 diseased ash trees.

SF values were calculated both from the static and dynamic tests. In addition, the ultimate uprooting torque was also estimated from the static pulling test, and compared to the measured ultimate torque. Unsurprisingly, the estimated and measured maximum torque showed very good correlation. On the other hand, static and dynamic safety factor values were in relatively poor agreement (**Fig 2a**). Since the static SF value is verified against static pulling test results only, it is not possible to how well it works for dynamic wind load conditions, and whether the static or dynamic SF is a better predictor of dynamic safety. One interesting result is that the dynamic SF was a better predictor of the measured uprooting torque than the static SF value (**Fig 2b**).

Case study nr. 2 – The effect of foliage changes

The foliage changes of broadleaved trees obviously effect their stability, which is expected to change between the summer and winter months. The torque from horizontal wind loading is calculated using the formula below:

$$M_{wind} = Ap_w c_w h_{cr}, \tag{3}$$

where A is the crown surface area, p_w is wind pressure, c_w is the aerodynamic drag factor and h_{cr} is the crown centerpoint height. Intuitively one might assume that stability will improve in the winter, when leaves are absent, and therefore the surface area (A) is lower. This, however, does not take crown shape into consideration. In the summer, trees tend to bend in the wind, which decreases the drag factor (c_w), and therefore the torque as well, as opposed to winter when the crown tends to deform less. The question is which effect is more influential.

Several trees were examined both in summer and winter conditions. The examination included 11 specimens of seven broadleaved species, as well as 5 coniferous trees of various species as control. SF values were measured in winter and also in spring or summer, at various times, but otherwise under similar conditions (e.g. wind direction, soil moisture content, etc. Then the SF values were compared between seasons.

Fig. 3 shows the comparison between winter and summer SF values. As expected, winter SF values are typically higher than their summer counterparts. However, there is considerable variation in the data, and in some cases, the two values were very close. This suggests that surface area in itself does not explain the differences between summer and winter safety, and the differing behavior of bare branches in the winter (which causes differences in the aerodynamic drag factor) also influences the results. **Table 1** shows the ratio of winter to summer SF values in case of coniferous species. All values are very close to 1, since these trees do not lose their leaves in the winter.

This study provided important practical learnings for dynamic tree testing. If possible, testing of broadleaved trees should take place between mid-spring and mid-autumn, when foliage is present. If we have to test in the winter, we should expect summer SF to be about 30 to 50 percent of the winter value, but there is a lot of variation in this, and measurements should be repeated in the summer for certainty. Finally, stability testing should never be done when the ground is frozen, stabilizing the roots and resulting in unrealistically high SF values.

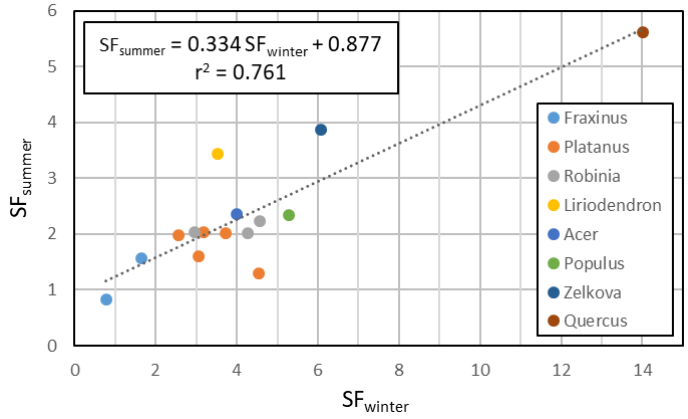

Figure 3—A comparison of winter and summer Safety Factor values in various broadleaved trees

Table 1—Winter to summer stability comparison in coniferous trees

Species	SF_{winter} / SF_{summer}
Cedar	0.95
Sequoia	1.03
Taxus	0.96
Abies grandis	0.92
Pinus nigra	1.36

Case study nr. 3 – Root cutting

This interesting study included a single pedunculate oak (*Quercus robur*) tree. The roots of the tree were excavated to reveal the root structure (**Fig. 4**), and the diameters of the main roots recorded. After that, several dynamic stability measurements were performed. In-between the measurements, more and more of the large roots were cut to decrease the stability of the tree, until almost all of the roots were finally severed. Thereby, the changes in dynamic stability due to weakening the root structure were monitored. Measurements were taken in the summer and autumn of 2021, over a 4-month period.

Fig. 5. shows the changes in the dynamic stability of the tree as a function of the percentage of the total cross sectional area that was severed before each measurement. There is a general decreasing trend in the results. However, in the early stages of the study, SF values increased, rather than decreased after cutting a small percentage of the roots. The four outlying points were measured after severing 2.6, 4.6, 6.9 and 8.8 percent of the roots, respectively.

The explanation for this anomaly is the variation in wind direction. The initial measurement, as well as the ones taken after cutting over 10 percent of the roots, were carried out in the prevailing wind SW wind direction. However, the three outlying points were recorded in crosswind conditions (SE). This shows that wind direction has a very important influence on dynamic stability measurements, as trees tend to optimize their root structure to resist prevailing wind, and may behave differently in crosswind. This observation agrees with earlier findings (Fathi 2019).

Figure 4—The exposed root structure of the oak tree before systematically severing each of the main roots

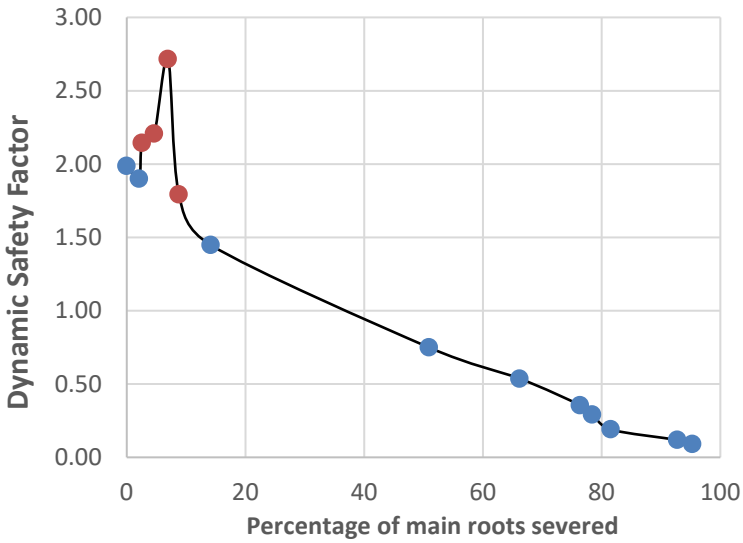

Figure 5—Safety factor values measured after progressively severing the roots of an oak tree. Blue points were measured in the prevailing SW wind direction. Orange points were measured in crosswind (SE).

Case study nr. 4 – High wind events

As mentioned earlier, direct verification of the reliability of dynamic stability is very difficult to achieve, as this requires observing the failure of trees under strong wind conditions during or soon after testing. Nevertheless, two examples in the past few years demonstrated the accuracy of the dynamic method:

1) In 2016, a weak maple tree was examined in the University Botanical Gardens in Sopron, Hungary. Dynamic measurements showed the Safety Factor of the tree to be below 1 in a reference wind velocity of 70 km/h. Within two weeks, a 63 km/h windstorm uprooted the tree. The exposed root structure was visibly very weak.
2) Very recently, dynamic measurements were taken on three Eucalyptus trees over several days by Tim Moya Associates near London, UK, during extremely strong winds approaching 120 km/h in velocity, which caused significant inclinations of more than 1.6 degrees (typically trees fail at 2 to 2.5 degrees of inclination). Trees were partially shaded from wind on one side by some buildings, and, as the wind direction changed gradually over the measurement period, the effect of shading is clearly visible when the wind direction was from that direction. The most important finding, however, was the direct observation of the loss of stability, as shown in **Fig. 6.** The red line marks the event, after which there is a marked increase in the inclination values, while wind intensity remains the same. This points to a significant loss in stability, and an increased likelihood of tree failure in the near future.

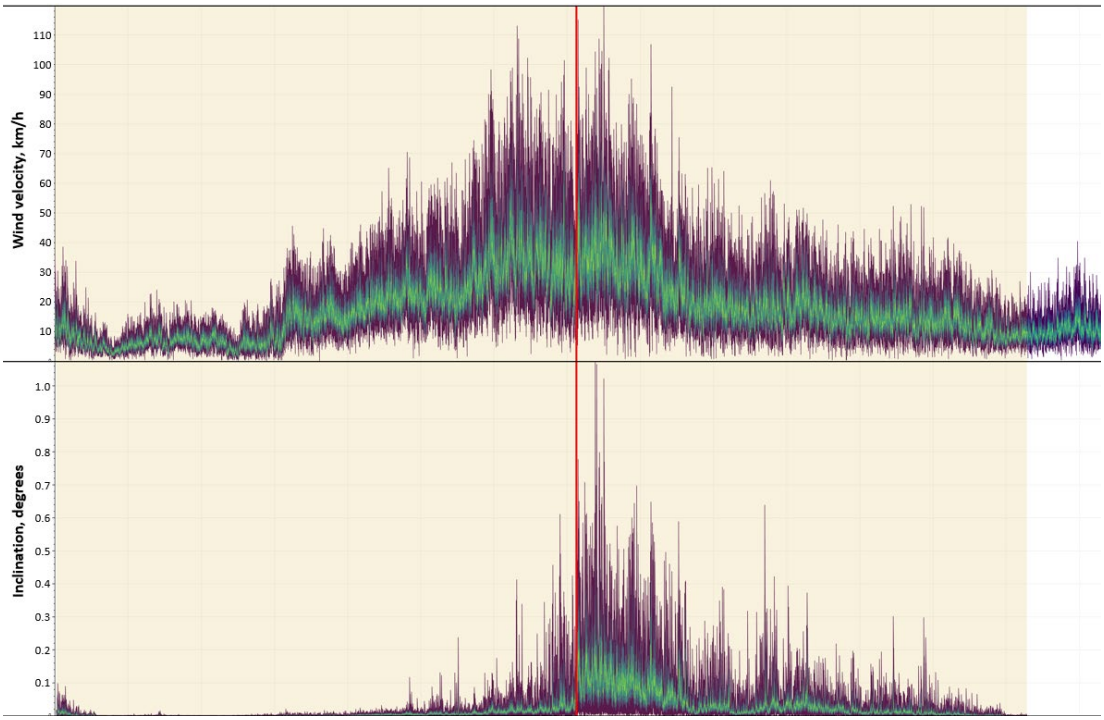

Figure 6—Concurrent wind velocity and inclination diagrams measured on a Eucalyptus tree near London, UK. The red line marks an event when there is a notable loss of stability and increase in the movement of the tree. Diagram courtesy of Mr. James Chambers, Tim Moya Associates, UK.

Conclusions

This paper introduced some of the improvements done to the evaluation of dynamic tree safety data over the last years, as well as some dynamic testing case studies. The results of the study lead to the following conclusions:

- Using the maximum, rather than the average values in each batch of data improves the correlation between wind intensity and inclination. Applying a median filter compensates for the slow creep in inclination data due to temperature variations, and using a linear approximation makes the evaluation much faster without significant losses in the accuracy when estimating the ultimate wind pressure required for uprooting the tree.

- Case studies, including the comparison of the dynamically measured parameters to static ultimate load testing results, detecting the effect of foliage change, tracking the effect of root cutting through measuring dynamic safety, and experiences during high-wind weather events dynamic tree stability testing is an accurate and reliable tool for tree stability assessment.
- Expertise regarding the effect of tree morphology and measurement conditions is required for the accurate interpretation of the results. Without the appropriate knowledge, results may be misinterpreted and may lead to incorrect decisions regarding risks and the necessary tree management and removal.

Acknowledgments

This study has been financed by Project no. TKP2021-NKTA-43, which has been implemented with the support provided by the Ministry of Innovation and Technology of Hungary from the National Research, Development and Innovation Fund, financed under the TKP2021-NKTA funding scheme.
The authors would like to acknowledge the contribution of Dr. Shadabeh Fathi, as well as Mr. James Chambers, Tim Moya Associates, UK, to the results presented in this paper.

References

Bejo L., F. Divos, S. Fathi 2017. Dynamic root stability assessment – basics and practical examples. In: X. Wang; C.A. Senalik; R.J. Ross ed. Proc. 20th International Nondestructive Testing and Evaluation of Wood Symposium Madison, Wisconsin, USA, pp. 262-269. , 1 p.

Buza, A.K., F. Divos. 2016. Root Stability Evaluation with Non-Destructive Techniques. Acta Silvatica et Lignaria Hungarica 12(2):125-134.

FAKOPP Ltd. 2021. Manual for the DynaTree dynamic root and trunk evaluation system. 47 pp.

Fahti, S. 2019. The reliability and applications of dynamic tree stability inspection. Doctoral Dissertation, University of Sopron, Hungary. 109. pp.

Fathi, S., L. Bejo, F. Divos 2020. Investigating the Effect of Weather and Seasonal Factors on Root Stability Using Dynamic Measurements. Open Journal of Forestry 10(1):124-134.

Fathi, S., Mag. K. Schwanda, R. Gschwandtner, N. Nemestothy, Nikolaus, L. Bejo, A. K. Buza, F. Divos 2019. Dynamic and Static Root System Evaluation. In: X. Wang, U. Sauter ed. Proc. 21st Int. Nondestructive Testing and Evaluation of Wood Symposium. USDA Forest Service pp. 394-400.

TMS – Tree Motion Sensors, http://www.argus-electronic.de/en/tree-inspection-technology/products/tms-tree-motion-sensors, Date: June 27, 2016

J. Kent, N. Haritos, and P.K. Addes. 2006. Mechanical stability of trees under dynamic loads. American Journal of Botany 93(10):1361–1369.

Moore, J.R., and D.A. Maguire. 2008. Simulating the dynamic behavior of Douglas-fir trees under applied loads by the finite element method. Tree Physiology 28:75–83

Shigo, A. 1986 A New Tree Biology: Facts, Photos, and Philosophies on Trees and their Problems and Proper Care. Shigo and Trees, Snohomish, Washington

Wessolly, L., and M. Erb 1998. Handbuch der Baumstatik und Baumkontrolle. Patzer Verlag, Berlin, Germany.

Comparing the Stability of the Trees in Different Seasonal and Weather Conditions by Using Nondestructive Method

Ferenc Divos
Head, FAKOPP Enterprise, Sopron, Hungary
divos@fakopp.hu

Laszlo Bejo,
Professor, Institute of Wood Based Products and Technologies, University of Sopron, Hungary.
bejo.laszlo@uni-sopron.hu

Shadabeh Fathi *
Graduated from Institute of Wood Based Products and Technologies, University of Sopron, Hungary.
shadabeh.fathi@gmail.com

* Corresponding author

Abstract

There are many available evaluations and equipment to measure the safety of live trees. Instead of static loading, dynamic technique uses actual wind loads. The goal of this study is assessing how dynamic tree stability is affected by various factors, including: soil moisture content, wind direction. Trees are considered natural capital. The biggest motivation to pursue non-destructive testing in the wood and wood product industries was the need to use them in the best way possible. In this research work DynaRoot system (Fakopp BT 2018) were used. A number of conifers specimens were chosen in the Botanical Gardens of the Sopron University, Hungary. Data was collected over a 2 year period, during which trees were measured in different conditions. With the dynamic method, there is a limitation on how well measurement conditions can be controlled. Measurements can only be taken in windy weather. Wind intensity and direction cannot be controlled, and sometimes there is no wind to measure trees in the chosen conditions. Results show, soil moisture content has a strong positive correlation with the dynamic Safety Factor of coniferous trees. On the other hand, Wind direction variation had less of an effect on the stability of coniferous trees than expected. It is likely that other factors are more influential on dynamic stability.

Keywords; Tree Stability, DynaRoot system, Safety Factor, Wind Direction

Introduction

Recognizing tree stability can be determined by many methods, the simplest one is visual inspection, which obtained from the tree crown requires special expertise and much anatomical knowledge and practical experience, whereas this method is not able to be very accurate about structural stability and leaves a lot of room for human error. Since trees are considered natural capital, there is an increased emphasis around the world to address forest and ecosystem health issues. The marketplace is becoming increasingly global in nature. The biggest motivation to pursue non-destructive testing in the wood and wood product industries was the need to use them in the best way possible. These challenges necessitate

accurate, cost-effective non-destructive tests (Brashaw et al 2014). Advancement in nondestructive testing (NDT) led to the development of a number of more reliable techniques and instruments in the past 75 years. Various methods and techniques have been advanced during these years, and various manufacturers offer equipment like Sound velocity evaluation, Acoustic tomography, Impedance tomography, Resistance drilling, Static pulling test, Acoustic root mapping, Electromagnetic radiation-based techniques and Ground penetrating radar (for root detection) for tree condition and safety. Ultrasonic testing was the latest to come to the industry approximately in 1912. The industrial use of ultrasonic testing started simultaneously in three countries: the USA, GB and Germany. In 1931, Saddik obtained a patent for using ultrasonic waves, using two transducers to detect flaws in solids. The traditional and accepted way to directly establish tree stability is the pulling test. It is a very well researched and established method, based on theoretical considerations of tree mechanics, as well as extensive practical experimentation (Brudi and Wassenaer 2002). A novel approach emerged recently for assessing tree stability and trunk safety. Instead of static loading, this technique uses actual wind loads. This is a more realistic loading scenario, but the interaction of the wind loads and the movement of the various part of the tree is a highly complex process, governed by many variables, and impossible to accurately describe or model at our current level of scientific advancement. There are other issues that need to be considered when employing dynamic testing. One of these is wind direction. Depending on the geographical area, winds most frequently blow from the same point of the compass. Such winds are called prevailing winds, and their direction depends on the geographical location. Prevailing winds are often strong, and therefore trees tend to develop their crown, trunk and root systems so as to be most resistant in this direction. The stability of trees can be markedly different in crosswinds than in prevailing winds, and the operator has no control over this factor. Since the dynamic method allows testing several trees at once with ease, it may be a useful tool to examine several trees in various conditions to extend our knowledge base about the behavior of trees in different circumstances, and examine the effect of factors such as wind direction, precipitation, temperature, pruning, etc. the goal of this research is Assessing how dynamic tree stability is affected by various factors, including: soil moisture content, wind direction.

Equipment and methods

Measuring trees in different weather and seasonal conditions to build a database and draw conclusions regarding the influence of various factors on the stability of coniferous and deciduous trees. The DynaRoot system is completely nondestructive method, while in the case of pulling test, the force is exerted mechanically, but, in normal cases, it does not cause any damage to the tree. The DynaRoot system consists of three components (Figure 1): Anemometer: an instrument for measuring wind velocity at or near the tree to be evaluated. The closer the anemometer is to the tree the better, but, depending on wind velocity DynaRoot may provide reliable data even with measurements taken several kilometers away. Ideally the anemometer should be clear of buildings or other objects that may obstruct the wind, at a height of at least 10 m. When measuring trees in the University’s botanical gardens, we used a modified TX20 ball anemometer permanently mounted on top of one of the University buildings (no farther than 800 m from the measured trees), with a sampling rate of 1 Hz. This instrument is set up to send the data directly to a web server, whence it can be retrieved later.

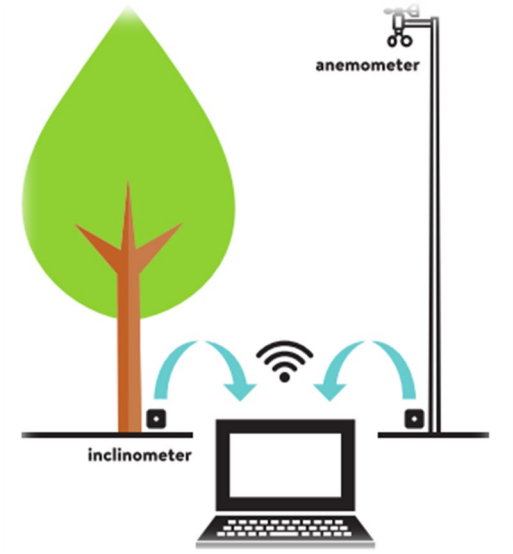

Figure 1 – Schematic of the DynaRoot system (with mobile anemometer tower)

The examined specimens included a wide range of species with different morphological characteristics, including the following Port-Orford-cedar (Chamaecyparis lawsoniana), Giant sequoia (Sequoiadendron giganteum), English Yew (Taxus baccata), Grand fir (Abies grandis), Black pine (Pinus nigra). One specimen of each species was chosen for investigation. Data was collected over a 2 year period (19.04.2018 to 24.11.2019), during which trees were measured in different conditions, i.e. in the winter, frozen ground conditions are likely, and in autumn and spring. With the dynamic method, there is a limitation on how well measurement conditions can be controlled. Measurements can only be taken in windy weather. Wind intensity and direction cannot be controlled, and sometimes there is no wind to measure trees in the chosen conditions.

Tree inclination and wind velocity were measured using the DynaRoot system. Wind measurement was monitored in one central place (on top of the NRRC building of the University of Sopron, Hungary), while tree inclination was measured using inclinometers affixed to the root collar of each tree. Inclinometer and anemometer readings were uploaded in the DynaRoot evaluation software, which calculated the Safety Factor, critical wind pressure for each measurement. Metadata for analyzing the results wind direction and soil moisture content. Therefore, dynamic measurements and the resulting SF values could only be compared to wind direction, and the database for the effect of moisture content was smaller. Moisture content was determined by drying the soil sample for approx. 24 h at 100 °C, until completely dry, and comparing the initial weight to the oven dry weight.

Evaluation and results

Measurements on different trees were taken in the autumn, winter and spring over a period of 2 years (spring 2018 and autumn 2019). Testing required wind velocities of at least 25 km/h, which limited the number of measurements. There were sometimes also technical difficulties with the anemometer that failed to send wind data, and also faulty inclinometers, and – in one case – deliberate vandalism. Because of these limitations and problems, a total of 15 measurements were taken on 5 trees in different weather and seasonal conditions. Since there was no way to control measurement conditions, these measurements include a wide variety of soil moisture content, wind velocity and direction, as well as diverse foliage conditions in the case of broadleaved trees. Tables 1 shows 5 conifers recorded information.

Table 1 – The stability of conifers measured under different weather and seasonal conditions

Species	Date	Soil MC (%)	WD (°)	Acrown (m2)	SF	r (%)	pcrit (Pa)	Height (m)	DBH (cm)
Cedar	08/06/18	20.1	294	159	7.69	83	6565	24.5	159
	08/12/18	20.9	262	159	7.33	71	6676		
	07/03/19	16.6	169	159	6.37	72	6410		
Sequoia	09/06/18	23.8	146	265.0	9.86	60	8721	29.7	118
	29/11/18	28.9	91	265.0	10.23	59	9000		
	27/02/19	17.8	290	265.0	6.17	70	5366		
Grand fir	19/04/18	11.0	45	117	2.56	57	5471	31.0	70
	01/12/18	18.5	100	117	3.51	91	3051		
	09/03/19	18.8	136	117	3.78	79	3326		
Yew	08/12/18	21.0	272	219.6	8.00	70	7652	27.8	63
	07/03/19	16.6	153	219.6	5.47	90	4609		
	10/06/19	13.0	87	219.6	5.34	90	4667		
Black Pine	09/03/19	15.2	118	162.9	4.45	80	4384	23.6	67
	12/04/19	11.0	299	162.9	3.76	62	3264		
	23/11/19	13.8	77	162.9	2.81	94	2397		

Legend: MC = moisture content; WD = Wind direction; r = correlation coefficient; DBH = diameter at breast height

This apparent lack of relationship is partly because of the relatively small number of measurement in each tree, and also because of the complex interaction of various factors (some of which, like the effect of frozen ground, shading or differences in root structure, could not be measured and factored in). Combining the results of the individual trees may highlight trends and tendencies not evident in tree-by-tree analysis.

The parameters calculated Table 1 allows us to compare the relative changes in Safety Factor to the changes in moisture content and wind direction, regardless of individual differences between trees.

The effect of soil moisture changes on the stability of conifers is shown in Figure 2. Moisture content appears to account for almost 80% of the variation in tree stability, while the remaining 20% may be caused by various other factors like wind direction, frozen ground, snow, etc. On the one hand, this is to be expected, since coniferous trees tend to be more similar in their gross anatomical features. However, the results contradict the expectation that moisture tends to loosen the soil, and therefore decrease tree stability.

The positive effect of soil moisture content increase on the stability of coniferous trees is most likely due to the root structure of the trees. Many coniferous trees (like pines and fir) have a taproot system, with the main root reaching deep into the ground. The compaction of the lower soil layers by the added weight of the topsoil may stabilize deep-reaching roots. Other trees (like sequoia) have a dense, matted root system, which incorporates large amounts of soil. The added weight of this soil helps anchoring the tree and, again, improves stability (Fathi et al. 2020).

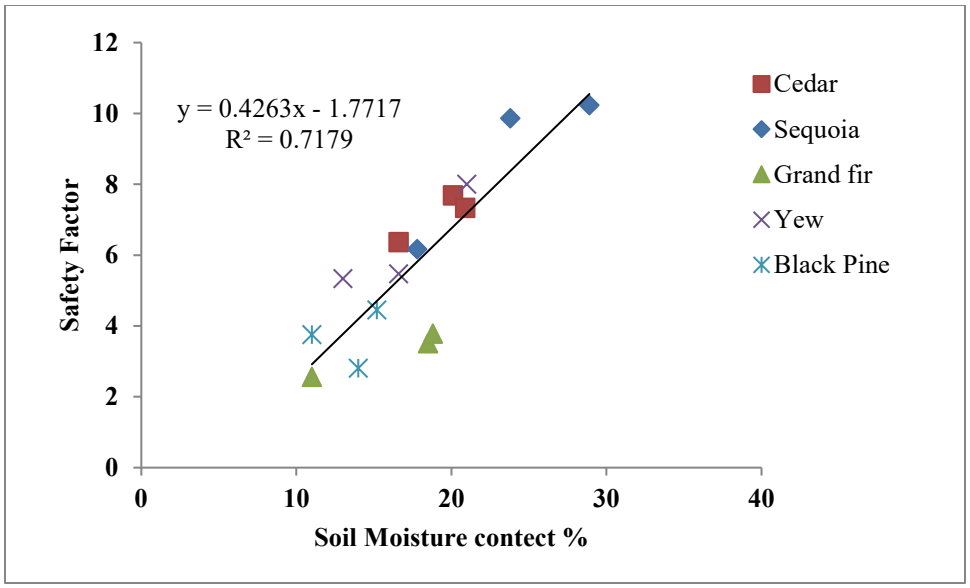

Figure 2 – The effect of changes in soil moisture content on the Safety Factor of coniferous

Wind direction also plays an important role on tree stability. Trees tend to be strongest in the prevalent direction, and get progressively less resistant as we move away from that point in the compass. The figure 3- shows how wind direction affect tree stability in different seosons. Horizintal axis expresses recorded data for every single tree in spring, autumn and winter respectively. The right vertical axis indicates the stability of trees, left vertical axis illustrate wind direction in degrees. As can be seen clearly in the graph, the trend for wind direction was different in 2 trees one of them was seqouia tree (mostly in spring and autumn) which is approximately the oldest and hence taller than most and the thickest of all. This may cause crosswind to reinforce its stability. Furthurmore, safety factor for black pine in spring, which had thiner trunk, was decreased by the crosswind

These two trees were exception in this measurement. for the rest, followed similar trends (SF and wind direction). This shows that prevalent winds are might be less effective than crosswind in reinforcing the stability of trees. As was mentioned, there are other factors such biological factors involved and these factors undoubtedly have influence on stability.

Conclusions

Soil moisture content has a strong positive correlation with the dynamic Safety Factor of coniferous trees. This is most likely explained by the root structure of these trees. On the other hand, Wind direction variation had less of an effect on the stability of coniferous trees than expected. It is likely that other factors are more influential on dynamic stability. This is an advantage from a practical application point-of-view, where arborists and other experts do not have to worry about the effect of wind direction variations.

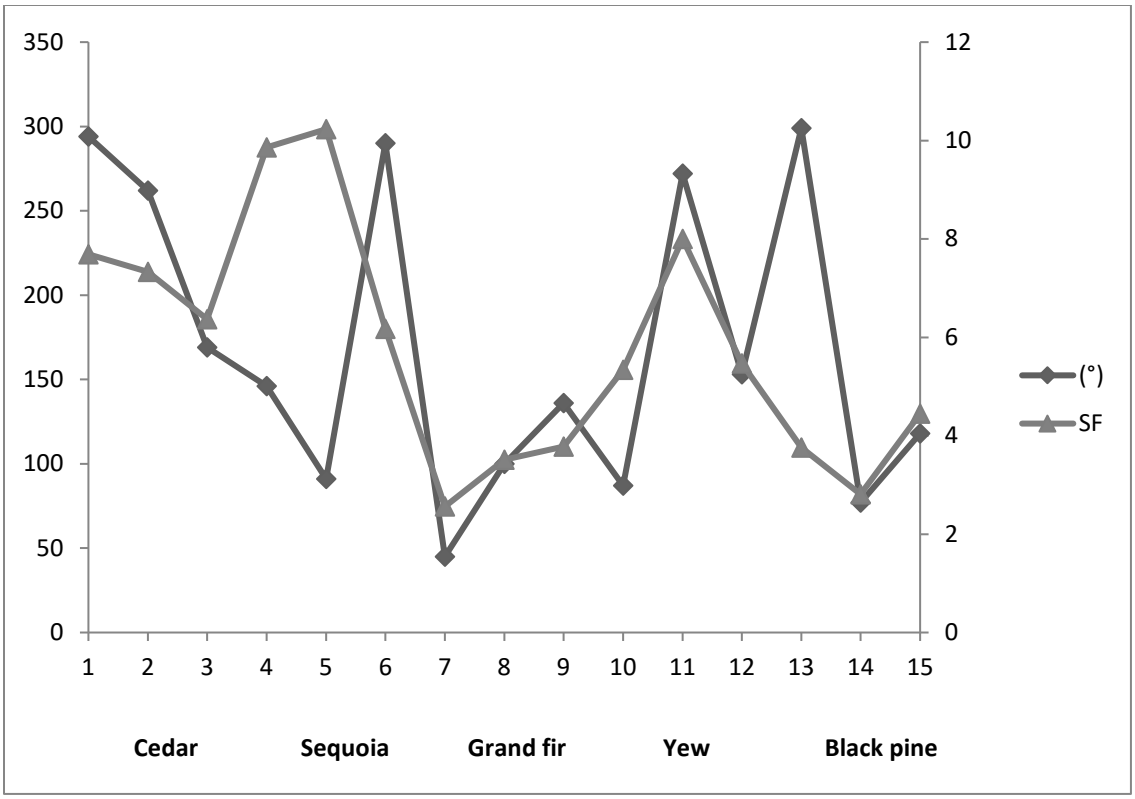

Figure 3- The effect of wind direction in the SF in different seasons

References

1. Brashaw , B. K., Bucur, B. V, Divos, F., Gonçalves, R., Lu, J., Meder, R., Pellerin, F. R., Potter, S., Ross, R. J., Wang, X., and Yin, Y. 2014. Nondestructive Testing and Evaluation of Wood: A Worldwide Research Update, Fores Products Journal 59(3): (35-43)
2. Brudi, E. and Wassenaer, P. V. 2002. Trees and Statics: Non-Destructive Failure Analysis, in How Trees Stand Up and Fall Down, Illinois, pp. 53–70.
3. Fakopp Ltd. 2018 DynaRoot Dynamic Root Evaluation System http://fakopp.com/docs/products/dynaroot/UserManualDynaRoot.pdf
4. Fathi, S., Bejo, L. and Divos, F. 2020. Investigating the Effect of Weather and Seasonal Factors on Root Stability Using Dynamic Measurements, Open Journal of Forestry 10:124–134
5. Saddik, G., 2015. Ultrasound Imaging System. Ph.D. thesis. University of California, Los Angeles, CA Bioengineering Department.

Identification of Wood Decay and Hollowness in Standing Tress using Electric Resistance Tomograph: A Nondestructive Testing Approach

B.N. Divakara*
Department of Silviculture Forest Management, Institute of Wood Science and Technology, Bangalore, Karnataka, India, bndsira@gmail.com

S. Chaithra
Department of Silviculture Forest Management, Institute of Wood Science and Technology, Bangalore, Karnataka, India, greenivyscarlet14@gmail.com

C. Balaji
Department of Silviculture Forest Management, Institute of Wood Science and Technology, Bangalore, Karnataka, India, balajich95216@gmail.com

*Corresponding author

Abstract

The term nondestructive evaluation is well established in wood science research, representing "the process by which selected physical properties of a material is being tested without damage or alteration to its end-use capabilities." Nondestructive testing methods locate and quantify wood decay and defects or hollowness of large physical wooden structures, thereby analyzing the structural soundness of trees to estimate the probability of failure. Nondestructive testing equipment with advanced techniques provides extensive information on the internal integrity of trees. Proper tree health involves regular monitoring and using preventative measures to ensure the tree is free from fungal infections, avoiding tree failure. Visual inspections of fungal conks or open cavities for tree stability evaluation are limited. To measure the internal physical conditions of standing trees to make better decisions, a multisensor electric resistance tomograph (ERT) method can be carried out without disturbing the long-term health of the tree by determining the presence and extent of internal decay. Defects affect the internal energy flow leading to varying resistivity differences. ERT using the specific software PiCus Treetronic can sense the damaged or abnormal tree tissue, such as wood deterioration or hollowness, and identify it based on the measured resistivity patterns.

Keywords: electric resistance tomograph, nondestructive testing, tree decay, hollowness

Session 4

NDE of Sawn Logs for Optimal Utilization

Small-Diameter Logs from Oak for Structural Purposes—Determination of Mechanical Properties by Nondestructive and Destructive Testing

Nicolas Hofmann*
Forest Research Institute Baden-Württemberg, Department of Forest Utilisation, Freiburg, Germany, nicolas.hofmann@forst.bwl.de

Franka Brüchert
Forest Research Institute Baden-Württemberg, Department of Forest Utilisation, Freiburg, Germany, franka.bruechert@forst.bwl.de

Udo H. Sauter
Forest Research Institute Baden-Württemberg, Department of Forest Utilisation, Freiburg, Germany, udo.sauter@forst.bwl.de

Kay-Uwe Schober
Hochschule Mainz, University of Applied Sciences, Mainz, Germany, kay-uwe.schober@hs-mainz.de

Beate Hörnel-Metzger
Hochschule Mainz, University of Applied Sciences, Mainz, Germany, beate.hoernel-metzger @hs-mainz.de

* Corresponding author

Abstract

In Germany, only half of the annual increment is used in oak stands. Especially small-diameter oaks are currently either not used or only used as firewood. In order to achieve long-term carbon dioxide storage and higher added value, our research project aims on making small-diameter oak logs available as structural timber members, e. g. for columns, frameworks and agricultural buildings, like barns. For this purpose, the mechanical properties of the logs and factors influencing them have to be determined.

In the experimental program, static MOE/MOR (bending tests), dynamic MOE (Viscan), density/moisture content (CT-scanning, wood samples), internal and external wood defects (CT-scanning, visual quality grading) and geometry properties (DiShape) of 70 oak (*Quercus petraea* (Matt.) Liebl.) logs with a length of 5 m and an average mid diameter of about 25 cm have been investigated and statistically analyzed.

First results show that moisture content and wood density in fresh and dry condition are within the range found for oak in the literature. Most logs were graded in quality class C, which represents intermediate quality logs characterized by a larger number of medium sized to large knots, presence of curvature and other features. MOR varied between 27 MPa and 135 MPa, while the static MOE ranged from 4600 MPa to 30000 MPa (median 9683 MPa) and the dynamic MOE from 5480 to 15907 MPa (median 11941 MPa). Mean dynamic MOE was about 18 % higher than mean static MOE, which is in accordance to other studies comparing non-destructive and destructive methodologies for mechanical characterisation of timber.

These preliminary results indicate that small-diameter oak logs appear suitable for load-bearing structures. The results will be further discussed to develop strength grading procedures supported by machine testing for such irregular shaped small-diameter logs, which should to be used as structural elements.

Keywords: CT scanning, bending tests, structural timber, *Quercus petraea*

Acknowledgement: This project (support code 2218WK18C3) was funded by the Federal Ministry of Food and Agriculture (BMEL) through the Agency for Renewable Resources (FNR).

Distribution of Wetwood in Silver Fir (*Abies Alba* MILL.)—A Prerequisite for NDT Mechanical Characterization of Logs

Franka Brüchert*
Forest Research Institute Baden-Württemberg, Department of Forest Utilisation, Freiburg, Germany, franka.bruechert@forst.bwl.de

Guénaël Klotzbücher
Forest Research Institute Baden-Württemberg, Department of Forest Utilisation, Freiburg, Germany

Martin Huber
Forest Research Institute Baden-Württemberg, Department of Forest Utilisation, Freiburg, Germany, martin.huber@forst.bwl.de com

Udo H. Sauter
Forest Research Institute Baden-Württemberg, Department of Forest Utilisation, Freiburg, Germany, udo.sauter@forst.bwl.de

* Corresponding author

Abstract

Wetwood are confined zones with an extremely higher moisture content (MC) than the surrounding stem wood. Such wood abnormalities are a well-known feature in stem wood of the genus *Abies* and can usually be found in the heartwood core of older trees. Its water content strongly exceeds that of the adjacent normal wood and MC can be found to be even higher than that of water-saturated sapwood. Presence of wetwood in logs can cause severe problems in wood processing. Not only is timber drying quality strong-ly affected, but the deviation of MC can also lead to heavy distortions of the boards. As density and mechanical properties of timber vary with the moisture content, the presence of wetwood also interferes with those basics of non-destructive testing which are based on these material characteristics. Yet, the formation of wetwood is still not fully understood in detail. The size and distribution patterns of wetwood in the stem and logs vary to a large extent.

High resolution x-ray based computed tomography (CT) was found to be suitable for detection and analysis of the moisture distribution in trees and logs.

Logs of silver fir (4-5m length, mid diameter from 39 to 83cm) were CT scanned at 180kV and 14mA and images reconstructed to app. 1x1x5mm voxel resolution. With a new, automated algorithm, which is capable to cope with the irregular distribution of high moisture pockets, the shape and location of the wetwood zones were detected and the volumetric fraction per slice was calculated. The analysis of the logs and their CT scans showed the potential of CT scanning for the further optimisation of wood processing based on the overall wetwood level (up to 30 % volumetric fraction), and on the location as well as the identified 3D distribution patterns of wetwood within the logs.

Keywords: x-ray, CT, wetwood, *Abies alba*

Acknowledgement: This project (project number 22040418) was funded by the Federal Ministry of Food and Agriculture (BMEL) through the Agency for Renewable Resources (FNR e.V.).

Using X-ray Computed Tomography (CT) Scanning to Optimize Log Primary Breakdown in Plantation-Grown White Spruce (*Picea glauca* (Moench) Voss)

Isabelle Duchesne
Canadian Wood Fibre Centre, Canadian Forest Service, Natural Resources Canada, Quebec, Canada, isabelle.duchesne@nrcan-rncan.gc.ca

Queju Tong
Richmond, British Columbia, Canada, tessie.tong@gmail.com

Patrick Lenz
Canadian Wood Fibre Centre, Canadian Forest Service, Natural Resources Canada, Quebec, Canada, patrick.lenz@nrcan-rncan.gc.ca

Abstract

This study examined the effects of incorporating internal knot characteristics into log breakdown decision-making on lumber value for white spruce. Knot characteristic information was extracted from sawlogs using X-Ray computed tomography (CT) imaging to examine the impact of site, genetic provenance and sawing optimization strategy on lumber product recovery. Of the 79 trees sampled for this study, 48 came from two mature genetic trials (Baskatong, Quebec; Petawawa, Ontario), while 31 trees originated from a younger Nelder spacing trial (Woodstock, New Brunswick). The log and stem reconstructions were done using a knot-detection algorithm within the Optitek sawing simulator that applied three optimization strategies: sweep up (traditional), shape optimized, and knot optimized. The results indicated that the knot-optimized strategy consistently generated the highest value recovery, while the sweep-up strategy generated the lowest. The increase in lumber value recovery from sweep up to knot optimized was the highest in the Nelder plantation that had the smallest trees. Increase in lumber value was lowest amongst the largest trees in this study, suggesting that the knot-optimized strategy may provide more benefit for smaller trees than for larger trees. Overall, the results demonstrated that knot-optimized sawing strategies can help to extract more value from every tree, which presents an opportunity for the forest industry to augment its competitiveness in the face of reduced fibre supply.

Keywords: CT scanning, knots, sawing optimization, lumber value recovery

Introduction

Anticipating reduced timber availability due to natural and climate-related disturbances, forest professionals urgently need to optimize processes to extract maximum value from every tree harvested. In Canadian sawmills, the current sawing optimization applied to maximize lumber recovery only considers external characteristics of logs (Belley et al. 2019); however, knots are one of the major defects affecting lumber structural performance and value (Longuetaud et al. 2012). Recent studies have shown strong potential benefits (i.e., total product value increase of up to 24%) in using CT technology combined with optimal log rotation (Rinnhofer et al. 2003; Stängle et al. 2015; Rais et al. 2017). This study examines lumber value recovery potentials in plantation-grown trees in different locations in Eastern Canada.

Material and methods

Tree selection

Three white spruce plantations were analyzed in this study (Table 1). The first two plantations (Baskatong and Petawawa) were mature (age 55-56) whereas the third one was pre-mature (age 32) with small-diameter trees. Each provenance trial included four common seed sources that represented the eastern Canadian geographic range of the species. Seed sources had been collected in populations from Thunder Bay (west, Ontario), Chalk River (south, Ontario), Lac Baskatong (north, Quebec) and from Price (east, Quebec), and were planted in square plots according to a complete randomized bloc design. Initial spacing among trees was 1.8 m. The Nelder spacing trial had been established with standard reforestation seedlings provided by the province of New Brunswick. According to the Nelder design, initial spacing among trees varied from 0.9 m to 4 m.

Table 1— Descriptive statistics of the 79 trees selected for this study. Standard deviations are shown in italics. Average values followed by the same letter in the same column are not significantly different at 0.05 significance level.

Trial	Site	DBH [1]	Tree height	Stem taper	Stem sweep	Merchant. length	Merchant. volume
	(nb of trees)	(cm)	(m)	(cm/m)	(cm/m)	(m)	(dm^3)
Provenance	Baskatong, QC	18.2 ^{B}	16.4 ^{B}	1.1 ^{A}	0.3 ^{B}	10.1 ^{B}	186 ^{B}
Tree age: 55	(n=24)	*2.81*	*1.58*	*0.24*	*0.23*	*2.03*	*76.0*
Provenance	Petawawa, ON	22.4 ^{A}	18.8 ^{A}	1.1 ^{A}	0.3 ^{B}	13.5 ^{A}	363 ^{A}
Tree age: 56	(n=24)	*2.96*	*2.04*	*0.17*	*0.09*	*2.82*	*143.7*
Nelder Spacing	Woodstock, NB	16.2 ^{B}	12.6 ^{C}	1.3 ^{A}	0.5 ^{A}	6.9 ^{C}	115 ^{C}
Tree age: 32	(n=31)	*4.42*	*1.62*	*0.40*	*0.26*	*2.52*	*75.9*

[1]DBH: Diameter at breast height.

CT Scan, knot extraction and sawing simulations in Optitek

After harvest, trees were delimbed and cut into 2.5m long logs. The logs were then CT scanned with X-ray computed tomography (CT) in a Siemens Somatom Sensation 64 medical scanner (Siemens Medical Solutions USA, Inc.) located at the Institut national de la recherche scientifique in Quebec City (Canada). CT images were recorded at every millimetre along the logs with a 2 mm CT image thickness such that there was 1 mm-thick overlap between two consecutive images that ensured maximum knot detection from one image to the following one. All CT images obtained from the scanned logs were then fed into an image-processing tool CT2Opti (Vallerand et al. 2011) for external shape extraction, knot detection, and full-stem reconstruction (i.e., reconnecting consecutive sawlogs within each tree). Sawing simulations were performed on Optitek version 10, a sawing simulation software package developed by FPInnovations. In Optitek, optimization processes are performed to “saw” a set of input logs in a pre-built “sawmill” into a user-defined product list. A set of grading rules separates lumber into pre-defined grades based on lumber dimension and location of defects, according NLGA rules (National Lumber Grades Authority, NLGA 2017).

Optimization strategies

Three sawing optimization strategies were tested in this study: sweep up, shape optimized, and knot optimized, as described in Belley et al. 2019. With the first two strategies, Optitek generated the best solution based on the external shape of the stems only, while with the third strategy, it generated the best solution based on both the external shape and internal knottiness of the stems. Thus, the knot optimized strategy offered the highest level of optimization, taking both external stem shape and internal knot characteristics into consideration during optimization process.

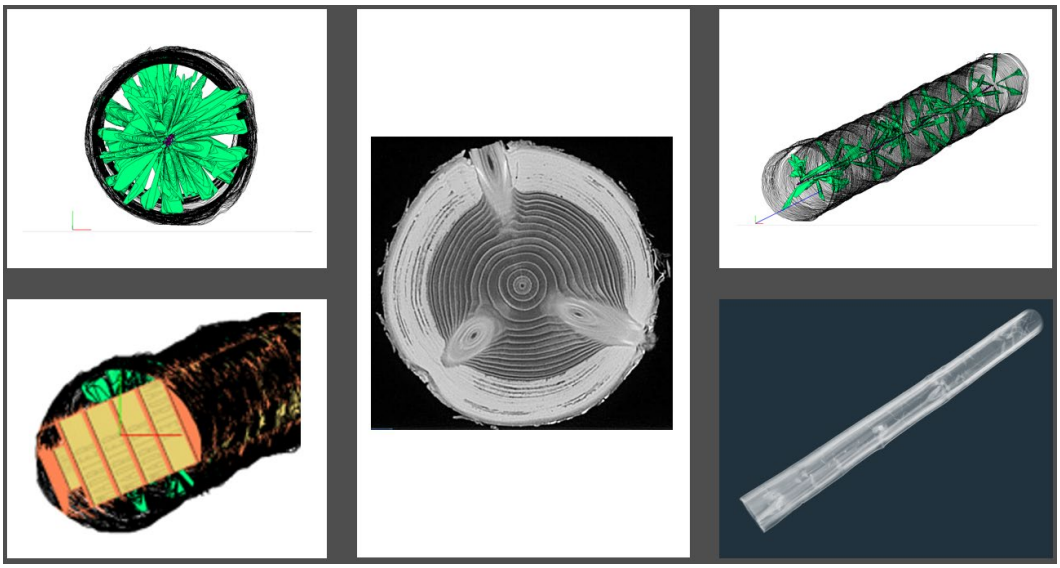

Figure 1— Diagram outlining data collection process. Logs were X-ray CT scanned and knots were extracted from the CT images using the CT2Opti software. The Optitek sawing simulation software simulated the optimal log sawing pattern that maximized lumber value considering the distribution of internal knots.

Results and discussion

Results from the 2-way analysis of deviance indicated the significant effects of stem size (as represented by 3 sites: Baskatong, Petawawa, and Woodstock) and optimization strategy (Table 2). No significant interaction effect was detected neither an influence of the seed source (i.e. provenance, results not shown). GLHT multiple comparisons revealed that among the 3 sites, Woodstock had the lowest total lumber value recovery per unit stem volume ($81.10/m^3) as compared to Baskatong ($92.27/m^3) and Petawawa ($102.60/m^3); and among the 3 optimization strategies, knot optimized had a higher total value recovery ($100.18/m^3) than shape optimized ($91.89/m^3), which in turn was higher than sweep up ($85.18/m^3).

Table 2—Two-way analysis of deviance table and general linear hypothesis (multiple comparisons) testing the effect of stem size (represented by 3 sites: Baskatong, Petawawa, and Woodstock) and sawing optimization strategies (sweep up, shape optimized, knot optimized) on the total lumber value per unit stem volume ($/m^3). Tested as linear mixed effect model with Type III Wald Chi-square Test, $P < 0.05$. LSMeans values followed by the same letter for the same source are not significantly different at 0.05 significance level.

Source	Analysis of deviance			GLHT Multiple comparison		
	Chi-square	DF	Pr > Chisq	Level	LSMeans	
Site	55.66	2	< 0.0001	Baskatong	92.27	B
				Petawawa	102.60	A
				Woodstock	81.10	C
Optimization	183.84	2	< 0.0001	Knot	100.18	A
				Shape	91.89	B
				Sweep up	85.18	C

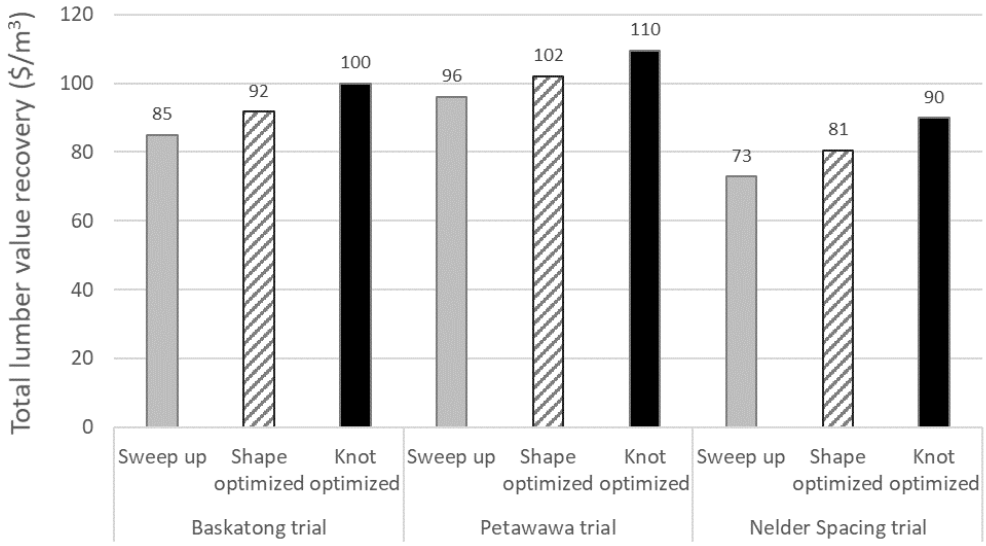

Figure 2— Total lumber value recovery per unit stem volume ($/m^3) from the three trials (Baskatong and Petawawa provenance trials and Nelder spacing trial in Woodstock) for the three levels of optimization (sweep up, shape optimized, and knot optimized).

When breaking down lumber value recoveries from the 3 strategies for each site, the increase in lumber value recovery from sweep up to knot optimized was 23.5% in Woodstock, 17.7% in Baskatong, and 14.1% in Petawawa (Figure 2). The increase from shape optimized to knot optimized was 11.6% in Woodstock, 9.0% in Baskatong and 7.4% in Petawawa. This result suggests that smaller stems have a higher potential benefit from employing knot-optimized strategy than larger stems. In the current context, where forest management practices aim to increase plantation productivity and reduce rotation age, which both increases the proportion of juvenile wood in the stem, it will be increasingly important to use advanced CT scan technology to optimize not only lumber value recovery, but also the mechanical properties of each piece of lumber produced.

Conclusions

Using CT scanning technology to determine internal knot distribution offers good opportunities to maximize forest resource utilization. The substantial gains obtained when simultaneously considering external and internal log attributes before sawing, provide baseline information for further research and development and potential investments. By increasing the maximum extraction value from every tree, the forest sector will contribute to a sustainable, value-added transformation of the resource, and be able to remain competitive in the global market in the face of reduced national fibre supply.

Acknowledgments

This research was funded by the Canadian Wood Fibre Centre of Natural Resources Canada through the Fibre Solutions Research Program. The authors thank Denis Belley for sharing datasets of CT scanned logs from the Nelder spacing trial, and Steve Vallerand and Mohammed Khachan (FPInnovations) for their invaluable help with CT2Opti and Optitek.

References

Belley D.; Duchesne, I.; Vallerand, S.; Barrette, J.; Beaudoin, M. 2019. Computed tomography (CT) scanning of internal log attributes prior to sawing increases lumber value in white spruce (*Picea glauca*) and jack pine (*Pinus banksiana*). Can. J. For. Res. 49: 1516-1524.

Longuetaud, F.; Mothe, F.; Kerautret, B.; Krähenbühl, A.; Hory, L.; Leban, J.-M.; Debled-Rennesson, I. 2012. Automatic knot detection and measurements from X-ray CT images of wood: a review and validation of an improved algorithm on softwood samples. Comput. Electron. Agric. 85: 77–89. doi:10.1016/j.compag.2012.03.013.

NLGA 2017. Standard grading rules for Canadian lumber. National Lumber Grades Authority, Vancouver, BC, Canada.

Rais, A.; Ursella, E.; Vicario, E.; Guidiceandrea, F. 2017. The use of the first industrial X-ray CT scanner increases the lumber recovery value: case study on visually strength-graded Douglas-fir timber. Ann. For. Sci. 74: 28. https://doi.org/10.1007/s13595-017-0630-5.

Rinnhofer, A.; Petutschnigg, A.; Andreu, J.-P. 2003. Internal log scanning for optimizing breakdown. Comput. Electron. Agric. 41: 7–21. doi:10.1016/S0168-1699(03)00039-5.

Stängle, S.M.; Brüchert, F.; Heikkila, A.; Usenius, T.; Usenius; A.; Sauter, U.H. 2015. Potentially increased sawmill yield from hardwoods using X-ray computed tomography for knot detection. Ann. For. Sci. 72: 57–65. doi:10.1007/s13595-014-0385-1.

User's Manuel, Optitek 10. FPInnovations, Pointe-Claire, QC, Canada.

Vallerand, S.; Belley, D.; Duchesne, I.; Beaudoin, M.; Swift, E. 2011. Utilisation d'images CT pour la modélisation 3D de billes réelles avec caractéristiques internes. Note de recherche no 2 ForêtValeur/ForValueNet, Université Laval, Québec, QC, Canada.

Nondestructive Testing of Timber Prior to Sawing Using Finite Element Models Based on X-Ray Computed Tomography Data—A Preliminary Study

Johannes A. J. Huber*
Wood Science and Engineering, Luleå University of Technology, Skellefteå, Sweden, johannes.huber@ltu.se

Olof Broman
Wood Science and Engineering, Luleå University of Technology, Skellefteå, Sweden, olof.broman@ltu.se

Johan Oja
Wood Science and Engineering, Luleå University of Technology, Skellefteå, Sweden, johan.oja@ltu.se

Lars Hansson
Department of Ocean Operations and Civil Engineering, Norwegian University of Science and Technology, Ålesund, Norway, laha@ntnu.no

Mats Ekevad
Wood Science and Engineering, Luleå University of Technology, Skellefteå, Sweden, mats.ekevad@ltu.se

* Corresponding author

Abstract

X-ray computed tomography (CT) of wood delivers internal density data of a scanned object, from which, depending on the resolution, internal features such as the pith, annual rings, and knots can be identified. Some sawmills use CT scanners in front of the saw line to determine optimal positioning of the log in the saw, to maximise the value yield of the sawn products. We envision that the gathered CT data also could be used for mechanical evaluations of the timber using numerical models of boards prior to sawing. In a recent study by the authors, a method was developed to create 3D and 1D finite element (FE) models based on CT scans of dried sawn timber, which could predict bending stiffness and strength in bending simulations with high accuracy. The objective of the present study is to explore how the method can be adapted to CT scans of logs before sawing. Our preliminary study was based on CT data of green Norway Spruce logs and the corresponding scans of dried sawn timber. The stiffness and strength were evaluated using four-point bending tests. Additionally, the resonance frequency of the logs was recorded. The corresponding volume of each piece of sawn timber was extracted from the log data, and an FE model was created. The model accounted for the pith, the annual rings, the knots, and the local fibre deviations around knots. Various laws for local stiffness and different failure criteria were tested. The study showed how FE models of virtual pieces of sawn timber can be created from CT data and what obstacles need to be overcome for further development of the presented method. The results indicated that more detailed evaluations of the relationship between local stiffness and density may be required, specifically for knots and for wood in green state.

Keywords: strength prediction, virtual grading, numerical modelling, sawmill optimisation

Evaluation of Sawmill Log Scanners Compared with Forest Harvester Measurements

Kari Hyll *
Skogforsk, the Forestry Research Institute of Sweden, Uppsala Science Park, 751 83, Uppsala, Sweden.
kari.hyll@skogforsk.se

Maria Nordström
Skogforsk, the Forestry Research Institute of Sweden, Uppsala Science Park, 751 83, Uppsala, Sweden.
maria.nordstrom@skogforsk.se

* Corresponding author

Abstract

A set of log scanners at Swedish sawmills were evaluated with regard to the random uncertainty when measuring top diameter and length of sawlogs during operational log scaling. The influence of some technical and environmental factors at the measurement sites was also investigated. The log scanner measurements were benchmarked against manual measurements by quality controllers. The variability in the difference between the log scanner and the quality-control measurement was used to evaluate the scanners. The results were compared to top diameter and length measurements performed by quality-controlled harvesters. The 3D X-ray scanner in the study had significantly lower variability than the other log scanner types. The length variability was less among different models than top diameter measurement. In general, 1D optical scanners had higher variability than 3D optical scanners, but performance could be similar given the right conditions. The harvesters' variability in top diameter and length measurement was generally equal to or less than that of the log scanners. However, the log scanner with the very lowest variability outperformed all the harvesters in top diameter measurement.

Keywords: Log scanner, log scaling, diameter, length, harvester, X-ray, optical, sawlogs, measurement uncertainty

Introduction

Swedish log scaling

Log scaling is the process of measuring and estimating the quantity and quality of timber. Measurements can be made for process control or as a basis for payment. Most log scaling in Sweden is performed by the third-party organization Biometria, which is jointly financed by the forest industry. Biometria also performs quality control and audits of their own and other parties' measurements. In Sweden, the majority of timber comprises spruce (*Picea abies*) and pine (*Pinus sylvestris*), and is traded by either top cylinder volume under bark or solid volume under bark. This volume is calculated from a diameter or combination of diameters, from which the bark thickness is deducted, and the length of the log (SDC 2017). Log scaling at the sawmill as the basis of payment is referred to as the ordinary measurement. The process is typically semi-automated, where the diameter, length, and in some cases additional parameters, are measured by an automated log scanner, while the tree species and quality class are assessed by a human log scaler (Table 1). In Sweden, only type-approved measurement equipment may be used to provide data that forms the basis of payment (VMK 2019).

Table 1 - Measurement of sawlog parameters used for payment in Swedish log scaling, and the technical requirements (Björklund and Edlund 2013, SDC 2018, Biometria 2019, VMK 2019).

Log parameter	Method
Diameter under bark (mm)	Fully automated with 3D optical or X-ray log scanner, or any type of log scanner in combination with manual bark estimation
Length (cm)	Conveyer, log scanner, data handling system
Sweep (cm)	Manual estimation or 3D log scanner
Metal occurrence	Metal detector or X-ray log scanner
Quality class	Manual estimation or automatic measurement by 3D X-ray or 3D optical + 1-2D X-ray log scanner
Tree species	Manual estimation
All other parameters	Manual estimation

For quality control and audit, also called the control measurement, the standard way of measuring diameter is by caliper and length by measurement tape. Since diameter is measured on bark, a value under bark is achieved by measuring and deducting the bark thickness. Two alternative approaches are used to measure bark thickness: 1) a bark thickness probe, or 2) removing the bark from the log with an axe at the point of measurement. The diameter is measured in two orthogonal directions, and the average of the two figures is used (SDC 2017).

Log scanners

Log scanners are designed to measure single logs before sawing, using optical light or X-ray radiation, or a combination of both. Dependent on the number of measurement directions, different shape parameters can be inferred. Sawmills are calling for new methods to measure additional log parameters, thereby increasing the degree of automation, seeing advantages such as higher objectivity and 24/7 capacity. One early example of automation was under-bark diameter measurement, instead of manual estimation of bark thickness. However, some models (mainly 1D optical) cannot perform automated under-bark measurement. Manual bark thickness estimation is also preferred over automated measurement for parts of the year, especially when logs are affected by snow and ice. Many factors influence the uncertainty of a log scanner measurement, such as air temperature and conveyer speed and technical status. For most log scanners, length is measured opto-mechanically through photocells connected to the conveyer belt. Consequently, the length measurement is less dependent on the log scanner and more dependent on the mechanical status of the conveyer.

According to an inventory of 165 sawmills in Sweden, 124 had a log scanner that provided data for payment (Biometria, 2019). Most of the sawmills without log scanners processed relatively low volumes. Studies have shown that sawmills with the most advanced log scanners also tend to be among those that produce the highest volumes of lumber (Edlund 2009, Strömgren 2015).

Harvester measurements

Timber in Sweden is harvested using the cut-to-length system, meaning that the stem is cut into logs of specific dimensions tailored to customer needs. The length and diameter of each log is measured by mechanical gauges in the harvester head. The diameter is measured on bark and converted to an under-bark value using a bark function, which calculates the double bark thickness to be subtracted from the diameter measured on bark. The length and diameter are then combined to produce a fixed volume under bark. The operator estimates and registers tree species for each stem. Many harvesters are quality controlled through a third-party inspection, performed by Biometria, whose quality technicians then continuously monitor the harvester's measurement by comparing submitted files with control measurements (Biometria 2019).

Motivation of the study

Timber is the most valuable forest product in Sweden. As log scanners are used both for sorting the timber before sawing and to provide basis for payment, assessing and improving their measurement is highly relevant. However, few studies have examined the performance of log scanner measurements (Strömgren 2016). Logs are measured at the time of harvest, which provides an alternate point in the value chain for regulating the agreement between seller and buyer. Consequently, there is strong motivation for comparing log scanner and harvester measurements.

Materials and methods

Materials

The material comprised sawmill log scanner and harvester control measurements and corresponding ordinary measurements, and sawmill metadata such as log scanner age.

Sawmills

Nineteen sawmills participated in the study, together representing a wide variety in log scanner manufacturer and model. Some consideration was also given to geographical spread (Figure 1) and tree species (Table 2).

Sawmill study period and number of data points

The target study period for the log scanner measurements was July 1, 2019, to June 30, 2020. Four sawmills changed log scanner during the study period, reducing the number of control logs representing those scanners. In those cases, the study period was extended about half a year backward and forward in time, and both the old and the new scanners were included in the study. On average, the sawmills had 849 control logs during the study period. The sawmill with the fewest control logs, 354, changed log scanner during the period. The sawmill with the most sawlogs had 1625. A minimum number of control logs is required, while the variation above that reflects different needs for quality control and feedback to log scalers at different sites.

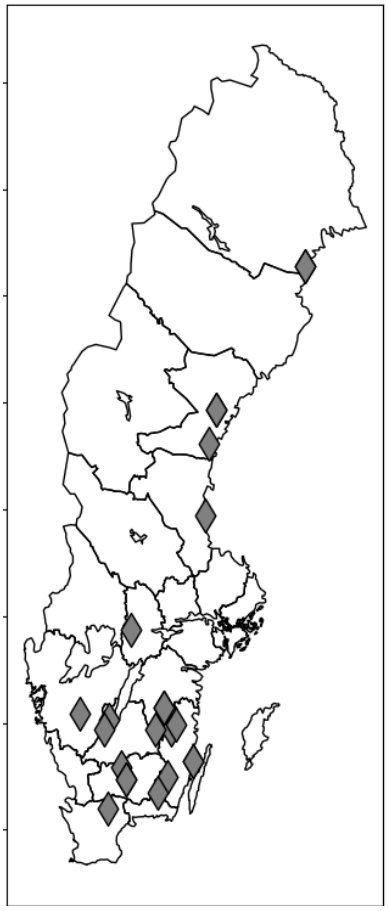

Figure 1 - Geographical location (gray diamonds) of the 19 sawmills in the study

Log scanners

As four of the sawmills changed scanner during the study period, the total number of scanners in the study was 23. Their characteristics are summarized in Table 2. The sample included models from all major manufacturers active on the Swedish market at the time of the study. It would have been desirable to have additional scanners of the Fusion 3GX and CT-Log models, but only a few scanners of those models were installed at Swedish sawmills at the time of the study.

Table 2 - Model, manufacturer, and measurement principle of the log scanners in the study. Note that the same mill can process both spruce and pine, thereby contributing to log scanner numbers for both species. *Rema and Sawco merged to become RemaSawco.

Model	Manufacturer	Principle	# Scanners	# measures spruce | pine
Elinova	Andor	1D optical	4	3 | 3
Rema 900X	Rema	1-2D optical	3	2 | 1
Proscan	Sawco*	3D optical	1	1 | 1
LogBark	Rema*	3D optical	4	3 | 3
RS-3D LogScanner	RemaSawco	3D optical	4	4 | 2
LogEye	Microtec	3D optical + 2D X-ray	3	1 | 2
RS-LogProfiler	RemaSawco	3D optical + 2D X-ray	2	2 | 2
Fusion 3GX	Finnos	3D optical + 2D X-ray	1	0 | 1
CT-Log	Microtec	3D X-ray	1	0 | 1

The analyzed parameters comprised top diameter under bark and length. It should be noted that only the CT-Log uses log scanner (non-contact) data to measure length (Franscesco Fontanini, Microtec, personal communication 2021). As opto-mechanical length measurement is used for the other models, the correlation between log scanner model/type and the uncertainty of the length measurement is expected to be weaker. However, there is a potential correlation between log scanner age and conveyer status/health, which in turn is expected to influence the length uncertainty. The ages of the log scanners ranged from 0 to 38 years, but some may have been upgraded during that time. In this study, scanner age was strongly correlated with scanner type, see Figure 2.

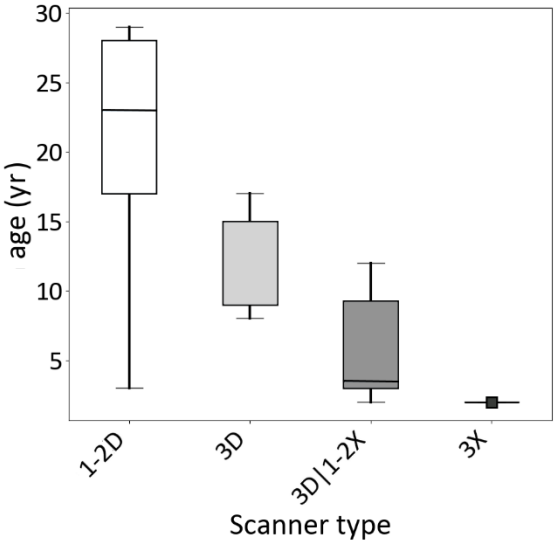

Figure 2 - Ages of the log scanners in the study. The vertical line is the median value. 1-2D stands for 1D/2D optical scanner, 3D stands for 3D optical scanner, 3D2X stands for 3D optical scanner with 1D/2D X-ray and 3X stands for 3D X-ray scanner. The 3X has no variability as it comprises only one scanner.

Harvesters

The harvester data comprised 31 quality-controlled harvesters operating in southern Sweden during 2020. Data from harvesters with fewer than ten control-measured logs was not used in the analysis. The average number of control-measured logs per harvester was 28, though four harvesters had only 10-15 control logs.

Methods for handling log scanner data

Filtering and outlier removals

If the number of control logs for a certain sawmill was less than 30 for a tree species, all control logs of that tree species were removed from the data. Thirty-one logs had their control measurement top diameter recorded as zero, so they were removed, and 21 logs had no registered bark type and were also removed. Outliers may be caused by logs that end up parallel with each other on the conveyer, thereby overlapping in width and/or length. If these logs are not removed, they may disproportionally influence the variability. Based on procedures used by Biometria, outliers in length and top diameter were defined as follows, and subsequently removed.

- Length outlier: abs(Ordinary length – Control length) > 10 cm
- Top diameter outlier: abs(Ordinary top diameter – Control top diameter) > 30 mm

where abs(…) stands for the absolute value. In addition, one single, very thick log (top diameter 600 mm, length 383 cm, gross volume 1247 liters) was removed, as it was a significant outlier in the gross volume. In total, 84 log scanner outliers were removed, an average of five per sawmill.

Calculation of variability

The evaluation of the ordinary measurement is based on the deviation between the control measurement and the ordinary measurement, referred to here as the *control difference*, CD:

CD = (Ordinary measurement – Control measurement) (1)

The mean of CD (the systematic uncertainty or bias) mainly reflects the calibration of the log scanner, rather than the scanner itself, and is not part of the analysis in the study. Instead, the analysis is based on the variability in CD (the contribution of random effects to uncertainty). The variability was calculated as a 1σ standard deviation, so 68% of the outcomes are expected to have a value within this deviation from the average.

Methods for handling harvester data

The data was filtered for outliers in the same way as for the log scanner data. Out of the section-measured diameters, only the top diameter value was used. Logs with top diameter of less than 130 mm were removed to enable a focus on timber dimensions.

To facilitate a comparison between the harvester-measured top diameter (on bark, ob) and that of a log scanner (under bark, ub), the standard deviation under bark was estimated for the harvester. This was done by adding an uncertainty for the bark thickness calculation using Skogforsk's bark functions. The standard deviation σ_{bark} between measured and calculated double bark thickness in the top end of the log was taken from Hannrup & Lundgren (2012) (Table 3).

Table 3 - Left: The variability σ_{bark} from the double bark thickness used to convert from diameter over bark to diameter under bark in harvester measurements. Right: Formula of the variability of the harvester's top diameter measurement.

Spruce	Pine
2.2 mm	2.5 mm

$$\sigma_{harvester,ub} = \sqrt{\sigma^2_{harvester,ob} + \sigma^2_{bark}} \quad (2)$$

Results and discussion

Results

Top diameter

In this section, top diameter always refers to top diameter under bark. The variability in the control difference of the top diameter of spruce and pine is shown in Figure 3.

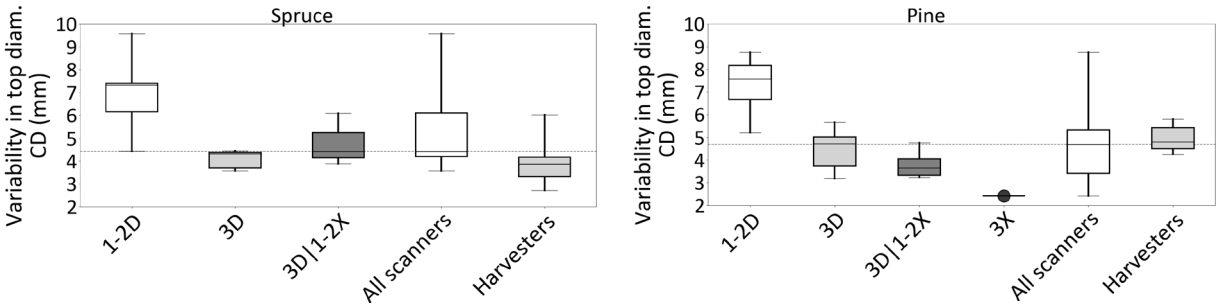

Figure 3 - The variability in the control difference (CD) of the top diameter (mm) of spruce (left) and pine (right) logs. The boxes comprise the 25th-75th percentile of data, while the whiskers comprise the full range of the data. The vertical line is the median value of all the log scanners. 1-2D stands for 1D/2D optical scanner, 3D stands for 3D optical scanner, 3D2X stands for 3D optical scanner with 1D/2D X-ray and 3X stands for 3D X-ray scanner. The 3X has no variability as it comprises only one scanner and is instead highlighted with a circle. Note that there are currently no 3D X-ray scanners installed in spruce sawmills in Sweden.

In general, newer log scanner types (Figure 2) have lower variability in control difference than older types. The harvester variability is similar to, and sometimes lower than, that of the log scanners. However 1-2D optical scanners can perform as well as the other log scanners given the right conditions, which highlights how technical and environmental factors contribute to the variability. Where the harvester variability is highest, it is still lower than the scanners with highest variability. For log scanners, the average top diameter measurements show no significant difference between spruce and pine. For the harvesters, spruce measurement has lower variability than pine measurement. Statistics independent of tree species and scanner type are shown in Table 4.

Table 4 – Statistics of the variability in control difference for top diameter (mm) for all control logs (independent of tree species) computed over the whole study period for each log scanner and harvester in the study.

Top diameter	Min (mm)	Median (mm)	Mean (mm)	Max (mm)
Log scanners	2.4	4.4	5.0	9.6
Harvesters	2.7	4.1	4.1	6.0

Length

The variability for the length measurement of spruce and pine is shown in Figure 4.

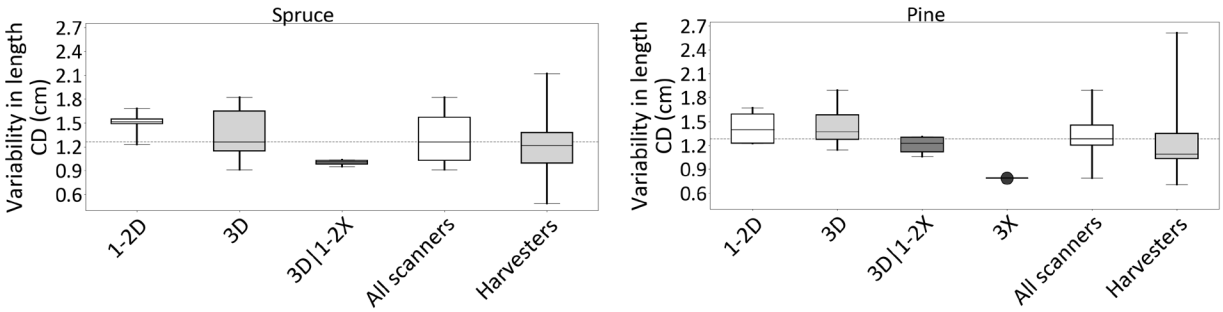

Figure 4 - The variability in the control difference (CD) of the length (cm) of spruce (left) and pine (right) logs, respectively. The boxes comprise the 25th-75th percentile of data, while the whiskers comprise the full range of the data. The vertical line is the median value of all the log scanners. 1D-2D stands for 1D/2D optical scanner, 3D stands for 3D optical scanner, 3D2X stands for 3D optical scanner with 1D/2D X-ray and 3X stands for 3D X-ray scanner. The 3X has no variability as it comprises only one scanner and is instead highlighted with a circle. Note that there are currently no 3D X-ray scanners installed in spruce sawmills in Sweden.

The length variability has a smaller range than top diameter variability, likely due to greater similarities between the measurement principles. The exception is the 3D X-ray log scanner, which shows

significantly lower variability compared to the other scanner types. On average, neither log scanners nor harvesters show a significant difference between spruce and pine average length measurements. However, the variability within the harvester group (the distance between the whiskers) is greater than the variability within the log scanner group, especially for pine. Statistics independent of tree species and scanner type are shown in Table 5.

Table 5 – Statistics of the variability in control difference for length (cm) for all control logs (independent of tree species) computed over the whole study period for each log scanner and harvester in the study.

Length	Min (cm)	Median (cm)	Mean (cm)	Max (cm)
Log scanners	0.8	1.3	1.3	1.8
Harvesters	0.5	1.2	1.2	2.6

Discussion

The datasets of this study have limitations. Some scanner types and models are only present in single examples, preventing the study of variability within that group. A certain amount of the variability in the log scanner result derives from the control measurement method (caliper handling, axe debarking, visual estimation, etc.), rather than from the ordinary measurement. For log length, this number is around 0.1 cm (Strömgren 2017b), corresponding to 8% of the mean variability. Ideally, this contribution should be subtracted. Because no corresponding value was available for top diameter, that operation was not performed. Finally, the study could not separate the technical and environmental factors of the measurement site from log scanner factors. This is both a weakness and a strength, as the dataset reflects actual production conditions.

Previous studies from Biometria reported that the mean variability in control difference of log scanners at Swedish sawmills was 5.7 mm for top diameter and 1.5 cm for length (Strömgren 2016, Strömgren 2017), higher figures than shown in this study. Those studies incorporated more log scanners, and it is possible that the log scanner sample in the present study has a technical status above the average. Since 2016, some old scanners have been replaced, which could also explain the reduced variability in the present study.

For the harvester data, the number of control logs is relatively low, resulting in more uncertain statistics. Additionally, only the top diameter was evaluated, and not the range of sectional diameter measurements that are usually averaged when the harvester measured volume is calculated. However, the results from this study correspond well to experience from dedicated harvester evaluations. Harvester variability is often similar to, or lower than that of log scanners, which opens up the possibility of using harvester measurements as a quality check on log scanner measurements, given that logs can be traced in sufficient detail from harvest to arrival at the mill.

It would have been interesting to study additional parameters that are automatically measured as a basis for payment (Table 1). However, those parameters are not recorded in sufficient detail in control log data. It would also have been interesting to study the influence of conveyer belt speed and log ovality on the variability in top diameter. However, that would have required saved historical data, which was not the case for the present study but could be planned for future studies.

Conclusion

Sawlog dimension measurements at two different points in the value chain, during harvest and at the sawmill, have been evaluated. For top diameter measurement, there is a large spread in the variability between different log scanner models and types, where newer types have lower variability. For measurement of length, the corresponding spread in variability is lower, as the technical principle for length measurement is similar for most models. The X-ray-based length measurement of the study's 3D X-ray scanner is an exception, which also shows a significantly lower variability of the length

measurement compared to other scanner types. Harvester measurement of log top diameter and length is comparable to, and sometimes better than, that of sawmill log scanners. The exception is the 3D X-ray log scanner, which had significantly lower variability than the harvesters.

Acknowledgments

The authors wish to thank the Södra Research Foundation for their financial contribution to this project. We also want to thank the staff at Biometria for their support with data and the analysis project, as well as the members of the reference group.

References

Biometria. 2019. Instruktion för kvalitetssäkring av längd- och diametermätning med skördare [Instruction for quality assurance of length and diameter meaurement in harvesters]. 1-15 p.

Biometria. 2019. Tillämpningsanvisning till Mätningsinstruktion för kvalitetsbestämning av sågtimmer av tall och gran [Guide to the application of the Measurement instruction for grading of pine and spruce sawlogs]. 1-28 p.

Björklund, L. and J. Edlund. 2013. Metodbeskrivning Semiautomatisk kvalitetsklassning av tallsågtimmer enligt VMR 1-07 [Method description for Semi-automatic grading of pine sawlogs according to VMR-1-07]. SDC. 17 p.

Edlund, J. 2009. Mätramar för sortering och vederlagsmätning vid sågverken 2008 [Log scanners for sorting, scaling and grading at Swedish sawmills 2008]. VMK. 1-3 p.

SDC. 2017. Mätning av stocks volym under bark [Measurement of log volume under bark]. 1-19 p.

SDC. 2018. Kvalitetsbestämning av sågtimmer av tall och gran [Grading of spruce and pine sawlogs]. SDC. 1-10 p.

Strömgren, M. 2015. Mätramar för sortering och ersättningsgrundande mätning vid svenska sågverk 2015 [Log scanners for sorting and payment-related measurement at Swedish sawmills 2015]. 1-6 p.

Strömgren, M. 2016. Mätosäkerheter vid mätning av sågtimmer [Sawlog measurement uncertainty]. SDC. 1-21 p.

Strömgren, M. 2017. Noggrannare längdmätning av sågtimmer [Improved uncertainty for sawlog length measurements]. 1-25 p.

VMK. 2019. Allmänt om typgodkännande av utrustning och metoder för ersättningsgrundande virkesmätning [On type-approval of equipment and methods for payment-related log scaling and grading]. 1-5 p.

VMK. 2019. Lista över typgkodkännanden [Measurement devices type-approved by VMK]. 1-4 p.

Session 5

Advanced Grading Technologies for Solid Wood and Engineered Wood Products

Prediction of Tensile Modulus of Elasticity from Longitudinal and Transverse Natural Frequencies in Hardwood Species

Gonzalo Moltini *
Cesefor, Soria, Spain, gonzalo.moltini@cesefor.com

Gonzalo Cabrera
Cesefor, Soria, Spain, gonzalo.cabrera@cesefor.com

Vanesa Baño
Cesefor, Soria, Spain, vanesa.bano@cesefor.com

* Corresponding author

Abstract

Currently, most of structural timber in Europe is graded with C classes, obtained from bending tests; however, many engineered wood products require the grading in T classes, from tensile tests. The increasing demand of wood for structures leads to the need of studying new timber species, mainly focused on both high strength capacity and/or fast-grown criteria. Then, the objective of this study is to evaluate the stiffness properties of different hardwood species by both non-destructive testing and tensile tests according to EN 408. Three high-, medium- and low- density hardwood species from Spain, named *Eucalyptus globulus*, *Fagus sylvatica* and *Populus x euramericana*, respectively, were studied and compared with a well-known and more commonly used species in structures in Europe (*Pinus sylvestris*). The first step was the measurement of both longitudinal and transverse vibration modes, following the standard ASTM C215-2, in 30 specimens of each species to estimate the dynamic moduli of elasticity obtained from: i) the longitudinal natural frequency; and ii) from the first, third and fifth transverse natural frequencies, using the Timoshenko beam theory. The second step was the comparison between the dynamic moduli of elasticity and the static modulus of elasticity in tension. The results showed different stiffness/density relationships for the four studied species, being poplar and pine grouped in the lower values and Eucalyptus in the higher values. Poplar showed a behaviour like a coniferous species. The values for dynamic modulus obtained from transverse vibration were higher than that obtained from longitudinal vibration for the medium- and low-density species. However, the Eucalyptus globulus, being the one with the highest values for both density and stiffness properties, showed a lower value.

Keywords: NDT, hardwood, vibration analysis

Introduction

General information

Currently we are experiencing an increased demand for timber and timber products worldwide (Dangel, 2016). The increasing demand of wood for structures leads to the need of studying new timber species, mainly focused on both high strength capacity and/or fast-grown criteria. Fast-growing criterium is mainly associated to softwood species and high strength capacity to hardwoods. There are species which combine

both of these qualities, such as, Eucalyptus sps. (Lara Bocanegra 2017; Vega 2020), among others. In Europe, softwood species are mainly graded in C classes and hardwood species in D classes (for bending) and T classes for tension (softwoods), these classes are defined by the standard EN 338:2016. Currently there are no classes defined for hardwoods tested in tension, even if the current criteria allow hardwoods to be classified as T classes if the mean density is lower than 600 kg/m^3. Thus, medium- and high- density hardwoods cannot be assigned to strength classes in tension. On the other hand, standard for the production of Glulam beams (EN 14080:2013), proposes a method to calculate the properties of Glulam beams based on the tensile properties of lamellas.

Therefore, the objective of this study is to evaluate the stiffness properties of three different Spanish high-, medium- and low- density hardwood species (*Eucalyptus globulus, Fagus sylvatica and Populus x euramericana*, respectively) obtained from longitudinal and transversal natural frequencies and from experimental tensile tests, comparing their potential grading yield with a well-known species (*Pinus sylvestris*).

Methodology

Four different species were studied, three high-, medium- and low- density hardwood species and one softwood species: Blue gum (*Eucalyptus globulus*), Beech (*Fagus sylvatica*), Poplar (*Populus x eruamericana*) and Scots pine (*Pinus sylvestris*) respectively. For each species, 30 specimens were tested.

Non-Destructive Testing

Vibration measurements were carried out using two different configurations, longitudinal and transversal, following the guidance of ASTM C215-19. In the longitudinal setup, the pickup accelerometer was placed in one end and the impulse given by a hammer was done in the other end. In the transverse setup, the supports were placed at a given distance from the end (matching the vibration node), the pickup was placed on one end and the impact was driven in the centre of the beam. The acceleration was registered in steps of 1x10-4 s over a time frame of 8 s. Measurements of moisture content were made with a handheld xylohigrometer (EN 13183-2: 2002). Mass and dimensions of each specimen were recorded. The set up for the non-destructive test is shown in Figure 1.

A pickup unidirectional accelerometer was used (PCB 352C33) connected to an USB oscilloscope (DS1M12 from Connective Peripherals). The signal is then registered and processed in a numerical analysis software, obtaining the Fast Fourier Transform.

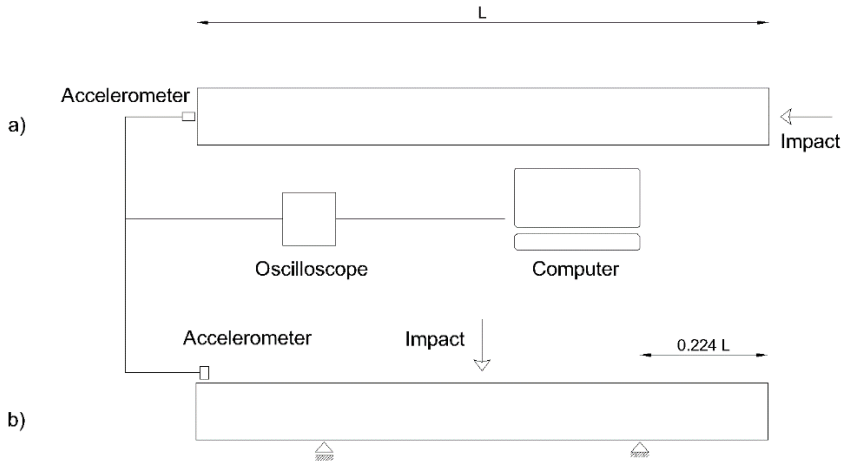

Figure 1: NDT setup for: a) longitudinal vibration, b) transverse vibration

Frequency analysis

Using the Fast Fourier Transform function from MATLAB, the FFT for each time-acceleration signal was obtained. For the longitudinal vibration modes, the frequency of the first longitudinal vibration mode was recorded. For transversal mode the frequencies for the first, third and fifth vibration modes were obtained. An example of the obtained FFT for transverse vibration is shown in Figure 4.

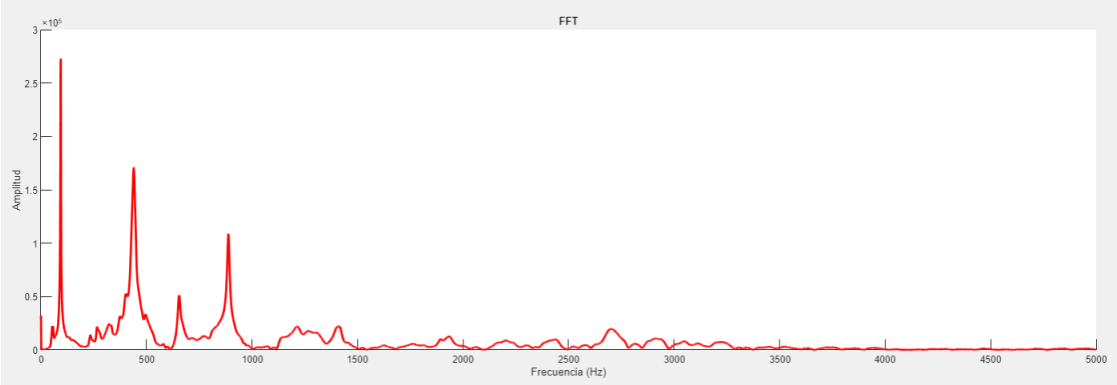

Figure 4: FFT of a transverse vibration signal for a Beech specimen

Dynamic elastic modulus determination

Two different analyses were used for the determination of the dynamic elastic modulus. The first one was a direct method, using the frequency of the first longitudinal vibration mode (1).

$$E_{dyn,L} = (2f_L L)^2 \rho \quad (1)$$

Where $E_{dyn,L}$ is the dynamic elastic modulus obtained from longitudinal frequency, the length L and the density ρ. The second approach involves optimizing the relationship for the elastic modulus and the shear modulus using the equations given by Majkut (Majkut 2009) for a beam using the Timoshenko beam theory.

Destructive Testing

Tension tests were carried out obtaining tension strength and elastic modulus. Protocol defined by EN 408:2011+A1:2012 was followed Density was determined following the procedure described in EN 408:2011+A1:2012 (Figure 2). Moisture content for destructive testing was determined following the oven dry method described in EN 13183-1:2002+AC:2003. Mass and dimensions were registered at this time as well.

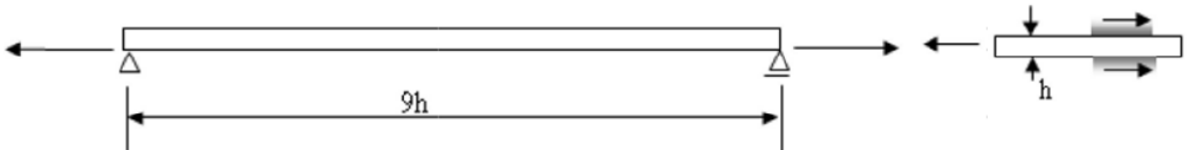

Figure 2: Tensile test configuration (EN 408:2011+A1:2012)

Where h is the width of the specimen. To calculate the static elastic modulus, two extensometers were placed at each side of the specimen as shown in Figure 3.

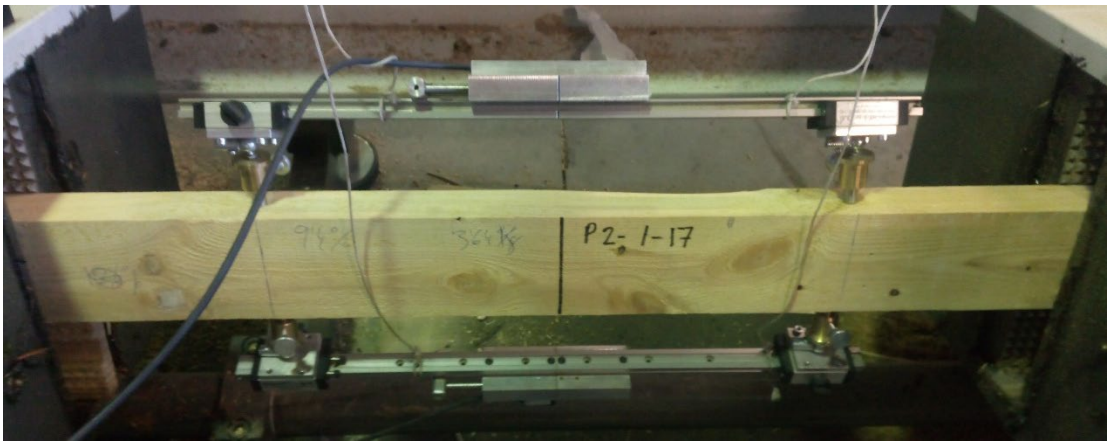

Figure 3: Tensile test of a Pinus sylvestris specimen

Results

Sample properties

The properties of the samples studied for each species is shown in Table 1.

Table 1: Summary of the sample data

Species	Value	$E_{dyn,L}$ (N/mm^2)	$E_{dyn,T}$ (N/mm^2)	$f_{t,0}$ (N/mm_2)	Et,0 (N/mm^2)	Density (Kg/m^3)
Pinus sylvestris	Mean	13287	13333	36.0	13072	548
	CoV (%)	19	20	29.0	18	11
Populus x euramericana	Mean	10813	11197	41.1	10698	455
	CoV (%)	16	17	36	15	10
Fagus sylvatica	Mean	14632	14845	64.7	13036	717
	CoV (%)	12	12	26	10	5
Ecualyptus globulus	Mean	20890	20688	75.1	20418	861
	CoV (%)	17	18	30	17	9

Where $E_{dyn,T}$ is the dynamic modulus of elasticity obtained from transversal frequencies, $f_{t,0}$ the tensile strength and $E_{t,0}$ is the static modulus of elasticity.

It was observed the different range of densities among the hardwood group, ranging from 455 to 861 Kg/m3, the same tendency was noted for the rest of the properties.

NDT testing vs. Grade Determining Properties

In this section the results the relationship between the non-destructive testing results and the grade determining properties are presented (Tensile strength, Elastic modulus and Density). In Figure 5 the relationship between tensile strength and both dynamic modulus of elasticity is shown. The results showed a normal correlation for pine, but the correlation was worse for the hardwoods (for eucalyptus the correlation coefficient was as low as 0.16 for the longitudinal dynamic elastic modulus). In hardwoods the transversal dynamic elastic modulus showed a minimal improvement compared to the longitudinal one.

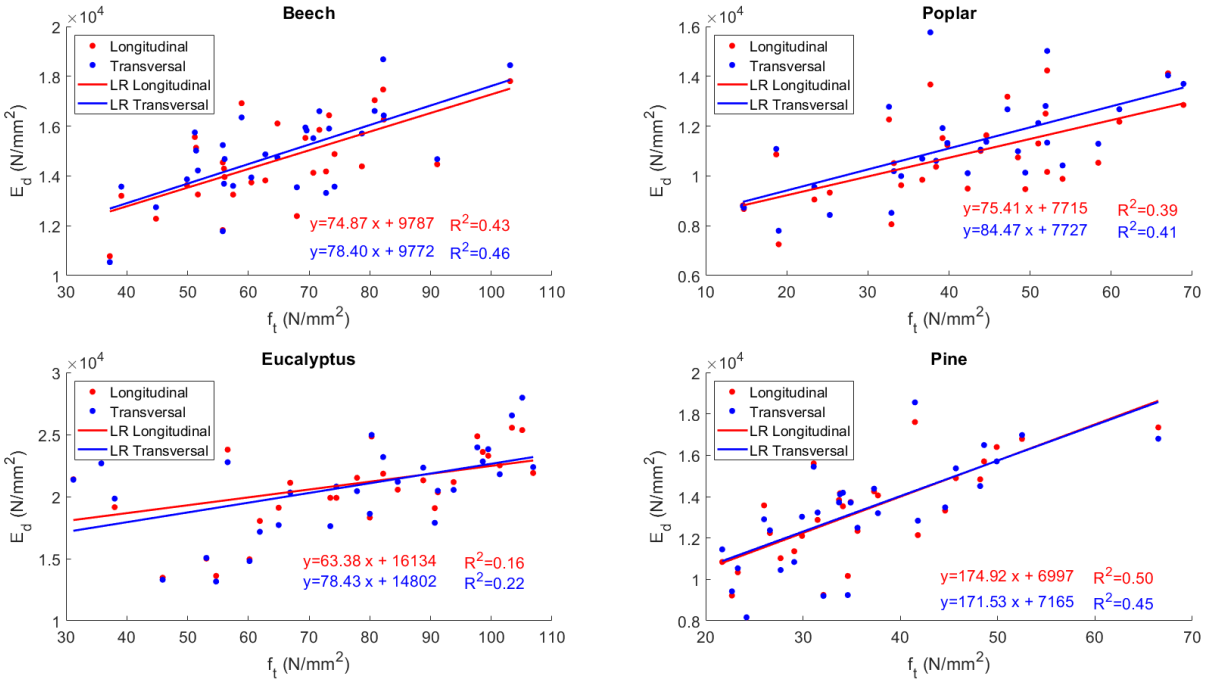

Figure 5: Relationships between tensile strength and dynamic modulus of elasticity

The relationship between dynamic and static elastic modulus is shown in Figure 6.

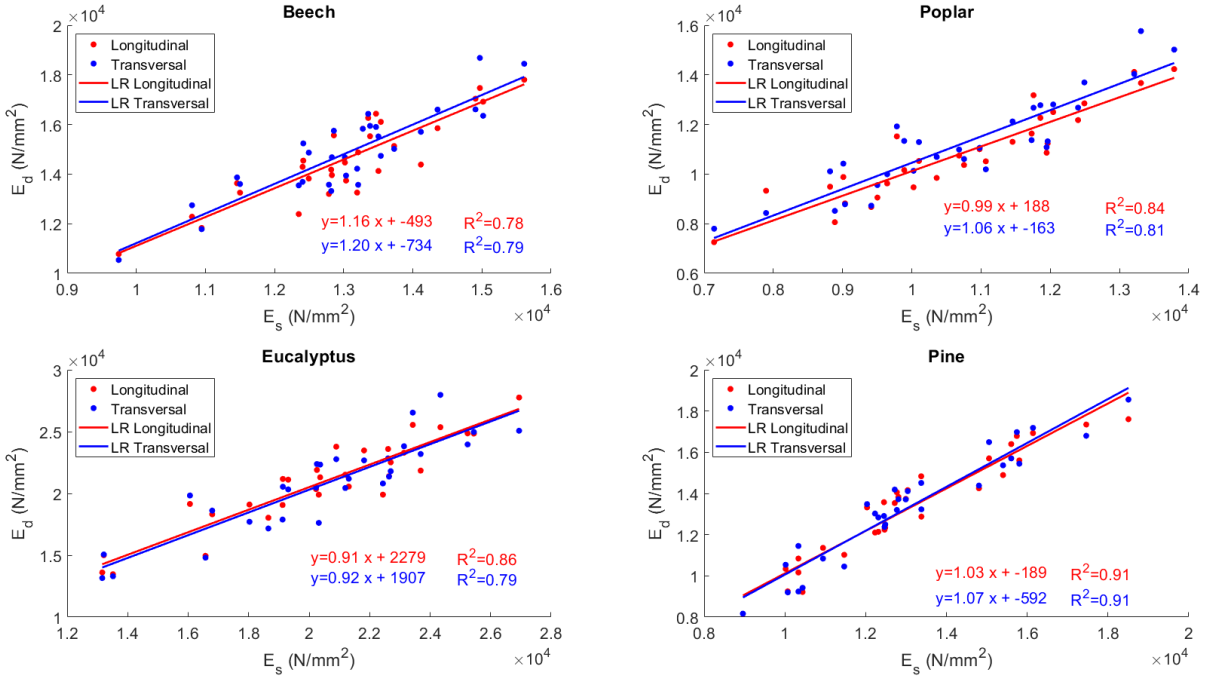

Figure 6: Relationships between tensile static elastic modulus and dynamic modulus of elasticity

Despite having lower correlation when compared to softwood, the dynamic elastic modulus showed to be a good prediction parameter for the static elastic modulus in hardwoods. The correlation coefficient did not change significantly among the hardwood group.

In figure 7 it is shown the relationship between density and dynamic elastic modulus.

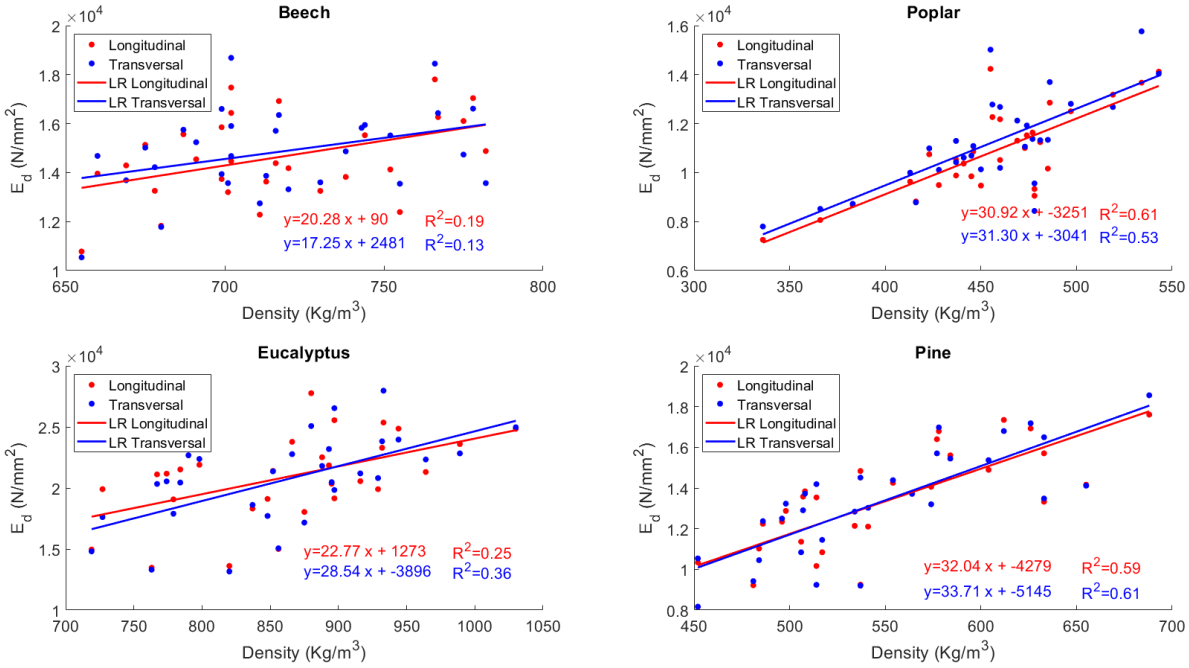

Figure 7: Relationships between density and dynamic elastic modulus

The density showed a normal correlation with the dynamic elastic modulus of elasticity for Pine and Poplar (low density hardwood), for the higher density hardwoods the correlation was as low as 0.13 (Beech).

Conclusions and future works

There is a high potential for the use of hardwoods for structural purposes. The growth rate of these species along with the high mechanical properties imply that they can be used to increase sustainability.

Both non-destructive methods studied showed similar prediction values, however, the computational cost of calculating the transversal modulus of elasticity is high and an optimization study is needed.

The transversal analysis also provides the shear modulus, static test needs to be performed to verify this method of prediction.

For hardwoods the dynamic modulus of elasticity is not a good predictor of tensile strength, specially for high density ones. Other non-destructive parameters such as fibre deviation should be studied.

The dynamic modulus of elasticity (for both methods) is a good method to predict the static elastic modulus despite the difference in species and densities.

For high density hardwoods, the dynamic elastic modulus showed poor correlations. It shows acceptable levels for low density hardwoods.

Acknowledgments

This research project has been sponsored by the project SOE4/P1/E1115 «Eguralt: Application and dissemination of innovative solutions for the promotion of mid-rise timber construction in the SUDOE area», co-financed by FEDER funds within the framework of the Interreg SUDOE program.

References

ASTM C215-19: Standard Test Method for Fundamental Transverse, Longitudinal, and Torsional Resonant Frequencies of Concrete Specimens

U. Dangel, Turning Point in Timber Construction, Birkhäuser, Basel, 2016

A.J. Lara-Bocanegra, A. Majano-Majano, J. Crespo, M. Guaita; Finger-jointed Eucalyptus globulus with 1C-PUR adhesive for high performance engineered laminated products. Construction and Building Materials, Vol 135, March 2017, Pages 529-537.

L. Majkut. Free and forced vibrations of Timoshenko beams described by single difference equation. Journal of Theoretical and Applied Mechanics. Vol 47. 2009. Pages 193-2010.

UNE-EN 13183-1: 2002 Moisture content of a piece of sawn timber-Part 1: Determination by oven dry method

UNE-EN 13183-2: 2002 Moisture content of a piece of sawn timber-Part 2: Determination by electrical resistance method

UNE-EN 408:2011+A1:2012 Structural timber and glued laminated timber: Determination of some physical and mechanical properties

UNE-EN 338:2016 Structural timber: Strength classes

UNE-EN 14080:2013 Structural timber – Glued laminated timber and glued solid timber - requirements

A. Vega, V. Baño, A. Cardoso, L. Moya: Experimental and numerical evaluation of the structural performance of Uruguayan Eucalyptus grandis finger-joint. European Journal of Wood and Wood Products, September 2020, Vol 78, Pages 923-932.

Influence of Board Geometry on the Determination of Dynamic Mechanical Properties of Structural Lumber

Aleš Straže *
University of Ljubljana, Biotechnical Faculty, Ljubljana, Slovenia, ales.straze@bf.uni-lj.si

Luka Krajnc
Slovenian Forestry Institute, Ljubljana, Slovenia, luka.krajnc@gozdis.si

Abstract

When using dynamic mechanical methods to grade structural lumber, significant differences in measured values have been observed, depending on the frequency range of the method and the geometry of the boards, and are also influenced by sound wave dispersion. To better understand these phenomena, spruce (*Picea abies* Karst.) lumber without visible anomalies with cross sections of 42×42 and 42×84 mm and a length of 4.0 m was dynamically tested and analyzed in longitudinal vibrations and by measuring of time of flight of bulk and surface ultrasonic waves. The sound velocity and the modulus of elasticity determined in longitudinal vibrations (v_L, E_L) and by the velocity of bulk ultrasonic waves (v_{USB}, E_{USB}) were independent of the length of the specimens. In contrast, the modulus of elasticity decreased with the shortening of the specimens when we measured the velocity of surface ultrasonic waves (v_{USS}, E_{USS}). We confirmed the characteristic differences in the measured velocities ($v_{USB} > v_{USS} > v_L$), the same here for the modulus of elasticity ($E_{USB} > E_{USS} > E_L$), in all studied samples. The geometry of the samples significantly affected the differences between the measured values of the moduli when the ratio between the sample length (L) and the wavelength (λ) was less than 20, or in samples shorter than 2 m.

Keywords: structural lumber, dynamic testing, modulus of elasticity, sample geometry

Introduction

Determination of elastic properties of materials based on the propagation velocity of sound waves in wood is one of the applied and proven methods for non-destructive material testing to assess the quality of wood material during wood processing, especially in the grading of structural timber. Although the concept of acoustic wood classification has been validated (Sandoz, 1989), it is important to note that acoustic measurements in wood are influenced by many factors, such as moisture content, temperature, dimensions of the wood piece, acoustic measurement systems, and instruments used (Bucur & Böhnke, 1994; Gerhards, 1982a; Gerhards, 1982b; Wang, 2013). The practical implementation of acoustic classification technology in the wood industry requires a comprehensive understanding of the effects of these physical and environmental conditions on the accuracy of acoustic measurements.

Previous research has investigated various factors that affect the accuracy and precision of dynamic mechanical measurements, as well as many types of measurement devices. Some studies (Arriaga et al., 2017) investigated sensor location, moisture content, and temperature, as well as wood orientation in different pine species. They concluded that the length of the sample was important for accuracy. However, as the length increased, the speed of the ultrasonic waves slightly decreased in general. For practical application, they recommended a minimum sample length of 1.5 m; otherwise, we would not get correct results. Ultrasound studies have also shown that when ultrasound passes through wood, we are

dealing with multiple types of waves. Research shows that ultrasound can propagate by compressive or bulk waves, shear waves, and also surface waves. The velocity of surface waves has been found to vary with the ratio of length (L) and wavelength (λ) up to a value of 5 ($L/\lambda < 5$) (Bartholomeu et al., 2003). However, for bulk ultrasound waves, the same study does not mention the influence of the length of the sample on the velocity of the ultrasound.

In the study of dynamic mechanical properties by vibration methods using frequency response, the influence of the geometry of the specimens on determined modulus of elasticity is well known, especially in flexural vibrations, where the natural frequency of shorter specimens is negatively affected by shear stresses (Bucur, 2006). Otherwise, studies report an increase of the modulus of elasticity with increasing frequency, which is accompanied by a shortening of the characteristic time (Divos & Tanaka, 2005; Ouis, 2002).

The aim of this study was to analyze the influence of the characteristic time and the type of dynamic mechanical method used in the determination of the dynamic modulus of elasticity of wood. The latter is generally inversely proportional to the frequency of the mechanical vibrations in the sample and depends on the characteristics of the forced external vibrations, generated mechanically or with ultrasound.

Material and methods

Sampling

For the study, we used air-dried elements with a length of 4 m, a nominal cross section of 42 × 42 mm (n = 13; small size specimens), and a cross section of 42 × 84 mm (n = 13; large size specimens). The elements were selected at the lumberyard based on their visual characteristics. They were free of growth peculiarities and anomalies (knot size only up to 10 mm in diameter), they were straight grained, and they belonged to the highest quality class (EN DIN 4074-1) (Fig. 1). Elements with narrow, medium and wide growth rings were equally included in the set. The specimens had radial or semi-radial orientation in cross-section and their dimensions were measured with an accuracy of ± 0.01 mm. Prior to measurement, the specimens were conditioned at 20 °C and 50 % relative humidity for 4 weeks.

Figure 1— Selection of small size- (42 × 42 mm) and large size (42 × 84 mm) test specimens with for the investigation of dynamic mechanical properties.

The elements were weighed on a laboratory balance (Δm = ± 0.1 g) before each measurement. The individual samples were then marked for cutting to length, which was done in steps (1... 7) so that each sample was removed by 250 mm on both sides, i.e. 500 mm in each step together. In this way, from the 4000 mm long basic element, we obtained 7 specimens with lengths of 3500 mm, 3000 mm, 2500 mm, 2000 mm, 1500 mm, 1000 mm and 500 mm.

Determination of dynamic mechanical properties of wood

Determination of elastomechanical properties of structural lumber with ultrasound

Ultrasound velocity was measured in the longitudinal direction of the board for each length tested (4000...500 mm) using a Proceq Pundit PL-200PE pulse ultrasound device equipped with 54 kHz exponential transducers. We tested 2 positions of the transducers - the frontal position to determine the velocity of ultrasound waves in the bulk (v_{USB}), and the lateral position to determine the velocity of ultrasound waves at the surface (v_{USS}) (Fig. 2). These velocities, multiplied by the wood density (ρ), were used to determine the ultrasonic moduli of elasticity from bulk (E_{USB}) and surface (E_{USS}) waves (Eq. 1,2).

$$E_{USB} = \rho \cdot v_{USB}^2 \quad (1)$$

$$E_{USS} = \rho \cdot v_{USS}^2 \quad (2)$$

Determination of elastomechanical properties of structural lumber by vibration resonant method

For longitudinal vibrations, specimens were placed on soft, thin rubber pads and were excited with a steel hammer (mass 100 g) from a free end. Sound was recorded with a unidirectional condenser microphone (PCB-130D20) and acquired by a NI-9234 DAQ module in 24-bit resolution at 51.2 kHz sampling frequency (Fig. 2). The measured natural frequency of the board (f_L) in the first longitudinal vibration mode was used to determine the sound velocity (v_L) and modulus of elasticity (E_L) in the longitudinal direction of the board (Eq. 3).

$$E_L = \rho \cdot (2 \cdot L \cdot f_l)^2 = \rho \cdot v_L^2 \quad (3)$$

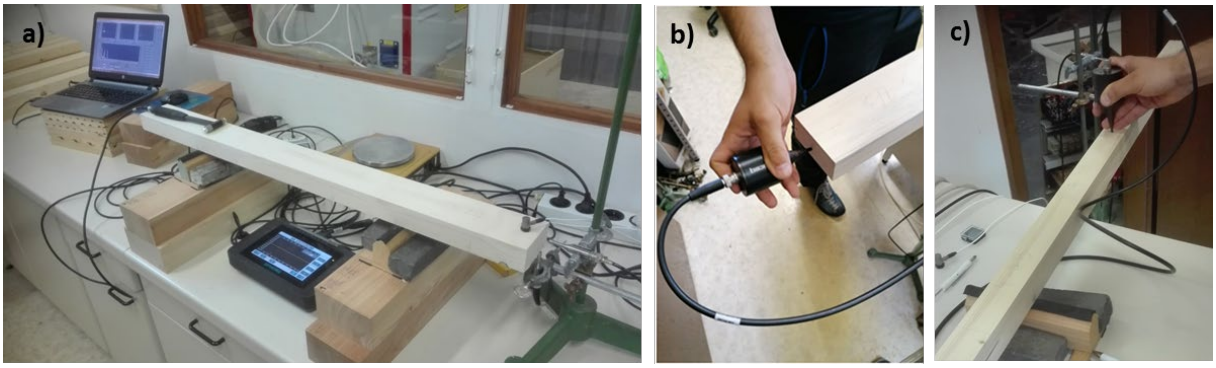

Figure 2— (a) Principle of the analysis of longitudinal vibration response of structural lumber specimens, (b) the experimental setup for determination of velocity of bulk ultrasound waves, (c) the experimental setup for determination of velocity of surface ultrasound waves.

Results and discussion

Sample characteristics and variation of density

For the small-sized samples, we determined a minimum density of 401 kg/m^3 and a maximum density of 580 kg/m^3, and an average value of 471 kg/m^3. The average density of the samples was slightly higher than the average reported in the literature for spruce (Wagenführ, 2014). In the large-sized samples, we measured a wide range of densities, but the average density of the wood in both groups was not significantly different (Tab. 1).

Table 1—Wood density and its variation in small size and large size specimens (n = 13)

	Small size 42 × 42 mm	Large size 42 × 84 mm
Average	**471.3**	**470.3**
Minimum	401.1	399.9
Maximum	580.0	645.5
Coef. of variation	12.0	13.5

In the total population of samples, we observed a low variability of wood density along the samples in the range of low, medium and high wood density (Fig. 3). The coefficient of variation averaged 1.1% for small-sized samples and 1.3% for large-sized samples and was independent of the density of each sample.

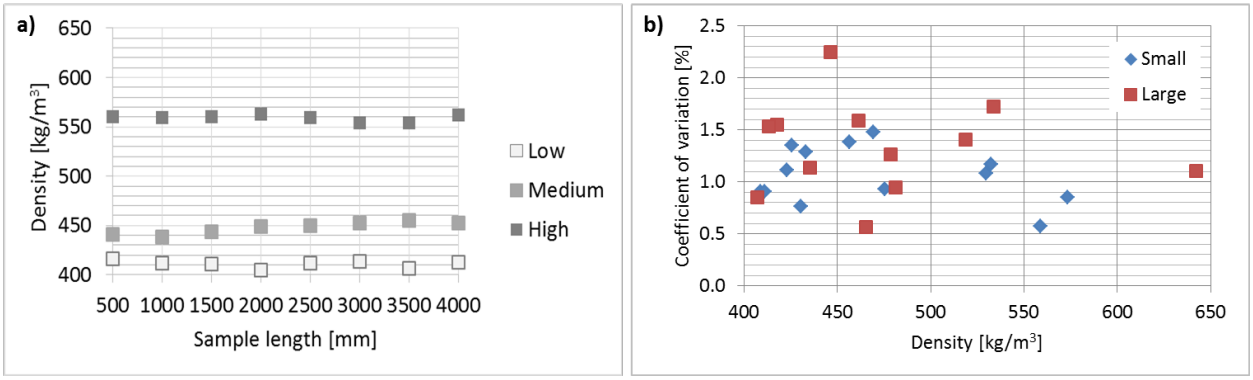

Figure 3— (a) Variation of wood density along the length of the samples from low, medium to high density class (b) Coefficient of variation of wood density in small-sized and large-sized samples

Samples from the lower density range (400 - 485 kg/m^3) generally had the widest growth rings and a low proportion of latewood. Medium density samples (485 - 570 kg/m^3) had medium-width annual rings, and the narrowest annual rings were found in samples from the highest density class (570 - 655 kg/m^3), as expected (Fig 4).

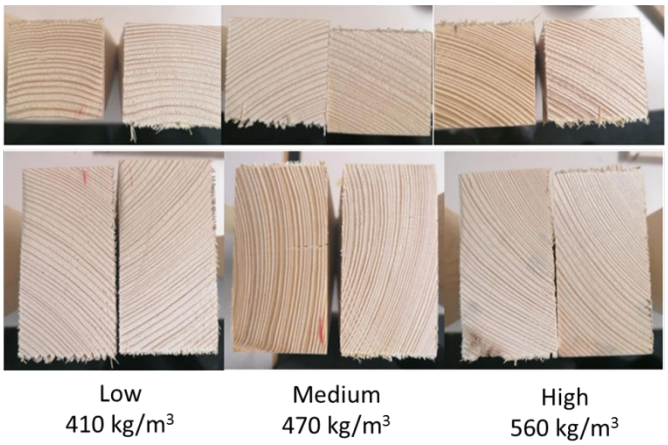

Figure 4— Cross section view of low density (left), medium density (middle) and high density samples (right).

Impact of wood density on the propagation of sound and ultrasound

For the small specimens with maximum length (L = 4000 mm), the average speed of sound was 4564 m/s (CV = 5.8%) for the vibration method. The average velocity of ultrasound was 11.2% higher and was 5079 m/s (CV = 9.5%) (Fig. 5). At the same length, we determined the average speed of sound 4423 m/s (CV = 7.8%) for large-sized specimens in the frequency response, and the average speed of ultrasound in this case was 26.1% higher and was as high as 5547 m/s (CV = 6.1%). However, in all cases we could not confirm the influence of wood density on the sound or ultrasound velocity in the axial direction of the wood, as it was found in other studies (Bucur, 2006). Studies on the increase of sound and ultrasonic velocity along the wood fibers are directly related to the length and orientation of the wood fibers as well as to microstructural features, e.g. the degree of crystallinity of the cellulose microfibrils in the cell walls (Baar et al., 2012; Obataya et al., 2000).

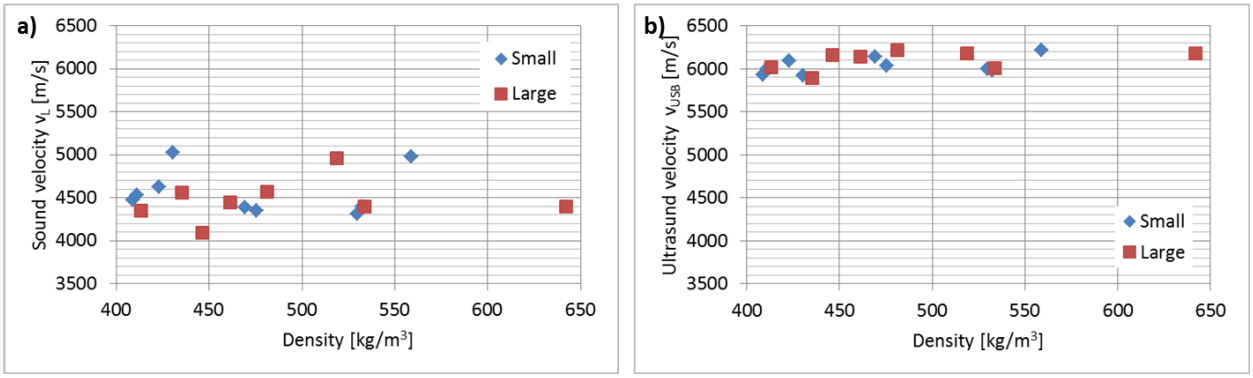

Figure 5— (a) Variation of sound velocity in relation to the wood density of small- and large-sized samples, (b) Variation of bulk ultrasound velocity in relation to the wood density of small- and large-sized samples.

Dependence of dynamic mechanical properties on the geometry of the boards

The constant value of the modulus of elasticity, regardless of the length of the specimens and the size of the cross section, was measured by the vibration resonance method. The values in the medium density specimens were comparable to those in the literature (small-sized: E_L = 9.60 GPa; large-sized: E_L = 9.64 GPa) and not much higher than the modulus of elasticity measured in static tests (Edlund et al., 2006; Holeček et al., 2017; Mania et al., 2015) (Fig. 6).

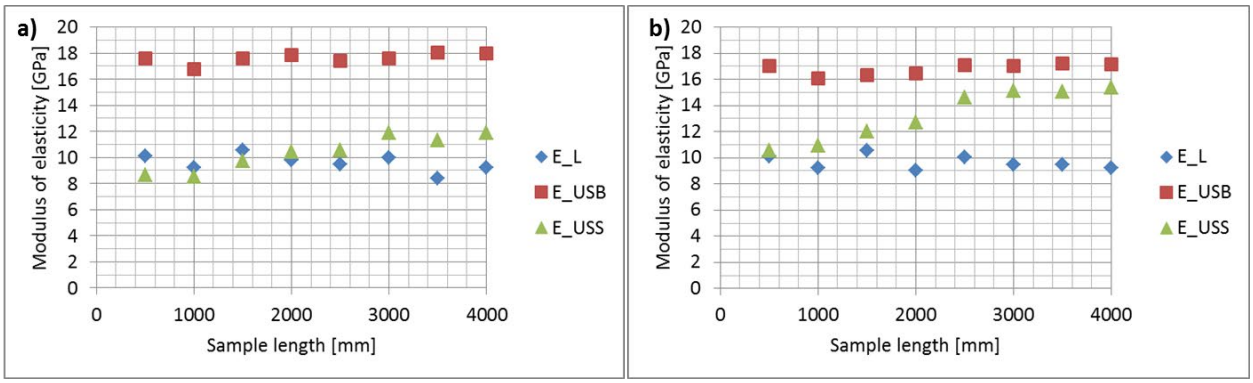

Figure 6— Variation of moduli of elasticity, determined by resonant vibration method (E_L) and bulk- (E_{USB}) and surface ultrasound velocity (E_{USS}) in medium dense small-sized samples (a), and in large-sized samples (b)

The largest modulus of elasticity was determined by measuring the velocity of bulk ultrasonic waves. The values determined for small samples of medium density were 84% (E_{USB} = 16.8 GPa) higher than the modulus of elasticity determined by the vibrational resonance method. However, for large-sized specimens, the difference was 75% (E_{USB} = 17.6 GPa). The difference, found also in some other studies (Baar et al., 2012), can be attributed to the shorter characteristic measurement time with the ultrasonic method (Divos & Tanaka, 2005; Ouis, 2002).

However, the elastic modulus determined by the surface ultrasonic waves increased with increasing length for both groups of specimens. For small specimens, it increased from 8.5 GPa (L = 500 mm) to 11.9 GPa (L = 4000 mm). For the large specimens, the change was even greater, from 10 GPa to 15.5 GPa. The result is consistent with some previous studies that emphasize the importance of a sufficiently large ratio between the sample length and the wavelength of the stress waves ($L/\lambda > 5$) (Bartholomeu et al., 2003; Oliveira et al., 2006).

Conclusions

The sound velocity and the modulus of elasticity determined in longitudinal vibrations (v_L, E_L) and by the velocity of bulk ultrasonic waves (v_{USB}, E_{USB}) are independent of the length of the specimens. Higher values of the latter are attributed to the shorter characteristic measurement time.

In contrast, the modulus of elasticity decreased with the shortening of the specimens when the velocity of surface ultrasonic waves (v_{USS}, E_{USS}) is used. The geometry of the samples significantly affected the differences between the measured values of the moduli when the ratio between the sample length (L) and the wavelength (λ) was less than 20, or in samples shorter than 1.5 m.

Acknowledgments

We thank the Ministry of Education, Science and Sports of the Republic of Slovenia and the Slovenian Research Agency (ARRS) for co-funding research from programs P4-0015 (Wood and lignocellulosic composites) and P4-0430 (Forest timber chain and climate change: the transition to a circular bioeconomy).

References

Arriaga, F., Llana, D.F., Esteban, M., Iniguez-Gonzales, G. 2017. Influence of length and sensor positioning on acoustic time-of-flight (Tof) measurement in structural timber. *Holzforschung*, **71**, 713-723.

Baar, J., Tippner, J., Gryc, V. 2012. The influence of wood density on longitudinal wave velocity determined by the ultrasound method in comparison to the resonance longitudinal method. *European Journal of Wood and Wood Products*, **70**, 767-769.

Bartholomeu, A., Goncalves, R., Bucur, V. 2003. Disperision of ultrasonic waves in Eucalyptus lumber as a function of the geometry of boards. *Scientia forestalis*, **63**, 235-240.

Bucur, V. 2006. *Acoustics of wood*. Springer-Verlag, Berlin.

Bucur, V., Böhnke, L. 1994. Factors affecting ultrasonic measurements in solid wood. *Ultrasonics*, **32**(5), 385-390.

Divos, F., Tanaka, T. 2005. Relation between static and dynamic modulus of elasticity of wood. *Acta silvatica & lignaria Hungarica*, **1**, 105-110.

Edlund, J., Lindström, H., Nilsson, F., Reale, M. 2006. Modulus of elasticity of Norway spruce saw logs vs. structural lumber grade. *Holz als Roh- und Werkstoff*, **64**, 273-279.

Gerhards, C.C. 1982a. Effect of moisture content and temperature on the mechanical properties of wood: An analysis of immediate effects. *Wood and Fiber*, **14**(4), 4-36.

Gerhards, C.C. 1982b. Longitudinal stress waves for lumber stress grading: Factors affecting applications: State of the art. *Forest Products Journal*, **32**, 20-25.

Holeček, T., Gašparik, M., Lagaňa, R., Borůvka, V., Oberhofnerová, E. 2017. Measuring the Modulus of Elasticity of Thermally Treated Spruce Wood using the Ultrasound and Resonance Methods. *BioResources*, **12**(1), 819-838.

Mania, P., Fabisiak, E., Skrodzka, E. 2015. Differences in the Modal and Structural Parameters of Resonance and Non-Resonance Wood of Spruce. *Acta Physica Polonica*, **127**, 110-113.

Obataya, E., Ono, T., Norimoto, M. 2000. Vibrational properties of wood along the grain. *Journal of Materials Science*, **35**, 2993-3001.

Oliveira, F.G.R., Miller, K.P., Canadian, M., Sales, A. 2006. Effect of the size of the specimen on ultrasonic velocity. *Revista Árvore*, **30**(1), 141-145.

Ouis, D. 2002. On the frequency dependence of the modulus of elasticity of wood. *Wood Science and Technology*, **36**, 335-346.

Sandoz, J.L. 1989. Grading of construction timber by ultrasound. *Wood Science and Technology*, **23**, 95-108.

Wagenführ, R. 2014. *Holzatlas*. *4th ed*. Fachbuchverlag, Leipzig.

Wang, X. 2013. Stress wave E-rating of structural timber – Size and moisture content effects. *18th International Nondestructive Testing and Evaluation of Wood Symposium*, Madisson. pp. 38-46.

Strength Grading Softwood Structural Lumber with MoE Low Point

Jon Shanks
TimberED Services, Fremantle, Western Australia, jonshanks@timbered.com.au

Richard Schaffner
Wespine, Bunbury, Western Australia, richard.schaffner@wespine.com

Geoff Boughton
TimberED Services, Fremantle, Western Australia, boughton@timbered.com.au

James Szabadics
Wespine, Bunbury, Western Australia, jamess@wespine.com

Abstract
Sawn structural radiata pine lumber commonly used in Australia is stress-graded prior to sale. The stress-grading process uses indicators of strength and measurements of modulus of elasticity (MoE) to assign individual pieces of timber to a stress-grade that most accurately represents its properties. Each stress-grade has a full suite of structural properties including bending MoE. This paper focuses on strength grading of structural softwood lumber using a number of different attributes of the timber and correlates the attributes with the tension strength. The research program used full length tension strength to correlate with various grading parameters. By testing the full graded length of the timber in tension, the region with the lowest strength will initiate failure. Typically, the failure initiates at or near knots where there is some local slope of grain near a corner. Grading parameters from commercial grading machines were used to correlate with tension strength and included knot size estimated by surface scanning and tracheid response; knot area ratio (KAR) from an aggregation of knot data across the cross section; and local MoE on-flat. Correlations between MoE on-flat and bending, compression, and beam shear strength were investigated using data from an in-grade study. The test results indicated that the best correlation was obtained using a mixture of all grading parameters, but it was only marginally higher than the correlation obtained from local MoE on-flat alone for the radiata pine resource processed in this study.

Keywords: strength grading, MoE low point, radiata pine, grading parameters

Introduction
Lumber grading in Australia

Australian stress grades for use in structural design are presented in *AS 1720.1-2010 Timber Structures, Part 1: Design methods* (Standards Australia 2010). Example 'MGP' grades with associated characteristic values from AS 1720.1 (Standards Australia 2010) are presented in Table 1. Average modulus of elasticity, MoE, is an important grade characteristic which often governs in design and can also be the limiting property in grading.

The majority of structural softwood lumber production nationally in Australia is from pinus radiata (2,000,000m^3pa), with some pinus caribbea/pinus elliottii hybrid 360,000m^3pa and other softwood species 50,000m^3pa. The predominant grade consumed by Australian house builders is MGP10.

Table 1 —Lumber grades to AS1720.1-2010

Stress grade	Depth	Breadth	Bending, f'_b	Tension parallel to grain, f'_t	Compression parallel to grain, f'_c	Shear in beam, f'_s	Average MoE, E
	(mm)	(mm)	(MPa)	(MPa)	(MPa)	(MPa)	(MPa)
MGP10	70 to 140	35 and 45	17	7.7	18	2.6	10 000
	190		16	7.1	18	2.5	
	240		15	6.6	17	2.4	
	290		14	6.1	16	2.3	
MGP12	70 to 140	35 and 45	28	12	4	3.5	12 700
	190		25	12	23	3.3	
	240		24	11	22	3.2	
	290		22	9.9	22	3.1	
MGP15	70 to 140	35 and 45	39	18	30	4.3	15 200
	190		36	17	29	4.1	
	240		33	16	28	4	
	290		31	14	27	3.8	

Mills producing structural softwood lumber in the MGP grades must both qualify the grading processes prior to production and verify lumber properties during production. These requirements are set out in *AS/NZS 1748.1:2011 Timber—Mechanically stress-graded for structural purposes Part 1: General Requirements* (Standards Australia 2011). Mills are individually responsible for their grading processes, thresholds, quality processes, and therefore product compliance. Individual mills throughout Australia have developed unique combinations of grading equipment and grading thresholds as they seek to improve processes and recoveries.

The research presented in this paper is from Wespine, a mill in south-west Australia producing structural radiata pine from 70x35 to 240x45mm in MGP10 and MGP12 along with proprietary structural grades. Drymill grading equipment includes USNR LHG surface scanner and Metriguard HCLT 7200 mechanical grader. Mill output is approximately 140,000m^3 of structural product per annum.

Importance of optimisation of grading for strength-limited products

The limiting characteristic in grading will vary depending on resource and product; production is either strength or stiffness-limited in the MGP grades. If production is stiffness-limited then grading can be well refined and recovery maximised with the MoE directly measured board-by-board in production with a Metriguard HCLT mechanical grader for example. However, even in those cases, a proportion of the production will be limited by the strength of the pieces. Strength is inferred from relationships with properties measured in grading such as MoE and KAR (Boughton and Juniper 2010) (Bailleres, Hopewell et al. 2012). If production is strength-limited, then refinement of these relationships in the context of the mill-specific resource and grading equipment represents a significant opportunity for improved recovery while managing risk of non-compliance.

The Wespine mill has determined that while most batches of lumber processed through its drymill are stiffness-limited in grading, strength-limited batches occur often and must be processed appropriately. The maximum possible recovery can be achieved in better differentiating stress-grading decisions at the low end; better sorting between low MGP10 and non-structural product. Figure 1 presents a diagram of production settings or grading thresholds against tested strength or production target. The target in optimising stress-grading is to identify a grading parameter with the best possible correlation with tested strength to minimise product in the 'Rejected but compliant' zone with control over how much product is in the 'Accepted & non-compliant' zone. The 'Accepted & non-compliant' zone contains material that has strength below the design values published in *AS 1720.1* (Standards Australia 2010) for a given stress grade. As the design value represents a population 5th percentile strength, in general, this region should contain no more than 5% of all pieces accepted into the grade during production for the lumber to be compliant.

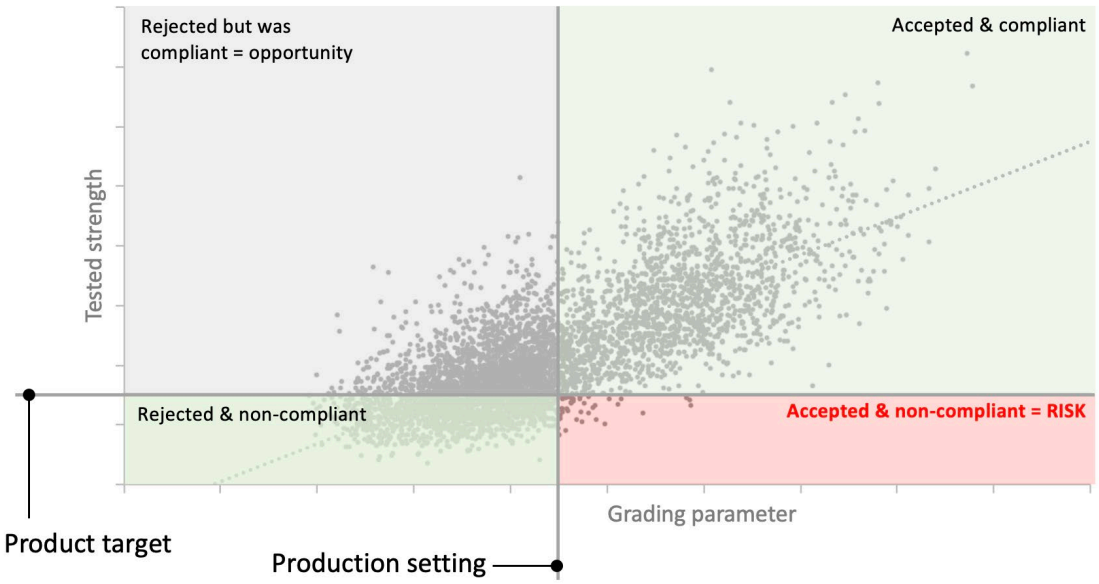

Figure 1—Grading thresholds and compliance

Quality Control testing

Typical quality control (QC) processes use random position edgewise four point MoE and bending strength testing over a span of 18*d* (where *d* is the nominal depth) to *AS/NZS 4063.1:2010 Characterization of structural timber, Part 1: Test methods* (Standards Australia 2010) from a random sample. Tension failure of the critical bottom face, usually in the middle third span, typically governs in four-point bending. The fibre in this region only represents around ~1/6 of the volume of the timber in the test span, and an even lower fraction of the timber in the full test board. Considering a 6m 90x35mm board this equates to only half the depth in a 540mm (6*d*) length or less than 5% of the volume of the board. A more efficient approach to find the weakest part of the tested board is to use the full board length in tension testing. Wespine uses full length tension tests for strength QC, recording the tensile failure stress, position of tension failure, and manually estimated Knot Area Ratio (KAR) at failure.

Annual checks by Wespine and third-party auditors confirm the relationship between full length tension testing and random position bending testing. National in-grade testing programs and qualification tests are used to establish the minor properties (compression, shear) by MGP grade.

Available grading data

Wespine has the following grading parameters on which to make grading decisions in production:

The complete on-flat MoE board profile from the mechanical grader (Figure 2). Average MoE (MoE_{avg}) and low point MoE (MoE_{lp}) can be established for the complete board, or for specific board portions or test spans in relating random position QC test results with grading parameters.

Defect size and location estimated by surface scanners. Knot data are used to plot knot size and position along the board length, Figure 2. KAR differentiated by edge and centre knot can be related to specific board portions or test spans.

This grade information was available for each board tested in a recent national in-grade test program and in QC testing.

Figure 2—Example board MoE profile and defect data

QC test data

Approximately 14,000 pieces of timber per year are tested in full length tension as part of the QC process. Approximately 620mm of timber is embedded in the jaws of the tension tester, but all of the MoE profile shown in Figure 2 and most of the defects shown in Figure 2 are included in the test span. The tension QC test data for four months were used in this project.

In-grade test data

An in-grade study was undertaken to supplement mill production data. Representative samples of 90x35mm boards were taken from four structural grades including MGP10 and MGP12 along with timber that failed to meet the lowest structural grade. These samples were split evenly between bending, tension, compression and beam shear tests resulting in ~210 boards per test across the grades. Tests were performed at random positions within the board lengths in accordance with *AS/NZS 4063.1* (Standards Australia 2010). Grading data was related to in-grade test span position.

Correlations with grading parameters

QC tension data

Full length tension test data was considered from 4740 boards randomly sampled through production across all sizes and grades over a representative four-month period (August to November 2021 inclusive). Correlations were drawn between the full-length tension strength and various grading parameters from the full-length boards to establish which grading parameter gave the best correlation with tension strength.

Figure 3 presents KAR plotted against tension strength. KAR_{man} is estimated manually at the failure during full-length tension testing with KAR_{grad} identified at or near the tension failure location from the surface scanners. A reasonable agreement can be seen between KAR_{man} and KAR_{grad}. The relationship between KAR_{grad} and full-length tension strength is not strong with a coefficient of determination R^2=8%. Correlating full-length tension strength against the maximum board edge KAR ($KAR_{max,edge}$) gives an R^2 of 15%. Equivalent for maximum board centre KAR ($KAR_{max,centre}$) gives R^2 of 8%. An optimized combination of $KAR_{optimized} = KAR_{max,edge} + 0.6* KAR_{max,centre}$ gives an R^2 of 21% (Figure 4). Figure 5 presents the correlation with full-length tension strength using the $KAR_{optimized}$ plus density (measured at the time of QC testing). This provides a stronger correlation (R^2=30%) than $KAR_{optimized}$ alone (R^2=21%) or density alone (R^2=13%). Other combinations of grading parameters were analysed including accumulated KAR over different accumulation lengths with density, MoE_{lp}, and MoE_{avg}. The strongest correlations are presented in this paper.

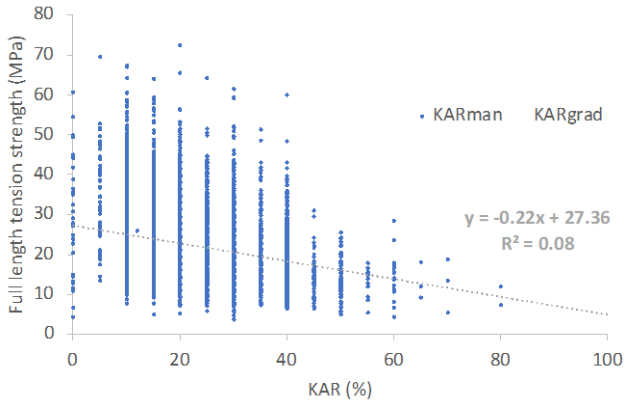

Figure 3—KAR_{man} and KAR_{grad} vs full-length tension strength

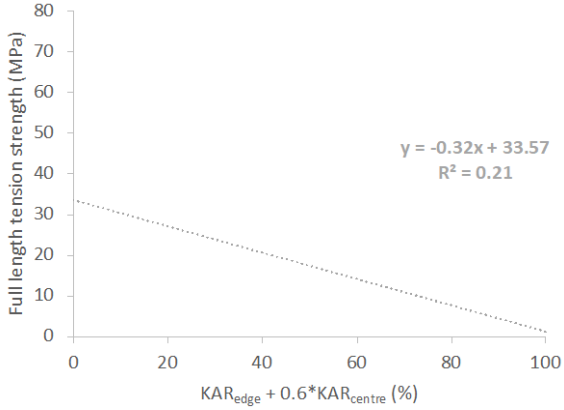

Figure 4—$KAR_{optimized}$ vs full-length tension strength

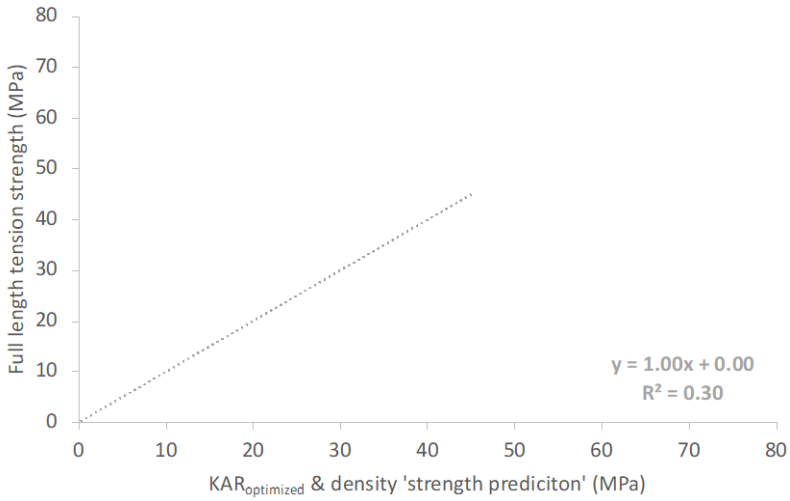

Figure 5—$KAR_{optimized}$ & density vs full-length tension strength

Figure 6 presents full-length board low point MoE established board-by-board on-flat through the mechanical grader (MoE_{lp}) in production plotted against the full-length board tension strength. Coefficient of determination is 58% presenting a good correlation between the grading parameter and a board test strength. Board average MoE established by the mechanical grader in production (MoE_{avg}) gives R^2=35% correlated with full-length tension strength. Figure 7 presents the best correlation developed from the grading data available considering an optimized combination of MoE_{lp} with KAR_{grad} weighted by the knot's proximity to the board edge. The improvement in correlation over MoE_{lp} alone was marginal (59% vs 58%) but includes a far more complex grading parameter to consider in production. Similar marginal gains are seen using MoE_{lp} and $KAR_{optimized}$ in combination.

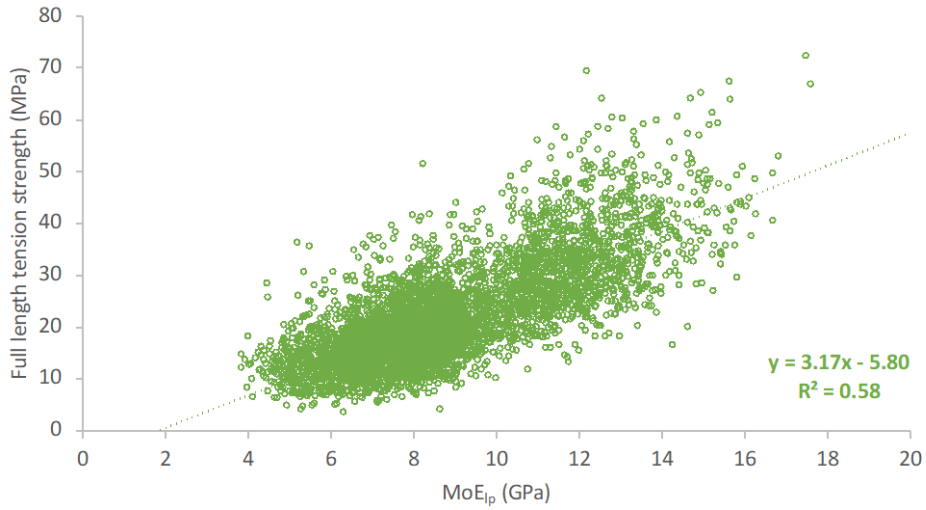

Figure 6—MoE$_{lp}$ in full board vs full-length tension strength

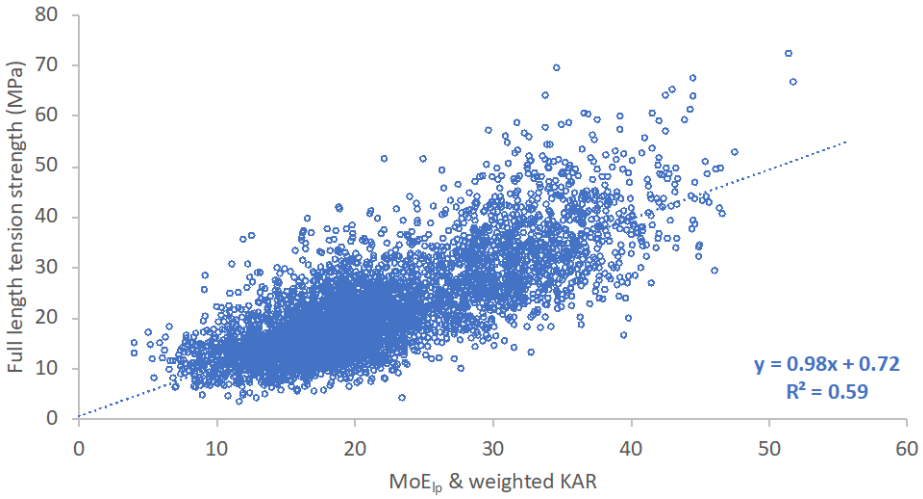

Figure 7—Optimized grading parameter vs full-length tension strength

In-grade test data

Tests in bending, tension, compression and beam shear were performed at random positions within the boards' lengths in accordance with *AS/NZS 4063.1* (Standards Australia 2010) and the results compared with the grading parameters within the test lengths (as opposed to full board length). Results are presented in Figure 8 and summarised below:

- Modulus of elasticity had an excellent correlation (R^2 = 86%) with the average grade MoE$_{avg}$ over the test span.
- All strengths had good correlation with the on-flat low point MoE (MoE$_{lp}$) in the test span calculated from grading data established through the mechanical grader in production:
    - Bending strength R^2 = 49%
    - Tension strength R^2 = 58%
    - Compression strength R^2 = 65%
    - Beam shear strength R^2 = 56%

Figure 8—Correlations between in-grade test properties and grading parameters

A separate series of bending tests was conducted by testing at the strength biased location determined by MoE_{lp} (Figure 9). In this series the bending test was centred on the predicted lowest strength location in the whole length. It gave a slight improvement in R^2 for strength with MoE_{lp} (from R^2 = 49% to R^2 = 55%), but the correlation between the low point grade MoE (MoE_{lp}) and the test MoE (MoE_{4pt}) (Figure 9) was around the same as that for the average grade MoE (MoE_{avg}) on the test span and test MoE (MoE_{4pt}) (Figure 8).

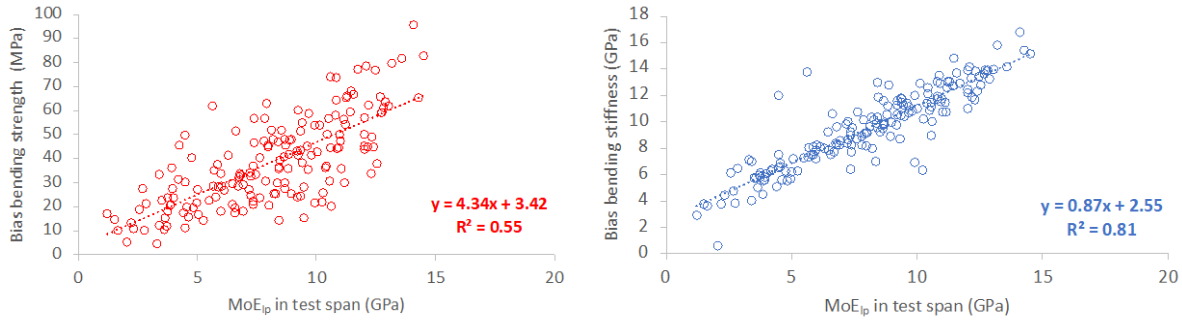

Figure 9—Biased bending correlations between in-grade test properties and grading parameters

Discussion

Full length tension testing provides a method of locating and evaluating the lowest strength portion of timber within a graded length that is not affected by decisions of test location or specimen orientation. An effective strength QC process has been developed around full-length tension testing on boards sampled throughout production. The results of these tests show that the best knot related grading parameter correlation from the board portion loaded in the test span uses an optimized combination of maximum KAR from the centre and edge knots in a board and gives R^2=21%. MoE$_{lp}$ established through the mechanical grader in production provides a significantly better correlation (R^2=58%) against full-length tension strength from QC data than knot related parameters. The correlation between MoE$_{lp}$ and all strength properties - tension, beam shear, compression and bending strength were all strong (R^2=49% to 65%).

Conclusion

Low point of on-flat MoE (MoE$_{lp}$) established through a mechanical grader for each test piece in production provides a good correlation with all tested strengths (bending, tension, compression and beam shear). The correlation of tension strength with the MoE$_{lp}$ established by the mechanical grader in grading is significantly better than the correlation between strength and grading parameters evaluated using a number of different knot parameters. Using MoE$_{lp}$ for strength grading improves recovery of compliant lumber significantly over other available grading parameters particularly for the key grading discrimination at low grades; separating non-structural from structural product. Wespine are continuing to optimize grading processes and algorithms using MoE$_{lp}$ alone and in combination with other available grading parameters, whilst continuing to pursue best possible value-recovery with compliant product.

Acknowledgments

Thanks to everyone at Wespine for making its production and QC systems together with data available for analysis and presentation in this paper. A particular thanks to Mark Stubbs QC Supervisor.

References

Bailleres, H., G. Hopewell, G. Boughton and L. Brancheriau (2012). "Strength and stiffness assesssment technologies for improving grading effectiveness of radiata pine wood." Bioresources **7**: 1264-1282.

Boughton, G. and P. Juniper (2010). Revision of Australian MGP Stress Grades 2009. 11th World Conference on Timber Engineering, WCTE**:** 41 to 46.

Standards Australia (2010). AS 1720.1-2010 Timber structures Part 1: Design methods, Standards Australia.

Standards Australia (2010). AS/NZS 4063.1:2010 Characterization of structural timber - Part 1: Test methods, Standards Australia.

Standards Australia (2011). AS/NZS 1748.1:2011 Timber - Mechanically stress-graded for structural purposes Part 1: General requirements, Standards Australia.

Challenges and Opportunities Toward the Use of Hardwood Species in Glued-Laminated Timber in Canada

Alexandre Morin-Bernard
Renewable Materials Research Center, Department of Wood and Forest Sciences, Laval University, Quebec, QC, Canada, alexandre.morin-bernard.1@ulaval.ca

Alexis Achim
Renewable Materials Research Center, Department of Wood and Forest Sciences, Laval University, Quebec, QC, Canada, alexis.achim@sbf.ulaval.ca

Pierre Blanchet
Industrial Research Chair on Eco-Responsible Wood Construction, Department of Wood and Forest Sciences, Laval University, Quebec, QC, Canada, pierre.blanchet@sbf.ulaval.ca

Abstract

Multiple challenges have limited the use of hardwood species in load-bearing applications in Canada. Yet, timber from those species offers the potential to manufacture products with outstanding strength. A recent project assessing the technical feasibility of glued-laminated timber made from hardwood species highlighted some of the reasons for their limited use. Strength grading of these species remains a major challenge, partly because of their complex and variable anatomical structure. While machine grading methods developed for softwoods are applicable to hardwoods, they lead to a conservative use of the resource. Developing processing parameters adapted to these species also represents a challenge for which recent research efforts have brought potential solutions. Glulam products made from hardwood species with mechanical properties equivalent to available softwood products represent a promising and high value-added outcome for undervalued species, but it appears essential to also offer products taking fully advantage of the higher strength of hardwood species.

Keywords: engineered wood products, glued-laminated timber, hardwoods, strength grading

Introduction

In a context where limiting the ecological footprint of the built environment has become a priority, wood has gradually established itself as the structural material best able to fulfill this task. In the province of Quebec, Canada, the market share of wood as the main structural material in commercial, industrial and multi-residential buildings under five floors rose from 15% in 2007 to 31% in 2018, and reached 44% when including hybrid structural systems (Cecobois 2019). Glued-laminated timber (glulam) is one of the most widespread structural engineered wood products, and is used in both light frame construction and post and beam systems. Glulam products are traditionally composed of softwood species, but there is also a sustained interest toward using hardwood species.

In 1985, the American Institute of Timber Construction has adopted a standard, updated in 1996, which allows the manufacture of structural glulam from various hardwood species, visually or machine graded

(AITC 119-96, 1996). In Europe, the work of Egner and Kolb (1966) demonstrated the possibility of using European beech timber (*Fagus sylvatica* L.) for the production of structural glulam. In recent decades, many studies have investigated the mechanical properties of such products, and since 2009, several technical approvals have been issued for products using European beech and oak (*Quercus robur* L., *Quercus petraea* (Matt.) Liebl.), as well as chestnut (*Castanea sativa* Mill.).

Yet, for the time being, no standards or technical approval allow the use of hardwood species in glulam in Canada. In 2018, we initiated a project aiming to assess the technical feasibility of glulam made from yellow birch (*Betula alleghaniensis* Britt.) and white ash (*Fraxinus americana* L.). This project included shear tests to assess the performance of different structural adhesives systems and tensile strength tests aiming to identify indicating properties allowing the strength grading of these species (Morin-Bernard et al. 2020a, 2020b). The project also aimed to identify the optimal geometric characteristics for the finger joints and to carry out preliminary bending tests on full-size beams (Morin-Bernard et al. 2021). Results confirmed the potential of the investigated species for load-bearing applications, but also revealed important challenges that will need to be addressed before northern hardwood species become widely used in Canadian glulam products. Here, we propose an overview of the opportunities and technical challenges toward the use of hardwood species in glued-laminated timber in Canada, with a focus on the importance of a dedicated strength grading method for an efficient and economically viable use of the resource.

Canadian hardwood lumber: an underutilized resource

Throughout Canada, the proportion of the allowable annual cut (AAC) in hardwood species that is actually harvested averaged only 46.4% for the 2013-2018 period (Natural Resources Canada 2021). Data from the province of Quebec are consistent with this assessment, with only 52.1% of the hardwood's AAC that was harvested during the same period. For Quebec alone, those unharvested volumes represent 12 947 093 m^3 over a five year period, and even reaches 17 739 138 m^3 when including aspen species (MFFP 2019). Birch is the species group for which the ratio of the harvest to AAC is the lowest, with only 21% of the AAC harvested between 2008 and 2013. The harvest ratio was slightly higher for the maple species, with an average of 42% of AAC actually harvested (Fig. 1; Durocher et al. 2019).

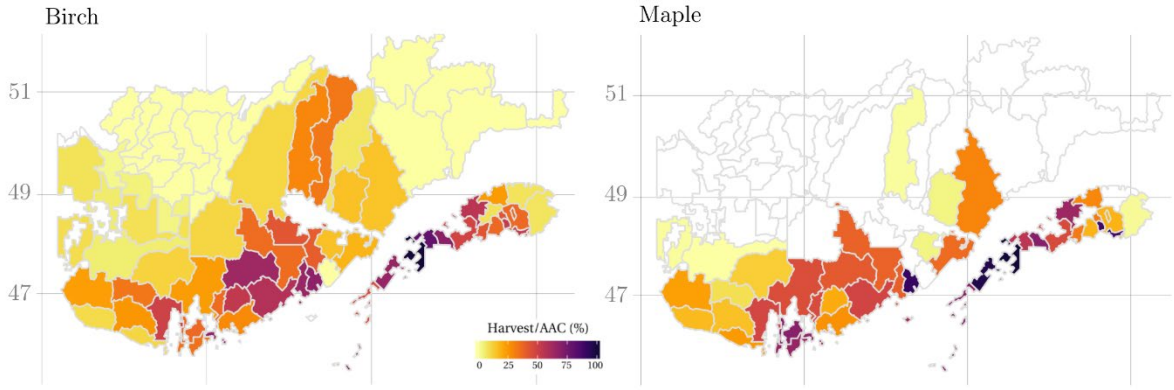

Figure 1 – Ratio of harvested volume over allowable annual cut for birch and maple in Quebec. Adapted from (Durocher et al. 2019)

Opportunities for hardwood lumber in load-bearing applications

Historically, the low utilization of hardwoods in structural applications was attributed to the low profit margins for commodity lumber and low market acceptance (Ross and Erickson 2020). With the increased interest in high value-added products such as structural engineered wood products, there is now a potential to overcome these issues. Manufacturing glulam would provide a high value-added outcome for hardwood lumber, in addition to making possible the use of smaller, lower quality timber that would have been less

interesting for the production of factory lumber. The interest of architects and engineers for wood as a building material is also a factor that can promote a greater use of hardwood species. Several studies have shown that building designers tend to choose wood products because of their aesthetics (Gaston 2014; Laguarda Mallo and Espinoza 2015; Markström et al. 2018). To that end, the noble and distinctive appearance of hardwoods, which favored their use in appearance products, could also foster their use in structural applications. This is especially true in the current context, where architects are increasingly making structural elements apparent.

The Challenging Task of Grading Hardwoods for Strength

Most Canadian hardwood species have, at least on paper, the mechanical properties required for load-bearing applications, with strength and stiffness values superior to most softwood species (Jessome 1977). However, one of the main challenges limiting their use in structural applications lies in the difficulty to efficiently use this potential through strength grading. Current grading standards for hardwood species are based on the appearance and on the possibility of manufacturing certain products rather than on their mechanical resistance (NHLA 2019). A machine grading approach appears essential for an efficient use of the resource. In the United States, the first grading methods allowing to use hardwoods in structural applications relied mainly on visual grading, which resulted in an inefficient use of the resource (Green and McDonald 1993). It has been demonstrated that despite fundamental anatomical differences with softwoods, it is possible to grade hardwood lumber using the machine grading procedures developed for softwoods, and this can result in a significant increase in structural lumber yield compared to visual grading alone (Green et al. 1994). Yet, this approach remains conservative, preventing from taking full advantage of the properties of hardwood species, due to fundamental differences with softwoods in the relationships between their different mechanical properties.

Distinct Property Relationships

While hardwood species have the potential to reach considerably higher strength classes than softwoods, they generally show a greater variability in their mechanical properties (Ehrhart et al. 2016; Green et al. 1994). The interrelationships between the properties of several hardwood species also appear to be different to those of softwoods (Sarnaghi et al. 2017). Most hardwood species have a higher bending strength for a given modulus of elasticity. However, this advantage could be offset by a lower correlation between bending strength and modulus of elasticity, as confirmed by studies on both North American (Green et al. 1994) and European (Ravenshorst 2015) hardwood species. Yet, this would not be the case for all species. Tests on American red oak lumber showed that the coefficient of determination between MOE and MOR (0.46) was close to that of coniferous species such as Southern pine, Douglas-fir and Hem fir (0.46 – 0.56). In contrast, species such as yellow poplar and trembling aspen appear to have a much weaker relationship ($0.25 < r^2 > 0.30$) between stiffness and strength (Green and McDonald 1993). This reality was accounted for in the European standard EN 338 (2016), which provides different strength classes for hardwoods, characterized by a lower MOE for a given MOR. This standard allows the grading of hardwoods to a characteristic bending strength reaching 80 MPa, compared to a maximum of 50 MPa for softwoods. These classes therefore consider the different property profiles of hardwoods compared to softwoods, although some hardwoods such as chestnut are instead classified according to softwood strength classes because of their similar behavior (Brunetti et al. 2019; Ridley-Ellis et al. 2016).

All of the above-mentioned strength classes are based on bending strength. Yet, when lumber is used for the manufacture of glulam, it is the tensile strength in the outer tension zone of the beam that is the determinant driver of beam strength (Brandner and Schickhofer 2008; Colling 1990). When using pieces sorted in bending grades to manufacture glulam, tension strength has to be estimated from bending strength using conservative relationships (Ridley-Ellis et al. 2016). This has led to the development of softwood tensile strength classes in European standard EN 338 (2016), which are directly based on tensile

tests. European glulam standard EN 14080 (2013) provides predefined glulam beam lay-ups specifying the required tensile strength classes of lamellae required to reach the targeted bending strength. For hardwood species, the development of strength classes based on tensile tests thus appears relevant. Indeed, several studies have revealed that for a given MOE, the ultimate tensile strength (UTS) of hardwoods would be, like MOR, higher than that of softwoods (Glos and Denzler 2006; Solli 2004). Recently, work conducted on European beech and European ash (*Fraxinus excelsior* L.) proposed new tensile strength classes for these species (Kovryga et al. 2020a). Considering the different property profiles of these species allowed reaching a characteristic tensile strength of 50 MPa, which is a modest yet significant improvement from the maximum characteristic tensile strength of the highest hardwood bending strength class of 48 MPa. Lamellae with such tensile strength allows the manufacture of glued-laminated timber beams of the GL48 class (Porteous and Kermani 2013).

Differences in the influence of knots, slope of grain and density

Most current strength grading procedures, such as machine stress rated (MSR) lumber, are based on a combination of machine grading followed by a visual inspection to ensure that strength reducing defects are kept within allowed limits for a given grade (Bendtsen and Youngs 1981; Ridley-Ellis et al. 2016). A common practice for softwood grading for structural purposes is to use the general slope of grain as an indicating property. Local grain deviations are accounted for indirectly, through the displacement of the cross section caused by knots and associated local grain deviation (ASTM 2011; Frühwald and Schickhofer 2005). While failure of softwood lumber is almost always initiated from knots, it is not the case for tropical hardwoods, because timber from these species often have very few or no knots (Ravenshorst 2015). Temperate hardwood species could be an intermediate case, since knots in hardwoods are less prevalent than in softwoods, especially in higher grades, but still generate strong local grain deviations when present. Fiber patterns around knots in hardwoods appear to be less uniform and less predictable than in softwoods (Sarnaghi et al. 2017). This is in line with what we experienced when investigating the most relevant indicating properties to predict the tensile of white ash and yellow birch timber. In the final models, one of the most powerful indicating properties was the maximum local grain deviation (Morin-Bernard et al. 2020a), while the general slope of grain, measured on various lengths, was a very weak predictor of tensile strength, as also revealed by studies on European hardwood species (Brunetti et al. 2019). The maximum local grain deviation was closely related to the UTS through the Hankinson equation, as revealed when plotting the measured UTS against the maximum local grain deviation (Fig. 2).

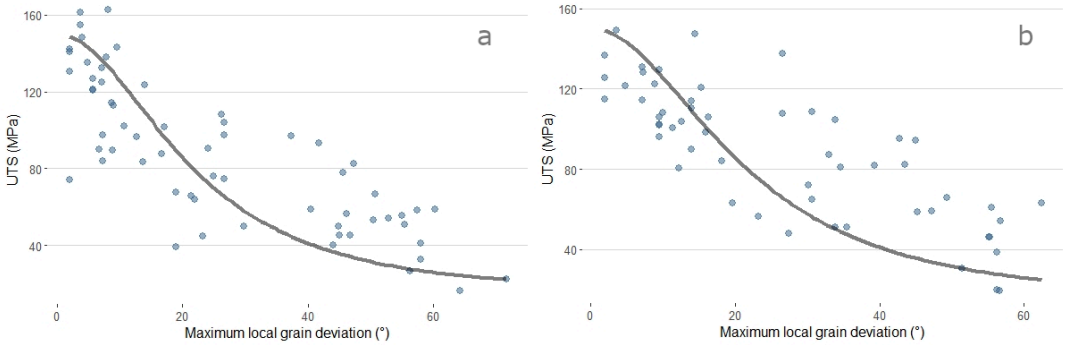

Figure 2 – Ultimate tensile strength of white ash (a) and yellow birch (b) lamellae as a function of the maximum local grain deviation. Dot represents observations and the solid line represents the predicted behavior using the Hankinson equation.

While we succeeded in visually assessing the local grain deviations in a research context, such task can be quite challenging in practice as this task is time consuming (Bollmus et al. 2017; Frühwald and Schickhofer 2005; Ravenshorst 2015). When a radial surface was present, we obtained satisfactory results

using the growth rings boundaries to determine the angle of the grain, as proposed by Koehler (1960). However, it was not possible to use this method for all specimens, which necessitated the use of a magnifying glass, a scribe and even required observation of the failure pattern. Alternative and more technologically advanced methods have been proven effective for some hardwood species, namely the tracheid effect, electrical field strength measurement, microwave scanning and transverse ultrasound scanning. What emerges from the studies carried out on the subject is the difficulty to identify a single method that would be universally applicable to all temperate hardwood species. For instance, Schlotzhauer et al. (2018) showed that the tracheid effect could be used on maple, basswood and to a lesser extent birch, but was not applicable to oak. For the latter, the electrical field strength system and the microwave scanning provided good results. For beech, the electrical field measurement method offered good results. However, none of these three methods, neither transverse ultrasound scanning, provided conclusive results on ash (Kovryga et al. 2020b). As a solution, it was proposed that, for some species, especially those belonging to the tropical hardwoods and softwoods groups, the influence of the slope of grain could be accounted for by only measuring the MOE (Ravenshorst 2015). However, as our results highlighted, the relationship between MOE and UTS appears to be relatively weak for temperate hardwood species, and there was no statistically significant relationship between the MOE and the maximum local grain deviation.

Processing related challenges and strength potential of full-scale beams

Our work on hardwood glulam also highlighted challenges related to the processing of timber into the finished product. The shorter fibers of hardwoods, along with their thicker cell walls and small lumen hinders the movement of fluids, such as adhesives, in the radial and tangential directions, more than in the case of softwoods (Bandel 1995; Ross 2010; Sellers 1988). For face bonding of lamellae, we succeeded in reaching high shear strength and wood failure in dry conditions (Morin-Bernard et al. 2020b). However, resistance to delamination in wet conditions is still a major challenge, mainly because dimensional changes in hardwoods in reaction to moisture content changes are greater than for softwood species, even at the same density (Ammann et al. 2016; Lehmann et al. 2018). Only few available adhesive systems can fulfill the delamination requirements included in glued-laminated timber standards, making machining parameters a critical element (Jiang et al. 2014). Surface preparation is also critical for finger jointing. Our tensile test campaign on finger jointed ash and yellow birch lamellae resulted in very low wood failure with yellow birch, a diffuse porous hardwood, mainly because of a poor adhesive penetration. With white ash, a ring porous species, higher wood failure levels were reached, because of an easier penetration of the adhesive in the large earlywood vessels (Morin-Bernard et al. 2021). However, the penetration of the adhesive was very superficial, or even non-existent, in the latewood portion of the growth rings, causing a discontinuity of the bondline, as revealed by X-ray tomography images of the finger joints (Fig. 3). This is a key issue because the width of the ring and any variation in the earlywood to latewood ratio will therefore affect the joint strength.

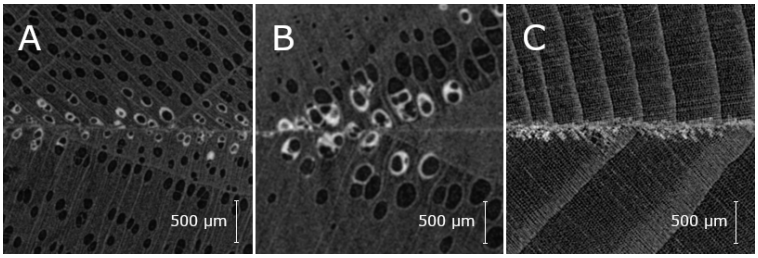

Figure 3 – Adhesive penetration at a finger joint bondline on white ash (A), yellow birch (B) and spruce (C) (Morin-Bernard et al. 2021)

In our preliminary bending tests on full-scale beams, these issues resulted in failure initiated in one of the finger joints located in the outermost lamellae in the tension-stressed side of the beams. The glulam

elements, with cross-section dimensions of 130 x 243 mm, still achieved a strength of around 40 MPa for yellow birch and 47 MPa for white ash (Morin-Bernard et al. 2021). It is impossible to derive a 5th percentile bending strength from the very limited number of beams tested, but these results are promising for beams that were manufactured in industrial conditions without extensive optimization of the processing parameters. For comparison purposes, the 5th percentile strength of the highest grade of softwood glulam available in Canada, once adjusted to the same dimensions is 37.03 MPa. Additional research efforts will be required to determine the appropriate manufacturing parameters for the species available in Canada, but the results obtained with European species suggests that this is quite achievable.

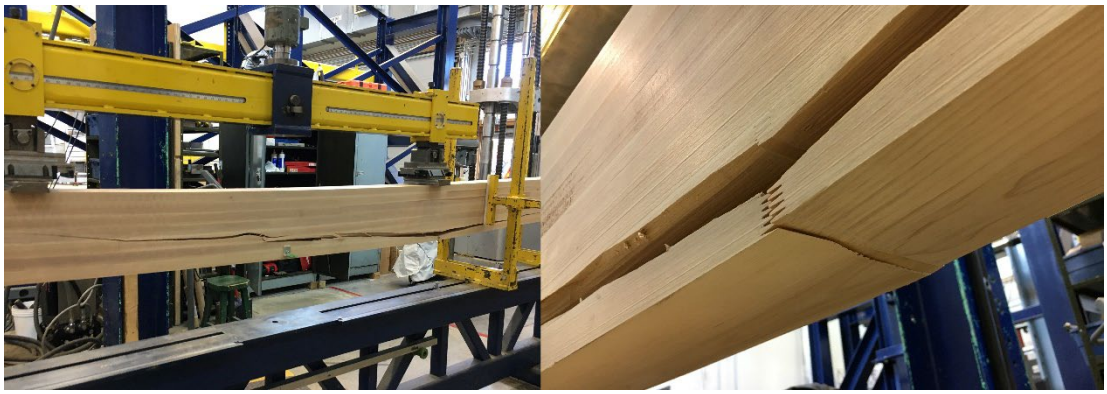

Figure 4 – Failure of yellow birch glulam beam initiating at a finger joint located in the bottom lamellae (Morin-Bernard et al. 2021)

In the United States, the highest strength class (24F-E2) of hardwood glued-laminated timber permitted in AITC 119-96 (1996) reaches comparable strength, with a 5th percentile bending strength of 36.37 MPa, once adjusted to the moisture content and dimensions of the beams tested in our project. Glulam products made from European beech timber can, however, reach much higher strength classes, with a 5^{th} percentile bending strength of 52.80 MPa, when adjusted to cross-section dimensions of 130 x 243 mm.

Beyond the bending strength, it is the potential stiffness properties of products made from hardwood species that are remarkable. Indeed, stiffness is frequently the limiting factor in the design of timber structures, because the deflection of floors must be kept within acceptable limits. Although glulam beams made from white ash and yellow birch achieved strengths comparable to products made from softwood species, the use of high-quality lamellae made it possible to achieve MOE values of 15 078 MPa for ash and over 16 000 MPa for yellow birch. These values are comparable to the average stiffness of European GL48 beech glulam (15 100 MPa) and far exceed that of products manufactured in conformity with AITC 119-96 (1996), which would be, when adjusted to the moisture content and dimensions of the beams tested in our study, under 13 000 MPa.

Complementary approaches for an efficient and economically viable utilization of the resource

The interest toward the use of hardwood species in glulam in the USA during the 1990s was driven by a concern for rationally using the resource, finding outcomes for lumber of all grades. The research that led to the publication of AITC 119-96 was initially focused on the production of glulam for bridge construction. Less importance is thus given to appearance, and more defects such as knots and grain deviations are accepted, especially in the central portion of the beams (Manbeck et al. 1996). Some bridges were even built from glulam whose lamellae were taken from log heart cants (Janowiak 1995), with relatively low strength and stiffness due to juvenile wood attributes. In Europe, hardwood glued-laminated timber products were developed under different considerations. Most of the available hardwood glulams for which technical approvals have been emitted originate from research and development efforts

conducted by private industries aiming to develop high-end products designed for use in applications where appearance is critical. Using high quality lamellae allows reaching strength classes that would not be attainable with softwood lumber, and most importantly, higher stiffness values. Such high stiffness and strength widen the potential applications of glulam, making it even more competitive against alternative structural materials. By offering the possibility to reduce the cross-section of structural elements, resulting in less encroachment into the habitable area of a building, those products fit well within the current architectural trends seeking for slender geometries (Uzelac Glavinić et al. 2020).

We argue that combining both above-mentioned approaches is crucial to increase the use of hardwood species in Canadian glulam. The importance of finding outcomes for lower quality material is evident, and essential to ensure an efficient utilization of the resource. So is the need to fully exploit the high mechanical properties of some hardwood species. Considering the cost of high-quality hardwood lumber, it is crucial to offer products whose benefits match the additional expense. In combination with the interest from the noble and distinctive appearance of hardwoods, succeeding in offering hardwood glulam products with mechanical properties superior to that of softwood products would represent a winning combination, likely to convince even more building designers to turn to wood as a structural material.

Of course, the road will be paved with additional challenges, particularly related to the regulatory framework and the inertia of the wood-processing industry. For instance, most hardwood mills are not designed to produce dimension lumber, and not all softwood mills can process large diameter hardwood stems. Furthermore, until effective and economic strength grading methods are developed specifically for hardwoods, it is unlikely that glulam standards will include hardwood beam lay-ups allowing to exploit the full strength potential of these species. The best way forward will likely come from companies that may develop proprietary hardwood glulam products, as was the case in Europe. Such task would, however, require considerable investments to demonstrate the safeness of the products through full-scale test campaign with the Canadian Construction Materials Centre. Nevertheless, in a context where wood is increasingly used in construction and where hardwood species are broadly available, the interest toward their use in load-bearing applications is unlikely to fade away.

References

AITC. 1996. Standard specifications for structural glued laminated timber of hardwood species AITC 119-96. American Institute of Timber Construction.

Ammann, S.; Schlegel S.; Beyer M. [and others]. 2016. Quality assessment of glued ash wood for construction engineering. European Journal of Wood and Wood Products. 74(1): 67-74.

ASTM. 2011. Standard Practice for Establishing Structural Grades and Related Allowable Properties for Visually Graded Lumber ASTM D245. West Conshohocken, PA.: American Society for Testing and Materials.

Bandel, Alberto. 1995. Gluing wood. Catas.

Bendtsen, B.A.; Youngs R.L. 1981. Machine stress rating of wood: an overview. in Proceedings of the XVIIIUFRO World Congress, Kyoto, Japan.

Bollmus, S.; Gellerich, A.; Schlotzhauer, P. [and others]. 2017. Hardwood research at the Georg-August University of Goettingen. P. 116-122 in Proceedings of the 6th International Scientific Conference on Hardwood Processing. Natural Resources Institute Finland Helsinki, Finland.

Brandner, R.; Schickhofer, G. 2008. Glued Laminated Timber in Bending: New Aspects Concerning Modelling. Wood Science and Technology. 42(5): 401-25. doi: 10.1007/s00226-008-0189-2.

Brunetti, M.; Nocetti, M.; Pizzo, B. [and others]. 2019. Glued structural products made of beech wood: quality of the raw material and gluing issues. P. 230-42 in Proceedings of the 7th International Scientific Conference on Hardwood Processing.

Cecobois. 2019. Étude sur les parts de marché du matériau bois dans la construction non résidentielle de 4 étages ou moins au Québec.

Colling, F. 1990. Bending strength of glulam beams—a statistical model. Proc., Int. Union of Forest Res. Org., Group S5 2.

Durocher, C.; Thiffault, E.; Achim, A. [and others]. 2019. Untapped Volume of Surplus Forest Growth as Feedstock for Bioenergy. Biomass and Bioenergy. 120: 376-86. doi: 10.1016/j.biombioe.2018.11.024.

Egner, K.; Kolb, H. 1966. Geleimte Träger und Binder aus Buchenholz. Bau. Mit Holz. 68(4) :147-54.

Ehrhart, T.; Fink, G.; Steiger, R. [and others]. 2016. Strength grading of European beech timber for the production of GLT & CLT. P. 29-44 in International Network on Timber Engineering Research: Proceedings of Meeting 49. Vol. 49. Timber Scientific Publishing, KIT Holzbau und Baukonstruktionen.

EN 14080. 2013. Timber structures—glued laminated timber and glued solid timber—requirements. British Standards Institution (BSI), London, UK.

EN, BSIBS. 2016. 338: 2016: Structural Timber—Strength Classes. BSI Standards Publication: London, UK.

Frühwald, K.; Schickhofer, G. 2005. Strength grading of hardwoods. P. 198-210. in Proceedings of the 14th International Symposium on Nondestructive Testing of Wood. Eberswalde, Germany.

Gaston, C.W. 2014. Visual Wood Product Trends in North American Nonresidential Buildings. Forest Products Journal. 64(3-4): 107-15. doi: 10.13073/FPJ-D-13-00077.

Glos, P.; Denzler, J.K. 2006. Allocation of Central European hardwoods into EN 1912. in Proceedings of the CIB W. Vol. 18.

Green, D.W.; McDonald, K.A. 1993. Investigation of the mechanical properties of red oak 2 by 4’s. Wood and fiber science. 25(1): 35-45.

Green, D.W.; Ross, R.J.; McDonald, K.A. 1994. Production of hardwood machine stress rated lumber. P. 141-150 in Proceedings of 9th lnternational symposium on nondestructive testing of wood 1993, Madison, WI.

Janowiak, J.J. 1995. Efficient utilization of red maple lumber in glued-laminated timber beams. Vol. 541. US Department of Agriculture, Forest Service, Forest Products Laboratory.

Jessome, A.P. 1977. Résistance et propriétés connexes des bois indigènes au Canada. Laboratoire des produits forestiers de l’Est.

Jiang, Y.; Schaffrath, J.; Knorz, M. [and others]. 2014. Applicability of various wood species in glued laminated timber-Parameter study on delamination resistance and shear strength. in Proceedings of the World Conference on Timber Engineering WCTE 2014.

Koehler, Arthur. 1960. Guide to determining slope of grain in lumber and veneer.

Kovryga, A.; Sarnaghi, K.A.; van de Kuilen, J.W.G. 2020b. Strength Grading of Hardwoods Using Transversal Ultrasound. European Journal of Wood and Wood Products. 78(5): 951-60. doi: 10.1007/s00107-020-01573-2.

Kovryga, A.; Stapel, P.; van de Kuilen, J.W.G. 2020a. Mechanical properties and their interrelationships for medium-density European hardwoods, focusing on ash and beech. Wood Material Science & Engineering. 15(5): 289-302. doi: 10.1080/17480272.2019.1596158.

Laguarda Mallo, M.F.; Espinoza, O. 2015. Awareness, Perceptions and Willingness to Adopt Cross-Laminated Timber by the Architecture Community in the United States. Journal of Cleaner Production. 94: 198-210. doi: 10.1016/j.jclepro.2015.01.090.

Lehmann, M.; Clerc, G.; Lehringer, C. [and others]. 2018. Investigation of the bond quality and the finger joint strength of beech glulam. in Proceedings of the World Conference on Timber Engineering (WCTE 2018). Seoul, Republic of Korea.

Manbeck, H.B.; Janowiak, J.J.; Blankenhorn, P.R.; Labosky Jr., P. 1996. Standard designs for Hardwood glued-laminated highway bridges. Madison, Wisconsin 351-360.

Markström, E.; Kuzman, M.K.; Bystedt, A. [and others]. 2018. Swedish architects view of engineered wood products in buildings. Journal of Cleaner Production. 181: 33-41.

MFFP. 2019. Bilan quinquennal de l'aménagement durable des forêts 2013-2018 - Calcul et respect des possibilités forestières. https://mffp.gouv.qc.ca/documents/forets/amenagement/reddition-comptes/BilanQuinquennalADF.pdf. [Date accessed unknown].

Morin-Bernard, A.; Blanchet, P; Dagenais, C.; Achim, A.. 2020a. Strength grading of northern hardwood species for structural engineered wood products: Identification of the relevant indicating properties. BioResources. 15(4): 8813.

Morin-Bernard, A.; Blanchet, P.; Dagenais, C.; Achim, A. 2020b. Use of northern hardwoods in glued-laminated timber: A study of bondline shear strength and resistance to moisture. European Journal of Wood and Wood Products. 78(5): 891-903.

Morin-Bernard, A.; Blanchet, P.; Dagenais, C.; Achim, A. 2021. Glued-laminated timber from northern hardwoods: Effect of finger-joint profile on lamellae tensile strength. Construction and Building Materials. 271: 121591.

Natural Resources Canada. 2021. Indicateur : Volume récolté par rapport à l'approvisionnement en bois durable. https://www.rncan.gc.ca/nos-ressources-naturelles/forets/letat-forets-canada-rapport-annuel/bois-recolte-facon-durable/16495. [Date accessed unknown].

NHLA. 2019. Rules for the measurement and inspection of hardwood and cypress. National Hardwood Lumber Association. Memphis. TN.

Porteous, J.; Kermani, A. 2013. Structural timber design to Eurocode 5. John Wiley & Sons.

Ravenshorst, G.J.P. 2015. Species independent strength grading of structural timber.

Ridley-Ellis, D.; Stapel, P.; Baño, V. 2016. Strength Grading of Sawn Timber in Europe: An Explanation for Engineers and Researchers. European Journal of Wood and Wood Products. 74(3): 291-306. doi: 10.1007/s00107-016-1034-1.

Ross, R.J. 2010. Wood handbook: wood as an engineering material. USDA Forest Service, Forest Products Laboratory, General Technical Report FPL-GTR-190, 509p.

Ross, R.J.; Erickson, J.R. 2020. Undervalued hardwoods for engineered materials and components. General Technical Report FPL-GTR-276. Madison, WI: US Department of Agriculture, Forest Service, Forest Products Laboratory. 108 p. 276.

Sarnaghi, A.K.; Gard, W.F.; van de Kuilen, J.W.G. 2017. 3D FE-numerical modelling of growth defects in medium dense European hardwoods. P. 116-122 in Proceedings of the 6th International Scientific Conference on Hardwood Processing.

Schlotzhauer, P.; Wilhelms, F.; Lux, C.; Bollmus, S. 2018. Comparison of Three Systems for Automatic Grain Angle Determination on European Hardwood for Construction Use. European Journal of Wood and Wood Products. 76(3): 911-923. doi: 10.1007/s00107-018-1286-z.

Sellers, Terry. 1988. Gluing of eastern hardwoods: a review.

Solli, K.H. 2004. Tensile strength of Nordic birch. in Proceedings of Meeting Thirty-seven of CIB-W18, paper 37. Vol. 6.

Uzelac Glavinić, I.; Boko, I.; Torić, N.; Lovrić Vranković, J. 2020. Application of Hardwood for Glued Laminated Timber in Europe. Journal of the Croatian Association of Civil Engineers. 72(07): 607-616. doi: 10.14256/JCE.2741.2019.

Local Modulus of Elasticity by Constrained Optimization

Friend K. Bechtel
Kierstat Systems LLC, Mead, Washington, USA, fbechtel@ieee.org

Abstract

Machine stress rating (MSR) is generally accepted as the preferred production-line process in the grading of lumber for structural applications. The most widely used MSR machinery measures bending stiffness, and from stiffness, modulus of elasticity (*E*), on a sequence of bending spans along a wood board. Strength is inferred from its correlation with *E*. The advantages of estimating local modulus of elasticity (local *E*), particularly regarding strength inferences, have been discussed in the literature along with three local *E* estimation methods. Each uses a sequence of *E* measurements as input. The first employs the Fourier transform, the second a Kalman filter, and the third chooses from among an infinite number of solutions for an underdetermined set of linear equations. All three methods yield similar results, but the last may be the easiest to implement. The present work uses the third method to optimize the choice of solution from among the available solutions. A Lagrange multiplier approach minimizes a measure of local compliance variation (compliance *C* being defined as the reciprocal of *E*, i.e. $C = 1/E$) all while constraining the solution to satisfy the set of linear equations. This method makes much better use of the *E* measurement sequence than does the usual MSR measurement process. Graphs of local *E* from the same piece of lumber with the same sequence of bending *E* measurement data studied in previous work allow the conclusion that constrained optimization is a practical method for estimating local *E*. All indications point toward efficient and beneficial production-line implementation from software modifications in existing MSR equipment.

Some related, but unpublished, additional material may be obtained from references in the report FPL-GTR-280 by opening that document with Adobe Acrobat and selecting the boxes labeled supplemental material at the ends of those references.

Keywords: local *E*, modulus of elasticity, compliance, span function, lumber grading, MSR, constrained optimization, Lagrange multipliers

Introduction

The production of machine stress rated (MSR) lumber typically uses overlapping sequences of bending modulus of elasticity (*E*) measurements. Past work used these measurements to estimate local *E* on short length increments of lumber (Bechtel 1985, 2009; Bechtel et al. 2006, 2007a, 2007b; Foschi 1987; Lam et al. 1993; Pope and Matthews 1995). The bending span is usually about 900 to 1200 mm long, and each measurement of *E* is therefore a composite of the local *E* values within the span. As a board is displaced longitudinally relative to a bending span, the next *E* measurement in the sequence is a composite of most of the same local values but from an incrementally displaced position in the span. As a new local value enters the span at one end, another exits at the other end.

The arithmetic of previous and present work to estimate local *E* from the measured *E* sequence uses compliance as the reciprocal of modulus of elasticity because we recognized that measured compliance is the convolution of a "span function" with unknown local compliance values. Span function (Bechtel 2007)

is a weighting function that weights each local compliance within a bending span into a measured compliance result. As a board moves through the bending span, we relate each compliance measurement with a position along the board, noting that each measurement is a weighted combination of local values.

We write the sequence of measured compliances as a set of linear equations, one equation for each measurement in the sequence. There are fewer measurements, hence fewer equations, than unknown local compliance values because the first measurement in the sequence is taken when the center of the bending span is half the bending span length from the leading end of the board, and the last occurs half this distance from the trailing end. For a typical bending span system of supports, it has long been obvious that the local E (or compliance C) values near the leading and trailing ends of the span contribute little to a measurement. The span function quantifies the contribution amounts.

Fewer equations than unknowns, leads to an infinite number of solutions in a manifold of solutions. We can obtain a unique solution by adding to the number of equations. One approach adds equations by requiring local compliance values near ends of the board to have the same value. Another would make additional measurements with different machine types having different span functions; thereby increasing the number of equations. So long as the span functions of the added equations satisfy conditions of linear independence from the existing span functions, this method can reduce the dimensionality of the solution space and yield improved results. Defining a bending span that would weight local compliance values more heavily near span ends would be ideal.

Instead of the above possibilities for adding equations, we use here the method of Lagrange Multipliers (Kaplan 1952) to choose a "best" solution from among the infinite number of available solutions. We treat the equations as constraints and minimize a function of the local compliances.

Compliance equations (the constraints)

Consider the length of a board to be regularly subdivided into n local length increments, each associated with a local compliance. The set of linear equations to solve is (Bechtel 2009):

$$\begin{aligned} h(p)C(1) + h(p-1)C(2) + \cdots + h(1)C(p) &= C_{\mathrm{M}}(1) \\ h(p)C(2) + h(p-1)C(3) + \cdots + h(1)C(p+1) &= C_{\mathrm{M}}(2) \\ &\vdots \\ h(p)C(n-p+1) + h(p-1)C(n-p+2) + \cdots + h(1)C(n) &= C_{\mathrm{M}}(m) \end{aligned} \tag{1}$$

Each of the m measurements, $C_{\mathrm{M}}(\cdot)$, is a weighted combination of the local compliances, $C(1)$, $C(2)$, . . . , $C(n)$ where we call the weights $h(1)$, $h(2)$, . . . , $h(p)$ span weights. The span weights, which sum to one, correspond to local increments of the bending span adjacent the board during the measurement. In Eqs. (1), there are n local compliances along the board, p span weights and m measurements. Span weights outside the span have zero values and may be omitted from the equations. We obtain span weights as discretized versions from a bending span function (Bechtel 2007), and these determine how much each local compliance contributes to a measurement. In some production-line machines (Bechtel and Allen 1995, Metriguard 2007), the number of bending span support points, and hence the span function along with the span weights, changes with board position relative to the span. This is a result of multiple rollers at span ends where leading and trailing ends of a board engage a different number of rollers (supports) as the board moves through the machine. Consequently, the span weights may differ in each of the m equations of Eqs. (1). That adds notational and bookkeeping complexity but does not affect the ideas we present here. For simplicity of presentation, and without loss of generality in the approach, we now restrict discussion to simply-supported, center-loaded bending spans. In this case, the span functions (and hence span weights) are identical for each measurement, and they remain unchanged other than in position from one equation to the next. The notation of Eqs. (1) is sufficient, and we can write the equations in matrix form as:

$$\boldsymbol{HC} = \boldsymbol{C}_{\mathrm{M}} \tag{2}$$

where the (m,n)-dimensional "span matrix" $\boldsymbol{H}$**,** the n-dimensional local compliance vector $\boldsymbol{C}$, and the m-dimensional measured compliance vector $\boldsymbol{C}_{\mathbf{M}}$ are defined as:

$$\boldsymbol{H} = \begin{bmatrix} h(p) & h(p-1) & \cdots & h(1) & 0 & \cdots & \cdots & 0 \\ 0 & h(p) & h(p-1) & \cdots & h(1) & 0 & \ddots & \vdots \\ \vdots & \ddots & \ddots & \ddots & \ddots & \ddots & \ddots & \vdots \\ \vdots & \ddots & 0 & h(p) & h(p-1) & \cdots & h(1) & 0 \\ 0 & \cdots & \cdots & 0 & h(p) & h(p-1) & \cdots & h(1) \end{bmatrix}, \quad \boldsymbol{C} = \begin{bmatrix} C(1) \\ C(2) \\ \vdots \\ C(\mathrm{n}) \end{bmatrix}, \quad \boldsymbol{C}_{\mathrm{M}} = \begin{bmatrix} C_{\mathrm{M}}(1) \\ C_{\mathrm{M}}(2) \\ \vdots \\ C_{\mathrm{M}}(\mathrm{m}) \end{bmatrix} \tag{3}$$

Entries in the j^{th} row of $\boldsymbol{H}$ are the p span weights of the span function used for the j^{th} measurement, arranged in reverse order, and shifted so that they multiply the correct local compliance values. The reversal is a result of the discrete convolution wherein the leading end of a board with local compliance $C(1)$ multiplies the last span function weight $h(p)$ in the span and then leaves the span.

Solution by method of Lagrange multipliers

The set of linear equations, Eqs. (1) or (2), is under-determined, i.e., there are more unknown local compliances than there are measurements ($n > m$). Then, there exists an infinite number of solutions to Eq. (2). A careful look at Eqs. 2 and definitions (3) reveals that $n = m + p$ -1, assuming there are an odd number p of increments in the test span.

Subject to the constraint $\boldsymbol{HC}$ - $\boldsymbol{C}_{\mathbf{M}} = \mathbf{0}$, which identifies the family of solutions, we minimize a scalar function of the local compliances.

As part of the scalar function definition, let $\boldsymbol{A}$ be an estimate of the n-dimensional mean vector for the unknown local compliance vector $\boldsymbol{C}$. While the mean vector is unknown, there is no reason to believe that any component of it would vary from any other. Because each measured compliance is a weighted average of the local compliances, a good estimator for each component is the sample mean of the components of $\boldsymbol{C}_{\mathbf{M}}$. Thus, the estimator $\boldsymbol{A}$ for the mean is taken as:

$$\boldsymbol{A} = \left(\frac{1}{m} \sum_{i=1}^{m} \boldsymbol{C}_{\mathrm{M}}(i) \right) [1 \quad 1 \quad \cdots \quad 1]^{\mathrm{T}} \tag{4}$$

where " T " indicates matrix transpose so that $[1 \quad 1 \quad \cdots \quad 1]^{\mathrm{T}}$ is an n-dimensional vector of ones. Let us assume that a reasonable covariance matrix for the local compliance vector $\boldsymbol{C}$ is the symmetric Toeplitz matrix $\boldsymbol{W}$, where:

$$\boldsymbol{W} = \sigma^2 \boldsymbol{R} \qquad \text{and} \qquad \boldsymbol{R} = \begin{bmatrix} 1 & \mathrm{r} & \mathrm{r}^2 & \cdots & \mathrm{r}^{n-1} \\ \mathrm{r} & 1 & \mathrm{r} & \ddots & \vdots \\ \mathrm{r}^2 & \mathrm{r} & 1 & \ddots & \mathrm{r}^2 \\ \vdots & \ddots & \ddots & \ddots & \mathrm{r} \\ \mathrm{r}^{n-1} & \cdots & \mathrm{r}^2 & \mathrm{r} & 1 \end{bmatrix} \tag{5}$$

The parameter σ^2 is the variance of each component of local compliance vector $\boldsymbol{C}$**,** and r is a correlation coefficient relating adjacent components of $\boldsymbol{C}$. Assumptions in Eqs. (5) are reasonable because they allow the components of $\boldsymbol{C}$ to be less closely correlated the farther they are apart. As will become apparent, the results are insensitive to r. The result does not depend on the variance σ^2 , and we do not discuss it further. We define the following scalar quadratic function of $\boldsymbol{C}$ and proceed to minimize it with respect to $\boldsymbol{C}$.

$$(\boldsymbol{C} - \boldsymbol{A})^{\mathrm{T}} \boldsymbol{W}^{-1} (\boldsymbol{C} - \boldsymbol{A}) \tag{6}$$

All values of $\boldsymbol{C}$ for which quadratic (6) is constant define the surface of an ellipsoid in n-dimensional space about the mean vector $\boldsymbol{A}$. We minimize this quadratic expression while satisfying Eq. (2) by using the method of Lagrange multipliers. This has the effect of minimizing the variation among the local compliance components of $\boldsymbol{C}$ while at the same time satisfying Eq. (2). We form the Lagrangian:

$$(\boldsymbol{C}-\boldsymbol{A})^{\mathrm{T}}\boldsymbol{W}^{-1}(\boldsymbol{C}-\boldsymbol{A})-\boldsymbol{\gamma}^{\boldsymbol{T}}(\boldsymbol{HC}-\boldsymbol{C}_{\mathrm{M}}) \tag{7}$$

$\boldsymbol{\gamma}$ is an m-dimensional vector of Lagrange multipliers. Set the gradient of the Lagrangian to zero.

$$2\boldsymbol{W}^{-1}(\boldsymbol{C}-\boldsymbol{A})-\boldsymbol{H}^{\mathrm{T}}\boldsymbol{\gamma}=\boldsymbol{0} \tag{8}$$

Solve Eq. (8) for $\boldsymbol{C}$:

$$\boldsymbol{C}=\frac{1}{2}\boldsymbol{W}\boldsymbol{H}^{\mathrm{T}}\boldsymbol{\gamma}+\boldsymbol{A} \tag{9}$$

Substitute Eq. (9) into Eq. (2) and solve for $\boldsymbol{\gamma}$:

$$\boldsymbol{\gamma}=2\left(\boldsymbol{HWH}^{\mathrm{T}}\right)^{-1}(\boldsymbol{C}_{\mathrm{M}}-\boldsymbol{HA}) \tag{10}$$

The inverse operation of Eq. (10) is allowed because we assume that the matrix $\boldsymbol{H}$ in def. (3) has rank m, a reasonable assumption if the bending span and span weights $h(\cdot)$ are typical of MSR production machinery.

Use Eq. (10) in Eq. (9) to obtain:

$$\boldsymbol{C}=\boldsymbol{W}\boldsymbol{H}^{\mathrm{T}}\left(\boldsymbol{HWH}^{\mathrm{T}}\right)^{-1}(\boldsymbol{C}_{\mathrm{M}}-\boldsymbol{HA})+\boldsymbol{A} \tag{11}$$

Finally, use Eq. (5) in Eq. (11) to cancel out the variance σ^2 :

$$\boldsymbol{C}=\boldsymbol{R}\boldsymbol{H}^{\mathrm{T}}\left(\boldsymbol{HRH}^{\mathrm{T}}\right)^{-1}(\boldsymbol{C}_{\mathrm{M}}-\boldsymbol{HA})+\boldsymbol{A} \tag{12}$$

Results

We used data from a previously studied 38 mm x 89 mm x 4500 mm piece of Douglas Fir lumber, selected for its large knots (Bechtel 2009). The compliance vector $\boldsymbol{C}_{\mathbf{M}}$ is from a sequence of 73 measurements on overlapping bending spans spaced 50 mm apart longitudinally. The apparatus had a simply-supported, center-loaded bending span 900 mm long. In this case, the vector and matrix size parameters in Eqs. (3) are m = 73, p = 19, and n = 91. We used the vector $\boldsymbol{C}_{\mathbf{M}}$ as input to Eq. (12); but, from Eq. (4) note that the entry for $\boldsymbol{A}$ also depends on $\boldsymbol{C}_{\mathbf{M}}$. Fig. 1 illustrates local E we obtained by taking the component-by-component reciprocal of $\boldsymbol{C}$. To combat the noise, obvious in Fig. 1, we locally filtered the measured compliances in $\boldsymbol{C}_{\mathrm{M}}$ and then applied Eq. (12) to the filtered $\boldsymbol{C}_{\mathbf{M}}$ to obtain the result in Fig. 2. We used the same filter (a Gaussian blur) as in the previous work and denote the filtered $\boldsymbol{C}_{\mathbf{M}}$ by $\boldsymbol{C}_{\mathbf{Mf}}$ to distinguish it from $\boldsymbol{C}_{\mathbf{M}}$.

In Figs. 1 and 2, r = 0.97. In Figs. 3 and 4, computations are identical to those of Fig. 2 except that r = 0 and r = 0.9 respectively. We observe only small differences from the result in Fig. 2 at the beginnings and ends of the computed local E curves. There are no discernable differences for r values larger than 0.97 until r is quite close to 1, and the matrix $\boldsymbol{R}$ is close to singular giving false results due to computational issues.

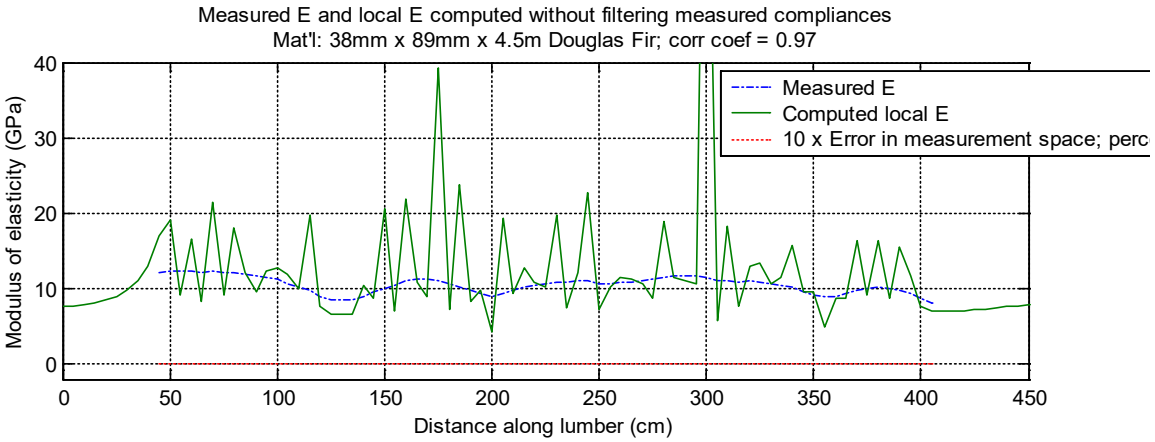

Figure 1. Measured E_M and computed local E without filtering measured compliances.

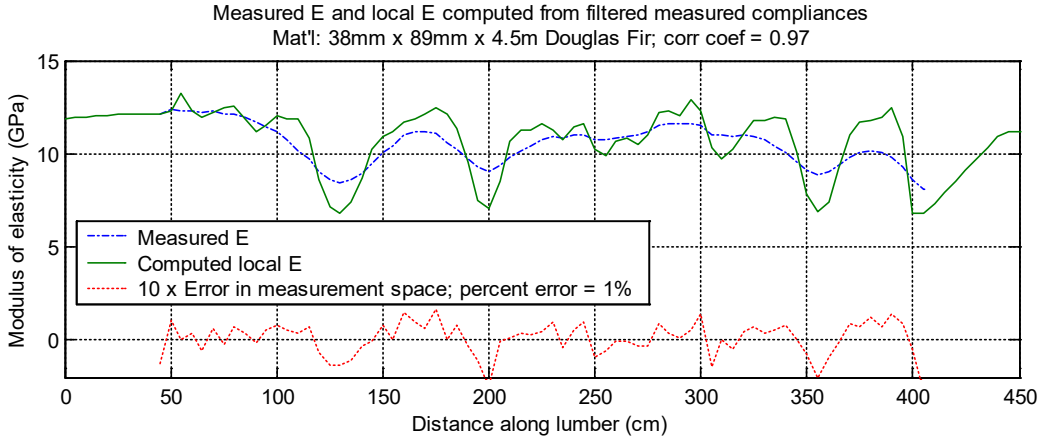

Figure 2. Measured E_M and computed local E after first filtering measured compliances.

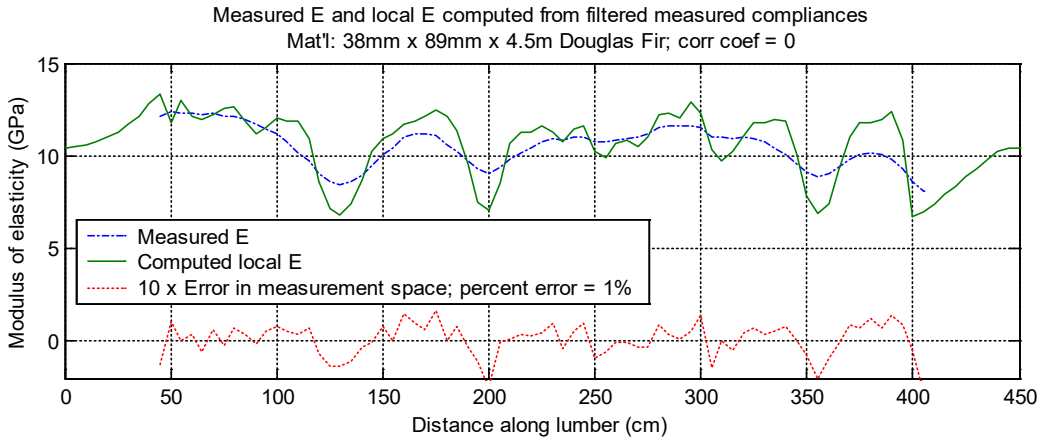

Figure 3. Same as Fig. 2, but with correlation coefficient = 0.

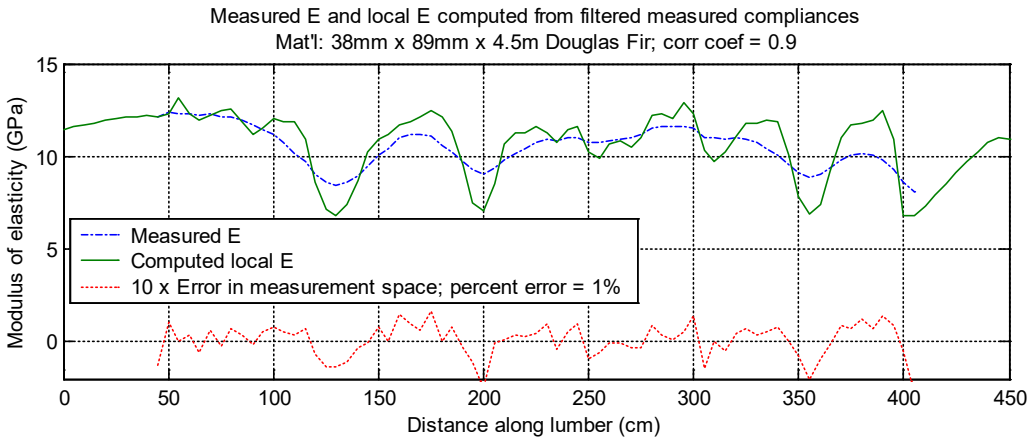

Figure 4. Same as Fig. 2, but with correlation coefficient = 0.9.

We set r = 0.97, and explored further the effect of filtering. It is a simple matter to pass the filtered measured compliance data through the filter again, and Fig. 5 shows the result.

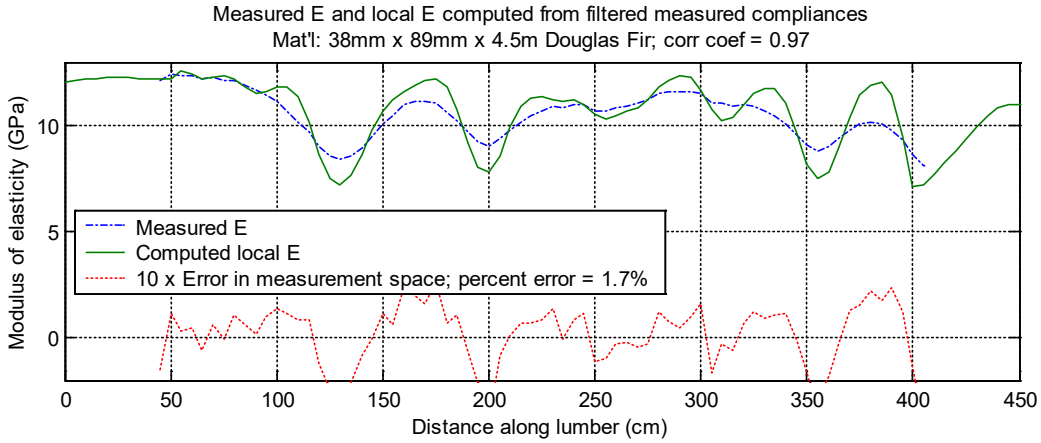

Figure 5. Same as Fig. 2, but measured compliances are passed twice through the filter.

Computed local *E* in Fig. 5 is smoother than for Fig. 2. Continuing in this manner, Fig. 6 shows the result of passing the measured compliance seven times through the filter before computing local *E*.

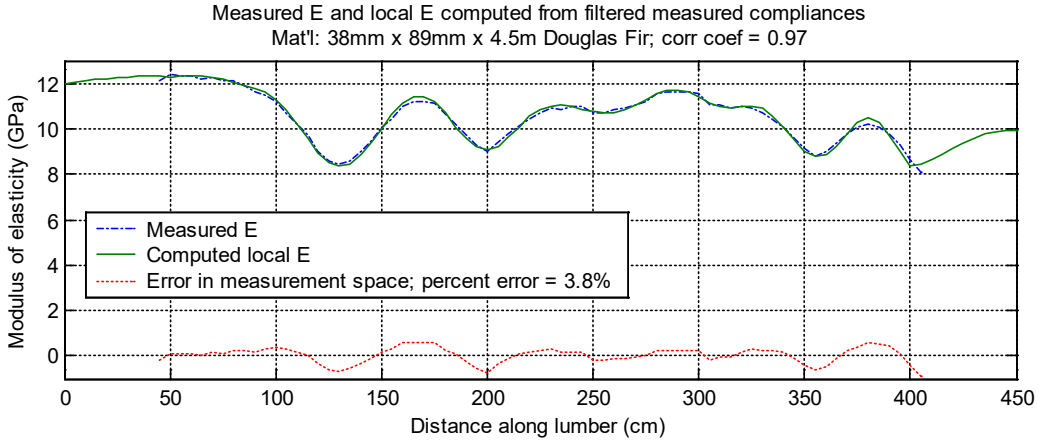

Figure 6. Same as Fig. 2, but measured compliances are passed seven times through the filter.

For Figs. 5 and 6, we do not actually pass the measured data through the filter multiple times, but the result is the same as if we had.

Because matrix $\boldsymbol{H}$ has rank m, both the m-dimensional vectors $\boldsymbol{C}_{\mathbf{M}}$ and $\boldsymbol{C}_{\mathbf{Mf}}$ must be in the column space of matrix $\boldsymbol{H}$. Therefore, both the local compliance vector $\boldsymbol{C}$ we obtain by using $\boldsymbol{C}_{\mathbf{M}}$ as input to Eq. (12) and the local compliance vector $\boldsymbol{C}_{\mathbf{f}}$ we obtain with filtered $\boldsymbol{C}_{\mathbf{Mf}}$ as input to Eq. (2) satisfy the equation. However, the unavoidable small quantization and other measurement noise errors in $\boldsymbol{C}_{\mathbf{M}}$ are amplified in the computations and give the unreasonable result of Fig. 1. We argue, therefore, that because of the noise, $\boldsymbol{C}_{\mathbf{M}}$ cannot be correct. Filtering reduces this measurement noise error, and the local E result of Fig. 2 that we obtain by applying Eq. (12) to filtered measurement vector $\boldsymbol{C}_{\mathbf{Mf}}$ is reasonable. Low areas align with observed knots in the measured board, and there are no unreasonably high values. We graph in the figures the noise as the difference of the reciprocals of $\boldsymbol{C}_{\mathbf{M}}$ and $\boldsymbol{C}_{\mathbf{Mf}}$, referring to it as noise in the measurement space. The errors (amount of smoothing) in Figs. 1-5 are small so the illustrated error curves show ten times the error. We state also a percent error computed as:

$$\text{Percent error} = 100\ \text{sqrt}(\text{var}(\boldsymbol{C}_{\mathbf{M}} - \boldsymbol{C}_{\mathbf{Mf}}))\ /\ \text{mean}(\boldsymbol{C}_{\mathbf{M}}) \tag{13}$$

where we compute variance (var) and mean from the components of the vectors $\boldsymbol{C}_{\mathbf{M}}$ and $\boldsymbol{C}_{\mathbf{Mf}}$.

Discussion

It is interesting to compare the computed local E with the measured E_{M} in the figures. In Fig. 1 we attribute the large discrepancy between the two curves to measurement noise, which the computation process amplifies. The question is: how much measurement noise is there? Repeatability studies (Bechtel 1993, Metriguard 2007) indicate that the so-called "low point" error expected in production-line machines is about one percent or less for a well-tuned machine. Low point E corresponds to the reciprocal of a component of measured compliance $\boldsymbol{C}_{\mathbf{M}}$. While we base our percent error on measured compliance (not on E), there is little difference between the two error measures for errors in the neighborhood of one percent.

We argue that we should set the amount of filtering so that the error in Eq. (13) agrees with the low point measurement error observed in practice. On this basis we argue in favor of the local E results of Figs. 2, 3 or 4 (note the factor of 10 in these figures for the plotted error). As more filtering is used, the local E result is even smoother and can be made to look quite similar to the measured E_{M} as shown in Fig. 6 where the error is 3.8 percent.

Suggested Implementation: Initially, to avoid disrupting the MSR measurement and quality control processes, implementation can begin with rather extensive filtering as in Fig. 6 where local E is practically identical with the usual measured E_{M}. Such implementation will have the added benefit of reducing noise in the result thereby improving yield on that basis alone. Successive reductions in the amount of filtering bring into focus the lower local E values along the board as in Figs. 2, 3, 4, and 5. For each reduction of filtering, we would couple small reductions in low-point E grade thresholds to take advantage of the improved accuracy in identifying the seriousness of low local E. Present rules for MSR lumber production equipment in North America allow efficient implementation of small changes in grade thresholds.

Benefits: With improved knowledge of local E, boards with poor local E will be removed even with reduced low point E thresholds. This will allow more good boards (those that otherwise would be downgraded) to pass into MSR grades and lead to better use of the forest resource, improved MSR yields and increased mill profits.

Conclusions

Local *E* estimation by constrained optimization is feasible and may be implemented in the production of MSR lumber with minimal disruption. Existing equipment can be upgraded with software modifications. Improved grading accuracy, increased high-grade yields, and greater profits to mills are anticipated. These benefits will be the result of a process that uses all measurements for which a local *E* value contributes. The present system uses only the measurement where that local *E* is at the center of a bending test span, thereby not using all the information generated by the measurements. It is important to correct this oversight and fully use available measurements to estimate local *E* values in the lumber resource. Lumber is a renewable and efficiently produced structural product that is strong and light. However, it is quite variable; improved local *E* estimation will help unlock the value in each piece produced.

References

Bechtel, F.K. 1985. Beam stiffness as a function of pointwise E, with application to machine stress rating. Proc. Int'l Symp. on Forest Products Research. CSIR. Pretoria, South Africa.

____. 1993. Estimating residual error by repeated measurements. Wood Fiber Sci. 25(1):46-60.

____. 2007. Estimating local compliance in a beam from bending measurements; Part I. Computing "span function". Wood Fiber Sci. 39(2):250-259.

____. 2009. Local modulus of elasticity-- Intuition and ramifications. Proc. 16th Int'l Sym. on Nondestructive Testing and Evaluation of Wood. Beijing, China. 130-136.

____ and J.R. Allen. 1995. Introduction to the Metriguard Model 7200 LS Lumber Tester. Pullman, WA.

____, C.S. Hsu, and T.C. Hanshaw. 2006. Method for estimating compliance at points along a beam from bending measurements. U.S. Patent No. 7,047,156.

____, ____, and ____. 2007a. Estimating local modulus of elasticity in a beam from bending measurements, an overview. Forest Products Journal. 57(1/2):118-126.

____, ____, and ____. 2007b. Estimating local compliance in a beam from bending measurements-- Part II: Optimal estimation of local compliance. Wood Fiber Sci. 39(2):260-270.

Foschi, R.O. 1987. A procedure for the determination of localized modulus of elasticity. Holz als Roh-und Werkstoff. 45:257-260.

Kaplan W. 1952. Advanced Calculus. Addison-Wesley. Reading MA. p128-129.

Metriguard Inc. 2007. Catalog 34-1. Pullman WA. Model 7200 HCLT p19, Repeatability p2.

Lam, F., R.O. Foschi, J.D. Barrett, and Q.Y. He. 1993. Modified algorithm to determine localized modulus of elasticity of lumber. Wood Science and Technology. 27:81-94.

Pope, D.J. and F.W. Matthews. 1995. A comparison of deconvolution techniques to improve MOR estimation from stress grading machine output. Wood Science and Technology 29. pp. 431-439.

Using Acoustic Tomography Techniques to Estimate Bending Properties of Cross-Laminated Timber

Frederico Jose Nistal França
Department of Sustainable Bioproducts, Mississippi State University, Starkville, Mississippi, USA, fn90@msstate.edu

Christopher Adam Senalik
USDA Forest Service, Forest Products Laboratory, Madison, Wisconsin, USA, christopher.a.senalik@usda.gov

R. Daniel Seale
Department of Sustainable Bioproducts, Mississippi State University, Starkville, Mississippi, USA, rds9@msstate.edu

Robert J. Ross
USDA Forest Service, Forest Products Laboratory, Madison, Wisconsin, USA, robert.j.ross@usda.gov

Rubin Shmulsky
Department of Sustainable Bioproducts, Mississippi State University, Starkville, Mississippi, USA, rs26@msstate.edu

* Corresponding author

Abstract

This research is focused on evaluating the bending stiffness and strength of cross-laminated timber (CLT) panels with acoustic tomography techniques. Eleven panels of Southern Pine three-ply CLT were acquired for this study. One test specimen was cut from each panel. Weight and dimensions were measured for each specimen. Each specimen measured approximately 0.11 m thick, 0.46 m wide, and 3.05 m long. The specimens were nondestructively tested (NDT) using multiple sensor tomography techniques comprised of up to 12 sensors. Panel density and wave velocity between sensors were calculated. Each specimen was then tested to failure in flatwise (third-point) static bending. Flatwise bending modulus of elasticity (MOE) and strength (modulus of rupture (MOR)) were determined. To predict the MOE and MOR using NDT variables, stepwise procedure was used for fitting models. It was found that the correlation between the acoustic technique outputs and bending properties varied based on which subset of 12 sensors was used. The highest coefficient of determination ($r^2 = 0.62$) was from using eight sensors (acoustic technique output) and strength (bending MOR).

Keywords: mechanical properties, mass timber products, modulus of rupture

Session 6

Condition Assessment of Historic Wood Artifacts and Structures

Mechanical Performances and Nondestructive Test with Demolished Timber Collected from a Wooden Building Several Hundred Years Old

Erina Kojima*
Department of wood engineering, Forest and Forest Products Research Institute, Tsukuba, Ibaraki, Japan, erinak@ffpri.affrc.go.jp

Hideo Kato
Department of wood engineering, Forest and Forest Products Research Institute, Tsukuba, Ibaraki, Japan, kato_hideo@ffpri.affrc.go.jp

Yasutaka Watanabe
Hiroshima Prefectural Technology Research Institute Forestry Research Center, Miyoshi, Hiroshima, Japan, y-watanabe73265@pref.hiroshima.lg.jp

Ken Yamamoto
Hiroshima Prefectural Technology Research Institute Forestry Research Center, Miyoshi, Hiroshima, Japan, k-yamamoto86252@pref.hiroshima.lg.jp

Ichirou Saitou
Hiroshima Prefectural Technology Research Institute Forestry Research Center, Miyoshi, Hiroshima, Japan, i-saitou81355@pref.hiroshima.lg.jp

Abstract

The long-term use and reuse of timber as a structural material are important from the viewpoint of the carbon storage effect. However, it is well known that timber often undergoes brittle fracture and decreases strength due to long-term use over time. Although this is a major concern from the perspective of safety and maintenance of wooden buildings, there are no scientifically based criteria for the reuse of timber as a structural material in the renovation of wooden buildings. Therefore, it is worthwhile to accumulate data on the strength of demolished timbers and to develop strength estimation techniques for nondestructive testing. In this study, the dynamic Young's modulus was measured by the longitudinal vibration method and stress waves method using demolished timber (red pine, *Pinus densiflora*) collected from a wooden building several hundred years old, and the relationship between the dynamic Young's modulus and the bending and compression strength properties of the full-scale wood was investigated. In addition, the effects of defects such as mortise holes and insect bites on the mechanical performance of the specimens were investigated. Specifically, the dynamic Young's modulus was measured by the longitudinal vibration method for the case where the mortise holes were removed and the case where all other damages such as insect bites and nail holes were removed. As a result, the correlation between the actual bending strength and compressive strength and the dynamic Young's modulus by the longitudinal vibration method was the highest. The results show that the longitudinal vibration method has potential as a strength estimation method. It was also shown that the effect of mortise holes and other damage on the dynamic Young's modulus was comparable.

Keywords: demolished timber, full-scale test, dynamic Young's modulus, *Pinus densiflora*

Introduction

Long-term use and reuse of wood as a structural material are important in terms of its carbon storage benefits. However, it is known that wood often undergoes brittle fracture and strength loss due to long-term use (Kránitz et al. 2016, Zeniya et al. 2019). This is a major concern in terms of the safety and maintenance of wooden buildings. Therefore, when renovating wooden buildings, the reuse of members is considered as well as replacing materials that are deemed to be no longer usable, thereby extending the overall service life of the building. However, there are no clear criteria for judging whether or not such materials can be reused. The establishment of nondestructive evaluation methods for reuse would not only further extend the service life of buildings but also significantly improve on-site work efficiency.

For this purpose, it is essential to accumulate data on the mechanical performance of demolition timbers, but there is insufficient data on demolition timbers compared to unused wood. In addition, although several studies have examined the mechanical properties of wood by cutting small defect-free specimens from demolition timbers (e.g., Kohara 1952, Attar-Hassan 1976, Yokoyama et al. 2009, Kránitz et al. 2014, Witomski et al. 2014), there have been few reports on full-scale tests using the demolition timbers as they are (Yamasaki et al. 2005). In order to further reuse demolition timber or to select appropriate materials, it is necessary to clarify the full-scale strength performance of demolition timbers and to study strength estimation techniques by nondestructive testing. In addition, defects in demolition timbers, such as mortise that were made during construction or insect holes (not termite damage in this study) that occurred during service, are thought to affect the mechanical performance of the demolition timbers.

In this study, we conducted bending and compression tests on full-size specimens of red pine taken from a wooden building more than several hundred years old. In addition, the relationship between the dynamic Young's modulus obtained by nondestructive testing and the mechanical performance was investigated. In addition, to examine the effect of defects on mechanical performance, the dynamic Young's modulus of the demolition timbers was measured when defects were removed from the demolition timbers.

Materials and Method

Test specimen

The specimens were structural timbers (red pine, *Pinus densiflora*) that were visually determined to be non-reusable during the renovation of a several hundred-year-old wooden building in Japan (Figure 1). Most of the specimens had defects such as wormholes mainly in the sapwood, in addition to mortise and nail holes that had been made during construction. The surfaces of the specimens were not smooth. There were a total of 123 specimens. The dynamic Young's modulus of all these specimens was measured by the longitudinal vibration method and by testing with a stress wave velocity measuring instrument (FAKOPP). Full-scale bending tests were conducted on the specimens with a length of 2700 mm or greater, and full-scale compression tests were conducted on the other specimens.

Test method

Nondestructive test

In this study, dynamic Young's modulus was measured by the longitudinal vibration method and by testing with a stress wave velocity measuring instrument (FAKOPP) before full-scale bending and full-scale compression tests. In the longitudinal vibration method, the natural frequency (fr) of the specimen was measured by tapping the specimen with a hammer, and the dynamic Young's modulus (E_{fr}) was calculated from the length (L) and density (ρ) using Equation (1).

$$E_{\mathrm{fr}} = 4 \times \rho \times (\mathrm{fr} \times L)^2 \quad (1)$$

In the test using FAKOPP, a hammer was used to strike the wood surface to propagate stress waves in the longitudinal direction, and the velocity of stress wave propagation (v) was measured. To obtain stable values, measurements were taken five times per specimen and the average value was obtained. In addition, dynamic Young's modulus was also measured by the MM method (Kiribayashi 2017), in which the specimens were struck with a device modified from a knocking ballpoint pen instead of a hammer. The dynamic Young's modulus (E_{sw}, $E_{sw\text{-}MM}$) in each method was calculated from the density and propagation velocity of the specimens using Equation (2).

$$E_{\mathrm{sw}} \text{ or } E_{\mathrm{sw-MM}} = \rho \times v^2 \quad (2)$$

Full-scale bending test

For full-scale bending tests, a 1000 kN full-scale strength test machine (IP-10B-B2, Maekawa Testing Machine MFG. Co., Ltd.) was used. A four-point load method with three equal load points was used, with the distance between the fulcrums set at 18 times the thickness of the specimen. The displacement of the specimen was measured by a displacement transducer (SDP-50, Tokyo Measuring Instruments Laboratory Co., Ltd.) attached to the center of the specimen in the length and thickness directions. From the obtained stress-strain curves, the static bending Young's modulus of elasticity (*MOE*) and bending strength (*MOR*) were calculated. The dimensions and density of the specimens are shown in Table 1.

Table 1—Specimen size and mechanical properties for bending test

n=75	Length (m)	Width (mm)	Thickness (mm)	ρ (kg/m^3)	MC (%)	E_{fr} (GPa)	E_{sw} (GPa)	$E_{sw\text{-}MM}$ (GPa)	*MOE* (GPa)	*MOR* (MPa)
Mean	4.03	109	95.5	474	12.0	7.43	8.54	7.75	6.99	17.8
CV (%)	10.3	8.58	9.45	14.1	6.74	25.6	22.7	24.5	41.0	45.9

n: Number of specimens, ρ: Density of specimen, MC: Moisture content, E_{fr}: Dynamic Young's modulus obtained by longitudinal vibration method, E_{sw}: Dynamic Young's modulus obtained by FAKOPP with hammer, $E_{sw\text{-}MM}$: Dynamic Young's modulus obtained by MM method, *MOE*: Bending Young's modulus, *MOR*: Bending strength.

Full-scale compression test

For full-scale compression tests, a 2000 kN full-scale compression testing machine (A-200-B1, Maekawa Testing Machine MFG. Co., Ltd.) was used. The length of the specimen was six times the shorter side. Displacement transducers (CDP-25, Tokyo Measuring Instruments Laboratory Co., Ltd.) were attached to the center of the two opposite surfaces in the direction of the length of the specimen at a distance of 180 mm between the points, and the amount of displacement was measured. The compressive Young's modulus (E_C) and compressive strength (σ_C) were calculated from the obtained stress-strain curves. The dimensions and density of the specimens are shown in Table 2.

Table 2—Specimen size and mechanical properties for compression test

n=48	Length (mm)	Long side (mm)	Short side (mm)	ρ (kg/m^3)	MC (%)	E_{fr} (GPa)	E_{sw} (GPa)	$E_{sw\text{-}MM}$ (GPa)	E_C (GPa)	σ_C (MPa)
Mean	540	105	88.1	500	13.1	8.25	9.20	8.20	8.79	23.2
CV (%)	0.137	5.42	4.64	9.92	13.5	16.7	17.6	27.2	41.2	29.0

n: Number of specimens, CV: Coefficient of variation, ρ: Density of specimen, MC: Moisture content, E_{fr}: Dynamic Young's modulus obtained by longitudinal vibration method, E_{sw}: Dynamic Young's modulus obtained by FAKOPP with hammer, $E_{sw\text{-}MM}$: Dynamic Young's modulus obtained by MM method, E_C: Compressive Young's modulus, σ_C: Compressive strength.

Effects of defects

The effects of defects such as mortise holes, nail holes, and insect holes in demolished timbers on the dynamic Young's modulus (E_{fr}) by the longitudinal vibration method were investigated. The measurement method for the longitudinal vibration method is the same as the method described above. The E_{fr} of the full-size specimen was used as the E_{fr} of the full-size bending specimen (Table 1). From the nondestructive portion of the subsequent full-scale bending test, the specimen defects were removed in two stages, and E_{fr} was determined for each stage.

In the first stage, the specimens were cut to remove relatively large defects such as mortises and notches (Figure 2a); in the second stage, all defects were removed from the specimens in the first stage, and then the specimens were dimensioned (Figure 2b). The defects removed in the second stage were mainly relatively small, such as insect holes and nail holes. Hereafter, for each defect stage of the specimens, the full-size specimens are referred to as "Actual size," the first stage specimens as "Small specimens," and the second stage specimens as "Clear specimens.

The dimensions and densities of the Small specimen and Clear specimen are shown in Table 3 (Actual size is the same as the full-scale bending specimens shown in Table 1). Density was calculated from the volume and weight of the rectangular specimens without considering gaps of defect, so density increased with the removal of defects.

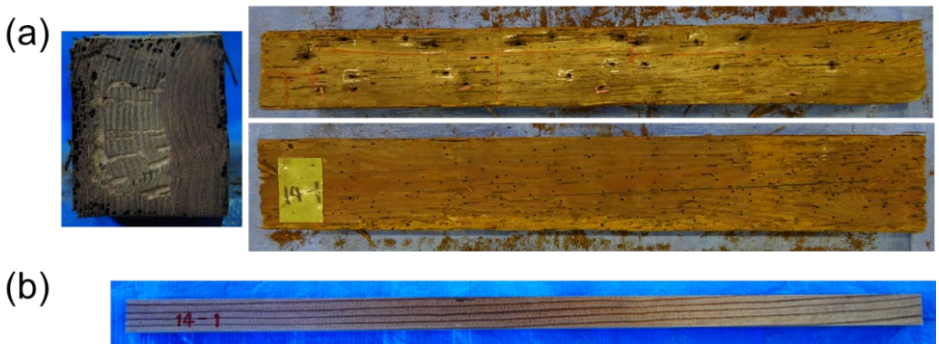

Figure 2—Example of test specimen. (a) Small specimen (b) Clear specimen

Table 3—Specimen size and mechanical properties for each specimen condition

Specimen condition		Length (mm)	Width (mm)	Thickness (mm)	ρ (kg/m^3)	E_{fr} (GPa)
Small Specimen *n*=106	Mean	853	107	89.5	503	9.10
	CV (%)	23.5	8.24	7.62	13.7	24.0
Clear Specimen *n*=102	Mean	500	20.2	15.2	533	11.3
	CV (%)	0.553	0.232	0.316	15.5	22.1

n: Number of specimens, CV: Coefficient of variation, ρ: Density of specimen, E_{fr}: Dynamic Young's modulus obtained by longitudinal vibration method.

Result and discussion

Bending performance

The relationship between Young's modulus (*MOE*, E_{fr}, E_{sw}, $E_{sw\text{-}MM}$) and bending strength (*MOR*) is shown in Figure 3. The coefficient of determination (R^2) for each correlation is organized in Table 4. First, the R^2 for the relationship between *MOE* and *MOR* was 0.73, indicating a good correlation. This means that

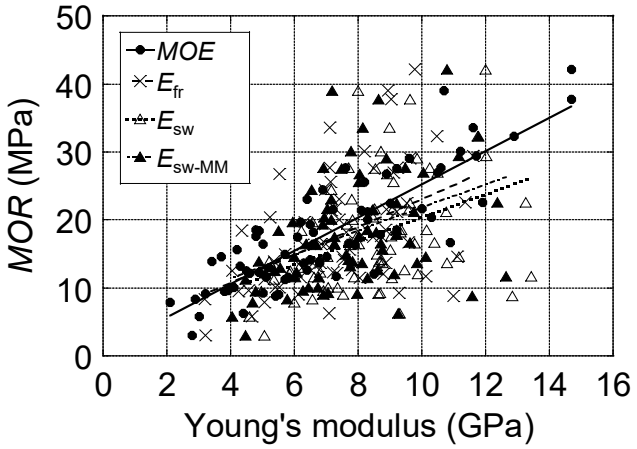

Figure 3—Relationships between Young's modulus and *MOR*. E_{fr}: Dynamic Young's modulus obtained by longitudinal vibration method, E_{sw}: Dynamic Young's modulus obtained by FAKOPP with hammer, $E_{sw\text{-}MM}$: Dynamic Young's modulus obtained by MM method, *MOE*: Bending Young's modulus, *MOR*: Bending strength.

Table 4— Coefficient of determination in each loading mode.

Loading mode	E_{fr}	E_{sw}	$E_{sw\text{-}MM}$	*MOE* or E_C[1)]
Bending	0.23	0.17	0.16	0.73
Compression	0.19	0.19	0.06	0.14

[1)] *MOE* is for bending static Young's modulus and E_c is for compressive static Young's modulus. E_{fr}: Dynamic Young's modulus obtained by longitudinal vibration method, E_{sw}: Dynamic Young's modulus obtained by FAKOPP with hammer, $E_{sw\text{-}MM}$: Dynamic Young's modulus obtained by MM method, *MOE*: Bending Young's modulus, E_C: Compressive Young's modulus.

MOR can be estimated from *MOE* even for full-size timbers with defects taken from wooden buildings that are several hundred years old. The correlation between the dynamic Young's modulus from non-destructive tests and *MOR* is weak compared to the correlation between *MOE* and *MOR*. Among the dynamic Young's modulus, E_{fr} and *MOR* had the highest R^2, and E_{sw} and $E_{sw\text{-}MM}$ using FAKOPP were comparable.

Compressive performance

The relationship between Young's modulus (E_C, E_{fr}, E_{sw}, $E_{sw\text{-}MM}$) and longitudinal compressive strength (σ_C) is shown in Figure 4. The respective coefficients of determination (R^2) are organized in Table 3. To begin with, the coefficient of determination in the relationship between E_C and σ_C is 0.14, which is significantly lower than the bending performance. The displacement measurement jig used in this study consisted of four knife edges that sandwiched the two facing surfaces of the specimen. Since the surfaces of the specimens were not smooth due to the presence of wormholes, etc., it is thought that some specimens could not be accurately measured because the knife edges were not pinched enough. This may have resulted in inaccurate measurement of E_C and a weak correlation with σ_C. Among the dynamic Young's modulus from non-destructive testing, E_{fr} and E_{sw} had the highest correlation with σ_C, while $E_{sw\text{-}MM}$ had the lowest coefficient of determination. According to previous studies (Kiribayashi 2017), $E_{sw\text{-}MM}$ by the MM method is considered to have better repeatability and measurement accuracy due to the uniformity of the striking force applied by the device modified from a knocking ballpoint pen.

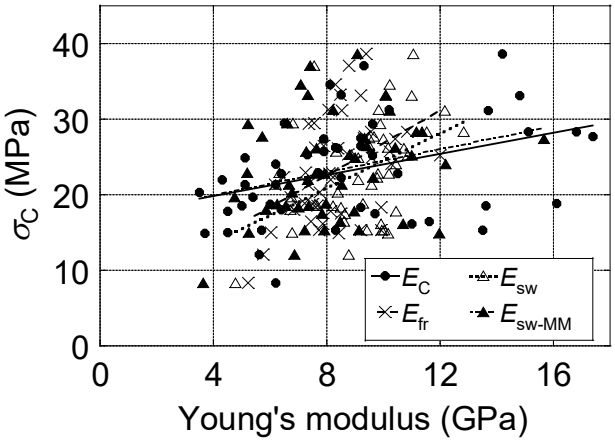

Figure 4—Relationships between Young's modulus and σ_C. E_{fr}: Dynamic Young's modulus obtained by longitudinal vibration method, E_{sw}: Dynamic Young's modulus obtained by FAKOPP with hammer, $E_{sw\text{-}MM}$: Dynamic Young's modulus obtained by MM method, E_C: Compressive Young's modulus, σ_C: Compressive strength.

Here, $E_{sw\text{-}MM}$ shown in Table 2 shows smaller values than E_{sw}, i.e., the propagation velocity is slower. This suggests that when the specimen contains many defects such as wormholes and mortise holes as in this study, the impact given by the device used in the MM method is weaker than the hammer used in the standard method, and the propagation velocity is significantly attenuated due to voids such as defects, resulting in a weaker correlation with σ_C.

Effect of defects

The defects were removed from the non-destructive portion after the full-scale bending test in two stages, and the E_{fr} at that time was examined. Figure 5 shows the relationship between density and E_{fr} under each condition. Since the densities of the Actual size and Small specimen were calculated without considering the gap of the defect, it was expected that the correlation between density and E_{fr} would be weak. However, contrary to expectations, the coefficient of determination for the Actual size specimen was the highest at 0.36, while the coefficient of determination for the Clear specimen with no defect was the

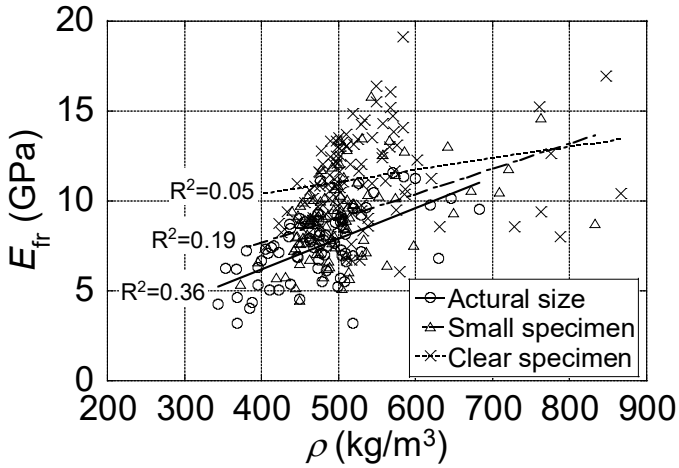

Figure 5—Effect of defects on the relationships between density and E_{fr}. ρ: Density of specimen, E_{fr}: Dynamic Young's modulus obtained by tapping method.

lowest at 0.05. This may be since there were several specimens in clear specimen with higher densities than normal red pine (here above 700 kg/m^3), and these specimens had relatively low E_{fr}. These specimens were found to contain more resin, which may be the cause of the higher density. In other words, densification by resin does not contribute to E_{fr}. Next, Figure 5 shows that E_{fr} and density increase with the removal of defects, and the regression line moves to the upper right. Here, E_{fr} is affected by density as shown in Equation (1). Therefore, it is necessary to evaluate the extent to which the increase in density and the removal of defects are responsible for the increase in E_{fr}. Therefore, the density and E_{fr} ratios before and after removal of defects were determined for each specimen. The results are shown in Figure 6. The line within each box indicates the median. The boxes indicate the range of the center 50% of the data for the population. The lines outside the boxes indicate the maximum and minimum values of the data. "○" indicates an outlier.The left half of the figure shows the density ratio and the right half shows the E_{fr} ratio. Also, A indicates Actual size, S indicates Small specimen, and C indicates Clear specimen. For example, S/A indicates the density ratio or E_{fr} ratio of the Small specimen to the Actual size. In the case of C/A, which has the highest degree of defect removal, the density ratio was 1.13 on average, while the E_{fr} ratio was 1.55. In other words, the E_{fr} ratios were much higher than the density ratios. This indicates that E_{fr} r increased not only due to the increase in density but also due to the removal of defects. Furthermore, when large defects such as mortise holes were removed (S/A) and when small defects as insect holes and nail holes were removed (C/A), the density ratio was 1.06 for both cases, and the E_{fr} ratio was 1.23 and 1.25, respectively, which were almost the same values. In other words, the type of defects did not affect E_{fr} in this study.

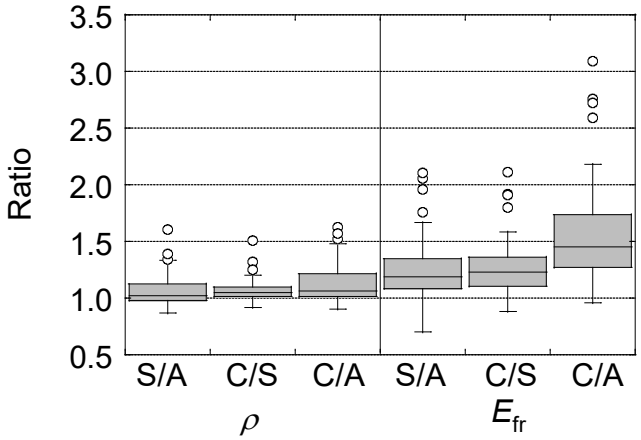

Figure 6—Density and E_{fr} ratio with defects removal. ρ: Density of specimen, E_{fr}: Dynamic Young's modulus obtained by longitudinal vibration method. A: Actual size, S: Small specimen, C: Clear specimen.

Conclusions

In this study, the full-scale bending and compression performance of demolition timbers taken from a several hundred-year-old wooden building was clarified, and the relationship with the dynamic Young's modulus was investigated by nondestructive testing. In addition, the effects of defects such as mortise holes on the mechanical performance were also examined.

As a result, the static Young's modulus is considered to be appropriate for estimating the bending strength of demolition materials with defects. In addition, E_{fr} for longitudinal vibration as a nondestructive testing method was shown to have potential as a method for estimating bending and compressive strength. The effects of relatively large defects such as mortise holes and notches and relatively small defects such as

wormholes and nail holes on E_{fr} were similar. E_{fr} was approximately 1.55 times higher when all defects in the demolished timber were removed.

References

Attar-Hassan, G. 1976. The effect of ageing on the mechanical properties of Eastern white pine. Bull Assoc Preserv Technol. 8(3):64–73.

Kiribayashi, M. 2014. The applicability of the stress-wave method to the nondestructive evaluation of the wood properties of standing trees and logs. Dissertation. Tottori University.

Kohara, J. 1952. Studies on the durability of wood I: mechanical properties of old timbers. Bull. Kyoto Prefectural Univ. 2: 116–131.

Kránitz, K.; Deublein, M.; Niemz, P. 2014. Determination of dynamic elastic moduli and shear moduli of aged wood by means of ultrasonic devices. Mater Struct. 47: 925–936.

Kránitz, K.; Sonderegger, W.; Bues, CT.; Niemz, P.; 2016. Effects of aging on wood: a literature review. Wood Sci Technol. 50:7–22.

Witomski, P.; Krajewski, A.; Kozakiewicz, P. 2014. Selected mechanical properties of scots pine wood from antique churches of central Poland. Eur J Wood Prod. 72: 293–296.

Yamasaki, M.; Hirashima, Y.; Sasaki, Y. 2005. Mechanical properties of the used wood recycled from old temples. J Struct Constr Eng AIJ. 588: 127–132.

Yokoyama, M.; Gril, J.; Matsuo, M.; Yano, H.; Sugiyama, J.; Clair, B.; Kubodera, S.; Mitsutani, T.; Sakamoto, M.; Ozaki, H.; Imamura, M.; Kawai, S. 2009. Mechanical chracteristics of aged hinoki wood from Japanese historical buildings. Comp Rend Phys. 10: 601–611.

Using Dielectric Orthotropy as an Indicator of Internal Decay of Wood Members

C. Adam Senalik
USDA, Forest Service, Forest Products Laboratory, Madison, WI, USA, christopher.a.senalik@usda.gov

Benjamin Farber
Mississippi State Univ., College of Forest Resources, Dept. of Sustainable Bioproducts, Starkville, MS, USA, bf720@msstate.edu

James P. Wacker
USDA, Forest Service, Forest Products Laboratory, Madison, WI, USA, james.p.wacker@usda.gov

Xiping Wang
USDA, Forest Service, Forest Products Laboratory, Madison, WI, USA, xiping.wang@usda.gov

Abstract

Several material properties of wood are directionally dependent. Mechanical properties such as tension, compression, and bending strength vary greatly for the same piece of wood when tested parallel to the grain (longitudinally), perpendicular to the grain and parallel to the annual rings (tangentially), or perpendicular to both the grain and rings (radially). For this reason, wood is often considered to be a cylindrically orthotropic anisotropic material. The orthotropy extends to dielectric properties of wood. However, in the presence of internal decay, the directional dependency of the dielectric qualities diminishes. By identifying and measuring the loss of directional dependency, the presence and extent of internal decay is evaluated. Ground penetrating radar (GPR) is used as the inspection tool. A bowtie, bistatic, dipole antenna with a center frequency of 2 GHz is used for measurement. The specimens are wood members of sizes typically used in bridge construction. The GPR technique has several advantages over existing non-destructive testing (NDT) techniques: it requires access to only one side of the specimen, no special methods are needed to couple the sensor to the specimen, and it uses a commercially available tool already accepted within the NDT industry. This study is part of a larger study to develop improved NDT tools for timber bridge inspection.

Keywords: Ground penetrating radar, GPR, glulam, bridge timbers

Introduction

Since the turn of the century, interest in ground penetrating radar (GPR) as an inspection tool for wooden structures has increased (Rodrigues, B. et al. 2021). GPR allows rapid scanning of the target specimen, detects several types of subsurface features, detects the presence of moisture, and does not require direct contact between the sensor and target (Mai et al 2015a, Cassidy 2009, Müller 2002, Müller 2003, Rodríguez-Abad 2008, Hans et al. 2015a, Hans et al. 2015b). Alongside the advantages are complicating factors. Wood is a dispersive material, so the radar wave frequency affects how the wave travels through the target specimen. In addition, the transmitting wave may be affected by any combination of temperature, moisture content, geometry of the specimen and/or internal features, and density (Mai et al 2015, Hans et al. 2015a, Hans et al. 2015b, Torgovnikov 1993). When the impact of the complicating

factors is understood, GPR becomes a powerful inspection tool. The United States Department of Agriculture (USDA), Forest Service (FS), Forest Products Laboratory (FPL), in conjunction with the U.S. Federal Highway Administration (FHWA) recently initiated a multiphase study to develop GPR into a viable inspection tool for wood structures (Senalik et al. 2016). The goal of the overall study is to develop improved NDT tool for timber bridge inspection.

Background

The ability of GPR to locate fungal decay is examined here. Normally fungal decay is collocated with pockets of moisture within the wood beam. In this study, the specimens were conditioned to 12% moisture content (MC) to remove the pockets of internal moisture to quantify the sensitivity of GPR to fungal decay alone. The method used to locate the decay monitors change in dielectric constant (DC) parallel to the grain ($DC_{//}$) relative to the DC perpendicular to the grain ($DC_{\perp}$). DC is the capacitance of a material relative to the capacitance of a vacuum. It is expressed as a unitless ratio with a range of values of 1 for air to over 80 for pure water. DC is affected by temperature, relative humidity, and wave frequency. The specimens in this study are constructed of Douglas-fir which has DC values around 2.3 parallel to the grain and 1.8 perpendicular to the grain at 22.8°C, 12% MC, and 2 GHz (Torgovnikov 1993, Wittkopf and MacDonald 1949, Mai 2015b, Rodríguez-Abad 2010). As wood decays, $DC_{//}$ decrease more quickly than $DC_{\perp}$. As a result, by monitoring the DC change relative to each direction, internal decay can be identified.

Materials and Methods

The specimens in this study are Douglas-fir (*Pseudotsuga menziesii (Mirb)Franco*) glued-laminated beams with rectangular cross sections typical of those used in bridge construction. The specimens are inoculated with brown rot fungus known to be aggressive against the Douglas-fir species (*Fomitopsis pinicola (Sw.) P.Karst. (1881)*) and exposed to field conditions for 46 months in the Harrison Experimental Forest in Mississippi, USA, which is approximately 40-km north of the Gulf of Mexico. The conditions at the exposure site promotes fungal growth. The treatment of the specimens is extensively described in (Senalik et al. 2016, Senalik et al. 2017). A diagram of a typical specimen is shown in Figure 1a. The four fungal cavities are shown: one in each end and two on the top face near the ends. Scan direction is relative to the metal identification (ID) tag on each specimen.

The specimens include two glulam beams: a six-layer glulam beam with cross-sectional dimensions of 13.0-cm × 22.7-cm and a five-layer glulam beam with dimensions of 13.0-cm × 17.8-cm. Both beams are 81.3-cm in length. After field exposure, the specimens are returned to FPL and inspected using X-ray computer tomography (CT) to identify areas of decay (Senalik et al. 2019, Bucur 2003). Hereafter, the six-layer glulam will be referred to as specimen A and the five-layer is specimen B. After CT, the specimens are stored in an environmentally controlled room (22.8°C and 50% relative humidity (RH)) for 28 months to reach an equilibrium moisture content (EMC) of 12%. At that time, the specimens are scanned using GPR with a center frequency of 2-GHz. The GPR and antenna which emits the radar waves are a commercially available unit from Geophysical Survey Systems, Inc. from Nashua, NH (GSSI). The unit is a GSSI SIR® 4000 GPR data acquisition system and a 2-GHz MHz dipole bowtie antenna (DBA) (GSSI 2014). A typical GPR output scan, a radargram, is shown in Figure 1b. The dark band at approximately 350 ns/$DC^{½}$ represents the far edge of the specimen. Note the distortion to the shape of the curve near the ends of the specimen.

Each face of each specimen is scanned with the GPR DBA oriented such that the electromagnetic field generated is parallel to the grain (this orientation is designated $ef_{//}$ for brevity; $ef_{\perp}$ for perpendicular). It is from these scans that $DC_{//}$ is determined. An aluminum plate is placed on the side of the specimen

opposite of the antenna to create a strongly reflective boundary which facilitates the identification of the far edge of the specimen in the GPR output. The scanning regime is shown in Figure 2. On the top face, the edge of the palm antenna is aligned with the edge of beam and scanned towards the ID tag. This produces a scan through the depth of the specimen (top to bottom). For the second scan, the DBA uses the same scan line, but scans away from the ID tag. Due to the design of the DBA, approximately 2-in of the end of the specimen where the scan begins are missed. The scan away from the metal ID tag provides the information on the lost 2-in. The data from both scans are merged to provide a single output for the entire length of the specimen. Since decay often enters wood at the cut ends, it is important that the overall scan contain as much information about the end of the specimens as possible. The third and fourth scans are in the same directions as the first and second, but the palm antenna is aligned with the opposite edge of the specimen.

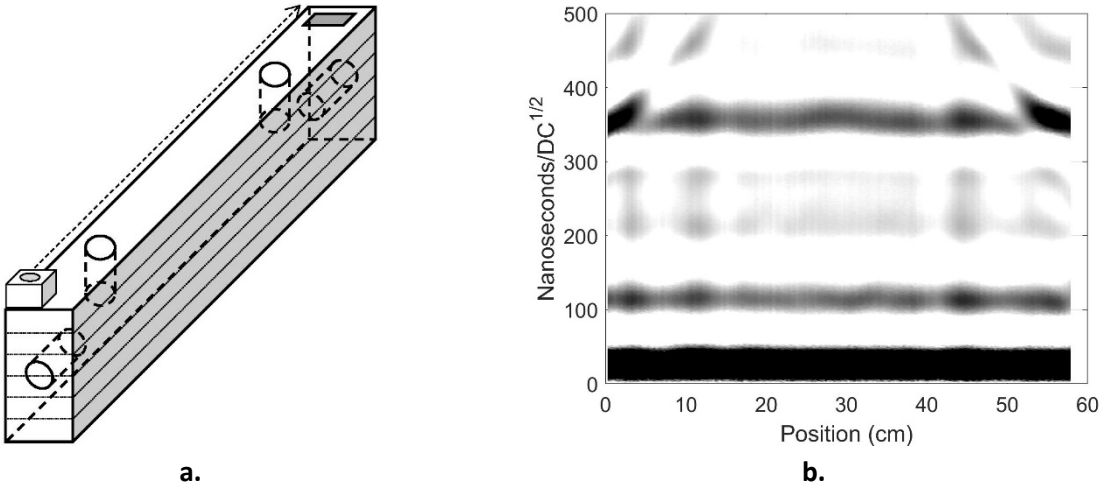

Figure 1 - Diagram of typical specimen and a typical radargram. a) Diagram of typical 6-layer glulam beam specimen. The white box with the gray circle on top represents the GPR antenna. The arrow represents the direction the antenna is moved during a GPR scan. b) Typical radargram from a longitudinal GPR scan. The prominent black line at approximately 350 ns/DC^{½} is the bottom edge of the specimen.

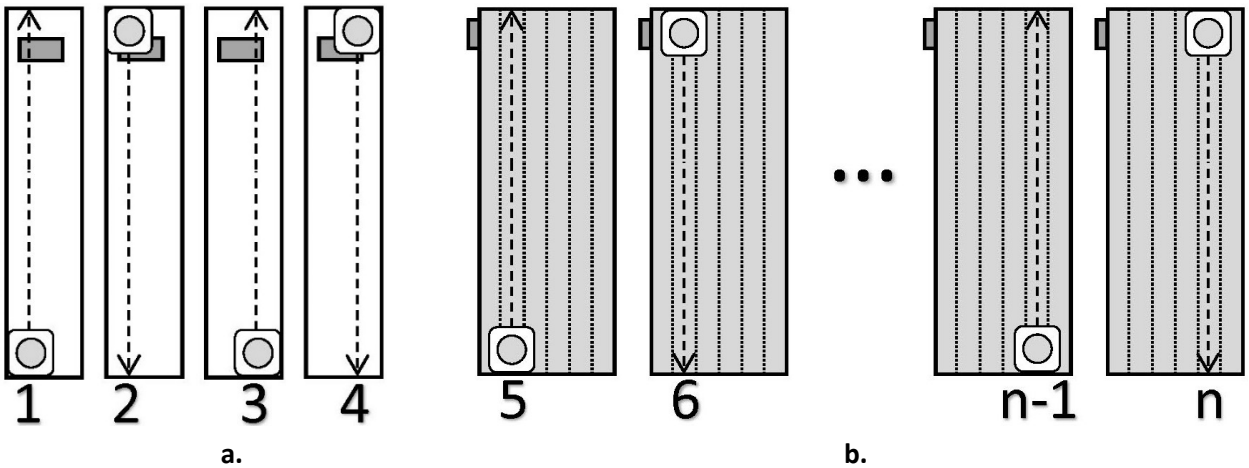

Figure 2 - GPR scanning regime of specimens. The dark rectangle at the top of the specimens represents the metal identification tag. The white box with the gray circle represents the GPR antenna. The arrow represents the direction of motion of the antenna during scanning a) Scanning of top and bottom surfaces. b) Scanning of side surfaces. Only the inner layers are scanned. The top and bottom layers are not scanned as the antenna will overhang the edge of the specimen.

On the sides of the specimen, the scan lines are along the centerline of each of the interior lamina. The top and bottom lamina are excluded from scanning as the antenna will overhang off the edge of the specimen causing the output to be some mixture of wood and air. The fifth specimen scan is the second lamina from the top in the direction towards the ID tag; the sixth is the same scan line away from the ID tag. Scans along the side are across the width of the specimen. The process is repeated for each of the interior lamina and for the same lamina with the antenna positioned on the opposite side of the specimen. GPR scans of the bottom of the specimen mirror those taken on the top. The entire scanning process is then repeated with the GPR DBA oriented such that $ef_{\perp}$ is generated and $DC_{\perp}$ is determined.

Decay detection makes use of the difference in DC parallel and perpendicular to the wood grain. Early in the study, there was an examination of the proportional reduction in DC parallel to the grain relative to the proportional change in DC perpendicular to the grain as a method of identifying decay regions. Unfortunately, the proportional change in $DC_{//}$ too close to that of $DC_{\perp}$ to make accurate predictions. At that point, the method was altered to look at the absolute change in $DC_{//}$ relative to the absolute change in $DC_{\perp}$. Since $DC_{//}$ is larger than $DC_{\perp}$ and the proportional change in DC for both directions was found to be similar, the absolute reduction is $DC_{//}$ must be greater than that of $DC_{\perp}$. At this point, a threshold differentiating sound and decayed wood is needed. The threshold is developed from control specimens. The decision to develop the threshold from control specimens rather than initial GPR of the specimens prior to field exposure is made as a consideration of the information that will be available to inspectors in the field. It is unlikely they will have early time GPR information of wood bridge timbers, and would rely upon information gleams from similar beams that have not been field exposed.

Threshold Development

Two five-layer glulam beams with the same cross-sectional dimensions as specimen B were used as control specimens. The control specimens were cut from the same beams that were used to make the five-lamina field exposed specimens. The control specimens are designated as C1 and C2. From the control specimens, two analysis methods were developed: compensation for geometric distortion of the GPR output caused by proximity to the end of the beam, and threshold value contour identifying likely areas of decay.

As the DBA nears the end of the specimens, reflections from the wood air boundary at the end of the specimen cause distortion of the GPR output. This distortion is a function of the thickness of the specimen under the DBA and the distance between the DBA to the end of the specimen. To compensate for this distortion, a shape factor based upon distance from the edge of the specimen is determined. Shape factors are generated for scans through the depth and across the width for $ef_{//}$. For brevity, the process of developing the shape factor is shown only for scans across the width with $ef_{//}$. When the DBA is far from the end of the specimen, the reflection for the far edge of the specimen is mostly constant (Region 1 in Figure 3a). As the DBA approaches the end of the specimen, the data recorded by the GPR is a combination of the reflection from the far edge and the reflection from the end of the specimen (Region 2). As the DBA continues to approach the end of the specimen, the reflection from the end of the specimen becomes the dominant source of information in the output (Region 3). While the compensation cannot recover specimen condition information that is both near the end and near the far edge, it does lessen the influence of the boundary effects on the output.

In Figure 3a the end distortion is shown for several scans through the width of the control specimens. The Regions described above are identified. The first step in compensating for the end effect distortion is to normalize each scan by the respective mean value of Region 1 to yield a factional value for each data point as shown in Figure 3b. The fractional values (ordinate or y-values) are averaged for at each location (abscissa or x-values) to form a single curve as shown in Figure 3c. The values along the curve are the

shape factor. Each point of the raw scan is divided by the fractional value of the shape factor to remove the end effect distortion. An example of the application of the shape factor curve is shown in Figure 3d and Figure 3e.

The next step is to develop a threshold criterion that differentiates between sound and decayed wood. After the shape factor is applied to the raw data, the region of the $DC_{//}$ curve with the lowest coefficient of variation across a window of 3.8-cm is located. The window length of 3.8-cm was chosen as it is the approximate width of the DBA. When the region is found, the mean of the region is subtracted from all points on the $DC_{//}$ curve. The same window is then applied to $DC_{\perp}$, and the mean of the values is subtracted from all points on the $DC_{\perp}$ curve. As a result, the two curves vary about the zero DC value, and any variation in the curves is due to variations in the wood or the presence of decay. The parallel and perpendicular curves that vary about the zero DC value are referred to as $DC^0_{//}$ and $DC^0_{\perp}$. An example is shown in Figure 4a and Figure 4b. The final step is to subtract the values of the DC^0// curve from the $DC^0_{\perp}$ curve. The resulting difference curve is used to locate areas decayed wood. An example is shown in Figure 4c.

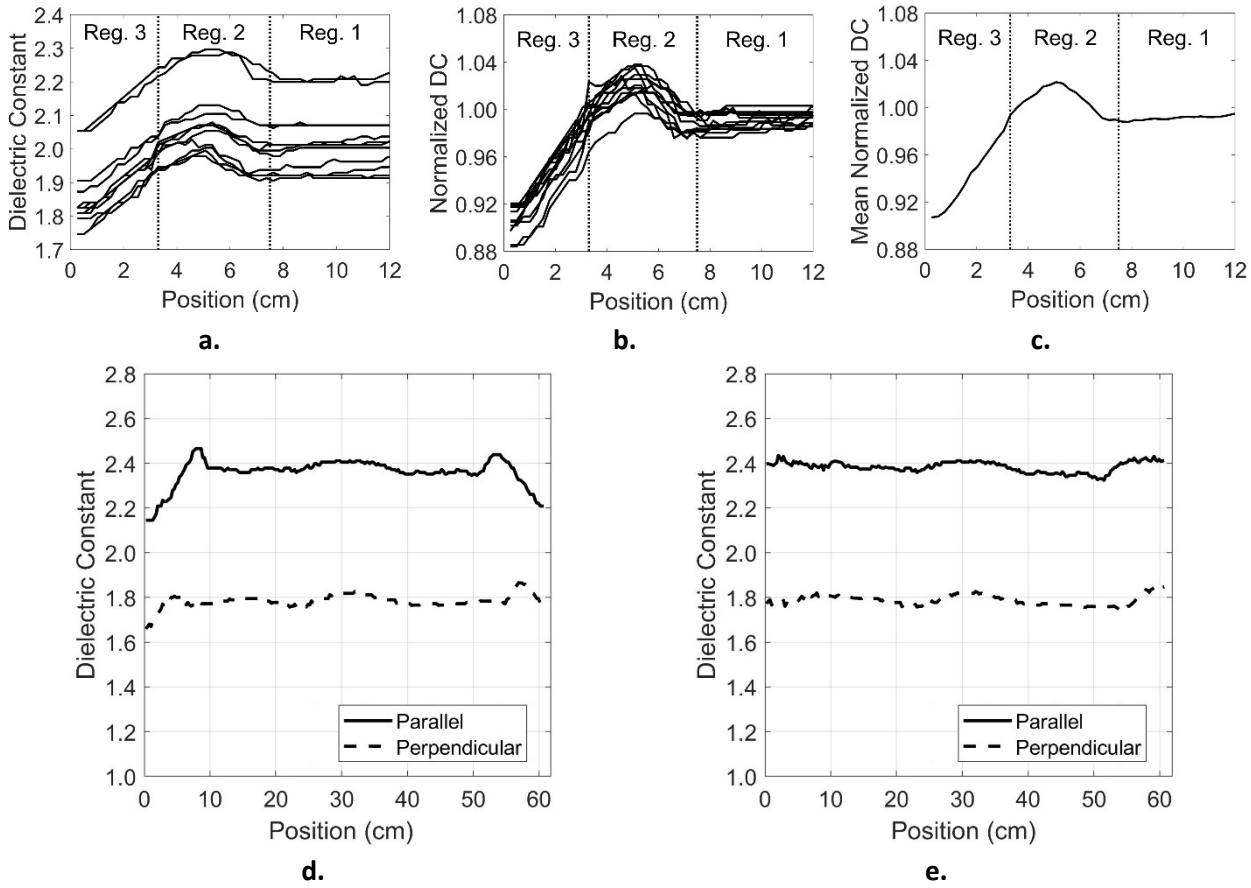

Figure 3 - Reducing end effect distortion with shape factor curve. a) Several scan outputs with end effect distortion. Region 1 is not affected by the end boundary. Region 2 is affected by both end boundary and the far edge. Region 3 is affected by the end boundary. b) Each scan is normalized by the mean value of Region 1. c) Normalized scans are averaged to yield the shape factor curve. d) A typical scan output with end effect distortion. e) The same scans when corrected by dividing the values by the shape factor curve values.

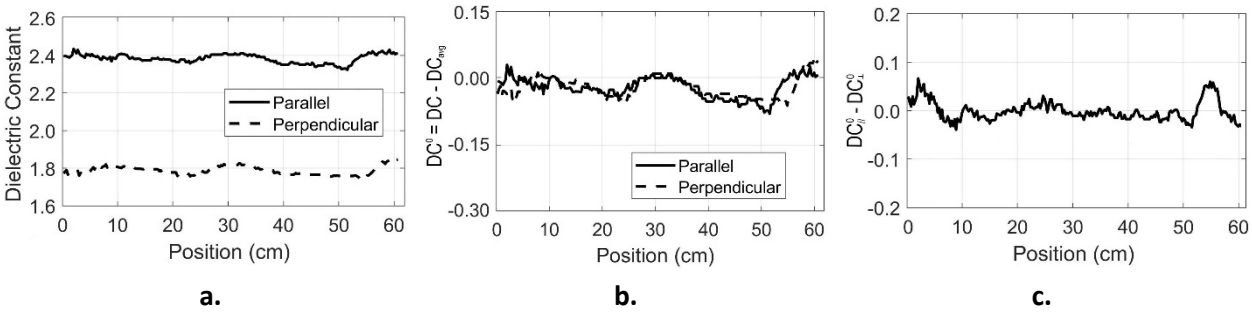

Figure 4 - Calculating difference in DC parallel and perpendicular to grain. a) DC curves with end adjustment (same as Figure 3e) b) Curves adjusted to remove average DC value ($DC^0 = DC - DC_{avg}$) c) Difference between curves ($DC^0_{//} - DC^0_{\perp}$)

The threshold criterion is developed using all the DC difference curves from the control specimens. As shown in Figure 5a the values for all the curves are combined into a single data set. For any given point along the beam length, all the data from all the curves within ±1.9-cm of the given data point are combined into a single data set. The average and standard deviation of the data set are calculated. The threshold is set at the mean minus two standard deviations. This process is repeated for every point along the beam length to generate the threshold curve. The threshold line is shown as a white line in Figure 5a. Figure 5b is an overhead view of Figure 5a; the threshold curve is shown as a dashed black line. Values that fall below the threshold line indicate decayed wood.

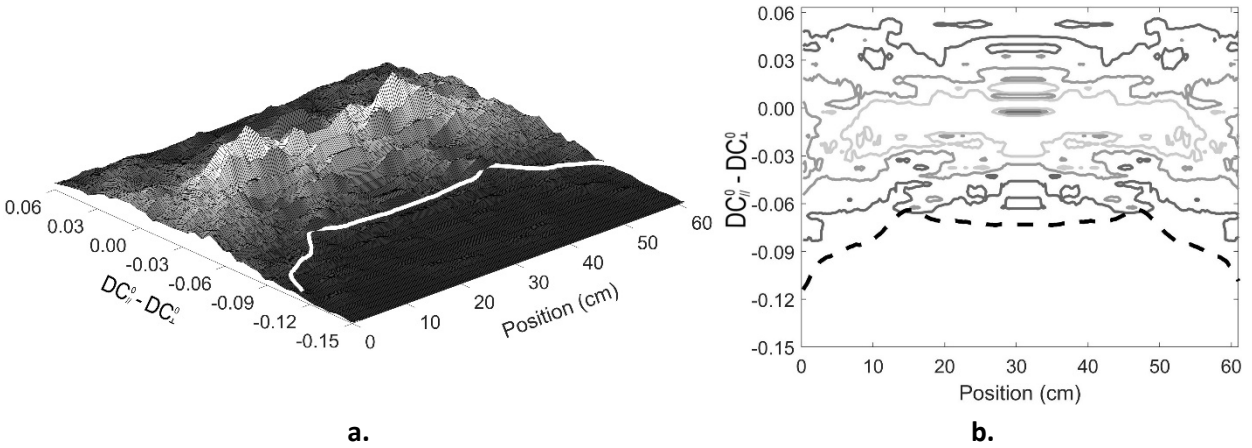

Figure 5 - Development of the threshold curve identifying decayed wood using control specimens. a) A histogram plot by location along the control specimens. The white line is the threshold curve which is determined as two standard deviations below the mean DC for that location. b) A plan view of Figure 5a. The threshold curve is shown here as a black dashed line.

Results

Figure 6a and Figure 6b shows a scan of the A and B specimen, respectively, as well as the threshold curve for each. Based upon the threshold curve for specimen A, it would be predicted that decay would be found within the ranges of 0 to 26-cm and above 66-cm. It would be expected that the decay would be more severe in the 0 to 26-cm range than above 66-cm. Figure 7 and Figure 8 show the decay map developed for the A and B specimen, respectively, using the X-ray CT. The method of developing the decay map is described in (Senalik 2019). For the A specimen, there is considerable advanced decay from top to bottom of the specimen from 0 to 26-cm. Also, at 66-cm and above, there is advanced decay at the top and middle of the specimen, but the lower portion of the specimen appears to be sound.

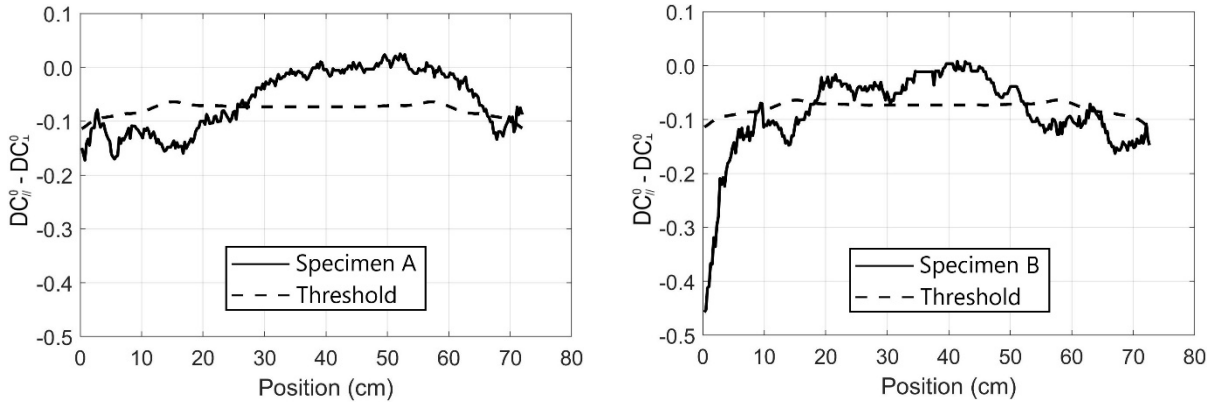

Figure 6 - DC difference plots for specimens A and B. a) The plot predicts decay from 0 to 26-cm and above 66-cm. b) The plot predicts decay below 18-cm and above 52-cm.

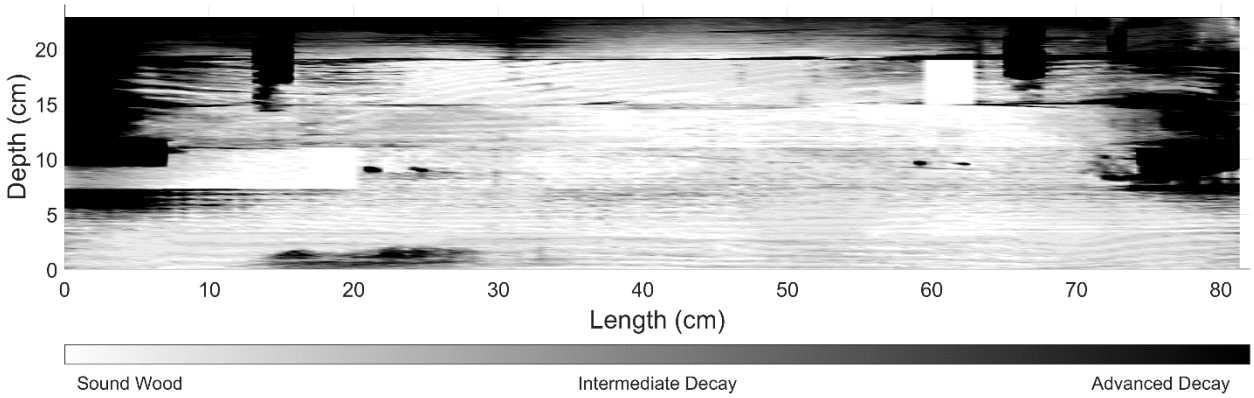

Figure 7 - Decay map of specimen A. In general, decay spreads out from the four fungal cavities and from the ends of the specimen. Advanced decay is present from top to bottom from 0 to 32-cm. There is advanced decay visible along the top surface. From 64 to 80-cm advanced decay is present in the top four lamina, but the bottom two lamina appear to be sound wood.

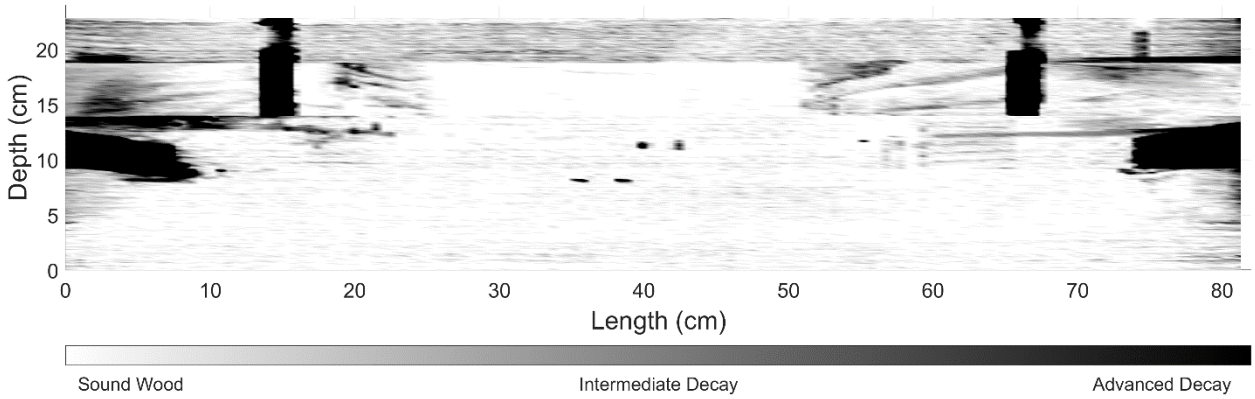

Figure 8 - Decay map of specimen B. In general, decay spreads out from the four fungal cavities and from the ends of the specimen. Advanced decay is present in the top three lamina from 0 to 23-cm. There is intermediate decay along some portions of the top lamina but it is only visible near the ends. There is a small region of advanced decay at 55-cm with larger areas at 67-cm and above.

Figure 6b shows a scan of the B specimen as well as the threshold curve. Based upon the threshold curve, it would be predicted that decay would be found within the ranges of 0 to 18-cm and above 52-cm. It would be expected that the decay would be more severe in the 0 to 5-cm range than any other region of specimen B. Figure 8 shows the decay map developed for the B specimen using the X-ray CT. From 0 to 23-cm, advanced decay is visible in the top three lamina with the highest concentration from 0 to 7-cm. There is intermediate decay along the top lamina, but it is only visible near the ends of the specimen. A small region of advanced decay is between 53 and 58-cm. Small regions of advanced decay are present between 65 and 80-cm.

Conclusions

For both specimens, A and B, there is good agreement between locations of interior decay and the difference in DC parallel versus perpendicular to the grain. As expected, wood decay decreases the DC of the wood and the DC parallel to the grain decreases quicker than DC perpendicular to grain in the presence of decay. A method is proposed for compensating for the distortion of the GPR signal near the end of the specimens using a shape factor. The shape factor method needs additional refinement to improve the performance for 6-lamina glulam. The coefficient of variation of the $DC_{//}$ values is used to identify the portion of the specimens that contain the least decayed wood. While COV results agree with X-ray CT scans, additional work is necessary to determine if this is the best method for identifying regions of sound wood. Finally, the DC difference values from control specimens are used to develop a threshold curve for decayed wood. The threshold of two standard deviations below the mean DC difference is used. Additional analysis may yield a better threshold estimate.

Acknowledgments

This study is part of the Research, Technology, and Education portion of the National Historic Covered Bridge Preservation (NHCBP) Program administered by the United States Department of Transportation, Federal Highway Administration. The NHCBP program includes preservation, rehabilitation, and restoration of covered bridges that are listed or are eligible for listing on the National Register of Historic places; research for better means of restoring and protecting these bridges; development of educational aids; and technology transfer to disseminate information on covered bridges to preserve the Nation's cultural heritage.

References

Bucur, V. 2003. Nondestructive characterization and imaging of wood. Berlin Heidelberg New York: Springer.

Cassidy, N.J. 2009. Electrical and Magnetic Properties of Rocks, Soils and Fluids. In Ground Penetrating Radar Theory and Applications; Elsevier: Amsterdam, The Netherlands; pp. 41–72.

Geophysical Survey Systems, Inc (2014) SIR 4000 manual. Geophysical Survey Systems, Inc., Nashua, NH. https://www.geophysical.com/wp-content/uploads/2017/10/GSSI-SIR4000-Manual.pdf .

Hans, G.; Redman, D.; Leblon, B.; Nader, J.; La Rocque, A. 2015a. Determination of log moisture content using early-time ground penetrating radar signal. Wood Mater. Sci. Eng. 2015, 10, 112–129.

Hans, G.; Redman, D.; Leblon, B.; Nader, J.; La Rocque, A. 2015b. Determination of log moisture content using ground penetrating radar (GPR). Part 1. Partial least squares (PLS) method. Holzforschung 2015, 69, 1117–1123.

Mai, T.C.; Razafindratsima, S.; Sbartaï, Z.M.; Demontoux, F.; Bos, F. 2015a. Non-destructive evaluation of moisture content of wood material at GPR frequency. Constr. Build. Mater. 77, 213–217.

Mai, T.C.; Sbartaï, Z.M.; Bos, F. 2015b. Non-destructive evaluation of wood moisture content using GPR technique—Effect of fiber direction and wood type. In Proceedings of the International Symposium Non-Destructive Testing in Civil Engineering (NDT-CE), Berlin, Germany, 15–17 September 2015.

Müller, W. 2002. Trial of ground penetrating radar to locate defects in timber bridge girders. In Proceedings of the Riding the Wave to Sustainability: IPWEAQ 2002 State Conference, Nossa Lakes, Queensland, Australia, 6–10 October 2002.

Müller, W. 2003. Timber girder inspection using ground penetrating radar. Insight Non Destr. Test. Cond. Monit. 2003, 45, 809–812, doi:10.1784/insi.45.12.809.52990.

Rodrigues, Brunela Pollastrelli; Senalik, Christopher Adam; Wu, Xi; Wacker, James. 2021. Use of Ground Penetrating Radar in the Evaluation of Wood Structures: A Review. Forests. 12(4): 492. https://doi.org/10.3390/f12040492.

Rodríguez-Abad, I.; Martínez Sala, R.; García-García, F.; Capuz Lladró, R.; Diez Barra, R. 2008. A non-destructive method for the evaluation of density and moisture content. In Proceedings of the 12th International Conference on Ground Penetrating Radar, Birmingham, UK, 16–19 June 2008.

Rodríguez-Abad, I.; Martínez-Sala, R.; García-García, F.; Capuz-Lladró, R. 2010. Non-destructive methodologies for the evaluation of moisture content in sawn timber structures: Ground penetrating radar and ultrasound techniques. Near Surf. Geophys. 2010, 8, 475–482, doi:10.3997/1873-0604.2010048.

Senalik, C.A.; Wacker, J.P.; Wang, X.; Jalinoos, F. 2016. Assessing the Ability of Ground Penetrating Radar to Detect Fungal Decay in Douglas-Fir Beams. In: 25th ASNT Research Symposium: Summaries and Abstracts. Paper presented at 25th Research Symposium, New Orleans (110-116). Columbus, OH: American Society for Non-destructive Testing, Inc. 7 p.

Senalik, C. Adam; Wacker, James P.; Wang, Xiping; Rodrigues, Brunella Pollastrelli; Jalinoos, Frank. 2017. Assessing ability of ground penetrating radar to detect internal moisture and fungal decay in Douglas-fir beams. In: Wang, X.; Senalik, C.A.; Ross, R.J., eds. Proceedings, 20th international non-destructive testing and evaluation of wood symposium. General Technical Report. FPL-GTR-249. Madison, WI: U.S. Department of Agriculture, Forest Service, Forest Products Laboratory: 286-300.

Senalik, Christopher Adam; Wacker, James; Wang, Xiping; Wu, Xi. 2019. Identifying incipient decay in Douglas-fir bridge components using x-ray computerized tomography. In: Wang, X.; Sauter, U.H.; Ross, R.J., eds. 2019. Proceedings: 21st International Nondestructive Testing and Evaluation of Wood Symposium. General Technical Report FPL-GTR-272. Madison, WI: U.S. Department of Agriculture, Forest Service, Forest Products Laboratory: 62-70.

Torgovnikov, G.I. 1993. Dielectric Properties of Wood and Wood-Based Materials; Springer-Verlag Berlin Heidelberg, 1993.

Wittkopf, J.J.; MacDonald, M.D. 1949. Dielectric Properties of Douglas Fir at High Frequencies. Oregon State Engineering Experiment Station Bulletin 28, July 1949.

Mixed Session (Online)

Relation of Ultrasonic Wave Velocity and Compression Strength of Artificially Decayed Wood

Kana Yamashita
Department of Wood Properties and Processing, Forestry and Forest Products Research Institute, Tsukuba, Ibaraki, Japan, zaikana@ffpri.affrc.go.jp

Hirofumi Ido
Department of Wood Engineering, Forestry and Forest Products Research Institute, Tsukuba, Ibaraki, Japan, ido@ffpri.affrc.go.jp

Yuko Ota
College of Bioresource Sciences, Nihon University, Kameino, Fujisawa, Japan, yuko.ota@nihon-u.ac.jp

Toshihiro Yamada
Graduate School of Agricultural and Life Sciences, The University of Tokyo, Chichibu, Saitama, Japan, yamari@uf.u-tokyo.ac.jp

Abstract

Sound velocity is used for detecting decay of trees and wood nondestructively. In order to improve the accuracy of estimating strength decrease from sound velocity, it is important to clarify the relations of decay degree, sound velocity and wood strength. In this study, artificially decayed specimens were prepared by inoculating *Fomitopsis palustris* on the compression strength specimens in tangential, radial and longitudinal directions of *Larix kaempferi*. The relations between mass loss, ultrasonic wave velocity loss and compression strength were obtained. With increase of the ultrasonic wave velocity loss, mass loss increased linearly and compression strength decreased curvilinealy in the three directions. The ultrasonic wave velocity loss was larger in the radial direction than in the tangential and longitudinal directions, which was suggested to be affected by the difference of decay degree of earlywood and latewood.

Keywords: brown rot, decay, mass loss, ultrasonic velocity, compression strength

Introduction

In order to maintain urban trees and wooden building while ensuring safety for a long period of time, it is important to evaluate the remaining strength of trees or wood damaged by biodeterioration in a nondestructive way as much as possible. The ultrasonic wave, which is safe and portable method, has been applied to evaluate physical properties or defects. The ultrasonic wave propagation within wood is affected not only by density, but also largely influenced by anisotropic structures depending on species and moisture content (Bucur 1988, Mishiro 1996, Sakai 1993). Therefore, it is important to examine how the velocity and strength decreased for different species and direction. The ultrasound propagation change have been examined using the wood with artifically made holes (Espinosa et al. 2020, Lee et al. 2011, Lin 2000). However, there are limited studies for ultrasonic sound propagataion and remining strength using bio-deteriorated wood, because it is necessary to consider the bio-deterioration process in living trees or building materials. In lab tests, Sumiya showed that bending strength loss was quite larger than mass loss

and decrease of velocity in radial direction using Japanese cedar treated with the brown rot fungi *Fomitopsis palustris* (Sumiya 1965). Goto et al. showed the negative correlations between the decrease of velocity in tangential direction and remaining partial compression strength in tangential direction for pillar-shaped wood samples of five species treated with *F. palustris* (Goto et al. 2011). Those studies have shown the possibility of ultrasonic wave velocity to evaluate remaining strength, but the information of anisotropy of velocity and strength is limited. The velocity and strength have anisotropy depending on species, so the relations between velocity and strength of decay wood could be varied by directions. Espinosa et al. showed that considering wood anisotropy in the imaging process led to a better defect detection compared to the use of a common imaging techniques (Espinosa et al 2020). Mcgovern et al. showed ultrasonic velocity decreased and attenuation increased with amount of decay using controlled decay specimens. They also showed that the attenuation anisotropy; the attenuation was larger in the radial direction, followed by the tangential direction and the lowest in the longitudinal direction (Mcgovern et al. 2011). In this study, we examined the relations between ultrasonic wave velocity and compression strength under decay progress in the tangential, radial and longitudinal directions using Japanese larch wood, which is used for construction and civil engineering.

Materials and methods

Materials

From air-dried heartwood of *Larix kaempferi*, three types of compression strength specimens, tangential compression strength specimen (T-specimen), radial compression strength specimen (R-specimen), and longitudinal compression strength specimen (L-specimen) were prepared and seasoned in a constant temperature and humidity room. The specimen sizes were 100 mm (T) x 30 mm (R) x 30mm (L) for T-specimen, 30 mm (T) x 100 mm (R) x 30mm (L) for R-specimen, and 30 mm (T) x 30 mm (R) x 100mm (L) for L-specimen. For each type of specimen, 29 specimens were prepared from the same tree. Their weights, dimensions and ultrasonic wave transmission times along the long axis were measured. The ultrasonic wave transmission time was measured using Pundit 7 (Proceq) with transducers of 54 kHz covered by rubber caps.

Artificial decay

The brown rot fungus *Fomitopsis palustris* (Berk. et Curt.) Gilbn & Ryb. FFPRI 0507, which is designated in Japanese Industrial Standards (Japanese Industrial Standards Committee 2009, 2010), was cultivated in the PDA medium. PDA medium without mycelia was also prepared for control specimens. In order to decay homogeneously, inoculation was conducted on lateral sides of specimens (Fujihira et al. 1997). Layers of paper with a size of 95 mm x 160 mm (Kim towel, Nippon Paper Crecia) were soaked in the 30 mL liquid medium containing glucose, malt extract, peptone and distilled water, and then wrapped around the long axis sides of each specimen. One set of three specimens (T-, R- and L-specimens) were put in a heat-resistant polypropylene bag. Totally 29 bags were prepared and sterilized in an autoclave for 60 minutes at 121°C. The bag edges were partly opened and five PDA disks containing mycelia with diameters of 5 mm were put on each specimen of 27 bags. PDA disks without mycelia were put on specimens of two bags which were served as control. The bags were sealed again and put in a room at 25 °C.

Evaluation of decayed specimens

Three bags each were taken out in nine batches: 30, 51, 61, 82, 103, 131, 156, and 246 days after inoculation. The specimens were sterilized with ethylene oxide and seasoned in a constant temperature humidity room. Their weights, dimensions and ultrasonic wave transmission times were measured using the same methods as before inoculation. The differences of weight and velocity before and after decay

were obtained as mass loss and velocity loss for each specimen. They were corrected by subtracting averages of control specimens.

Compression test was conducted using a universal testing machine until the load reached the maximum. For R-specimen, the load at 3 mm deformation was used as the maximum load. The maximum load was divided by the bearing area to obtain compression strength. In order to compare the strength decrease among directions, the relative compression strength was calculated using the average of control specimens as 100%. The specimens were oven-dried at 103°C to obtain moisture contents. The average and standard deviation of moisture content at testing were 14.3±0.6%.

Results and discussion

Trends with decay period

The mycelia inoculated on lateral sides continued to develop during the decay period. It covered the whole specimens after 51 days, therefore the mycelia could have entered from the all six faces. Figure 1 shows the trends of mass loss, velocity, and compression strength with decay period. The mass loss increased and velocity and compression strength decreased as the decay period became longer. Mass loss decreased similarly for the three types of specimens. On the other hand, decrease trends of velocity and compression strength were different among directions. The velocity decreased greatly in radial direction than in tangential and longitudinal directions. The velocity in radial direction was faster than that in tangential direction for non-decayed specimen and at early stage of decay, whereas it dropped to the similar level at late stage of decay. The compression strength decrease trends were slightly different among the three directions. Tangential and radial compression strength decreased rapidly at early stage of decay, whereas longitudinal compression strength kept decreasing until 194 days. Radial compression strength was larger than tangential compression strength for non-decayed specimen and at early stage of decay, whereas it dropped to the similar level at late stage of decay.

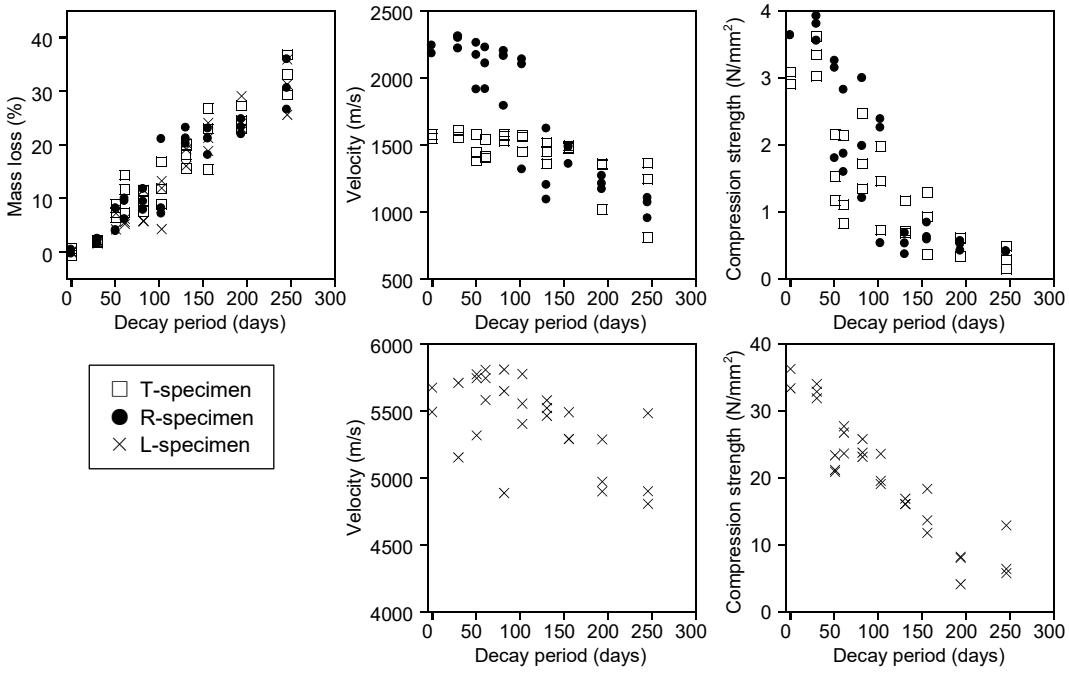

Figure 1—Trends with decay period for mass loss, velocity and compression strength.

Relations between density, velocity and compression strength

Figure 2 shows the relations of density, velocity and compression strength for decayed and control specimens. Table 1 shows the correlation coefficients regressed linearly and exponentially. Positive relations were found between density and velocity. The correlation coefficients of linear and exponential regressions were at the similar level. They were the highest for the radial direction, followed by the tangential direction, and lowest for the longitudinal direction.

Positive correlations were found between density and compression strength. The correlation coefficients were higher for exponential regressions in tangential and radial directions, whereas, higher for linear regression in longitudinal direction. These correlations were higher than those for velocity in tangential and longitudinal directions.

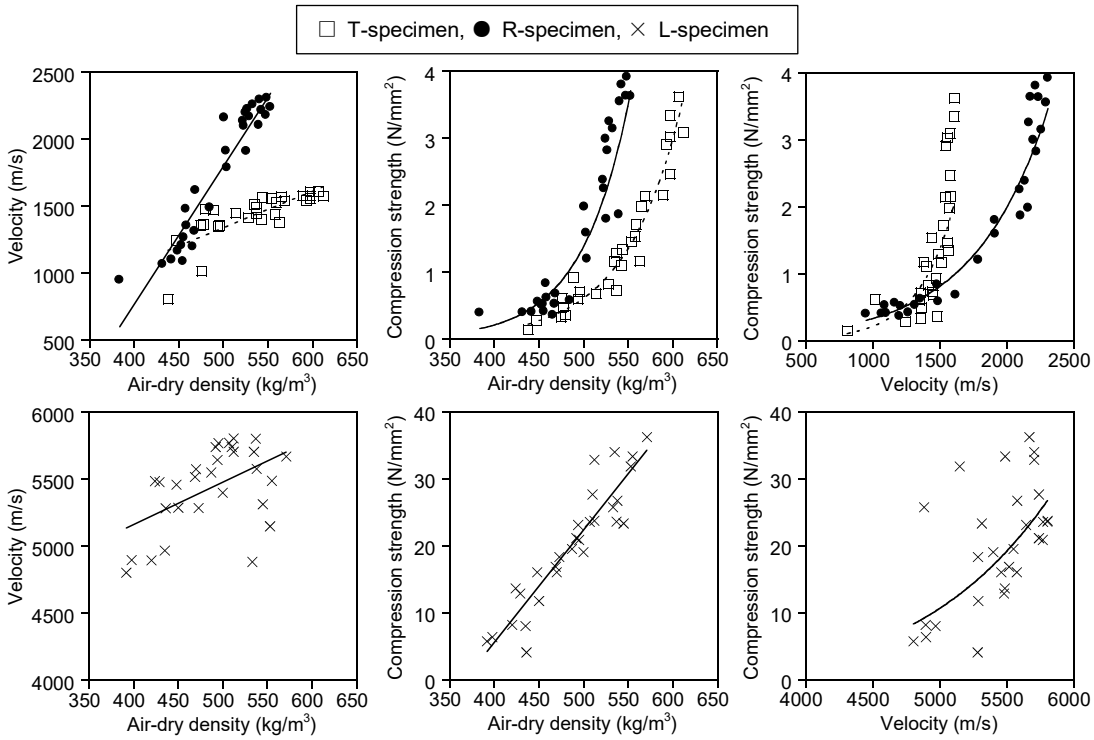

Figure 2—Correlation coefficients between density, velocity and compression strength.

Table 1—Correlation coefficients among density, velocity, and compression strength

Explanatory and objective variables	Specimen	Linear		Exponential	
		r	P	r	P
Density and velocity	T	0.772	<0.0001	0.757	<0.0001
Density and velocity	R	0.949	<0.0001	0.950	<0.0001
Density and velocity	L	0.509	0.0048	0.502	0.0047
Density and compression strength	T	0.914	<0.0001	0.967	<0.0001
Density and compression strength	R	0.892	<0.0001	0.948	<0.0001
Density and compression strength	L	0.926	<0.0001	0.904	<0.0001
Velocity and compression strength	T	0.663	<0.0001	0.832	<0.0001
Velocity and compression strength	R	0.921	<0.0001	0.966	<0.0001
Velocity and compression strength	L	0.564	0.0014	0.563	0.0003

Positive relations were also found between velocity and compression strength. The correlation coefficients were higher in exponential regression than linear regression for the tangential and radial directions, whereas those of linear and exponential regression were at the similar level for the longitudinal direction. When compared by direction, they were highest for the radial direction, followed by the tangential direction and the lowest for the longitudinal direction, which was as same as the relations between density and velocity.

The correlations were high between density and radial velocity (r=0.950), and density and longitudinal compression strength (r=0.926) (Table 1), which suggests that radial velocity is useful to predict density, and density is useful to predict longitudinal compression strength. Therefore, high accuracy is expected to predict the longitudinal strength from radial velocity. On the other hand, the correlations between density and velocity were lower in the longitudinal or tangential direction. It might be because the cell wall degradation preceded in earlywood ahead in latewood as suggested by Smith and Graham for Douglas-fir (Smith and Graham 1983). The latewood remained undegraded until late stage of decay, therefore the ultrasonic wave could have passed the latewood. Predicting density from velocity in tangential and longitudinal direction might not be so reliable as from the velocity in radial direction. Anisotropic differences obtained in this study is thought to reflect the anatomical and physical structures of larch which has distinct latewood. The tree ring structures consisting of earlywood and latewood, and biodegradation progress might be varied within or among trees. Therefore, the regression equations might be variable for other trees grown in different environment or species that have different structures, which might be future study.

Relations between mass loss, velocity loss and compression strength

Figure 3 shows the relations of velocity loss and relative compression strength against mass loss. Table 2 shows their regression equations and correlation coefficients. Linear correlations were obtained between mass loss and velocity loss, and curvilinear correlations were obtained between velocity loss and relative compression strength.

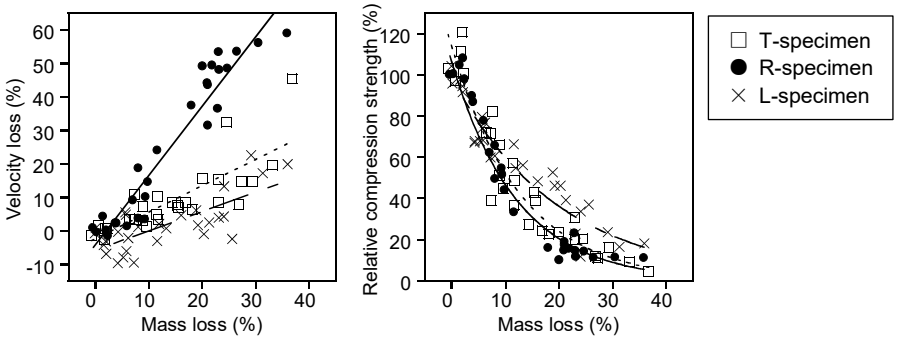

Figure 3—Relations between mass loss, velocity loss and relative compression strength

Table 2—Regression equations and correlation coefficients among mass loss, velocity loss and relative compression strength

Explanatory and objective variables	Specimen	Regression equations	Correlation coefficients	
			r	P
Mass loss and velocity	T	y=0.792x-2.501	0.800	<0.001
Mass loss and velocity	R	y=2.074x-4.288	0.959	<0.001
Mass loss and velocity loss	L	y=0.5768x-5.817	0.743	<0.001
Mass loss and relative compression strength	T	$y=113.5e^{(-0.07778x)}$	0.952	<0.001
Mass loss and relative compression strength	R	$y=106.1e^{(-0.08226x)}$	0.980	<0.001
Mass loss and relative compression strength	L	$y=98.66e^{(-0.05017x)}$	0.953	<0.001

Janzen and Nicholas showed that compression strength in brown-rotted wood was more sensitive than mass loss as a measure of wood decay in lab tests, and radial compression was more sensitive than tangential compression to extent of decay for *Pinus glabra* (Janzen and Nicholas 2016). In this study, compression strength dropped to around 50% at mass loss of 10%. The decrease of compression strength was larger than mass loss from the early stage of decay. Sumiya showed that bending strength dropped largely at early decay, whereas velocity in radial direction decreased gently for *Cryptomeria japonica* (Sumiya 1965). In this study, velocity loss was smaller than compression strength loss in the three directions. Compared with mass loss, the velocity loss was a little larger for the radial direction, and smaller for the tangential and longitudinal directions.

In this study, cracks were observed on the decayed specimens after drying, which was also observed in Takahashi et al. in the *L. kaempferi* wood decayed by *F. palustris* (Takahashi et al. 2012). The decreases of velocity and strength in this study might have been affected not only by the cell wall biodegradation but also by drying checks. In order to apply the relations between velocity and strength for the living trees or building materials with different levels of moisture, it is desirable to get the relations between velocity and strength in green wood, which might be future study.

Conclusions

Considering anisotropy is important to evaluate remaining strength from velocity loss. For predicting mass loss from velocity loss, radial velocity is more reliable than tangential velocity for larch decayed wood, because the ultrasound wave might pass faster in the sound latewood. Predicting mass loss from longitudinal velocity is difficult unless the decay precedes at a considerable level.

Acknowledgments

This work was supported by JSPS Kakenhi Grant Number 26292079. We thank Dr. Kohei Kambara and Mr. Hiroto Toyofuku for their assistant in experiments.

References

Bucur, V. 1988. Wood structural anisotropy estimated by acoustic invariants. IAWA Bulletin 9(1): 67-74.

Mishiro, A. 1996. Effect of density on ultrasonic velocity in wood. Mokuzai Gakkaishi 42(9): 887-894.

Sakai, H.; Takaghi, K. 1993. Ultrasonic propagation and the mechanism of water absorption in woods. Mokuzai Gakkaishi 39(7): 757-762.

Espinosa, L.; Brancheriau, L.; Cortes, Y. [and others] 2020. Ultrasound computed tomography on standing trees: accounting for wood anisotropy permits a more accurate detection of defects. Annals of Forest Science 77: 68.

Lee, S.; Lee, S.J.; Lee, J.S. [and others]. 2011. Basic study on nondestructive evaluation of artificial deterioration of a wooden rafter by ultrasonic measurement. J Wood Sci 57(5): 387-394.

Lin, C.J.; Chiu, C.M.; Wang, S.Y. 2000. Application of ultrasound in detecting wood decay in squirrel-damaged standing trees of Luanta China Fir. Taiwan J For Sci 15(2): 267-279.

Sumiya, K. 1965. Relations between defects in wood and velocity of ultrasonic wave. Wood Research. 34: 22-36.

Goto, T.; Tomikawa, Y.; Nakayama, S.; Furuno, T. 2011. Changes of propagation velocity of ultrasonic waves and partial compression strength of decay-treated woods: relationship between decrease of propagation velocity of ultrasonic waves and remaining strength. Mokuzai Gakkaishi 57(6): 359-369.

Espinosa, L.; Brancheriau, L.; Prieto, F.; Lasaygues, P. 2018. Sensitivity of ultrasonic wave velocity estimation using the Christoffel equation for wood non-destructive characterization. Bioresouces 13(1): 918-928.

McGovern, M; Senalik, A; Chen, G; [and others] 2011. Effect of decay on ultrasonic velocity and attenuation measurements in wood. Proc. of SPIE 7981:79810N-1.

Japanese Industrial Standars Committee. Japanese Industrial Standard, Method of test for woods. JIS Z 2101:2009.

Japanese Industrial Standars Committee. Japanese Industrial Standard, Wood preservatatives-Performance requirements and their test methods for determining effectiveness. JIS K 1571:2010.

Fujihira, M.; Nakamura, Y.; Isoda, N; Hikita, Y. 1997. Relationship between decay resistance and changes of bending strength of structural lumber of wood-framing construction by fungal attack. Mokuzai Gakkaishi. 43(7): 589-594.

Smith, S.M.; Graham, R.D. 1983. Relationship between early decay and radial compression strength of Douglas-fir. Forest Products Journal. 33(6): 49-52.

Janzen, S.; Nicholas, D.D. 2016. Relation of transverse compression properties and the degree of brown rot biodeterioration of Pinus glabra in the soil block test. Holzforschung 70(11): 1067-1071.

Takahashi, T.; Tanaka, K.; Togashi, I.; [and others]. 2012. Material characteristics and residual strength for decay of compressed wood made of Japanese larch. Transaction of the JSME. 794(78): 1400-1410.

Combining Nondestructive Testing Technology and Digital Twin for Preventive Conservation of Wooden Cultural Relics

Xueyi Ma
School of Technology, Beijing Forestry University, Beijing, China, maxueyi@bjfu.edu.cn

Jian Zhao *
School of Technology, Beijing Forestry University, Beijing, China, zhaojian1987@bjfu.edu.cn

Puxiang Wang
School of Technology, Beijing Forestry University, Beijing, China, xiangzi@bjfu.edu.cn

Yuankai Weng
School of Technology, Beijing Forestry University, Beijing, China, yuankai96bfu@163.com

Lihua Fei
Quanzhou Maritime Museum Fujian, Quanzhou, Fujian, China, fjqzflh@163.com

Dong Zhao *
School of Technology, Beijing Forestry University, Beijing, China, zhaodong68@bjfu.edu.cn

* Corresponding author

Abstract

Large movable cultural relics are constantly subject to degradation due in particular to atmospheric and environmental agents. As an advanced protection scheme, preventive strategies have been gradually preferred to the curative approaches for the conservation of large movable cultural relics, especially wooden cultural relics, because of their ability to maintain their significance. Non-destructive monitoring methodologies based on image sensors and data analysis methodologies based on digital technologies play a key role for the analysis of cultural relics degradation. This study aims to present a framework for the analysis of the state of degradation of cultural relics, exploiting an approach including a combination of monitoring database, inverse dynamics problems and digital twins. In this regard, a preliminary case-study is presented, based on the stern of the Quanzhou Bay Song wooden shipwreck, China. Such an approach starts with the 3D survey of the stern structure and culminates with the definition of a detailed finite element model that can be exploited to predict future scenarios. In order to reduce uncertainties in analytical the stern structure models and obtain a proper digital twin, the scan-based 3D model is imported into the finite element environment and then calibrated the material properties through monitoring database and inverse dynamics problems, which using material characteristics identified from field displacement data recorded before and after the modification intervention as reference indicators. After evaluating the effectiveness of the reinforcement measures, the digital twin ability of the reconstruction of the past and future damage scenarios of the stern is verified by nonlinear static analysis. The results highlight the great advantages of combining non-destructive testing technology and data analysis methodologies in the field of heritage conservation.

Keywords: nondestructive testing technology, digital twin, the finite element model updating, 3D-DIC, wooden cultural relics

1 Introduction

The Song Dynasty shipwreck in Quanzhou Bay (AD 960-1279) is one of the most important archaeological discoveries in China (Fei 2014). The shipwreck is suffering from increasing deformation over time, which is caused by the time-dependent deformation of the wood members, as well as the damage accumulation due to chemical degradation and physical shrinkage and swelling. Aging and weakening wooden structures of cultural relic requires a potent support in the process of conservation (Afshar et al. 2021). On the one hand, a sensible design of the support structure requires a numerical model of the structure to calculate displacements and stresses to assess a support rational design. Finite element numerical modeling has become the preferred method for the design and modeling analysis of the improved supported and strengthened structures for historical cultural heritage (Afshar et al. 2017). On the other hand, 3D structural deformation monitoring is increasingly becoming useful tools for in-situ preservation of large cultural heritage and to constantly update the deformation condition report of the cultural relics.

The application of the DT concept to the protection and conservation of the cultural heritage (CH) implies the possibility to accurately simulate the structural response over time in order to understand its behavior and prevent future problems. But generating digital replicas of CH structures is a challenging and often burdensome task. Due to the evolution of geomatics methodologies, laser scanning and digital photogrammetry (Guarnieri et al. 2012; Yastikli 2007; Remondino 2011) can be used to generate the refined models of real-world CH, which is known as Scan-to FEM. In order to effectively use the geometric data derived by 3D laser scanning for structural purposes, it is necessary to perform operations that transform a point cloud into a continuum model (Barazzetti et al. 2015; Castellazzi et al. 2015; Fortunato et al. 2017; Pepe et al. 2020). The complete DT model contains not only the FEM but also the real material properties. In addition, accuracy of DT analysis prediction strongly depends on the properties of materials evaluated experimentally. By combining with full-field deformation measurement technology, virtual field method (VFM) (Pierron and Grédiac 2012; Ma et al. 2020) and finite element model updating (FEMU) method (Lecompte et al. 2007; He and Liu 2018) have been used to extract elastic properties in a constitutive model. As the most general and intuitive method for identifying the material constitutive parameters, the FEMU method is based on full-field displacement measurements and allows characterizing complex constitutive laws. In-situ deformation monitoring of shipwreck structure can be used to compensate for the differences in material properties between recent and archaeological wood, which can be used as input for the necessary FE analysis of the shipwreck during the design of the supporting structure. Meanwhile, the deformation monitoring data can better understand the structural behavior of the ship and provide accurate data support for the design of improved support structure.

Considering the growing threats faced by heritage places, monitoring physical factors that can potentially threaten the integrity of tangible features of significance can be particularly helpful in supporting preventive conservation strategies (Mesas-Carrascosa et al. 2016). Devices to monitor specific factors influencing internal and external conditions of assets to support preventive conservation approaches have for long been used by specialist in heritage conservation (Elfadaly et al. 2018). Based on observation, control, and recording of a wide variety of critical physical parameters, sensors allow experts to detect abnormal changes in environmental conditions that could threaten buildings and sites' integrity. in addition to the obvious short-term benefits, long-term storage of data provided by the sensors can contribute to a better understanding of interference between CH assets and their environment by comparing such data to the information collected along with the different phases of conservation projects. And the data monitored at the same time can also be used to update the DT model to make better predictions.

Optical-based monitoring techniques are getting more and more attention along with the acceleration of optics and image processing because of its advantages of non-contact and high precision. Several non-contact optical measurement methods have been applied in the areas of structural monitoring (Balletti et al. 2016; Wang et al. 2018; Galantucci and Fatiguso 2019; Sabato et al. 2020). Due to the size of the object to be monitored, the complexity of the shape, the required measurement accuracy, the time required for operation, and the cost of the system, not all available optical techniques can be applied to monitoring the deformation of wooden structures of archaeological shipwrecks.

This research presents a method combining nondestructive testing technology and DT for preventive conservation of wooden cultural relics, which can generate the refined models of real-world stern. The generated 3D mirror model can be used to predict deformation and design structural intervention. Meanwhile the in situ monitoring was used to update the 3D mirror model and improve its predictive performance. Section 2 presents the progress of generate the 3D mirror model; Section 3 presents DT was used to structural intervention; and Section 4 is the conclusion.

2 Digital twin of Quanzhou Bay Song

2.1 Case Study Description and in Situ Investigations

The 13th-century oceangoing merchant ship Quanzhou Bay Song, shown in Figure 1(a), is the earliest and larger three-masted wooden ship salvaged from the marine mud and conserved in China. Since 1959, the ship has been on display to the public at the Quanzhou Maritime Museum. The residue length of the shipwreck is 24.20 m, and its maximum residue width is 9.15 m. Three types of wood were used in the shipwreck: fir, pine and camphor wood. Most of the hull, including hull boards and bulkheads, were made of fir, the keel and bottom plate were made of pine, and the mast base, lutchet, ribs and stern post were made of camphor wood.

2.2 Structural Intervention

Currently, the shipwreck is suffering from increasing deformation over time, which is caused by the time-dependent deformation of the wood members, as well as the damage accumulation due to chemical degradation and physical shrinkage and swelling. Quanzhou Bay Song shipwreck is currently placed on a steel support rig of 6 herringbone cradles and 6 reinforcing ribs connected by large I-beams and concrete box girders. The cradles fit as close to the hull in order to provide good contact and even support. The weight of the shipwreck is therefore concentrated at point loads, which has resulted in the bending of the weakened wood structure between the cradles. This is especially true in the stern, where the lutchet is heavy and lies beyond the herringbone cradle, causing the stern to sag (as shown in Figure.1(b)).

With the aim of reinstating the sound condition of the Quanzhou Bay Song, strengthening works were carried out between May 2021 and June 2021. The design of the structural intervention was conceived not only to contain the existent damage, but also to prevent its further occurrence and to meet both conservation and economic requirements. Therefore, a stern reinforcement project implemented by the Quanzhou Maritime Museum as part of a larger project to secure the long-term stability of the shipwreck structure was to use the same type of steel support to improve the stern support structure to slow or even eliminate the sagging of the stern (as shown in Figure 1(c)).

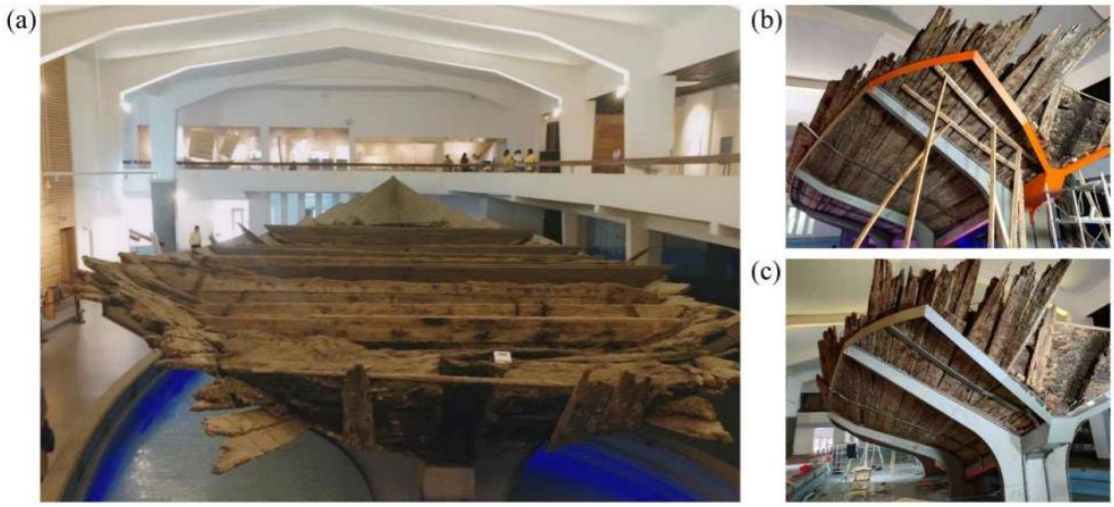

Figure 1—(a)The 13th-century oceangoing merchant ship Quanzhou Bay Song. (b) The constructed steel support frame. (c)The finished steel support frame.

2.3 Establish the geometry model of digital twin

2.3.1 Laser Scanner Acquisition

Before the structural intervention, advanced digital tools were exploited to achieve a more detailed knowledge of the ship and to keep track of its current condition for future comparative analysis. Particularly, in December 2016, a laser scanner survey was performed aiming at obtaining high-resolution spatial data for both accurate geometrical representation and geo-referenced damage mapping. Thanks to this powerful digital tool, a valuable reference 3D model featuring 2641995 points, and stern of the model featuring 42161 points and carrying precise volumes of information of the ship was obtained and herein exploited to build the geometry of its digital twin.

2.3.2 Scan-to -FEM

The software industry Geomagic Studio 2015 is currently focusing on the definition of parametric-based modelling approaches, which allow performing in no time the transition from half-raw survey data (point clouds) to 3D geometrical entities, i.e., CAD or BIM elements. Such approaches may be widely applicable to heritage buildings because they are frequently characterized by architectural layouts consisting of regular modules and repetition of architectural orders (Serlio 1982; Alberti 1992). The point cloud data obtained by laser scanning was processed by the software to obtain a 3D surface model of the hull, which is hollow. The 3D surface model was then processed to obtain a 3D digital mirror of the hull.

2.4 Estimation of material parameters

In our study, FEMU method was used to estimate the material parameters. And the elastic properties of recent wood are used as the initial parameters are to carry out the calculations. Nodal displacements are collected and compared to the experimental counterparts. Accordingly, an objective function $Q(\bar{r})$ can be indicated unweighted least squared difference between the experimentally determined and numerically calculated displacements:

$$Q(\bar{r}) = \sum_{i=1}^{n} \left[\left(u_i^{FEM}(\bar{r}) - u_i^{DIC}(\bar{r}) \right)^2 + \left(v_i^{FEM}(\bar{r}) - v_i^{DIC}(\bar{r}) \right)^2 + \left(w_i^{FEM}(\bar{r}) - w_i^{DIC}(\bar{r}) \right)^2 \right] \quad (1)$$

where $\{\bar{r}\}$ indicate a set of unknown material properties consisting of the material density and nine elasticity constants, u_i^{FEM} and u_i^{DIC} are the FEM-calculated displacement component and DIC-extracted displacement

component at the position of the i-th finite element node along the x-direction respectively, v_i^{FEM} and v_i^{DIC} are the FEM-calculated displacement component and DIC-extracted displacement component at the position of the i-th finite element node along the y-direction respectively and n is the number of data used for calculation. For orthotropic materials, the compliance matrix $[C]$ can be written in terms of nine engineering elasticity constants as follow:

$$[C] = \begin{bmatrix} \frac{1}{E_1} & \frac{-\upsilon_{21}}{E_2} & \frac{-\upsilon_{31}}{E_3} & 0 & 0 & 0 \\ \frac{-\upsilon_{12}}{E_1} & \frac{1}{E_2} & \frac{-\upsilon_{32}}{E_3} & 0 & 0 & 0 \\ \frac{-\upsilon_{13}}{E_1} & \frac{-\upsilon_{23}}{E_2} & \frac{1}{E_3} & 0 & 0 & 0 \\ 0 & 0 & 0 & \frac{1}{G_{12}} & 0 & 0 \\ 0 & 0 & 0 & 0 & \frac{1}{G_{13}} & 0 \\ 0 & 0 & 0 & 0 & 0 & \frac{1}{G_{23}} \end{bmatrix} \tag{2}$$

Levenberg-Marquardt nonlinear least squares optimization method was used to identify the parameters. The sensitivities of the displacements to the properties of these material can be extracted by finite difference approximations. The partial derivative of displacement extracted by DIC with respect to material characteristics is defined as the sensitivity matrix. And the changes in material properties, can be associated through the sensitivity matrix.

$$\begin{bmatrix} \frac{\partial\{u\}}{\partial E_1} & \frac{\partial\{u\}}{\partial E_2} & \cdots & \frac{\partial\{u\}}{\partial \upsilon_{12}} & \cdots & \frac{\partial\{u\}}{\partial G_{23}} & \frac{\partial\{u\}}{\partial \rho} \\ \frac{\partial\{v\}}{\partial E_1} & \frac{\partial\{v\}}{\partial E_2} & \cdots & \frac{\partial\{v\}}{\partial \upsilon_{12}} & \cdots & \frac{\partial\{v\}}{\partial G_{23}} & \frac{\partial\{v\}}{\partial \rho} \\ \frac{\partial\{w\}}{\partial E_1} & \frac{\partial\{w\}}{\partial E_2} & \cdots & \frac{\partial\{w\}}{\partial \upsilon_{12}} & \cdots & \frac{\partial\{w\}}{\partial G_{23}} & \frac{\partial\{w\}}{\partial \rho} \end{bmatrix} \begin{Bmatrix} \Delta r_1 \\ \Delta r_2 \\ \vdots \\ \Delta r_{10} \end{Bmatrix} = \begin{Bmatrix} \{u^{FEM}\} - \{u^{DIC}\} \\ \{v^{FEM}\} - \{v^{DIC}\} \\ \{w^{FEM}\} - \{w^{DIC}\} \end{Bmatrix} \tag{3}$$

The parameters are updated iteratively. The residual error vector at any iteration change to the suggested parameter r. Finally, a new $\{r\}$ is computed using $\{r\}_{i+1} = \{r\}_i + \{\Delta r\}_i$. The iterative process is repeated until the square of the error between the displacements calculated by FEM and the displacements extracted by DIC (shown as Eq. (1)) is lower than the predetermined error margin and material properties are updated together.

3 DT for structural intervention

After establishing the 3D mirror model of shipwreck stern, the deformation of the stern was predicted through this system, and an ideal structural interference was designed.

3.1 DT for structural intervention design

The ideal structural interference for shipwreck stern designed by the system is to add support on both sides of the stern (Figure 2(a)), which based on the prediction results of the 3D mirror model. Figure 2 (c) and Figure 1(c) show the structural intervention for stern with 3D mirror model and real-world object, respectively.

Figure 2(b) shows the deformation prediction of stern after structural intervention. Compared with nonintervention, the maximum deformation of the stern decreased from 0.254mm to 0.115mm, and the maximum deformation of the stern rudder decreased from 0.084mm to 0.002mm, which effectively prevented the deformation of the hull and the sinking of the stern rudder under the influence of gravity. Due the complexity of the surface of the stern, the reinforcement structure of compound space curved surface was designed (Figure 2 (c)).

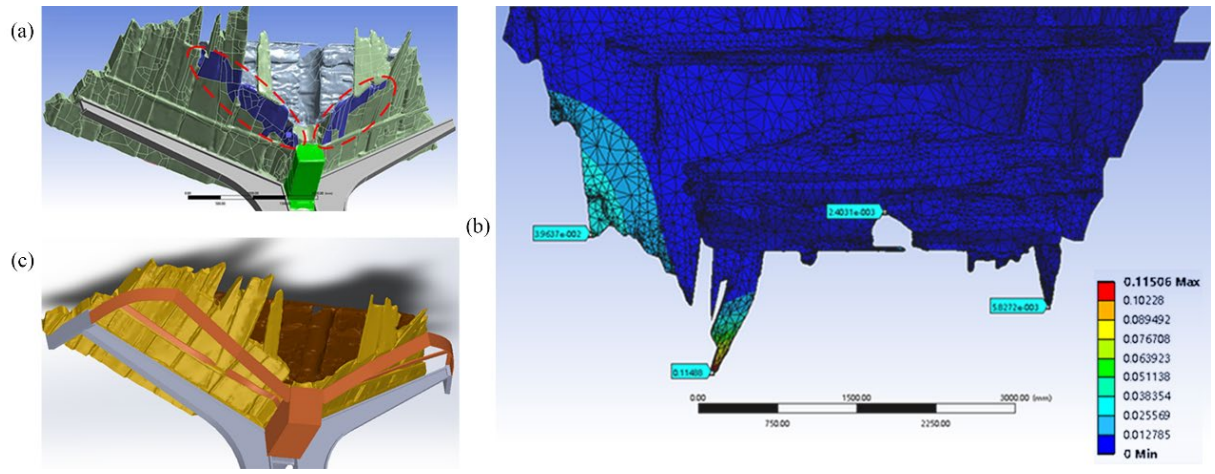

Figure 2—(a) Schematic diagram of the area to be reinforced (b) Deformation displacement with structural intervention (c) Schematic diagram of stern reinforcement scheme.

3.2 Results with structural interference

The deformation of shipwreck stern was extracted by stereo-DIC during the structural interference. And before the structural interfering, the stern was supported by wooden frame. As shown in Figure 3, the monitoring results show that the average horizontal displacement in the three areas of the stern rudder varied within the range between -0.3mm and 0.2mm and the vertical displacement varied within the range between -0.4mm and 0mm. The stern had a slightly "outward expansion" deformation in the horizontal direction, and a slightly displacement in the vertical direction. The deformation indicates that the stern was supported by the wooden frame, and the deformation was conducive to structural interference and would not affect the stability of the overall structure.

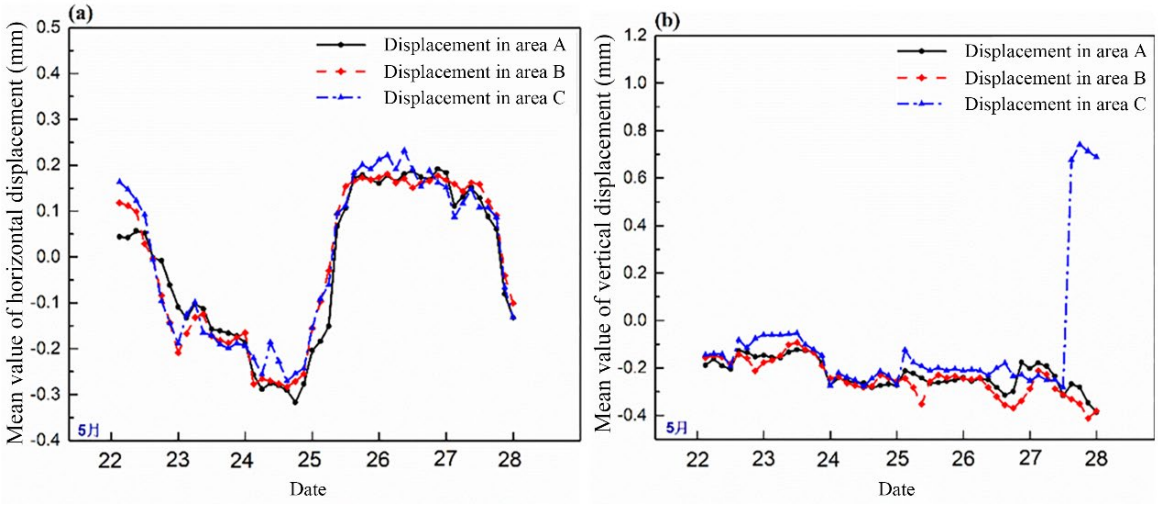

Figure 3—Monitoring results of stern rudder after structural strengthened. (a) Horizontal displacement. (b) Vertical displacement.

As shown in Figure 1(c), the designed structural interference was fixed to support the stern. The monitoring results were shown in Figure 3(a), and the outward expansion trend of the stern was effectively prevent. As shown in Figure 3 (b), the mean value of displacement in the vertical direction of area C sharply changed in the after structural interfering, and its displacement increased from -0.2mm to

0.7mm. The stern had a deformation with a small clockwise rotation, which eliminated the uneven stress on the left and right sides of the stern. The left side of the stern was slightly raised, while the right side was relatively reduced. And the monitoring results verifies the effectiveness of the designed structural interference.

4 Conclusions

In this paper, a method combining nondestructive testing technology and DT for preventive conservation of wooden shipwreck stern is proposed to monitor and predict the current situation of shipwreck stern. In order to obtain a proper digital twin of this structure, the generated parametric model is imported into an FE environment and then calibrated via an inverse dynamic problem, using as reference metrics the material properties identified from field deformation data monitored before and after a retrofitting intervention. In addition, it can not only update the material properties of the stern but also can be used to design the reasonable structural interference. The validity of the designed structural interference is verified by in situ monitoring, which an also verify the validity of the DT.

Acknowledgments

This work was supported by the Fundamental Research Funds for the Central Universities (2021ZY67).

References

Afshar, R.; Alavyoon, N.; Ahlgren, A. [and others]. 2021. Full scale finite element modelling and analysis of the 17th-century warship Vasa: A methodological approach and preliminary results. Engineering Structures. 231. https://doi.org/10.1016/j.engstruct.2020.111765.

Afshar, R.; Van Dijk, N.P.;Bjurhager, I. [and others]. 2017. Comparison of experimental testing and finite element modelling of a replica of a section of the Vasa warship to identify the behaviour of structural joints. Engineering Structures. 147:62-76. https://doi.org/10.1016/j.engstruct.2017.05.051.

Alberti, L.B. 1992. De re Aedificatoria. Ediciones Akal: Madrid, Spain.

Balletti, C.; Beltrame, C.; Costa, E. [and others]. 2016. 3D reconstruction of marble shipwreck cargoes based on underwater multi-image photogrammetry. Digital Applications in Archaeology and Cultural Heritage. 3(1):1-8. https://doi.org/10.1016/j.daach.2015.11.003.

Barazzetti, L.; Banfi, F.; Brumana, R.[and others]. 2015. Cloud-to-BIM-to-FEM: Structural simulation with accurate historic BIM from laser scans. Simul. Model. Pract. Theory. 57:71–87. https://doi.org/10.1016/j.simpat.2015.06.004.

Castellazzi, G.; D'Altri, A.M.; Bitelli, G.[and others]. 2015. From laser scanning to finite element analysis of complex buildings by using a semi-automatic procedure. Sensors . 15:18360–18380. https://doi.org/10.3390/s150818360.

Elfadaly, A.; Attia, W.; Qelichi, M.M. [and others]. 2018. Management of Cultural Heritage
Fei, L.H. 2014. An investigation of the state of conservation of the Song Dynasty Shipwreck in Quanzhou Bay.China Cult. Herit. 2:74–79.

Fortunato, G.; Funari, M.F.; Lonetti, P. 2017. Survey and seismic vulnerability assessment of the Baptistery of San Giovanni in Tumba (Italy). J. Cult. Herit. 64-78. https://doi.org/10.1016/j.culher.2017.01.010.

Galantucci, R.A.; Fatiguso, F. 2019. Advanced damage detection techniques in historical buildings using digital photogrammetry and 3D surface anlysis. Journal of Cultural Heritage. 36:51-62. https://doi.org/10.1016/j.culher.2018.09.014.

Guarnieri, A.; Remondino, F.; Vettore, A. 2012. Digital photogrammetry and tls data fusion applied to cultural heritage 3D modeling. Int. Arch. Photogramm. Remote Sens. Spat. Inf. Sci. 36:1–6.
He, T.; Liu, L.; Makeev, A. 2018. Uncertainty analysis in composite material properties characterization using digital image correlation and finite element model updating. Composite Structures. 184:337-351. https://doi.org/10.1016/j.compstruct.2017.10.009.

Lecompte, D.; Smits, A.; Sol, H. [and others]. 2007. Mixed numerical-experimental technique for orthotropic parameter identification using biaxial tensile tests on cruciform specimens. International Journal of Solids and Structures. 44(5):1643-1656. https://doi.org/10.1016/j.ijsolstr.2006.06.050.
Ma, X.Y.; Wang, Y.; Zhao, J. 2020. Optimized Polynomial Virtual Fields Method for Constitutive Parameters Identification of Orthotropic Bimaterials. Advances in Materials Science and Engineering, 2974723. https://doi.org/10.1155/2020/2974723

Mesas-Carrascosa, F.J.; Verdú Santano, D.; de Larriva, J.E.M.[and others]. 2016. Monitoring heritage buildings with open source hardware sensors: A case study of themosque-cathedral of Córdoba. Sensors 16:1620. https://doi.org/10.3390/s16101620

Pepe, M.; Costantino, D.; Garofalo, A.R. 2020. An efficient pipeline to obtain 3D model for HBIM and structural analysis purposes from 3D point clouds. Appl. Sci. 10:1235. https://doi.org/10.3390/app10041235.

Pierron F, Grédiac M. 2012. The Virtual Fields Method. New York: Springer.
Remondino, F. 2011. Heritage recording and 3D modeling with photogrammetry and 3D scanning. Remote Sens. 3:1104–1138. https://doi.org/10.3390/rs3061104.

Sabato, A.; Valente, N. A.; Niezrecki, C. 2020. Development of a Camera Localization System for Three-Dimensional Digital Image Correlation Camera Triangulation. IEEE Sensors Journal. 20(19):11518-11526. https://doi.org/10.1109/JSEN.2020.2997774.

Serlio, S. 1982. The Five Books ofArchitecture. Dover publication: New York, NY, USA.
Sites Using Remote Sensing Indices and Spatial Analysis Techniques. Surv. Geophys. 39:1347–1377.

Wang, Z.Q.; Zhao, J.; Fei, L.H. [and others]. 2018. Deformation Monitoring System Based on 2D-DIC for Cultural Relics Protection in Museum Environment with Low and Varying Illumination. Mathematical Problems in Engineering. 13:2018. https://doi.org/10.1155/2018/5240219.

Yastikli, N. 2007. Documentation of cultural heritage using digital photogrammetry and laser scanning. J. Cult. Herit.8:423–427. https://doi.org/10.1016/j.culher.2007.06.003.

Influence of Moisture Content on Mechanical Properties and Damage Forms of Ancient Timber Members

Zhenbo Xin*
School of Technology, Beijing Forestry University, Beijing, China, zb_xin6@163.com

Houjiang Zhang
School of Technology, Beijing Forestry University, Beijing, China, hjzhang6@bjfu.edu.cn

Dongfang Ke
School of Technology, Beijing Forestry University, Beijing, China, qingdaoyxqz@163.com

Yongzhu Yu
School of Technology, Beijing Forestry University, Beijing, China, yu_yongzhu@163.com

Abstract

Timber members are the key load-bearing components and indispensable parts of the ancient wooden architecture, and their physical and mechanical properties affect the safety and stability of the structure. Moisture content (MC) is one of the most important factors for mechanical properties and damage forms of timber. Ancient larch (*Larix principis-rupprechtii Mayr*) timber, and ancient nanmu (*Phoebe zhennan S. Lee*) timber, two kind main specie timbers used for northern China royal wooden architectures, were used to analyze the effect of MC on mechanical properties and damage forms in this paper. The mechanical properties and damage forms of specimens with 3 levels MC were used in the mechanical tests. Total 36 small clear specimens were obtained from ancient and current timber of both larch and nanmu timber. Firstly, 3 groups were divided equally of 36 specimens processed, and MC of 3 groups was adjusted to high, medium, and low levels respectively by using constant temperature and humidity chamber and drying oven. And then, the load-displacement curves were obtained using a universal material testing machine to analyze the effect of MC on the damage forms. Modulus of rigidity (MOR), modulus of elasticity (MOE) and compressive strength parallel to grain (CSPG) were calculated to analyze the influence of MC on mechanical property parameters.

The results indicated that there was a significant influence of MC on the bending damage form of larch timber specimens, however, the damage forms of compressive parallel to grain for both larch and nanmu specimens were less affected by MC. In addition, the MOR, MOE and CSPG of specimens both decreased with the increase of MC and showed a clear negative correlation.

Keywords: ancient timber members, mechanical properties, damage forms, moisture content

Introduction

Wooden structure architecture in China has a distinctive national style and artistic characteristics with a history of more than several hundred years, which is a valuable cultural heritage. Timber members are the most basic components, and their physical and mechanical properties affect the safety of the wooden

structure building. Nowadays, modulus of rigidity (MOR), modulus of rigidity (MOE) and compressive strength parallel to grain (CSPG) are mainly evaluation factors in the detection of ancient timber members (Xin et al.2021). They are the important mechanical performance parameters for evaluating the main load-bearing structures of wooded ancient architectures, which can be used to the safety assess of beams and columns, respectively. And it can be used for the maintenance, conservation restoration and analysis of the causes of damage and even in the reconstruction of the damaged architecture (Feio et al.2015).

The effect of MC on mechanical properties cannot be ignored. Wood is inherently hygroscopic, and moisture changes make it easy to structural variations that can affect a variety of properties (Dietsch et al. 2015). Generally, an increase in strength and stiffness due to the reduction in MC below fibre saturation point (FSP) is assumed (Dietsch et al.2015; Brandner et al.2016;Skaar 1988). As the MC can affect the wood microstructure and the mechanical properties as well as the damage forms (Harada et al.2005), and they are the key points to affect the safety of ancient wooden structure architecture. Thus, there is a significant interest in studying the effect of MC on the mechanical properties and damage forms of timber in ancient buildings.

In resent years, there have been many studies on the effects of MC on the physical, mechanical and chemical properties of wood and wood products as the important effect of MC on the properties of timber (Nocetti et al. 2015; Shirmohammadi, et al. 2021; Zhong et al.2021). Meanwhile, the physical and mechanical properties of ancient timbers have been irreversibly changed during hundreds of years of service, such as physical and mechanical properties, color parameters and equilibrium moisture content (EMC) (Kranit et al.2016; Zhang 2022). It has been shown that there is a significant difference between the moisture behavior of aged timber and that of the corresponding current timber, but comparative studies of moisture effects on mechanical property parameters and damage forms of aged and current timber are relatively rare.

In this study, ancient larch (*Larix principis-rupprechtii Mayr*) timber and ancient nanmu (*Phoebe zhennan S. Lee*) timber, obtained from a dismantled ancient building, were conducted to obtaied the small clear specimens. At the same time, the corresponding current timber were used to comparative analysis. Firstly, the specimens were kept in a constant temperature and humidity chamber and drying oven to adjust their MC. And then, the MC of the specimen was adjusted to low, medium and high levels. Next, standard mechanical tests were carried out to obtain displacement-load curves and mechanical properties of the specimens under three levels MC. The effect of MC on damage forms and mechanical property parameters was analyzed in the end.

Materials and methods

Materials

Larch (*Larix principis-rupprechtii Mayr*) timber and nanmu (*Phoebe zhennan S. Lee*) timber were commonly used in ancient Chinese royal architecture, being used as key timber elements such as beams and columns. In this study, each of the 18 larch and nanmu small clear specimens were processed for the study of the effects of MC on mechanical properties and damage forms, where each 9 specimens were from ancient timber and corresponding current timber, and with dimensions of 20 × 20 × 300 mm ($R \times T \times L$), as shown in Figure 1.

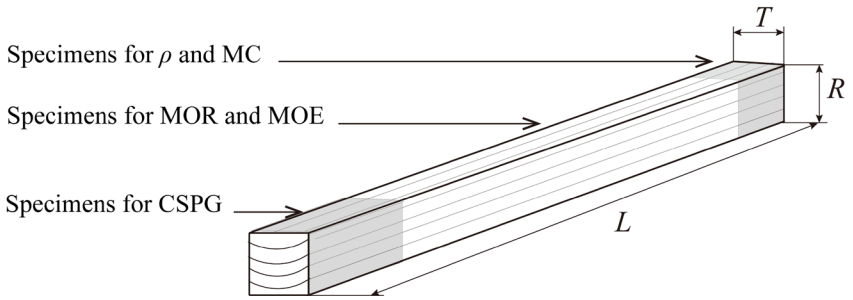

Figure 1 Small clear specimens

Drying ovens and constant temperature and humidity chambers were used to adjust the MC of the specimens, which were adjusted to 3 levels. First, the first group of specimens were adjusted to a moisture content in the range of 2-5% by drying ovens to simulate timber members in warm rooms in northern China in winter. In the second group, the specimens were placed in a constant temperature and humidity chamber at 65% relative humidity and 20°C for 7 days and the specimens were adjusted to a MC of about 12% [Ross 2021]. In the third group, the specimens were placed in a constant temperature and humidity chamber at 90% relative humidity and 40°C for 7 days, and the specimens were adjusted to a MC of around 15-20% to simulate the timber members in the rainy and hot summer months in China.

Testing method

The universal mechanical testing machine was used to test the MOE, MOR and CSPG, at the same time, the load-displacement curves of each specimen were obtained by the universal material testing machine. Meanwhile, in order to analyse the effect of MC on the mechanical properties parameters quantitatively, the MC and mechanical properties parameters of each specimen were calculated by the following formulas.

$$\mathrm{MC} = \frac{m_1 - m_0}{m_0}, \quad MOR = \frac{3p_{\max} l}{2RT}, \quad MOE = \frac{23pl^3}{108RT^3 f}, \quad CSPG = \frac{p_{\max}}{RT}$$

Where R and T are the dimensions of R and T direct of small clear specimens, p_{max} is the force by fracture, l is the distance between the middle supports of universal material testing machine, f is the strain of specimens, p is the force at f strain. where m_1 was the weight of the specimen when tested, m_0 was the total dry weight of the specimens.

Results and discussion

Effect of MC on bending damage

As shown in Figure 2, there are the load-displacement curves of the larch specimen during bending damage, where the solid line correspond to the current timber specimen and the dashed line represent the ancient timber specimen. Firstly, it can be seen that the displacements and loads at damage of the ancient timber specimens are significantly lower than those of the current timber. At the same time, the displacements were increased and the load were reduced of bending damage as the MC increases, and this phenomenon can be observed more evidently from the current timber. On the other hand, there is a more pronounced difference in the damage form for ancient and current specimens. The ancient larch specimens showed a clear brittle fracture accompanied by a large ringing sound at the time of damage under three levels MC. In contrast, the current timber specimens only showed a slight rattling at the lower-level MC. Consequently, it can be found that there is a higher breaking load but smaller displacement that can be withstood for larch specimens at lower MC, while as the MC increases, the displacement that the specimen can withstand increases, but its ultimate breaking load decreases significantly.

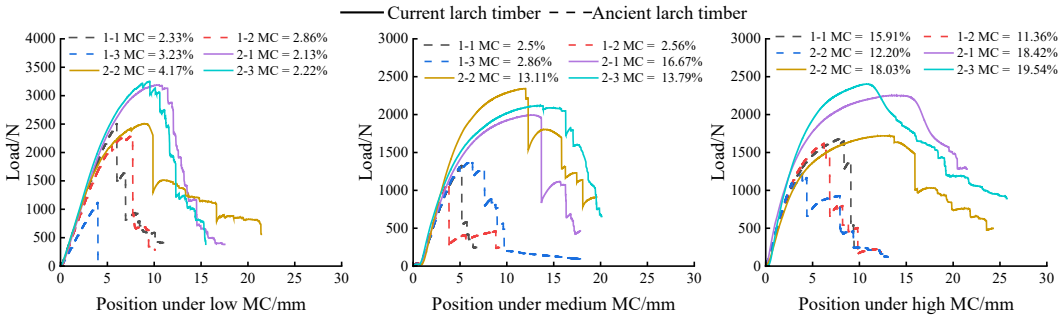

Figure 2 Load-displacement curves of larch bending damage

The load-displacement curves of the nanmu specimen is shown in Figure 3, with the solid line being the current timber and the dashed line being the ancient timber. It can be observed firstly that there is little difference in the maximum displacement between the ancient and current nanmu specimens under three levels MC. However, in contrast, the maximum load that both ancient and current nanmu specimens showed a significant decrease as the MC increased. At the same time, there was a similar form of damage in the ancient and current nanmu specimens, both showed a clear brittle fracture with a sound at breakage under the three levels MC, which showed a obvious difference from that phenomenon of the larch specimens.

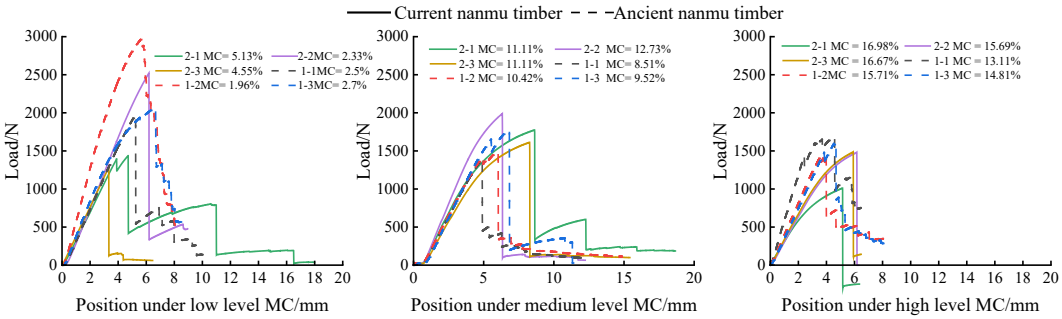

Figure 3 Load-displacement curves of nanmu bending damage

Effect of MC on compressive damage of parallel to grain

Figure 4 shows the load-displacement curves during the compressive damage of parallel to grain of the larch specimen. It can be found that the ultimate loads of the current larch specimens are slightly higher than those of the ancient larch timber specimens, but there is no significant difference in their displacement at damage. The damage form at all three levels MC is shown similar, as a rapid increase in load with increasing displacement at the beginning, and there was a small decrease in load with the increase in displacement, and then no further increase in load with further increase in displacement until the specimen is destroyed. And it can also be found that there is no significant effect on the damage form by the MC.

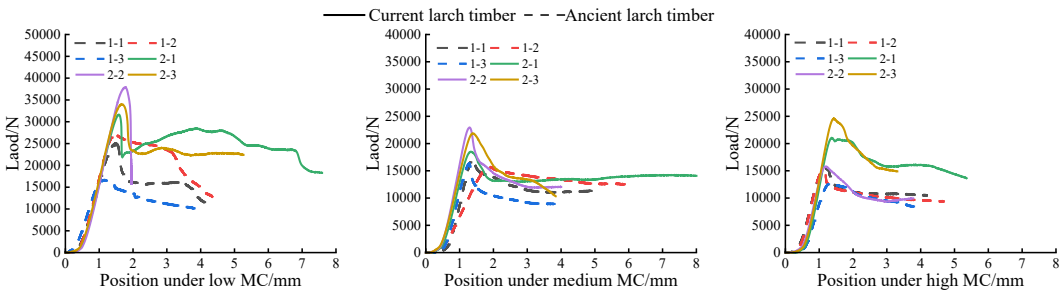

Figure 4 Load-displacement curves of larch compressive damage of parallel to grain

Figure 5 shows the load-displacement curves during the compressive strength parallel to grain of the nanmu specimen. As can be seen in Figure 5, there is no significant difference in the displacement of the ancient and current nanmu specimens, but a significant decrease of their ultimate load with the increase of MC. At the same time, there was no significant effect of MC on the damage form of the nanmu specimens, which was similar to that of the larch specimens.

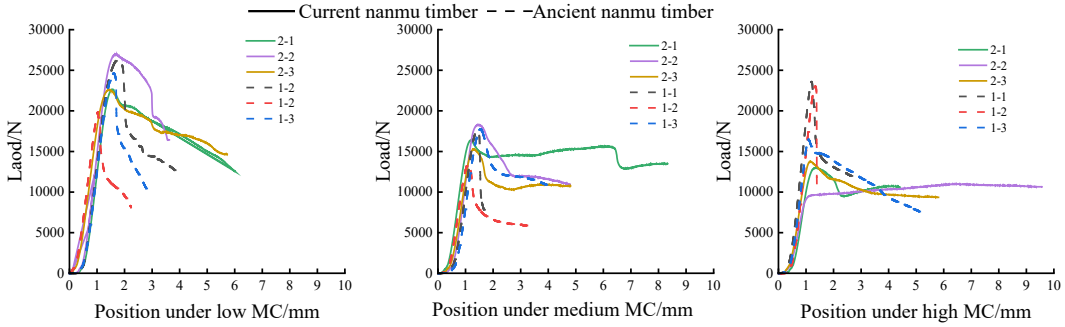

Figure 5 Load-displacement curves of nanmu compressive damage of parallel to grain

Effect of MC on mechanical property parameters

MOR, MOE and CSPG of the larch specimens were calculated and used to analyses the effect of MC on the mechanical properties parameters. The relationships between mechanical property parameters and MC of ancient and current larch specimens are shown in Figure 6. Firstly, it can be found that the mechanical properties of the current larch specimens are significantly higher than those of the ancient wood members at the same MC, whereas it can also be noticed that the mechanical property parameters decrease significantly with increasing MC.

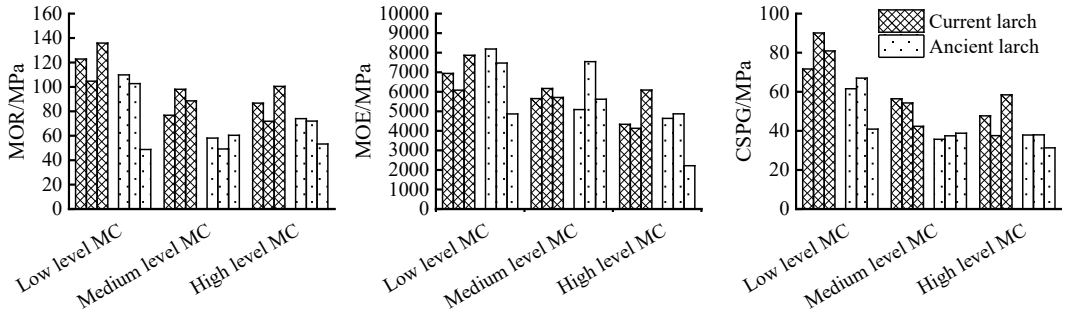

Figure 6 Relationships between mechanical property parameters and MC of larch specimens

Figure 7 shows the mechanical properties of nanmu ancient and current specimens under three levels MC. Firstly, it can be noted that the mechanical properties of new and old heather are similar at the same MC. In contrast, the mechanical property parameters of the current and ancient nanmu specimens were shown a significant negative correlation with MC.

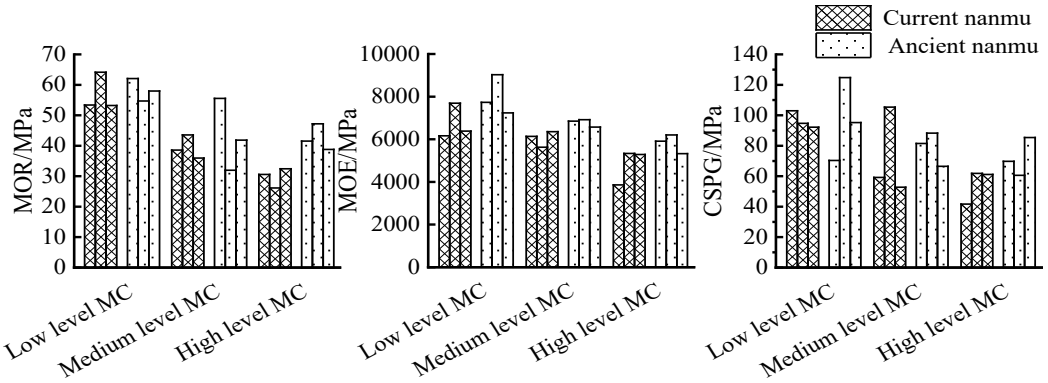

Figure 7 Relationships between mechanical property parameters and MC of nanmu specimens

Discussion

The main purpose of this study is to investigate the effect of MC on the mechanical properties and damage forms of timber members. For timber members of ancient architecture, the high MC increases the displacement of the timber members of ancient buildings, but their ultimate load is reduced. Obviously, the higher MC has a more pronounced negative effect on the mechanical properties parameters. The main reason for this phenomenon may be that water molecules are more easily accessible to the wood microstructure at relatively high MC, causing the amorphous areas of the wood to wet up and the microstructure to be more loosely organized. In this condition, crystallinity of the wood easily decreases and more susceptible to stress relaxation at a macroscopic level, which leads the mechanical property parameters to be reduced (Chen 2018). At the same time, as the MC of the specimen increases, the water molecules are connected to the hydroxyl groups on the cellulose macromolecule chains in a hydrogen bonding mode. Therefore, it is easier for the wood filaments to break and more prone to slip and fracture. In the case of ancient timeber members, the cellulose and hemicellulose are degraded and the relative content is reduced under the effect of natural ageing. Therefore the change in MC has a weaker effect for ancient timber than that for current timber.

Therefore, it can be seen that an appropriate reduction in the MC of timeber members of ancient buildings will help to increase their ultimate load, and reduce the probability the decay and insects or other diseases. Yet, the precursor warning function of timber members in ancient architecture will reduce owing to low MC, timber members are easily susceptible to more severe brittle fractures, especially facing larger random loads. Consequently, suitable human control of the MC is necessary, in the routine maintenance of timber members of ancient buildings.

Conclusions

The objective of this study is to investigate the effect of MC on the mechanical properties parameters and damage forms of ancient timber member. The conclusions are shown as follows:

(1) There is a significant effect of MC on the form of bending damage for timber specimens, with the ultimate load decreasing and the displacement increasing as the MC increases for both larch and nanmu specimens. At the same time, with the MC decreases, the degree of brittle fracture increased and the early warning ability of the larch specimens decreased, yet there is weak influence on the nanmu specimen.
(2) There is a significant effect of MC on the load of compressive damage for both larch and nanmu specimens. Whereas, there is a weak effect on displacement and the damage form of MC for larch and nanmu specimens.
(3) The MC has a significant negative effects on the mechanical property parameters, as the MOE, MOR and CSPG decrease significantly with increasing MC.

References

Xin, Z.B.; Guan, C.; Zhang, H.J. [and others].2021. Assessing the density and mechanical properties of ancient timber members based on the active infrared thermography, Constr. Build. Mater. 304.

Feio, A.; Machado,J.S. 2015. In-situ assessment of timber structural members: Combining information from visual strength grading and NDT/SDT methods – A review, Constr. Build. Mater. 101.1157-1165.

Dietsch, P.; Gamper, A.; Merk, M. [and others]. 2015. Monitoring building climate and timber moisture gradient in large-span timber structures, Journal of Civil Structural Health Monitoring 5(2). 153-165.

Dietsch,P.; Franke,S.; Franke,B. [and others]. 2015. Methods to determine wood moisture content and their applicability in monitoring concepts, Journal of Civil Structural Health Monitoring 5(2) 115-127.

Brandner, R.; Flatscher,G.; Ringhofer,A. [and others]. 2016. Cross laminated timber (CLT): overview and development, European Journal of Wood and Wood Products 74(3). 331-351.

Skaar,C. 1988. Wood-Water Relations, Springer Series in Wood Science.

Nocetti, M.; Brunetti, M.; Bacher,M. 2015. Effect of moisture content on the flexural properties and dynamic modulus of elasticity of dimension chestnut timber, European Journal of Wood and Wood Products. 73(1).51-60.

Shirmohammadi,M.; Leggate, W.; Redman, A. 2021. Effects of moisture ingress and egress on the performance and service life of mass timber products in buildings: a review, Constr. Build. Mater. 290.

Zhong,X.; Zhang, S.J.; Ma, N.E. 2021. Variation in pore size distribution of wood cell wall under different moisture states, Journal of Beijing Forestry University, 2021, 43(11): 128−136.

Chen, S.Y. 2018. Micro-analysis of wood under different percentage of moisture, Inner Mongolia Agricultural University.

Harada,M.; Hayashi,Y.; Hayashi,T. [and others]. 2005. Effect of moisture content of members on mechanical properties of timber joints, Journal of Wood Science 51(3) 282-285.
Kranitz,K.; Sonderegger,W.; Bues,C.T. [and others]. 2016. Effects of aging on wood: a literature review, 50(1) 7-22.

Zhang, D. 2022. Properties change under natural aging of ancient building larch members, Journal of Civil and Environmental Engineering.

Ross, R. 2021. Wood handbook: wood as an engineering material. General Technical Report FPL-GTR-282. Madison, WI: U.S. Department of Agriculture, Forest Service, Forest Products Laboratory. 543 p

Nondestructive Evaluation of the Concealed Wood Columns in Historic Buildings

Houjiang Zhang *
School of Technology, Beijing Forestry University, Beijing, China, hjzhang6@bjfu.edu.cn

Zhenbo Xin
School of Technology, Beijing Forestry University, Beijing, China, zb_xin6@163.com

Yongzhu Yu
School of Technology, Beijing Forestry University, Beijing, China, yu_yongzhu@163.com

Dian Zhang
The Palace Museum, Beijing, China, zhangdian126@126.com

Hui Wang
The Palace Museum, Beijing, China, 2827904490@qq.com

* Corresponding author

Abstract

The supporting wood columns in the ancient buildings in China are normally partialy or completely wrapped within the wall systems. Decay can occure on the contact areas between the wood columns and the wall, and there is limited access for physical testing and inspection operation. Through the field inspection of an ancient building complex in Beijing, we investigated the use of nondestructive testing and evaluation methods for assessing the conditions of the concealed or partially concealed wood columns and determined the location and extent of the defects within the wood columns. The inspection results of this study provides basis for repairing the wood columns in the building complex, and also provides proved nondestructive testing procedures for evaluating the concealed wood columns in similar ancient wood buildings.

Sixty-eight wall wood columns in the Main Hall, East Hall and West Hall of the building were used as the investigation objects. First of all, the exposed face, air vent and opening of wood columns were used for field detection, which includes external defect detection, sounding detection, internal defect detection and moisture content detection. Then, the data of wood column sizes, surface defect types and sizes, micro drill resistance curves and so on were collected and analyzed to evaluate the defects status of each wood column tested, and the decay distribution law of the wall wood columns were summed.

The main forms of external defects were external decay and material loss, and the main forms of internal defects were internal decay and cavity. For a single wood column, the decay mainly occurred in the area where the wood columns were in contact with the wall at the cross sections. In the longitudinal, decay mainly occurred in the bottom of the wood column, and the decayed decreased with the height.

Keywords: wall wood columns, defects, evaluation, decay

Introduction

China has a large number of historic wood structure buildings. Wood columns are one of the key load-bearing components of those buildings, supporting the full load on the top of the building. However, as a biomaterial, wood is prone to decay and other defects after many years of service. Common defects of wood columns mainly include decay, cavity, cracks and overall deformation. These defects will reduce the carrying capacity of the columns, and then affect the stability and safety of the whole building (Guo et al. 2019, Wang 2017). From their relationship with the building walls, they can be divided into wall wood columns and independent wood columns. Wall wood column refers to the column that contacts the wall, partially or completely wrapped by the wall, and the independent wood column refers to the column that has a certain distance from the wall with no obstacles around.

NDT refers to method which detects the properties, states and defects of the surface and interior of the tested object by means of physical or chemical means and by using modern technology and equipment, without damaging or affecting the performance of the tested object (Duan et al. 2002, Zhang et al. 2016). At present, the commonly used NDT methods for ancient building wood components mainly include tapping detection, micro-drill resistance detection, stress wave detection and others (Zhu et al. 2011).

The historic building courtyard tested in this paper was built in 1540, and eight emperors used it as their office and residence in the Qing Dynasty (Figure 1). A research protection with systematic research and repair was officially started in 2018, in which the detection and repair of the wood columns is one of the important works (Zhang 2019). There are 94 wood columns in the main hall, east hall and west hall, including 68 wall wood columns and 26 independent wood columns. Wall wood columns account for 72.3% of the total number of wood columns. These wall wood columns directly contact brick, soil and other wall materials, poor ventilation conditions, easy to wet, produce decay and other defects. How to use nondestructive methods to effectively detect and evaluate their defects, is a key task that needs to be carefully solved, which related to the smooth progress of the renovation project.

This paper takes the 68 wall wood columns as investigation objects to carry out nondestructive testing and evaluation of their defects, especially the existence law of decay. It can provide reference for nondestructive testing and evaluation of other ancient wood buildings.

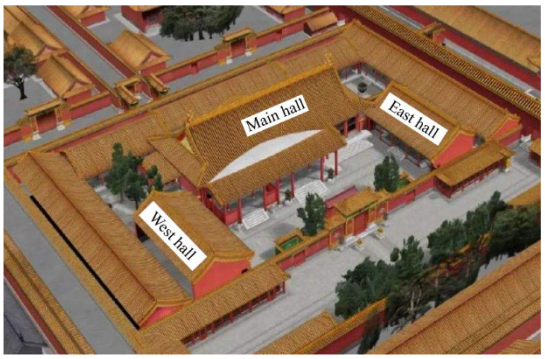

Figure 1—The historic wood building courtyard

Inspecting objects

For the 68 wall wood columns in this study, some wood columns have two exposed surfaces, some have one exposed surface, and some are completely wrapped by the wall without an exposed surface. In the latter two cases, some wood columns have one air vent (at the bottom of the column) or two air vents (at the bottom and upper part of the column) on the wall. Therefore, from perspective of degree of the

wooden column wrapped by the wall and whether there one or two vents, the 68 wall wood columns can be divided into five categories: double-sided exposed, single-sided exposed with vent, single-sided exposed without vent, completely wrapped with vent, and completely wrapped without vent. The schematic diagram is shown in Figure 2. Table 1 shows the number of wood columns of each type in the three buildings.

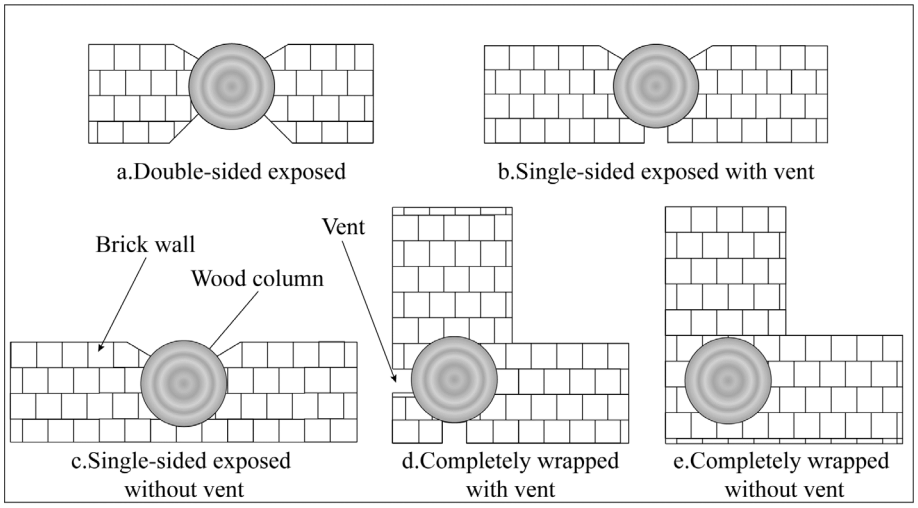

Figure 2—Schematic diagram of 5 types of the wall wood columns

Table 1—Type and quantity of wall wood columns

Building name	Double-sided exposed	Single-sided exposed with vent	Single-sided exposed without vent	Completely wrapped with vent	Completely wrapped without vent	Total
Main Hall	8	1	15	10	2	36
East Hall	4	4	6	0	2	16
West Hall	4	4	6	0	2	16
Total	16	9	27	10	6	68

Study metheds

On-site inspection

For four types of wood columns, i.e. double-sided exposed, single-sided exposed with vent, single-sided exposed without vent, completely wrapped with vent, make full use of the appearance and air vents to observe, detect and evaluate the external and internal defects of the wood columns. For the fifth type of wood columns, completely wrapped without vent, one or more holes on the wall near the middle and lower part of the wood columns were opened, to observe and use instruments to inspect and evaluate the defects. On-site inspection processes and methods include external defect detection, sounding, internal defect detection, moisture content detection and tree species sampling. The inspection was conducted on five sunny days in October 2020, with a temperature of 7-18℃ and wind class 1-2.

The instruments used include micro-drilling resistance meter, moisture meter, increment core, etc., and general tools used include probe, hammer, tape measure, awl, etc. The micro-drilling resistance meter used was Resistograph 4452-P developed by Rinntech, Germany, and the moisture meter used was a probe-type wood moisture content meter. The increment core used was Haglof with 80 cm length, which was used to detect and sample the wood columns through the vents or opening holes.

Laboratory analysis and evaluation

The data of column sizes, surface defect types and sizes, micro drill resistance curves and moisture content obtained by the field inspection were summarized and analyzed to evaluate the defects of each wood column tested. Tree species of wood columns were identified. According to the evaluation results, the wood columns were classed and the defect status were drawn.

The formulation of classification criteria refers to Chinese national standard GB / T 50165-2020, GB / T 13942.2-2009, DB11 / T 1190.1-2015, and combined with actual situation of the wood columns. Four parameters are defined as shown in the following formulas.

$$k = \frac{S_e}{S}, \quad p = \frac{S_i}{S}, \quad m = \frac{l_c}{l}, \quad n = \frac{h_c}{d}$$

Where, S_e is cross-section area of the external defects and S_i is cross-section area of the internal defects, S is cross-section area of the wood columns, k is external defect area proportion coefficient, p is internal defect area proportion coefficient. For crack defects, l_c and h_c are crack length and depth respectively, l and d are length and diameter of the wood columns respectively, and m and n are crack length and depth proportion coefficients respectively.

The classification criteria of wood columns are shown in Table 2. Grade A columns are in good condition and need no intervention, grade B columns have certain defects and require regular review or appropriate intervention, grade C columns should not be used, suggesting replacement or pier connection. Grade B includes grade B1 and Grade B2. Grade B1 columns do not need repair, but require regular review. Grade B2 also have certain defects, need making a dry environment or a proper reinforcement.

Table 2—Classification criteria of wood columns

Defect types	Grade A	Grade B1 and B2	Grade C
External defect	$k < 0.05$	$0.05 < k < 0.45$	$k > 0.45$
Internal defect	$p = 0$	$0 < p < 0.15$	$p > 0.15$
Crack	$m \leq 0.1$ $n \leq 0.1$	$0.1 < m < 0.8$ $0.1 < n < 0.8$	$m > 0.8$ $n > 0.8$

Results and analysis

Overall situation of wood column defects

Forms of the wood column defects

The defects of ancient wood members usually can be divided into external defects and internal defects. The external defects usually include cracks, surface decay, material loss and overall deformation, while the internal defects mainly include internal decay, internal cavities and internal cracks, etc.

It is found that main forms the external defects of the wood columns in this yard are external decay and material loss caused by decay, and secondary form is crack. Main form of internal defect is internal decay, and secondary form is internal crack. The external defects of wood columns can be directly observed and measured through visual inspection, while the internal defects of wood columns need to be inferred by detection results of the micro-drilling resistance, which cannot be directly observed. Figure 3 shows three external forms of defects of the wood columns.

Surface decay Material loss Surface crack

Figure 3—External defects of the wall wood columns

Classification results of the wall wood columns

Total 68 wall wood columns of the historic buildings were inspected, and it was found 31 wood columns are grade A, 22 wood columns are grade B1, 13 wood columns are grade B2 and 2 wood columns are grade C. It means the overall preservation of wall wood columns of this yard is good, in which 53 columns are grade A and B1, without intervention, accounting for 77.9% of the total, 13 grade B2 columns require proper intervention and regular observation, accounting for 19.2% of the total, only 2 grade C columns need to be replaced in time, accounting for 2.9% of the total.

Decay regularity of the wall wood columns

Decay distribution of a single wood column

Figure 4 is schematic diagram of decay distribution law of the single-sided exposed wood columns. As shown in Figure 4a, from cross sections of a single wood column, decay is mainly external, less internal. The external decay mainly occurs on contact area with the wall, and there basically is no decay appear on exposed area of the wood column. As shown in Figure 4b, from the vertical perspective of a single wood column, decay mainly occurs on the lower part, and the root decay is the most serious, with the rise of height, the decay gradually weakens. In theory, around wrapped part by the wall, there should be about 1 cm gap between the wood column surface and the wall, namely so-called "skirt" structure, which used for the surface air flow. But in the actual detection process, it was found that the most columns have no skirt structure exist, while a small number of the columns got the skirt structure, because of the age, the gaps between the columns and the walls are filled with dust and soil. i.e. water of the walls is directly transmitted to the wood columns, resulting in a large moisture contents of the contact area of the wood, which make the wood columns wrapped by the wall prone to decay. Furthermore, the closer to the ground, the greater humidity of the wall, resulting in higher moisture content in the lower part of the wood columns, so that more serious the root decay. Because the air vents have small sizes, and usually covered by window bricks, so vent part surfaces of the wood columns should be similar as the surface wrapped by the wall, which are also prone to decay.

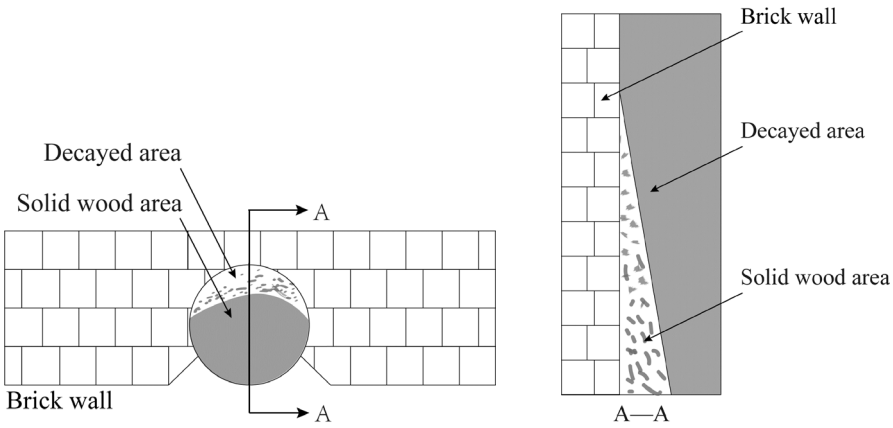

a. Transverse decay distribution b. Vertical decay distribution

Figure 4—Schematic diagram of decay law of a single-sided exposed wood column

Relationship between decay and wrapped degree of the wood columns

If existence of the vents is not considered, the wall wood columns can be divided into double-sided exposed, single-sided exposed and completely wrapped of three categories. The double-sided exposed wood column has the least wrapped degree by the wall, the completely wrapped wood column has the most wrapped degree by the wall and the single-sided exposed wood column has middle level wrapped by the wall. Figure 5a shows number of three type wood columns with various grades. It can be seen that all 16 double-sided exposed wood columns are grade A, total 36 single-sided exposed wood columns have 10 grade A, 17 grade B1, 8 grade B2 and 1 grade C, and total 16 completely wrapped wood columns have 5 grade A, 5 grade B1, 5 grade B2 and 1 grade C.

Each category of wood columns is divided into grade A + B1 (without intervention) and grade B2 + C (requiring intervention), then proportions of wood columns with the two grades is shown in Figure 5b. Where all double-sided exposed wood columns are grade A + B1 with the highest proportion, the single-sided exposed wood columns have 75% grade A + B1 with second proportion, and the fully wrapped wood columns have 62.5% grade A + B1 with the lowest proportion. The proportions of grade B2 + C of the three category wood columns are 0%, 25% and 37.5% respectively. It can be seen that decay probability of double-sided exposed wood columns is the lowest, decay probability of single-sided exposed wood columns is higher and completely wrapped wood columns are most likely to decay.

The reason for this phenomenon is that contact area between a double-sided exposed wood column and the wall is the smallest, its overall ventilation performance is good, and the flowing air easily takes away the moisture to keep the column dry, so that reducing the probability of decay occurring. For single-sided exposed and completely wrapped wood columns, the contact area between the column surface and the wall gradually increases, and more water transmit from the wall into the wood column. The moisture in the column cannot be discharged in time, resulting in a high moisture content in the contact area, which is prone to fungal growth and increases probability of the wood decay.

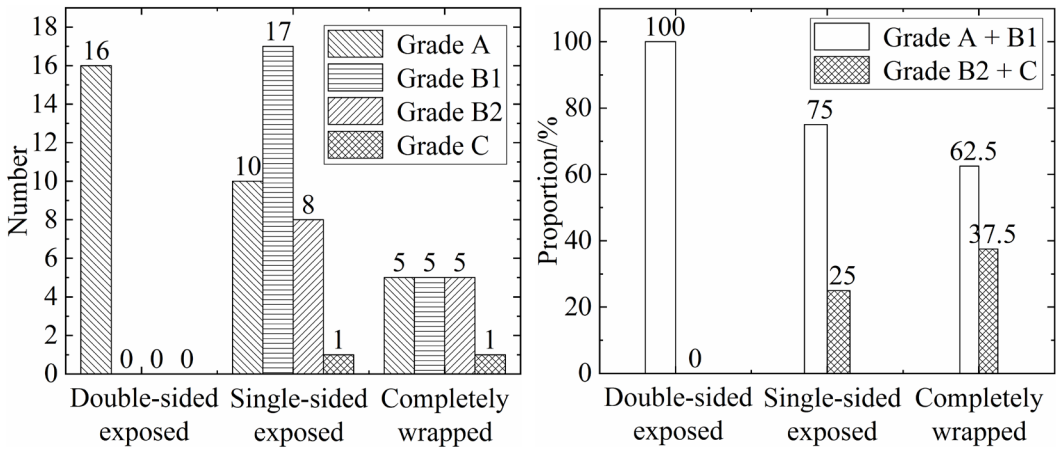

a. Number of wood columns of various grades b. Proportions of wood columns of various grades

Figure 5—Effects of different wrapped degree on the grade of wall wood columns

Conclusions

Wall wood columns of historic buildings are partly or totally wrapped by wall, the contact area of the columns with the walls are easy to decay, and the detection operation spaces are poor. Therefore, this paper takes wall wood columns of main hall, east hall and west hall of a yard of historic buildings as research object to carry out nondestructive testing and evaluation of defects of the wood columns. The main conclusions were obtained as following.

1) The practice has proved that it is feasible to detect and evaluate external and internal defects of wall wood columns using combination of visual inspection, sounding, micro-drilling resistance, moisture content measuring, through exposed faces, air vents and openings of the columns.
2) Main forms the external defects of the wood columns in this yard are external decay and material loss caused by decay, and secondary form is crack. Main form of internal defect is internal decay, and secondary form is internal crack.
3) The overall preservation of wall wood columns of this yard is good, in which 53 columns are grade A and B1, without intervention, accounting for 77.9% of the total, 13 columns are grade B2, requiring proper intervention and regular observation, accounting for 19.2% of the total, 2 columns are grade C, needing to be replaced in time, accounting for 2.9% of the total.
4) For a single wood column, in the transverse sections, decay mainly exists in contact area with the wall, while on the longitudinal direction, decay mainly occurs at the lower part, usually the root decay is serious then gradually decreases upward.
5) For the entire wall wood columns, decay probability of double-sided exposed wood columns is the lowest, decay probability of single-sided exposed wood columns is higher and completely wrapped wood columns are most likely to decay.

References

Duan X F, Li Y D, Wang P. 2002. Review of NDE Technology as applied to wood preservation. China wood industry, 16(5): 14-16.

DB11 / T 1190.1 – 2015 Technical code for appraiser of structural safety of ancient building Part 1: timber structure. 2015.

Guo K L, Zhang H J, Guan C, et al. 2019. Time domain analysis and research on local coin-tap signals of wood members. Forestry Machinery & Working Equipment, 47(2): 42-46.

Ministry of Development of the People's Republic of China. GB / T 28990 – 2012 Code for non-destructive evaluation of interior decay and modulus of elasticity of historic building wood members by stress wave methods. Beijing: Standards Press of China, 2012.

Ministry of Development of the People's Republic of China. GB / T 50165 – 2020 Technical code for maintenance and strengthening of ancient timber buildings. Beijing: China Architecture & Building Press, 2020.

State Bureau of Technical Supervision. GB / T 13942.2 – 2009 Durability of wood-Part 2: Method for field test of natural durability. Beijing: Standards Press of China, 2009.

Wang X. 2017. Analysis on the degradation of mechanical properties of damaged timber columns [D]. Xi'an: Xi`an University of Architecture and Technology, M.S. thesis.

Zhang D. 2019. The story of the renovation of Yangxin Hall. Forbidden City, (12): 54 - 61.

Zhang H J, Guan C, Wen J. 2016. Applications and research development of nondestructive testing of wood based materials. Journal of Forestry Engineering, 1(6): 1-9.

Zhu L, Zhang H J, Shun Y L, et al. 2011. Research status of Non-destructive Testing technology for wooden components of ancient architectures. Forestry Machinery & Working Equipment, 39(3): 24-27.

Flexible Machine Strength Grading: Using Acoustic NDT of Green Sawn Timber to Calculate Grading Settings for Individual Batches of Spruce Sawn Timber

Andreas Weidenhiller *
Holzforschung Austria, Franz-Grill-Str. 7, 1030 Vienna, Austria, a.weidenhiller@holzforschung.at

Andreas Neumüller
Holzforschung Austria, Franz-Grill-Str. 7, 1030 Vienna, Austria, a.neumueller@holzforschung.at

Abstract

Machine strength grading is an efficient method to achieve sawn timber of homogeneous quality. In the European machine-controlled approach, settings for machine strength grading need to be calculated in advance, based on a representative sample of destructively tested sawn timber which may need to encompass a thousand or more pieces. If an industrially graded batch deviates strongly from the characteristics of the representative sample, the grading becomes less efficient. This paper introduces and evaluates a modified approach to settings calculation which adapts the settings to the quality of the batch to be graded. The aim is to thus maintain a high grading efficiency even on deviating batches. To achieve this, the new method adjusts the original representative sample to match the current batch by means of statistical simulation. The quality of the batch is assessed by means of acoustic NDT of the green sawn timber, which can simultaneously be used to segregate the timber by quality. In contrast to the method currently in use, the new method could maintain a high grading efficiency even for batches with substantially lower quality than the representative sample. This method opens up new and interesting options for machine strength grading, especially in combination with different kinds of pre-grading. Further research should be directed towards the potential and the limitations of simulation approaches to machine strength grading.

Keywords: acoustic NDT, dynamic modulus of elasticity, green sawn timber, machine strength grading, settings for individual batches, spruce (Picea abies)

Introduction

Due to the variability inherent in the natural construction material wood, strength grading is an indispensable prerequisite for using timber for load-bearing purposes. Beside the traditional approach of visual strength grading by outer characteristics such as shape and size of knot clusters or other visible defects, in the last decades, machine strength grading has evolved as a new and highly reliable method to assess the strength of sawn timber (Ridley-Ellis et al. 2016). Based on various NDT techniques such as eigenfrequency measurement, x-rays, or imaging, estimates for the grade determining properties (GDPs) strength, stiffness and density are derived (Viguier et al. 2015). These estimates are called "indicating properties" (IPs). Timber is assigned to strength grades based on thresholds on one or more of such IPs. These thresholds are also called "settings". Several approaches to determine appropriate settings are in use. One widely used approach is based on regular destructive testing of randomly selected graded timber to make sure that the GDPs are still achieved by the graded material ("output control").

In Europe, a different approach is dominant (Ridley-Ellis et al. 2016): the so called "machine control" approach relies on initial testing of large representative quantities of sawn timber (at least 450 pieces

according to EN 14081-2:2018; in practice, often more than 1000 or even several thousand), based on which thresholds are derived which can then be used for all timber of the tested species and the designated countries of origin without almost any further testing necessary. To account for variations in the quality of the timber from these origins, EN 14081-2:2018 also provided an option for "adaptive settings", allowing the settings derived according to the procedures laid down in EN 14081-2:2018 to be adjusted in a clearly defined manner according to the previously obtained IP values for the currently graded batch.

In a simulation study, Weidenhiller (2021) did not find evidence that these "adaptive settings" could effectively improve the grading results for tension strength classes. Weidenhiller (2021) showed that a different approach based on simulation to extrapolate the timber quality from the previously obtained IP values was able to adjust much better to the timber quality, at the cost of a high computational burden.

In the present paper, we introduce an alternative method to adjust strength grading to the quality of the graded material. Strength grading usually is done almost at the end of the production process, after sawing, drying and planing of the material. This makes sense because drying and machining operations can change the shape (e.g. warping), properties (e.g. cracks) and dimensions of the timber, whereby some correlation of the strength grading result with the properties of the final product is lost. Furthermore, the moisture in the green sawn timber prevents accurate determination of density, which is an important GDP, and local variations in density can point to weak spots in the timber. Also, the density contrast in green sawn timber between wood and knots is low, so that knots can be detected by x-ray much less reliably than in the dry timber. On the other hand, a lot of energy has to be used for drying of material that then may turn out to be unsuitable for the designated purpose during the final strength grading. One solution for this dilemma is to pre-grade the material, either before (cf. Brännström 2009; Weidenhiller et al. 2021) or after sawing. Such a pre-grading step could help to reduce the variability of the sawn timber, improve the accuracy of the final machine strength grading and reduce the amount of energy required for drying and processing of material that will ultimately prove unsuitable for construction purposes. One possibility for pre-grading of the green sawn timber is by using the dynamic modulus of elasticity of the green timber ($E_{dyn,u}$). Weidenhiller (2019) showed that it was possible to predict the GDPs based on $E_{dyn,u}$.

The present paper used the results from Weidenhiller (2019) and showed how these results can be combined with simulation methods to determine individual settings for each batch of sawn timber. Thus, two objectives could be achieved simultaneously: First, it became possible to apply machine strength grading to pre-graded sawn timber, even to batches where the strongest boards had been removed, without compromising the representativity requirement of EN 14081-2:2018. Second, variations in the quality between batches of sawn timber could be taken into account, not only based on IPs measured on part of the material as is the case in adaptive settings approaches, but based on measurements performed on the entire batch in the green state. For evaluation, this approach was applied to machine strength grading data from about two million pieces of sawn timber measured by eight different wood processing companies, enhanced by simulated values for the GDPs.

Material and methods

Overview

In Figure 1, an overview of the modelling process for the current paper is given, including the raw data, which will be discussed in more detail in the Materials subsection, and the various processing steps by which the data were transformed and combined, which will be discussed in subsections with names as given in the second row of Figure 1. All calculations were performed in the open statistics platform R (R Core Team 2018).

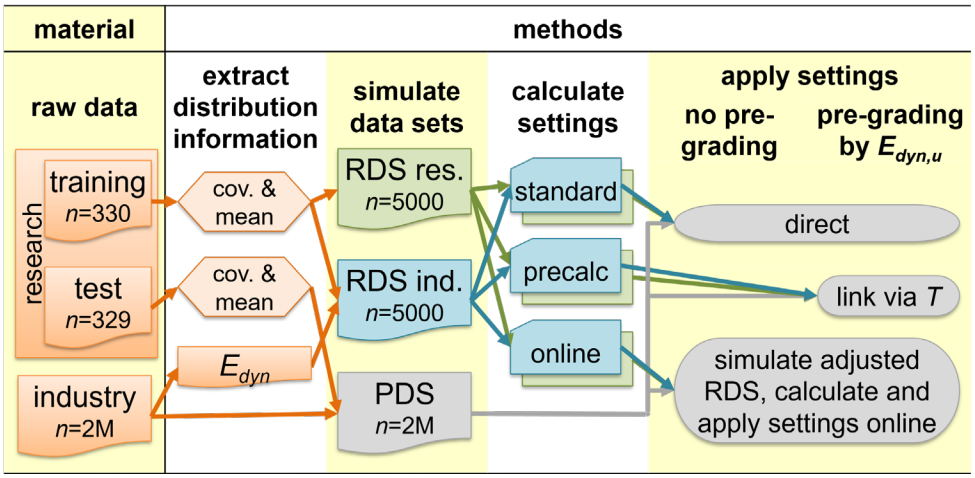

Figure 1— Overview over the link between the raw data (material) and how they were further processed (methods). RDS = reference data set, PDS = production data set.

Material

There were two main data sets, called "research" and "industry", from which processing started. The research data consisted of 659 spruce boards collected at three sites in Austria. For these boards, the dynamic modulus of elasticity was measured on the green boards ($E_{dyn,u}$), machine strength grading data was recorded on the dry boards (Microtec GoldenEye 702 and 706) and destructive tensile tests were performed. The research data set was split equally into training and test (first column of Figure 1).

The industry data set consisted of about two million spruce boards for which machine strength grading data was recorded on the dry boards in the production facilities of the supporters of the project InnoGrading (see acknowledgements). Two supporters provided data from Microtec Goldeneye 702 machines (x-ray scanner), six supporters provided data from Microtec Goldeneye 706 machines (x-ray scanner plus measurement of the dynamic modulus of elasticity E_{dyn}). Artificial production batches were defined by repeatedly grouping together 2000 consecutive pieces, which resulted in a total of 1080 batches.

Extract distribution information

The training part of the research data was split into four sub-samples to fulfill the required number of samples for settings calculation according to EN 14081-2:2018. As the material was collected from only three different sites, the boards from one site were split to form two sub-samples. For each of these sub-samples, covariance and mean information of the recorded variables were calculated. Covariance and mean information of the recorded variables were also calculated on the whole training part and the whole test part of the research data (first two entries in the second column of Figure 1). The tensile strength was log-transformed before calculating the means and covariances. The mean and covariance were the main input for the simulation described in the next section.

For each of the six wood processing companies which provided data from a Goldeneye 706, the distribution of the measured E_{dyn} values was extracted by calculating 833 or 834 equally distributed quantile values across the entire range of the E_{dyn} values (last entry in the second column of Figure 1). Four times, 833 values were calculated, and two times 834 values, to achieve a total of 5000 (target sample size according to the next section). This was also an input for the simulation.

Simulate data sets

For calculating machine strength grading settings, a representative data set consisting of at least 450 boards in at least four sub-samples was required according to EN 14081-2:2018 (see also next subsection). Such a data set will be called a "reference data set" (RDS) in the following.

In the present work, RDS data was created using simulation, supported by the package WoodSimulatR (Weidenhiller and Wegscheider 2020), an extension to the open statistics platform R (R Core Team 2020). For the method "precalc" presented in this work (see section "Calculate settings"), it was expected that a much larger RDS than the required 450 boards would be necessary. To be on the safe side, we simulated RDS with 5000 boards.

To study the effect of the RDS on the results, two RDS were simulated. "RDS research" (first entry in the third column of Figure 1) was only based on the training part of the research data set. Four times 1250 pieces were simulated based on the means and covariances of the four sub-samples of the training data.

For "RDS industry" (second entry in the third column of Figure 1), a total of 5000 E_{dyn} values from six sub-samples (i.e., the different wood processing companies) had been calculated according to the previous section. Based on the means and covariances calculated on the entire training part of the research data, matching values for $E_{dyn,u}$, as well as data from machine strength grading and destructive testing were conditionally simulated using WoodSimulatR.

While the RDS were used to calculate settings, a further data set was required to independently evaluate the accuracy of the different strength grading methods discussed in this study. The basis for this "production data set" (PDS) was the industry data. However, for the industry data, neither $E_{dyn,u}$ nor data from destructive testing were available. For the data recorded on Goldeneye 702 machines, also E_{dyn} was missing. Based on the means and covariances calculated on the entire test part of the research data, matching values for these quantities were conditionally simulated using WoodSimulatR.

Calculate settings

Three different methods for settings calculation were used (see fourth column of Figure 1): "standard" settings on the entire RDS according to EN 14081-2:2018, "precalc" precalculated settings on the RDS after applying pre-grading, and "online" settings which were calculated on a simulated data set that matched the respective batch to be graded. Details on the different methods follow below.

While in practice, settings are frequently calculated to grade timber into several strength grades in parallel, the present study focused on settings to grade into only one strength grade. This removed a lot of complexity and sufficed to compare the properties of the different settings calculation methods.

It is also possible to use multiple IPs in parallel for strength grading by defining parallel thresholds, one per grade and per IP. To simplify calculations, only one IP was considered in this work – we used (and simulated) the IP calculated by Microtec Goldeneye 706 as a predictor for tensile strength.

Settings calculation according to EN 14081-2:2018 works almost without parametric assumptions, which also means that settings for a single grade can be strongly influenced by a small number of boards. To reduce the dependency on random effects influencing the performance on a single grade, we calculated settings for an entire range of strength grades – always for grading only into one strength grade at a time.

We focused on the tension strength grades from EN 338:2016 in the range from T12 to T26. The 95% factor on the mean modulus of elasticity as defined in EN 384:2018 for the calculation of characteristic values for machine strength grading was applied. In EN 338:2016, not all integer grades between T12 and T26 are defined; e.g. T17 is missing. To maintain homogeneity for our analyses, required values for such missing grades were linearly interpolated.

For "standard" settings calculation, one has to define thresholds so that the characteristic values calculated on that part of the RDS which is within the thresholds satisfy the requirements for the desired strength grade (cf. EN 338:2016). The requirements (multiplied by a factor 0.95 for the mean and 0.90 for the fifth percentile) must also be satisfied for each sub-sample in the thresholded RDS – this is called "sub-sample verification". There are some piece count requirements (in the grade, at least 20 pieces; in the reject, at least 5 pieces and 0,5% of the total number of pieces), and there is something called "cost matrix requirement". This last requirement in EN 14081-2:2018 was the only one we didn't apply in our calculations. It usually only has minor effects. The "standard" settings calculation led to 15 different settings for the 15 target grades from T12 to T26 for each of the two RDS.

The "precalc" settings calculation worked exactly like the "standard" settings application, but with a reduced RDS. By thresholds of T with 9000 N/mm² to 13000 N/mm² in steps of 1000 N/mm² on the $E_{dyn,u}$, the RDS was split in two parts – in one "below T" and in one "above T". For each value of T, settings were calculated both for "below T" and for "above T". To maintain a sufficient number of pieces in the reduced RDS for all thresholds T, a much larger RDS was required than is usual for method "standard". The "precalc" settings calculation led to $15 \times 5 \times 2 = 150$ different settings per RDS: for the 15 different target grades, for the five thresholds T, and for both "below T" and "above T".

For "online" settings calculation, the preparation just consisted in storing means and covariances of the variables for each sub-sample of the RDS. In practical application in the industry, the actual settings calculation for method "online" would be done for a batch after the dynamic modulus of elasticity $E_{dyn,u}$ has been measured for all boards of the batch in the green state, and after any splitting of the batch, e.g. in a sub-batch "below T" and in a sub-batch "above T". "Online" settings calculation would then be done separately on each sub-batch. This was also simulated in the present study. For each such sub-batch, an adapted RDS (aRDS) was simulated which was 200 times as large as the sub-batch, but with at most 5000 boards. The simulated aRDS was randomly split in as many sub-samples as were in the original RDS (in the study: four for the research RDS, six for the industry RDS). Simulation was performed conditional on the measured distribution of the $E_{dyn,u}$ values from the sub-batch using WoodSimulatR. On this simulated aRDS, settings calculation again was performed just as in the "standard" settings calculation. "Online" settings calculation was performed both without pre-grading (15 target grades for 1080 batches and the two RDS) and with pre-grading (15 target grades for five thresholds, for both "below T" and "above T", for 1080 batches and two RDS).

Apply settings

Settings for methods "standard" and "online" were applied both without pre-grading and with pre-grading. For settings of method "precalc", pre-grading was a prerequisite; therefore, application without pre-grading was not possible for this method (see fifth and sixth column of Figure 1).

For each batch (or sub-batch) and each applied setting, the following quantities were stored for further analysis: the number of pieces in the batch (always 2000 without pre-grading, but less than 2000 with pre-grading), the number of pieces in the grade, and the actual characteristic values of the in-grade timber of this batch.

Evaluate the results

Based on the actual characteristic values of the in-grade timber of a batch (or sub-batch), the highest grade was selected for which the characteristic values still satisfied the requirements defined in EN 338:2016. This grade was called the "achieved grade". This achieved grade ideally would be equal to the "target grade" for which the settings had been calculated, but due to the variability in the material properties, this will not always be the case. Therefore, the "deviation from the target grade" was calculated, as the numerical difference $deviation = grade_{achieved} - grade_{target}$. Due to our choice of grades T12 to T26 in steps of 1 N/mm², these deviations were integer values. The batches were grouped into five groups according to their deviation values: "-2-" meant two grades or more below the target grade, "-1" meant one grade below the target grade, "0" meant equal to the target grade, "1" meant one grade above the target grade, and "2+" meant two grades or more above the target grade.

For each application of a single setting, a certain batch would fall into exactly one of these five groups. For all application results in a certain category, e.g. all "standard" settings applied without pre-grading, the number of pieces in each of the five groups was added up, giving a total amount of in-grade-timber in each group. As the timber was graded multiple times into different grades and with pre-grading by different thresholds T, each batch and each piece of timber contributed to this count multiple times. If one divided the count of the in-grade timber by the sum of all in-grade timber in this category, one got the share that each of the five groups had relative to the total amount of in-grade timber. If one divided the count by the sum of the sizes of the involved batches, one got the share that each of the five groups had relative to the total grade yield. These two quantities, the share of the in-grade timber and the share of the grade yield, were used to visualize and compare the grading accuracy of the methods "standard", "online" and "precalc".

Results and discussion

In Figure 2, the accuracy of the methods "standard", "online" and "precalc" is compared both without pre-grading (left panels) and with pre-grading (shown separately for sub-batches "below T" and "above T" in the center and right panels). The methods are given on the horizontal axis. For each method, the share of timber in batches with different deviations from the target grade is shown, both relative to the total amount of in-grade timber (top panels) and relative to the total amount of timber in the batches (bottom panel).

For grading without pre-grading (left panel) and for the sub-batches "above T" (right panel), the accuracy of the methods was very similar. But for the sub-batches "below T" (center panel), the accuracy of method "standard" was much lower. This is as expected, and it highlights the importance of the requirement in EN 14081-2:2018 that the RDS has to be representative of the material which is to be graded with the settings calculated based on this RDS. The sub-batches "below T" only contained timber with an $E_{dyn,u}$ below a certain threshold T – in other words, the strong boards had been removed. This shifted the distribution of the properties in such a way that the "standard" settings were no longer valid for sub-batches "below T". Using method "precalc" instead of method "standard", the representativity requirement could be fulfilled within the framework of the current standard EN 14081-2:2018. Figure 2 clearly shows that in this way, the share of in-grade timber with a negative deviation from the target grade (achieved grade lower than the target grade) could be brought back to the level of the scenario without pre-grading.
The downside of the method "precalc" was that the number of settings to be calculated in advance was nine times larger than for method "standard", and in the practical application, one can only choose one of the five pre-grading thresholds defined during settings calculation. Moreover, for the calculation of the settings, only a potentially small part of the RDS could be used, because the threshold had to be applied to

the RDS, as well. Depending on the thresholds one wants to calculate settings for, a very large RDS may be required. As the creation of an RDS requires destructive testing of all the involved timber, this may become prohibitively expensive.

The method "online" used a radically different approach. As described in the section "Calculate settings", this method relies on simulation and may, therefore, require much less destructive testing. On the other hand, the accuracy of the method crucially depends on the way the simulated aRDS is created and on whether this aRDS truly matches the batch for which the settings are to be calculated. According to Figure 2, method "online" was as accurate as method "standard" without pre-grading and almost as accurate as method "precalc" for sub-batches "below *T*". The downside of method "online" in comparison to method "standard" was that all timber needed to be scanned twice: once, for example, in the green state, and once during the final strength grading. Further, each sub-batch needed to be individually tracked through the production so that the results from the first scan could be used as input for the final strength grading.

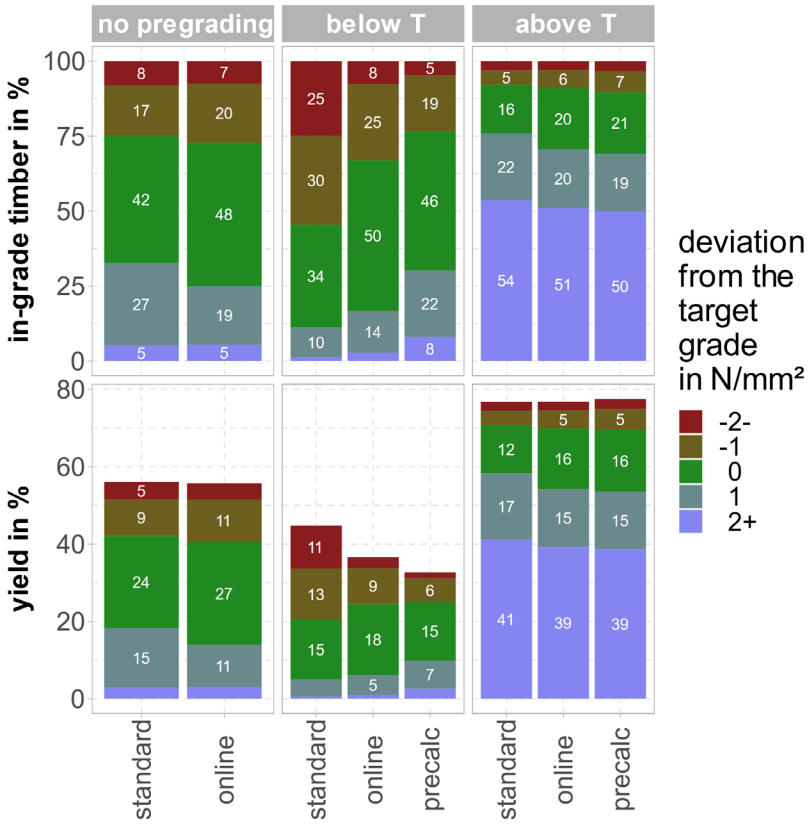

Figure 2— Comparison of grading accuracy between the standard method and the new methods "online" and "precalc". Timber share by deviation from the target grade for the different methods, relative to the total amount of in-grade timber (top panel) and relative to the total amount of timber (bottom panel).

While method "standard" in the scenario without pre-grading was equally accurate as method "online", it is important to note that for both methods, about 25% of the in-grade timber were in batches where the achieved grade was lower than the target grade (top left panel of Figure 2). However, this doesn't necessarily imply that in current industrial practice, also one quarter of the batches don't reach the target grade. The settings for this study were calculated on artificial data sets based on destructively tested timber originating in Austria (although no doubt part of the material processed by the sawmills and

included in the industry RDS was imported), so the different sub-samples from both RDS used in this study possibly were less heterogeneous than is the case for RDS used for calculating settings for practical applications. Thanks to the sub-sample verification required by EN 14081-2:2018, such heterogeneity leads to more conservative settings.

To determine how the grading results depended on the RDS used, Figure 3 contrasts the accuracy observed when using settings calculated on the industry RDS (also shown in Figure 2) with the accuracy when using settings calculated on the research RDS. For this, the horizontal axis was modified in comparison to Figure 2. The method names were abbreviated to "std", "on" and "pre" and were suffixed with the abbreviations "ind" and "res" for the industry RDS and the research RDS, respectively.

Comparing just the accuracy of the methods on the research RDS with one another leads to similar results as for the industry RDS discussed above: The accuracy of all three methods was comparable except for "below *T*", where method "standard" was much less accurate. However, compared to the settings from the industry RDS, the yield increased (bottom panels of Figure 3) and the share of in-grade timber with an achieved grade below the target grade increased even more. This implies that a good sampling to achieve a representative RDS is as important for methods "online" and "precalc" as it is for method "standard".

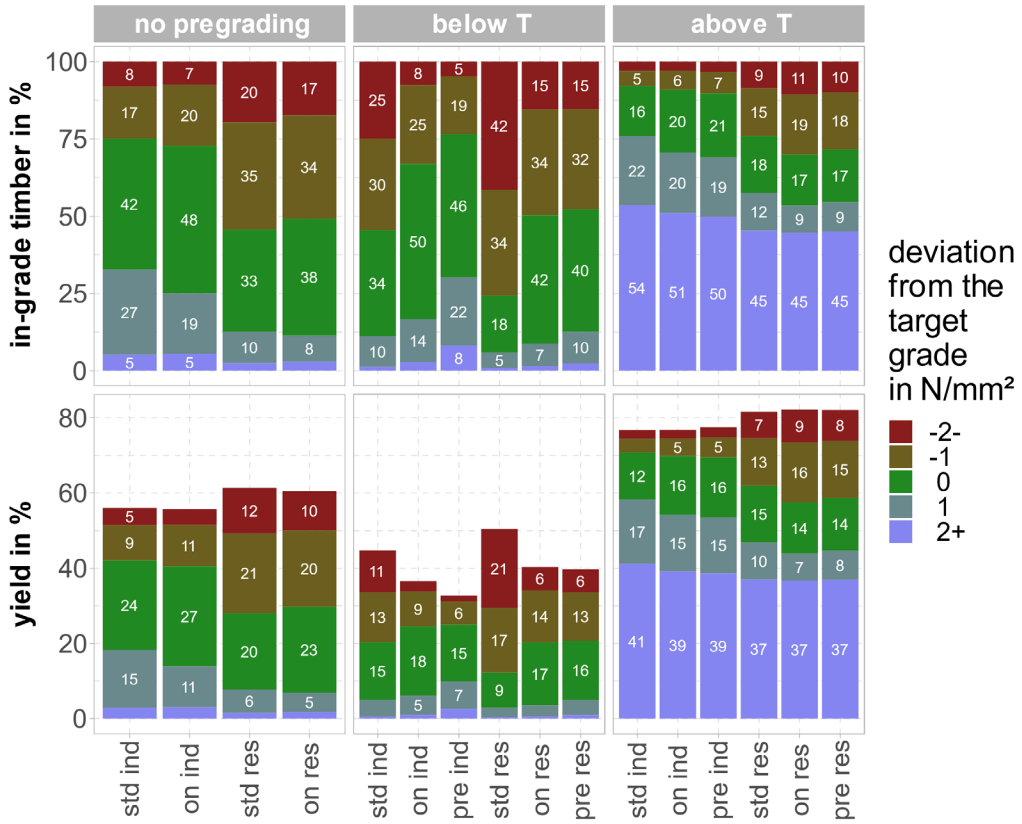

Figure 3— Comparison of grading accuracy between the standard method ("std") and the new methods, abbreviated "on" and "pre", for settings calculation based on the two different reference datasets industry ("ind") and research ("res"). Timber share by deviation from the target grade for the different methods, relative to the total amount of in-grade timber (top panel) and relative to the total amount of timber (bottom panel).

Conclusions

In this paper, we introduced two methods for machine strength grading which are compatible with pre-grading of the material. Method "precalc" worked by calculating a large number of settings a priori for a pre-defined set of pre-sorting thresholds at the cost of requiring a potentially huge number of destructive tests to achieve adequate reference data for settings calculation. Method "online" worked by simulating artificial reference data which matches the characteristics of the batch to be graded; the basis for the simulation was formed by determining the dynamic modulus of elasticity of all boards in the batch in the green state. The new methods were at least as accurate as the "standard" method according to EN 14081-2:2018.

For the case where the part of the batch with the high-strength material was removed, the method "standard" showed a much worse accuracy than the methods "online" and "precalc", which means (as is known to all experts in machine strength grading) that the "standard" method must not be used on a batch from which the high-strength material has been removed.

The study also revealed that all three methods were sensitive to the statistical properties of the data set on which the settings have been calculated – it is essential that this data set is sampled representatively for the material which is to be graded with these settings.

The methods "online" and "precalc" could thus be used to implement more flexible strength grading procedures in the industry. Method "online" is promising because it offers high flexibility while requiring only a moderate (but representative) number of destructive tests to form the statistical basis. As method "online" depends on accurate statistical simulation of the timber properties and their dependencies, further research should focus on such simulation methods.

Acknowledgments

The research for this article was done within the InnoGrading project funded by the Austrian Research Promotion Agency (FFG, grant no. 869170). We thank the wood processing companies Binderholz GmbH, Doka GmbH, Hasslacher Holding GmbH, Mayr-Melnhof Holz Leoben GmbH, Pfeifer Holz GmbH & Co KG, Rubner Holzindustrie GmbH, Stora Enso Wood Products GmbH and Wiehag GmbH for supporting the project by providing sawn timber NDT data from their sites and for their feedback and discussion. We also thank Microtec srl. for data processing, feedback and discussions. The dataset of destructively tested spruce was created within the SiOSiP project (funded by FFG in the research program "Production of the Future", grant no. 843678) with the support of the project partners Rubner Holzindustrie and the Association of the Austrian Wood Industries.

References

Brännström, M. 2009. The impact of a strength grading process on sawmill profitability and product quality. BioResources 4:1430–1454

EN 338: 2016. Structural timber – Strength classes. CEN European Committee for Standardization, Brussels

EN 384: 2018. Structural timber – Determination of characteristic values of mechanical properties and density. CEN European Committee for Standardization, Brussels

EN 14081-2: 2018. Timber structures – Strength graded structural timber with rectangular cross section – Part 2: Machine grading; additional requirements for type testing. CEN European Committee for Standardization, Brussels

R Core Team 2018. R: A Language and Environment for Statistical Computing. https://www.R-project.org/

R Core Team 2020. R: A Language and Environment for Statistical Computing. R 4.0.3. https://www.R-project.org/

Ridley-Ellis, D.; Stapel, P.; Baño, V. 2016. Strength grading of sawn timber in Europe: an explanation for engineers and researchers. Eur. J. Wood Prod. 74:291–306. doi: 10.1007/s00107-016-1034-1

Viguier, J.; Jehl, A.; Collet, R.; Bleron, L.; Meriaudeau, F. 2015. Improving strength grading of timber by grain angle measurement and mechanical modeling. Wood Material Science and Engineering 10:145–156. doi: 10.1080/17480272.2014.951071

Weidenhiller, A. 2019. Towards flexible machine strength grading: Predicting the outcomes of destructive tension tests for spruce by acoustic NDT of the green sawn timber. In: Wang X, Sauter UH, Ross RJ (eds) Proceedings of 21st International Nondestructive Testing and Evaluation of Wood Symposium, Freiburg im Breisgau, pp 176–184

Weidenhiller, A. 2021. Evaluation of the European adaptive settings approach and comparison with a new simulation-based method. In: Proceedings of the World Conference on Timber Engineering WCTE 2021

Weidenhiller, A.; Huber, J.A.J.; Broman, O.; Fredriksson, M.; Brüchert, F.; Sauter, U.H.; Lycken, A.; Ziethen, R.; Oja, J. 2021. Improved strength grading based on log and board measurements – review and outlook: the research project READiStrength. In: Proceedings of the World Conference on Timber Engineering WCTE 2021

Weidenhiller, A.; Wegscheider, A. 2020. WoodSimulatR: Generate Simulated Sawn Timber Strength Grading Data. https://cran.r-project.org/package=WoodSimulatR. Accessed 21 December 2020

Nondestructive Detection and 3D Mapping of Root System of Ancient Camphor Tree Based on Ground-Penetrating Radar

Zhang Xiaowei
Joint International Research Institute of Wood Nondestructive Testing and Evaluation, School of Technology, Beijing Forestry University, Beijing 100083, China, email: zhangxw@bjfu.edu.cn

Wang Zepeng
Joint International Research Institute of Wood Nondestructive Testing and Evaluation, School of Technology, Beijing Forestry University, Beijing 100083, China, email: wangzepeng@bjfu.edu.cn

Xue Fangxiu
Joint International Research Institute of Wood Nondestructive Testing and Evaluation, School of Technology, Beijing Forestry University, Beijing 100083, China, email: fangxiuxue@bjfu.edu.cn

Li Haibin
Joint International Research Institute of Wood Nondestructive Testing and Evaluation, School of Technology, Beijing Forestry University, Beijing 100083, China, email: lihaibin@bjfu.edu.cn

Li Shuang
Joint International Research Institute of Wood Nondestructive Testing and Evaluation, School of Technology, Beijing Forestry University, Beijing 100083, China, email: beilinls@163.com

Wen Jian *
Joint International Research Institute of Wood Nondestructive Testing and Evaluation, School of Technology, Beijing Forestry University, Beijing 100083, China, email: wenjian@bjfu.edu.cn

* Corresponding author

Abstract

Hundred-year-old trees are a precious heritage left by nature and have very important historical, cultural, ecological, scientific research and high economic values. As one of the important organs of ancient trees, the root system provides important support and material exchange with the soil. But due to the complex of soil environment and root spatial distribution, it caused difficulties in obtaining the three-dimensional structure of the root system. The object of this paper is to achieve nondestructive and accurate in situ detection and 3D mapping of the root system of a 150-year-old camphor tree in Deqing, Huzhou, Zhejiang Province with ground penetrating radar (GPR), an efficient geophysical detection technique. Firstly, FK migration and Hilbert transform were employed to recognize the root on the pre-processed GPR B-scan image of the camphor tree root system. And the effectiveness and accuracy of root detection were verified by simulation experiments and fresh grapevine control experiments. After that, with considering the growth characteristics of the root system and the impact of root orientation on root detection using GPR, the root system spatial structure of camphor tree was mapped in three-dimensional space using OpenGL by combining the detected roots in the GPR B-scan images and their circular scanning traces. Finally, the spatial discretization method was adopted to obtain and analyze the distribution density map of the root system at different depths.The experiment result shows the effectiveness of the scheme in root detection and its 3D structure mapping, demonstrates the future of root nondestructive detection based on GPR and provides important data support for ancient tree conservation.

Keywords: non-destructive detection, ground penetrating radar, root detection, 3D structure mapping

Introduction

Ancient and famous trees contain rich natural, social, historical and cultural information. They play an irreplaceable role and important value in the study of natural change, climate change, the protection of forest genetic genes, the study of social history and the inheritance of traditional culture. They are also important tourism resources to show the harmony between man and nature. As one of the important organs in the growth of ancient trees, the root system not only supports the whole stem, but also participates in the exchange of water and nutrients between trees and soil (Ma et al., 2018). Accurate root detection and reconstruction of three-dimensional spatial structure can not only contribute to the study of root function, but also provide important data support for the study of inter-root soil environment and ancient tree protection. However, because the roots of ancient trees are mostly buried underground and their spatial distribution is huge and complex, it is difficult to sample and measure them in a large range. The traditional research methods for root structure are to directly obtain root samples from the soil (such as excavation method, soil column method and container method), which can directly obtain more accurate root location and distribution data. However, they would cause the destruction of soil environment and root system.

As a nondestructive testing technology widely used in underground object detection, GPR has been widely used in root detection(Liu et al., 2018 , Molon et al., 2017) with its efficient sampling, convenient use and large detection area. The high-frequency electromagnetic wave (200MHz-2GHz) emitted by GPR to the underground would produce emission, refraction and scattering phenomena when passing through the interface of media with different electrical or magnetic characteristics such as air, soil and roots. Hruska (Stokes et al., 2002) and Butnor (Butnor et al., 2001 , Butnor et al., 2003) used 450MHz antenna radar to scan the roots of oak trees, which verified the effectiveness of GPR technology in detecting the coarse roots of trees. In radar wave one-dimensional scanning data (A-Scan), the position, size, moisture content and growth direction of roots would affect the signal reflection intensity, reflection area and response time interval of A-Scan data. By analyzing the data from the embedded and screened root samples using statistical methods, the researchers(Barton and Montagu, 2004 , Guo et al., 2013) verified that the root related parameters are closely related to the A-Scan signal parameters. According to the imaging principle of ground penetrating radar, in the two-dimensional scanning image (B-scan) composed of multiple A-Scan data, The root system usually has a hyperbolic shape due to the diffraction waves that appear during the scanning of the common offset radar. Some scholars(Li et al., 2016 , Zhang et al., 2021) combine computer vision and machine learning methods to detect roots by identifying and fitting hyperbola in the preprocessed B-Scan image from the perspective of physical imaging and geometric relationship. According to the roots detected from the B-Scan data and combined with the corresponding scanning trajectory, early researchers (Wu et al., 2014 , Xiao et al., 2021) determined the connection relationship of root points on adjacent scanning surfaces according to their personal experience, and obtained the topological relationship between root detection points. In recent years, with the help of considering root parameters and three-dimensional visualization software, researchers(Butnor et al., 2016 , Zhu et al., 2014) have obtained three-dimensional images of measured tree roots and estimated root biomass.

According to the related research for tree root detection, this paper employed the GPR for the root nondestructive detection of ancient trees, presented a root nondestructive detection scheme combined with root in-situ recognition and three-dimensional mapping, and applied to an ancient camphor tree with a tree age of 150 years in Deqing County, Huzhou City, Zhejiang Province. Based on the B-scan image of the root circumference measurement section, the three-dimensional spatial distribution map of the root and the distribution density map at different depths were drawn.

Data collection

In the scheme, the common offset TRU tree radar system (SIR3000, GSSI, USA) was employed to measure the roots of ancient trees which are underground and difficult to observe. The system includes radar antenna with center frequency of 900MHz, data collector and measuring wheel. And its track interval and number of samples are 5mm and 512 respectively. For in situ root measurements, the current trajectory methods for nondestructive measurement of tree underground root systems include parallel line method, grid method, circumferential method and combined scheme were shown in the figure 1. Owing to the root system is centered on the tree trunk and grows in all directions, and the effective detection angle of the tree radar system is 45° (Cui et al., 2020), in order to ensure the effective detection and measurement simplicity and efficiency for most of the root systems, this scheme samples the circumferential measurement scheme shown in Figure 1-d. During the measurement process, starting from the track with the smallest perimeter of the trunk regarded as the geometric center, the radius of the perimeter of each measurement track increases fixedly until the area corresponding to the largest measurement circle is comparable to its canopy coverage. And for each measurement circle, the starting point is from due north and along clockwise. After the measurement, Root radar data with multiple sets of concentric circular trajectory measurement profiles with different radius could be obtained for root recgnition and its 3D mapping. Figure 1-f showed the measurement site for an ancient camphor tree with a radius of 0.78 m. In this measurement, nine circumferential scans in total were acquired and they radius increased from 0.88m by 0.5m to 4.88m.

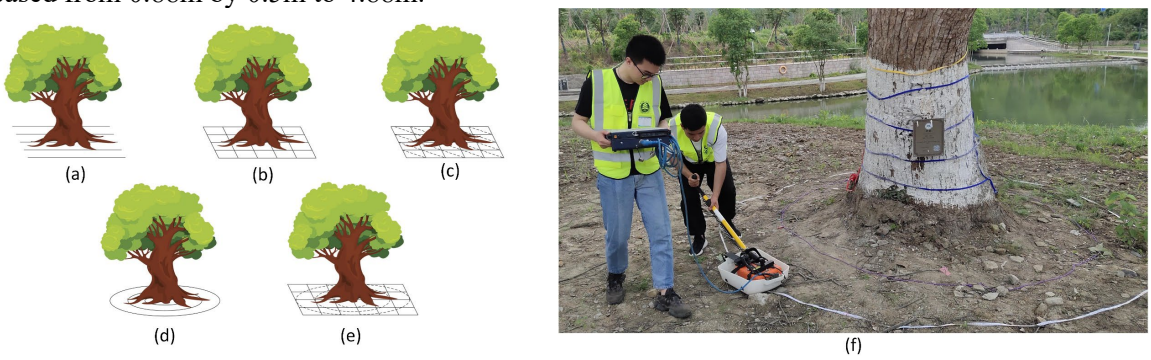

Figure 1—Camphor root system measurement program and measurement site. a),b),c),d),e) the GPR root system measurement scheme, f) the camphor measurement site

Root Recognition

To obtain the root position from the GPR B-Scan image, a three-stage process including preprocessing, FK migration, and Hilbert transform was adopted. The figure 2 showed the whole process for a controled expriment designed and detected in the Practice Base (40°29″ N, 116°20′27″ E) of Beijing Forestry University. In this detection, there are three grapevine buried 30 cm deep and 50 cm apart. The following are the details.

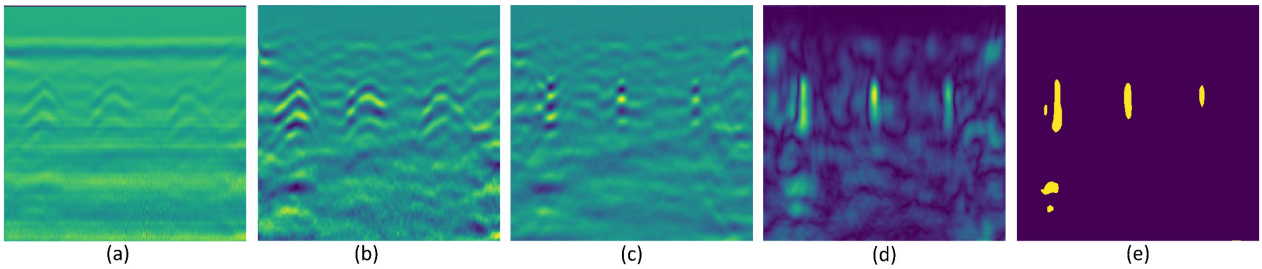

Figure 2— the process for root recognition for a controled expriment. a) the raw B-Scan image, b) the image after pre-processing, c) the image after FK migriation, d) the image after hilbert transform, e) The image after binarization.

Pre-processing

The electromagnetic waves emitted by ground-transmitting radar would emit reflection, transmission, scattering, bypassing and attenuation phenomena at the partition interface of the medium when they propagate underground. And besides the real data, the raw data of radar waves including external random noise and coherent noise caused by inter-media reflection. In order to reduce the noise in the measurement environment, the effects of direct waves and background noise are removed by averaging methods. To remove the low-frequency noise introduced by direct air-to-ground waves and the electronic saturation generated, a dewow filter was used to retain the high-frequency waves above 47.8 MHz for all data. At the same time, a trapezoidal bandpass filter was designed according to the center frequency of the antenna, which allows signals whose frequencies range from 250-500 to 1000-2000 MHz to pass through in order to remove high and low frequency noise from the amplitude spectrum corresponding to the radar data. And the median filtering in image processing based on statistical theory was adopted, which sets the filter kernel size as 5x5 to eliminate the discrete noise points in the ground-penetrating radar image data. The result after preprocessing was shown in Figure 2-b.

FK Migration

When recognizing root in GPR B-Scan image, root systems usually showed as hyperbolic pattern due to the presence of the bypassing effect. Due to the bypassing effect which affects the identification of root location, FK migration technique based on fluctuation equation was emplyed to weaken the hyperbolic bypassing effect of root. In radar data migration processing, the propagation velocity of electromagnetic waves in the soil medium is a key parameter. But due to the complex distribution of the subsurface medium and the large measurement range, the method based on the propagation velocity estimation of sampling points was difficult to obtain a better focusing effect. The image entropy was used to evaluate the chaotic state of the image after migration shown in the equation 1, and the minimum entropy was adopted to estimate the propagation speed of electromagnetic waves and obtained the best focusing effect. The figure2-c showed the result after FK migration.

$$E(X)=\sum_{j=1}^{T}\left\{\frac{\sum_{i=1}^{S}x_{ij}^{4}}{\left[\sum_{i=1}^{S}x_{ij}^{2}\right]^{2}}\right\} \quad (1)$$

Where the T and S are the number of columns and rows of the B-Scan image, respectively. X_{ij} represents the pixel value of the i-th row and j-th column of the image.

Hilbert Transform

Compared with the migration technique to eliminate the bypassing effect, the Hilbert transform converted the radar wave response pulse into the root envelope by phase-shifting the radar wave signal in the frequency domain and constructing its analytic signal. In this paper, the Fourier transform was first used to convert the radar wave signal to the frequency domain, then the frequency domain representation of the analytic signal was constructed by using the relationship between the original signal, the Hilbert transform signal and its analytic signal, followed by the Fourier inverse transform to obtain the analytic signal, and finally the one-half threshold method is used to obtain the root response region. the whole process was shown in the equation 2. The result after Hilbert transform was shown in Figure 2-d and 2-e.

$$x(t)\xrightarrow{FFT}X(\omega)\rightarrow Y(\omega)\xrightarrow{IFFT}y(t) \quad (2)$$

where $x(t)$ and $y(t)$ are the radar signal and its analytic signal.

Root system architecture mapping

Reconstructing the three-dimensional structure of tree root system is an important goal of root detection. Based on the root points recognized in the B-Scan image, the 3D position of the root points could be recovered in combination with the corresponding circular scan trajectory. Then the root points of different scan profiles according to the sequence of trajectories with increasing radius of the scan circumference could be connected and the distribution of root points and density distribution in different depth ranges could be drawn. The 3D structure mapping and density map of root system were shown in Figure 3. Here are the detailed steps for drawing the 3D structure and density map of the camphor root system.

1) Sorting the 9 circumferential scan profiles by radius from smallest to largest.
2) restore the 3D coordinates of the detected root points on the 9 circumferential scan profiles and plot the root point distribution.
3) traverse the circumferential sequence and calculate the geometric distance between the root points of adjacent profiles.
4) Obtain the root connection sequence from inside-out according to the shortest distance principle.
5) Calculate root curves using cubic spline interpolation.
6) Discretize the measurement area using 1 mm as the minimum unit and draw the root distribution density map.

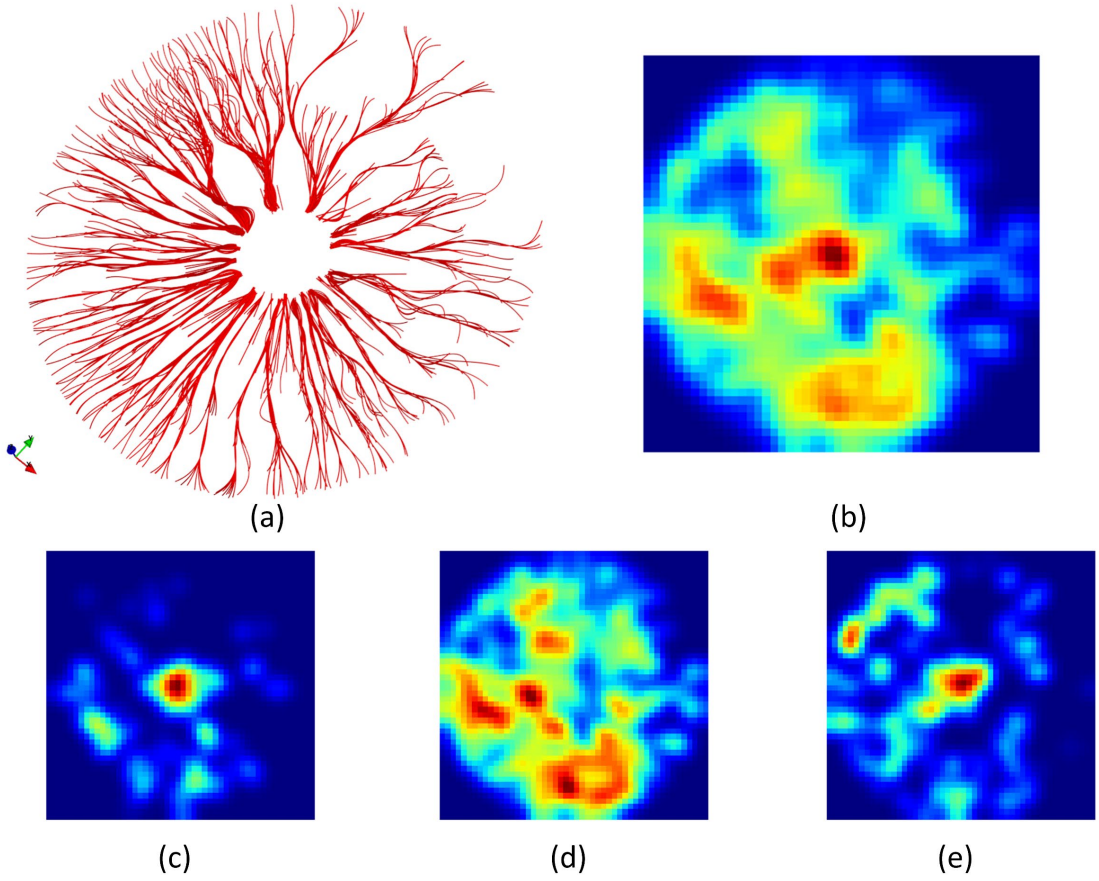

Figure 3—The 3D structure mapping and density map of Camphor root system. a) the root system 3D structure diagram, b) Root density map of the measurement domain, c), d), e) Root density maps in the range of 0-20 cm, 20-40 cm, and 40-60 cm

Conclusions

In order to study the spatial distribution of the underground root system in an ancient tree, GPR technology was applied to circumferentially measure the root system of an ancient camphor tree. In this paper, a 3D reconstruction scheme of ancient tree root system with radar wave image sequences was presented, the spatial structure of the root system of Camphor tree was mapped, and the stratified density distribution of the root system was obtained. First, the position of the roots was identified on the pre-processed radar B-Scan images using FK migration and Hilbert transform, and the fine accuracy was verified by simulation experiments and pre-buried control experiments. Then the detected root points were then combined with the corresponding scan trajectories to recover their 3D coordinates. And the 3D topology of the root system was drawn by the minimum distance method. Finally, the distribution density of the root system was analyzed at different depth ranges.

In practice, root system detection would be influenced by soil distribution and physical parameters of the root system. By accurately estimating the root system physical parameters, such as root location, root diameter, water content and direction, etc., from radar B-Scan images, the root system 3D structure mapping would be more accurate.

Acknowledgments

This research was funded by the Fundamental Research Funds for the Central Universities (Grant No. 2021ZY73), the Beijing Municipal Natural Science Foundation (Grant No. 6202023) and the National Natural Science Foundation of China (Grant No. 32071679). We thank all authors for their cooperation.

References

BARTON C V M, MONTAGU K D 2004. Detection of tree roots and determination of root diameters by ground penetrating radar under optimal conditions. Tree Physiology [J], 24: 1323-1331.

BUTNOR J R, DOOLITTLE J A, JOHNSEN K H, et al. 2003. Utility of Ground-Penetrating Radar as a Root Biomass Survey Tool in Forest Systems. Journal of Soil Science Society of America [J], 67: 1607-1615.

BUTNOR J R, DOOLITTLE J A, KRESS L, et al. 2001. Use of ground-penetrating radar to study tree roots in the southeastern United States. Tree Physiology [J], 21: 1269-1278.

BUTNOR J R, SAMUELSON L J, STOKES T A, et al. 2016. Surface-based GPR underestimates below-stump root biomass. Plant and Soil [J], 402: 47-62.

CUI X, LIU X, CAO X, et al. 2020. Pairing dual-frequency GPR in summer and winter enhances the detection and mapping of coarse roots in the semi-arid shrubland in China. European Journal of Soil Science [J], 71: 236-251.

GUO L, LIN H, FAN B, et al. 2013. Impact of root water content on root biomass estimation using ground penetrating radar: evidence from forward simulations and field controlled experiments. Plant and Soil [J], 371: 503-520.

LI W, CUI X, GUO L, et al. 2016. Tree Root Automatic Recognition in Ground Penetrating Radar Profiles Based on Randomized Hough Transform. Remote Sensing [J], 8.

LIU X, DONG X, XUE Q, et al. 2018. Ground penetrating radar (GPR) detects fine roots of agricultural crops in the field. Plant and Soil [J], 423: 517-531.

MA Z Q, GUO D L, XU X L, et al. 2018. Evolutionary history resolves global organization of root functional traits. Nature [J], 555: 94-+.

MOLON M, BOYCE J I, ARAIN M A 2017. Quantitative, nondestructive estimates of coarse root biomass in a temperate pine forest using 3-D ground-penetrating radar (GPR). Journal of Geophysical Research-Biogeosciences [J], 122: 80-102.

STOKES A, FOURCAUD T, HRUSKA J, et al. 2002. An evaluation of different methods to investigate root system architecture of urban trees in situ. I. Ground-penetrating radar. Journal of Arboriculture [J], 28: 2-10.

WU Y, GUO L, CUI X, et al. 2014. Ground-penetrating radar-based automatic reconstruction of three-dimensional coarse root system architecture. Plant and Soil [J], 383: 155-172.

XIAO L, LI C, CAI Y, et al. 2021. Preliminary Application of Ground-Penetrating Radar for Reconstruction of Root System Architecture in Moso Bamboo. Remote Sensing [J], 13.

ZHANG X, XUE F, WANG Z, et al. 2021. A Novel Method of Hyperbola Recognition in Ground Penetrating Radar (GPR) B-Scan Image for Tree Roots Detection. Forests [J], 12: 1019.

ZHU S, HUANG C, SU Y, et al. 2014. 3D Ground Penetrating Radar to Detect Tree Roots and Estimate Root Biomass in the Field. Remote Sensing [J], 6: 5754-5773.

Nondestructive Timber Testing as a Tool to Detect Depletion of Carbon Storage in Stem of Aspen

Linda Čakša
Forest tree breeding and climate change, Latvian State Forest Research Institute "Silava", Salaspils, Latvia, linda.caksa@silava.lv

Laura Ķēniņa
Forest tree breeding and climate change, Latvian State Forest Research Institute "Silava", Salaspils, Latvia, laura.kenina@silava.lv

Nauris Siksna
Forest tree breeding and climate change, Latvian State Forest Research Institute "Silava", Salaspils, Latvia, nsiksna@gmail.com

Kristaps Ozoliņš
Forest tree breeding and climate change, Latvian State Forest Research Institute "Silava", Salaspils, Latvia, kristaps.ozolins@silava.lv

Ieva Jaunslaviete
Forest tree breeding and climate change, Latvian State Forest Research Institute "Silava", Salaspils, Latvia, ieva.jaunslaviete@silava.lv

Āris Jansons*
Forest tree breeding and climate change, Latvian State Forest Research Institute "Silava", Salaspils, Latvia, aris.jansons@silava.lv

Abstract

Carbon sequestration and storage are increasingly important forest ecosystem services, even so much that forests can be established and maintained only for this purpose, which can be easily implemented by using widespread and fast-growing tree species, such as Eurasian Aspen (*Populus tremula* L.). However, aspen is considered to be particularly prone to biotic agents, which can notably reduce the life span of aspen even in stand level. Therefore, determination of the optimal rotation period for this species in terms of carbon sequestration could facilitate evaluation of the role of old aspen stands in climate-change mitigation. The study was carried out in European hemiboreal forests of Latvia, where wood density of stem basal part (determined by a resistograph) was compared with actual wood density and carbon content (after felling) for 1305 trees in aspen-dominated old-growth (104 to 135 years) stands. Most of the tested aspen had stem-rot, leading to 17% lower wood density for moderately decomposed stage, while strongly decayed stems had up to 5 times lower wood density than that of a healthy aspen. For moderately decomposed stems, carbon concentration did not differ from unaffected wood, while for strongly decayed stems it was 4% higher. However, stem rot led to only 2% to 9% reduction of carbon storage on old-growth aspen stands. A resistograph can be used as the identification of stem decay levels in any aspen stand. Further studies shall address the amplitude of presence of stem-rot in mid-aged stands as the old-growth stands may represent an outlier from the average trend due to aging effect.

Keywords: Eurasian aspen, *Populus tremula*, resistograph, Carbon sequestration, stem-rot, hemiboreal forests.

Loading Resistance of Silver Birch (*Betula pendula* Roth.) and Eurasian Aspen (*Populus tremula* L.) in Urban and Peri-urban Forests

Oskars Krišāns
Forest tree breeding and climate change, Latvian State Forest Research Institute "Silava", Salaspils, Latvia, oskars.krisans@silava.lv

Linda Čakša
Forest tree breeding and climate change, Latvian State Forest Research Institute "Silava", Salaspils, Latvia, linda.caksa@silava.lv

Roberts Matisons
Forest tree breeding and climate change, Latvian State Forest Research Institute "Silava", Salaspils, Latvia, roberts.matisons@silava.lv

Steffen Rus
Faculty of Resource Management, University of Applied Sciences and Arts, Göttingen, Germany, steffen.rust@hawk.de

Didzis Elferts
Faculty of Biology, University of Latvia, Riga, Latvia, didzis.elferts@lu.lv

Andris Seipulis
Forest tree breeding and climate change, Latvian State Forest Research Institute "Silava", Salaspils, Latvia, andris.seipulis@silava.lv

Āris Jansons*
Forest tree breeding and climate change, Latvian State Forest Research Institute "Silava", Salaspils, Latvia, aris.jansons@silava.lv

Abstract

In urbanized areas, wind disturbances can be intensified by anthropogenic stresses under which trees may become hazardous, creating serious threats and damages to near targets. Therefore, species with notably lower wood mechanical properties and compartmentalization, such as pioneers, are considered to have higher wind damage risk if subjected to unfavorable growing conditions. Eurasian aspen (*Populus tremula* L.) and silver birch (*Betula pendula* Roth.) are frequently found in both urban and peri-urban forests in northeastern and central parts of Europe, which strengthens the necessity for the evaluation of mechanical stability of such species. Therefore, static pulling tests were performed to compare the mechanical stability of the studied species in urban and peri-urban forests. The loading resistance of the studied species differed, with birch being more stable than aspen, indicating that aspen is more prone to wind damage. Also, the mechanical stability of birch did not differ between trees growing in urban forests and those growing in peri-urban forests, suggesting that static pulling tests are a suitable method for comparison of trees from completely different growing conditions.

Keywords: Eurasian aspen, *Populus tremula*, silver birch, *Betula pendula* Roth., static tree-pulling test, urban forests, peri-urban forests

Near-Infrared Spectroscopy Coupled with Chemometric Analysis as a Valuable Nondestructive Tool for Prediction of Carbon Content in Wood Samples

Iris Beatriz Vega Erramuspe*
Forest Products Development Center, School of Forestry and Wildlife Sciences, Auburn University, Auburn, Alabama, USA, ibv0002@auburn.edu

Dana Mitchel
USDA Forest Service Laboratory, Auburn, Alabama, USA

Jason Thompson
USDA Forest Service Laboratory, Auburn, Alabama, USA, jason.d.thompson@usda/gov

Thomas Elder
USDA Forest Service Laboratory, Auburn, Alabama, USA, thomas.elder@usda.gov

Brian Via
Forest Products Development Center, School of Forestry and Wildlife Sciences, Auburn University, Auburn, Alabama, USA, brianvia@auburn.edu

* Corresponding author

Abstract

As interest in wood as one of the primary feedstocks for the materials, energy, and chemicals of the future continues to grow, the need for an accurate estimation of the amount of wood available for consumption becomes more evident. Carbon-Nitrogen-Hydrogen (CHN) elemental analyzers are used in routine analysis to quickly determine the carbon, nitrogen, and hydrogen content in lignocellulosic biomass. Near-infrared (NIR) spectroscopy is widely used to study the chemical composition of these samples also. The chemometric analysis of large and complex data from NIR spectroscopy measurements is a powerful tool for predicting the carbon content in woody biomass samples. This study was carried out with more than one hundred samples from the same tree species. The ground samples were analyzed using a Thermo Scientific Flash2000 Series Elemental Analyzer and a Perkin Elmer Spectrum 400 FT-NIR spectrophotometer equipped with a 10-mm sample spinner accessory in a near-infrared reflectance accessory (NIRA). Partial least square (PLS) and principal components regression (PCR) algorithms were used in the chemometric analysis. The results show the potential of NIR spectroscopy as a quick and nondestructive method to predict the C content of woody biomass. Additionally, the results clearly show the importance of sample collection and preparation.

Keywords: near-infrared reflectance accessory, FT-NIR spectroscopy, chemometrics, template near infrared reflectance accessory

Assessment of Incipient Decay on Wood Using Stress Wave Technique

Tamara Franca*
Department of Sustainable Bioproducts, Mississippi State University, Starkville, Mississippi, USA, tsf97@msstate.edu

Brianna Duquette
Department of Sustainable Bioproducts, Mississippi State University, Starkville, Mississippi, USA, bad477@msstate.edu

Adam Senalik
Engineering Properties of Wood, Wood based Materials and Structures, USDA Forest Service, Forest Products Laboratory, Madison, Wisconsin, USA, christopher.a.senalik@usda.gov

Robert Ross
Engineering Properties of Wood, Wood based Materials and Structures, USDA Forest Service, Forest Products Laboratory, Wisconsin, USA, robert.j.ross@usda.gov

* Corresponding author

Abstract

Wood is a biological, sustainable, and renewable material. However, because of its nature, it is susceptible to degradation. To fully achieve the capacity of wood structures, it is important to understand the behavior of the material and to monitor in-service wood, consequently enhancing safety and avoiding unnecessary replacement. The objective of this work was to evaluate the performance of nondestructive testing (NDT) to detect early decay in wood structures. This work is part of a larger study that focuses on improvement of in-service condition assessment of wood structures such as timber bridges and mass timber structures. A total of 320 specimens of untreated southern yellow pine measuring 0.5 by 0.5 by 11.25 in. (tangential by radial by longitudinal directions) were exposed to natural conditions. The NDT method used in this study was stress wave speed. Time of flight (TOF) was also recorded. For this work, the variables presented included mass loss, TOF, and ultimate tension strength (UTS). NDT was the most consistent method in identifying early decay in wood, and it was able to identify decay before any significant changes in mass loss or UTS. The results of this project will help improve on-site assessment of wood structures and increase scientists', builders', and end-users' knowledge of wood used as a building material.

Keywords: early degradation, fungi damage, detection of decay, evaluation, wood structures

Poster Session

Approved Method for Efficient Inspection and Documentation of Not Only Historic Timber Structures based on Results Obtained in Hundreds of Successful Projects Since 1988

Frank Rinn*
Court registered Expert for Tree and Timber Inspection, Heidelberg, Germany

* Corresponding author

Abstract

Caring about historic buildings is not only important for preserving a society's cultural heritage and for attracting tourists, but it also brings other benefits: a 700-year-old roof structure of a church in Germany, for example, not only teaches us how to build stably and sustainably for a long usage time but also what needs to be done to ensure that such a structure survives for centuries without significant damage. A special combination of conventional inspection (visual and tapping) and electronically regulated, high-resolution resistance drilling was shown to be affordable and efficient in reliably examining the condition of old wood in structures. But, how the results are presented is critical, so that administrations, architects, engineers, and repairing carpenters quickly and fully understand the condition of the structure. For this, we developed a special concept for mapping the condition (very different from just showing defects) and successfully used it in hundreds of projects (church roofs, multistory half-timbered buildings, timber bridges, timber towers, playground toys, harbor structures, etc.). Compared with previous common procedures, our inspections help preserve more historic integrity and at the same time typically lead to reduced repair costs of about 50% due to various reasons. For example, we find ‘hidden’ defects and we can examine even invisible beams behind stucco or in ceilings. Based on our condition sketches, the renovation measures can be well planned, organized, and optimized beforehand. In addition, our results help with designing better new timber structures that last longer with less defects.

Keywords: resistance drilling, timber structures, condition mapping

Urban Green Spaces and How They Affect Woody Species Diversity and Biomass Carbon Stock in Hawassa, Ethiopia

Abel Woldeyohanis*
Faculty of Science, Addis Ababa University, Addis Ababa, Ethiopia. abel.feyisa@aau.edu.et

Mesele Negash
Wondo Genet College of Forestry and Natural Resources, Hawassa University, Hawassa, Ethiopia, kelemuamesele@yahoo.com

Yoseph Melka
Wondo Genet College of Forestry and Natural Resources, Hawassa University, Hawassa, Ethiopia, yosef.melka@gmail.com

Abstract

Urbanization tends to alter the ecosystem. Urban green spaces are established to reduce impacts of urbanization. However, in developing regions, this is often neglected. The city of Hawassa, Ethiopia, has been greatly affected by rapid urbanization. Hence, this study's aim was to assess the role of green infrastructure in woody species diversity and carbon stock in Hawassa. A cluster sampling method was used to classify the existing green infrastructure. In this study, 240 sample plots were used to compile a woody species inventory and for soil sampling. Also, 58 woody species belonging to 44 genera and 28 families were recorded; 67.25% of these were exotics. The highest Shannon–Wiener diversity was in private and public institution compounds (mean 1.35) and the least diversity was in street trees (0.68). The highest mean biomass carbon was recorded in street trees (167.5 t C ha^{-1}) and the lowest was in urban forests (11.4 t C ha^{-1}). Soil organic carbon accounted for 90% of ecosystem carbon stocks for urban forests, 60% for private and public institutions, 57% for urban church forests, and 37% for street trees. Generally, there is lower species diversity and a dominance of exotic species. Planting diverse and indigenous species should be the next priority.

Keywords: carbon stock, Ethiopia, Hawassa, urban green infrastructure, woody species diversity